

**DNA-Ferrocene Covalent Adducts for Studying  
DNA Conductance and Engineering Molecular  
Recognition Switch of DNA Base Pairing**

**THESIS SUBMITTED TO  
THE UNIVERSITY OF PUNE  
FOR THE DEGREE OF  
DOCTOR OF PHILOSOPHY  
IN  
CHEMISTRY**

**BY  
AMIT NARESHKUMAR PATWA**

**DIVISION OF ORGANIC CHEMISTRY  
NATIONAL CHEMICAL LABORATORY  
PUNE 411008  
INDIA**

**APRIL 2009**



# राष्ट्रीय रासायनिक प्रयोगशाला

(वैज्ञानिक तथा औद्योगिक अनुसंधान परिषद)

डॉ. होमी भाभा मार्ग पुणे - 411 008. भारत

## NATIONAL CHEMICAL LABORATORY



(Council of Scientific & Industrial Research)

Dr. Homi Bhabha Road, Pune - 411 008. India.

### CERTIFICATE

This is to certify that the work presented in the thesis entitled “DNA-Ferrocene Covalent Adducts for Studying DNA Conductance and Engineering Molecular Recognition Switch of DNA Base Pairing” submitted by **Amit N. Patwa**, was carried out by the candidate at the National Chemical Laboratory, Pune, under our supervision. Such materials as obtained from other sources have been duly acknowledged in the thesis.

**Prof. K. N. Ganesh, FNA, FNASc.**  
(Research Guide)

**Director, IISER Pune,**  
**Pune-411008.**


**J. C. Bose Fellow**  
**National Chemical Laboratory,**  
**Pune-411008.**

**Dr. (Mrs.) Vaijayanti A. Kumar**  
(Research Co-Guide)

**Division of Organic Chemistry,**  
**National Chemical Laboratory,**  
**Pune-411008.**

**APRIL 2009**

**Communication  
Channels**

  
NCL Level DID : 2590  
NCL Board No. : +91-20-25902000  
EPABX : +91-20-25893300  
+91-20-25893400

**FAX**

Director's Office : +91-20-25902601  
COA's Office : +91-20-25902660  
COS&P's Office : +91-20-25902664

**WEBSITE**

[www.ncl-india.org](http://www.ncl-india.org)



**NATIONAL CHEMICAL LABORATORY**

---

---

## **CANDIDATE'S DECLARATION**

---

---

I hereby declare that the thesis entitled **“DNA-Ferrocene Covalent Adducts for Studying DNA Conductance and Engineering Molecular Recognition Switch of DNA Base Pairing”** submitted for the degree of Doctor of Philosophy in Chemistry to the University of Pune has not been submitted by me to any other University or Institution. This work was carried out at the National Chemical Laboratory, Pune, India.

**Amit N. Patwa**  
**Senior Research Fellow**  
**Division of Organic Chemistry,**  
**National Chemical Laboratory,**  
**Pune – 411008.**  
**INDIA.**

**APRIL 2009**

*DEDICATED  
TO  
MY BELOVED PARENTS  
AND  
FAMILY MEMBERS*



---

---

## Acknowledgement

---

---

Where would I be without my family? My parents deserve special mention for their inseparable support and prayers. My Father, Nareshbhai Patwa, is the person who put the fundament to my learning character, showing me the joy of intellectual pursuit ever since I was a child. My Mother, Lataben Patwa, is the one who sincerely raised me with her caring, gentle and unconditional love.

There are so many people, whose support, encouragement & inspiration are very much essential to accomplish major achievements in life, especially, if it involves the elements of fulfilling one's cherished dreams. This Thesis is by far the most significant scientific accomplishment in my life and it would be impossible without people who supported me and believed in me. I have worked with a great number of people whose contribution in assorted ways to the research and the making of the thesis deserves special mention. It is a pleasure to convey my gratitude to them all in my humble acknowledgment.

In the first place I would like to record my gratitude to Prof. K. N. Ganesh, my research supervisor, for his supervision, advice, and guidance from the very early stage of this research as well as giving me extraordinary experiences through out the work. Above all and the most needed, he provided me unflinching encouragement and support in various ways. His truly scientist intuition has made him a constant oasis of ideas and passions in science, which exceptionally inspire and enrich my growth as a student, a researcher and a scientist want to be. I thank him from the bottom of my heart for introducing me to the science of bioorganometallic chemistry. I am indebted to him more than he knows.

My special thanks go to Dr. (Mrs.) Vaijayanti A. Kumar, my research co-guide, for her untiring support, valuable guidance and critical suggestions. I value her concerns and motivation. Discussion with her has been very stimulating and helped to make most logical plan of action for work.

I am grateful to Dr. Mohan M. Bhadbhade and Dr. Rajesh G. Gonnade without whose expertise in X-ray crystallography the second chapter would not have been possible. Their scientific temper and pleasing personalities make them great people to work with. I take this opportunity to place on record my thanks to Dr. K. Vijayamohanan and P. Meera for recording and interpreting cyclic voltammograms of ferrocene-nucleobase conjugates as well as ferrocene-oligonucleotide conjugates.

I am very much grateful to Mrs. Anita Gunjal for providing synthesized DNA as well as for synthesis of ferrocene modified oligonucleotides. I also thank to Mrs. M. V. Mane and Mrs. S. S. Kunte for carrying out HPLC analysis. My special thanks for Mrs. M. V. Mane who taught me HPLC technique. I wish to thank my senior Dr. Moneesha D'costa for teaching me Gel Electrophoresis technique. She was always there to help me. I also thank Dr. (Mrs.) Susmita Gupta with whom I have worked during initial stage of my research career. I also thank to Dr. B. G. Hazara, Dr. Vandana S. Pore and their research group.

The kind support from NMR group is greatly acknowledged and thanks to Dr. Rajmohanan and Mrs. Kavitha. I wish to thank Mrs. Shanthakumari and Dr. Mahesh Kulkarni for their help in recording the LC-MS and MALDI-TOF spectra.

It is my privilege to thank Dr. Ganesh Pandey, Head, OCD, for his constant encouragement and interest shown during the progress of my work. I am also grateful to Dr. H. V. Thulasiram, Dr. N. P. Argade, Dr. D. D. Dhavale, Dr. Srinivas Hotha, Dr. V. R. Pedireddi, for their help and encouragement.

I express my sincere thanks to my chemistry teacher Fatima madam and my tutor A. K. Shah for developing interest in chemistry field at school days. I also thank Dr. S. M. Desai and Prof. A. C. Shah (The former Head-Chemistry Department and Dean-Science Faculty), M. S. University of Baroda, Vadodara, Gujarat, for their concern and guiding in my M. Sc. course.

It is hard to find a lab better well-knit as a unit than the one I was blessed with an opportunity to work in. I had wonderful seniors Pallavi, Nagendra, Dinesh, Govindraju, Praveen, Sunil, Umashankar, Gourishankar, Raman and Khirud, who have extended their friendship and helped me with various capacities. The co-operation and support extended by Ashwani, Sreedhar, Gitali, Roopa, Pradnya, Manaswini, Mahesh, Nasrin, Satish, Madhuri, Sachin, Seema, Parameshwar, Namrata, Harshal, Venu, Kiran and Harshit have been exemplary, to say the least, and I cherished their company throughout. If there was never a dull moment when I was in the lab it was due to the amazing atmosphere filled with humour & harmony that prevailed there. I also thank organic chemistry office staff – Mrs. Deshpande, P. V. Iyer, Catherine, Kulkarni, Pawar, Bhumkar and Fernandes for their assistance in many ways throughout my tenure at NCL.

My stay here was made livelier by GJ hostel, a hostel unique in ways more than one. It provided the perfect atmosphere to spend leisure time and I thoroughly enjoyed all the sports & cultural activities that abounded in the hostel. I owe a big “thanks” to all my friends who made GJH such a wonderful place to stay in. I also thank to Chakru et al. for the delicious food. I also enjoyed my stay at New Hostel and I thank to all the member of New Hostel for developing and maintaining friendly atmosphere. I was lucky to have some really nice seniors and colleagues in all of NCL during my stay here. My table mates: Mahesh Thakkar, Kishor (Bhaiya), Sambhaji, Baag (Sheru), Aarif (Captain), Bhalchandra, Shivanand Pai, Ganesh Kokate (with whom I have seen many marathi movies) and Nilesh.

I also thank to seniors and colleagues of Lab 288 – Murugan, Kapoorji, Prabalda, Dumbre, Sanjay, Balaji, Tiwariji, Nishant (Guptaji), Sujit, Ravi, Kesari, Debasish (maharaj), Debasis Dey, Priyanka, Rajendra, Prasanna, Swaroop, Srikant and Deepak for all their kind help I needed. I will never forget those wonderful and memorable picnic days which I have spent with them.

I am lucky enough to have the support of many good friends and seniors. Life would not have been the same without them. Thanks to my roommate M. Sankar and my other friends: Easwar, Pashupathy, Mallikarjun, Subramanium, Selvakannan, Devraj, Anirban, Mandar Bodas, Bidhan, Vijayraj, Prathap, Nitin Pagar, Mukulesh,

*Dholakiya Saheb, Shrojal, Shilendra, Pratheep(PK), Satyanarayan Reddy, Govande, Ramesh Patel, Pinak and Pushpesh for their cheerful company and making my life in NCL very lively and enjoyable.*

*I am thankful to BCCGJ, NCL sports community and all the cricket playing members and friends Sudhir, Ashish, S. Rao, Atul, Amol, Subramaniam, Ramanujan, Kannan, Ganya, Sarvesh, Kamendra, Dilip, Nishant V., Ramesh, Sameer, Somesh, Sushbhai, Mudit, Mishra (Don), Dharna, Sudhakar, Ankush, Abhijit, Mandeep, Varun and all the member of NCL Cricket Team essentially Balmiki M.(Dhoni), Ganeshbhai, Sharik Inamdar, Sunil Pate, Sankar Mane, Prashant Kulkarni, Atul Mahajan and M. Vadnere, which made my stay a memorable one, which always took me away from distress and never let me feel alone.*

*O! Oh!! How can my "Kalitiri" group friends be left out?... How can I forget the real gems in my life?... Such friends rarely occurs. . . these rare-earth elements Mehul-Kavita, Chaku-Divya, Sunil-Shilpa, Nimit-Birva, Jigar-Ami, Siddharth-Khyati, Zankar-Komal, Daxesh-Manisha and Keyur-Hiral get full marks. My school friends Samrat-Priyanka, Mehul-khyati, Dongre-Sonal, Mahek, Pinal, Sonal, Sujal, Umang and Virat-Nimisha also deserve citation at this juncture.*

*I am grateful to UGC-CSIR, New Delhi, Government of India, for awarding the junior and senior research fellowships, IISER-PUNE for financial support, Dr. S. Sivaram, Director, and Dr. B. D. Kulkarni, Deputy Director, National Chemical Laboratory to carry out my research works, extending all infrastructural facilities and to submit this work in the form of a thesis for the award of Ph. D. degree.*

*It has been a difficult task to capture and express my feelings for my family members. What I am and intend to be in the future is because of the good will and unstinted support of my parents, elder brother, Niraj, my bhabhi, Archana and my nephew-a little champ-nishil without knowing much what I am doing exactly, just wishing me all the time with no expectations. No words are enough to acknowledge them for their patience and sacrifice which were always remain a source of inspiration and will remain throughout my life. Words fail me to express my appreciation to my wife Aashka whose dedication, love and persistent confidence in me, has taken the load off my shoulder. I am also grateful to my wife for the unconditional support and encouragement in all my effort and being always there for me. My success now and always will be dedicated to my family. I would also thank my father-in-law (Nipunbhai Shah), mother-in-law (Shobhanaben Shah) and brother-in-law (Rushit) for letting me take her hand in marriage, and accepting me as a member of the family, warmly.*

*Finally, my acknowledgement would not be complete without thanking the Almighty, for the strength and determination to put my chin up when faced with hardships in life.*

***Amit Nareshkumar Patwa***

# CONTENTS

<b>ABBREVIATIONS</b>	<b>i</b>
<b>ABSTRACT</b>	<b>v</b>
<b>PUBLICATION / PRESENTATION</b>	<b>xix</b>

---

## CHAPTER 1 INTRODUCTION: BIOCONJUGATES OF FERROCENE AND THEIR APPLICATIONS

---

<b>1.1 Nucleic Acids: Chemical Structure</b>	<b>01</b>
1.1.1 Shapes of nucleotides	03
1.1.2 Sugar pucker in nucleosides	04
1.1.3 Base pairing via hydrogen bonding	04
1.1.4 DNA secondary structures	06
1.1.5 Molecular recognition in the major and minor grooves of duplex DNA	08
1.1.6 Bioorganometallic chemistry of DNA	10
<b>1.2 Ferrocene: A Sandwich Compound</b>	<b>10</b>
1.2.1 Methods of synthesis of ferrocene	12
1.2.2 Structure and physical properties of ferrocene	12
1.2.3 Chemical properties of ferrocene	14
<b>1.3 Bioorganometallic Chemistry of Ferrocene</b>	<b>15</b>
1.3.1 Ferrocene-nucleobases conjugates	19
1.3.2 Ferrocene-oligonucleotide conjugates	23
1.3.3 Applications of ferrocene-labeled DNA oligomers as gene sensors	28
<b>1.4 Present Work</b>	<b>31</b>
<b>1.5 References</b>	<b>33</b>



---

---

## CHAPTER 2

### FERROCENE-NUCLEOBASE CONJUGATES: SYNTHESIS AND X-RAY CRYSTAL STRUCTURE STUDIES

---

---

<b>2.1</b>	<b>Introduction</b>	38
<b>2.2</b>	<b>Present Work: A Rationale and Objective</b>	39
<b>2.3</b>	<b>Synthesis of Ferrocene-Nucleobase Conjugates</b>	40
2.3.1	Synthesis of ferrocene-linked mono and bis-thymine/ uracil/5-bromouracil conjugates with <i>n</i> -butyl spacer	40
2.3.2	Synthesis of ferrocene-linked thymine and uracil conjugates at different chain end with <i>n</i> -butyl spacer	44
2.3.3	Synthesis of ferrocene-linked bis thymine/uracil conjugates with methylene spacer	45
2.3.4	Synthesis of ferrocene-linked thymine and uracil conjugates at different chain end with methylene spacer	47
2.3.5	Synthesis of ferrocene-linked mono and bis adenine conjugates with <i>n</i> -butyl spacer	48
2.3.6	Synthesis of ferrocene-linked chimeric thymine /adenine conjugates end with <i>n</i> -butyl spacer	49
2.3.7	Attempts towards synthesis of ferrocene linked bis(cyanuric acid (CA)) conjugate with <i>n</i> -butyl spacer	50
<b>2.4</b>	<b>X-ray Crystal Structure Analysis</b>	52
2.4.1	X-ray crystal structures and self-assembly in ferrocene bis(nucleobase) conjugates with <i>n</i> -butyl spacer	52
2.4.2	X-ray crystal structures and self-assembly in ferrocene mono nucleobase conjugates with <i>n</i> -butyl spacer	57
2.4.3	X-ray crystal structures and self-assembly in ferrocene bis(nucleobase) conjugates with methylene spacer	60
2.4.4	X-ray crystal structures and self-assembly in ferrocene mono adenine conjugate with <i>n</i> -butyl spacer	67
2.4.5	X-ray crystal structures and self-association properties in ferrocene-cyanuric acid conjugates with <i>n</i> -butyl spacer	70

<b>2.5</b>	<b>Conclusions</b>	78
<b>2.6</b>	<b>General Experimental Methods</b>	82
<b>2.7</b>	<b>Experimental</b>	83
<b>2.8</b>	<b>References</b>	102
<b>2.9</b>	<b>Appendix</b>	105

---

**CHAPTER 3**  
**FERROCENE-OLIGONUCLEOTIDE CONJUGATES: SYNTHESIS,**  
**CHARACTERIZATION AND BIOPHYSICAL STUDIES**

---

<b>3.1</b>	<b>Introduction</b>	168
	3.1.1 Spectroscopic methods for studying DNA interaction	168
	3.1.2 Gel electrophoresis	170
<b>3.2</b>	<b>Present Work: A Rationale and Objective</b>	171
<b>3.3</b>	<b>Synthesis of Ferrocene-Phosphoramidite Monomer Unit</b>	172
<b>3.4</b>	<b>Synthesis, Purification and Characterization of Ferrocenyl-Modified Oligonucleotides</b>	173
<b>3.5</b>	<b>Results and Discussion</b>	175
	3.5.1 Gel shift assays	175
	3.5.2 UV- <i>T<sub>m</sub></i> studies	182
<b>3.6</b>	<b>Conclusions</b>	185
<b>3.7</b>	<b>General Experimental Methods</b>	186
<b>3.8</b>	<b>Experimental</b>	186
<b>3.9</b>	<b>References</b>	191
<b>3.10</b>	<b>Appendix</b>	193

**CHAPTER 4  
FERROCENE-NUCLEOBASE AND FERROCENE-  
OLIGONUCLEOTIDE CONJUGATES: ELECTROCHEMICAL  
INVESTIGATION**

<b>4.1</b>	<b>Introduction</b>	204
4.1.1	Bioelectrochemistry: DNA and nucleobase electrochemistry trends	204
4.1.2	Redox labeling approach for direct electrochemistry of DNA	206
4.1.3	Why ferrocene?	207
<b>4.2</b>	<b>Electrochemical Investigation of Ferrocene-Nucleobase Conjugates and Ferrocene-Oligonucleotide Conjugates</b>	<b>209</b>
4.2.1	Ferrocene-nucleobase conjugates	209
4.2.2	Ferrocene-oligonucleotide conjugates	210
<b>4.3</b>	<b>Electrochemical Techniques</b>	<b>212</b>
4.3.1	Cyclic voltammetry	212
4.3.2	Ultramicroelectrode Voltammetry (Steady State Voltammetry)	216
<b>4.4</b>	<b>Present Work: Experimental Section</b>	<b>219</b>
4.4.1	Electrochemical experiments for ferrocene-nucleobase conjugates	219
4.4.2	Electrochemical experiments for ferrocene-oligonucleotide conjugates	222
<b>4.5</b>	<b>Results and Discussion</b>	<b>223</b>
4.5.1	Ferrocene-nucleobase conjugates: electrochemical investigation	223
4.5.2	Ferrocene-oligonucleotide conjugates: electrochemical investigation	227
<b>4.6</b>	<b>Conclusions</b>	<b>230</b>
<b>4.7</b>	<b>References</b>	<b>231</b>

---

---

**ABBREVIATIONS**

---

---

Å	Angstrom
Br-U	5-Bromouracil
°C	Degree Celsius
A	Adenine
Ac	Acetyl
Ac <sub>2</sub> O	Acetic anhydride
AlCl <sub>3</sub>	Aluminum chloride
aq.	Aqueous
bp	Base pair
BPB	Bromophenol Blue
BSA	Bovine Serum Albumin
Bz	Benzoyl
C	Cytosine
Calcd.	Calculated
CD	Circular Dichroism
Cp	Cyclopentadienyl
CTG	Cholne transport gene
CV	Cyclic Voltammetry
dA	2'-Deoxyadenosine
DAAO	D-Amino Acid Oxidase
dC	2'-Deoxycytidine
DCM	Dichloromethane
ddUTP	Dideoxynucleotide triphosphate
decomp.	Decompose
deg. / °	Degree centigrade
dG	2'-Deoxyguanosine
DCM	Dichloromethane
DIAD	<i>N,N'</i> -Diisopropylazadicarboxylate
DIPEA	Diisopropylethylamine
DMAP	4',4'-Dimethylaminopyridine

DME	1,2-Dimethoxyethane
DMF	<i>N,N</i> -Dimethylformamide
DMSO	Dimethylsulfoxide
DMT	Dimethoxytrityl
DMT-Cl	4,4'-Dimethoxytrityl chloride
DNA	2'-Deoxyribonucleic acid
ds	Double stranded
dT	2'-Deoxythymidine
dU	2'-Deoxyuridine
dUTP	Deoxynucleotide triphosphate
ECD	Electrochemical detector
EDTA	Ethylenediaminetetraacetic acid
Et	Ethyl
EtOAc	Ethyl acetate
EtOH	Ethanol
FAD	Flavin adenine dinucleotide
FADH <sub>2</sub>	reduced FAD
Fc	Ferrocene
fmol	Femtomole
FTIR	Fourier Transform Infrared
G	Guanine
g	gram
GOD/Gox	Glucose Oxidase
h / hr	Hours
H <sub>2</sub> SO <sub>4</sub>	Sulfuric acid
HG	Hoogsteen
HPLC	High Performance Liquid Chromatography
Hz	Hertz
I	Ionosine
ISE	Ion-Selective electrode
K <sub>2</sub> CO <sub>3</sub>	Potassium carbonate
KOH	Potassium hydroxide
LC-MS	Liquid Chromatography-Mass Spectrometry

LiAlH <sub>4</sub> / LAH	Lithium aluminum hydride
LiOH	Lithium hydroxide
M	Molar
m.p.	Melting point
MALDI-TOF	Matrix Assisted Laser Desorption Ionisation-Time of Flight
MeOH	Methanol
mg	milligram
MHz	Megahertz
min	minutes
μL	micro liter
mL	milliliter
μm	Micro meter
μM	Micro molar
μs	Micro second
mM	Millimolar
mmol	Millimoles
MO	Molecular Orbital
<i>m</i> -RNA	Messenger RNA
Ms	Methanesulfonyl
MS	Mass Spectrometry
MsCl	Methanesulfonyl chloride
MW	Molecular Weight
N	Normal
NaH	Sodium Hydride
NH <sub>3</sub>	Ammonia
nm	nanometer
NMR	Nuclear Magnetic Resonance
ODNs	Oligodeoxynucleotides
ox	oxidation
P <sub>2</sub> O <sub>5</sub>	Potassium pentoxide
Pd	Palladium
PNA	Peptide Nucleic Acid
PPh <sub>3</sub>	Triphenylphosphine

ppm	Parts per million
Py	Pyridine
q	quartet
QCM	Quartz Crystal Microbalance
QRE	Quasi Reference Electrode
r.t. / rt	Room Temperature
red	reduction
RNA	Ribonucleic acid
RP-HPLC	Reversed Phase-HPLC
rWC	reverse Watson-Crick
S	second
SECM	Scanning Electrochemical Microscope
SPM	Scanned Probe Microscope
SPR	Surface Plasmon Resonance
ss	single strand / single stranded
STM	Scanning Tunneling Microscopy
T	Thymine
TBAF	Tetrabutylammonium fluoride
TBDMS	<i>tert</i> -Butyldimethylsilyl
TEA / Et <sub>3</sub> N	Triethylamine
THF	Tetrahydrofuran
TLC	Thin layer chromatography
T <sub>m</sub>	Melting temperature
TMEDA	<i>N,N,N',N'</i> -Tetramethylethylenediamine
TMS	Tetramethylsilane
TMS-	Trimethylsilyl
<i>t</i> -RNA	Transfer RNA
U	Uracil
UME	Ultramicroelectrode
UV-Vis	Ultraviolet-Visible
WC	Watson-Crick

---

---

## ABSTRACT

---

---

**Research Student: Amit Nareshkumar Patwa**

**Research Guide: Prof. K. N. Ganesh**

**Research Co-Guide: Dr. (Mrs.) Vaijayanti A. Kumar**

---

---

The thesis entitled **“DNA-Ferrocene Covalent Adducts for Studying DNA Conductance and Engineering Molecular Recognition Switch of DNA Base Pairing”** comprises studies towards the design, synthesis and X-ray crystal structure studies of ferrocene-nucleobase conjugates. The synthesis and biophysical studies of ferrocene-oligonucleotide conjugates are also discussed. The thesis also focuses on an electrochemical investigation of ferrocene-nucleobase and ferrocene-oligonucleotide conjugates using cyclic voltammetry. The thesis has been divided into four chapters.

**Chapter -1:** The first chapter gives an overview on background literature for undertaking the research work, briefly reviews the literature and recent advancements in the area of ferrocene conjugation to nucleobases, nucleosides, nucleotides, amino acids and peptides, proteins, etc. and their applications.

**Chapter -2:** This chapter describes synthesis, characterization and X-ray crystal structure studies of ferrocene-linked mono and bis-nucleobase conjugates with different spacer.

**Chapter-3:** This chapter depicts synthesis of a new ferrocenyl-phosphoramidites monomer as well as synthesis, characterization and biophysical study of ferrocene-modified oligonucleotide.

**Chapter-4:** This chapter presents an electrochemical investigation of ferrocene-nucleobase conjugates and ferrocene-oligonucleotide conjugates using cyclic voltammetry to understand the redox behavior of the systems.

---

---

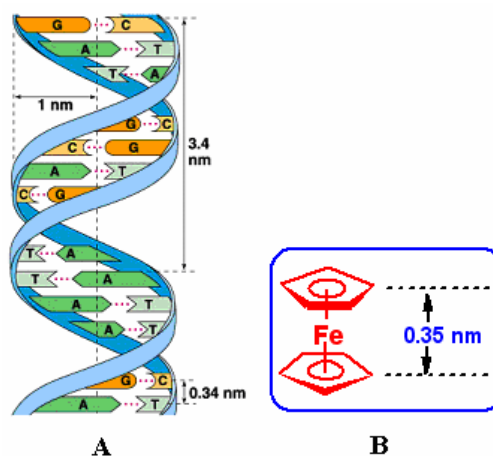
### **Chapter 1: Introduction: Bioconjugates of ferrocene and their applications**

The discovery of ferrocene and elucidation of its remarkable structure is arguably the starting point for modern organometallic chemistry. Currently *bioorganometallic chemistry* is growing rapidly, networking classical organometallic chemistry to biology,



medicine, and molecular biotechnology. The stability of the ferrocenyl group in aqueous, aerobic media, the accessibility of a large variety of derivatives, and its favorable electrochemical properties have made ferrocene and its derivatives very popular molecules for biological applications and for conjugation with biomolecules. However, ferrocene conjugates with nucleobases, nucleosides and nucleic acids is a relatively less explored field compared to the studies of its interaction with amino acids and proteins, peptides and more recently, peptide nucleic acids.

An attractive feature of ferrocene is that the two cyclopentadienyl (Cp) rings can rotate around the Fe atom, which can act as a ball bearing, and the vertical distance between the two Cp rings in ferrocene is 0.35 nm, which is similar to the distance between the stacked base pairs in DNA (Figure 1).



**Figure 1:** (A) Distance between the stacked base pairs in DNA double helix (B) Interring spacing in ferrocene

The redox active ferrocene units linked to self-base pairing nucleobases or DNA/RNA with a designed spacer could therefore be useful building blocks in supramolecular chemistry coupling molecular recognition with electrochemistry, leading to novel applications for the electrochemical recognition of a large variety of DNA/RNA binding substrates. In this chapter the discussion has been limited to conjugates in which ferrocene is covalently bonded to the biomolecule.

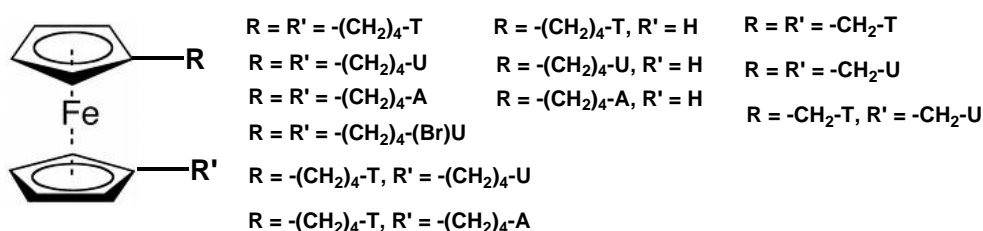
Thus first chapter gives an overview on background literature for undertaking the research work, briefly reviews the literature and recent advancements in the area of bioconjugates of ferrocene and their applications

The work presented in this thesis involves the design, synthesis, characterization and X-ray crystallographic analyses of the redox active ferrocene-nucleobase conjugates

with a designed spacer. This thesis also involves the design, synthesis, and biophysical evaluation of ferrocenyl-modified oligonucleotides. Thesis also focused on an electrochemical investigation of ferrocene-nucleobase conjugates and ferrocenyl-oligonucleotide conjugates.

## Chapter 2: Ferrocene-nucleobase conjugates: Synthesis and X-ray crystalstructure studies

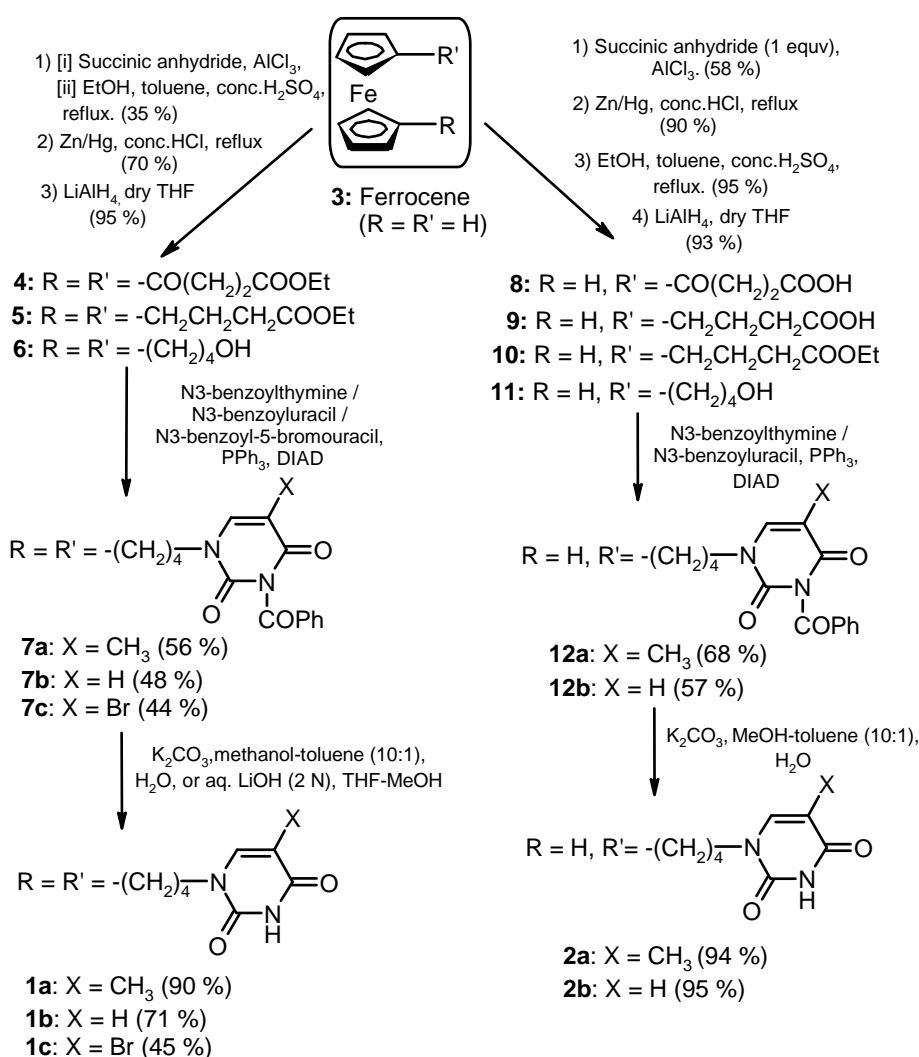
Development of supramolecular assemblies into well-defined architecture has been a subject of great interest in recent years in view of both its importance in the synthesis of artificial models for natural processes and its significance to obtain insight into the conformational features of biomolecules such as proteins, lipids, and nucleic acids. A system of evolutionary perfection for molecular self-assembly is DNA/RNA. The two antiparallel strands of DNA are held together by A:T and C:G base pairs to form the double helix where hydrogen bonding between complementary bases and  $\pi$ -stacking interactions between the adjacent and stacked base pairs stabilize the double helical architecture. Hydrogen bond mediated supramolecular interactions have provided inspiration to design a number of novel self-assembling systems. Incorporation of the common nucleobases A, G, C, and T (or U) in the supramolecular environment enables exploration of different pairing characteristics of these nucleobases. Synthesis and self-association motifs of ferrocene-linked mono-(nucleobase) conjugates with a single carbon methylene spacer have been reported in literature.



**Figure 2:** Ferrocene-linked mono and bis-nucleobase derivatives with different spacer. T = thymine, U = uracil, Br-U = 5-bromouracil, A = adenine

Thus the synthesis of conjugates in which ferrocene is covalently bonded to the nucleobases is of great interest because the redox active ferrocene units linked to self-base pairing nucleobases or DNA/RNA with a designed spacer could therefore be useful building blocks in supramolecular chemistry coupling molecular recognition with

electrochemistry, leading to novel applications for the electrochemical recognition of a large variety of DNA/RNA binding substrates. In this chapter the construction of a series of new ferrocene-linked mono and bis-nucleobase conjugates with different spacer has been described. A complete series of thymine, uracil, 5-bromouracil and adenine derivatives (mono and bis), with *n*-butyl spacer, has been synthesized (Figure 2) and comprehensively characterized, also by X-ray analysis. Synthesis and X-ray crystal structure studies of ferrocene-linked bis-thymine or uracil conjugates with methylene spacer has also been described (Figure 2).

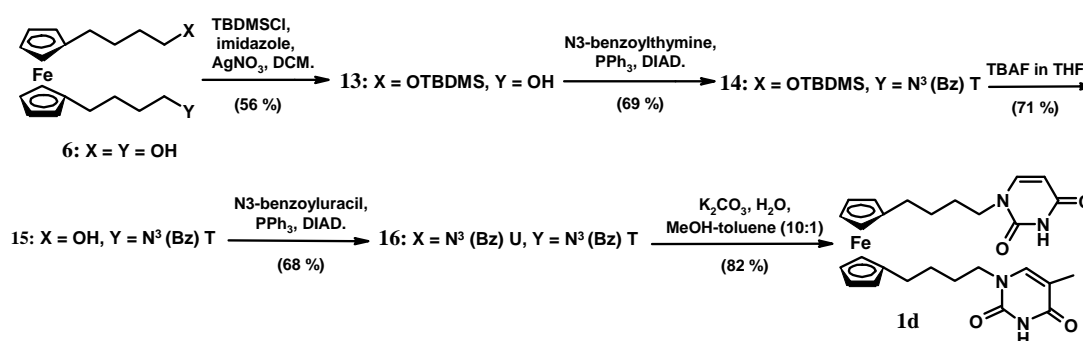


**Scheme 1:** Synthesis of ferrocene-linked mono and bis thymine/uracil conjugates with *n*-butyl spacer.

First it was chosen a simple *n*-alkyl spacer to connect ferrocene with the nucleobases T and U and *n*-butyl chain provided the appropriate hydrophobicity to

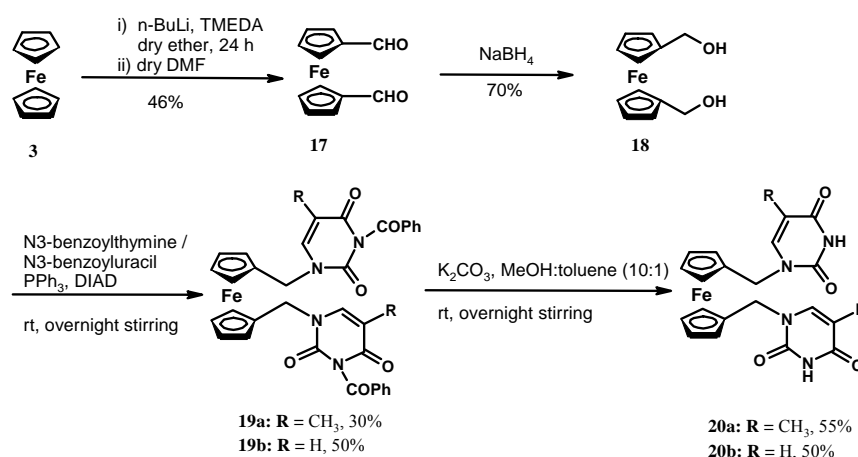
enhance the solubility of the ferrocene linked bis(nucleobase) conjugates in common organic solvents. The synthetic route for the bis(nucleobase) ferrocene target compounds involved the key intermediate 1,1'-bis(4-hydroxybutyl)ferrocene **6** while the mono nucleobase ferrocene was synthesized from 1-(4-hydroxybutyl)ferrocene **11** (Scheme 1).

Chimeric mixed base ferrocene derivative **1d** (thymine(T) and uracil (U) bases at different chain end) was also synthesized (Scheme 2).



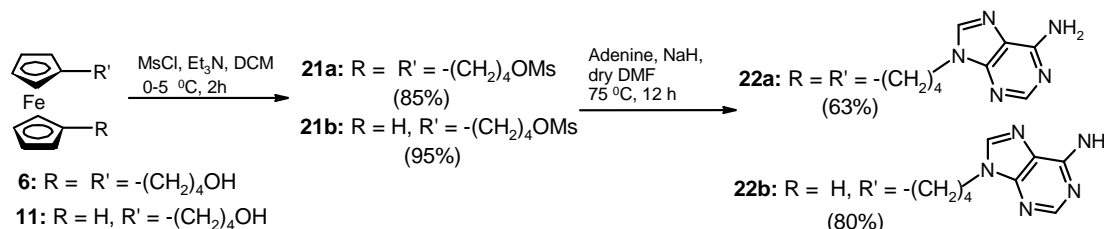
**Scheme 2:** Synthesis of synthesis of chimeric mixed base ferrocene derivatives with *n*-butyl spacer.

Then it was decided to synthesize ferrocene linked bis(thymine (T)/ uracil (U)) conjugate with methylene spacer to study the difference between the crystal structure by changing the chain length (Scheme 3).

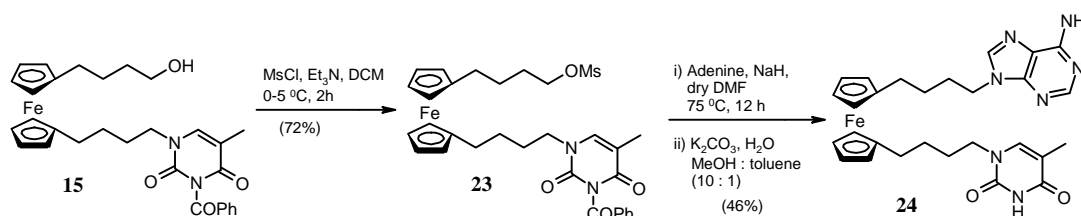


**Scheme 3:** Synthesis of ferrocene-linked bis thymine/uracil conjugates with methylene spacer.

Later it was planned to synthesize ferrocene linked mono and bis adenine conjugates (Scheme 4) and chimeric conjugate in which one of the chains of ferrocene carried a thymine residue and the other bearing an adenine moiety (Scheme 5).



**Scheme 4:** Ferrocene linked mono and bis (adenine (A)) conjugate with n-butyl spacer

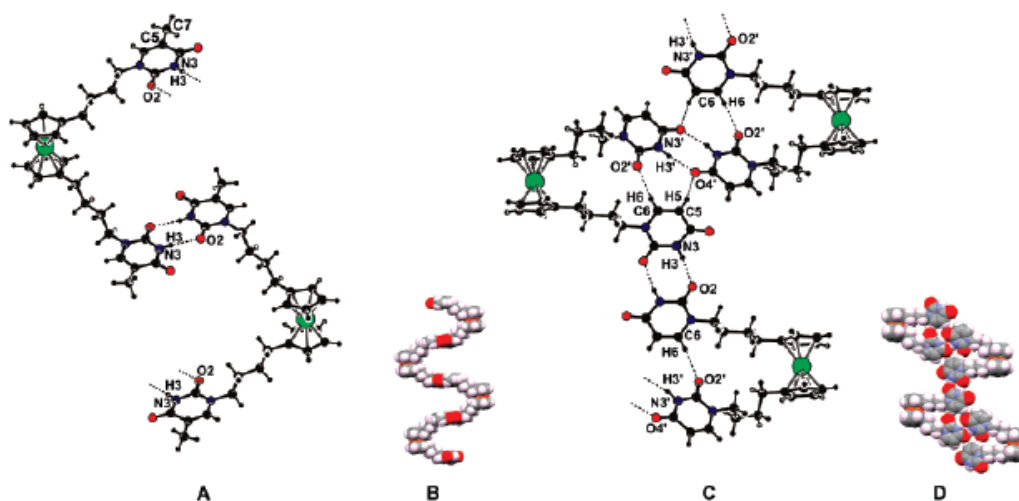


**Scheme 5:** Ferrocene linked thymine (T) and adenine (A) conjugate at different chain end with n-butyl spacer

### X-ray crystal structure studies

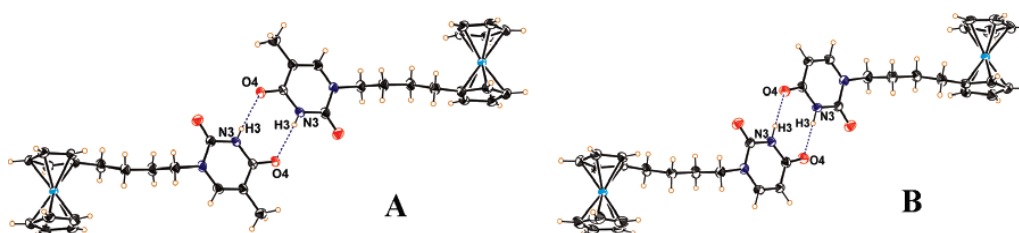
The bis thymine ferrocene compound **1a** occupies crystallographic two fold symmetry axis passing through the central Fe atom of the ferrocene moiety with the n-butyl chains in the extended conformation. A contiguous centrosymmetric, self base pairing constituting ‘reverse Watson-Crick’ (rWC defined as pairing involving O2 of T/U) type pairing (Figure 3A).

The structure of bis(uracil) conjugate **1b** (Figure 3C) is devoid of two-fold symmetry, with one of the n-butyl chains adopting an extended conformation and the other chain in folded state. The U of the folded chain exhibited WC type self-pairing through O4 rather than O2 and making N3'-H3'...O4' interaction with U on the folded chain of the next molecule. Interestingly, the U on the extended chain formed a rWC type pairing with the U of the extended chain of the neighbouring molecule *via* N3-H3...O2 hydrogen bond, in comparison to the WC type base pairing of U in the folded chains. The crystal structure of **1c** was found to be almost identical to that of **1a**. Additionally, the crystal structure of the chimeric conjugate **1d** was also examined. Remarkably, the structure of **1d** was isomorphous to that of **1a**.



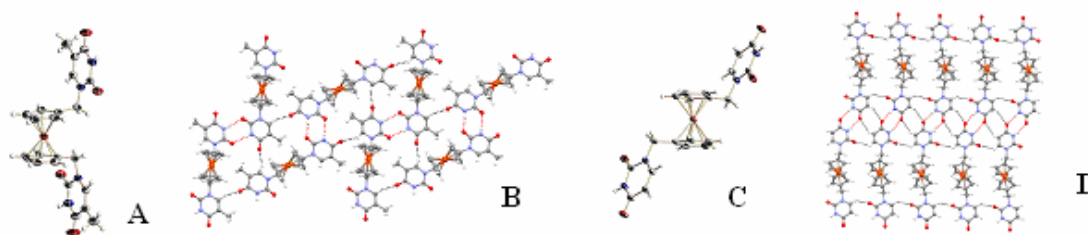
**Figure 3:** T.T and U.U self-base pairing in **1a** (A) and **1b** (C). Molecule **1b** makes an intramolecular C6-H6...O2' contact. Inlay shows the CPK model of a single helical strand for **1a** (B) and **1b** (D).

Crystal structures of mono(thyminyl) ferrocene **2a** and mono(uracilyl) ferrocene **2b** were also determined by single crystal X-ray diffraction method. Both the compounds are almost isostructural. Notably, molecules in both **2a** and **2b** form dimeric centrosymmetric self base pairing of WC type (Figure 4). The methyl group at C5 in **2a** did not make much effect in molecular packing.



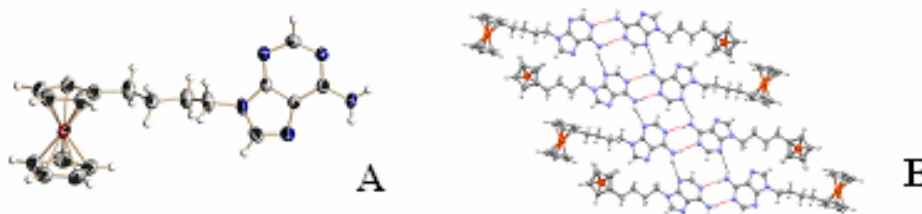
**Figure 4:** Self-base pairing in monosubstituted ferrocene conjugates **2a** (A) and **2b** (B).

In the crystal structure of **20a**, intermolecular hydrogen bonding takes place to reverse Watson-Crick sites via two centrosymmetric hydrogen bonding. While in **20b**, intermolecular hydrogen bonding takes place through Watson-Crick sites. Beside this, other remarkable difference between the crystal structure of **20a** and **20b** is that in **20a** both the thymine moiety are on the same side of the ferrocene ring while in **20b** both the uracil moiety are on the opposite side (Figure 5).



**Figure 5:** [(A) and (C)] ORTEP view and [(B) and (D)] molecular packing diagram of **20a** and **20b** respectively.

In the crystal structure of **22b**, Intermolecular hydrogen bonding takes place to Watson-Crick sites. Molecular packing diagram shows that there are two different molecules present in asymmetric unit (Figure 6).

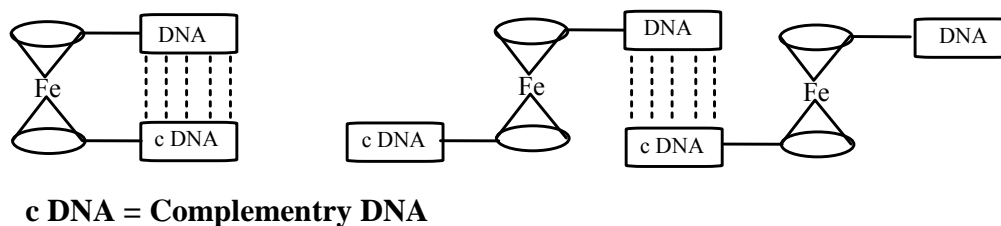


**Figure 6:** (A) ORTEP view and (B) molecular packing diagram of **22b**

Thus this chapter describes synthesis, characterization and X-ray crystal structure studies of ferrocene-linked mono and bis-nucleobase conjugates with different spacer.

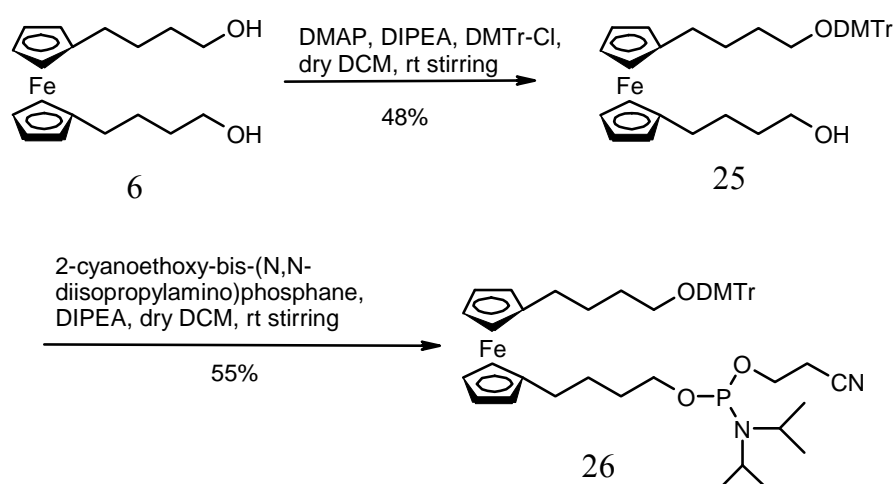
### **Chapter 3: Ferrocene-oligonucleotide conjugates: synthesis, characterization and biophysical studies**

Recently there has been a great interest in investigating DNA molecules for electrical/charge conductance. Several theories have been formulated to understand the mechanism of conductance. In present research, it is proposed to conjugate ferrocene to DNA at desired positions to influence the conductance ability of DNA and these molecules may help to test some of the hypothesis in mechanism of electron conduction in DNA. Accordingly the aim was to prepare suitable ferrocenyl-phosphoramidites, these can be incorporated into DNA sequence (Figure 7) and the property of resulting DNA conjugate investigated using various techniques such as UV- $T_m$ , Gel electrophoresis and cyclic voltammetry. The results are aimed at understanding the mechanism of DNA conductance.



**Figure 7:** Ferrocene unit incorporated in DNA sequences (ferrocene-linked oligonucleotide).

The Ferrocenyl-phosphoramidite monomer unit **26** has been synthesized from **6** in two steps (Scheme 6).



**Scheme 6:** Synthesis of ferrocenyl-phosphoramidite **26**.

The monomer **26** is necessary for incorporating into DNA sequence. These ferrocenyl-phosphoramidites have been directly employed in an automated solid-phase DNA synthesizer using phosphoramidite chemistry to synthesize ferrocenyl-modified oligonucleotide (**FcODNs**) (entry **3-5**, Table 1). The oligomers were synthesized in 3' to 5' direction on polystyrene solid support under standard condition. These oligomers were subsequently purified by reverse phase-HPLC on a preparative column and their integrity was confirmed by MALDI-TOF mass spectrometric analysis (Table 1).



**Table 1:** HPLC and MALDI-TOF mass spectral analysis of oligonucleotides.

Entry	Code No.	Sequences	Retention time (min)	Calculated MW	Measured MW
1	ODN-1	5'-AGA AAA GGA-3'	6.344	2804.97	2807.67
2	ODN-2	5'-TCC TTT TCT-3'	7.474	2630.81	2633.12
3	FcODN-1	5'-AGA AAA GGA—Fc--TCC TTT TCT-3'	10.823	5889.85	5889.27
4	FcODN-2	5'-Fc-AGA AAA GGA-3	14.698	3197.18	3198.57
5	FcODN-3	5'-TCC TTT TCT-Fc-T-3'	13.144	3327.17	3328.28

### A) UV-*T<sub>m</sub>* studies

The hybridization studies of ferrocenyl-modified oligonucleotides with complementary DNA sequence were done by temperature dependent UV-absorbance experiments. The complexes were prepared in 10 mM sodium phosphate buffer, pH 7.4 containing NaCl (10 mM) and were annealed by keeping the samples at 85 °C for 5 minutes followed by slow cooling to room temperature (annealing). Absorbance versus temperature profiles were obtained by monitoring at 260 nm with *UV-Vis* spectrophotometer scanning from 5 to 85 °C and *T<sub>m</sub>* values derived from the derivative curves (Table 2).

**Table 2:** UV-Melting temperature (*T<sub>m</sub>* values) of complementary oligonucleotide duplexes.

Entry	Code No.	Sequences	Melting Temperature (°C)
1	FcODN-1 (1.0 μM)	5'-AGA AAA GGA-Fc-TCC TTT TCT-3'	52.4
2	FcODN-1 ODN-1	5'-AGA AAA GGA----Fc----TCC TTT TCT-3' 3'-AGG AAA AGA-5'	55.4
3	FcODN-1 ODN-2	5'-AGA AAA GGA----Fc----TCC TTT TCT-3' 3'-TCT TTT CCT-5'	57.0
4	FcODN-1 FcODN-2	5'-AGA AAA GGA----Fc----TCC TTT TCT-3' 3'-AGG AAA AGA-Fc-5'	54.0
5	FcODN-1 FcODN-3	5'-AGA AAA GGA----Fc----TCC TTT TCT-3' 3'-T-Fc-TCT TTT CCT-5'	51.7
6	FcODN-1 ODN-2 ODN-1	5'-AGA AAA GGA----Fc----TCC TTT TCT-3' 3'-TCT TTT CCT-5'    3'-AGG AAA AGA-5'	56.2
7	FcODN-1 FcODN-3 FcODN-2	5'-AGA AAA GGA----Fc----TCC TTT TCT-3' 3'-T-Fc-TCT TTT CCT-5'    3'-AGG AAA AGA-Fc-5'	50.9
8	FcODN-1 FcODN-3 ODN-1	5'-AGA AAA GGA----Fc----TCC TTT TCT-3' 3'-T-Fc-TCT TTT CCT-5'    3'-AGG AAA AGA-5'	55.4
9	FcODN-1 ODN-2 FcODN-2	5'-AGA AAA GGA----Fc----TCC TTT TCT-3' 3'-TCT TTT CCT-5'    3'-AGG AAA AGA-Fc-5'	56.2

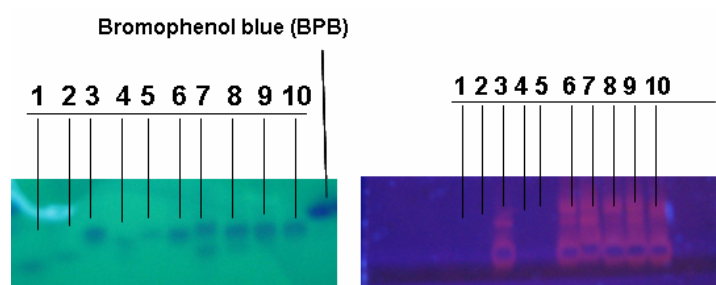
## B) Electrophoretic Gel shift assay

Electrophoretic gel mobility assay was used for the hybridization studies of different ferrocenyl-modified oligonucleotide to the complementary oligonucleotide (DNA). Gel electrophoresis was performed on 20 % nondenaturing polyacrylamide gel (acrylamide:*N,N'*-methylenebisacrylamide, 29:1) at constant power supply of 200 V and 10 mA. During electrophoresis the temperature was maintained at 10 °C. The spots were visualized through UV shadowing.

**Table 3:** Ferrocenyl-modified oligonucleotide and DNA sequences used for gel electrophoresis.

Entry	Code No.	Entry	Code No.
1	ODN-1	6	FcODN-1
2	ODN-2	7	FcODN-1 ODN-1
3	FcODN-1	8	FcODN-1 ODN-2
4	FcODN-2	9	FcODN-1 FcODN-2
5	FcODN-3	10	FcODN-1 FcODN-3

The formation of duplexes between ferrocenyl-modified oligonucleotide and complementary DNA were accompanied by the disappearance of the single strand and appearance of a lower migrating band due to duplexes. Further, the formation of duplexes was confirmed by ethidium bromide staining, where only the duplexes were observed as fluorescent bands because of intercalation, while the single strands were not stained (Figure 8). This chapter depicts synthesis of a new ferrocenyl-phosphoramidites monomer as well as synthesis, characterization and biophysical study of ferrocene-modified oligonucleotide.



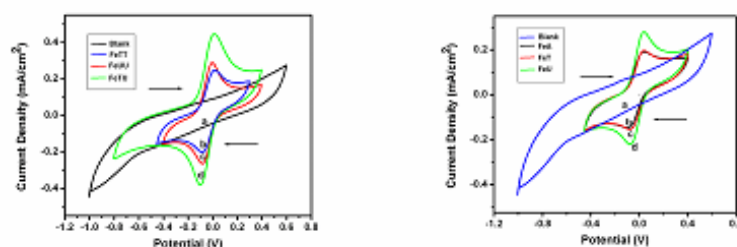
**Figure 8:** Gel shift assay (A) under UV shadow (B) after stained with ethidium bromide: only duplex was observed as fluorescent bands.

## Chapter 4: Ferrocene-nucleobase and ferrocene-oligonucleotide conjugates: electrochemical investigation

This chapter deals with the electrochemical studies of ferrocene of mono and bis-functional ferrocene-nucleobase conjugates using cyclic voltammetry in non-aqueous media. The redox behavior of the systems is understood in terms of the quantitative functional parameters derived from experimental electrochemical data, which is correlated with their chemical structure. This is followed by electrochemical investigation of ferrocene-oligonucleotide conjugates using steady state voltammetry. The electrochemical properties of these ferrocene-oligonucleotide conjugates were analyzed before and after hybridization with different oligonucleotides. The ability of using these ferrocenyl-labeled oligonucleotides in DNA sensors has been demonstrated.

### Ferrocene-nucleobase conjugates

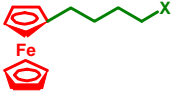
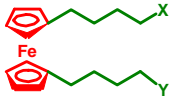
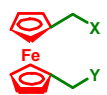
Cyclic voltammetry (CV) is an important technique to study the redox behavior of a system. The electrochemical behavior of ferrocene-linked mono and bis-nucleobase conjugates with different spacer has been examined using cyclic voltammetry.



**Figure 9:** Superimposed CVs of ferrocene nucleobase conjugates. [0.1M LiClO<sub>4</sub> - supporting electrolyte, potential scan rate of 50 mV/s, working electrode - 1mm Pt disk, counter electrode - Pt flag, reference electrode - Pt wire].

Within butylene spacers there is no effect of change in bases and mono or di substitution on potentials but the potentials are 70 mV less positive than that for ferrocene. The same trend was observed in ferrocene conjugates within methylene spacer but the potentials are 200 mV more positive than that of ferrocene. There is a significant shift between methylene and butylenes compounds by +300 mV, which is very interesting (Table 4).

**Table 4:** Electrochemical data for ferrocene-nucleobase conjugates.

	Entry	Compound(calibrated to DMF)	$E_{1/2}$ (V) vs Pt QRE
	1	X = T	+ 0.29
	2	X = A	+ 0.29
	3	X = U	+ 0.30
	4	X = Y = T	+ 0.28
	5	X = Y = U	+ 0.27
	6	X = T, Y = U	+ 0.27
	7	X = Y = (Br)U	+ 0.26
	8	X = T, Y = A	+ 0.30
	9	X = Y = A	+ 0.27
	10	X = Y = T	+ 0.57
	11	X = Y = U	+ 0.55
	12	X = T, Y = U	+ 0.54
	13	Ferrocene (Acetonitrile)	+ 0.23
	14	Ferrocene (DMF)	+ 0.34

**Ferrocene-oligonucleotide conjugates**

Steady-state cyclic voltammetry was performed to study electrochemical behaviour of ferrocene-oligonucleotide conjugates. Steady state cyclic voltammograms were recorded by fixing the ultramicroelectrode (UME) as tip. The tip signal is a Faradaic current from electrolysis of solution species.

**Table 5:** Electrochemical data for ferrocene-oligonucleotide conjugate

Oligonucleotides	$E_{1/2}$ (vs Ag/AgCl) (V)	OCV (V)	Oligonucleotides	$E_{1/2}$ (vs Ag/AgCl) (V)	OCV (V)
FcODN-1	- 0.09	0.23	FcODN-1...FcODN-3	- 0.18	0.14
FcODN-2	- 0.12	0.12	FcODN-1...ODN-1...ODN-2	- 0.10	0.16
FcODN-3	- 0.14	0.17	FcODN-1...FcODN-2...FcODN-3	- 0.15	0.15
FcODN-2...FcODN-3	- 0.2	0.06	FcODN-1...ODN-1...FcODN-3	- 0.13	0.15
ODN-1...FcODN-3	- 0.12	0.05	FcODN-1...ODN-2...FcODN-2	- 0.13	0.14
ODN-2...FcODN-2	- 0.15	0.03	ODN-1	- 0.13	0.19
FcODN-1	- 0.10	0.03	ODN-2	- 0.04	0.18
FcODN-1...ODN-1	- 0.13	0.02	ODN-1...ODN-2	- 0.07	0.05
FcODN-1...ODN-2	- 0.15	0.10	Ferrocene methanol std	+ 0.28	0.16
FcODN-1...FcODN-2	- 0.13	0.15			

[working electrode-25  $\mu$ m diameter Pt ultramicro-electrode, counter electrode-Pt wire, reference electrode-Ag/AgCl, ferrocene-oligonucleotide in phosphate buffer (pH 7.4), NaCl 10 mM]

In the case of ferrocene-conjugated oligonucleotides, there is a significant shift in the  $E_{1/2}$  value with hybridization. In a given buffer, there is a shift in  $E_{1/2}$  by about 70 mV after incorporating ferrocene to a simple oligonucleotide. All the ferrocene-tethered oligonucleotides have a more negative redox potential compared to ferrocene methanol standard indicating that there is an overall decrease in redox activity of the ferrocene moiety after attaching to the oligonucleotides strands. In most of the cases, the redox potential becomes more positive after adding an extra ferrocene unit by hybridizing two ferrocene containing strands. These results demonstrate that all ferrocene-modified oligonucleotides are electrochemically detectable and can be used as signaling probes in the electronic detection of nucleic acids.

---

---

**PUBLICATION**

---

---

1. Ferrocene linked thymine/uracil conjugates: Base pairing directed self assembly and supramolecular packing. **Amit N. Patwa**; Susmita Gupta; Rajesh G. Gonnade; Vaijayanti A. Kumar; Mohan M. Bhadbhade and Krishna N. Ganesh. *J. Org. Chem.* **2008**, 73, 1508-1515.

---

---

**Symposia attended / Poster presented / Oral presentation**

---

---

1. **Patwa, A. N.**; Gupta, S, Gonnade, R. G.; Kumar, V. A.; Bhadbhade, M. M.; Ganesh K. N., **Ferrocene-(bis)thymine/uracil conjugates: Base pairing directed helical assembly and supramolecular packing**; Oral presentation in “Royal Society of Chemistry-West India Section Student Symposium 2006” held on 13<sup>th</sup> and 14<sup>th</sup> October 2006 at Department of Chemistry, Faculty of Science, The Maharaja Sayajirao University of Baroda, Vadodara (Gujarat)-India.
2. **Patwa, A. N.**; Gupta, S, Gonnade, R. G.; Kumar, V. A.; Bhadbhade, M. M.; Ganesh K. N., **Ferrocene-(bis)thymine/uracil conjugates: i) Base pairing induced self – assembly of helical backbones ii) Base pairing geometry dependent differential supramolecular packing**; was presented as Poster in “Asia Academic Seminar On Molecular, Supramolecular Materials with Designed Functions” held between 24<sup>th</sup> and 28<sup>th</sup> February 2007 at National Chemical Laboratory, Pune (Maharashtra)-India.
3. **Patwa, A. N.**; Gupta, S, Gonnade, R. G.; Kumar, V. A.; Bhadbhade, M. M.; Ganesh K. N., **Ferrocene linked thymine/uracil conjugates: Base pairing directed self-assembly and supramolecular packing**; was presented a Poster in “US-India Nanoscience and Engineering Institute (USINSEI)” held between 9<sup>th</sup> and 18<sup>th</sup> January 2008 at MGM Beach Resorts, Chennai-India.

4. Attended “4<sup>th</sup> INSA-KOSEF Symposium in Organic Chemistry: Contemporary Organic Chemistry and its Future Directions” held between 12<sup>th</sup> and 13<sup>th</sup> January 2009 at National Chemical Laboratory, Pune-India.

# **CHAPTER 1**

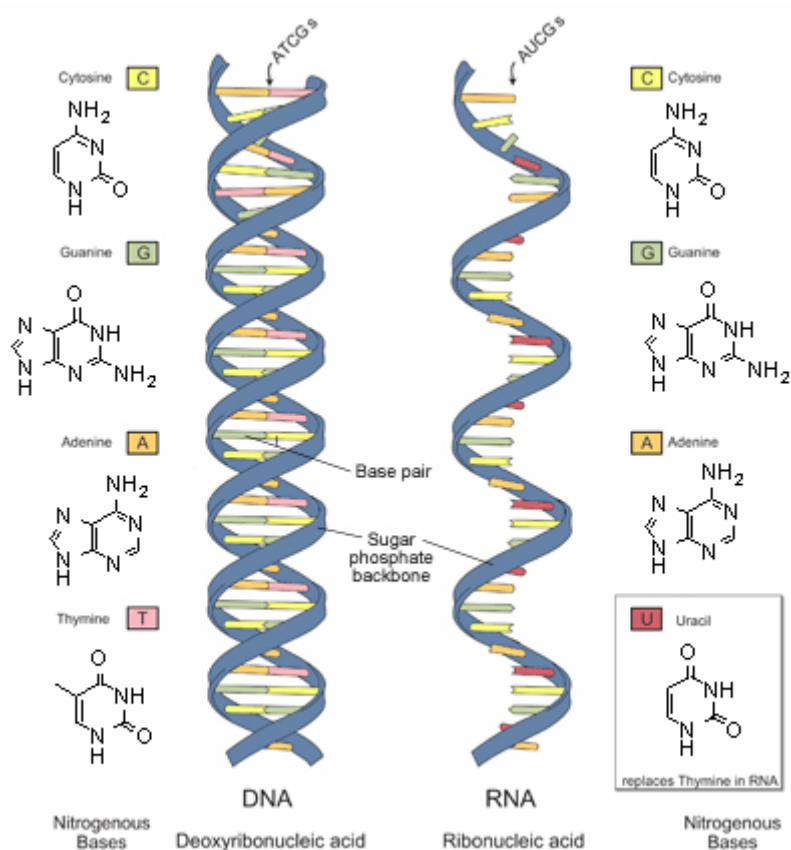
## **INTRODUCTION: BIOCONJUGATES OF FERROCENE AND THEIR APPLICATIONS**



## INTRODUCTION

The work presented in this thesis consists of studies on synthesis and structural conjugates of ferrocene with nucleobases and nucleic acids. This chapter gives an overview on background literature for undertaking the research work and gives an account of its recent advancements in the chemistry of ferrocene conjugates of nucleobases, nucleosides, nucleotides, amino acids and peptides, proteins with emphasis on their synthesis and applications. A brief introduction to nucleic acids structure and bonding, synthesis, physical and chemical properties of ferrocene is presented in next section.

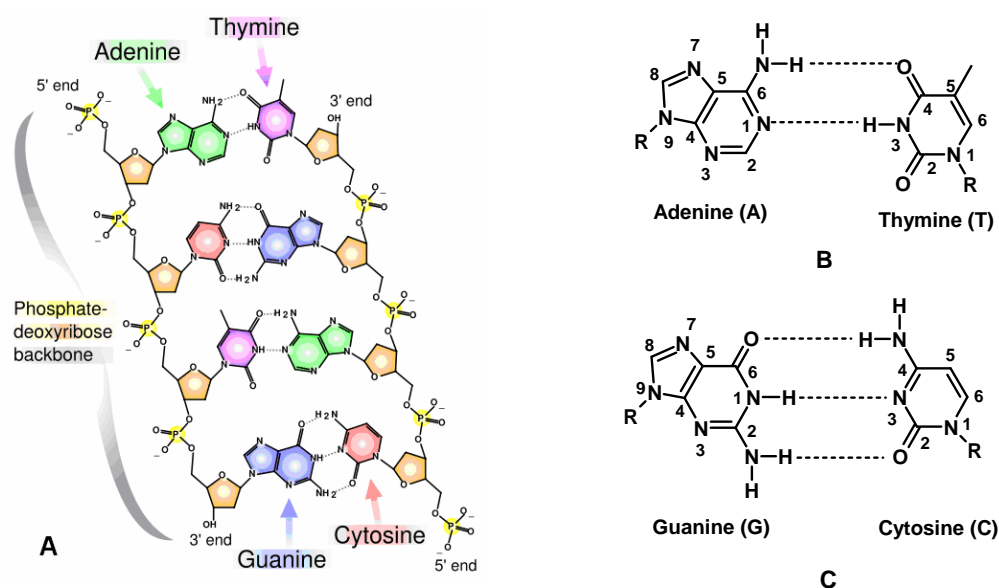
### 1.1 Nucleic Acids: Chemical Structure



**Figure 1.1** Models of DNA and RNA. Image adapted from: National Human Genome Research Institute. For image visit following website: [http://images2.clinicaltools.com/images/gene/dna\\_versus\\_rna\\_reversed.jpg](http://images2.clinicaltools.com/images/gene/dna_versus_rna_reversed.jpg)

Nucleic acids (DNA, RNA) are the most important of all biopolymers. DNA is the basic hereditary material in all cells and contains all information necessary to make proteins. It is present in the nucleus of organisms and contains the genetic instructions

specifying the biological development of all cellular forms of life and many viruses.<sup>1</sup> It has been 55 years since Watson and Crick proposed the double-helical structure for duplex DNA (Figure 1.1).<sup>2</sup> The molecular architecture of DNA consists of a double-stranded helix, of uniform diameter, with right handed twist. DNA is a polymer made up of nucleotide units. Each nucleotide unit consists of a nitrogenous base, a deoxyribose sugar, and a phosphate. The main chemical constituents of DNA are the sugar-phosphate unit present on the outer side of the helix which constitutes the backbone of each strand and the nitrogenous bases adenine (A), thymine (T), guanine (G) and cytosine (C) which are pointed towards the center of the helix. Each base is connected to a sugar *via* a  $\beta$ -glycosyl linkage (Figure 1.2). The adjacent nucleoside units (base + sugar) are connected *via* the O3' of one nucleoside to O5' atoms of other forming phosphodiester linkages. Hydrogen bonds between complementary base pairs (A:T; G:C) hold the two strands together (Figure 1.1). RNA contains ribose rather than deoxyribose sugars and the base composition are: adenine (A), uracil (U), guanine (G) and cytosine (C).



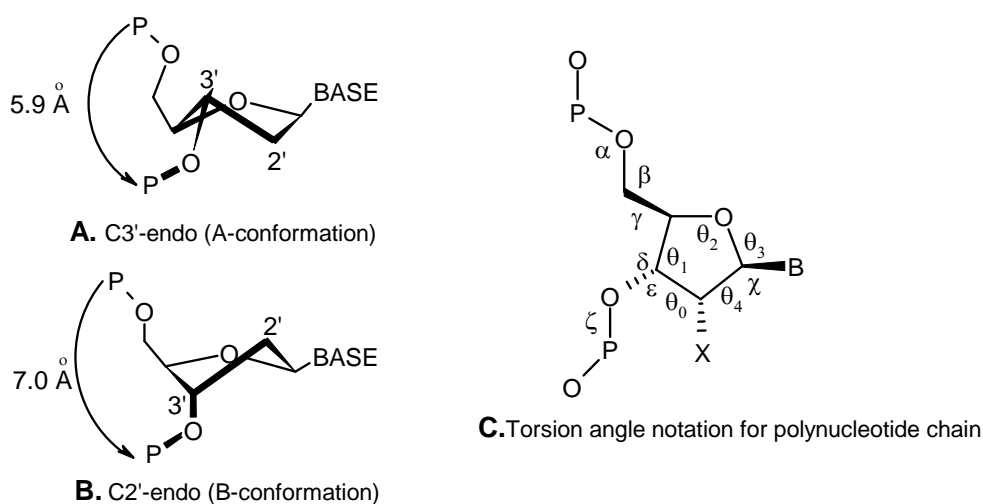
**Figure 1.2** (A) Chemical structure of DNA; Watson-Crick hydrogen-bonding scheme for (B) A:T and (C) G:C base pairs.

The double helix of DNA is nature's simple and elegant solution to the problem of storing, retrieving, and communicating the genetic information of living organism.<sup>3</sup> The specificity and the reversibility of the hydrogen bond formation between the complementary nucleobases is one of the most important characteristic features, which

allow the strands of the double helix to be unwound and then rewound in exactly the same configuration. The construction of DNA and design of its analogues for use in the recognition of specific DNA and RNA sequences has emerged as intellectual and practical assignment for synthetic and structural organic chemists. The recognition of DNA and RNA sequences by complementary oligonucleotides is a central feature of biotechnology and is vital for hybridization based biological applications. The study of such complementary recognition is possible with the widely used experimental techniques and diagnostic protocols.

### 1.1.1 Shapes of nucleotides

The molecular geometry of an individual nucleotide is very closely related to that of the corresponding nucleotide units in oligomers and nucleic acid helical structure. The details of the conformational structure of nucleotides are accurately defined by the torsional angles  $\alpha$ ,  $\beta$ ,  $\gamma$ ,  $\delta$ ,  $\varepsilon$  and  $\zeta$  in the phosphate backbone,  $\theta_0$  to  $\theta_4$ , in the furanose ring, and  $\chi$  for the glycosidic bond (Figure 1.3). Because many of these torsional angles are interdependent, one can simply describe the shapes of nucleotides in terms of four parameters: the sugar pucker, the *syn-anti* conformation of the glycosidic bond, the orientation of C4'-C5' bond and the phosphodiester backbone.



**Figure 1.3** Structures of A) C3'-endo, B) C2'-endo preferred sugar pucker and C) torsion angle notation for polynucleotide chain

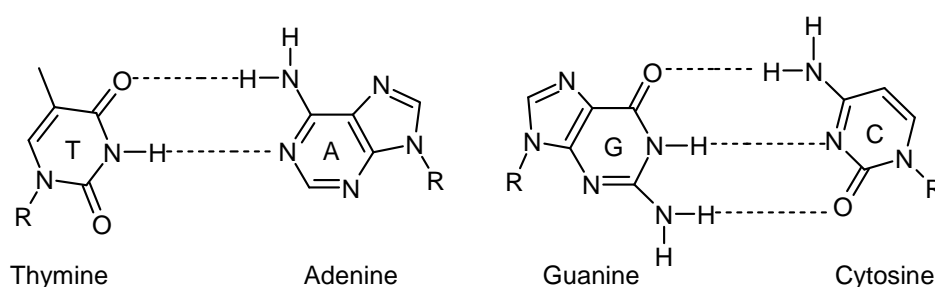
### 1.1.2 Sugar pucker in nucleosides

The pentose sugar rings in nucleosides are twisted or puckered in order to minimize non-bonded interactions between their substituents. This ‘*puckering*’ is described by identifying the major displacement of carbon C2’ and C3’ from the median plane of C1’-O4’-C4’. Thus, if the *endo*-displacement of C2’ is greater than the *exo*-displacement of C3’, the conformation is called C2’-*endo* and so on for other atoms of the ring (Figure 1.3A and 1.3B). The *endo*-face of the furanose is on the same side as C5’ and the base; the *exo*-face is on the opposite face to the base. The sugar puckers are located in the north (N) and south (S) domains of the pseudorotation cycle of the furanose ring.<sup>4</sup> In solution, N and S conformations are in rapid equilibrium and are separated by low energy barrier. The average position of the equilibrium is influenced by (i) the preference of the electronegative substituents at C2’ and C3’ for axial orientation, (as in the case of RNA the C2’-OH interact with backbone phosphate, C3’-*endo* is preferable conformation), (ii) the orientation of the base (*syn* goes with C2’-*endo*), and (iii) the formation of an intra-strand hydrogen-bond from O2’ in one RNA residue to O4’ in the next, which favors C3’-*endo*-pucker. The rise in the sugar phosphate backbone for each monomeric unit is 5.9 Å in case of RNA and 7.0 Å for DNA.

### 1.1.3 Base pairing *via* hydrogen bonding

The mutual recognition of A by T and of C by G uses hydrogen bonds to establish the fidelity of DNA transcription and translation. The N-H groups of the bases are potent hydrogen donors (d), while the *sp*<sup>2</sup>-hybridized electron pairs on the oxygens of the base C=O groups and on the ring nitrogens are much better hydrogen bonding acceptors (a) than are the oxygens of either the phosphate or the pentose. The acceptors:donors (a:d) hydrogen bonds so formed are largely ionic in character.

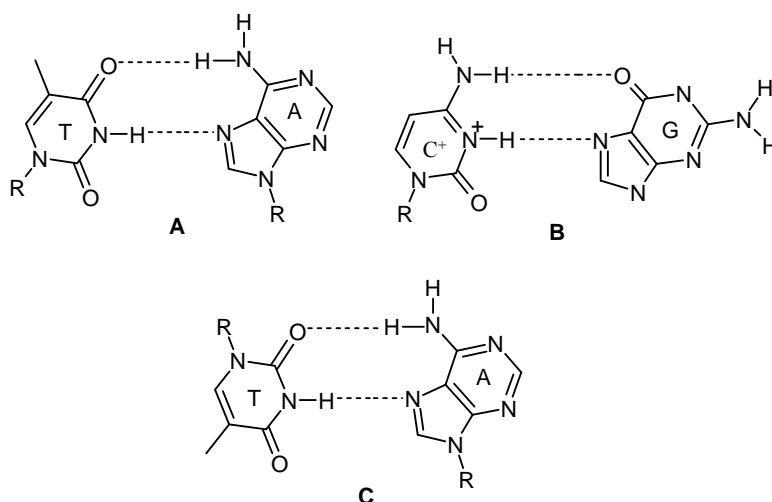
Watson and Crick recognized the complementarities in hydrogen-bonding capability of A:T and G:C base pairs during DNA model-building studies in 1952. This base pairing pattern known as Watson-Crick pairing (Figure 1.4) consists of two hydrogen bonds in an A:T base pair and three hydrogen bonds in a C:G base pair.<sup>2</sup>



**Figure 1.4** Watson and Crick hydrogen-bonding scheme for A: T and G: C base pair

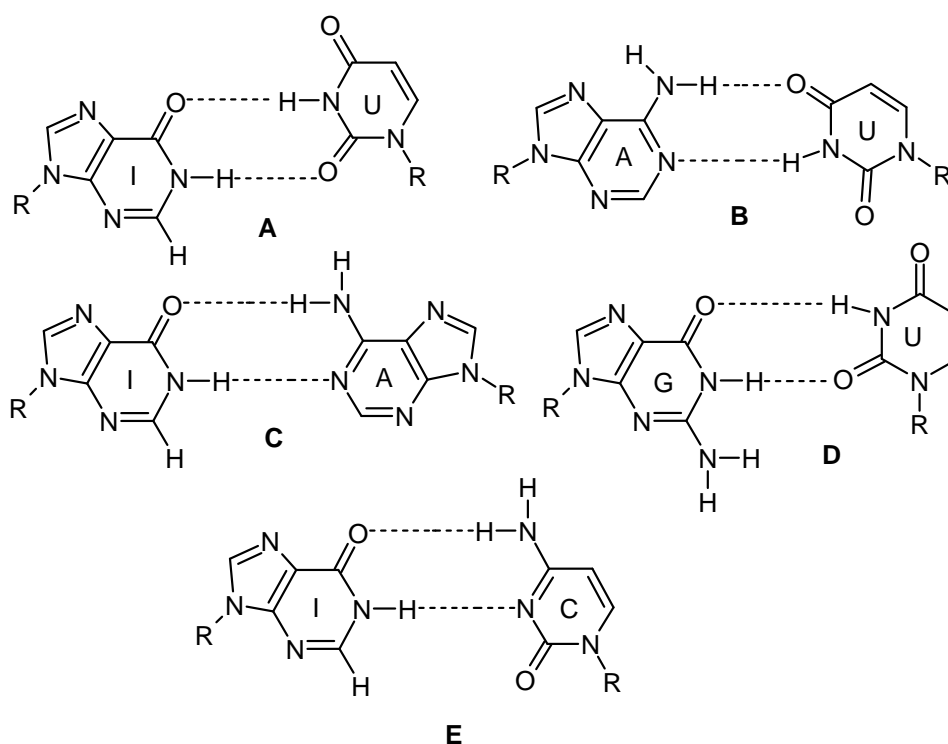
While Watson-Crick base pairing is the dominant pattern between the nucleobases, other significant pairings are Hoogsteen (HG)<sup>5</sup> and Wobble base pairs.<sup>6</sup> A Hoogsteen A:T base pair (Figure 1.5) has the N7 position of the purine base as a hydrogen bond acceptor and C6 amino group as a donor, binding to the Watson-Crick (N3-O4) face of the pyrimidine base. Hoogsteen pairs have quite different properties from Watson-Crick base pairs. The angle between the two glycosylic bonds (ca. 80° in the A:T pair) is larger and the C1'–C1' distance (ca. 8.6 Å) is smaller than in the regular geometry. In reversed Hoogsteen base pairs, one base is rotated through 180° with respect to the other.

Hoogsteen base-pairing allows binding of pyrimidine third strand in the major groove (Section 1.1.5) of Watson-Crick purine: pyrimidine duplexes to form triple-helical structures in 1:2 stoichiometry of (poly(dA):2poly(dT)) and (poly(rG):2poly(rC)). The triplexes do occur in DNA and RNA in polypurine:polypyrimidine structures.



**Figure 1.5** Hoogsteen hydrogen-bonding scheme for A) T:A and B) C<sup>+</sup>:G base pairs. C) Reverse Hoogsteen hydrogen-bonding scheme for T:A base pair

In Wobble base pairing (Figure 1.6), a single purine base is able to recognize different pyrimidines (e.g. I:U and I:A where I = inosine, U = uracil, A = adenine) and have importance in the interaction of messenger RNA (*m*-RNA) with transfer RNA (*t*-RNA) on the ribosome during protein synthesis (codon-anticodon interactions). Several mismatched base pairs and anomalous hydrogen bonding patterns have been seen in X-ray studies of synthetic oligodeoxynucleotides.<sup>7</sup>

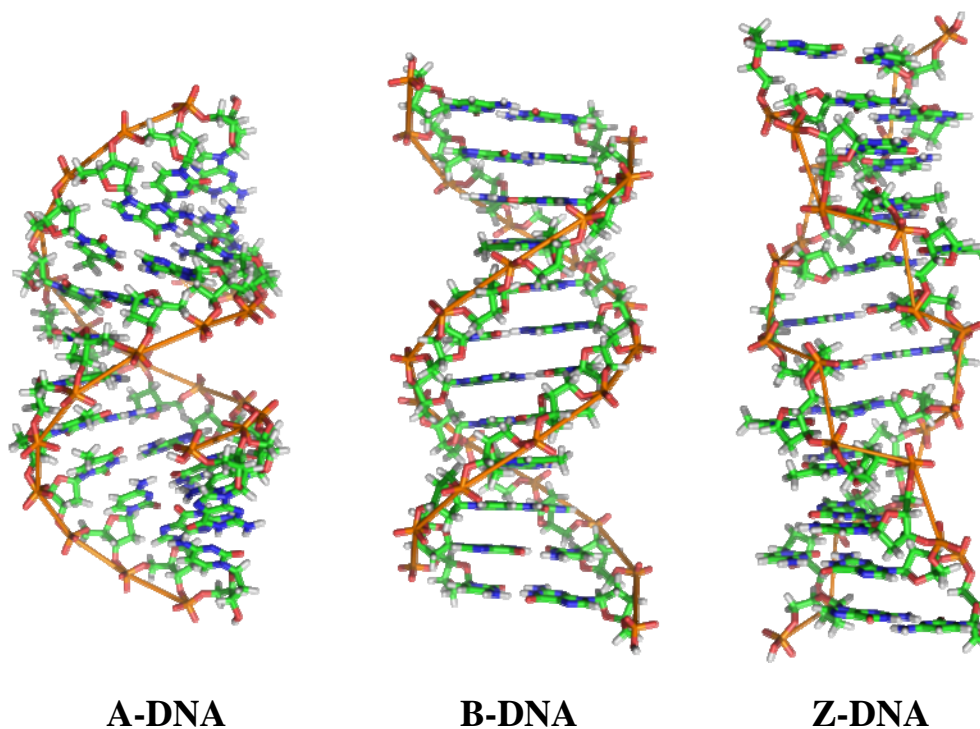


**Figure 1.6** Wobble base pairings for A) I:U, B) A:U, C) I:A, D) G:U and E) I:C. I = Inosine.

#### 1.1.4 DNA secondary structures

Three DNA conformations are normally found in nature, A-DNA, B-DNA, and Z-DNA (Figure 1.7). The "B" type described by Watson and Crick predominates in cells.<sup>8,9</sup> B-DNA is a right-handed double helix with a wide major-groove and a narrow minor-groove, where the bases are perpendicular to the helical axis. It is 23.7 Å wide and extends in a helical form over 34 Å per 10 bp of sequence. A-DNA and Z-DNA differ significantly in their geometry and dimensions from B-DNA, although still forming helical structures. At low humidity and high salt, the favored conformation is highly crystalline A-DNA while at high humidity and low salt, the dominant conformation is B-

DNA. In both A-DNA and B-DNA the Watson-Crick base pairing is maintained by *anti* glycosidic conformation of the nucleobases. The sugar conformation however, is different in both conformations with the B-DNA showing C2'-*endo* puckered sugar and the A-DNA exhibiting C3'-*endo* sugar- pucker.



**Figure 1.7** The structures of A, B and Z-DNA

A very unusual conformation of DNA-duplex is the left-handed Z-DNA.<sup>10</sup> This conformation of DNA is stabilized by high concentrations of  $MgCl_2$ ,  $NaCl$  and ethanol, and is favored for alternating purine:pyrimidine sequences of high G:C content. In Z-DNA the Watson-Crick base pairing is achieved by purines adopting *syn* glycosidic conformation with C3'-*endo* sugar-pucker<sup>8</sup> leading to characteristic zig-zag phosphate backbone. The characteristic features of major DNA conformations are summarized in Table 1.1.

RNA can also form double stranded duplexes. The most important structural feature of RNA that distinguishes it from DNA is the presence of a hydroxyl group at the 2'-position of the ribose sugar. The presence of this functional group enforces C3'-endo sugar conformation (as opposed to the C2'-endo conformation of the deoxyribose sugar in DNA) causing the helix to adopt the A-type geometry rather than the B-type which is

most commonly observed in DNA. In A-DNA the major groove is very deep and narrow and the minor groove is shallow and wide.

**Table 1.1** Salient features of the three major forms of DNA and RNA strands

Geometry attribute	A-DNA	B-DNA	Z-DNA
Helix sense	right-handed	right-handed	left-handed
Repeating unit	1 bp	1 bp	2 bp
Rotation/bp	33.6°	35.9°	60°/2bp
Mean bp/turn	11	10.0	12
Inclination of bp to axis	+19°	-1.2°	-9°
Rise/bp along axis	2.3 Å	3.32 Å	3.8 Å
Pitch/turn of helix	24.6 Å	33.2 Å	45.6 Å
Mean propeller twist	+18°	+16°	0°
Glycosyl angle	anti	anti	C: anti, G: syn
Sugar pucker	C3'-endo	C2'-endo	C: C2'-endo, G: C3'-endo
Diameter	25.5 Å	23.7 Å	18.4 Å
Conditions	Low humidity & High salt	Dilute aqueous solutions	High salt & alternating GC sequences
Major groove	Narrow & deep	Wide and deep	Flat
Minor groove	Wide	Narrow and deep	Narrow and deep

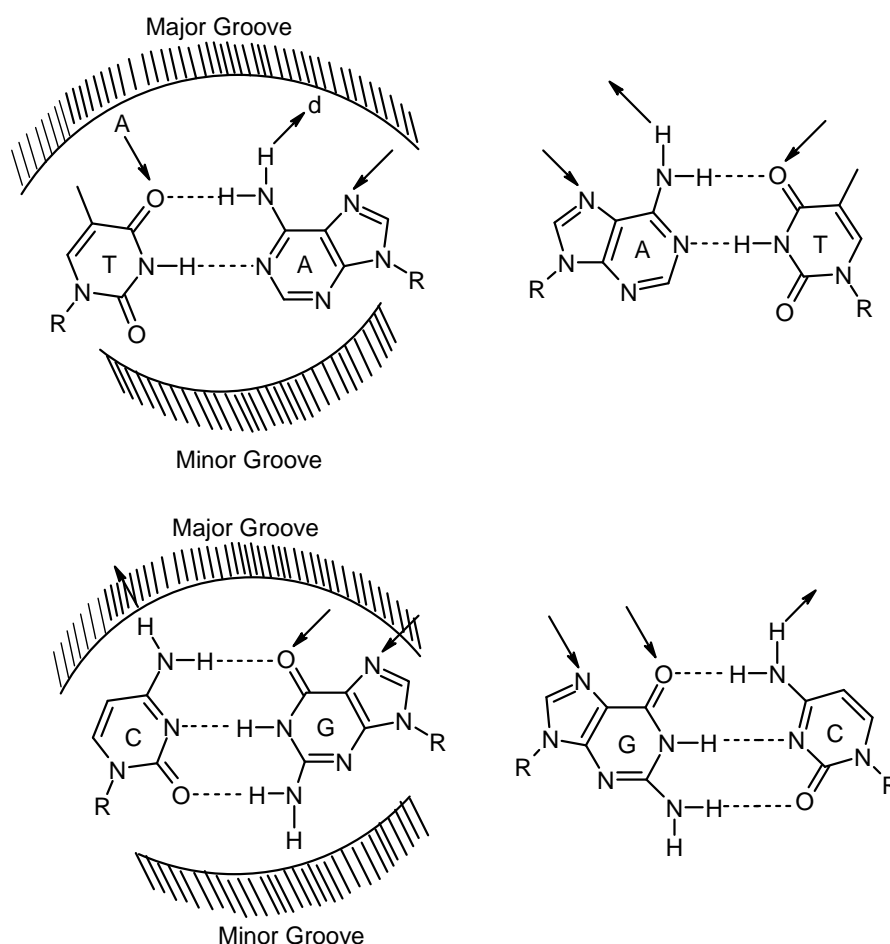
Other DNA conformations such as<sup>11</sup> C-DNA, D-DNA, E-DNA, L-DNA, P-DNA, and S-DNA are variations of A or B-type of DNA and have not been observed in naturally occurring biological systems.

### 1.1.5 Molecular recognition in the major and minor grooves of duplex DNA

The major and the minor grooves of DNA differ significantly in their electrostatic potential, steric effects, hydration<sup>4a</sup> and dielectric strength.<sup>12</sup> This is because of differing exposure of H-bonding sites in grooves.<sup>7</sup> A:T and T:A base pairs can accept additional hydrogen bonds from ligands bound in the major groove *via* the C4 carbonyl of T and N7 of A, while in the minor groove hydrogen bonding occurs through the C2 carbonyl of T and N3 of A (Figure 1.8). The only hydrogen bond donor in the major groove for the



A:T base pair is the N6 amino group of A, while none exists in the minor groove. For C:G and G:C duplexes, the H-bond acceptors in the major groove are N7 and O6 for G and in the minor groove are O2 of C and N3 of G. The hydrogen bond donor in the major groove for C:G is the N4 amino of C and in the minor groove, the N2 amino of G.



**Figure 1.8.** Hydrogen bond donor and acceptor sites in the major groove of duplex DNA at T:A, A:T, C:G and G:C base pairs. Arrows pointing to the atoms indicate acceptor sites; arrows pointing away from the atoms indicate donor sites.

The salient outcome of this pattern of hydrogen bond donors and acceptors in the grooves is that the molecules binding in groove can discriminate the A:T base pair from C:G efficiently from the major groove side but not so well in the minor groove.<sup>7</sup> Two additional features of molecular discriminations are also noteworthy. In A:T and T:A base pairs, the C5 methyl of T offers substantial hydrophobic recognition in the major groove which is absent for C:G and G:C base pairs. However, in the C:G and G:C duplexes, the N2 amino group of G presents a steric block to hydrogen bond formation at

N3 of G and the C2 carbonyl of C in the minor groove. It is possible to distinguish A:T from T:A and G:C from C:G in the major groove since the horizontally ordered array of hydrogen bonding sites and hydrophobic centers differ among the four pairs (Figure 1.8). The negative electrostatic potential due to phosphate charges is greater in the A:T minor groove than in G:C-rich regions of DNA and this provides an additional important source for A:T-specific minor groove recognition.<sup>4a</sup>

### 1.1.6 Bioorganometallic chemistry of DNA

The preceding sections of this chapter gave an overview on a brief introduction to structure and bonding of nucleic acids.

The redox active units linked to self-base pairing nucleobases or DNA/RNA could be useful building blocks in supramolecular chemistry coupling molecular recognition with electrochemistry, leading to novel applications for the electrochemical recognition of a large variety of DNA/RNA binding substrates. The main interest in redox labeled oligonucleotide derivatives is for electrochemical DNA sensors and is also important in studies over DNA mediated electron transfer processes, which has large potential for biomedical application, which have resulted in the synthesis of numerous transition metal (Ru, Os, Fe, Rh and Cu complexes) modified oligonucleotides.

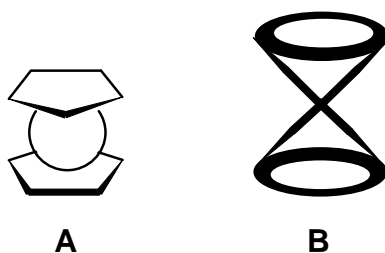
In this context, ferrocene has received considerable attention due to its good stability, enabling convenient synthetic chemistry. Further, ferrocene and its derivatives have received a lot of importance in molecular recognition research, due to their redox characteristics. As a part on this chapter the following section gives a brief introduction to synthetic approaches, physical and chemical properties of ferrocene as well as recent advancements in the chemistry of ferrocene conjugates of nucleobases, nucleotides, nucleosides, amino acids, peptides and proteins.

## 1.2 Ferrocene: A Sandwich Compound

In 1951, a new compound containing iron and two cyclopentadienide ligands was reported. Two independent groups of chemists Kealy and Pauson<sup>13</sup> and Miller *et al.*<sup>14</sup> almost simultaneously arrived at the same conclusions, albeit accidentally. Both groups noted that the new compound was insoluble in water, air-stable and sublimable with excellent solubility in organic solvents. Although even the first reports noted its high and

unexpected stability, the correct structure was only soon afterward suggested independently by Wilkinson and Fischer. To elucidate the correct structure of dicyclopentadienyl iron, Wilkinson used chemical, physical and spectroscopic methods while Fischer used X-ray crystallography to characterize the compound.

Wilkinson proposed a possible structure where the iron atom was placed between the two cyclopentadienyl (Cp) ligands. This reveals very strong bonding due to excellent overlap of the metal  $d$  orbitals and the  $\pi$ -electrons in the  $p$  orbitals of the Cp ligands. Wilkinson, Woodward and co-workers began to characterize the material and concluded that the  $\pi$ -complexed sandwich structure had to be correct<sup>15</sup> (Figure 1.9.A). Wilkinson discovered that the iron centre of the compound could be readily oxidized from +2 to +3 and formed a number of  $[(C_5H_5)_2Fe]^+X^-$  derivatives from the blue cation. Fischer's X-ray diffraction studies gave indisputable evidence of the 'sandwich' structure and postulated a 'double-cone' shape (Figure 1.9.B).



**Figure 1.9** (A) 'Sandwich' structure and (B) 'double cone' shape of cyclopentadienyl-iron

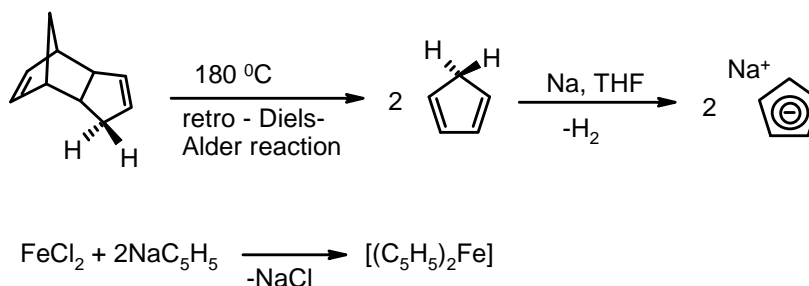
Woodward discovered that the aromatic nature of cyclopentadienyl rings were similar to benzene to carry out electrophilic aromatic substitution reactions. This, and a number of other aromatic similarities of the Cp rings to the benzene moiety, led one of Woodward's postdoctoral fellows, Mark Whiting, to coin the name '*ferrocene*'.<sup>16</sup> The entire class of transition metal dicyclopentadienyl compounds became rapidly known as the '**metallocenes**'. Wilkinson and Fischer shared the Nobel Prize for Chemistry in 1973 for pioneering work in organometallic chemistry. The term "sandwich compound" for this compound is today universally accepted for a much wider class of compounds. The discovery and recognition of this new type of bonding between metals and organic unsaturated molecules gave organometallic chemistry a whole new lease of life.

### 1.2.1 The methods of synthesis of ferrocene

There are two main routes that are normally employed in the formation of ferrocene.<sup>17</sup>

#### 1.2.1.A Using a metal salt and cyclopentadienyl reagents

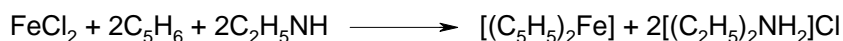
The synthesis starts with the ‘cracking’ of dicyclopentadiene through a retro Diels-Alder reaction to produce the monomeric cyclopentadiene ( $C_5H_6$ ). Cyclopentadiene, a weak acid with  $pK_a = 15$ , can be deprotonated by strong bases or alkali metals. Sodium cyclopentadienide (NaCp) upon reaction with ferrous chloride yields ferrocene (Figure 1.10).



**Figure 1.10** The ‘cracking’ of dicyclopentadiene and synthesis of ferrocene.

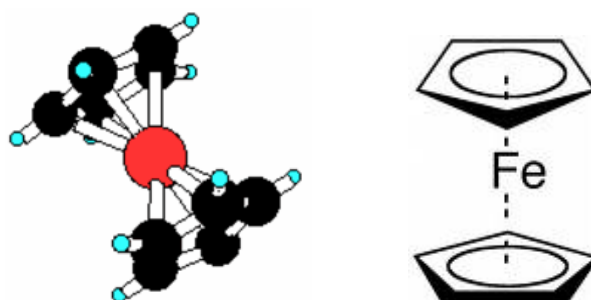
#### 1.2.1.B Using a metal salt and cyclopentadiene

If the salt anion has poor basicity and cannot deprotonate cyclopentadiene, an auxiliary base can be utilized to generate the cyclopentadienyl anions *in situ* which can sometimes be more convenient.



### 1.2.2 Structure and physical properties of ferrocene

Ferrocene sublimes readily above 100 °C. It is soluble in most of the organic solvents. It is insoluble in, and apparently unattacked by, water, 10 % caustic soda and concentrated hydrochloric acid even at the boiling point. It dissolves in dilute nitric or concentrated sulphuric acid.



**Figure 1.11** Structure of ferrocene

**Table 1.2** Physical properties of ferrocene

IUPAC name	bis( $\eta^5$ -cyclopentadienyl)iron(II)	Density	2.69 g/cm <sup>3</sup> (20 °C)
Molecular formula	C <sub>10</sub> H <sub>10</sub> Fe	Melting point	174 °C
Molar mass	186.04 g/mol	Boiling point	249 °C
Appearance	light orange powder	UV- $\lambda_{\max}$	326 m $\mu$ ( $\epsilon = 50$ ) 440 m $\mu$ ( $\epsilon = 87$ )

Ferrocene can be crystallized from solution in the monoclinic, triclinic, and orthorhombic crystal modifications, depending on the temperature. Original X-ray diffraction studies indicated a staggered configuration of the rings with a molecular centre of symmetry ( $D_{5d}$ ). However, gas-phase electron diffraction observations projected a  $D_{5h}$  geometry with C-C = 1.440(2)Å and Fe-C = 2.064(3) Å.<sup>18</sup> It is known in literature that below 164 K, the triclinic form persists and show virtual  $D_5$  symmetry, the rings being rotated by about 9° from the eclipsed orientation. The room temperature monoclinic crystalline form is a disordered species, indicating a staggered conformation ( $D_{5d}$ ), whilst in the orthorhombic form the rings are fully eclipsed ( $D_{5h}$ ). Although the orthorhombic form is thermodynamically stable up to 242 K, crystallization of this phase from solution occurred in only at much lower temperatures ( $\leq 110$  K).<sup>19</sup>

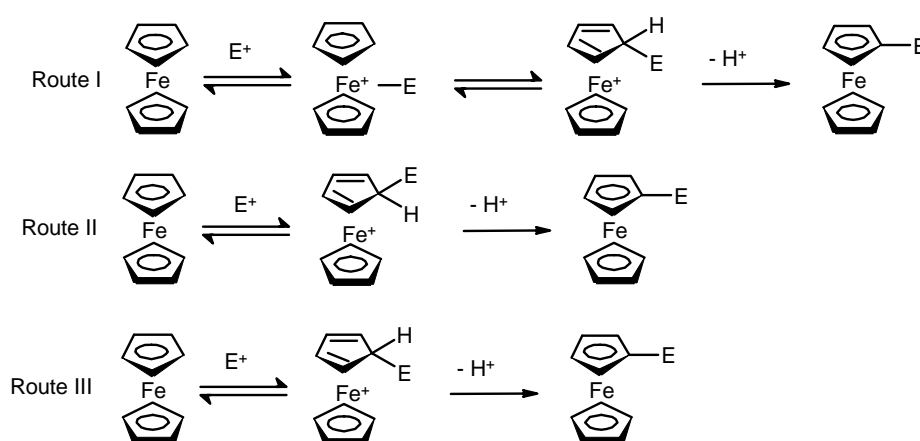
It is readily oxidized to a blue cation  $[\text{Fe}(\text{C}_5\text{H}_5)_2]^+$  (called ‘ferrocenium’), which is blue or green in dilute solution or blood red when concentrated. Upon oxidation there is a slight increase in Fe-C bond lengths and also within the rings, as is to be expected for removal of a bonding electron.

### 1.2.3 Chemical properties of ferrocene

The cyclopentadienyl rings are aromatic and, in general, most of the chemistry of ferrocene and its derivatives may be predicted on this basis. It is possible to carry out a variety of transformations on the cyclopentadienyl ligands due to its great stability and the ability to maintain the ligand-metal bonding under harsh condition.

#### 1.2.3A General electrophilic substitution

Ferrocene is more reactive towards electrophilic substitution than benzene indicating that more electrons are readily available. In fact compared to benzene, ferrocene reacts  $3 \times 10^6$  faster. It has been proposed that the electrophilic substitution takes place *via* three possible mechanisms. The electrophilic substituents ( $E^+$ ) interact first with the weakly bonding electrons of the iron atom and then transfer to the Cp ring with E in the *endo* (i.e. metal side) position which upon proton elimination gives substituted ferrocene (Route I) (Figure 1.12). Alternatively, it is thought that electrophilic attack takes places on the ring to the less hindered *exo* face of the ligand, and does not involve direct participation of the metal, which then loses a proton to give the product (Route II) (Figure 1.12). There is a third possible mechanism which involves addition of the electrophile to the *endo* face of the ligand but not *via* any metal interaction (Route III) (Figure 1.12).



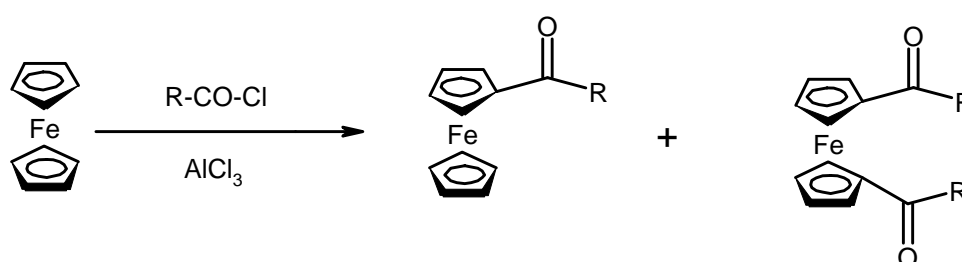
**Figure 1.12** Proposed mechanisms for electrophilic substitution of ferrocene.

In fact, each route is plausible and probably all do occur, but it has been suggested that the stereochemistry of the product of electrophilic substitution and the

kinetic features of the reaction are governed by the nature of the electrophile. In the proton-exchange reaction, it seems that the *exo* and *endo* pathways are equally likely.

### 1.2.3B Friedel-Crafts reaction

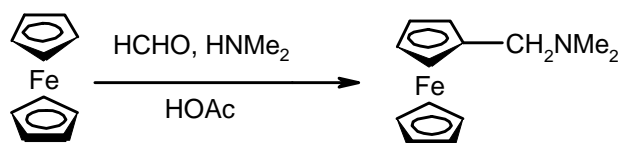
Ferrocene readily undergoes Friedel-Crafts acylation reaction on one ring and less readily on both the rings (Figure 1.13). It gives only one 1,1'-disubstituted compound due to free rotation of two Cp rings. Ferrocene also undergoes Friedel-Crafts alkylation on treatment with alkyl halide or alkenes. However, such reactions are not synthetically useful because of side reactions and poor yields.



**Figure 1.13:** Friedel-Crafts acylation of ferrocene.

### 1.2.3C Mannich reaction

Ferrocene undergoes Mannich reaction as it demonstrates the reactivity of its rings and resembles the reactive thiophene and phenol species rather than benzene which does not undergo Mannich condensations.



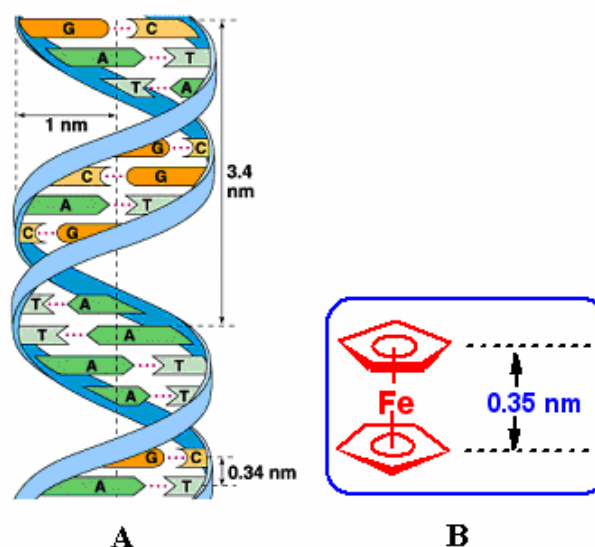
**Figure 1.14:** Mannich reaction of ferrocene.

## 1.3 Bioorganometallic Chemistry of Ferrocene

The discovery of ferrocene and elucidation of its remarkable structure is arguably the starting point for modern organometallic chemistry. Currently *bioorganometallic chemistry* is growing rapidly, networking classical organometallic chemistry to biology, medicine, and molecular biotechnology.<sup>20-22</sup> Ferrocene and its derivatives have numerous

medicinal applications. Ferrocene itself shows properties as an anti-anemic or cytotoxic agent.<sup>23,24</sup> It was found, by Neuse *et al.*, that there is a great enhancement in activity of cytotoxic metal compounds including ferrocene when these were bound to polymers as pro-drugs.<sup>25</sup> Conjugates of ferrocene with well-known drugs, antibiotics such as penicillins and cephalosporins, were reported.<sup>26</sup> In addition, structural variations of established drugs with the ferrocenyl moiety were reported, such as the anti-malarial drugs chloroquine (termed ferroquine), quinine, mefloquine, artemisinin,<sup>27</sup> ferrocenyl aspirin,<sup>28</sup> and the anti-cancer drug tamoxifen to give ferrocifen.<sup>29</sup>

The work presented in this thesis is mainly focused on the synthesis and characterization of conjugates in which ferrocene is covalently bonded to the biomolecule. The stability of the ferrocenyl group in aqueous, aerobic media, the accessibility of a large variety of derivatives, and its favorable electrochemical properties have made ferrocene and its derivatives very popular molecules for biological applications and for conjugation with biomolecules. Bioconjugates of ferrocene with amino acids and peptides, proteins, DNA, RNA, PNA, carbohydrates, and hormones have received significant attention. An attractive feature of ferrocene is that the two cyclopentadienyl (Cp) rings can rotate around the Fe atom, which can act as a ball bearing.<sup>30</sup> Further, the vertical distance between the two Cp rings in ferrocene is 0.35 nm, which is similar to the distance between the stacked base pairs in DNA<sup>31,32</sup> (Figure 1.15).



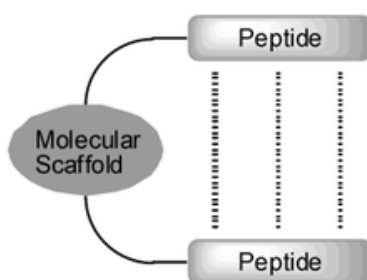
**Figure 1.15:** (A) Distance between the stacked base pairs in DNA double helix (B) Interrring spacing in ferrocene



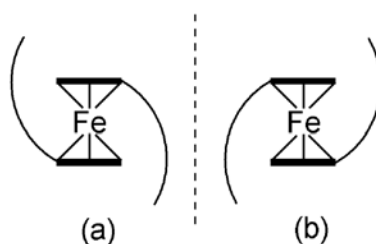
Bioconjugates of ferrocene with amino acid and peptides received considerable attention. Amino acids and peptides often assemble, by hydrogen bonding between individual molecules,<sup>33,34</sup> into extended supramolecular three-dimensional structures.

The properties of such extended peptide networks are related to the molecular arrangement of the individual molecules and offer fascinating array of structures. The utilization of a ferrocene unit as a molecular scaffold is considered to be one approach to study the hydrogen bonding ability of various peptide strands (Figure 1.16).<sup>35</sup> It's so because the inter-ring spacing of ferrocene is suitable for hydrogen bonding of the attached peptide strands. Hydrogen bonds play a crucial role in regulating the three-dimensional structure and function of biological systems. The utilization of self-assembling properties of short peptides, which possess chiral centers and hydrogen bonding sites, is considered to be a relevant approach to highly ordered molecular assemblies.

Conformational enantiomers based on the torsional twist about the Cp(centroid)-Fe- Cp(centroid) axis are possible in the case of the 1,1'-disubstituted ferrocene (Figure 1.17).<sup>36</sup> These conformational enantiomers are easily interconvertible because of the low energy barrier of Cp ring twisting. The incorporation of peptide chains into a ferrocene scaffold is envisaged to induce conformational enantiomerization by restriction of the torsional twist through the intramolecular hydrogen bonding. This bioorganometallic chemistry is envisioned to provide not only a peptidomimetic base for protein folding, but also pharmacologically useful compounds, artificial receptors, asymmetric catalysts, and new materials with functional properties.<sup>37</sup> Recently, significant efforts have been aimed at equipping non-covalent supramolecular peptide assemblies with redox active groups and giving them specific electric properties that may be exploited as biomolecular wires.



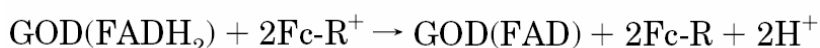
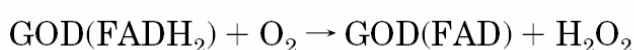
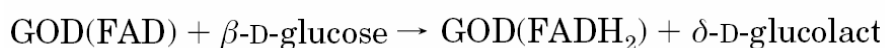
**Figure 1.16:** Schematic representation of ordered structure of peptides with molecular scaffolds.<sup>35</sup>



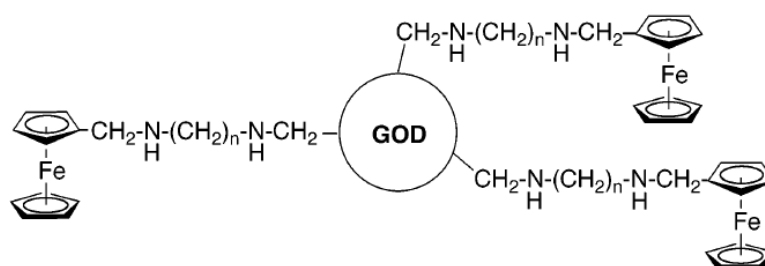
**Figure 1.17:** Enantiomorphous conformations of the 1,1'-disubstituted ferrocene peptide, related by a mirror plane

In past, significant efforts have been directed at the side-chain-selective and covalent labeling of proteins with organometallic complexes. Various conjugates of ferrocene with proteins are known and such redox labeled proteins can be used as biosensors. The rationale behind the derivatization was to make direct electrochemical communication possible between protein and the electrode. The glucose sensor is one of the most important biosensors for glucose detection. This is vital not only in the field of biotechnology for fermentation process control but also in medical services.<sup>38</sup>

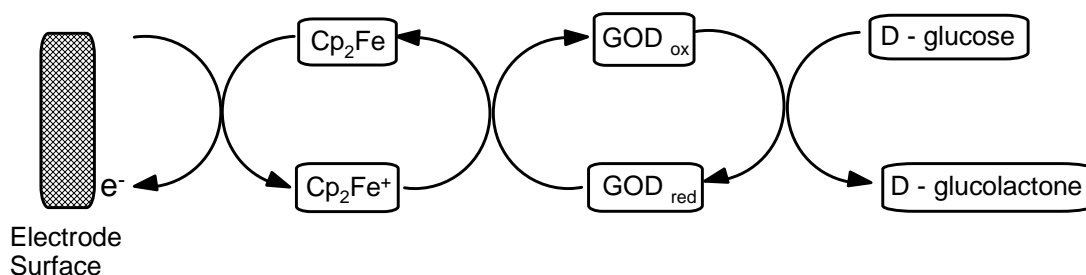
Glucose oxidase (GOD) is a dimeric glycoprotein which oxidizes  $\beta$ -D-glucose to  $\delta$ -D-glucolactone via two-electron process which is sensitive and specific. The current generated from the biochemical reaction between the enzyme and glucose can be computed by measuring the consumed oxygen or hydrogen peroxide produced in the reaction.



However, the direct electrochemical measurement of the amount of oxidized product is hindered since the enzyme does not react with electrode surfaces directly and as there can be dissolved oxygen in the samples. A redox-active mediator can be used to facilitate the quantitative oxidation of glucose under catalytic conditions. The glucose oxidase enzyme, labeled with ferrocene derivatives (Figure 1.18), is commonly used in biosensors to detect levels of glucose by keeping track of the number of electrons passing through the enzyme by connecting it to an electrode and measuring the resulting charge.<sup>39,40</sup> The use of ferrocene or its derivatives, as a mediator, avoid the effect of any dissolved oxygen (Figure 1.19).



**Figure 1.18** Modified glucose oxidase on the peripheral carbohydrate part of the enzyme



**Figure 1.19** The use of ferrocene as a mediator in a glucose sensor.

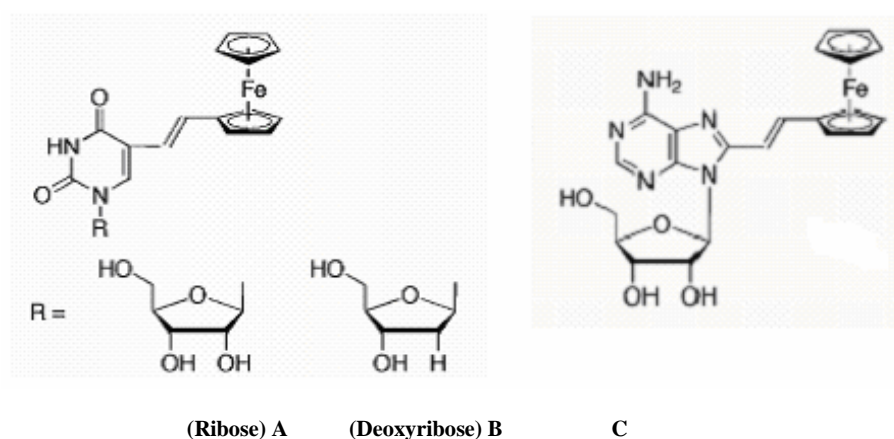
D-Amino acid oxidase (DAAO) is a flavoprotein which catalyzes the oxidative deamination of D-amino acids. DAAO, isolated from two different sources, pig kidney and *Rhodoturula gracilis* (yeasts), were labeled with ferrocene derivatives. The addition of D-alanine to either conjugate resulted in an electrochemical response. A linear relationship was observed between the D-alanine concentration and the current, thus making the use of the modified enzymes in amperometric D-amino acid sensors possible.<sup>41,42</sup> Bovine serum albumin (BSA) is a protein which was first labeled with ferrocene derivative in 1969. Ferrocenyl-BSA conjugates were applied as efficient diffusing macromolecular mediators between the enzyme glucose oxidase and the electrode. The tetrameric protein avidin (isolated from egg white) is remarkable for its ability to bind up to four molecules of biotin with high affinity. These ferrocenyl avidin conjugates were used to construct an enzyme-based biotin sensor by immobilizing them on an electrode.

### 1.3.1 Ferrocene-nucleobase conjugates

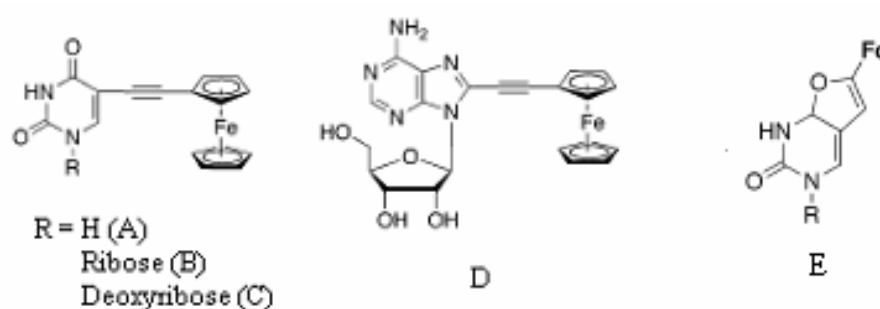
Ferrocene-nucleobase conjugate is a relatively new and less explored field in bioorganometallic chemistry as compared to the ferrocene conjugates with amino acids

and proteins described in previous section. Studies of interaction of ferrocene compounds with nucleobases can be categorized as (1) those involving Metal-Carbon bonds derived from carbon atoms of the biomolecule,<sup>43-45</sup> (2) ferrocene fragments coordinated at N- and O- donor sites of the nucleobases,<sup>46</sup> and (3) conjugates in which ferrocene is covalently bonded to the biomolecules with no direct interaction between biomolecules and metal ion. This last group of compounds is of interest as they represent a novel class of redox-active ligands with potential co-ordination chemistry.

Gautheron *et al.* have reported the first synthesis of ferrocene derivatives of nucleosides in 1991.<sup>47</sup> They used a variety of different Pd-catalyzed C-C coupling reactions to synthesize ferrocene derivatives of uridine, 2'-deoxyuridine, and adenosine derivatives<sup>47</sup> (Figure 1.20). They carried out a reaction of TMS-protected 5-iodouridine, 5-iodo-2'-deoxyuridine, and 8-bromoadenosine with zirconylated compound  $\text{Cp}_2\text{Zr}(\text{Cl})\text{CH}=\text{CH}\text{-Fc}$  (derived from ethynylferrocene and  $\text{Cp}_2\text{Zr}(\text{Cl})\text{H}$  (Schwartz's reagent)) and  $(\text{C}_6\text{H}_5\text{CN})_2\text{PdCl}_2$  as a catalyst. A reaction was also carried out with ethynylferrocene and 5-iodouracil, 5-iodouridine, 5-iodo-2'-deoxyuridine, and bromoadenosine giving 5-ethynylferrocenyluracil, 5-ethynylferrocenyluridine, 5-ethynylferrocenyldeoxyuridine, and ethynylferrocenyladenosine *via* Sonogashira coupling<sup>48</sup> (Figure 1.21).

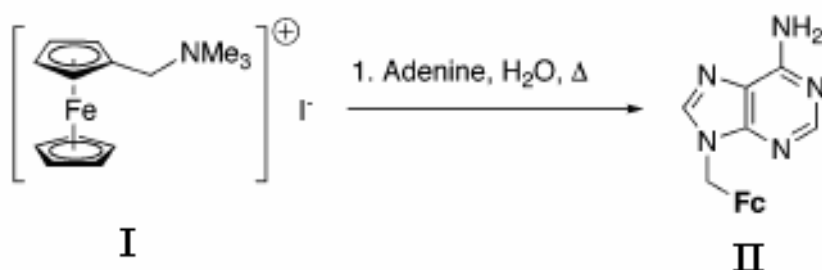


**Figure 1.20:** Ferrocenylated nucleosides with uridine (A), 2'-deoxyuridine (B), and adenosine (C).<sup>47</sup>

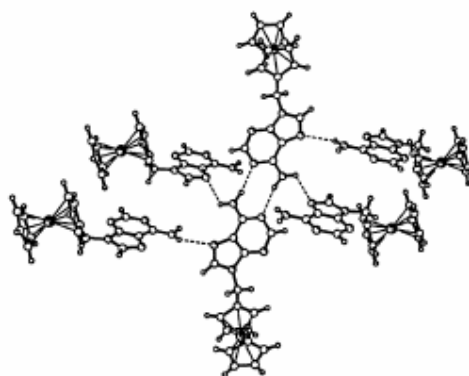


**Figure 1.21:** (A) 5-ethynylferrocenyluracil, (B) 5-ethynylferrocenyluridine, (C) 5-ethynylferrocenyldeoxyuridine, (D) ethynylferrocenyladenosine, and (E) cyclized ferrocenyl derivative obtained *via* Sonogashira coupling.<sup>48</sup>

Houlton *et al.* have published another approach for synthesis of metal nucleobases derivatives.<sup>49</sup> Trimethyl(ferrocenylmethyl)ammonium iodide **I** (Figure 1.22) was used as a convenient source of the ferrocenylmethyl cation in the reaction with various nucleobases and nucleobase derivatives. Complete range of cytosine, thymine, uracil, guanine, and adenine derivatives have been synthesized and characterized by X-ray analysis. X-ray single crystal analysis shows interesting intermolecular hydrogen bonding pattern in solid state for some of the compounds. Houlton *et al.* synthesized 9-ferrocenylmethyladenine **II**.<sup>49a</sup> The first synthesis of this compound was reported by Chen in 1980 who obtained a mixture of isomeric compounds, *N*<sup>6</sup>-ferrocenylmethyladenine and 7-ferrocenylmethyladenine.<sup>50</sup> The X-ray single-crystal structure analysis of **II** reveals that the hydrogen bonding between the adenine rings are formed by combination of Watson-Crick (two hydrogen bonds, central) and Hoogsteen sites (peripheral, one hydrogen bond each) (Figure 1.23).

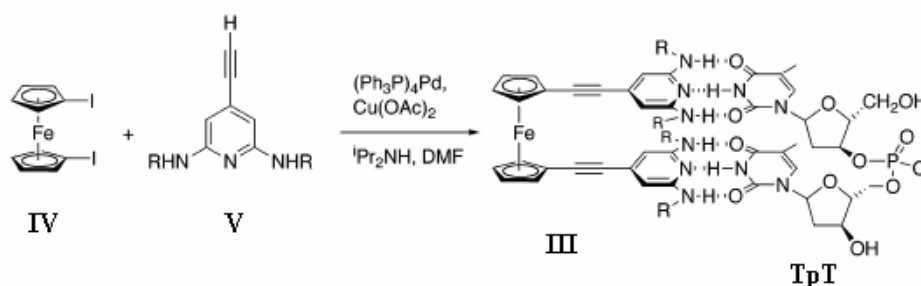


**Figure 1.22:** Synthesis of 9-ferrocenylmethyladenine<sup>49a</sup>



**Figure 1.23:** Intermolecular hydrogen bonding in compound **II**.<sup>49a</sup>

An interesting application of hydrogen bonding involving nucleobases was reported by Inouye and Takase<sup>51</sup> who synthesized ferrocene-modified artificial receptors and showed the strong binding of these designed receptors for dinucleotides. Thymidylyl(3'→5')thymidine (TpT) was synthesized as a target dinucleotide. The molecular design of ferrocene-modified artificial receptor **III** (Figure 1.24) for TpT was based on the inter-ring spacing between two cyclopentadienyl (Cp) rings in ferrocene (0.35 nm), which is almost the same as the distance between stacked base pairs in DNA. The receptor **III** (Figure 1.24) was synthesized by Sonogashira coupling of 1,1'-diiodoferrocene **IV** (Figure 1.24) with two equivalent of 2,6-diamido-4-ethynylpyridine **V**<sup>51</sup> (Figure 1.24).

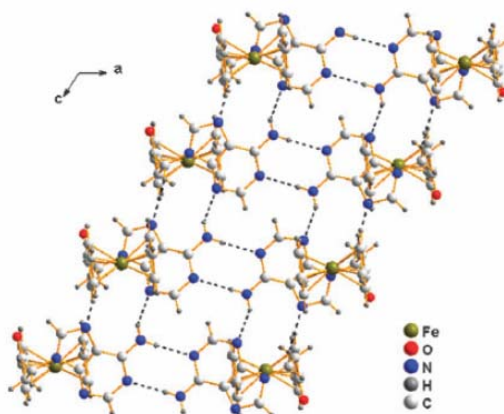


**Figure 1.24:** Synthesis of a molecular receptor for the dinucleotide TpT.<sup>51</sup>

An induced CD signal was observed when ferrocene moiety was associated with TpT. This induced CD signal can only be explained by a twisted orientation of the two Cp rings as consequence of strong hydrogen bonding to the chiral TpT molecule because the receptor **III** (Figure 1.24) is achiral. This is similar to the work of Hirao and Moriuchi, where hydrogen bonds between adjacent amino acids and peptides were

restricting the torsional twist of Cp rings on ferrocene, thus introducing an element of helical chirality.<sup>35</sup> This is useful for highly selective extraction of the dinucleotides into nonpolar solvents by using the receptors. Although it is not clear how this principle can be extended to longer oligonucleotides, such selective receptors may certainly play a role in identification and purification of oligonucleotides in the future.

After our initial publication on X-ray crystal structure studies of ferrocene-nucleobase conjugates,<sup>52a</sup> Verma *et al.* reported the synthesis and crystal structure of an adenine-ferrocene conjugate<sup>52b</sup> (Figure 1.25). The nucleobase forms a ribbon-like motif with the help of intermolecular hydrogen bonds. Hydrogen bonding,  $\pi$ - $\pi$  stacking and CH- $\pi$  interactions play an important role in the stability of the homoadenine tetrad structure, which facilitates ferrocenyl moieties to adopt an interesting spatio-temporal arrangement in the lattice superstructure.



**Figure 1.25:** View of ferrocenylated adenine ribbons.<sup>52b</sup>

In view of the above literature, the work presented in this thesis involves synthesis and characterization of conjugates in which redox active ferrocene is covalently bonded to the self pairing nucleobases or DNA/RNA with a designed spacer. These could be useful building blocks in supramolecular chemistry wherein molecular recognition is coupled with electrochemistry, and may also lead to novel applications for the electrochemical recognition of DNA/RNA binding substrates.

### 1.3.2 Ferrocene-oligonucleotide conjugates

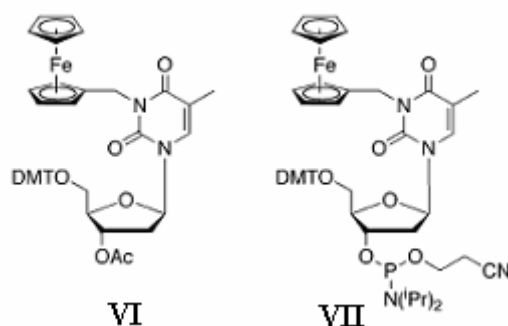
The main interest in ferrocene oligonucleotide derivatives is for electrochemical DNA sensors and is also important in studies on DNA mediated electron transfer. The

detection of specific DNA sequences using real-time methods has received increasing attention for applications in clinical diagnostics, food quality control, environmental protection and forensic science. Among the several detection techniques in literature, those based on radioactive isotopes is sensitive but unsafe due to their hazardous nature and short shelf life. Non-radioactive detection methods such as luminescence, fluorescence<sup>53</sup> or quartz crystal microbalance measurements<sup>54</sup> have been reported. The most common method of detection today is fluorescence, due to its high sensitivity and ease of handling both chemically and spectroscopically. Electrochemical detection offers an alternative means of detection due to their high sensitivity and the simplicity of the detection apparatus. Compared to fluorescence spectroscopy, electrochemical detection is probably more robust and less prone to errors. Therefore electrochemical methods have received particular attention in the development of inexpensive and compact devices. Electrochemical sensors can be built much smaller in size than fluorescence spectrometer. For all these reasons, there is a high interest in electrochemical DNA sensors.<sup>55</sup> One of the approaches of screening the DNA hybridization with a complementary strand is based on the change of the electrochemical response of labeling DNA with redox active compounds. In this context, ferrocene has received particular attention due to its high stability in aqueous aerobic media and facilitating convenient synthetic chemistry.

There are several methods for synthesis of ferrocene-oligonucleotide conjugates. In one instance, Mitsunobu reaction of ferrocenyl methanol with 5'-*O*-(4,4'-dimethoxytriphenylmethyl)-3'-*O*-acetylthymidine gives product **VI**, which was readily converted to the phosphoramidite **VII** (Figure 1.26) which was used as a monomer in automated oligonucleotide synthesis of DNA.<sup>56</sup>

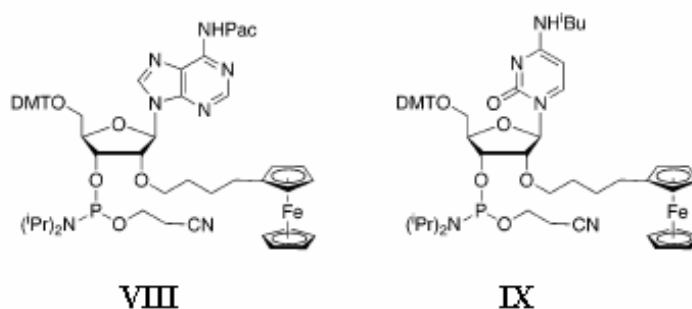
In other work, Gautheron and coworkers used a variety of different Pd-catalyzed C-C coupling reactions to synthesize ferrocene derivatives of uridine, 2'-desoxyuridine, and adenosine derivatives<sup>47</sup> (Figure 1.20). Sonogashira coupling of ethynylferrocene or related ferrocene derivatives with an ethynyl groups to iodouridin or bromoadenosine yields ferrocenylated nucleosides<sup>48</sup> (Figure 1.21), which in turn can be easily transformed into phosphoramidites and subjected to automated oligomer synthesis.





**Figure 1.26:** Ferrocenylated T monomers **VI** and **VII**.<sup>56</sup>

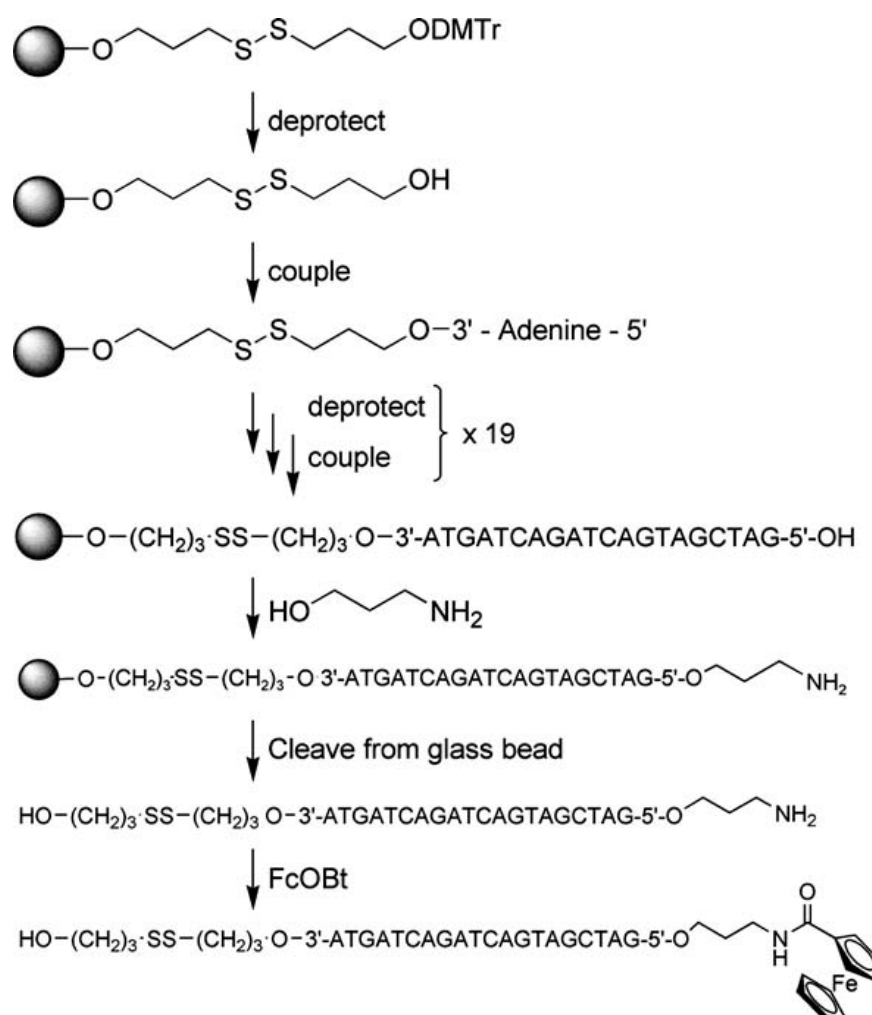
Yu *et al.*<sup>57</sup> synthesized a new type of ferrocene-containing phosphoramidite where a ferrocenyl group was linked to the 2'-position of ribose ring such as **VIII** and **IX** (Figure 1.27). These compounds were the first ferrocenyl-RNA derivatives that may be incorporated into an oligonucleotide strand at any position with possibilities for multiple ferrocenyl incorporation into the oligomer.



**Figure 1.27:** Electronically active 2'-modified phosphoramidite nucleotides **VIII** and **IX**.<sup>57b</sup>

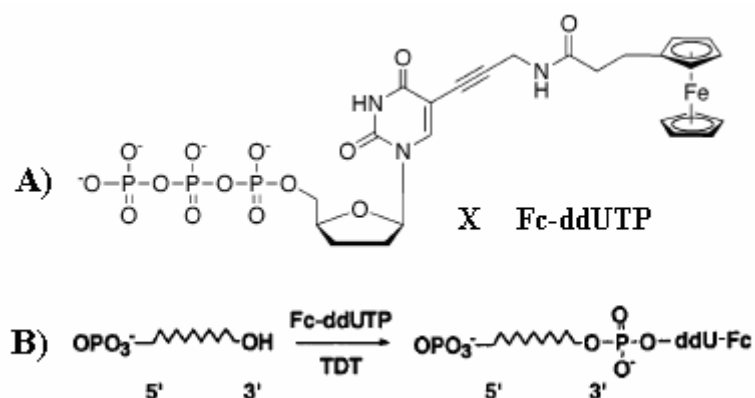
Ferrocenylated nucleotides were synthesized by direct coupling of active ester of ferrocenecarboxylic acid to an end tagged primary amine on the DNA oligonucleotide in solution<sup>58</sup> (Figure 1.28).

In all cases reported so far, the ferrocene label has been introduced at the monomer stage by metal catalyzed reaction (Sonogashira), and then employed in an automated solid-phase DNA synthesizer using phosphoramidite chemistry. Alternatively these may be introduced after the assembly of the oligomers sequence at the 5'-end.



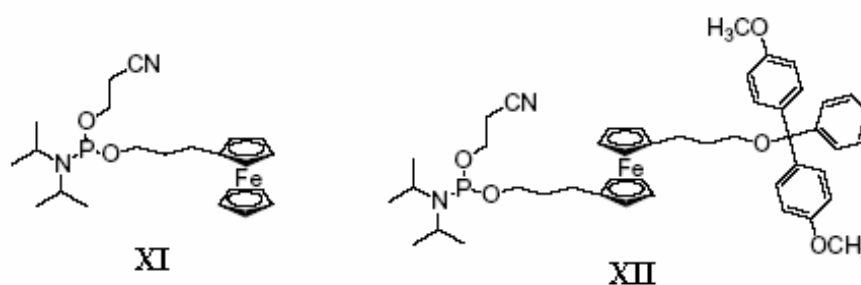
**Figure 1.28:** 5'-labeling of the oligonucleotide with the active ester of ferrocene carboxylic acid.<sup>58</sup>

Anne *et al.* have presented an interesting alternative for the labeling at the 3'-end of an oligonucleotide through a transformable 5'-monophosphate on a monomer.<sup>59</sup> The phosphate group at 5'-end is of importance since it can be profitably exploited for diverse bioconjugations and extension modifications.<sup>60</sup> Dideoxynucleotide triphosphate Fc-ddUTP **X** (Figure 1.21) was used as a building block to extend the 3' terminus of an oligonucleotide resulting in enzymatically 3'-end-labeling by presynthesized 5'-phosphorylated oligonucleotides. This leaves the 5'-end of oligonucleotides intact.<sup>59</sup> (Figure 1.29).



**Figure 1.29:** (A) Ferrocenylated dideoxynucleotide triphosphate (Fc-ddUTP) (B) the enzymatic incorporation reaction of the Fc-ddUTP at the 3'-terminus of the oligonucleotide.<sup>59</sup>

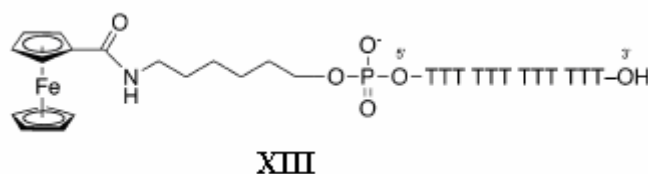
Brisset *et al.*<sup>61</sup> have synthesized monofunctional ferrocene containing phosphoramidite group **XI** and new type of bisfunctional ferrocene derivatives **XII** containing phosphoramidite and demethoxytrityl (DMT) groups (Figure 1.30). These ferrocenyl-phosphoramidites have been directly employed in an automated solid-phase DNA synthesizer using phosphoramidite chemistry for synthesis of ferrocene-labeled oligonucleotides, as potent markers of DNA hybridization, without the need for nucleotide chemistry. The advantage of this method is that it allows a non-specialist in nucleotide chemistry to access labeled oligonucleotides. Ferrocene labeled oligonucleotides, modified at the 3' and/or 5' extremities, with ferrocenyl moiety in the main backbone rather than in side chain was synthesized. It was demonstrated, that a ferrocenyl group at the 3' or 5' position has no drastic effect on the thermal stability of oligonucleotides. The 5' position appears to be more important<sup>62</sup> due to the increase in the electrochemical signal for ferrocene arising only due to binding with the exact target, and hence important for applications in DNA chip technology.



**Figure 1.30:** Structure of ferrocene phosphoramidites.<sup>61</sup>

### 1.3.3 Applications of ferrocene-labeled DNA oligomers as gene sensors

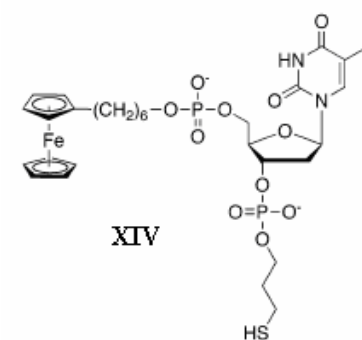
Ihara *et al.*<sup>63</sup> have demonstrated the detection of DNA and RNA at femtomole levels using HPLC, equipped with an ordinary electrochemical detector (ECD). Ferrocene-oligonucleotide **XIII** was synthesized by coupling of amino-terminated oligonucleotide with an activated ester of ferrocene-carboxylic acid<sup>64</sup> (Figure 1.31). The electrochemically active probe DNA **XIII** was hybridized to the complementary DNA, and the conjugate was identified electrochemically by HPLC-ECD.<sup>63-65</sup> In more practical case, the same probe was hybridized with a plasmid containing a choline transporter gene (CTG) fragment of 3693 bp in which the promoter of CTG fragment region contained one A<sub>13</sub> sequence, enabling the detection at concentration as low as 20 fmol.<sup>63</sup>



**Figure 1.31** Structure of a ferrocene-labeled (dT)<sub>12</sub> oligonucleotide.<sup>63</sup>

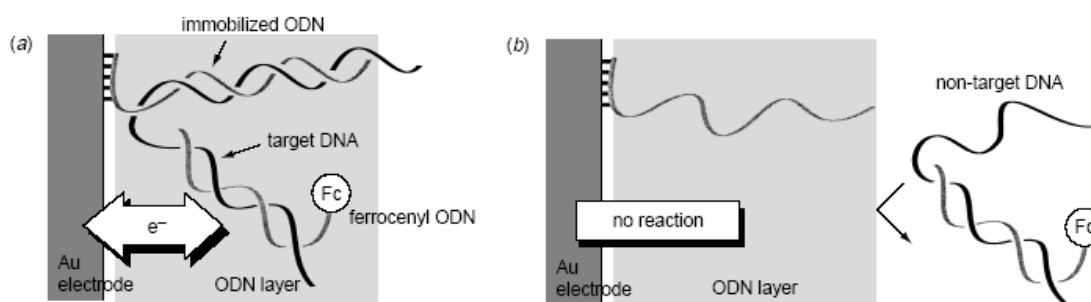
The development of chip technology has modernized the genetic analysis. On a single chip, thousands of oligonucleotides of different sequences can be immobilized in a spatially addressable manner. A fluorescent signal is generated when complementary DNA or RNA binds to these oligonucleotides. For detecting hybridization process in a chip format with electrochemical techniques, the surface of the electrode should serve as a chip on which the oligonucleotides are immobilized. Letsinger *et al.*<sup>66</sup> immobilized the ferrocenylated oligonucleotides in a self-assembled redox-active monolayer on a Au surface. Ferrocenylated thymidine monomer **XIV** (Figure 1.32) with 3'-thiol group was adsorbed on the surface of Au electrodes as a monolayer. The system exhibits a reversible redox signal due to the ferrocene label, which allowed the characterization of the modified surface.

Anne *et al.*<sup>59</sup> have shown that single stranded DNA molecules on gold surfaces are very flexible and become significantly stiffened by hybridization of a complementary strand to form duplex DNA.<sup>59</sup> The conformational changes lead to changes in the mobility of the ferrocenyl reporter group, which in turn changes its electron-transfer properties.<sup>67</sup>



**Figure 1.32:** 5'-Ferrocenylated thymine monomer with a 3'-thiol group for immobilization on a Au surface.<sup>66</sup>

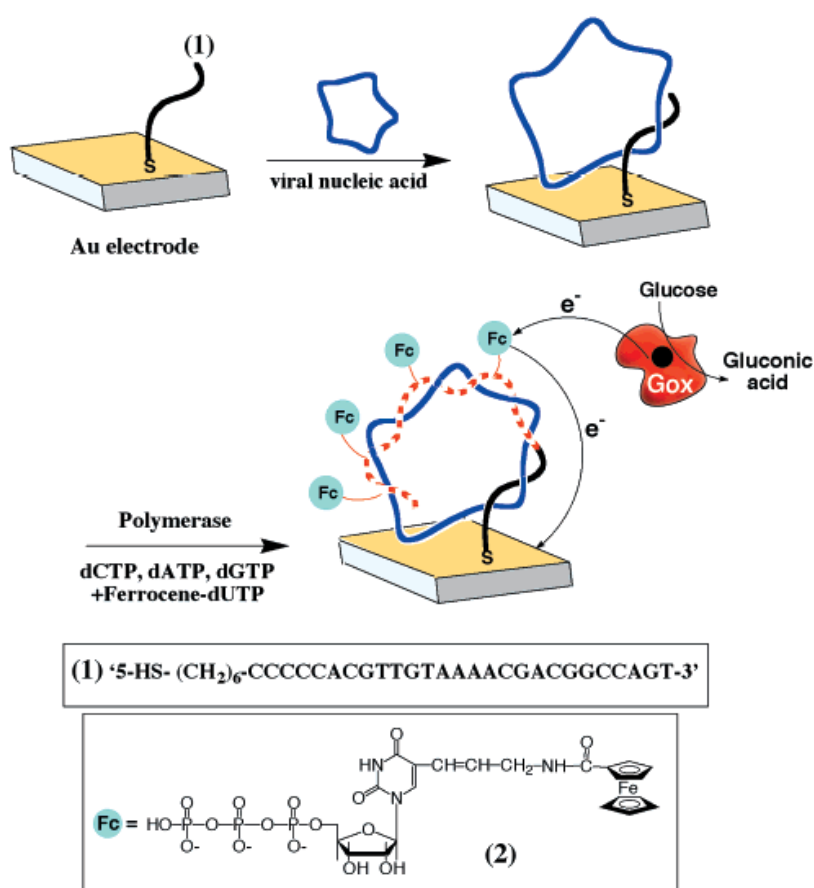
Ihara *et al.* have published a slightly different approach to an immobilized electrochemical gene sensor, using three oligonucleotide systems,<sup>68</sup> in a “sandwich assay” (Figure 1.33).<sup>69</sup> First, an oligonucleotide capture probe, possessing five successive thiophosphate groups was immobilized on an Au electrode surface. The target DNA strand was then hybridized to the immobilized capture probe through the presence of the complementary sequence. This was followed by the hybridization of a ferrocene-oligonucleotide to a complementary sequence on the single strand DNA target to result in a ternary complex. During this process the ferrocene was brought close to the electrode which resulted in a detectable electrochemical signal.



**Figure 1.33:** Schematic illustration of principle of the “sandwich assay” for electrochemical DNA sensors.<sup>68</sup>

The amperometric detection of DNA was examined by Ihara *et al.*<sup>68</sup> using redox-labeled nucleic acids as probes, e.g. ferrocene-labeled nucleic acids. Willner *et al.*<sup>70</sup> extended this work through a bioelectrocatalytic amplification of the DNA detection process. The scheme for the generation of the redox-active DNA replicas and the amperometric amplified bioelectrocatalytic analysis of the gene is outlined in Figure

1.34. Viral DNA interacts with a thiolated oligonucleotide assembled on an Au electrode. The thiolated monolayer of oligonucleotide is complementary to the cyclic viral DNA (M13 $\Phi$ ) and thus the viral DNA binds to the DNA film. The partially double-stranded assembly was then allowed to interact with a nucleotide mixture that includes the synthetic ferrocene tethered dUTP<sup>71</sup> as a redox-label. In the presence of polymerase, Klenow fragment I, the viral DNA was replicated incorporating the ferrocene-modified DNA. This was confirmed by quartz crystal microbalance. With ferrocene unit as electron-transfer mediators between the electrode surface and glucose oxidase to convert glucose to gluconic acid, a bioelectrocatalytic amplification of the DNA detection process was achieved. This system provides a new aspect in DNA bioelectronics with an ability to form redox-active DNA replicas that may be activated through a bioelectrocatalytic cascades.



**Figure 1.34:** Polymerase induced generation of a redox-active nucleic acid replica for amplified detection of viral DNA and the bioelectrocatalyzed oxidation of glucose to gluconic acid by glucose oxidase (Gox).<sup>70</sup>

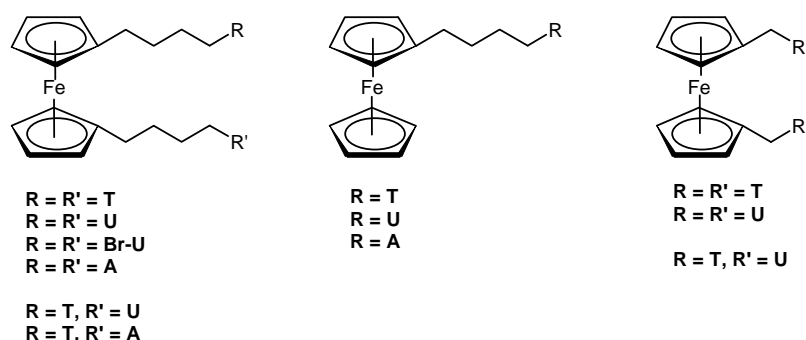
## 1.4 Present Work

The preceding sections of this chapter give an overview on bioorganometallic chemistry of ferrocene with emphasis on bioconjugates of ferrocene with amino acids and peptides, proteins, DNA, and RNA. Ferrocene-nucleobase conjugates (conjugates in which ferrocene is covalently bonded to the nucleobases with no direct interaction between nucleobases and metal ion) is a relatively new and less explored field of bioorganometallic chemistry. These conjugates represent a novel class of redox-active ligands which shows an interesting intermolecular hydrogen bonding.

Strategies for synthesis of ferrocenyl-modified oligonucleotides have been discussed. The ferrocene-oligonucleotide conjugates have applications as gene sensors with electrochemical detection.

The work presented in this thesis involves the design, synthesis, characterization and X-ray crystallographic analyses of the redox active ferrocene-nucleobase conjugates with designed spacers. This is followed by synthesis of ferrocenyl-phosphoramidite monomer, its incorporation into oligonucleotides, characterization and biophysical evaluation of ferrocenyl-modified oligonucleotides. Electrochemical investigation of ferrocene-nucleobase conjugates and ferrocene-oligonucleotide conjugates have been done using cyclic voltammetry.

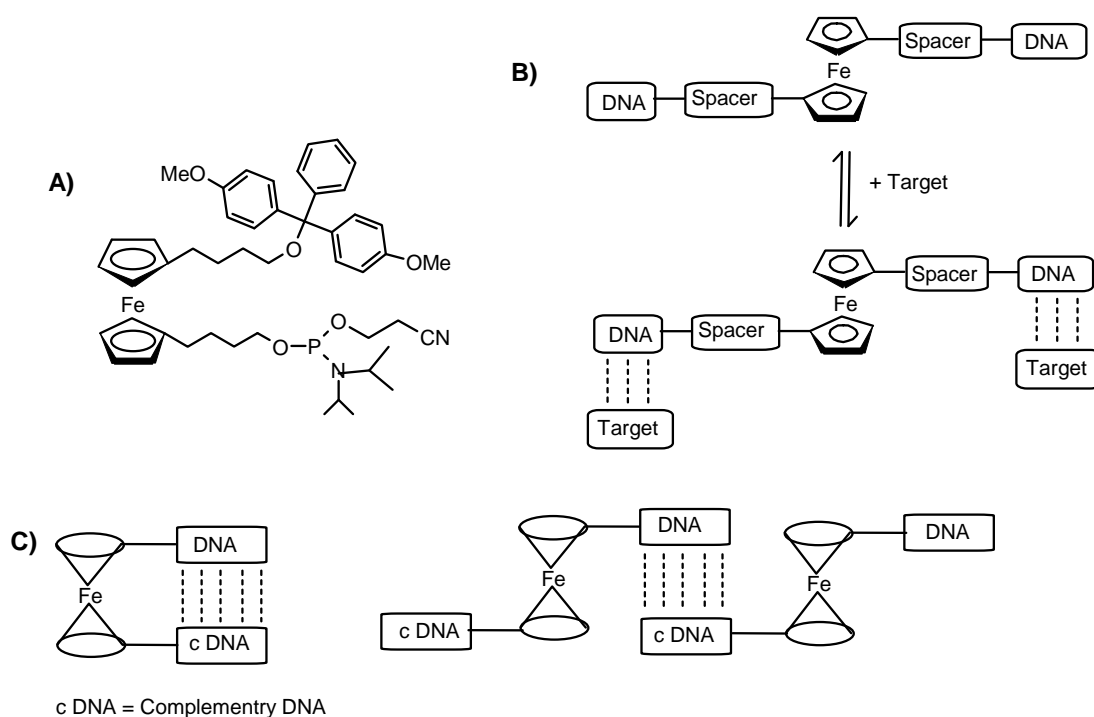
**Chapter 2** describes the construction of a series of new ferrocene-linked mono and bis-nucleobase conjugates with different spacer. A complete series of thymine, uracil, 5-bromouracil and adenine derivatives (mono and bis), with *n*-butyl and methylene spacer was synthesized (Figure 1.35) and comprehensively characterized, by X-ray analysis.



**Figure 1.35:** Ferrocene-linked mono and bis-nucleobase derivatives. T = thymine, U = uracil, (Br)U = 5-bromouracil, A = adenine

The synthesis of chimeric mixed base ferrocene derivatives (Figure 1.35) and X-ray crystallographic analyses are presented. The newly designed ferrocene-linked mono and bis-nucleobase conjugates show different supramolecular assemblies mediated *via* centrosymmetric reverse Watson-Crick (rWC) base pairings.

**Chapter 3** describes the synthesis and characterization of bifunctional ferrocene containing phosphoramidite and dimethoxytrityl (DMT) groups **XV** (Figure 1.36) useful for incorporation in an automated solid-phase DNA synthesizer and for synthesis of 3' and/or 5' modified oligonucleotides. Electrophoretic gel shift assay was used to establish the binding of different ferrocenyl modified oligonucleotides to the complementary DNA. The thermal stability of double strand oligonucleotides was studied by its melting temperature ( $T_m$ ).



**Figure 1.36:** A) Ferrocene-phosphoramidite (monomer unit), B & C) Ferrocene unit incorporated in DNA sequences (ferrocene linked oligonucleotide)

**Chapter 4** deals with the electrochemical studies of ferrocene of mono and bis-functional ferrocene-nucleobase conjugates using cyclic voltammetry in non-aqueous media. The redox behavior of the systems is understood in terms of the quantitative functional parameters derived from experimental electrochemical data, which is



correlated with their chemical structure. This is followed by electrochemical investigation of ferrocene-oligonucleotide conjugates using steady state voltammetry. The electrochemical properties of these ferrocene-oligonucleotide conjugates were analyzed before and after hybridization with different oligonucleotides. The ability of using these ferrocenyl-labeled oligonucleotides in DNA sensors has been demonstrated.

## 1.5 References

1. Blackburn, G. M.; Gait, M. J. In *Nucleic acids in chemistry and biology*. University Press: Oxford **1990**.
2. Watson, J. D.; Crick, F. H. C. *Nature* **1953**, *171*, 737–738.
3. Crooke, S. T. In *Therapeutic Applications of oligonucleotide*. Springer-Verlag: Heidelberg **1995**.
4. (a) Saenger, W. In *Principles of nucleic acid structure*. Springer-Verlag: New York **1984**.
5. Hoogsteen, K. *Acta. Crystal.* **1963**, *16*, 907-916.
6. (a) Crick, F. H. C. *J. Mol. Biol.* **1966**, *19*, 548-555. (b) Soll, D.; Cherayil, J. D.; Bock, R. M. *J. Mol. Biol.* **1967**, *29*, 97-112.
7. Seeman, N. C.; Rosenberg, J. M.; Rich, A. *Proc. Natl. Acad. Sci. USA.* **1976**, *73*, 604-807.
8. (a) Hayashi, G.; Hagihara, M.; Nakatani, K. *Nucleic Acids Symp Ser. (Oxf)* **2005**, *49*, 261-262. (b) Vargason, J. M.; Eichman, B. F.; Ho, P. S. *Nature Structural Biology* **2000**, *7*, 758-761.
9. Wang, G., Vasquez, K. M. *Mutat. Res.* **2006**, *598*, 103-119.
10. Berg, J. M.; Tymoczko, J. L.; Stryer, L. *Biochemistry*, 5<sup>th</sup> Edition, WH Freeman and Company, **2002**, 781-808.
11. (a) Weiss, B. (ed.) *Antisense Oligodeoxynucleotides and Antisense RNA: Novel Pharmacological and Therapeutic Agents*. CRC Press, Boca Raton, FL **1997**. (b) Stein, C. A. *Nat. Med.* **1995**, *1*, 1119-1121.
12. Barawkar, D. A.; Rajeev, K. G.; Kumar, V. A.; Ganesh, K. N. *Nucleic Acid Res.* **1996**, *24*, 1229-1237.
13. Kealy, T. J.; Pauson, P. L. *Nature* **1951**, *168*, 1039-1040.
14. Miller, S. A.; Tebbboth, J. A.; Tremain, J. F. *J. Chem. Soc.* **1952**, 632-635.

15. Wilkinson, G.; Rosenblum, M.; Whiting, M. C.; Woodward, R. B. *J. Am. Chem. Soc.* **1952**, *74*, 2125-2126.
16. Woodward, R. B.; Rosenblum, M.; Whiting, M. C. *J. Am. Chem. Soc.* **1952**, *74*, 3458-3459.
17. Wilkinson, G. *Org. Synth.* **1956**, *36*, 31-34.
18. Haaland, A. *Acc. Chem. Res.* **1979**, *12*, 415-422.
19. Seiler, P.; Duntz, J. D. *Acta. Cryst.* **1982**, *b38*, 1741-1745.
20. Jaouen, G.; Vessières, A.; Butler, I. S. *Acc. Chem. Res.* **1993**, *26*, 361-369.
21. (a) Fish, R. H.; Jaouen, G. *Organometallics* **2003**, *22*, 2166-2177. (b) Schlotter, K.; Boeckler, F.; Hußner, H.; Gmeiner, P. *J. Med. Chem.* **2005**, *48*, 3696-3699. (c) Pike, A. R.; Ryder, L. C.; Horrocks, B. R.; Clegg, W.; Elsegood, M. R. J.; Connolly, B. A.; Houlton, A. *Chem. Eur. J.* **2002**, *8*, 2891-2899. (d) Van Staveren, D. R.; Metzler-Nolte, N. *Chem. Rev.* **2004**, *104*, 5931-5986.
22. Metzler-Nolte, N. *Angew. Chem., Int. Ed.* **2001**, *40*, 1040-1043.
23. Köpf-Maier, P.; Köpf, H. *Chem. Rev.* **1987**, *87*, 1137-1152.
24. Köpf-Maier, P.; Köpf, H. *Struct. Bond.* **1988**, *70*, 103-185.
25. Shen, W. -C.; Beloussow, K.; Meirim, M. G.; Neuse, E. W.; Caldwell, G. *J. Inorg. Organomet. Polym.* **2000**, *10*, 51-60.
26. (a) Edwards, E. I.; Epton, R.; Marr, G. *J. Organomet. Chem.* **1979**, *168*, 259-272. (b) Simionescu, Cr.; Lixandru, T.; Scutaru, D.; Vata, M. *J. Organomet. Chem.* **1985**, *292*, 269-273. (c) Scutaru, D.; Mazilu, I.; Tataru, L.; Vata, M.; Lixandru, T. *J. Organomet. Chem.* **1991**, *406*, 183-187. (d) Scutaru, D.; Mazilu, I.; Vata, M.; Tataru, L.; Vlase, A.; Lixandru, T.; Simionescu, Cr. *J. Organomet. Chem.* **1991**, *401*, 87-90.
27. (a) Biot, C.; Glorian, G.; MacIejewski, L. A.; Brocard, J. S.; Domarle, O.; Blampain, G.; Millet, P.; Georges, A. J.; Abessolo, H.; Dive, D.; Lebibi, J. *J. Med. Chem.* **1997**, *40*, 3715-3718. (b) Delhaes, L.; Biot, C.; Berry, L.; MacIejewski, L. A.; Camus, D.; Brocard, J. S.; Dive, D. *Bioorg. Med. Chem.* **2000**, *8*, 2739-2745. (c) Beagley, P.; Blackie, M. A. L.; Chibale, K.; Clarkson, C.; Meijboom, R.; Moss, J. R.; Smith, P. J.; Su, H. *Dalton Trans.* **2003**, 3046-3051.
28. (a) Epton, R.; Marr, G.; Rogers, G. K. *J. Organomet. Chem.* **1978**, *150*, 93-100.

29. (a) Top, S.; Vessie`res, A.; Cabestaing, C.; Laios, I.; Leclercq, G.; Provot, C.; Jaouen, G. *J. Organomet. Chem.* **2001**, 637-639, 500-506. (b) Top, S.; Vessie`res, A.; Leclercq, G.; Quivy, J.; Tang, J.; Vaissermann, J.; Huche', M.; Jaouen, G. *Chem. Eur. J.* **2003**, 9, 5223-5236.
30. Hulton, A.; Isaac, C. J.; Gibson, A. E.; Horrocks, B. R.; Clegg, W.; Elsegood, M. R. *J. J. Chem. Soc., Dalton Trans.* **1999**, 3229-3234.
31. Leonard, G. A.; Zhang, S.; Peterson, M. R.; Harrop, S. J.; Helliwell, J. R., Cruse, W. B.; d'Estaintot, B. L.; Kennard, O.; Brown, T.; Hunter, W. N. *Structure* **1995**, 3 (4), 335-340.
32. Deeming, J. In *Comprehensive Organometallic Chemistr.* Wilkinson, G., Stone, F. G. A., (ed.) Pergamon: Oxford, UK, **1982**; Vol. 4, p 475.
33. (a) Hauser, C. R.; Lindsay, J. K. *J. Org. Chem.* **1957**, 22, 1246-1247. (b) Osgerby, J. M.; Pauson, P. L. *J. Chem. Soc.* **1958**, 656-660.
34. Petka, W. A.; Harden, J. L.; McGrath, K. P.; Wirtz, D.; Tirrell, D. A. *Science*, **1998**, 281, 389-392.
35. Moriuchi, T.; Hirao, T. *Chem. Soc. Rev.* **2004**, 33, 294-301.
36. Cerichelli, G.; Floris, B.; Ortaggi, G. *J. Organomet. Chem.* **1974**, 76, 73-79.
37. (a) Severin, K.; Bergs, R.; Beck, W. *Angew. Chem., Int. Ed.* **1998**, 37, 1634-1654. (b) Saweczko, P.; Enright, G. D.; Kraatz, H. -B. *Inorg. Chem.* **2001**, 40, 4409-4419. (c) Moriuchi, T.; Yoshida, K.; Hirao, T. *Org. Lett.* **2003**, 5, 4285-4288.
38. Wang, J. *Electroanalysis*, **2001**, 13, 983-988.
39. Bartlett, P. N.; Whitaker, R. G.; Green, M. J.; Frew, J. *J. Chem. Soc., Chem. Commun.* **1987**, 1603-1604.
40. Degani, Y.; Heller, A. *J. Phys. Chem.* **1987**, 91, 1285-1289.
41. Degani, Y.; Heller, A. *J. Am. Chem. Soc.* **1988**, 110, 2615-2620.
42. Riklin, A.; Katz, E.; Willner, I.; Stocker, A.; Buckmann, A. F. *Nature* **1995**, 376, 672-675.
43. Schollhorn, H.; Thewalt, U.; Lippert, B. *J. Chem. Soc., Chem. Commun.* **1986**, 258-260.
44. Zamora, F.; Sabat, M.; Lippert, B. *Inorg. Chem.* **1996**, 35, 4858-4864.
45. Price, C.; Elsegood, M. R. J.; Clegg, W.; Rees, N. H.; Houlton, A. *Angew. Chem., Int. Ed.* **1997**, 36, 1762-1764.

46. (a) Agnew, N. H.; Applton, T. G.; Hall, J. R.; Kilmister, G. F.; McMahon, I. J. *J. Chem. Soc., Chem. Commun.* **1979**, 324-326. (b) Toney, J. H.; Brock, C. P.; Marks, T. J. *J. Am. Chem. Soc.* **1986**, *108*, 7263-7274. (c) Smith, D. P.; Griffin, M. T.; Olmstead, M. M.; Maestre, M. F.; Fish, R. H. *Inorg. Chem.* **1993**, *32*, 4677-4678. (d) Chen, H.; Olmstead, M. M.; Smith, D. P.; Maestre, M. F.; Fish, R. H. *Angew. Chem., Int. Ed.* **1995**, *34*, 1514-1517.
47. Meunier, P.; Ouattara, I.; Gautheron, B.; Tirouflet, J.; Camboli, D.; Besancon, J.; Boulay, F. *Eur. J. Med. Chem.* **1991**, *26*, 351-362.
48. Sonogashira, K.; Tohda, Y.; Hagihara, N. *Tetrahedron Lett.* **1975**, *16*, 4467-4470.
49. (a) Price, C.; Aslanoglu, M.; Isaac, C. J.; Elsegood, M. R. J.; Clegg, W.; Horrocks, B. R.; Houlton, A. *J. Chem. Soc., Dalton Trans.* **1996**, 4115-4120 (b) Houlton, A.; Isaac, C. J.; Gibson, A. E.; Horrocks, B. R.; Clegg, W.; Elsegood, M. R. *J. Chem. Soc., Dalton Trans.* **1999**, 3229-3234.
50. Chen, S.-C. *J. Organomet. Chem.* **1980**, *202*, 183-189.
51. Inouye, M.; Takase, M. *Angew. Chem., Int. Ed.* **2001**, *40*, 1746-1748.
52. (a) Patwa, A. N.; Gupta, S.; Gonnade, R. G.; Kumar, V. A.; Bhadbhade, M. M.; Ganesh, K. N. *J. Org. Chem.* **2008**, *73*, 1508-1515. (b) Kumar, J.; Purohit, C. S.; Verma, S. *Chem. Commun.* **2008**, 2526-2528.
53. Abel, A. P.; Weller, M.G.; Duvencak, G. L.; Ehrat, M.; Widmer, H. M. *Anal. Chem.* **1996**, *68*, 2905-2912.
54. Fawcett, N. C.; Evans, J. A.; Chien, L. C.; Flowers, N. *Anal. Lett.* **1988**, *21*, 1099-1114.
55. Wilson, E. K. *Chem. Eng. News* **1969**, *47*, 7.
56. Bucci, E.; De Napoli, L.; Di Fabio, G.; Messere, A.; Montesarchio, D.; Romanelli, A.; Picciallia, G.; Varra, M. *Tetrahedron* **1999**, *55*, 14435-14450.
57. (a) Yu, C. J.; Wan, Y.; Yowanto, H.; Li, J.; Tao, C.; James, M. D.; Tan, C. L.; Blackburn, G. F.; Meade, T. J. *J. Am. Chem. Soc.* **2001**, *123*, 11155-11161. (b) Yu, C. J.; Wang, H.; Wan, Y.; Yowanto, H.; Kim, J. C.; Donilon, L. H.; Tao, C.; Strong, M.; Chong, Y. *J. Org. Chem.* **2001**, *66*, 2937-2942.
58. Kraatz, H. B. *J. Inorg. Organomet. Polym. Mater.* **2005**, *15*, 83-106.
59. Anne, A.; Blanc, B.; Moiroux, J. *Bioconjugate Chem.* **2001**, *12*, 396-405.

60. (a) Kamaike, K.; Ogawa, T.; Ishido, Y. *Nucleosides and Nucleotides* **1993**, *12*, 1015-1032. (b) Hermanson, G. T. Nucleic Acid and Oligonucleotide Modification and Conjugation. In *Bioconjugate Techniques*, Academic Press, Inc., London, **1996**; pp 643-671.
61. (a) Navarro, A-E.; Spinelli, N.; Chaix, C.; Moustrou, C.; Mandrand, B.; Brisset, H. *Bioorg Med. Chem. Lett.*, **2004**, *14*, 2439–2441. (b) Navarro, A-E.; Spinelli, N.; Moustrou, C.; Chaix, C.; Mandrand, B.; Brisset, H. *Nucleic Acids Res.*, **2004**, *32*, 5310-5319.
62. Long, Y-T.; Li, C-Z.; Sutherland, T.C.; Chahma, M.; Lee, J.S.; Kraatz, H-B. *J. Am. Chem. Soc.* **2003**, *125*, 8724–8725.
63. Takenaka, S.; Uto, Y.; Kondo, H.; Ihara, T.; Takagi, M. *Anal. Biochem.* **1994**, *218*, 436–443.
64. (a) Ihara, T.; Maruo, Y.; Takenaka, S.; Takagi, M. *Nucleic Acids Res.* **1996**, *24*, 4273-4280.
65. Takenaka, S.; Yamashita, K.; Takagi, M.; Uto, Y.; Kondo, H. *Anal. Chem.* **2000**, *72*, 1334-1341.
66. Mucic, R. C.; Herrlein, M. K.; Mirkin, C. A.; Letsinger, R. L. *Chem. Commun.* **1996**, 555-557.
67. Anne, A.; Bouchardon, A.; Moiroux, J. *J. Am. Chem. Soc.* **2003**, *125*, 1112-1113.
68. Ihara, T.; Nakayama, M.; Murata, M.; Nakano, K.; Maeda, M. *Chem. Commun.* **1997**, 1609-1610.
69. Takenaka, S. *Bull. Chem. Soc. Jpn.* **2001**, *74*, 217-224.
70. Patolsky, F.; Weizmann, Y.; Willner, I. *J. Am. Chem. Soc.* **2002**, *124*, 770-772.
71. Adamczyk, M.; Fishpaugh, J. R.; Heuser, K. J. *Bioconj. Chem.* **1997**, *8*, 253-255.

## **CHAPTER 2**

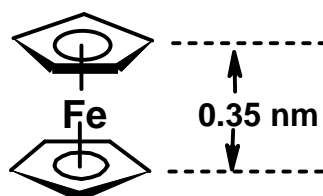
# **FERROCENE-NUCLEOBASE CONJUGATES: SYNTHESIS AND X-RAY CRYSTAL STRUCTURE STUDIES**

## 2.1 Introduction

Development of supramolecular assemblies into well defined architecture has been a subject of great interest in recent years in view of both its importance in the synthesis of artificial models for natural processes and its significance to get insight into the conformational features of biomolecules such as proteins, lipids and nucleic acids.<sup>1</sup> A system of evolutionary perfection for molecular self assembly is DNA / RNA.<sup>2</sup> The two antiparallel strands of DNA are held together by A:T and C:G base pairs to form the double helix where hydrogen bonding between complementary bases and  $\pi$ -stacking interactions between the adjacent, stacked base pairs stabilize the double helical architecture.<sup>2</sup> Given the four natural nucleobases A, G, C and T/U, at least 28 types of base pair modes are possible involving all combinations of self and complementary base pairing through the diverse hydrogen bond donor–acceptor sites.<sup>2</sup> However, nature prefers only two types in the form of the canonical Watson-Crick (WC) and Hoogsteen (HG) complementary base pairing in most DNA/RNA structures. Hydrogen bond mediated supramolecular interactions have provided inspiration to design a number of novel self assembling systems.<sup>3</sup> Incorporation of the common nucleobases A, G, C and T (or U) in supramolecular environment enables exploration of different pairing characteristics of these nucleobases.<sup>4</sup> Guanine derivative self-assemble through Hoogsteen interaction into either linear tapes or macrocycles.<sup>5</sup> Self pairing of adenine<sup>6</sup> as well as the 1-dimensional i-motif from C:C<sup>+</sup> base pairing *via* non Watson-Crick base pairing in DNA<sup>7</sup> and PNA<sup>8</sup> have been reported. In view of these observations, there has been a great interest in developing novel approaches to self assembled superstructures directed by nucleobase pairing in systems where the sugar-phosphate backbone is modified or replaced by synthetic linkers.<sup>9</sup> Studies of such designed systems are unraveling the formation of non-canonical, unusual modes of base pairing of the nucleobases, which have been recently detected in abundance in continuous 3-dimensional DNA lattice<sup>10</sup> and in DNA complexes having interstrand crosses.<sup>11</sup> Hence the study of unusual base pairings in nucleic acids and their model systems have assumed recent significance.

## 2.2 Present Work: A Rationale and Objective

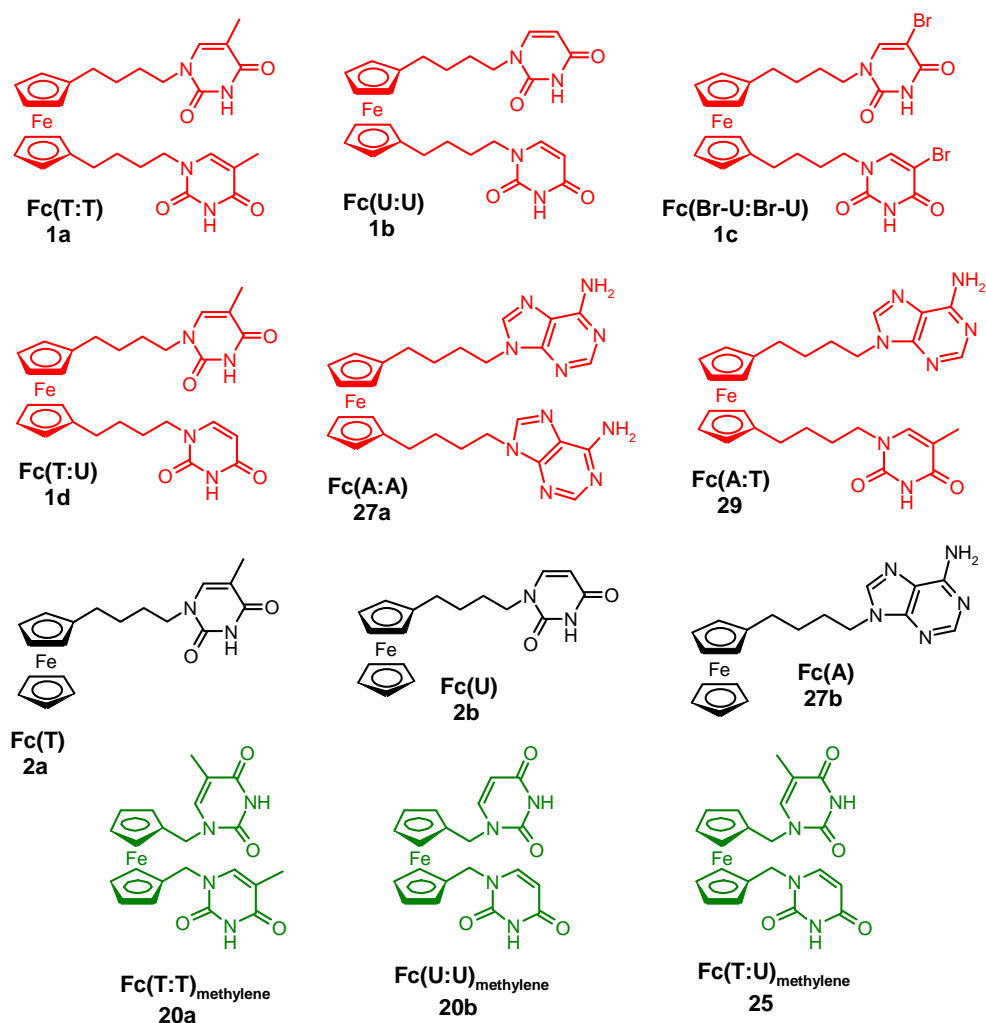
Currently bioorganometallic chemistry is growing rapidly, networking classical organometallic chemistry to biology, medicine and molecular biotechnology.<sup>12-15</sup> Ferrocene and its derivatives have received a lot of importance in molecular recognition research, due to their redox characteristics.<sup>3,15,16</sup> Synthesis and self association motifs of ferrocene linked mono-nucleobase conjugates with methylene spacer have been reported by Houlton's group.<sup>17</sup> After our initial publication on X-ray crystal structure studies of ferrocene-nucleobase conjugates,<sup>18a</sup> Verma *et al.* have reported the synthesis and crystal structure of an adenine-ferrocene conjugate with propionyl (-CO-CH<sub>2</sub>-CH<sub>2</sub>-) spacer.<sup>18b</sup> An attractive feature of ferrocene is that the two cyclopentadienyl (Cp) rings can rotate around the Fe atom which can act as a ball bearing<sup>17</sup> and the vertical distance between the two Cp rings in ferrocene is 0.35 nm which is similar to the distance between the stacked base pairs in DNA.<sup>2,19</sup> The redox active ferrocene unit linked to self base pairing nucleobases or DNA/RNA with designed spacer could therefore be useful building blocks in supramolecular chemistry coupling molecular recognition with electrochemistry, leading to novel applications for the electrochemical recognition of a large variety of DNA/RNA binding substrates. Thus the synthesis of conjugates in which ferrocene is covalently bonded to the nucleobases is of great interest.



This chapter describes the construction of a series of new ferrocene-linked mono and bis-nucleobase conjugates with different spacer. A complete series of thymine (T), uracil (U), 5-bromouracil (Br-U) and adenine (A) derivatives (mono and bis), with *n*-butyl, spacer was synthesized (Figure 2.1) and comprehensively characterized by X-ray analysis. Also described are the synthesis and X-ray crystal structure studies of ferrocene-linked bis-thymine or uracil conjugates with methylene spacer and mixed base ferrocene derivatives (Figure 2.1).

Attempts for synthesis of ferrocene-linked bis(cyanuric acid) derivatives with *n*-butyl spacer are also described, wherein instead of desired product, novel side products were obtained.





**Figure 2.1:** Ferrocene-linked mono and bis-nucleobase derivatives: Target molecules

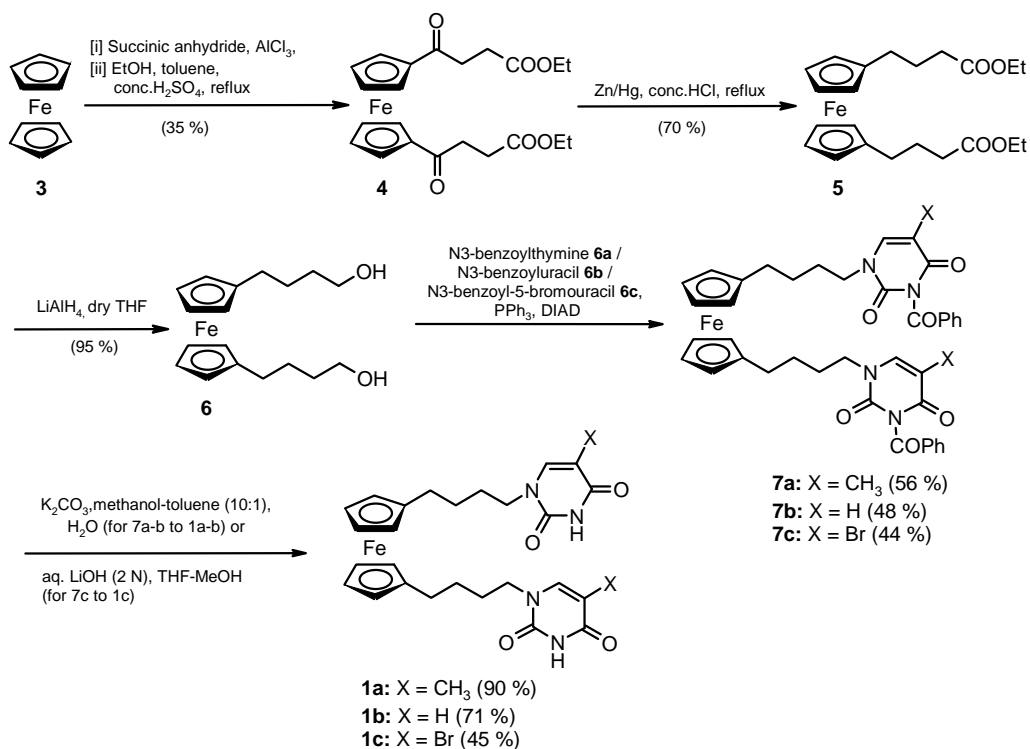
## 2.3 Synthesis of Ferrocene-Nucleobase Conjugates

This section describes the procedures pertaining to the synthesis of the ferrocene-nucleobase conjugates listed in Figure 2.1.

### 2.3.1 Synthesis of ferrocene-linked mono and bis-thymine/uracil/5-bromouracil conjugates with *n*-butyl spacer<sup>18a</sup> (1a-c and 2a-b)

The construction of a series of new ferrocene-linked bis conjugates 1,1'-bis(*N*1-butylthymine) **1a**, 1,1'-bis(*N*1-butyluracil) **1b** and 1,1'-bis(*N*1-butyl-5-bromouracil) **1c** derivatives was envisaged (Scheme 2.1). In addition, it was aimed to synthesize mono conjugates 1-(4-(thyminyl)butyl)ferrocene **2a** and 1-(4-(uracilyl)butyl)ferrocene **2b** (Scheme 2.2).

First simple *n*-alkyl spacer was chosen to connect ferrocene with the nucleobases thymine, uracil and 5-bromouracil. It was thought that *n*-butyl chain would provide the appropriate hydrophobicity to enhance the solubility of the ferrocene linked bis(nucleobase) conjugates in common organic solvents. The planned synthetic route for the bis(nucleobase) ferrocene target compounds involved the key intermediate 1,1'-bis(4-hydroxybutyl)ferrocene<sup>20</sup> **6** while the mono nucleobase ferrocene was synthesized from 1-(4-hydroxybutyl)ferrocene **11**. Ferrocene diol **6** was obtained from ferrocene in four steps. Ferrocene on treatment with 2 equivalents of succinic anhydride under Friedel-Craft reaction conditions and subsequent esterification gave ketoester **4**. This was followed by Zn/Hg reduction of the carbonyl group and LiAlH<sub>4</sub> reduction of the ester gave desired diol **6**, which was reacted with *N*3-protected T/U/5-(Br-U), under Mitsunobu reaction conditions, to yield **7a-c**. **7a** and **7b** on *N*3-debenzoylation using aq. K<sub>2</sub>CO<sub>3</sub> in methanol-toluene provided **1a** and **1b** respectively. The use of aq. K<sub>2</sub>CO<sub>3</sub> in methanol-toluene for debenzoylation of **7c** was not successful. However when LiOH in THF-methanol was used as the base for debenzoylation of **7c**, the desired product **1c** was obtained (Scheme 2.1).



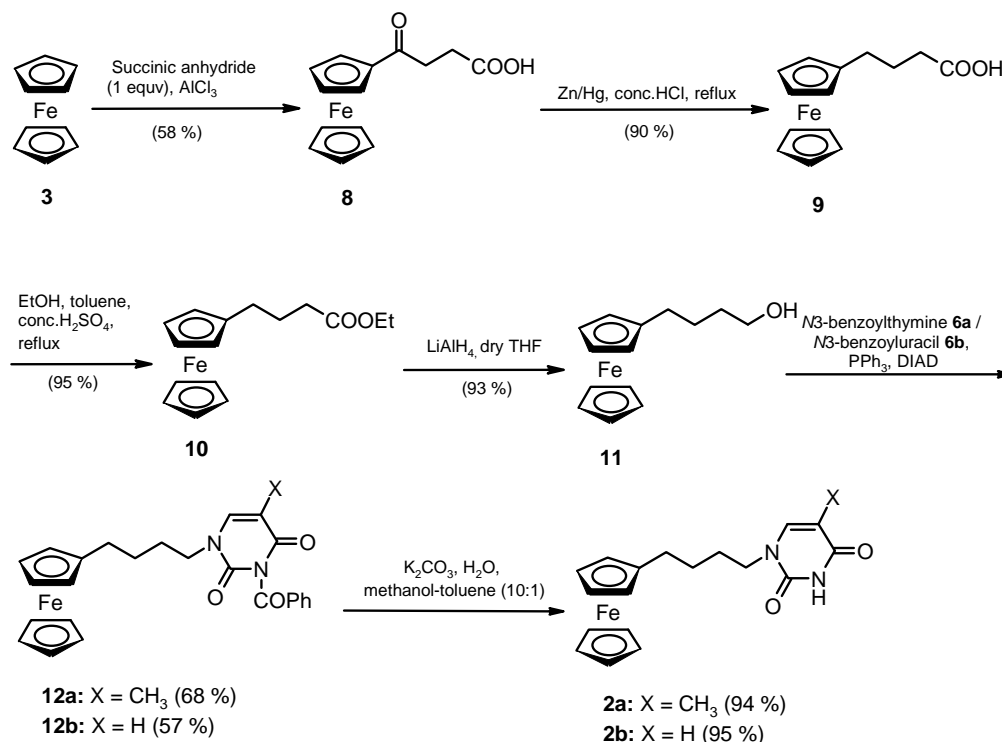
**Scheme 2.1:** Synthesis of ferrocene-linked bis thymine/uracil/5-bromouracil conjugates with *n*-butyl spacer.

The diketoester **4** was confirmed by  $^1\text{H}$  NMR spectrum showing triplet at  $\delta$  1.27 and quartet at  $\delta$  4.18 for ethyl ester group. Further, the formation of diester **5** was confirmed by appearance of four more protons at  $\delta$  1.78 for two  $-\text{CH}_2$  group. Diol **6** was characterized by disappearance of ethyl ester protons ( $\delta$  1.27 and 4.18) and appearance of four more protons at  $\delta$  3.58 for two  $-\text{CH}_2\text{-OH}$  group. Formation of benzoyl protected ferrocene nucleobase conjugates **7a-c** were confirmed by  $^1\text{H}$  NMR spectrum showing aromatic protons of benzoyl group at  $\delta$  7.89-7.45. Further, formation of conjugate **7a** was confirmed by showing singlet at  $\delta$  1.93 for  $-\text{CH}_3$  group of thymine, formation conjugate **7b** was confirmed by showing doublet at  $\delta$  5.77 for  $-\text{H}$  (proton) at fifth position of uracil and conjugate **7c** was confirmed by showing singlet at  $\delta$  7.55 for  $-\text{H}$  (proton) at sixth position of 5-bromouracil. Formation of conjugates **1a-c** was confirmed by disappearance of benzoyl (aromatic) protons ( $\delta$  7.89-7.45) in  $^1\text{H}$  NMR spectrum. The structures of compound **1a-c** were confirmed by X-ray crystallographic analysis.

Similarly, ferrocene alcohol **11** was obtained from ferrocene. Ferrocene on treatment with one equivalent of succinic anhydride under Friedel-Craft reaction conditions gave ketoacid **8**. This was followed by Zn/Hg reduction of the carbonyl group and esterification of carboxyl group yield ferrocene-ester **10**, which on  $\text{LiAlH}_4$  reduction gave desired alcohol **11**. This was followed by reaction of alcohol **11** with *N*3-protected T/U, under Mitsunobu reaction conditions, yield **12a-b**. **12a** and **12b** on *N*3-debenzoylation using aq.  $\text{K}_2\text{CO}_3$  in methanol-toluene provided **2a** and **2b** respectively (Scheme 2.2).

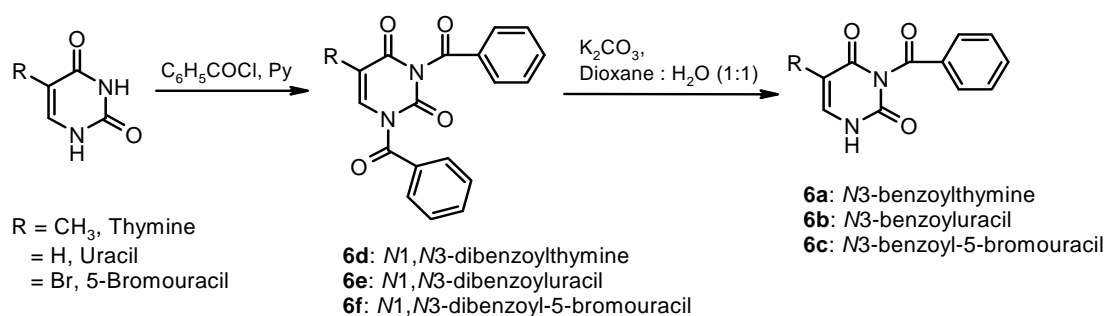
The ketoacid **8** was confirmed by  $^1\text{H}$  NMR spectrum showing two triplets at  $\delta$  3.07 and 2.75 for two  $-\text{CH}_2$  group (adjacent to carbonyl group). Acid **9** was confirmed by disappearance of triplet at  $\delta$  3.07 and showing four protons at  $\delta$  2.39 with one more triplet at  $\delta$  1.88 for two protons of another  $-\text{CH}_2$  group. Formation of ester **10** was confirmed by triplet at  $\delta$  1.27 and quartet at  $\delta$  4.16 for ethyl ester group. Further, the reduction of ester **10** to alcohol **11** was confirmed by disappearance of ethyl ester protons and appearance of two more protons  $\delta$  3.64 for one more  $-\text{CH}_2$  group. Formation of benzoyl protected ferrocene nucleobase conjugates **12a-b** were confirmed by  $^1\text{H}$  NMR spectrum showing aromatic protons of benzoyl group at  $\delta$  7.97-7.48. Further, formation of conjugate **12a** was confirmed by showing singlet at  $\delta$  1.97 for  $-\text{CH}_3$  group of thymine

and formation of conjugate **12b** was confirmed by showing doublet at  $\delta$  5.78 for  $-H$  (proton) at fifth position of uracil. Formation of conjugates **2a-b** were confirmed by disappearance of benzoyl (aromatic) protons ( $\delta$  7.97-7.48) in  $^1H$  NMR spectrum. The structures of compound **2a-b** were confirmed by X-ray crystallographic analysis.



**Scheme 2.2:** Synthesis of ferrocene-linked mono thymine/uracil conjugates with *n*-butyl spacer.

One step conversion of  $-OH$  group in **6** to the corresponding pyrimidinyl conjugates **7a-c** and **11** to the corresponding pyrimidinyl conjugates **12a-b** can be achieved under Mitsunobu conditions. As the reactivities of *N1* and *N3* of thymine are comparable towards alkylation, this reaction may in principle produce both *N1*-alkylated and *N1*, *N3*-dialkylated products. Hence, *N3* of thymine/uracil/5-bromouracil was first protected as benzoyl group, the synthesis of which is shown in Scheme 2.3. *N1,N3*-dibenzoyl derivatives **6d-f** of thymine/uracil/5-bromouracil was prepared following literature procedure<sup>21</sup> by treating thymine/uracil/5-bromouracil with more than 2 equiv. of benzoylchloride in pyridine. The treatment of *N1,N3*-dibenzoyl derivatives **6d-f** with  $K_2CO_3$  (0.25 N) in 1:1 mixture of dioxane:water for 5 h under carefully controlled conditions resulted in selective hydrolysis of *N3*-benzoyl group in **6d-f** to yield the *N1*-benzoyl products **6a-c** (Scheme 2.3)<sup>21</sup>.



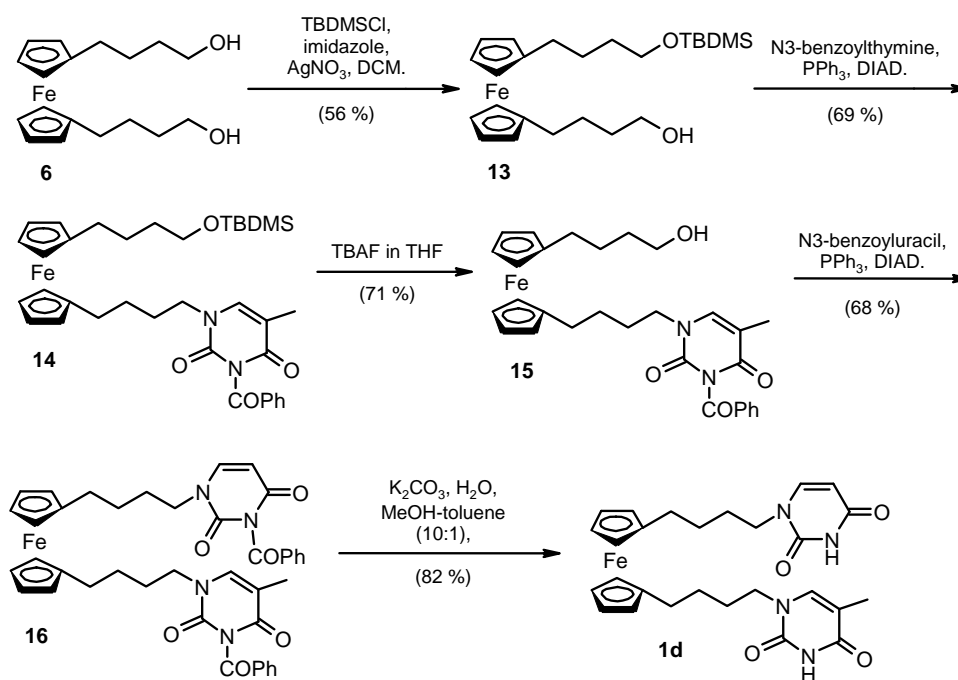
**Scheme 2.3:** Synthesis of N3-benzoyl derivatives of thymine/uracil/5-bromouracil.

### 2.3.2 Synthesis of ferrocene-linked thymine and uracil conjugates at different chain end with *n*-butyl spacer (**1d**)

Chimeric mixed base ferrocene bis conjugate of thymine (T)/uracil (U) **1d** was synthesized according to Scheme 2.4. Compound **1d** was obtained from compound **6** via the benzoyl derivative **16** in four steps. First step involves protection of one of the hydroxyls in bis alcohol **6** with TBDMS group to desymmetrize the molecule, to give compound **13**. The reaction gave some unreacted starting material **6** and the disilyl derivative **13a** which was separated by chromatography. Mitsunobu reaction of the second hydroxyl of **13** with N3-benzoylthymine gave **14**, which upon desilylation with TBAF yielded **15**. The reaction of resulting hydroxyl with N3-benzoyluracil under Mitsunobu conditions provided the mixed base conjugate **16** which was debenzoylated to result in the desired chimeric mixed base ferrocene conjugate **1d** (Scheme 2.4).

Formation of TBDMS protected alcohol **13** was confirmed by <sup>1</sup>H NMR spectrum showing singlet at  $\delta$  0.89 for nine protons of *tert*-butyl group and by mass spectra analysis having mass ( $m/z$ ) at 444.30 [ $M^+$ ]. Formation of Benzoyl protected thyminyll conjugate **14** was confirmed by showing aromatic protons of benzoyl group at  $\delta$  7.92-7.43 and singlet at  $\delta$  1.94 for  $-\text{CH}_3$  group of thymine. Deprotection of TBDMS group and formation of thyminyll alcohol **15** was confirmed by disappearance of singlet at  $\delta$  0.89 for nine protons of *tert*-butyl group. Successful synthesis and formation of benzoyl protected chimeric thymine/uracil conjugate of ferrocene **16** was confirmed by showing singlet at  $\delta$  1.93 for  $-\text{CH}_3$  group of thymine and showing doublet at  $\delta$  5.76 for  $-\text{H}$  (proton) at fifth position of uracil. Formation of desired mixed base conjugate **1d** was

confirmed by disappearance of benzoyl (aromatic) protons ( $\delta$  7.92-7.43) in  $^1\text{H}$  NMR spectrum. Further, the structure of compound **1d** was confirmed by X-ray crystallographic analysis.

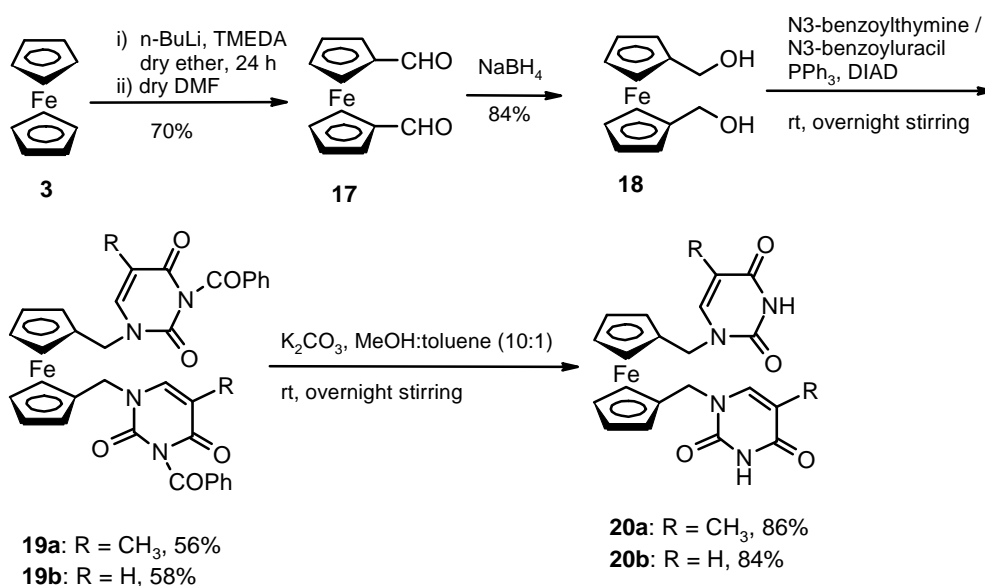


**Scheme 2.4:** Synthesis of chimeric mixed base ferrocene conjugates with *n*-butyl spacer.

### 2.3.3 Synthesis of ferrocene-linked bis thymine/uracil conjugates with methylene spacer (20a-b)

It was decided to synthesize the ferrocene-linked bis thymine/uracil conjugate with one carbon methylene spacer to study the differences in the properties (crystal structures, redox potentials, etc.) as a function of the chain length. The target compounds were 1,1'-bis(thyminylmethyl)ferrocene **20a** and 1,1'-bis(uracilylmethyl)ferrocene **20b**.

1,1'-Ferrocene dicarbaldehyde **17** was synthesized from ferrocene in good yield by treating the dilithioferrocene-TMEDA complex with dimethylformamide (DMF).<sup>22</sup> Compound **17** on reduction with  $\text{NaBH}_4$  gives 1,1'-bishydroxymethylferrocene **18**, which was reacted with *N*3-protected thymine/uracil, under Mitsunobu reaction conditions, to yield the ferrocene conjugates **19a-b**. *N*-Debenzoylation of **19a-b** using aq.  $\text{K}_2\text{CO}_3$  in methanol-toluene yielded the target compound **20a-b** (Scheme 2.5).



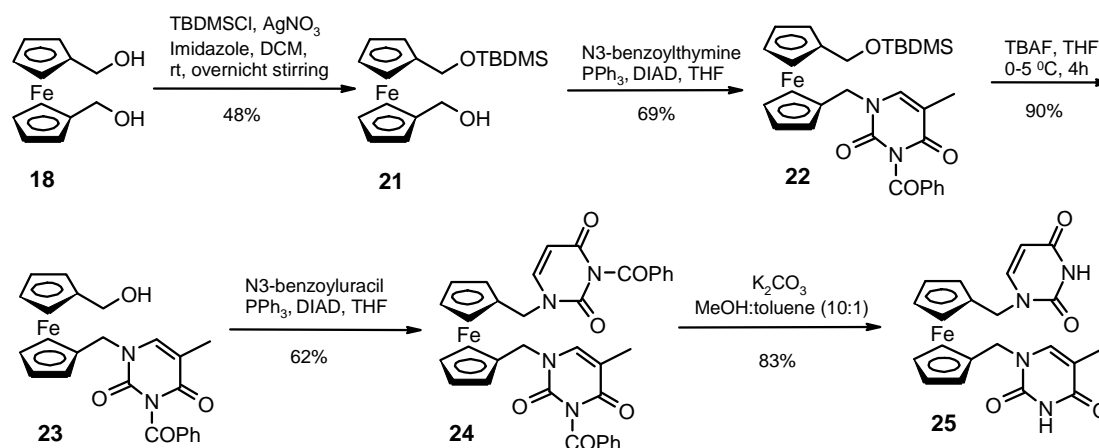
**Scheme 2.5:** Synthesis of ferrocene-linked bis thymine/uracil conjugates with methylene spacer.

Formation of dialdehyde **17** was confirmed by <sup>1</sup>H NMR spectrum showing singlet at  $\delta$  9.95 for two protons of two aldehyde groups. Reduction of dialdehyde and formation of diol **18** was confirmed by disappearance of singlet at  $\delta$  9.95 for two protons of two aldehyde groups and appearance of singlet at  $\delta$  4.40 for two methylene group attached to hydroxyl group. Incorporation of benzoyl protected thymine/uracil and formation of conjugates **19a-b** were confirmed by <sup>1</sup>H NMR spectrum showing aromatic protons of benzoyl group at  $\delta$  7.93-7.45. Further, formation of conjugate **19a** was confirmed by showing singlet at  $\delta$  1.91 for -CH<sub>3</sub> group of thymine, formation conjugate **19b** was confirmed by showing doublet at  $\delta$  5.76 for -H (proton) at fifth position of uracil. Formation of conjugates **20a-b** was confirmed by disappearance of benzoyl (aromatic) protons ( $\delta$  7.93-7.45) in <sup>1</sup>H NMR spectrum. The structures of compound **20a-b** were confirmed by X-ray crystallographic analysis.

### 2.3.4 Synthesis of ferrocene-linked thymine and uracil conjugates at different chain end with methylene spacer (25)

It was planned to synthesize chimeric conjugate **25** in which one of the chains of ferrocene carried a thyminylyl residue and the other bearing a uracil moiety with methylene spacer.

This was synthesized from diol **18** (prepared as in Scheme 2.5) in four steps involving protection of one of the hydroxyls with TBDMS group to desymmetrize the molecule, followed by Mitsunobu reaction of the second hydroxyl with *N*3-benzoylthymine. The *O*-desilylation was done using TBAF to yield the alcohol **23** which was reacted with *N*3-benzoyluracil under Mitsunobu condition, to obtain the mixed base conjugate **24**. The *N*-debenzoylation of **24** with aq.  $K_2CO_3$  in methanol-toluene gave the chimeric mixed base ferrocene conjugate **25** (Scheme 2.6).



**Scheme 2.6:** Synthesis of chimeric mixed base ferrocene derivatives with methylene spacer.

Formation of TBDMS protected alcohol **21** was confirmed by  $^1H$  NMR spectrum showing singlet at  $\delta$  0.95 for nine protons of *tert*-butyl group and by mass spectra analysis having mass ( $m/z$ ) at 360.22 [ $M^+$ ]. Formation of Benzoyl protected thyminylyl conjugate **22** was confirmed by showing aromatic protons of benzoyl group at  $\delta$  7.91-7.43 and singlet at  $\delta$  1.88 for  $-CH_3$  group of thymine. Deprotection of TBDMS group and formation of thyminylyl alcohol **23** was confirmed by disappearance of singlet at  $\delta$  0.95 for nine protons of *tert*-butyl group. Successful synthesis and formation of benzoyl protected chimeric thymine/uracil conjugate of ferrocene **24** was confirmed by showing

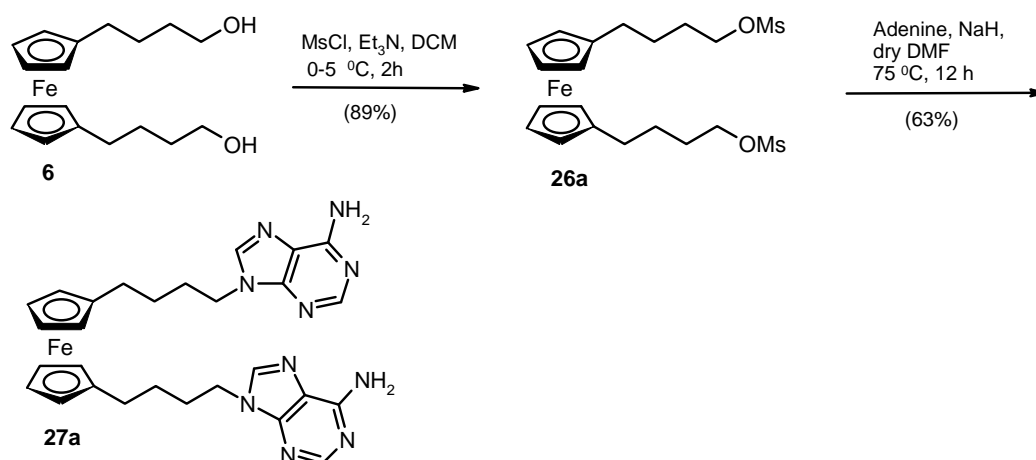


singlet at  $\delta$  1.90 for  $-\text{CH}_3$  group of thymine and showing doublet at  $\delta$  5.76 for  $-\text{H}$  (proton) at fifth position of uracil. Formation of desired mixed base conjugate **25** was confirmed by disappearance of benzoyl (aromatic) protons ( $\delta$  7.91-7.43) in  $^1\text{H}$  NMR spectrum and by mass spectra analysis having mass ( $m/z$ ) at 449.05 [ $\text{M}^+ + 1$ ].

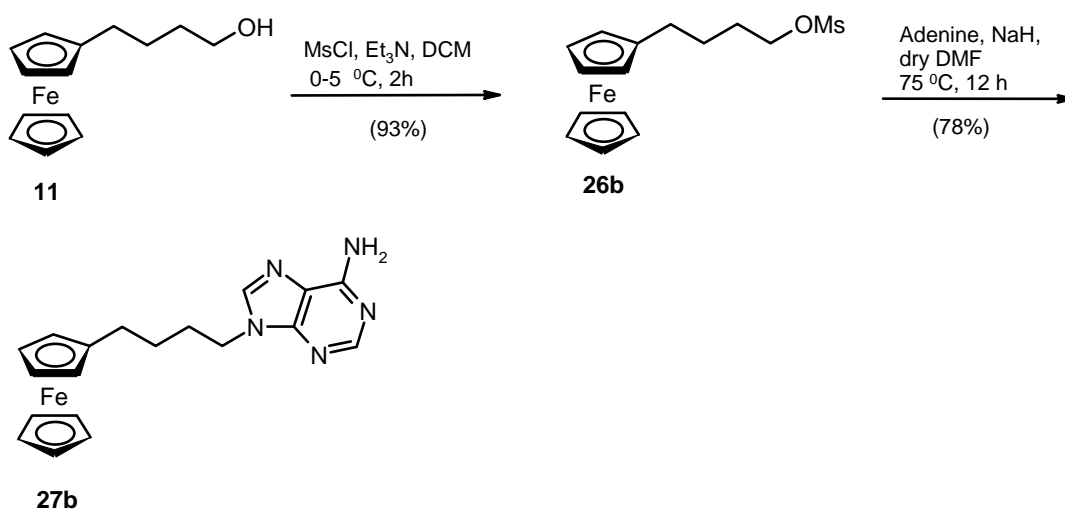
### 2.3.5 Synthesis of ferrocene-linked mono and bis adenine conjugates with *n*-butyl spacer (27a-b)

So far the synthesis of conjugates in which ferrocene is linked to mono and bis pyrimidine bases (thymine/uracil/5-bromouracil) with methylene or butyl spacer chains have been described. Triggered by X-ray crystallographic analyses (section 2.4) which showed interesting self assembling structures it was thus worthwhile to synthesize ferrocene-linked mono and bis purine nucleobase conjugates to study the self association properties as a function of bases.

The target compounds **27a** and **27b** were synthesized from diol **6** and alcohol **11** whose synthesis has already been reported (Scheme 2.1 and Scheme 2.2 respectively). The bis and mono hydroxyl compounds **6** and **11** were converted to corresponding mesyl derivatives 1,1'-bis(4-(methanesulfonyloxy)butyl)ferrocene **26a** and 1-(methanesulfonyloxybutyl)ferrocene **26b** respectively, by treatment with mesylchloride. Adenine was treated with NaH in DMF to give sodium adenylide, which was then reacted with **26a** and **26b** to obtain the desired 1,1'-bis(4-(adeninyl)butyl)ferrocene **27a** and 1-(4-(adeninyl)butyl)ferrocene **27b** (Scheme 2.7 and Scheme 2.8 respectively).



**Scheme 2.7:** Synthesis of ferrocene-linked bis adenine conjugates with *n*-butyl spacer.



**Scheme 2.8:** Synthesis of ferrocene-linked mono adenine conjugates with *n*-butyl spacer.

Both the products **26a** and **26b** were confirmed by  $^1\text{H}$  NMR spectrum showing singlet at  $\delta$  2.99 for  $-\text{CH}_3$  of mesyl group. Desired ferrocene bis and mono adeninyl conjugates **27a** and **27b** were confirmed by  $^1\text{H}$  NMR spectrum showing singlet at  $\delta$  7.64 and  $\delta$  7.78 for proton at eighth position of adenine moiety respectively. The structure of compound **27b** was further confirmed by X-ray crystallographic analysis.

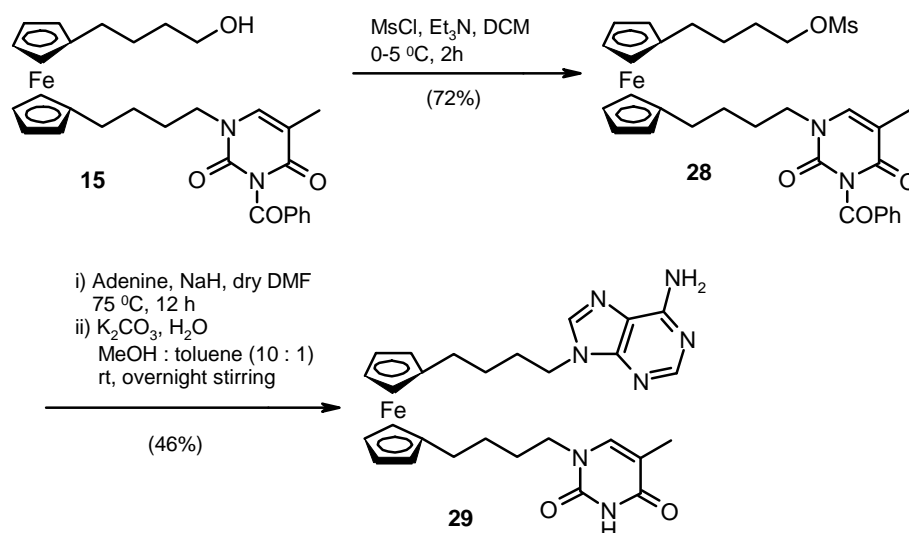
### 2.3.6 Synthesis of ferrocene-linked chimeric thymine/adenine conjugates with *n*-butyl spacer (**29**)

After the successful synthesis of ferrocene-linked mono and bis adenine conjugates it was decided to synthesize chimeric conjugate **29** in which one of the chains of ferrocene carried a thyminyl residue and the other bearing adenine moiety.

The chimeric conjugate **29** was synthesized from mono thymine substituted ferrocene conjugate **15** in two steps (Scheme 2.9). Compound **15** was first reacted with mesyl chloride to yield 1-(4-(*N*3-benzoylthyminyl)butyl)-1'-(4-(methylsulfonyloxy)butyl)ferrocene **28** which on subsequent treatment with sodium adenylide (prepared by treatment of adenine with NaH in DMF) gave the desired 1-(4-(thyminyl)butyl)-1'-(4-(adeninyl)butyl)ferrocene **29**.

Formation of mesyl derivative **28** was confirmed by  $^1\text{H}$  NMR spectrum showing singlet at  $\delta$  2.99 for  $-\text{CH}_3$  of mesyl group. Successful synthesis of target adenine/thymine mixed base conjugate **29** was confirmed by showing singlet at  $\delta$  7.54 for proton at eighth position of adenine moiety and at  $\delta$  1.75 for  $-\text{CH}_3$  group of thymine. Formation of

conjugate **29** was further confirmed by mass spectra analysis having mass ( $m/z$ ) at 555.46 [ $M^+$ ].



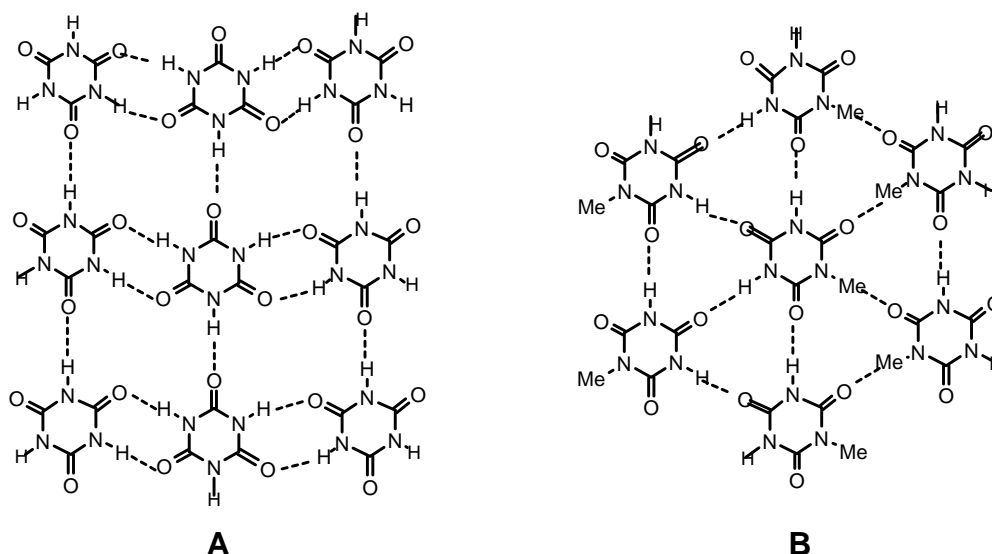
**Scheme 2.9:** Ferrocene linked thymine (T) and adenine (A) conjugate at different chain end with *n*-butyl spacer

### 2.3.7 Attempts towards synthesis of ferrocene linked bis(cyanuric acid (CA)) conjugate with *n*-butyl spacer

X-ray crystal structure studies (described later) of ferrocene-linked mono and bis pyrimidine nucleobase conjugates along with chimeric conjugates (with two different nucleobase at two different chains in same ferrocene unit) showed some unusual self assembling properties and hydrogen bonding pattern between nucleobases. These nucleobases can form hydrogen bonding from only one side. At this point, it was hypothesized that a modified nucleobase with equal propensity for hydrogen bonding from each face would statistically double the probability of efficient hydrogen bonding, leading perhaps to more interesting self assemblies.

Cyanuric acid is a six-membered cyclic imide with alternate arrangement of hydrogen bond donors and acceptors and it is potentially well suited for hydrogen bonding from either side. In its free form, it is known to form a network of well-defined robust hydrogen-bonded system through self assembly leading to a molecular tape.<sup>23,24</sup> Each tape is formed by continuous formation of double hydrogen bonds in one direction, while the tapes are held together in the other direction by single hydrogen bonds (Figure

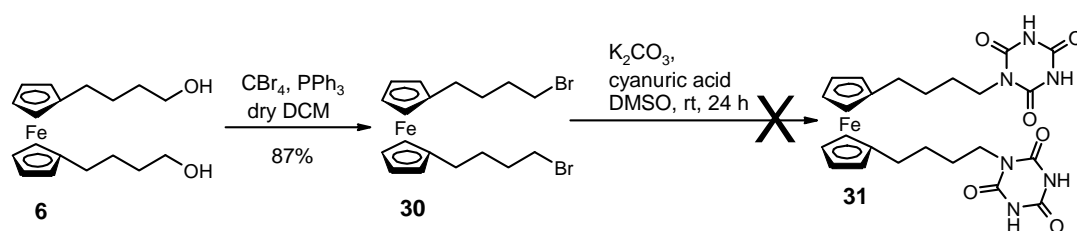
2.2A). Mono *N*-substitution of cyanuric acid perturbs this hydrogen-bonding network, as shown for *N*-methylcyanuric acid, which forms a hexagonal network<sup>25a</sup> (Figure 2.2B), with the interaction of C-H...O bonds. Thus cyanuric acid and *N*-methylcyanuric acid show different supramolecular structures with complete saturation of all H-bonding donor and acceptor sites.



**Figure 2.2:** Hydrogen bond arrangements in (A) cyanuric acid (B) *N*-methyl cyanuric acid

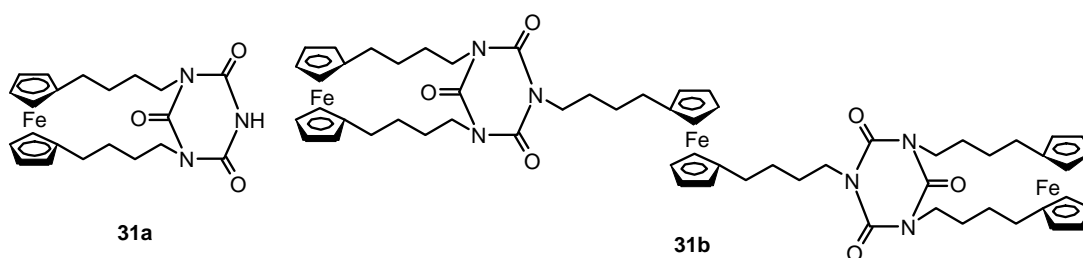
Cyanuric acid (CA) and *N*-methylcyanuric acid (MCA) have close structural resemblance to uracil and form a variety of hydrogen-bonded base pairs.<sup>25b</sup> Adenine, the complementary nucleobase for uracil also can base pair with cyanuric acid.<sup>26a</sup> In view of these facts, synthesis of ferrocene-linked bis(cyanuric acid) conjugates with *n*-butyl spacer would be interesting from formation of novel hydrogen bonding and self association patterns.

1,1'-Bis(4-hydroxybutyl)ferrocene **6** was treated with carbon tetrabromide in the presence of  $\text{PPh}_3$  in  $\text{DCM}$ <sup>26b</sup> to yield dibromo derivative **30**. To obtain the required ferrocene-linked bis(cyanuric acid) conjugate, dibromide **30** was reacted with cyanuric acid in the presence of base  $\text{K}_2\text{CO}_3$  in DMSO. After usual work up of the reaction mixture, the products were purified by column chromatography (Scheme 2.10).



**Scheme 2.10:** Proposed synthesis of ferrocene-linked bis(cyanuric acid (CA)) conjugate with *n*-butyl spacer

Two different products (one was major and the other was minor) were isolated and characterized by  $^1\text{H}$  NMR, mass spectroscopy and the structures were confirmed by X-ray crystallography. Instead of the required bis conjugate product **31**, the minor product was formed to be the compound **31a** have a cyclic structure of ferrocene with cyanuric acid. The major product was characterized as **31b** having two units of **31a** crosslinked to the ferrocene di butyl moiety as a spacer. The formation of these products was reproducible with failure to get any of **31**. The crystal structure of **31a** has described in this chapter, section 2.4.5.



**Figure 2.3:** Structure of **31a** and **31b**.

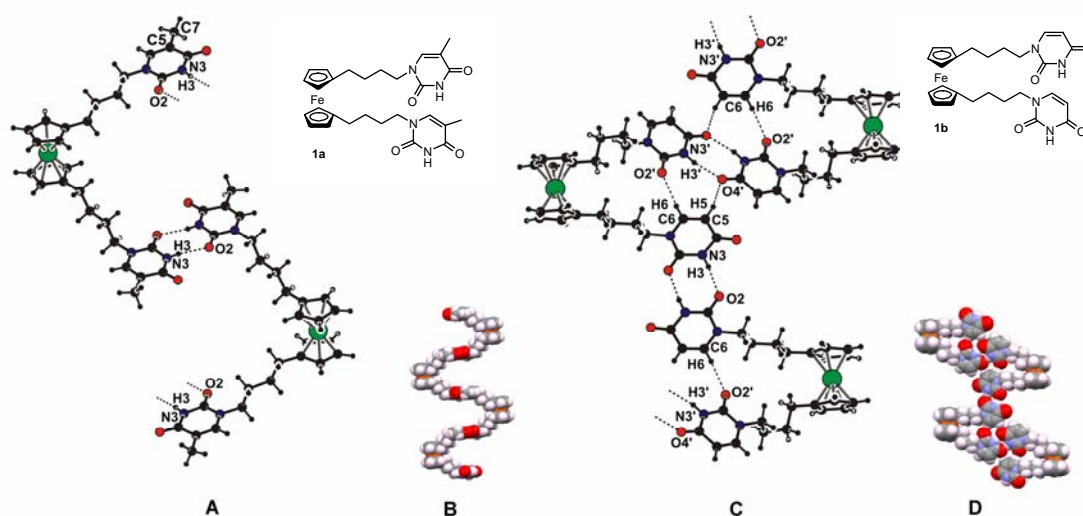
## 2.4 X-ray Crystal Structure Analysis

This section describes the X-ray crystallographic studies of ferrocene-nucleobase conjugates. The crystal structures of all the crystalline molecules were determined by single-crystal X-ray diffraction analysis.

### 2.4.1 X-ray crystal structures and self-assembly in ferrocene bis(nucleobase) conjugates with *n*-butyl spacer 1a-d

The bis(thyminyl) ferrocene conjugate Fc(T:T) **1a** occupies crystallographic two fold symmetry axis passing through the central Fe atom of the ferrocene moiety with the

*n*-butyl chains in the extended conformation. A contiguous centrosymmetric, self base pairing was seen via two N3-H3...O2 hydrogen bonds (H3...O2 = 2.14(3), N3...O2 = 2.913(3) Å and N3-H3...O2 = 169(3)°, constituting ‘reverse Watson-Crick’ (rWC defined as pairing involving O2 of T/U) type pairing (Figure 2.4A).<sup>2,15,17</sup> This self-pairing motif seems to be a dominant synthon in the self-assembly process during crystallization that leads to a regular helical backbone (Figure 2.4B).

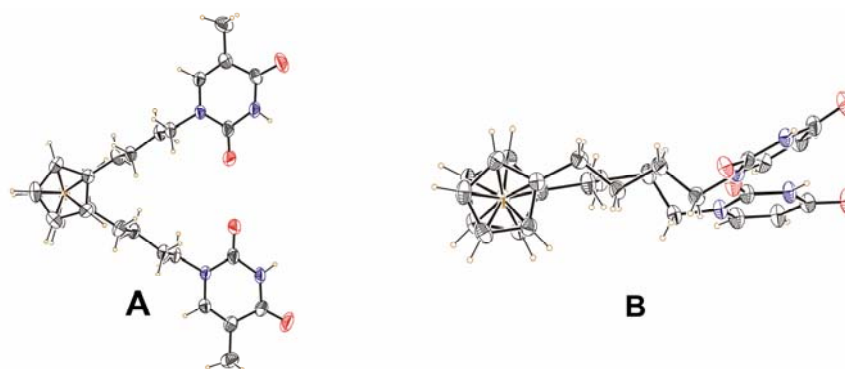


**Figure 2.4:** T:T and U:U self-base pairing in Fc(T:T) **1a** (A) and Fc(U:U) **1b** (C). Molecule Fc(U:U) **1b** makes an intramolecular C6-H6...O2' contact. Inlay shows the CPK model of a single helical strand for Fc(T:T) **1a** (B) and Fc(U:U) **1b** (D).

The bis substituents linked to the Cp rings of ferrocene are staggered by  $\sim 67^\circ$  around the ferrocene ring, with the methyl groups attached to C5 atom of thymine bases pointing away from each other (Figure 2.5A).

The structure of bis(uracil) conjugate Fc(U:U) **1b** (Figure 2.4C) was devoid of two-fold symmetry, with one of the *n*-butyl chains adopting an extended conformation and the other chain in folded state. The U of the folded chain exhibited ‘Watson-Crick’ WC type self-pairing through O4 rather than O2 and making N3'-H3'...O4' interaction with U on the folded chain of the next molecule. Interestingly, the U on the extended chain formed a rWC type pairing with the U of the extended chain of the neighbouring molecule via N3-H3...O2 hydrogen bond, in comparison to the WC type base pairing of U in the folded chains. This contiguous, alternating WC and rWC pairing motif formed the synthon of the bis(uracil) ferrocene helical backbone. The folded spacer chain

conformation leads to additional intramolecular C6-H6...O2' interaction, which is absent in Fc(T:T) **1a** and results in relatively eclipsed orientation (~19 deg.) of the two spacer chains in Fc(U:U) **1b** (Figure 2.5B).

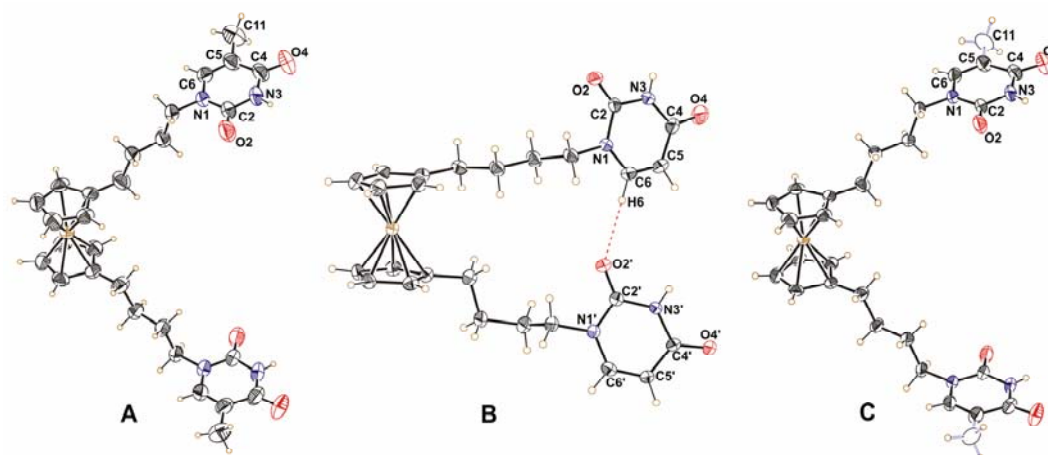


**Figure 2.5:** ORTEP of Fc(T:T) **1a** (A) and Fc(U:U) **1b** (B) viewed perpendicular to Cp rings.

The presence of 5-methyl group in Fc(T:T) **1a**, seems to sterically preclude the intermolecular (C5-H5...O4') and intramolecular (C6-H6...O2') interactions seen in Fc(U:U) **1b**, which perhaps leads to two different base pairings in the helical assembly of Fc(U:U) **1b**. To examine this, the 5-methyl in Fc(T:T) **1a** was replaced by 5-bromo in Fc(Br-U:Br-U) **1c**, whose crystal structure was found to be almost identical to that of Fc(T:T) **1a**, reiterating the steric role of 5-substituent in preventing the additional interactions seen in U:U pairings.

In order to understand the specific differences among the T:T and U:U pairs and how it governs the self assemblies, we examined the crystal structure of the chimeric conjugate Fc(T:U) **1d**, in which one of the chains carried a thymynyl residue and the other bearing a uracil moiety. Remarkably, the structure of Fc(T:U) **1d** was isomorphous to that of Fc(T:T) **1a**. The chimeric Fc(T:U) **1d** which chemically lacks a two-fold symmetry, acquired it in crystal structure by statistically distributing itself over two equally occupied orientations with the methyl group C7 (in Figure 2.6 it is C11) having only half the occupancy. Unlike Fc(U:U) **1b** that had alternate WC and rWC type pairings, compound Fc(T:U) **1d** exhibited only rWC type hydrogen bonding, inspite of having U:U base pairs as in analogous Fc(U:U) **1b**. There can be four possibilities of base pairings in Fc(T:U) **1d** namely T:T, U:U, T:U and U:T, but the observed structure corresponded to an average base pairing of 1/2(T+U)...1/2(T+U). Molecules of Fc(T:T)

**1a (A)** and Fc(T:U) **1d (C)** occupy crystallographic 2-fold axis passing through Fe atom. Molecule of Fc(T:U) **1d** acquires 2-fold symmetry by statistical disorder, methyl C7 (in Figure 2.6 it is C11) shown as open boundary ellipsoid has only half occupancy. Molecule of Fc(U:U) **1b (B)** lacking this 2-fold symmetry adapts a different conformation making an intramolecular C6-H6...O2' contact (Figure 2.6).



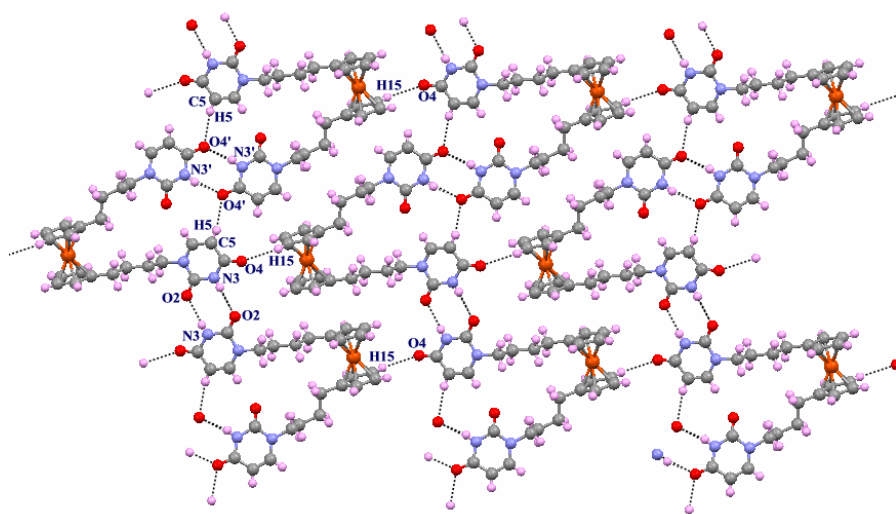
**Figure 2.6:** ORTEP views of Fc(T:T) **1a (A)**, Fc(U:U) **1b (B)** and Fc(T:U) **1d (C)**.

**Refinement of 1d:** Unit cell parameters of Fc(T:U) **1d** were almost identical to that of Fc(T:T) **1a**, suggesting the isostructurality between them; although unit cell volume of Fc(T:U) **1d** was lesser than that of Fc(T:T) **1a** ( $V = 2737.1(17) \text{ \AA}^3$  for Fc(T:T) **1a** and  $2683.6(9) \text{ \AA}^3$  for Fc(T:U) **1d**). Structure refinement carried out with the full occupancy to methyl group carbon C7 (in Figure 2.6 it is C11) atom showed significant increase in the thermal parameters (Uiso 0.18 for full occupancy, which was 0.05 a normally observed value for half occupancy) as well as increase in R-value (R-value 5.27 for full occupancy, which was 4.73 a normally observed value for half occupancy). The chemical analysis also supported the formulation.

The accurate geometries of the T:T, U:U and T:U base pairings are of considerable structural interest because of their presence in nucleic acids.<sup>2,27</sup> Very interestingly, the bisuracil derivative Fc(U:U) **1b** shows two different types of U:U base pairings in the same crystal form: a centrosymmetric rWC type with two N3-H3...O2 intermolecular contacts ( $\text{H3...N2} = 2.13(3)$ ,  $\text{N3...O2} = 2.915(4) \text{ \AA}$  and  $\text{N3-H3...O2} = 176(3)^\circ$  as in Fc(T:T) **1a**/ Fc(Br-U:Br-U) **1c**/ Fc(T:U) **1d** and the other being centrosymmetric WC type pairing through two N3'-H3'...O4' H-bonds ( $\text{H3'...O4'}$



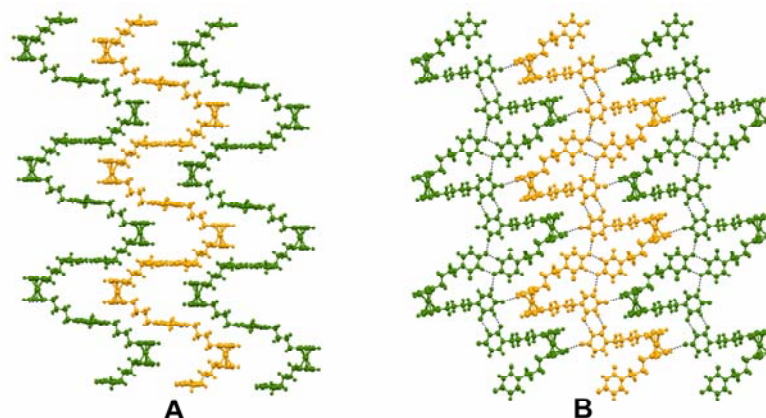
$=2.05(3)$ ,  $N3' \dots O4' = 2.845(4)$  Å and  $N3'-H3' \dots O4' = 169(3)^\circ$  (Figure 2.4C).  $O4'$  participating in WC motif is involved in bifurcated hydrogen bonding *via*  $C5-H5 \dots O4'$  interactions ( $H5 \dots O4' = 2.41$ ,  $C5 \dots O4' = 3.265(4)$  Å and  $C5-H5 \dots O4' = 152^\circ$ ). A weak C-H...O interaction of C5-H5 in uracil, possible due to the absence of the methyl group, seems to cause a bending of one of the side chains in bisuracil Fc(U:U) **1b** causing additional helical twist (Figure 2.7).



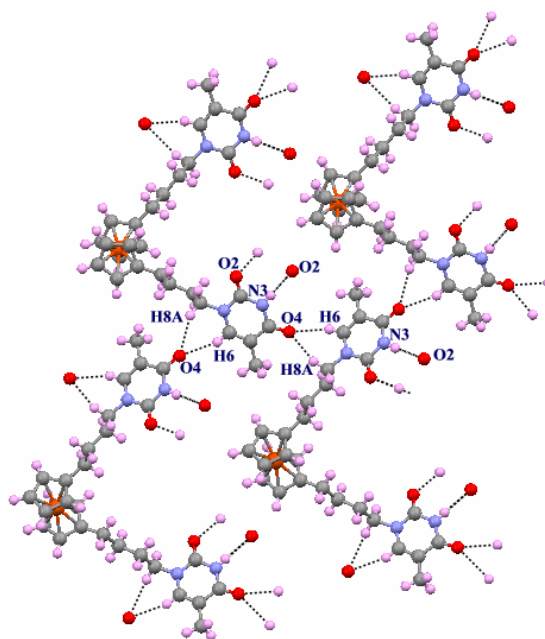
**Figure 2.7:** The various C-H...O interactions in Fc(U:U) **1b**

Sheets of infinite one-dimensional chains, self-assembled *via* base pairings are shown (Figure 2.8). In Fc(T:T) **1a**, a regular helix with a pitch of  $\sim 20.33$  Å has its bases almost perpendicular to the helical axis with no significant inter helical interactions in the sheet (Figure 2.8A). However, there are various C-H...O interactions made by a perpendicular interpenetrated sheet (Figure 2.9). The various C-H...O interactions are also seen in Fc(U:U) **1b** (Figure 2.7). The planar sheet in Fc(U:U) **1b** with each helix having two types of U:U pairings almost in plane of the sheet makes one C15-H15...O4 inter helical adhesion in this planar arrangement (Figure 2.8B) with a lower helical pitch  $\sim 17.9$  Å. Fc(T:T) **1a**/ Fc(Br-U:Br-U) **1c**/ Fc(T:U) **1d** show a single string of a regular helix (Figure 2.4B) while in Fc(U:U) **1b**, the helix is of ‘zig-zag’ type (Figure 2.4D); the absence of C5-methyl in Fc(U:U) **1b** provides possibilities for additional interactions. Although co-ordination induced self-assembly of helical chains are well known, this is a novel example where self base pairing present within the backbone leads to helical assemblies. The slight different geometries of T:T and U:U base pairs lead to variations

in interchain contacts causing different supramolecular structures. Crystal data of **1a**, **1b**, **1c** and **1d** are given in Appendix (Table 1.1, Table 1.2 and Table 1.3)



**Figure 2.8:** A sheet of chain assemblies showing differences in their architecture in Fc(T:T) **1a** (A) and Fc(U:U) **1b** (B).

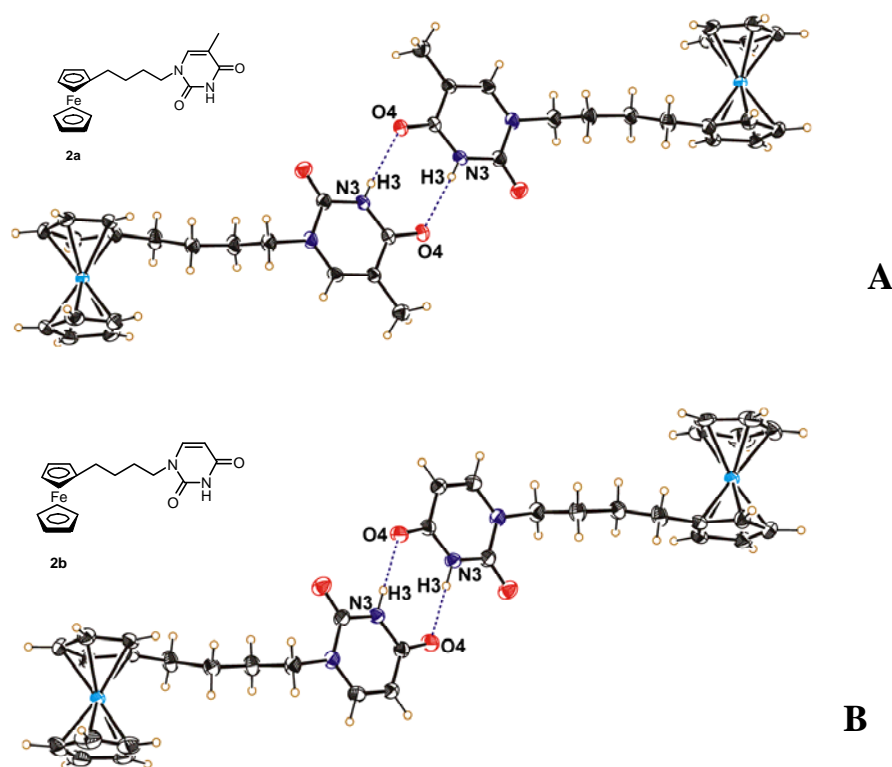


**Figure 2.9:** The various C-H...O interactions in Fc(T:T) **1a**

#### 2.4.2 X-ray crystal structures and self-assembly in ferrocene mono nucleobase conjugates with *n*-butyl spacer **2a-b**

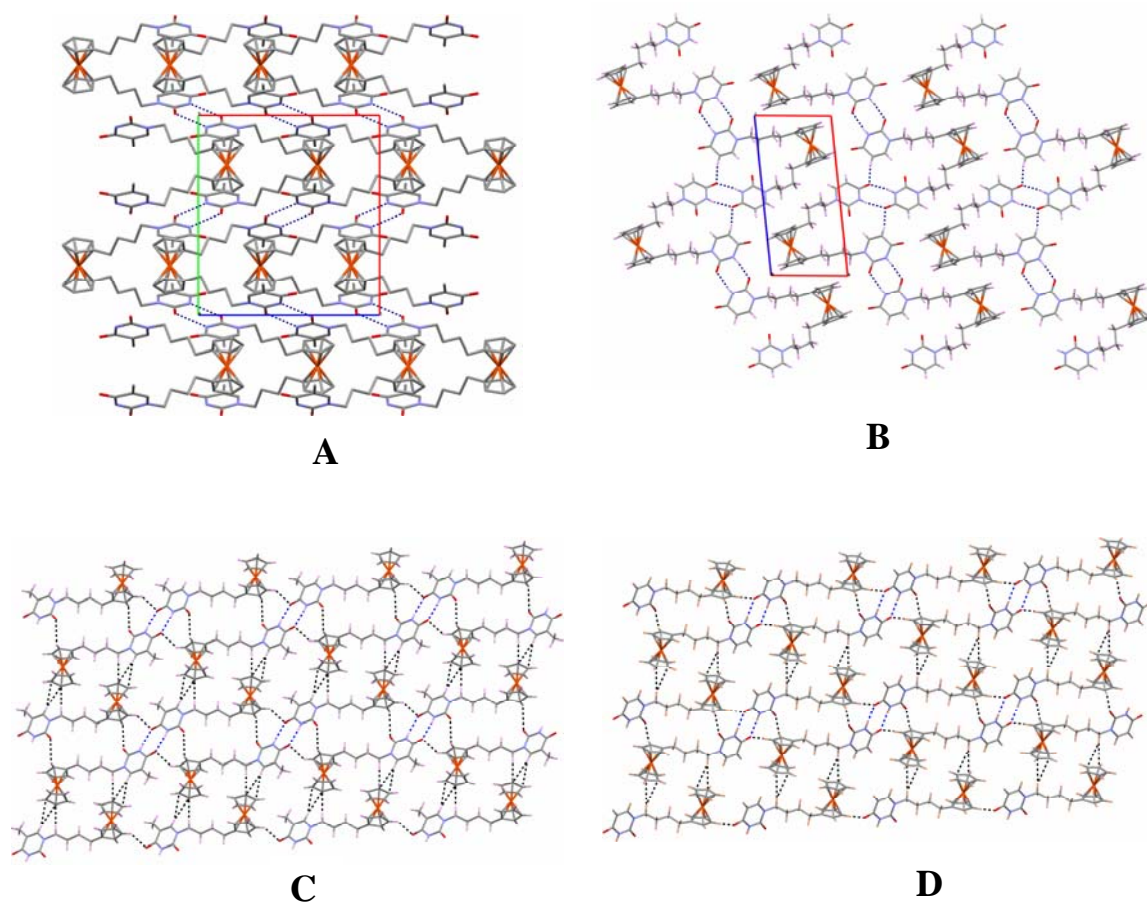
Crystal structures of mono(thyminy) ferrocene Fc(T) **2a** and mono(uracily) ferrocene Fc(U) **2b** were also determined by single crystal X-ray diffraction method. Both the compounds are almost isostructural. Notably, molecules in both Fc(T) **2a** and

Fc(U) **2b** form dimeric centrosymmetric self base pairing of WC type *via* N3-H3...O4 (H3...O4 = 2.14(3), N3...O4 = 2.847(3) Å and N3-H3...O4 = 173(3)°) for Fc(T) **2a** and (H3...O4 = 2.02, N3...O4 = 2.878(4) Å and N3-H3...O4 = 173°) for Fc(U) **2b** hydrogen bond (Figure 2.10).



**Figure 2.10:** Self-base pairing in monosubstituted ferrocene conjugates Fc(T) **2a** (A) and Fc(U) **2b** (B).

These dimeric base pairs in Fc(T) **2a** and Fc(U) **2b** are held together with various C-H...O and C-H... $\pi$  interactions forming planar sheet unlike Fc(T:T) **1a** and Fc(U:U) **1b** where molecules form helical assembly (Figure 2.11). The methyl group at C5 in Fc(T) **2a** did not make much effect in molecular packing. In Fc(U) **2b**, the side chain is in extended form involved in WC type base pairing while in the corresponding bis conjugate Fc(U:U) **1b**, the WC type base pairing is observed with the side chain in folded form. The T:T and U:U base pairing seen in mono substituted *n*-butyl spacer ferrocene conjugates are similar to that seen earlier in the mono(cytosinyl) ferrocene conjugates with methylene spacer chain.



**Figure 2.11:** Molecular packing diagram of (A) Fc(T:T) **1a**, (B) Fc(U:U) **1b**, (C) Fc(T) **2a** and (D) Fc(U) **2b**.

Thus, the newly designed ferrocene linked mono and bis(nucleobase) conjugates show different supramolecular assemblies mediated via centrosymmetric base pairings [T:T, (Br-U):(Br-U), T:U] of rWC type and U:U pairings of both WC and rWC types. The structure of ferrocene-bis(uracil) Fc(U:U) **1b** is perhaps the first example of WC and rWC like pairings being simultaneously present within the same crystal lattice. The comparison of structures clearly delineate the steric role of 5-substituent in influencing the supramolecular packing by inhibiting specific inter and intramolecular C-H...O contacts. The base pairing directed self assemblies are seen only in bis substituted ferrocene conjugates and this topology is influenced by the C5 substituents. The self assembly occurs through the use of all available hydrogen-bonding donors in the solid state. Such self-assembling organometallic units have utility in inducing chain reversal<sup>28</sup>

and build supramolecular scaffolds. Crystal data of **2a** and **2b** are given in Appendix (Table 1.2 and Table 1.4).

### 2.4.3 X-ray crystal structures and self-assembly in ferrocene bis(nucleobase) conjugates with methylene spacer **20a-b**

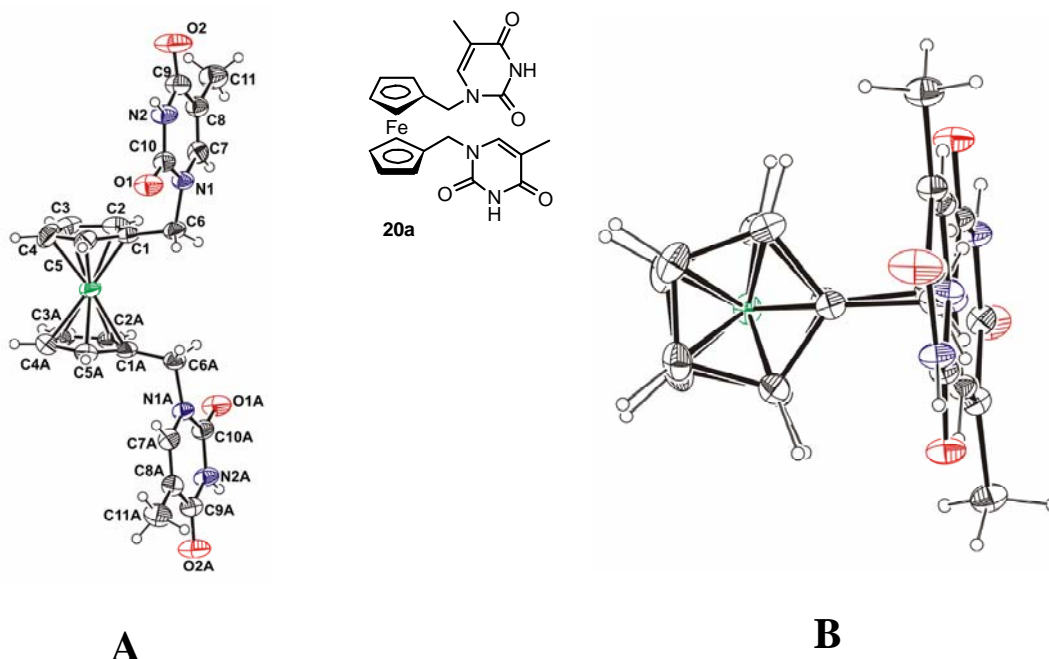
In order to examine the role of spacer chain in self assembly induced supramolecular structure and effect on base pairing, Fc(T:T) and Fc(U:U) were synthesized with a single methylene spacer, [Fc(T:T)<sub>methylene</sub>] **20a** and ) [Fc(U:U)<sub>methylene</sub>] **20b**, instead of butyl spacer (Figure 2.12).



**Figure 2.12:** Structures of A) ferrocene bis(thymine) [Fc(T:T)<sub>methylene</sub>] **20a** (B) ferrocene bis(uracil) [Fc(U:U)<sub>methylene</sub>] **20b** conjugates with single methylene spacer.

#### Crystal Structure of Fc(T:T)<sub>methylene</sub> **20a**

Slow evaporation of Fc(T:T)<sub>methylene</sub> **20a** in dichloromethane-methanol solution produced yellow colored good quality single crystals. The crystal structure of Fc(T:T)<sub>methylene</sub> **20a** was determined by single crystal X-ray diffraction, which revealed that the crystals belong to the monoclinic unit cell in the  $P2_1/c$  space group containing one molecule in the asymmetric unit along with two molecules of water, each disordered over four positions. The two-cyclopentadienyl (Cp) rings of the ferrocene moiety are almost eclipsed (staggered only by  $\sim 4^\circ$ ) and both the thymine group with methylene spacer are in extended conformation but are on the same side (Figure 2.13). The thymine base makes almost perpendicular orientation with the torsion twist of  $\sim 108^\circ$  about methylene carbon C6 and the methyl group attached to C8 atom of the thymine base pointing away from each other. The centroid-centroid separation of the Cp rings is 3.298(2) Å with the dihedral angle  $5.43^\circ$  and the Cp-Fe-Cp angle is  $174.89(7)^\circ$ .



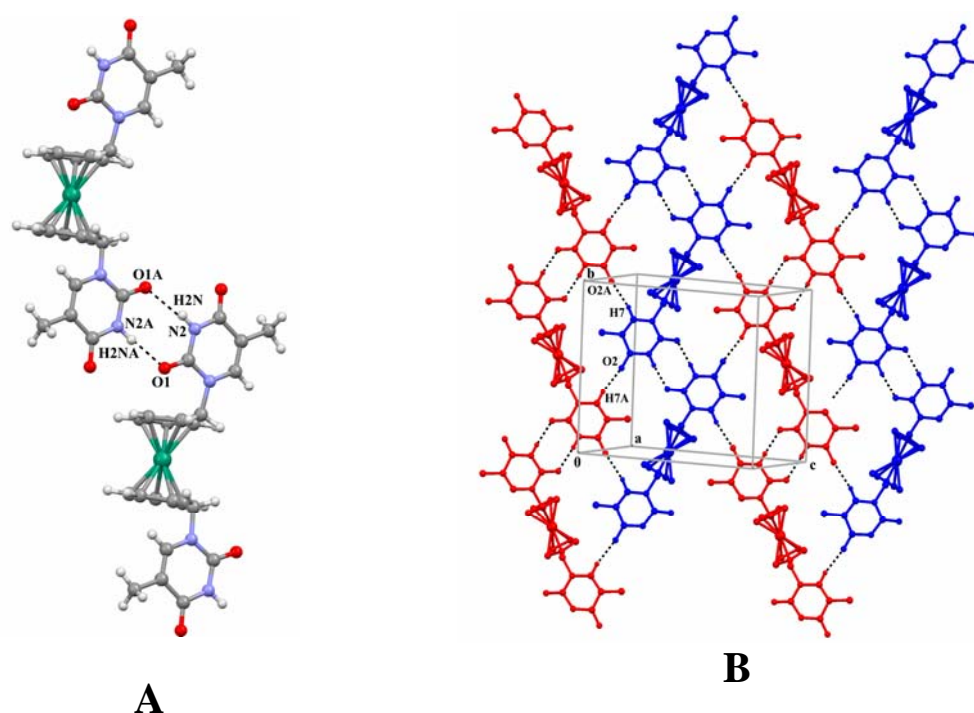
**Figure 2.13:** (A) ORTEP of  $\text{Fc}(\text{T:T})_{\text{methylene}}$  **20a** and (B) viewed perpendicular to Cp rings of  $\text{Fc}(\text{T:T})_{\text{methylene}}$  **20a**.

The neighboring molecules exhibit self-base pairing and are linked *via* two conventional  $\text{N2A-H2NA}\dots\text{O1}$  and  $\text{N2-H2N}\dots\text{O1A}$  hydrogen bonds comprising ‘reverse Watson-Crick’ (rWC) type pairing (Figure 2.14A). The thymine at C1 of Cp is engaged in hydrogen bond formation with the other thymine substituted at C1A of Cp of unit-translated molecule along 010 axis creating pseudo-centrosymmetric dimers. The geometry of the former hydrogen bond ( $\text{H2NA}\dots\text{O1} = 1.99 \text{ \AA}$ ,  $\text{N2A}\dots\text{O1} = 2.847(3) \text{ \AA}$  and  $\angle\text{N2A-H2NA}\dots\text{O1} = 174.9^\circ$ ) is slightly better compared to the later ( $\text{H2N}\dots\text{O1A} = 2.03 \text{ \AA}$ ,  $\text{N2}\dots\text{O1A} = 2.869(3) \text{ \AA}$  and  $\angle\text{N2-H2N}\dots\text{O1A} = 164.9^\circ$ ).

The self-pairing motif seems to be a dominant synthon in the self-assembly process during crystallization that leads to a regular ribbon formation (Figure 2.14B). These neighboring ribbons are related by *n*-glide symmetry and are stitched together *via* strong C-H...O hydrogen bond. The C7-H7 of thymine at C1 of Cp form almost linear C-H...O hydrogen bond with the carbonyl oxygen O2A of thymine at C1A of Cp ( $\text{H7}\dots\text{O2A} = 2.20 \text{ \AA}$ ,  $\text{C7}\dots\text{O2A} = 3.115(3) \text{ \AA}$ ,  $\angle\text{C7-H7}\dots\text{O2A} = 167^\circ$ ). In turn C7A-H7A of thymine at C1A forms short and linear hydrogen bond with the carbonyl oxygen O2 of thymine at C1 ( $\text{H7A}\dots\text{O2} = 2.18 \text{ \AA}$ ,  $\text{C7A}\dots\text{O2} = 3.089(3) \text{ \AA}$ ,  $\angle\text{C7A-H7A}\dots\text{O2} = 165^\circ$ ), thus forming two-dimensional sheet that extend within 101 plane while all the

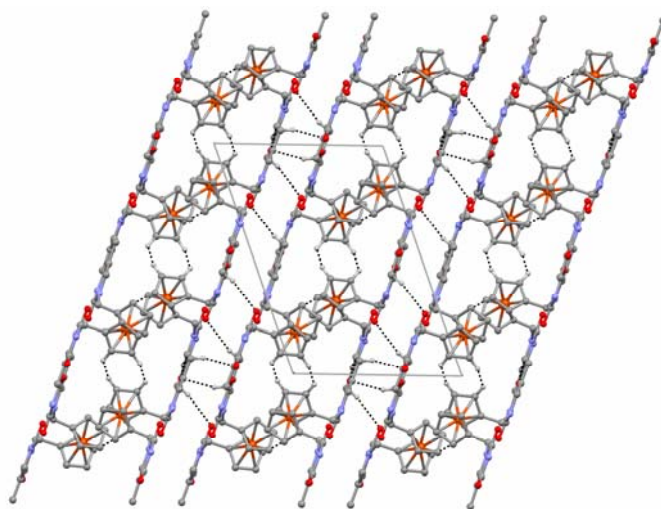
ferrocene moieties remain at one side of the sheet (Figure 2.14B). These sheets are further linked centrosymmetrically to another parallel sheet with the help of two weak C-H...O hydrogen bonds engaging carbonyl oxygens (O1 and O2) and both methyl groups (C11 and C11A) of thymine (C11-H11B...O2 and C11A-H11E...O1).

Although the H...O and C...O distances are long the angle of approach is close to linearity for both the C-H...O bonds (H11B...O2 = 2.65 Å, C11...O2 = 3.577(4) Å,  $\angle$  C11-H11B...O2 = 164°; H11E...O1 = 2.68 Å, C11A...O2 = 3.600(3) Å,  $\angle$  C11A-H11E...O2 = 160°). Thus carbonyl oxygens O1 and O2 are involved in bifurcated H-bond formation; O1 in self base pairing (N2A-H2NA...O1) and linking of parallel sheets (C11A-H11E...O1) while O2 in linking of base pairs (C7A-H7A...O2) and bridging of parallel sheets (C11-H11B...O2). Crystal data of **20a** are given in Appendix (Table 1.5 and Table 1.6).



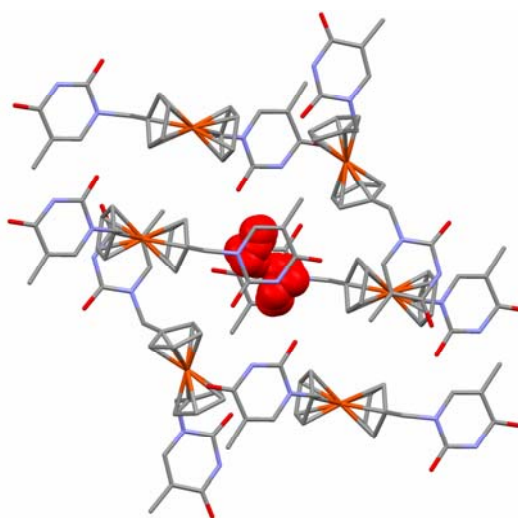
**Figure 2.14:** (A) N-H...O linked molecules formed ribbon through reverse ‘Watson-Crick’ type base pairing in Fc(T:T)<sub>methylene</sub> **20a** and (B) association of the ribbons via C-H...O contacts forming sheet in 2D in Fc(T:T)<sub>methylene</sub> **20a**

Each sheet exhibits interactions with another sheet running parallel to it on one side, these sheets create a channel embedding ferrocene moieties in close proximity *via* weak van der Waal’s interactions whereas in the other side these parallel sheets directly connected to each other *via* weak C-H...O interactions (Figure 2.15).



**Figure 2.15:** Molecular packing diagram of Fc(T:T)<sub>methylene</sub> **20a** viewed down *b*-axis.

The disordered water molecules are included in the cage formed by the thymine base and the ferrocene moiety with no significant interactions between the host and the guest molecules (Figure 2.16).



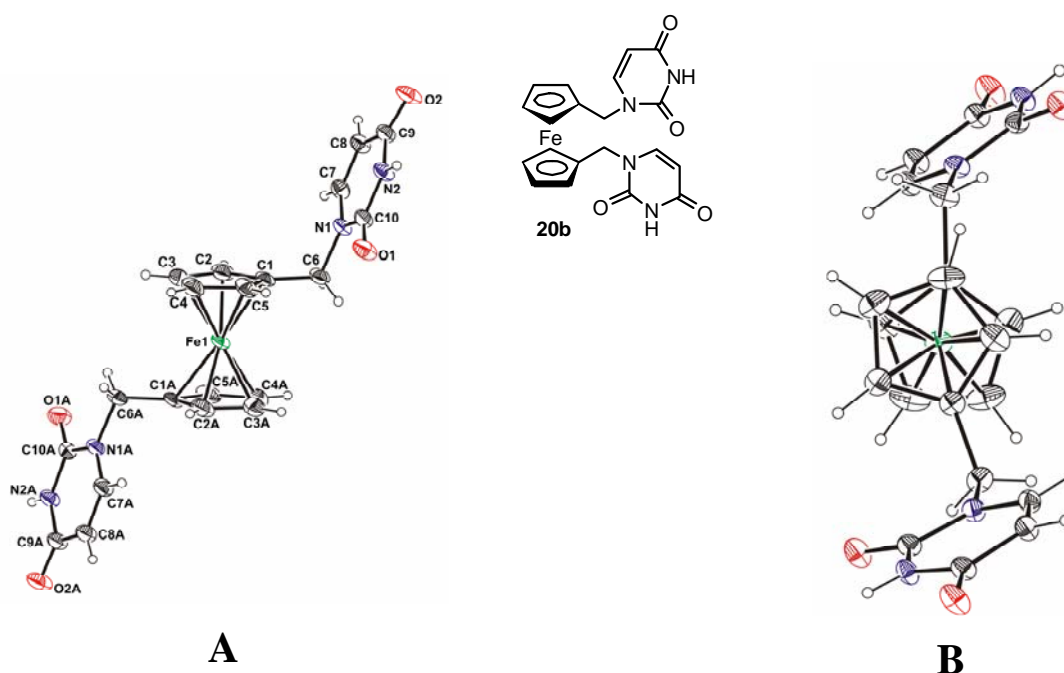
**Figure 2.16:** View of molecular packing showing water molecules (red) occupying the cage formed by the host molecules Fc(T:T)<sub>methylene</sub> **20a**.

### Crystal Structure of Fc(U:U)<sub>methylene</sub> 20b

The crystals of Fc(U:U)<sub>methylene</sub> **20b** when crystallized from DCM methanol mixture, revealed monoclinic unit cell in the  $P2_1/c$  space group containing one molecule in the asymmetric but without inclusion of water molecules. The two-cyclopentadienyl (Cp) rings of the ferrocene moiety are staggered by  $\sim 19^\circ$  and both the uracil groups with



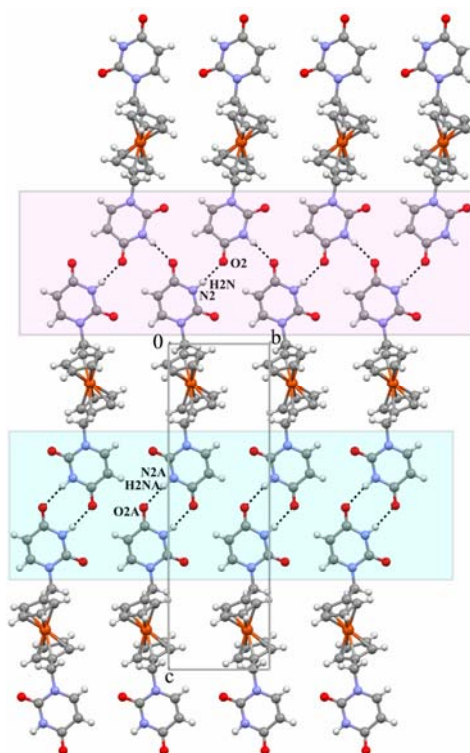
methylene spacer adopting extended conformation but are trans to each other (Figure 2.17) unlike  $\text{Fc}(\text{T}:\text{T})_{\text{methylene}}$  **20a**. Similar to TT, the both the uracils take a torsion twist of  $\sim 112^\circ$  about methylene carbon C6. The centroid–centroid separation of the Cp rings is 3.294(3) Å with the dihedral angle  $1.35^\circ$  and the Cp–Fe–Cp angle is  $178.96(11)^\circ$ .



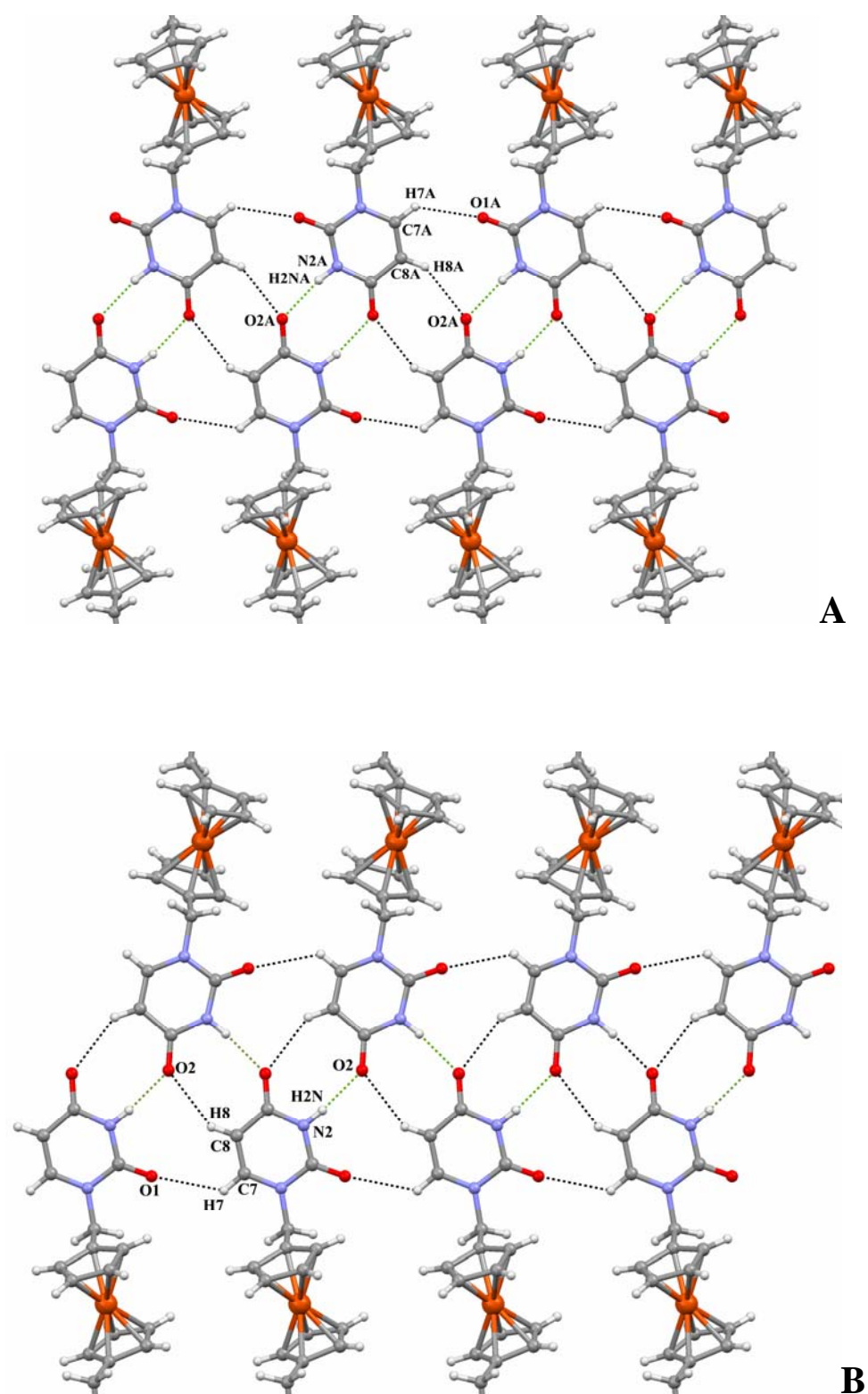
**Figure 2.17:** A) ORTEP of  $\text{Fc}(\text{U}:\text{U})_{\text{methylene}}$  **20b** and (B) viewed perpendicular to Cp rings of  $\text{Fc}(\text{U}:\text{U})_{\text{methylene}}$  **20b**.

The accurate geometries of the T.T and U.U base pairings are of considerable structural interest because of their presence in nucleic acids. Interestingly in the bis-uracil derivative  $\text{Fc}(\text{U}:\text{U})_{\text{methylene}}$  **20b**, only one U chain (labeled with trailer A) engaged in self-base pairing of ‘Watson-Crick’ (WC) motif *via* conventional centrosymmetric  $\text{N2A}\cdots\text{H2NA}\cdots\text{O2A}$  hydrogen bonds ( $\text{H2NA}\cdots\text{O2A} = 2.01$ ,  $\text{N2A}\cdots\text{O2A} = 2.853(4)$  Å and  $\text{N2A}\cdots\text{H2NA}\cdots\text{O2A} = 165^\circ$ ) while the other U chain was not involved in base pairing. Instead, the other U chain links the adjacent centrosymmetric base pairs *via*  $\text{N}\cdots\text{H}\cdots\text{O}$  hydrogen bond ( $\text{H2N}\cdots\text{O2} = 1.96$ ,  $\text{N2}\cdots\text{O2} = 2.807(4)$  Å and  $\text{N2}\cdots\text{H2N}\cdots\text{O2} = 170^\circ$ ) along the *b*-axis. The carbonyl oxygen O2A participating in WC motif is further involved in centrosymmetric hydrogen bonding *via*  $\text{C8A}\cdots\text{H8A}\cdots\text{O2A}$  interactions ( $\text{H8A}\cdots\text{O2A} = 2.57$ ,  $\text{C8A}\cdots\text{O2A} = 3.347(4)$  Å and  $\text{C8A}\cdots\text{H8A}\cdots\text{O2A} = 141^\circ$ ), thus O2A is simultaneously bonded to  $\text{N2A}\cdots\text{H2NA}$  and  $\text{C8A}\cdots\text{H8A}$ . The carbonyl oxygen O1A of

uracil is also centrosymmetrically bonded *via* C-H...O interactions to C7A-H7A ( $H7A...O1A = 2.55$ ,  $C7A...O1A = 3.247(5)$  Å and  $C7A-H7A...O1A = 132^\circ$ ). These two C-H...O interactions connect the two WC type base pairs revealing formation of tetrad with the help of N2A-H, C8A-H and C7A-H sites as hydrogen bond donors, while O2A and O1A acting as hydrogen bond acceptors. Similarly at other uracil chain, the carbonyl oxygen O2 is further bonded to C8-H8 to form centrosymmetric C8-H8...O2 hydrogen bond ( $H8...O2 = 2.53$ ,  $C8...O2 = 3.321(4)$  Å and  $C8-H8...O2 = 143^\circ$ ), thus involved in bifurcated hydrogen-bonding interaction. The other carbonyl oxygen O1 accepts the H-atom from C7 to form C7-H7...O1 hydrogen bond ( $H7...O1 = 2.62$ ,  $C7...O1 = 3.260(5)$  Å and  $C7-H7...O1 = 127^\circ$ ). Thus, four uracil moieties connected to each other forming a quartet structure *via* centrosymmetric N-H...O and C-H...O interactions. Linking of these uracil moieties at both sides of the ferrocene generate a continuous sheet formation in two-dimensional space (Figure 2.18). Crystal data of **20b** are given in Appendix (Table 1.5 and Table 1.6).

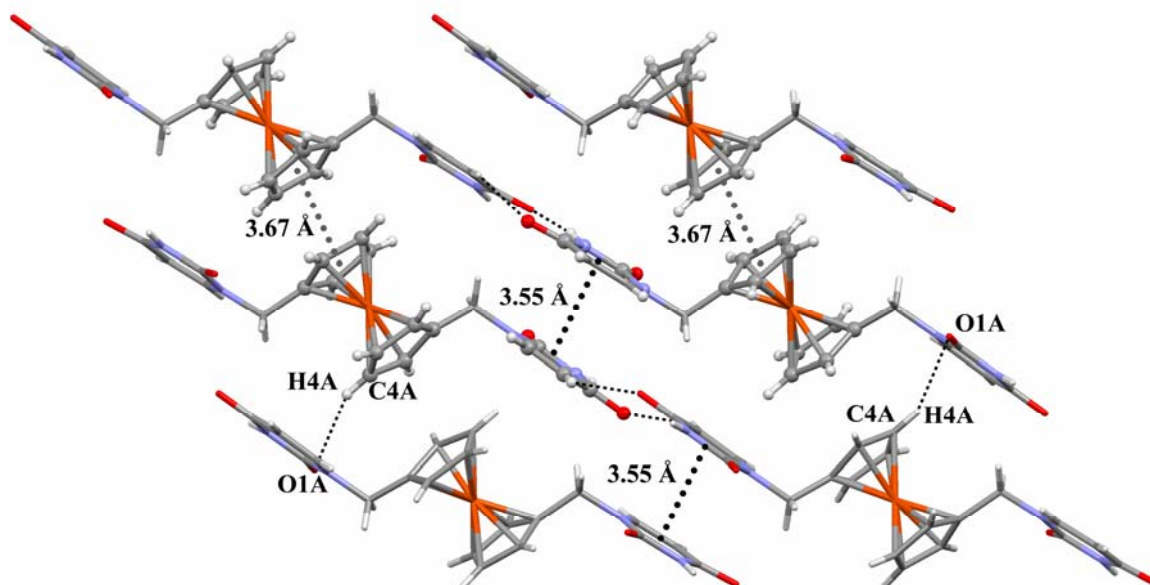


**Figure 2.18:** ‘Watson-Crick’ type self-base pairs associated *via* centrosymmetric N-H...O hydrogen bonds (highlighted with cyan) are connected through catemeric N-H...O hydrogen bond (shaded with pink) in  $Fc(U:U)_{\text{methylene}}$  **20b** forming 2D sheet pattern.



**Figure 2.19:** Zoom in view of (A) the base pair and (B) linking of base pair in Fc(U:U)<sub>methylene</sub> **20b**.

The adjacent sheets along the *b*-axis are linked *via*  $\pi\cdots\pi$  stacking interaction between the substituted Cp rings of ferrocene as well as between the uracil moiety as shown in Figure 2.20. In addition, one more weak C-H...O interaction C4A-H4A...O1A binds the neighboring sheets (Figure 2.20).

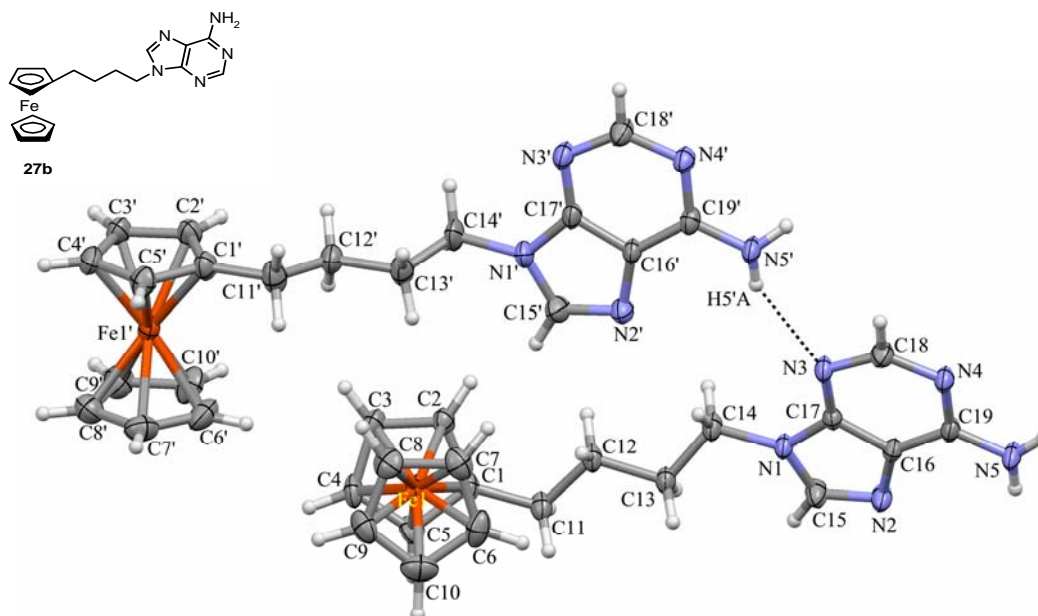


**Figure 2.20:** Perpendicular view of the sheet in  $\text{Fc}(\text{U}:\text{U})_{\text{methylene}}$  **20b** viewed down *b*-axis revealing association of the adjacent sheets *via*  $\pi\cdots\pi$  and C-H...O interactions.

#### 2.4.4 X-ray crystal structures and self-assembly in ferrocene mono adenine conjugate with *n*-butyl spacer **27b**

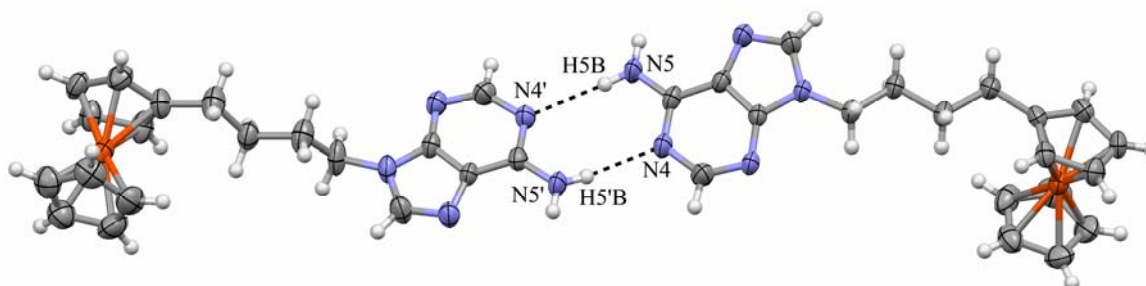
The crystal structure of the ferrocene linked mono(adenine) conjugate [ $\text{Fc}(\text{A})$ ] **27b** with *n*-butyl spacer chain was determined. The crystal belongs to triclinic unit cell in the *P*-1 space group containing two independent molecules in the asymmetric unit (Figure 2.21) which are interacting *via* N5'-H5'A...N3 hydrogen bond. The two-cyclopentadienyl rings (Cp) of the ferrocene moiety in both the molecules are almost eclipsed and the adenine group with *n*-butyl chain spacer adopting folded conformation in both the molecules. The centroid-centroid separation of the Cp rings is 3.295(4) Å with the dihedral angle 2.54° and the Cp-Fe-Cp angle is 177.89(12)° for the unprime

molecule and is 3.315(4) Å with the dihedral angle 5.18° and the Cp–Fe–Cp angle is 176.61(11)° for the prime molecule.



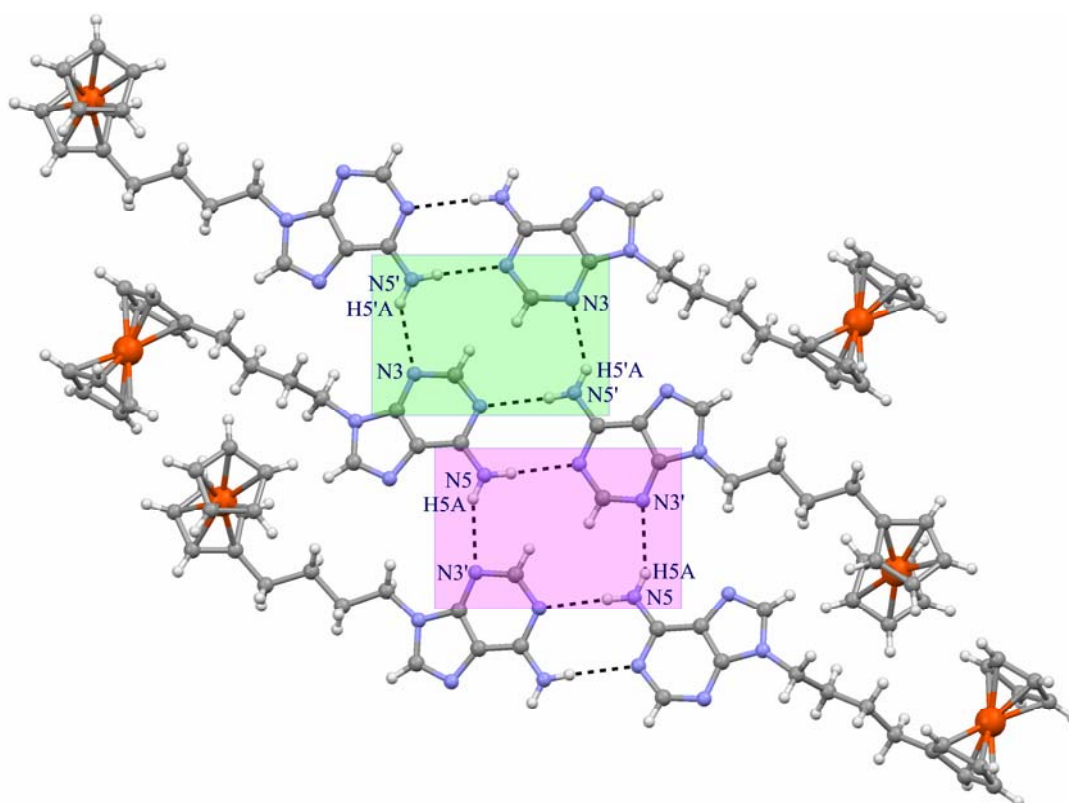
**Figure 2.21:** ORTEP of two symmetry independent molecules of Fc(A) **27b** showing intermolecular hydrogen bond.

Interestingly in the mono adenine derivative, both the symmetry independent molecules (prime and unprime) are engaged in self-base pairing of ‘Watson-Crick’ (WC) motif with each other *via* conventional N5'-H5'B...N4 and N5-H5B...N4' hydrogen bonds (N5'-H5'B...N4, N5'-H5'B = 0.850(18) Å, H5'B...N4 = 2.23(2) Å, N5'...N4 = 3.061(5) Å,  $\angle$ N5'-H5'B...N4 = 166(4)° and N5-H5B...N4', N5-H5B = 0.837(19) Å, H5B...N4' = 2.31(2) Å, N5...N4' = 3.142(5) Å,  $\angle$ N5-H5B...N4' = 175(4)°) forming the dimeric assembly across the pseudo inversion center (Figure 2.22).



**Figure 2.22:** ORTEP showing base pairing in Fc(A) **27b**

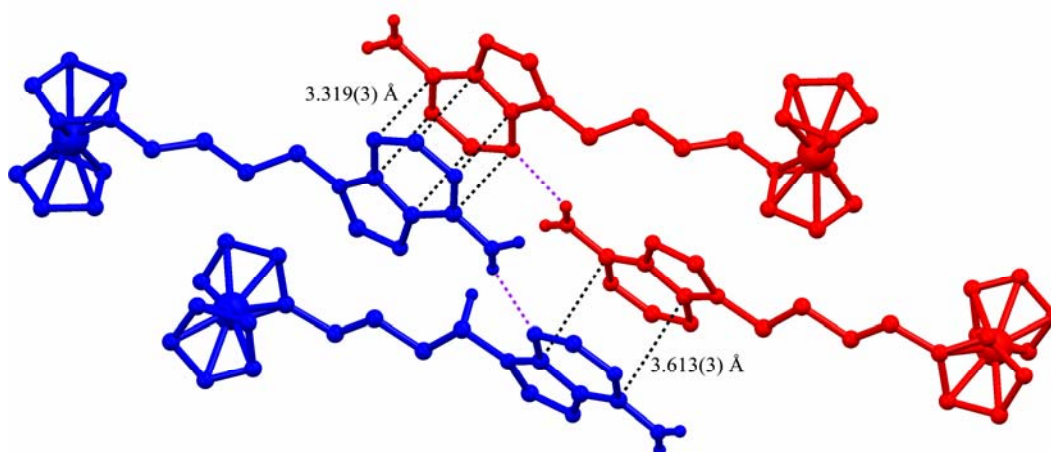
These self-base pairing dimers are bridged alternately *via* two different long and not so linear centrosymmetric N-H...N hydrogen bonds creating two different tetrads. One involving self-base pairing dimers associated *via* N5'-H5'A...N3 (N5'-H5'A = 0.836(18) Å, H5'A...N3 = 2.41(2) Å, N5'...N3 = 3.174(5) Å,  $\angle$ N5'-H5'A...N3 = 153(3)°) hydrogen bond and the other containing self-base pairs linked *via* N5-H5A...N3' N5-H5A...N3' (N5-H5A = 0.837(18) Å, H5A...N3' = 2.34(3) Å, N5...N3' = 3.041(5) Å,  $\angle$ N5-H5A...N3' = 142(3)°) hydrogen bond (Figure 2.23).



**Figure 2.23:** Bridging of the base pairs *via* two different N-H...N bonds forming 2D sheet pattern in Fc(A) **27b**. Shaded boxes (green and magenta) show two different tetrad formation within the sheet.

The adjoining sheets are centrosymmetrically stitched *via* short  $\pi$ ... $\pi$  stacking interaction between the six-member nucleobase of the adenine moiety as shown in Figure 2.24. Both the molecules form short  $\pi$ ... $\pi$  stacking interaction with their respective centrosymmetric partner thereby binding the sheets together. The geometry of the  $\pi$ ... $\pi$  interaction is better in prime molecules (Cg...Cg = 3.313(3) Å) compared to the unprimed molecules (3.613(3) Å) where Cg...Cg is the distance between ring

centroids. In addition, two more weak C-H...N interactions C14-H14A...N4' and C2'-H2'...N3 binds the neighboring sheets.

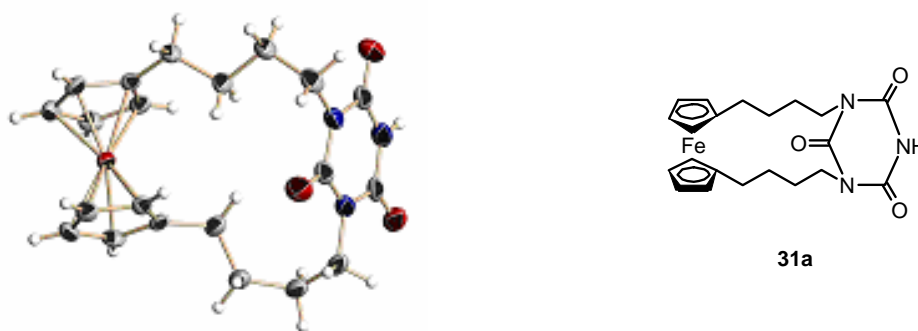


**Figure 2.24.** View of the neighboring sheets in Fc(A) **27b** revealing close association via  $\pi \dots \pi$  interactions.

#### 2.4.5 X-ray crystal structures and self-association properties in ferrocene-cyanuric acid conjugates with *n*-butyl spacer **31a**

X-ray crystal structure studies of ferrocene-linked mono and bis pyrimidine nucleobase conjugates along with chimeric conjugates (with two different nucleobase at two different chains in same ferrocene unit) showed some unusual self assembling properties and hydrogen bonding pattern between nucleobases. These nucleobases can form hydrogen bonding from only one side. At this point, it was hypothesized that a modified nucleobase with equal propensity for hydrogen bonding from each face would statistically double the probability of efficient hydrogen bonding, leading perhaps to more interesting self assemblies.

The crystal structure of the ferrocene linked cyanuric acid conjugate [Fc(CA)] **31a** with *n*-butyl spacer chain was determined. Fc(CA) **31a** have a cyclic structure of ferrocene with cyanuric acid (CA) bridged between the two *n*-butyl chain of the dibutyl ferrocene unit to form the complex illustrated in Figure 2.25.



**Figure 2.25:** ORTEP view of **31a**.

Slow evaporation of Fc(CA) in dichloromethane-methanol solution produced two concomitant polymorphs, blocks (**Form I**) and needle type crystals (**Form II**) at room temperature (Figure 2.26).



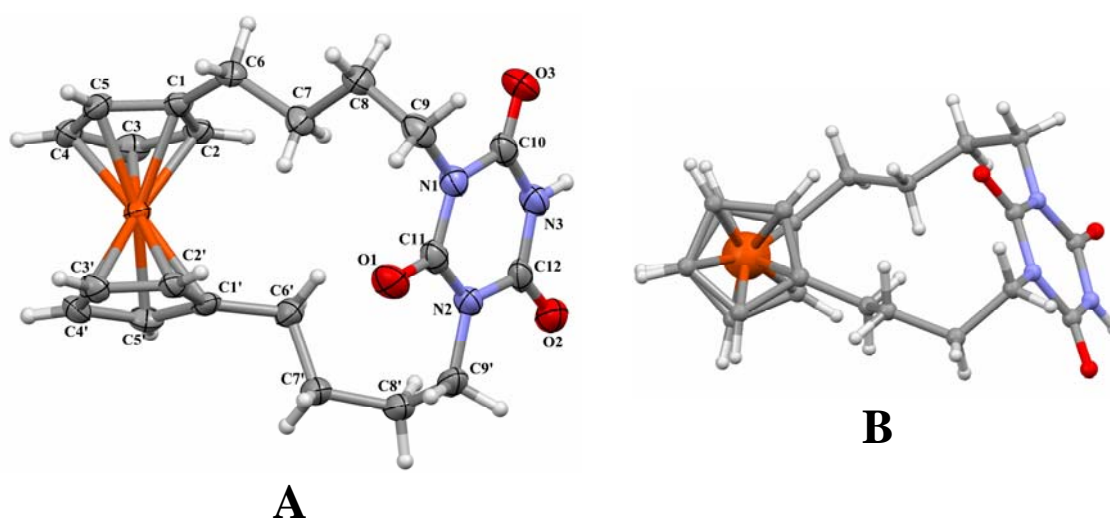
**Figure 2.26:** Photomicrographs of polymorphs of Fc(CA) complex, blocks (**Form I**) and needles (**Form II**).

The crystallographic data for dimorphs of Fc(CA) **31a** are summarized in Appendix (Table 1.7 and Table 1.8). Crystal structure determination revealed that **Form I** crystals belonged to triclinic space group  $P-1$  whereas the **Form II** crystals were monoclinic space group  $P2_1/c$  containing three independent molecules in the asymmetric unit. Single crystal X-ray data (Appendix, Table 1.7 and Table 1.8) revealed that the length of the  $a$ -axis in both forms is almost similar, whereas the difference is seen in the other two axes,  $b$  and  $c$ . In both the forms the structure revealed cyanuric acid is bridged



between the two *n*-butyl chains of the dibutyl ferrocene unit to form the complex illustrated in Figure 2.24.

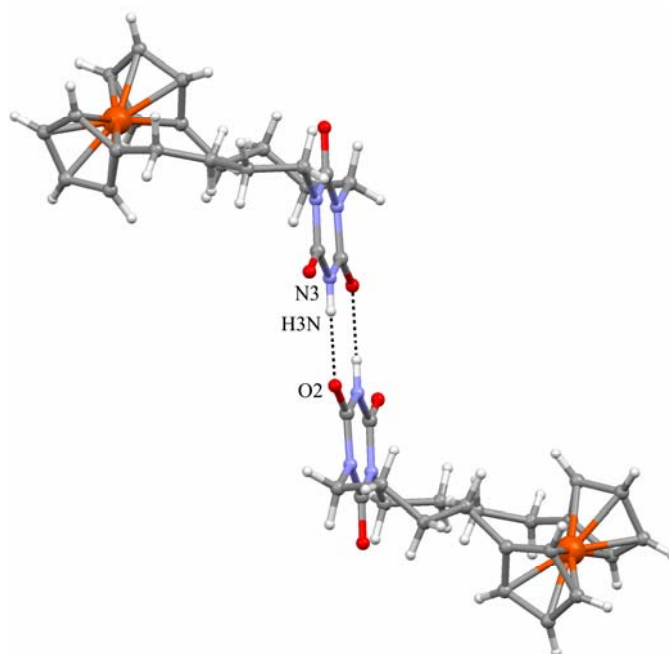
In **Form I** crystals, the two cyclopentadienyl (Cp) rings of the ferrocene moiety are staggered by  $\sim 9^\circ$  and the cynuric acid moiety is almost parallel to the ferrocene group. The bis substituents linked to the Cp rings of ferrocene are staggered by  $\sim 63^\circ$  around the ferrocene ring. The centroid–centroid separation of the Cp rings is 3.319(2) Å with the dihedral angle  $5.11^\circ$  and the Cp–Fe–Cp angle is  $176.82(8)^\circ$  (Figure 2.27).



**Figure 2.27:** (A) ORTEP of Fc(CA) **31a** and (B) viewed perpendicular to Cp rings.

In **Form II** crystals, the two-cyclopentadienyl (Cp) rings of the ferrocene moiety in all the three molecules show different orientation. In molecule A, the two Cp rings are staggered by  $\sim 5.5^\circ$  and the bis substituents linked to the Cp rings of ferrocene are staggered by  $\sim 66^\circ$  around the ferrocene ring. In molecule B, the staggering between the two Cp rings increased ( $\sim 21^\circ$ ) results in relatively decrease of staggering between the two spacer chains ( $48.5^\circ$ ). In molecule C the two Cp of the ferrocene moiety are almost eclipsed (staggered by only  $2^\circ$ ) leading to maximum separation between the spacer chains. In all the three molecules the CA molecules have almost parallel orientation with respect to the ferrocene moiety. The centroid–centroid separation of the Cp rings in molecule A, molecule B and molecule C are 3.311(3) Å, 3.318(3) Å and 3.300(3) Å with the dihedral angles  $4.8^\circ$ ,  $3.8^\circ$  and  $2.1^\circ$  respectively and the respective Cp–Fe–Cp angles are  $177.30(13)^\circ$ ,  $177.82(12)^\circ$  and  $178.75(14)^\circ$ .

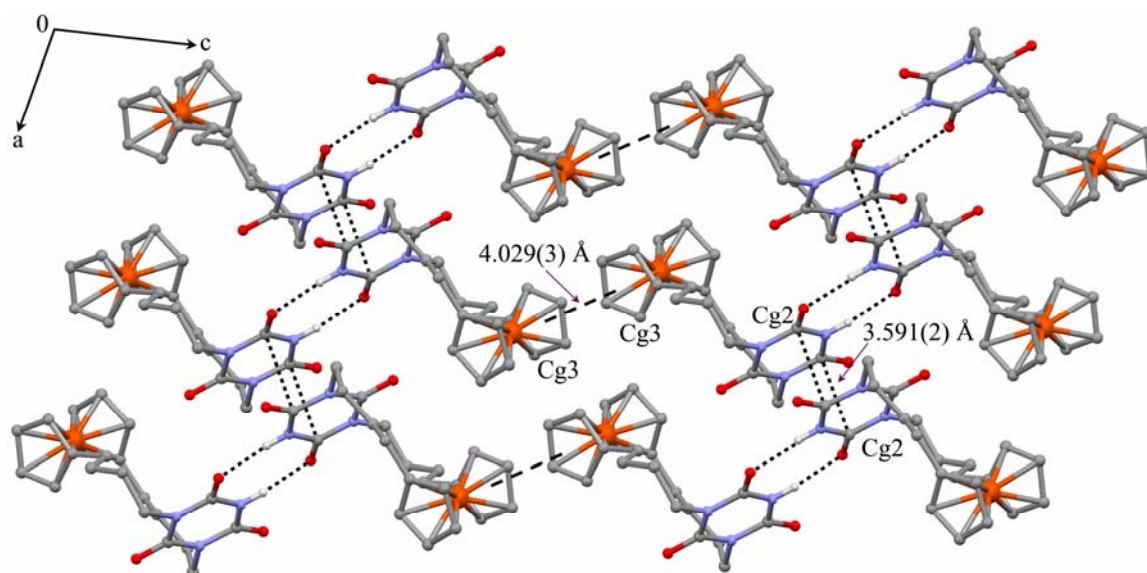
A common significant feature in both the forms is the linking of adjacent molecules *via* the strongest and conventional hydrogen bond, N-H...O, resulting self-base pairing. In **Form I** crystals the molecule exhibits self-base pairing *via* centrosymmetric N3-H3N...O2 hydrogen bond ( $H3N...O2 = 1.99 \text{ \AA}$ ,  $N3...O2 = 2.836(4) \text{ \AA}$  and  $\angle N3-H3N...O2 = 170^\circ$ ) across the inversion center. The two CA rings are engaged in hydrogen bond formation whereas ferrocene group along with the spacer chain of each molecule remain away from the hydrogen bond junction in trans orientation and make almost  $\sim 90^\circ$  angle with the hydrogen bonded pair thus forming Z-shape geometry (Figure 2.28).



**Figure 2.28:** Close pair of interacting molecules showing base pair formation *via* conventional N-H...O interactions in Fc(CA) **31a Form I**.

In **Form II** crystals, out of the three molecules, molecule A and molecule B form pseudocentrosymmetric self base pairs *via* two N-H...O hydrogen bonds [ $N3A-H3'A...O2B$ , ( $H3'A...O2B = 1.99$ ,  $N3A...O2B = 2.842(6) \text{ \AA}$  and  $\angle N3A-H3'A...O2B = 171^\circ$ ) and  $N3B-H3'B...O2A$  ( $H3'B...O2A = 1.96$ ,  $N3B...O2A = 2.815(6) \text{ \AA}$  and  $\angle N3B-H3'B...O2A = 171^\circ$ )] whereas in molecule C centrosymmetric self-base pairing was seen *via* two  $N3C-H3'C...O3C$  hydrogen bonds ( $H3'C...O3C = 2.00$ ,  $N3C...O3C = 2.858(7) \text{ \AA}$  and  $\angle N3C-H3'C...O3C = 172^\circ$ ). The geometry of these centrosymmetric synthons is similar to that observed in **Form I** crystals.

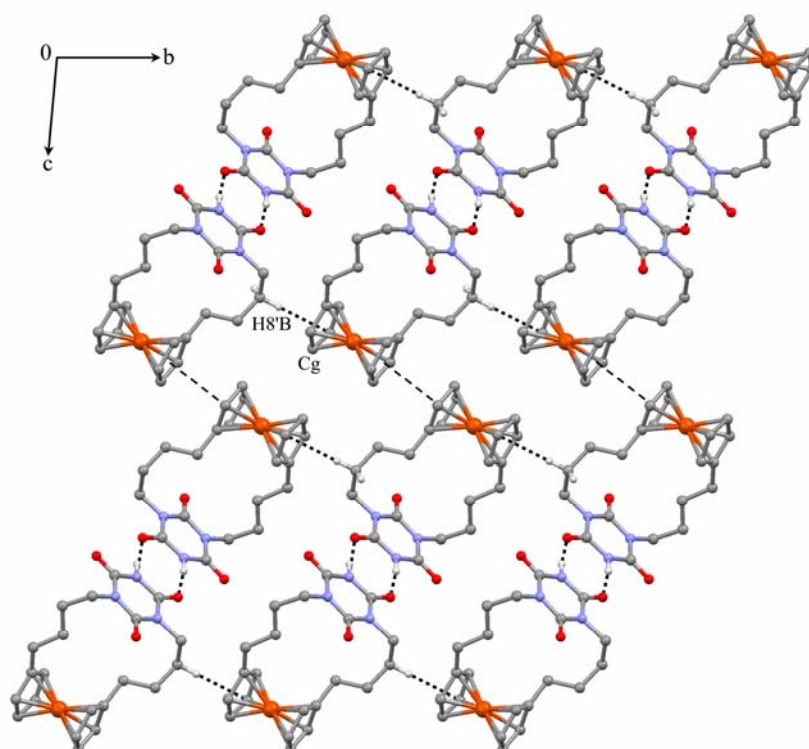
This self-pairing motif seems to be a dominant synthon in the self-assembly process during crystallization but these synthons weave differently *via* different intermolecular interactions leading to different path of nucleation resulted in dimorph formation. In **Form I** crystals the neighboring base pairs form a layered arrangement linked *via* centrosymmetric  $\pi\cdots\pi$  stacking interactions between the cyanuric acid moieties along the direction of *a*-axis while another centrosymmetric  $\pi\cdots\pi$  stacking interactions between the Cp rings of the adjacent ferrocene moieties bridge them along the direction of *c*-axis (Figure 2.29). The geometry of  $\pi\cdots\pi$  interaction between the cyanuric acid moieties being the stronger one having  $\text{Cg2}\cdots\text{Cg2} = 3.591(2)$  Å (Symmetry code:  $-x, 1-y, 1-z$ ) while  $\pi\cdots\pi$  interaction between Cp rings have  $\text{Cg3}\cdots\text{Cg3} = 4.029(3)$  Å for Form II (Symmetry code:  $-x, 1-y, 2-z$ ) where Cg2 and Cg3 are the centroids of Cp ring (C1'-C5') and cyanuric acid moiety (N1-C12) respectively. The two cyanuric acid ring are exactly parallel (dihedral angles 0) and the same is for Cp rings (dihedral angle  $0.03^\circ$ ) and the corresponding distances between planes are 3.330 and 3.910 Å for cyanuric acid and Cp rings respectively.



**Figure 2.29:** Association of the centrosymmetric dimers along *ac*-plane in Fc(CA) **31a Form I**.

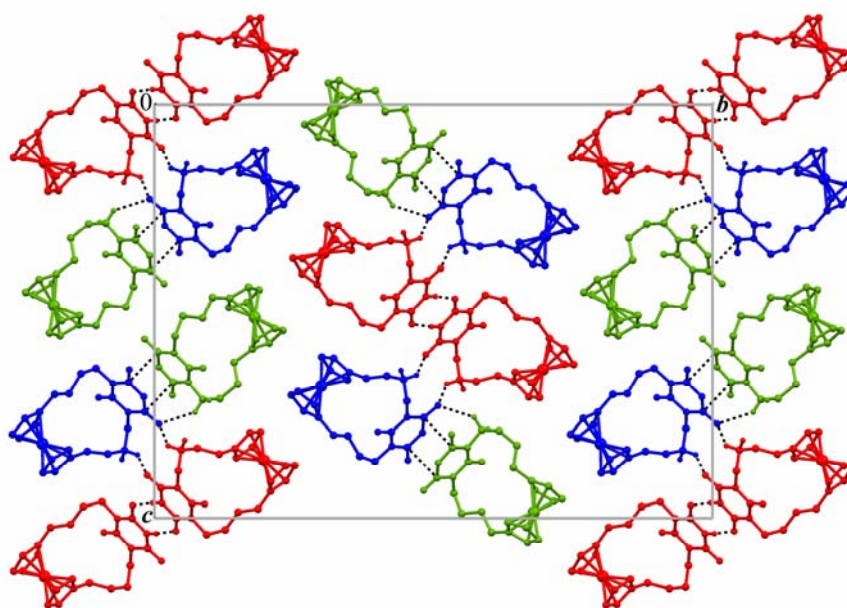
The molecular packing viewed down the *a*-axis revealed (Figure 2.30) the linking of the base pairs along the direction of *b*-axis *via* somewhat off centered C-H... $\pi$  interaction involving C-H of the butyl chain and Cp ring (C1-C5) the ferrocene group

(H8'B...Cg = 2.98 Å, C8'...Cg = 3.692(4) Å,  $\angle$ C8'-H8'B...O2A = 131°. Along the directions of *c*-axis they are stitched *via*  $\pi$ ... $\pi$  interaction between Cp rings of adjacent molecules as discussed earlier. Thus in **Form I** crystals, the base pairs are purely linked *via* weak intermolecular interactions such as  $\pi$ ... $\pi$  and C-H... $\pi$  interactions in all the three directions, which played a major role assembling the centrosymmetric synthons in the absence of other strong interactions.



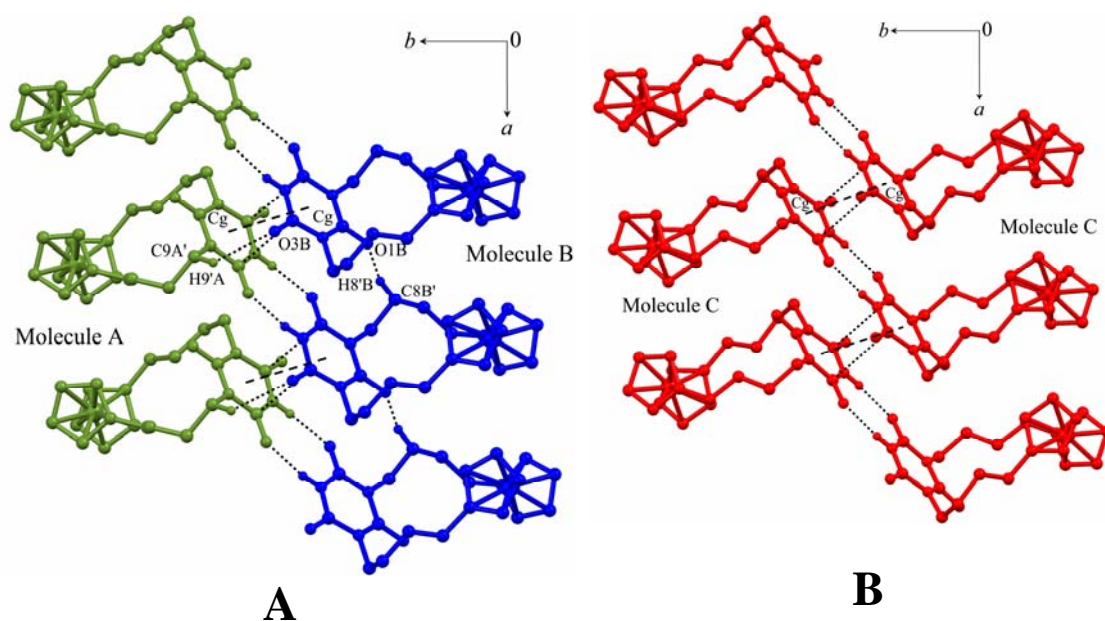
**Figure 2.30:** Molecular packing viewed down *a*-axis showing bridging of the base pairs *via*  $\pi$ ... $\pi$  and C-H... $\pi$  interactions in Fc(CA) **31a Form I**.

In **Form II** crystals, although the  $\pi$ ... $\pi$  stacking interaction between the cyanuric acid moieties is conversed, the association of base pairs in other dimension differs and no  $\pi$ ... $\pi$  and C-H... $\pi$  interactions between the Cp rings were observed in comparison with **Form I** crystals. Figure 2.31 shows the overall packing of the molecules in **Form II** crystals. As discussed earlier, the molecules A (green) and B (blue) are involved in base-pair formation whereas molecule C (red) forms its own base pair. Each base pair are arranged helically along the direction *b*-axis and are related by  $2_1$ -screw axis.



**Figure 2.31:** Molecular packing viewed down *a*-axis showing associations of different base pairs in Fc(CA) **31a Form II**.

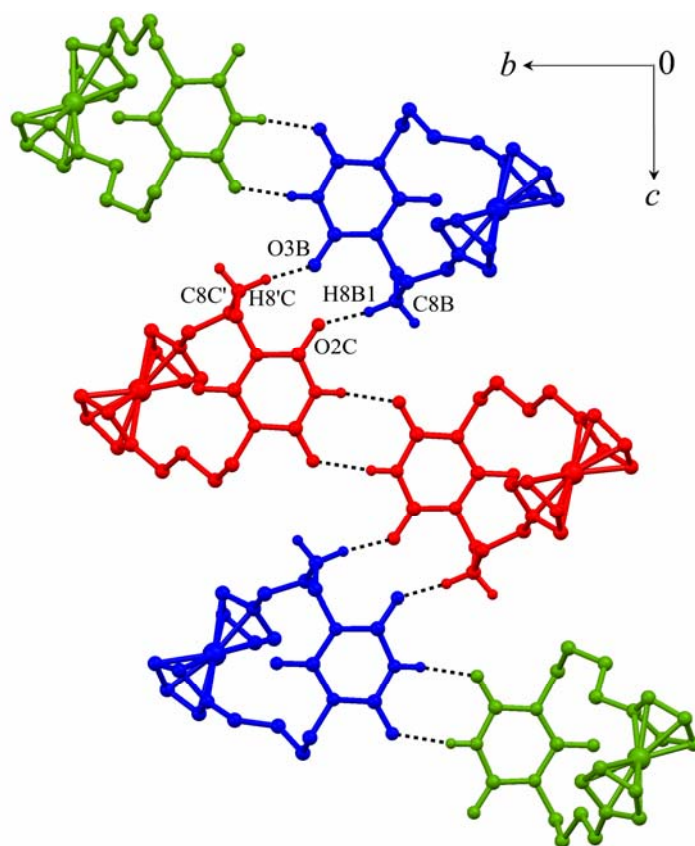
The adjacent base pairs along the direction of *a*-axis form a layered arrangement linked *via* centrosymmetric  $\pi\cdots\pi$  stacking interactions between the cyanuric acid moieties in **Form II** are similar to the **Form I** crystals, explaining the near equality of *a*-axis in both the polymorphs. The base pairs formed by molecules A and B are linked to other similar base pairs *via*  $\pi\cdots\pi$  stacking interactions between the cyanuric acid moieties of molecules A and B. Similarly the cyanuric acid moieties of molecule C is involved in centrosymmetric  $\pi\cdots\pi$  stacking interactions thereby connecting the base pairs of molecule C (Figure 2.32). The geometry of  $\pi\cdots\pi$  interaction between the cyanuric acid moieties of molecules C is better than that of molecules A and B (Cg $\cdots$ Cg = 3.582(3) Å, dihedral angles 0°, symmetry code: -x, 1-y, 1-z for molecule C and Cg $\cdots$ Cg = 3.665(3) Å, dihedral angles 3.96°, symmetry code: 1-x, -1/2+y, 1/2-z for molecule A and B). Additionally, two more C-H $\cdots$ O interactions involving C9A'-H9'A of butyl chain of molecule A and carbonyl oxygen O3B of molecule B (C9A'-H9'A $\cdots$ O3B, H9'A $\cdots$ O3B = 2.64 Å, C9A' $\cdots$ O3B = 3.347(7) Å,  $\angle$ C9A'-H9'A $\cdots$ O3B = 131°) and C8B'-H8'B of butyl chain and carbonyl oxygen O1B of molecule B (C8B'-H8'B $\cdots$ O1B, H8'B $\cdots$ O1B = 2.56 Å, C8B' $\cdots$ O1B = 3.391(7) Å,  $\angle$  C8B'-H8'B $\cdots$ O1B = 144°) also strengthened the layered arrangement in molecules A and B.



**Figure 2.32:**  $\pi$ ... $\pi$  stacking interactions between CA moieties of the base pairs in Fc(CA) **31a Form II**, (A) in molecules A and B and (B) in molecules C.

Along the directions of the *c*-axis the base pairs are linked *via* two long C-H...O contacts (Figure 2.33). The C8C' of butyl chain of molecule C (red) donates its proton H8'C to carbonyl oxygen O3B of cyanuric acid moiety of molecule B (blue); in turn the carbonyl oxygen O2C of cyanuric acid moiety of molecule C (red) accepts H-atom (H8B1) methylene carbon C8B of butyl chain of molecule B (blue). The H...O distances of these two C-H...O interactions are very long and also they deviate too much from the linearity (C8C'-H8'C...O3B, H8'C...O3B = 2.70 Å, C8C'...O3B = 3.418(8) Å,  $\angle$ C8C'-H8'C...O3B = 131° and C8B-H8B1...O2C, H8B1...O2C = 2.72 Å, C8B...O2C = 3.453(9) Å,  $\angle$ C8B-H8B1...O2C = 133°). No significant interactions were seen along the direction of *b*-axis between base pairs.

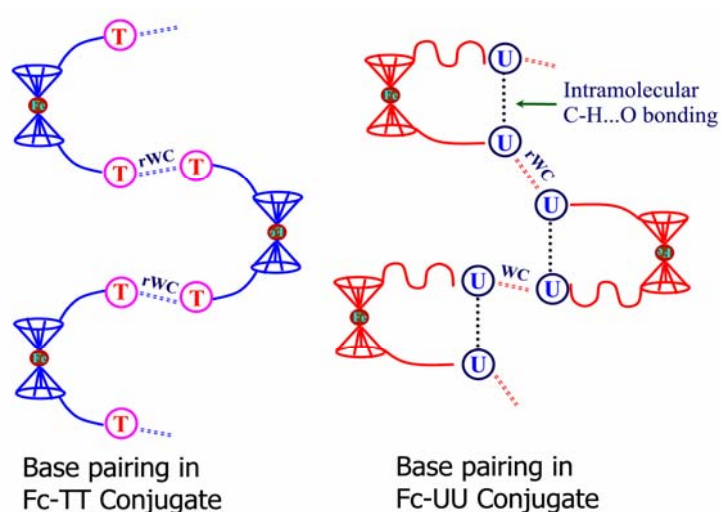
Thus self-pairing motif *via* strongest intermolecular hydrogen bond (N-H...O) seems to be a dominant synthon in the self-assembly process of both the polymorphs. But the engagement of the lone N-H group in N-H...O hydrogen bonding gave opportunity for the weaker interactions such as C-H...O, C-H... $\pi$ ,  $\pi$ ... $\pi$  to play their role in bridging of base pairs in other dimensions. Thus, nucleation pathways have diverged although various options of intermolecular interactions of similar strength were available leading to polymorph formations.



**Figure 2.33:** Associations of base pairs along the directions of *c*-axis linked *via* C-H...O interactions in Fc(CA) **31a Form II**.

## 2.5 Conclusions

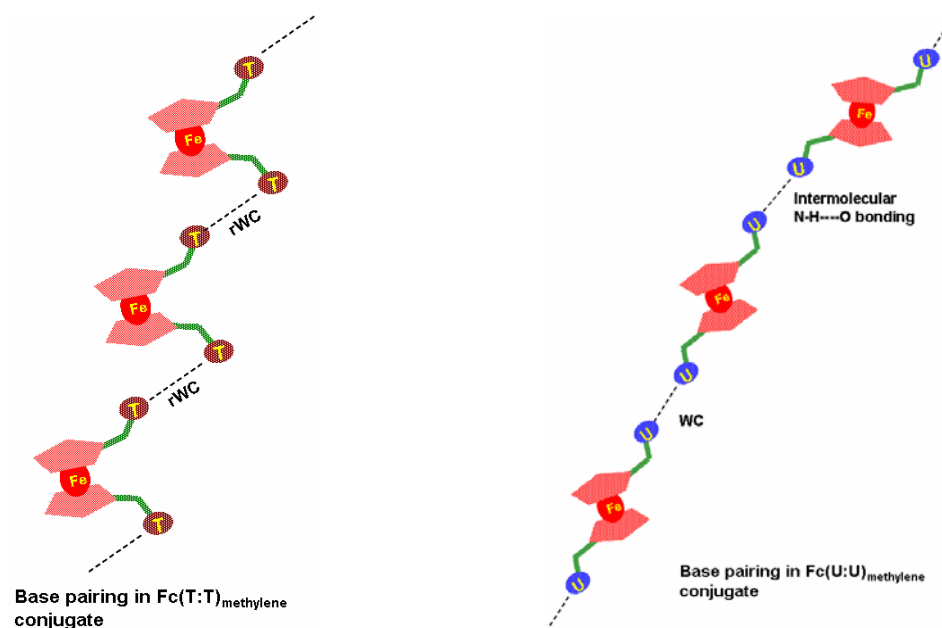
In conclusion, The synthesis of the newly designed ferrocene-linked mono and bis(nucleobase) conjugates with different spacer chain have been reported. Conjugates Fc(TT) **1a**, Fc(Br-U:Br-U) **1c** and Fc(T:U) **1d** show different supramolecular assemblies mediated via centrosymmetric base pairings of rWC type and Fc(U:U) shows pairing of both WC and rWC types. The structure of Fc(U:U) **1b** is perhaps the first example of WC and rWC like pairing being simultaneously present within the same crystal lattice. The comparison of structures clearly delineates the steric role of the 5-substituent in influencing the C-H...O contacts.



**Figure 2.24:** Graphical representation of H-bondings in Fc(T:T) and Fc(U:U) conjugates with *n*-butyl spacer.

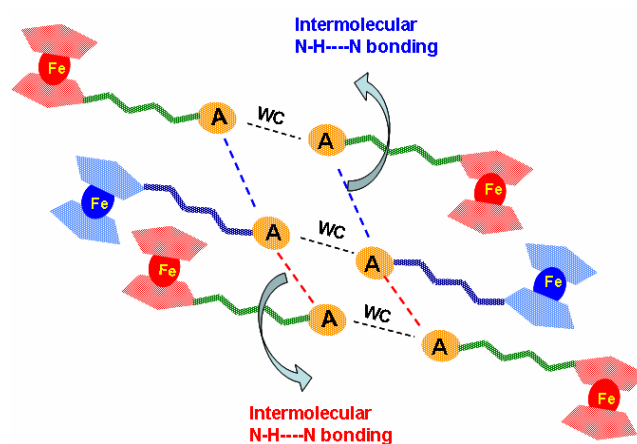
[Fc(T:T)<sub>methylene</sub>] **20a** and [Fc(U:U)<sub>methylene</sub>] **20b** have been synthesized to examine the role of spacer chain in self assemble induced supramolecular structure and effect on base pairing. In Fc(T:T)<sub>methylene</sub> **20a** the self-pairing of thymine leads to a regular ribbon formation. These neighboring ribbons are stitched together *via* strong C-H...O hydrogen bond. Fc(T:T)<sub>methylene</sub> **20a** forms two-dimensional sheet, with the help of two weak C-H...O hydrogen bonds, having ferrocene moieties remain at one side of the sheet. The interesting thing in Fc(T:T)<sub>methylene</sub> **20a** is that the water molecules are trapped in the self-assembly process during the crystallization. These disordered water molecules are included in the cage formed by the thymine base and the ferrocene moiety with no significant interactions between the host and the guest molecules. In the crystal structure of Fc(U:U)<sub>methylene</sub> **20b** both the uracil groups with methylene spacer adopting extended conformation but are trans to each other unlike Fc(T:T)<sub>methylene</sub> **20a**. Interestingly in the bisuracil derivative Fc(U:U)<sub>methylene</sub> **20b**, only one U chain engaged in self-base pairing of ‘Watson-Crick’ (WC) motif *via* conventional centrosymmetric hydrogen bonds while the other U chain was not involved in base pairing. In the crystal structure of Fc(U:U)<sub>methylene</sub> **20b** the adjacent sheets along the *b*-axis are linked *via*  $\pi$ ... $\pi$  stacking interaction between the substituted Cp rings of ferrocene as well as between the uracil moiety. The accurate geometries of the T.T and U.U base pairings are of considerable structural interest because of their presence in nucleic acids.





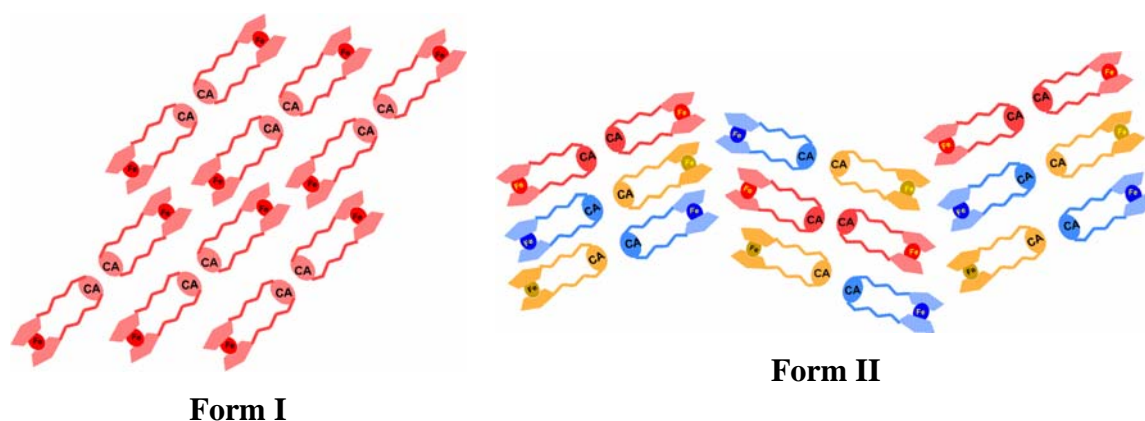
**Figure 2.25:** Graphical representation of H-bondings in  $\text{Fc}(\text{T}:\text{T})_{\text{methylene}}$  and  $\text{Fc}(\text{U}:\text{U})_{\text{methylene}}$  conjugates.

The crystal structure of ferrocene-adenine conjugate  $[\text{Fc}(\text{A})]$  **27b** have two independent molecules in the asymmetric unit. Interestingly in the  $[\text{Fc}(\text{A})]$  **27b**, both the symmetry independent molecules are engaged in self-base pairing of ‘Watson-Crick’ (WC) motif with each other forming the dimeric assembly across the pseudo inversion center. These self-base pairing dimers are bridged alternately *via* two different centrosymmetric N-H...N hydrogen bonds creating two different tetrads. The adjoining sheets are centrosymmetrically stitched *via* short  $\pi\cdots\pi$  stacking interaction between the six-member nucleobase of the adenine moiety.



**Figure 2.26:** Graphical representation of H-bondings in  $\text{Fc}(\text{A})$  conjugate with *n*-butyl spacer.

The crystal structure studies of ferrocene-cyanuric acid conjugate Fc(CA) **31a** revealed that crystallization of Fc(CA) **31a** produced two concomitant polymorphs. Self-pairing motif *via* strongest intermolecular hydrogen bond (N-H...O) seems to be a dominant synthon in the self-assembly process of both the polymorphs. But the engagement of the lone N-H group in N-H...O hydrogen bonding gave opportunity for the weaker interactions such as C-H...O, C-H... $\pi$ ,  $\pi$ ... $\pi$  to play their role in bridging of base pairs in other dimensions. Nucleations pathways have diverged due to various options of intermolecular interactions of similar strength were available leading to polymorph formations.



**Figure 2.27:** Graphical representation of molecular packing for Fc(CA) conjugates **Form I** and **Form II**.

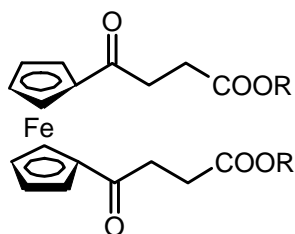
Thus the tethering of metal complexes to nucleobases is clearly synthetically viable for a wide range of systems. The self-assembly fascinatingly occurs through the use of all available hydrogen-bonding donors in the solid states. Such self-assembling organometallic units have utility in inducing chain reversal<sup>37</sup> and may also have more potential in biomimetic applications, in terms of the generation of supramolecular scaffolds. Analysis of supramolecular structures in directing the crystal packing helps one in understanding a hierarchy even in weak molecular interactions.

## 2.6 General Experimental Methods

Melting points of samples were measured on a Thermonik Campbell melting point apparatus in Celsius degrees and are uncorrected. Melting points of some of the samples were determined in open capillary tubes using Buchi Melting point B-540 apparatus and are uncorrected. Infrared spectra (IR) were recorded on Shimadzu 8400 series FTIR instrument.  $^1\text{H}$  and  $^{13}\text{C}$  NMR spectra were recorded on a Bruker AC-200, AC-400 and AC-500 NMR spectrometers. The chemical shifts are given in delta ( $\delta$ ) ppm values and relative to internal standard tetramethylsilane for  $^1\text{H}$ . Spin-spin coupling constants (J value) recorded in Hz. Peak multiplicities were denoted by s (singlet); br s (broad singlet), d (doublet), dd (double doublet), t (triplet), q (quartet), m (multiplet). Mass spectra were recorded on LC-MS/MS-TOF API QSTAR PULSAR spectrometer. Elemental analyses were performed by CHNS-O EA1108 elemental analyser. All reactions were monitored by analytical thin-layer chromatography (TLC) on Merck Aluminium precoated plates of silica gel 60 F<sub>254</sub> (Product Code. 1.05554.0007) with detection by either viewing under UV light or treating with an ethanolic solution of phosphomolybdic acid. Column chromatography was performed on silica gel column, packed with pet ether/triethylamine (98:2) and eluted with different composition of ethyl acetate/pet ether mixture. All reagents and solvent were general reagent grade unless otherwise stated. THF was freshly distilled from Na/benzophenone under nitrogen. Dichloromethane was freshly distilled from P<sub>2</sub>O<sub>5</sub> under nitrogen. Thymine, uracil and 5-bromouracil were purchased from Aldrich. N<sup>3</sup>-benzoylation of thymine/uracil/5-bromouracil were performed according to literature procedure.<sup>21</sup>

## 2.7 Experimental

**1, 1'-Bis-(3-carbethoxypropionyl)ferrocene (4):**<sup>20</sup> **(A)** A mixture of anhydrous aluminium chloride (96 g, 0.72 mol) in DCM (200 mL) was



**4:** R = Et

**4a:** R = H

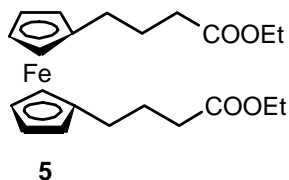
treated with succinic anhydride (36 g, 0.36 mol). The mixture was stirred and shaken a few minutes and a solution of ferrocene **3** (33.3 g, 0.18 mol) in DCM (200 mL) was added in small portions over a 10-minute period. Hydrogen chloride gas was evolved and the heat of reaction brought the mixture to 35 °C. The dark violet viscous solution was

allowed to stand 7 h at room temperature, poured onto ice, and filtered. The air-dried solid (yield 46 g) was extracted once with 800 mL of boiling water and twice with 150 mL of boiling water. The combined extract were cooled in an ice-bath and filtered to obtain crystalline 1,1'-bis-(3-carboxypropionyl)ferrocene (19.7 g 38 % yield, **4a**), m.p. 164-166 °C (decomp).

**(B)** The above diacid was converted to the corresponding diethyl ester **4** by slow distilling a solution of the acid (21.3 g, 0.055 mol), sulfuric acid (1.5g, 0.015 mol), ethyl alcohol (200 mL) and toluene (250 mL) through a small still. After slow distillation for 4 h, the remaining solution was cooled to room temperature and washed with 10 % aqueous sodium carbonate solution (75 mL). The toluene solution was dried over magnesium sulfate, filtered and evaporated at room temperature to obtained 23 g (94 %) of red brown crystals of **4**. This was recrystallized from ethyl alcohol as shiny orange-brown platelets: mp 134-136 °C (ethyl alcohol). Yield 35 % (combine two steps). <sup>1</sup>H-NMR (CDCl<sub>3</sub>, 200 MHz) δ: 1.27 (t, 6H, J = 7.1 Hz), 2.67 (t, 4H, J = 6.2 Hz), 3.01 (t, 4H, J = 6.0 Hz), 4.18 (q, 4H, J = 7.1 Hz), 4.57 (2, 4H), 4.87 (s, 4H). <sup>13</sup>C NMR (CDCl<sub>3</sub>, 50 MHz) δ: 14.0, 27.5, 34.2, 60.3, 70.4, 73.5, 79.7, 172.7, 201.1; MS (LC-MS): (*m/z*) Calcd for C<sub>22</sub>H<sub>26</sub>O<sub>6</sub>Fe 442.28 [M<sup>+</sup>], Found 443.36 [M<sup>+</sup> + 1], 465.42 [M<sup>+</sup> + Na]; Anal. calcd for C<sub>22</sub>H<sub>26</sub>O<sub>6</sub>Fe: C, 59.73; H, 5.92, Found: C, 60.1; H, 5.81.

**1, 1'-Bis-(3-carbethoxypropyl)ferrocene (5):** To zinc amalgam (5.0 g) in water (3.0 mL), conc. HCl (7.0 mL), benzene (5.0 mL) and ethanol (4.0 mL) was added **4** (2.5 g, 5.65 mmol). The mixture was refluxed briskly for 24-30 h, during which time conc. HCl

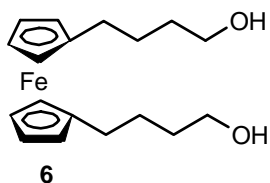
(2.5 mL) was added every six hours. The solution was cooled to room temperature; the aqueous layer was separated, diluted with water (5.0 mL), and extracted with ether (3 x



3.0 mL). The combined ether and benzene extract was washed with water and dried over calcium chloride. The solvents were removed by distillation under diminished pressure, and the residue was purified by column chromatography on silica gel, and eluted with pet ether/ethyl

acetate (8:2) to give **5** as reddish yellow oil. Yield 70 %.  $^1\text{H-NMR}$  ( $\text{CDCl}_3$ , 200 MHz)  $\delta$ : 1.24 (t, 6H,  $J = 7.0$  Hz), 1.85-1.71 (m, 4H), 2.26-2.33 (m, 8H), 4.02 (s, 8H), 4.13 (q, 4H,  $J = 7.0$  Hz).  $^{13}\text{C NMR}$  ( $\text{CDCl}_3$ , 50 MHz)  $\delta$ : 14.2, 26.3, 28.8, 33.9, 60.1, 68.1, 68.8, 88.2, 173.4; MS (LC-MS): ( $m/z$ ) Calcd for  $\text{C}_{22}\text{H}_{30}\text{O}_4\text{Fe}$  414.32 [ $\text{M}^+$ ], Found 414.13 [ $\text{M}^+$ ]; Anal. calcd for  $\text{C}_{22}\text{H}_{30}\text{O}_4\text{Fe}$ : C, 63.76; H, 7.24, Found: C, 63.61; H, 7.62.

**1, 1'-Bis-(4-hydroxybutyl)ferrocene (6):**  $\text{LiAlH}_4$  (1.22 g, 32.1 mmol) in dry THF (40



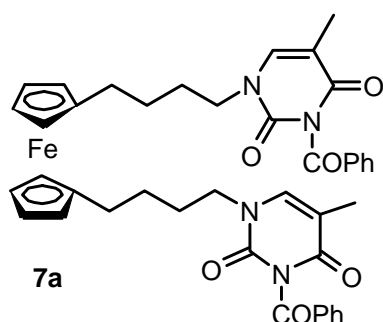
mL) was stirred for 10 minutes and a solution of **5** (2.2 g, 5.3 mmol) in dry THF (15 mL) was added drop by drop at such a rate that THF reflux gently. The reaction mixture was stirred for 3 to 4 h at room temperature followed by cooling in ice-bath, quenching with slow addition of ice and stirring for 1 h.

The reaction mixture was filtered and washed it with ether. The solvents are removed by distillation under diminished pressure, and the residue is purified by column chromatography on silica gel, and eluted with pet ether/ethyl acetate (3:2) to give **6** as reddish-yellow oil: Yield 95 %.  $^1\text{H-NMR}$  ( $\text{CDCl}_3$ , 200 MHz)  $\delta$ : 1.53 (m, 8H), 2.26 (m, 4H), 3.58 (m, 4H), 4.08 (s, 8H).  $^{13}\text{C NMR}$  ( $\text{CDCl}_3$ , 50 MHz)  $\delta$ : 27.1, 28.6, 32.3, 62.3, 69.1, 70.1, 91.4; MS (LC-MS): ( $m/z$ ) Calcd for  $\text{C}_{18}\text{H}_{26}\text{O}_2\text{Fe}$  330.24 [ $\text{M}^+$ ], Found 330.11 [ $\text{M}^+$ ]; Anal. calcd for  $\text{C}_{18}\text{H}_{26}\text{O}_2\text{Fe}$ : C, 65.45; H, 7.87, Found: C, 65.11; H, 8.22.

**General procedure for the preparation of 7a-c via Mitsunobu reaction:** *N*3-benzoylthymine/*N*3-benzoyluracil (1.89 mmol) and triphenylphosphine (0.60 g, 2.27 mmol) were dissolved in dry THF (10 mL) and the solution was cooled to 0 °C. At this temperature, alcohol **6** (0.25 g, 0.75 mmol) dissolved in dry THF (4 mL) was added to the stirred solution followed by dropwise addition of DIAD (0.45 mL, 2.27 mmol). The

solution was allowed to gradually reach room temperature and stirring was continued overnight. The solvent was removed under reduced pressure and the resulting solid was purified by flash chromatography on silica gel, packing with pet ether/triethylamine (98:2) and eluted with pet ether/ethyl acetate (7:3) to give ferrocene linked *N*3-benzoylprotected nucleobase **7a-c**.

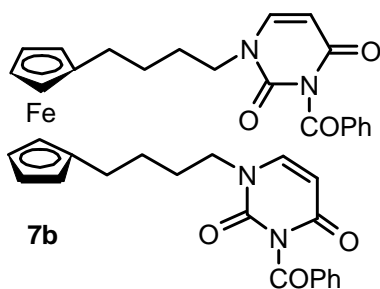
**1, 1'-Bis-(4-(*N*3-benzoylthyminy)butyl)ferrocene (7a).** Yellow foam: Yield 56%. IR



(thin film): 1745, 1695, 1650  $\text{cm}^{-1}$ .  $^1\text{H-NMR}$  ( $\text{CDCl}_3$ , 200 MHz)  $\delta$ : 1.51-1.36 (m, 4H), 1.80-1.60 (m, 4H), 1.93 (s, 6H), 2.42-2.18 (m, 4H), 3.69 (t, 4H,  $J = 6.9$  Hz), 4.02 (br s, 8H), 7.04 (s, 2H), 7.51-7.43 (m, 4H), 7.67-7.60 (m, 2H), 7.90 (d, 4H,  $J = 7.8$  Hz).  $^{13}\text{C NMR}$  ( $\text{CDCl}_3$ , 50 MHz)  $\delta$ : 12.3, 28.0, 28.6, 28.8, 48.4, 67.9, 68.7, 88.1, 110.4, 129.1, 130.3, 131.6, 134.9, 140.2,

149.7, 163.1, 169.2; MS (LC-MS): ( $m/z$ ) Calcd for  $\text{C}_{42}\text{H}_{42}\text{N}_4\text{O}_6\text{Fe}$  754.66 [ $\text{M}^+$ ], Found 754.32 [ $\text{M}^+$ ], 777.31 [ $\text{M}^+ + \text{Na}$ ].

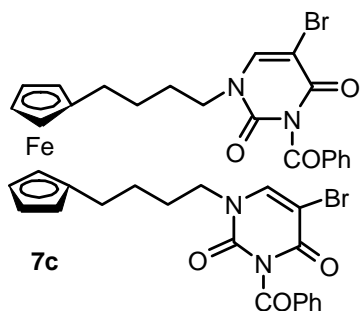
**1, 1'-Bis-(4-(*N*3-benzoyluracily)butyl)ferrocene (7b).** Orange foam: Yield 48%. IR



(thin film): 1745, 1703, 1660  $\text{cm}^{-1}$ .  $^1\text{H-NMR}$  ( $\text{CDCl}_3$ , 200 MHz)  $\delta$ : 1.58- 1.41 (m, 4H), 1.78-1.65 (m, 4H), 2.40-2.26 (m, 4H), 3.79-3.66 (m, 4H), 3.99 (s, 8H), 5.76 (d, 2H,  $J = 8.1$  Hz), 7.21 (d, 2H,  $J = 8$  Hz), 7.51-7.46 (m, 4H), 7.67-7.62 (m, 2H), 7.91 (d, 4H,  $J = 7.4$  Hz).  $^{13}\text{C NMR}$  ( $\text{CDCl}_3$ , 50 MHz)  $\delta$ : 28.0, 28.6, 28.9, 48.9, 68.0, 68.8, 88.1, 101.9, 129.2, 130.4, 131.4,

135.1, 144.3, 149.8, 162.5, 169.0; MS (LC-MS): ( $m/z$ ) Calcd for  $\text{C}_{40}\text{H}_{38}\text{N}_4\text{O}_6\text{Fe}$  726.61 [ $\text{M}^+$ ], Found 727.27 [ $\text{M}^+ + 1$ ], 749.27 [ $\text{M}^+ + \text{Na}$ ]; Anal. calcd for  $\text{C}_{40}\text{H}_{38}\text{N}_4\text{O}_6\text{Fe}$ : C, 66.12; H, 5.27; N, 7.71, Found: C, 65.93; H, 5.38; N, 7.69.

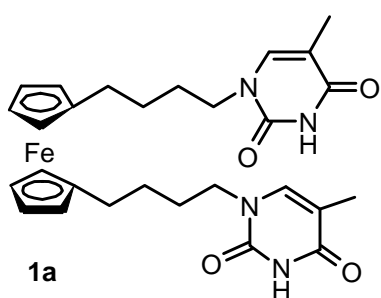
**1, 1'-Bis-[(4-(*N*3-benzoyl)-5-bromouracily)butyl]ferrocene (7c):** Yellow powder: mp 175-177  $^\circ\text{C}$  (DCM/pet ether). Yield 44 %. IR (thin film): 1741, 1695, 1660  $\text{cm}^{-1}$ .  $^1\text{H-NMR}$  ( $\text{CDCl}_3$ , 200 MHz)  $\delta$ : 1.55-1.35 (m, 4H), 1.78-1.65 (m, 4H), 2.4-2.2 (m, 4H),



3.79-3.65 (m, 4H), 4.08 (br s, 8H), 7.53-7.45 (m, 4H), 7.55 (s, 2H), 7.70-7.62 (m, 2H), 7.89 (d, 4H,  $J = 7$  Hz).  $^{13}\text{C}$  NMR ( $\text{CDCl}_3$ , 50 MHz)  $\delta$ : 27.2, 27.9, 28.1, 48.4, 67.3, 68.1, 87.5, 94.7, 128.6, 129.7, 130.3, 134.7, 143.9, 148.4, 157.7, 167.2; MS (LC-MS): ( $m/z$ ) Calcd for  $\text{C}_{40}\text{H}_{36}\text{N}_4\text{Br}_2\text{O}_6\text{Fe}$  884.40 [ $\text{M}^+$ ], Found 883.98 [ $\text{M}^+$ ], 906.98 [ $\text{M}^+ + \text{Na}$ ]; Anal. calcd for  $\text{C}_{40}\text{H}_{36}\text{N}_4\text{Br}_2\text{O}_6\text{Fe}$ : C, 54.32, H, 4.10, N, 6.33, Found: C, 54.27; H, 3.77; N, 6.42.

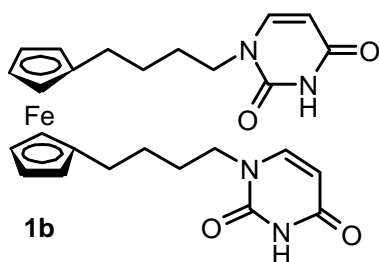
**General procedure for debenzoylation for preparation of 1a-b:** To a stirred solution of dibenzoyl derivative **7a-b** and (0.14 mmol) in methanol/toluene mixture (10:1, 80 mL) was added saturated solution of  $\text{K}_2\text{CO}_3$  in water. The resultant mixture was then stirred overnight at room temperature. The solvent was removed under reduced pressure and the residual material was extracted with DCM/methanol (30:1,  $3 \times 35$  mL). The combined organic phases were washed with brine solution, dried over  $\text{Na}_2\text{SO}_4$  and concentrated. The crude product was chromatographed on a silica gel column using ethyl acetate/pet ether (7:3) as eluent to give ferrocene linked nucleobase compounds **1a-b** and which were recrystallized from appropriate solvent.

**1, 1'-Bis-(4-(thyminy)butyl)ferrocene (1a):** Yellow needle: mp 208-209 °C (DCM/methanol). Yield 90 %. IR (thin film): 3174,



1670  $\text{cm}^{-1}$ .  $^1\text{H}$ -NMR ( $\text{CDCl}_3$  +2 drops  $\text{DMSO-}d_6$ , 200 MHz)  $\delta$ : 1.45-1.30 (m, 4H), 1.65-1.48 (m, 4H), 1.78 (s, 6H), 2.23-2.07 (m, 4H), 3.55 (t, 4H,  $J = 7.1$  Hz), 3.96 (br s, 8H), 6.86 (s, 2H), 9.79 (s, 2H).  $^{13}\text{C}$  NMR ( $\text{DMSO-}d_6$ , 50 MHz)  $\delta$ : 12.1, 27.7, 28.5, 28.5, 47.2, 67.7, 68.6, 88.6, 108.6, 141.7, 151.1, 164.5; MS (LC-MS): ( $m/z$ ) Calcd for  $\text{C}_{28}\text{H}_{34}\text{N}_4\text{O}_4\text{Fe}$  546.44 [ $\text{M}^+$ ], Found 546.14 [ $\text{M}^+$ ], 569.14 [ $\text{M}^+ + \text{Na}$ ]; Anal. calcd for  $\text{C}_{28}\text{H}_{34}\text{N}_4\text{O}_4\text{Fe}$ : C, 61.54; H, 6.27; N, 10.25, Found: C, 61.15; H, 6.04; N, 10.01.

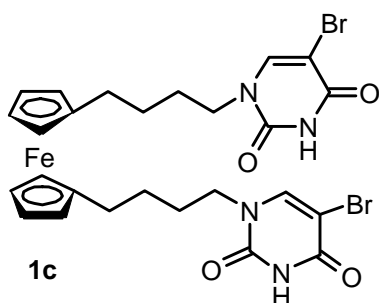
**1,1'-Bis-(4-(uracily)butyl)ferrocene (1b):** Orange solid: mp 165-167 °C (DCM/methanol/toluene). Yield 71 %. IR (thin film): 3020, 1681  $\text{cm}^{-1}$ .  $^1\text{H}$ -NMR ( $\text{CDCl}_3$



+ 2 drops DMSO-*d*<sub>6</sub>, 200 MHz)  $\delta$ : 1.53-1.28 (m, 4H), 1.77-1.54 (m, 4H), 2.38-2.20 (m, 4H), 3.64 (t, 4H, *J* = 6.6 Hz), 3.97 (s, 8H), 5.60 (d, 2H, *J* = 7.2 Hz), 7.07 (d, 2H, *J* = 7.4 Hz), 9.61 (br s, 2H). <sup>13</sup>C NMR (DMSO-*d*<sub>6</sub>, 50 MHz)  $\delta$ : 27.7, 28.5, 47.5, 67.7, 68.6, 88.6, 101.0, 145.9, 151.2, 164.0; MS (LC-MS): (*m/z*)

Calcd for C<sub>26</sub>H<sub>30</sub>N<sub>4</sub>O<sub>4</sub>Fe 518.39 [M<sup>+</sup>], Found 518.21 [M<sup>+</sup>], 541.21 [M<sup>+</sup> + Na]; Anal. calcd for C<sub>26</sub>H<sub>30</sub>N<sub>4</sub>O<sub>4</sub>Fe: C, 60.24; H, 5.83; N, 10.81, Found: C, 60.33; H, 5.86; N, 10.88.

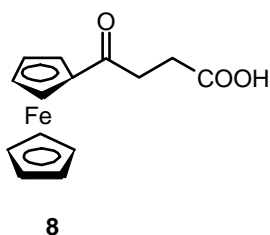
**1, 1'-Bis-[4-(5-bromouracil)butyl]ferrocene (1c):** To a stirred solution of compound



**7c** (0.1 g, 0.11 mmol) dissolved in THF/methanol mixture (3:2, 54 mL) was added LiOH (2N) solution in water. The reaction was monitored by checking TLC. After 6 h the solvent was removed under reduced pressure and the residual material was treated with ice cold water, acidified with dilute HCl and

extracted with ethyl acetate/methanol (50:1, 3 × 40 mL). The combined organic phases were washed with water, 5 % NaHCO<sub>3</sub>, brine solution, dried over Na<sub>2</sub>SO<sub>4</sub> and concentrated. The crude product was chromatographed on a silica gel column using pet ether/ethyl acetate (3:7) as eluent to give compound **1c** (35 mg, 45 %). Yellow needle: mp 228 °C ignited (THF/methanol). Yield 45 %. IR (thin film): 3188, 1693, 1674 cm<sup>-1</sup>. <sup>1</sup>H-NMR (CDCl<sub>3</sub> + 2 drops of DMSO-*d*<sub>6</sub>, 200 MHz)  $\delta$ : 1.41-1.21 (m, 4H), 1.62-1.43 (m, 4H), 2.21-2.05 (m, 4H), 3.55 (t, 4H, *J* = 7.1 Hz), 3.91 (br s, 8H), 7.41 (s, 2H), 11.08 (br s, 2H); MS (MALDI-TOF): (*m/z*) Calcd for C<sub>26</sub>H<sub>28</sub>N<sub>4</sub>Br<sub>2</sub>O<sub>4</sub>Fe 676.18 [M<sup>+</sup>], Found 676.98 [M<sup>+</sup>]; Anal. calcd for C<sub>26</sub>H<sub>28</sub>N<sub>4</sub>Br<sub>2</sub>O<sub>4</sub>Fe: C, 46.18; H, 4.17; N, 8.28, Found: C, 46.37; H, 4.23; N, 8.36.

**1-(3-Carboxypropionyl)ferrocene (8):** This was synthesized using procedure A as for **4**



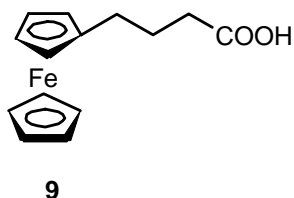
using the following reagents. Anhydrous aluminium chloride (48 g, 0.36 mol), succinic anhydride (18 g, 0.18 mol), ferrocene **3** (16.65 g, 0.09 mol). Orange powder: mp 164-165 °C (water). Yield 58 %. <sup>1</sup>H-NMR (CDCl<sub>3</sub>, 200 MHz)  $\delta$ : 2.75

**8**



(m, 2H), 3.07 (m, 2H), 4.22 (s, 5H), 4.50 (s, 2H), 4.80 (s, 2H); MS (LC-MS): ( $m/z$ ) Calcd for  $C_{14}H_{14}O_3Fe$  286.11 [ $M^+$ ], Found 287.07 [ $M^+ + 1$ ], 309.07 [ $M^+ + Na$ ]; Anal. calcd for  $C_{14}H_{14}O_3Fe$ : C, 58.74; H, 4.89, Found: C, 58.38; H, 4.94.

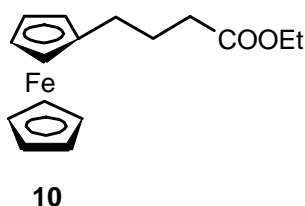
**1-(3-Carboxypropyl)ferrocene (9):** Experimental procedure is same as that for **5**. The



only difference is here acetic acid was used instead of ethanol. Yellow powder: mp 115-116 °C (ethyl acetate/pet ether). Yield 90 %.  $^1H$ -NMR ( $CDCl_3$ , 200 MHz)  $\delta$ : 1.92-1.78 (m, 2H), 2.43-2.36 (m, 4H), 4.06 (s, 4H), 4.11 (s, 5H).  $^{13}C$  NMR ( $CDCl_3$ , 50 MHz)  $\delta$ : 25.9, 28.8, 33.7, 67.3, 68.1, 68.5,

88.0, 179.9; MS (LC-MS): ( $m/z$ ) Calcd for  $C_{14}H_{16}O_2Fe$  272.12 [ $M^+$ ], Found 272.13 [ $M^+$ ], 295.04 [ $M^+ + Na$ ]; Anal. calcd for  $C_{14}H_{16}O_2Fe$ : C, 61.76; H, 5.88, Found: C, 61.88; H, 5.94.

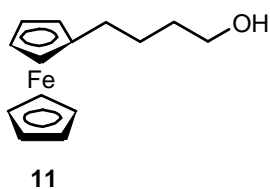
**1-(3-Carbethoxypropyl)ferrocene (10):** Experimental procedure and set up is same as



**4(B)**. Reddish-yellow oil: Yield 95 %.  $^1H$ -NMR ( $CDCl_3$ , 200 MHz)  $\delta$ : 1.27 (t, 3H,  $J = 6.7$  Hz), 1.92-1.77 (m, 2H), 2.42-2.29 (m, 4H), 4.07 (bs, 4H), 4.11 (s, 5H), 4.16 (m, 2H).  $^{13}C$  NMR ( $CDCl_3$ , 50 MHz)  $\delta$ : 14.1, 25.9, 28.7, 33.7, 59.9, 67.1, 68.0, 68.4, 88.1, 173.1; MS (LC-MS): ( $m/z$ )

Calcd for  $C_{16}H_{20}O_2Fe$  300.17 [ $M^+$ ], Found 300.24 [ $M^+$ ], 323.25 [ $M^+ + Na$ ]; Anal. calcd for  $C_{16}H_{20}O_2Fe$ : C, 64.0; H, 6.67, Found: C, 64.21; H, 6.35.

**1-(4-Hydroxybutyl)ferrocene (11):** Experimental procedure and set up is same as **6**.

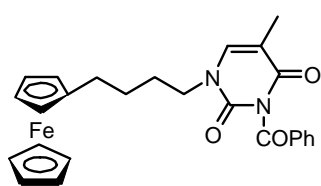


Reddish-yellow oil: Yield 93 %.  $^1H$ -NMR ( $CDCl_3$ , 200 MHz)  $\delta$ : 1.62-1.56 (m, 4H), 2.38 (t, 2H,  $J = 7.3$  Hz), 3.64 (t, 2H,  $J = 6.7$  Hz), 4.07 (s, 4H), 4.12 (s, 5H).  $^{13}C$  NMR ( $CDCl_3$ , 50 MHz)  $\delta$ : 27.1, 29.2, 32.5, 62.5, 67.1, 68.1, 68.5, 89.1; MS (LC-MS):

( $m/z$ ) Calcd for  $C_{14}H_{18}OFe$  258.14 [ $M^+$ ], Found 258.15 [ $M^+$ ]; Anal. calcd for  $C_{14}H_{18}OFe$ : C, 65.11; H, 6.97, Found: C, 64.73; H, 7.19.

**General procedure for the preparation of 12a-b via Mitsunobu reaction:** The experimental procedure employed was same as for Mitsunobu reaction. The following quantities of reagents were used. *N*3-benzoylthymine/*N*3-benzoyluracil (4.03 mmol), triphenylphosphine (1.22 g, 4.65 mmol), alcohol **11** (0.80 g, 3.10 mmol), DIAD (0.92 mL, 4.65 mmol). The resulting solid was purified by flash column using pet ether / ethyl acetate (4:1) to give ferrocene linked *N*3-benzoylprotected nucleobase **12a-b**.

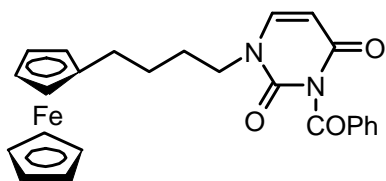
**1-(4-(*N*3-Benzoylthyminy)butyl)ferrocene (12a):** Yellow needles: Yield 68 %. mp



12a

142-143 °C; IR (thin film): 1745, 1697, 1650  $\text{cm}^{-1}$ ;  $^1\text{H}$ -NMR ( $\text{CDCl}_3$ , 200 MHz)  $\delta$ : 1.55 (m, 2H), 1.74 (m, 2H), 1.97 (s, 3H), 2.41 (t, 2H), 3.73 (t, 2H), 4.10 (s, 4H), 4.14 (s, 5H), 7.10 (s, 1H), 7.52 (t, 2H,  $J = 8$  Hz), 7.68 (t, 1H,  $J = 8$  Hz), 7.95 (d, 2H,  $J = 8$  Hz);  $^{13}\text{C}$ -NMR( $\text{CDCl}_3$ , 50 MHz)  $\delta$ : 12.2, 27.9, 28.6, 29.0, 48.4, 67.3, 68.1, 68.6, 88.3, 110.4, 129.0, 130.2, 131.7, 134.7, 140.1, 149.7, 163.0, 169.1; MS (LC-MS): ( $m/z$ ) Calcd for  $\text{C}_{26}\text{H}_{26}\text{N}_2\text{O}_3\text{Fe}$  470.34 [ $\text{M}^+$ ], Found 471.19 [ $\text{M}^+ + 1$ ], 493.16 [ $\text{M}^+ + \text{Na}$ ]; Anal. calcd for  $\text{C}_{26}\text{H}_{26}\text{N}_2\text{O}_3\text{Fe}$ : C, 66.38; H, 5.53; N, 5.95, Found: C, 65.75; H, 5.47; N, 5.85.

**1-(4-(*N*3-Benzoyluracily)butyl)ferrocene (12b):** Brown oil: Yield 57 %. IR (thin

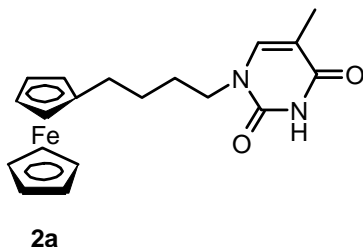


12b

film): 1747, 1703, 1660  $\text{cm}^{-1}$ ;  $^1\text{H}$ -NMR ( $\text{CDCl}_3$ , 200 MHz)  $\delta$ : 1.55-1.43 (m, 2H), 1.84-1.66 (m, 2 H), 2.46-2.27 (m, 2H), 3.72 (t, 2H,  $J = 6.4$  Hz), 4.12 (s, 9H), 5.78 (d, 1H,  $J = 7.2$  Hz), 7.19 (d, 2H,  $J = 7.4$  Hz), 7.52-7.45 (m, 2H), 7.68-7.61 (m, 1 H), 7.92 (d, 2H,  $J = 7.2$  Hz);  $^{13}\text{C}$ -NMR( $\text{CDCl}_3$ , 50 MHz)  $\delta$ : 28.0, 28.6, 29.1, 48.9, 67.2, 68.1, 68.5, 88.0, 101.9, 129.1, 130.3, 131.5, 135.0, 144.1, 149.7, 162.4, 168.8; MS (LC-MS): ( $m/z$ ) Calcd for  $\text{C}_{26}\text{H}_{26}\text{N}_2\text{O}_3\text{Fe}$  456.32 [ $\text{M}^+$ ], Found 456.10 [ $\text{M}^+$ ], 479.09 [ $\text{M}^+ + \text{Na}$ ].

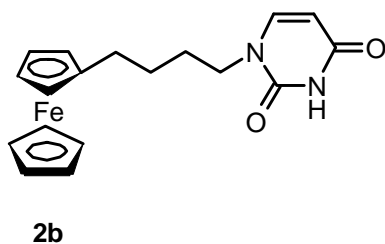
**General procedure for debenzoylation for preparation of 2a-b:** Experimental procedure and set up is same as **1a-b**.

**1-(4-(Thyminyl)butyl)ferrocene (2a):** Yellow needle: Yield 94 %; mp 199-200 °C (ethyl acetate/pet ether); IR (thin film): 3149, 1704,



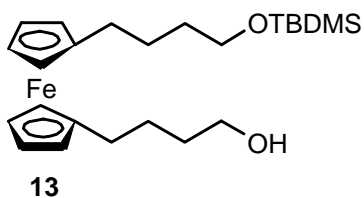
1666  $\text{cm}^{-1}$ ;  $^1\text{H-NMR}$  ( $\text{CDCl}_3$ , 200 MHz)  $\delta$ : 1.52-1.42(m, 2H), 1.76-1.61(m, 2H), 2.35(t, 2H), 3.66 (t, 2H), 4.12 (s, 9H), 6.92(s, 1H), 8.71(s, 1H); MS (LC-MS): ( $m/z$ ) Calcd for  $\text{C}_{19}\text{H}_{22}\text{N}_2\text{O}_2\text{Fe}$  366.24 [ $\text{M}^+$ ], Found 366.32 [ $\text{M}^+$ ]; Anal. calcd for  $\text{C}_{19}\text{H}_{22}\text{N}_2\text{O}_2\text{Fe}$ : C, 62.29; H, 6.01; N, 7.65, Found: C, 62.00; H, 6.06; N, 7.66.

**1-(4-(Uracilyl)butyl)ferrocene (2b):** Orange needles: Yield 95 %; mp 146-147 °C (ethyl acetate/pet ether); IR (thin film): 1747, 1703,



1665  $\text{cm}^{-1}$ ;  $^1\text{H-NMR}$  ( $\text{CDCl}_3$ , 200 MHz)  $\delta$ : 1.55-1.43 (m, 2H), 1.75-1.64 (m, 2H), 2.42-2.31 (m, 2H), 3.72-3.65(m, 2H), 4.13 (s, 9H), 5.66 (d, 1H,  $J = 8$  Hz), 7.09 (d, 1H,  $J = 8$  Hz), 8.49 (s, 1H);  $^{13}\text{C}$  NMR ( $\text{CDCl}_3$ , 50 MHz)  $\delta$ : 28.0, 28.7, 29.2, 48.6, 67.2, 68.1, 68.4, 88.1, 102.1, 144.3, 150.9, 164.0; MS (LC-MS): ( $m/z$ ) Calcd for  $\text{C}_{18}\text{H}_{20}\text{N}_2\text{O}_2\text{Fe}$  352.21 [ $\text{M}^+$ ], Found 352.05 [ $\text{M}^+$ ]; Anal. calcd for  $\text{C}_{18}\text{H}_{20}\text{N}_2\text{O}_2\text{Fe}$ : C, 61.36; H, 5.68; N, 7.95, Found: C, 61.53; H, 5.52; N, 7.62.

**1-(4-Hydroxybutyl)-1'-(4-(tert-butyl)dimethylsilyloxy)butylferrocene (13):**

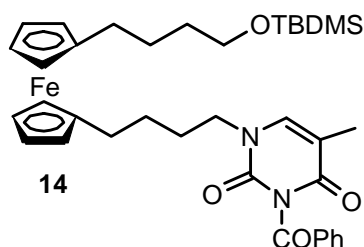


Compound **6** (0.68 g, 2.06 mmol), imidazole (0.42 g, 6.18 mmol) and  $\text{AgNO}_3$  (0.17 g, 1.03 mmol) were dissolved in DCM (20 mL) and the resulting mixture was stirred at 0 °C. Then TBDMSCl (0.34 g, 2.266 mmol) in DCM (10 mL) was added dropwise and the

reaction mixture was allowed to come at rt and stirred overnight. The reaction mixture was extracted with DCM ( $3 \times 20$  mL) and the combined organic layer was washed with water and brine, dried over  $\text{Na}_2\text{SO}_4$  and concentrated. The crude product was

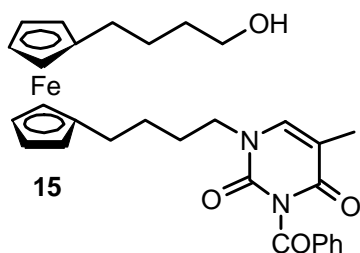
chromatographed on a silica gel column, packing with pet ether/triethylamine (98:2) and eluted with ethyl acetate/pet ether (1:19) to give compound **13** (515 mg, 56 %). Reddish-yellow oil: Yield 56 %.  $^1\text{H-NMR}$  ( $\text{CDCl}_3$ , 200 MHz)  $\delta$ : 0.04 (s, 6H), 0.89 (s, 9H), 1.27 (br s, 1H), 1.69-1.37 (m, 8H), 2.39-2.16 (m, 4H), 3.70-3.51 (m, 4H), 4.01 (s, 8H).  $^{13}\text{C}$  NMR( $\text{CDCl}_3$ , 50 MHz)  $\delta$ : -5.3, 18.3, 26.0, 27.4, 29.2, 29.2, 32.6, 32.7, 62.8, 63.1, 67.66, 67.72, 68.6, 88.8, 89.2; MS (LC-MS): ( $m/z$ ) Calcd for  $\text{C}_{24}\text{H}_{40}\text{O}_2\text{SiFe}$  444.51 [ $\text{M}^+$ ], Found 444.30 [ $\text{M}^+$ ].

**1-(4-(*N*3-Benzoylthyminy)butyl)-1'-(4-(*tert*-butyldimethylsilyloxy)butyl)ferrocene**



**(14)**. Experimental procedure and set up is same as Mitsunobu reaction. The quantities of reagents used are as follow. *N*3-benzoylthymine (0.70 g, 3.03 mmol), triphenylphosphine (0.92 g, 3.50 mmol), alcohol **13** (1.03 g, 2.33 mmol), DIAD (0.69 mL, 3.50 mmol). The resulting solid was purified by flash chromatography on silica gel, eluted with ethyl acetate/pet ether (1:4) to give ferrocene linked benzoyl protected nucleobase **14** (1.05 g, 69 %). Brown oil: Yield 69 %. IR (KBr): 1747, 1697, 1658  $\text{cm}^{-1}$ .  $^1\text{H-NMR}$  ( $\text{CDCl}_3$ , 200 MHz)  $\delta$ : 0.04 (s, 6H), 0.88 (s, 9H), 1.57-1.45 (m, 6H), 1.78-1.64 (m, 2H), 1.94 (s, 3H), 2.43-2.21 (m, 4H), 3.60 (t, 2H,  $J = 5.4$  Hz), 3.69 (t, 2H,  $J = 7$  Hz), 3.97 (s, 8H), 7.02 (s, 1H), 7.51-7.43 (m, 2H), 7.67-7.59 (m, 1H), 7.90 (d, 2H,  $J = 7.3$  Hz).  $^{13}\text{C}$  NMR ( $\text{CDCl}_3$ , 50 MHz)  $\delta$ : -5.3, 12.3, 18.3, 21.9, 25.9, 27.4, 28.2, 28.6, 29.0, 29.1, 32.7, 48.6, 63.0, 67.7, 67.9, 68.6, 87.9, 89.2, 110.5, 129.1, 130.3, 131.6, 134.9, 140.1, 149.7, 163.1, 169.1; MS (LC-MS): ( $m/z$ ) Calcd for  $\text{C}_{36}\text{H}_{48}\text{N}_2\text{O}_4\text{SiFe}$  656.71 [ $\text{M}^+$ ], Found 656.25 [ $\text{M}^+$ ], 679.24 [ $\text{M}^+ + \text{Na}$ ].

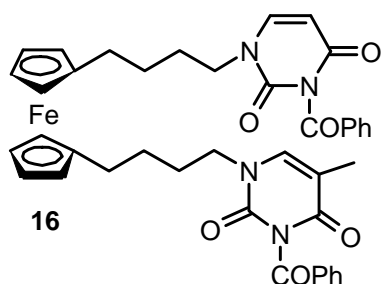
**1-(4-(*N*3-Benzoylthyminy)butyl)-1'-(4-hydroxybutyl)ferrocene (15)**. To a stirred,



cooled (0-5 °C) solution of **14** (0.29 g, 0.44 mmol) in THF (5 mL) was added 1M solution of TBAF (1.3 mL, 1.32 mmol) in THF and the resulting mixture was stirred at 0-5 °C for 3 h. Solvent was removed under reduced pressure and extracted with DCM (3 × 10 mL). The combined organic layer was washed with water,

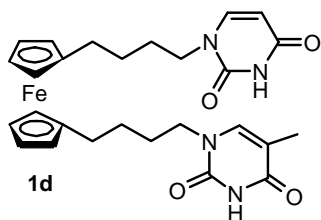
brine, dried over  $\text{Na}_2\text{SO}_4$  and concentrated. The crude product was chromatographed on a silica gel column, packing with pet ether/triethylamine (98:2) and eluted with ethyl acetate/pet ether (1:1) as eluent to give compound **15** (170 mg). Brown oil: Yield 71 %. IR (KBr): 3431, 1747, 1697, 1650  $\text{cm}^{-1}$ .  $^1\text{H-NMR}$  ( $\text{CDCl}_3$ , 200 MHz)  $\delta$ : 1.56-1.34 (m, 4H), 1.81-1.61 (m, 4H), 1.93 (s, 3H), 2.34-2.16 (m, 4H), 3.61-3.47 (m, 2H), 3.67 (t, 2H,  $J = 6.95$  Hz), 4.10 (s, 8H), 7.02 (s, 1H), 7.51-7.43 (m, 2H), 7.67-7.60 (m, 1H), 7.89 (d, 2H,  $J = 7.7$  Hz).  $^{13}\text{C NMR}$  ( $\text{CDCl}_3$ , 50 MHz)  $\delta$ : 12.3, 27.3, 28.1, 28.6, 28.9, 29.1, 32.5, 48.5, 62.6, 67.7, 67.9, 68.6, 88.0, 89.0, 110.5, 129.1, 130.3, 131.6, 134.9, 140.1, 149.8, 163.1, 169.1; MS (LC-MS): ( $m/z$ ) Calcd for  $\text{C}_{30}\text{H}_{34}\text{N}_2\text{O}_4\text{Fe}$  542.46 [ $\text{M}^+$ ], Found 542.14 [ $\text{M}^+$ ], 565.14 [ $\text{M}^+ + \text{Na}$ ].

**1-(4-(*N*3-Benzoylthyminy)butyl)-1'-(4-(*N*3-benzoyluracily)butyl)ferrocene (16).**



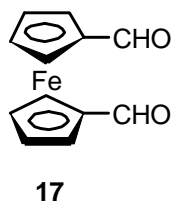
Experimental procedure and set up is same as Mitsunobu reaction. The quantities of reagents used are as follow. *N*3-benzoyluracil (0.17 g, 0.78 mmol), triphenylphosphine (0.24 g, 0.90 mmol), alcohol **15** (0.32 g, 0.60 mmol), DIAD (0.18 mL, 0.90 mmol). The resulting solid was purified by flash chromatography on silica gel, eluted with pet ether/ethyl acetate (7:3) to give ferrocene linked *N*3-benzoylprotected nucleobase **16**. Yellow foam: Yield 68 %. IR (thin film): 1747, 1699, 1660  $\text{cm}^{-1}$ .  $^1\text{H-NMR}$  ( $\text{CDCl}_3$ , 200 MHz)  $\delta$ : 1.53-1.38 (m, 4H), 1.77-1.62 (m, 4H), 1.93 (s, 3H), 2.36-2.15 (m, 4H), 3.76-3.62 (m, 4H), 4.06 (br s, 8H), 5.76 (d, 1H,  $J = 7.8$  Hz), 7.03 (s, 1H), 7.20 (d, 2H,  $J = 7.8$  Hz), 7.54-7.41 (m, 4H), 7.69-7.58 (m, 2H), 7.96-7.85 (m, 4H).  $^{13}\text{C NMR}$  ( $\text{CDCl}_3$ , 50 MHz)  $\delta$ : 12.2, 27.9, 28.5, 28.6, 28.8, 48.4, 48.8, 68.0, 68.8, 88.2, 88.3, 101.8, 110.4, 129.1, 129.1, 130.3, 131.4, 131.6, 134.9, 135.0, 140.2, 144.3, 149.7, 149.7, 162.4, 163.1, 168.9, 169.2; MS (MALDI-TOF): ( $m/z$ ) Calcd for  $\text{C}_{41}\text{H}_{40}\text{N}_4\text{O}_6\text{Fe}$  740.63 [ $\text{M}^+$ ], Found 740.03 [ $\text{M}^+$ ].

**1-(4-(Thyminy)butyl)-1'-(4-(uracily)butyl)ferrocene (1d).** Experimental procedure and set up is same as **1a-b**. Yellow needle: mp 162-164 °C (DCM/methanol/toluene). Yield 82 %. IR (thin film): 3184, 1697, 1674  $\text{cm}^{-1}$ .  $^1\text{H-NMR}$  ( $\text{CDCl}_3 + 3-4$  drops of  $\text{DMSO-}d_6$ , 200 MHz)  $\delta$ : 1.52-1.42 (m, 4H), 1.75-1.60 (m, 4H), 1.88 (s, 3H), 2.33-2.20



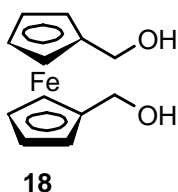
(m, 4H), 3.70-3.61 (m, 4H), 4.04 (br s, 8H), 5.62 (dd, 1H,  $J = 2$  Hz &  $J = 7.8$  Hz), 6.95 (s, 1H), 7.13 (d, 1H,  $J = 7.8$  Hz), 9.93 (br s, 1H), 10.06 (br s, 1H).  $^{13}\text{C}$  NMR (DMSO- $d_6$ , 50 MHz)  $\delta$ : 12.1, 27.7, 28.5, 47.2, 47.5, 67.7, 68.6, 88.56, 88.60, 101.0, 108.6, 141.7, 145.9, 151.1, 151.2, 164.0, 164.5; MS (LC-MS): ( $m/z$ ) Calcd for  $\text{C}_{27}\text{H}_{32}\text{N}_4\text{O}_4\text{Fe}$  532.42 [ $\text{M}^+$ ], Found 532.13 [ $\text{M}^+$ ], 555.13 [ $\text{M}^+ + \text{Na}$ ]; Anal. calcd for  $\text{C}_{27}\text{H}_{32}\text{N}_4\text{O}_4\text{Fe}$ : C, 60.90; H, 6.05; N, 10.52; Found: 60.58, 6.05, 10.33.

**1,1'-Ferrocenecarboxaldehyde 17.** The reaction was carried out in a Schlenk-type apparatus under argon. Ferrocene (5 g, 26 mmol) in dry ether (60



mL) was treated with 1.6 M solution of *n*-butyllithium (35.3 mL, 56 mmol) in hexane and subsequent addition of *N,N,N',N'*-tetramethylethylenediamine (TMEDA) (8.5 mL, 56 mmol). The reaction mixture was stirred for 20 h, and then dry DMF (6.5 mL) was added drop wise at  $-78$  °C. After 2 h stirring, the mixture was hydrolyzed at  $-78$  °C. The organic phase was extracted with dichloromethane, dried over  $\text{MgSO}_4$ , and concentrated which was recrystallized from cyclohexane to give 1,1'-ferrocenecarboxaldehyde **17** as shiny red crystals. Yield 70%; mp  $154$ - $156$  °C (cyclohexane);  $^1\text{H}$  NMR ( $\text{CDCl}_3$ , 200 MHz)  $\delta$  4.67 (s, 4H), 4.89 (s, 4H), 9.95 (s, 2H); MS (LC-MS) ( $m/z$ ) Calcd for  $\text{C}_{12}\text{H}_{10}\text{O}_2\text{Fe}$  242.06 [ $\text{M}^+$ ], Found 243.15 [ $\text{M}^+ + 1$ ], 265.15 [ $\text{M}^+ + \text{Na}$ ]; Anal. calcd for  $\text{C}_{12}\text{H}_{10}\text{O}_2\text{Fe}$ : C, 59.54; H, 4.16; Found: C, 59.47; H, 4.32.

**1,1'-Bis(hydroxymethyl)ferrocene 18.** The dialdehyde **1** (1.55 g, 6.4 mmol) in distilled MeOH (25 mL) was stirred at  $0$  °C for 10 min and  $\text{NaBH}_4$  (0.54 g,

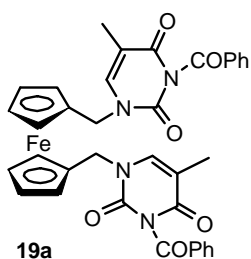


14.1 mmol) was added portion wise at such a rate that temperature should not go above  $0$  °C. The reaction mixture was stirred for 1 h at room temperature. The solvent was removed under reduced pressure and the residual material was extracted with ethyl acetate (3 x 75 mL). The combined organic phase were washed with brine solution, dried over  $\text{Na}_2\text{SO}_4$ , and concentrated. The crude product was chromatographed on a silica gel column with ethyl acetate/petroleum ether (2:3) as eluent to give **18** as yellow solid, which was

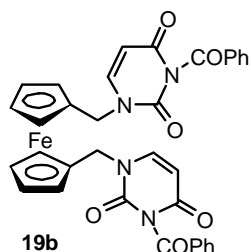
recrystallized from ethyl acetate/petroleum ether to give **18** as Yellow needles. Yield 84%; mp 106-108 °C (ethyl acetate/petroleum ether);  $^1\text{H}$  NMR ( $\text{CDCl}_3$ , 200 MHz)  $\delta$  3.54 (s, 2H), 4.19 (s, 4H), 4.22 (s, 4H), 4.40 (s, 4H);  $^{13}\text{C}$  NMR ( $\text{CDCl}_3$ , 50 MHz)  $\delta$  60.2, 66.9, 67.9, 89.3; MS (LC-MS) ( $m/z$ ) Calcd for  $\text{C}_{12}\text{H}_{14}\text{O}_2\text{Fe}$  246.08 [ $\text{M}^+$ ], Found 246.08 [ $\text{M}^+$ ]; Anal. calcd for  $\text{C}_{12}\text{H}_{14}\text{O}_2\text{Fe}$ : C, 58.57; H, 5.73; Found: C, 58.49; H, 5.81.

**General procedure for the preparation of 19a and 19b via Mitsunobu reaction:** *N*3-Benzoylthymine/*N*3-benzoyluracil (3.75 mmol) and triphenylphosphine (1.18 g, 4.5 mmol) were dissolved in dry THF (25 mL) and the solution was cooled to 0 °C. At this temperature alcohol **18** (0.37 g, 1.5 mmol), dissolved in dry THF (10 mL), was added to the stirred solution followed by drop wise addition of DIAD (0.9 mL, 4.5 mmol). The solution was allowed to gradually reach room temperature and stirring was continued overnight. The solvent was removed under reduced pressure and resulting solid was purified by flash chromatography on silica gel, packing with petroleum ether/triethylamine (98:2) and eluting with petroleum ether/ethyl acetate (1:1) to give ferrocene-linked *N*3-benzoylprotected nucleobases **19a** and **19b**.

**1,1'-Bis(*N*3-benzoylthyminylmethyl)ferrocene 19a.** Yellow needle; Yield 56%; mp 146-148 °C (DCM); IR (nujol) 1741, 1697, 1651  $\text{cm}^{-1}$ ;  $^1\text{H}$  NMR ( $\text{CDCl}_3$ , 500 MHz)  $\delta$  1.91 (s, 6H), 4.23 (s, 4H), 4.28 (s, 4H), 4.66 (s, 4H), 7.07 (s, 2H), 7.53-7.45 (m, 4H), 7.70-7.61 (m, 2H), 7.89-7.94 (m, 4H);  $^{13}\text{C}$  NMR ( $\text{CDCl}_3$ , 125 MHz)  $\delta$  12.4, 14.2, 47.1, 69.8, 82.3, 110.9, 129.1, 130.4, 131.6, 135.0, 139.2, 149.9, 162.9, 169.1; MS (LC-MS) ( $m/z$ ) Calcd for  $\text{C}_{36}\text{H}_{30}\text{N}_4\text{O}_6\text{Fe}$  670.50 [ $\text{M}^+$ ], Found 670.14 [ $\text{M}^+$ ]; Anal. calcd for  $\text{C}_{36}\text{H}_{30}\text{N}_4\text{O}_6\text{Fe}$ : C, 64.49; H, 4.51; N, 8.35; Found: C, 64.41; H, 4.63; N, 8.29.



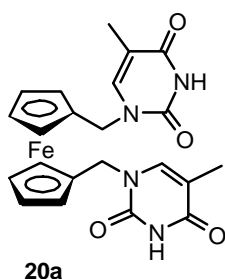
**1,1'-Bis(*N*3-benzoyluracilylmethyl)ferrocene 19b.** Yellow needle; Yield 58%; mp 223-225 °C (melt and decomp) (DCM); IR (nujol) 1745, 1699, 1651  $\text{cm}^{-1}$ ;  $^1\text{H}$  NMR ( $\text{CDCl}_3$ , 500 MHz)  $\delta$  4.25 (s, 4H), 4.28 (s, 4H), 4.68 (s, 4H), 5.75 (d, 2H,  $J = 8.3$  Hz), 7.22 (d, 2H,  $J = 7.8$  Hz), 7.52-7.48 (m, 4H), 7.67-7.64 (m, 2H), 7.93-7.91 (m, 4H);  $^{13}\text{C}$  NMR ( $\text{CDCl}_3$ , 125 MHz)  $\delta$  47.4, 70.4, 81.9, 102.3, 129.2, 130.5, 131.4, 135.2, 143.1,



149.9, 162.2, 168.8; MS (LC-MS) ( $m/z$ ) Calcd for  $C_{34}H_{26}N_4O_6Fe$  642.45 [ $M^+$ ], Found 642.03 [ $M^+$ ]; Anal. calcd for  $C_{34}H_{26}N_4O_6Fe$ : C, 63.56; H, 4.08; N, 8.72; Found: C, 63.39; H, 4.21; N, 8.66.

**General procedure for debenzoylation for preparation of 20a and 20b:** To a stirred solution of dibenzoyl derivative of **19a** and **19b** (0.3 mmol) in a THF:methanol:H<sub>2</sub>O mixture (1:1:0.05, 100 mL) was added K<sub>2</sub>CO<sub>3</sub> (0.34 g, 2.4 mmol). The resultant mixture was then stirred at room temperature overnight. The solvent was removed under reduced pressure and the residual material was extracted with DCM/methanol (30:1, 3 x 50 mL). The combined organic phase were washed with brine solution, dried over Na<sub>2</sub>SO<sub>4</sub>, and concentrated to give crude ferrocene-linked nucleobases **20a** and **20b**. The crude products were recrystallized from the appropriate solvent.

**1,1'-Bis(thyminylmethyl)ferrocene 20a.** Yellow needle; Yield 86%; mp 250 °C



(decomp) (DCM/methanol); IR (nujol) 3153, 1681, 1668 cm<sup>-1</sup>;

<sup>1</sup>H NMR (DMSO-*d*<sub>6</sub>, 500 MHz)  $\delta$  1.77 (s, 6H), 4.42 (s, 4H),

4.37 (s, 4H), 4.61 (s, 4H), 7.61 (s, 2H); <sup>13</sup>C NMR (DMSO-*d*<sub>6</sub>,

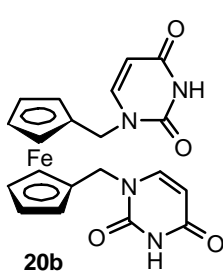
125 MHz)  $\delta$  12.2, 46.1, 69.2, 69.8, 83.7, 108.8, 141.0, 151.1,

164.6; MS (LC-MS) ( $m/z$ ) Calcd for  $C_{22}H_{22}N_4O_4Fe$  462.52 [ $M^+$ ],

Found 485.27 [ $M^+$  + Na]; Anal. calcd for  $C_{22}H_{22}N_4O_4Fe$ : C,

57.13; H, 4.79; N, 12.11; Found: C, 57.33; H, 4.92; N, 12.23.

**1,1'-Bis(uracilylmethyl)ferrocene 20b.** Yellow flakes; Yield 84%; mp 260 °C



(decomp) (DCM/methanol); IR (nujol) 3138, 1697, 1658 cm<sup>-1</sup>; <sup>1</sup>H

NMR (DMSO-*d*<sub>6</sub>, 500 MHz)  $\delta$  4.23 (s, 4H), 4.37 (s, 4H), 4.65 (s,

4H), 5.58 (d, 2H,  $J = 7.8$  Hz), 7.74 (d, 2H,  $J = 7.8$  Hz), 11.28 (br s,

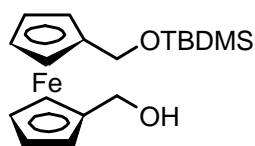
2H); <sup>13</sup>C NMR (DMSO-*d*<sub>6</sub>, 125 MHz)  $\delta$  46.4, 69.3, 69.8, 83.6,

101.2, 145.4, 151.0, 163.9; MS (LC-MS) ( $m/z$ ) Calcd for

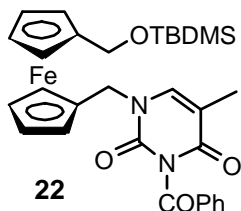
$C_{20}H_{18}N_4O_4Fe$  434.23 [ $M^+$ ], Found 434.30 [ $M^+$ ]; Anal. calcd for

$C_{20}H_{18}N_4O_4Fe$ : C, 55.32; H, 4.18; N, 12.90; Found: C, 55.45; H, 4.32; N, 12.77.

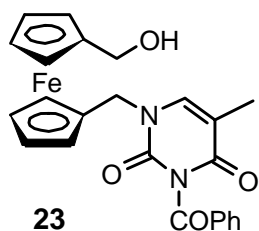


**1-(Hydroxymethyl)-1'-(*tert*-butyldimethylsilyloxymethyl)ferrocene 21.** Alcohol **18****21**

(0.65g, 2.65 mmol), imidazole (0.54 g, 7.95 mmol), and AgNO<sub>3</sub> (0.23 g, 1.33 mmol) were dissolved in DCM (20 mL) and the resulting mixture was stirred at 0 °C. Then TBDMSCl (0.44 g, 2.92 mmol) in DCM (10 mL) was added dropwise and the reaction mixture was allowed to come to room temperature and stirred overnight, then extracted with DCM (3 x 30 mL), and the combined organic layer was washed with water and brine, dried over Na<sub>2</sub>SO<sub>4</sub>, and concentrated. The crude product was chromatographed on a silica gel column, packing with petroleum ether/triethylamine (98:2) and eluted with ethyl acetate/petroleum ether (1:4) to give compound **21** as reddish-yellow oil. Yield 48%; IR (thin film) 3419 cm<sup>-1</sup>; <sup>1</sup>H NMR (CDCl<sub>3</sub>, 200 MHz) δ 0.12 (s, 6H), 0.95 (s, 9H), 4.17-4.13 (m, 8H), 4.32 (d, 2H, *J* = 6.7 Hz), 4.47 (s, 2H); <sup>13</sup>C NMR (CDCl<sub>3</sub>, 50 MHz) δ -5.3, 18.5, 26.0, 60.3, 61.3, 66.7, 67.3, 67.7, 68.2, 88.8, 90.1; MS (LC-MS) (*m/z*) Calcd for C<sub>18</sub>H<sub>28</sub>O<sub>2</sub>SiFe 360.35 [M<sup>+</sup>], Found 360.22 [M<sup>+</sup>]; Anal. calcd for C<sub>18</sub>H<sub>28</sub>O<sub>2</sub>SiFe: C, 59.99; H, 7.83; Found: C, 59.83; H, 7.98.

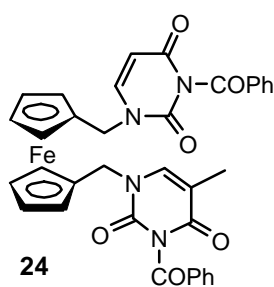
**1-(*N*3-Benzoylthyminylmethyl)-1'-(*tert*-butyldimethylsilyloxymethyl)ferrocene 22.****22**

Experimental procedure is same as Mitsunobu reaction. The quantities of reagents used are as follow. *N*3-benzoylthymine (0.92 g, 3.98 mmol), triphenylphosphine (1.20 g, 4.59 mmol), alcohol **21** (1.1 g, 3.06 mmol), DIAD (0.9 mL, 4.59 mmol). The resulting solid was purified by flash chromatography on silica gel column, packing with petroleum ether/triethylamine (98:2) and eluted with ethyl acetate/pet ether (1:9) to give ferrocene linked benzoyl protected nucleobase **22** as yellow solid. Yield 69%; mp 112-114 °C; IR (thin film) 1747, 1697, 1651 cm<sup>-1</sup>; <sup>1</sup>H NMR (CDCl<sub>3</sub>, 200 MHz) δ 0.06 (s, 6H), 0.91 (s, 9H), 1.88 (s, 3H), 4.12-4.10 (m, 2H), 4.20-4.18 (m, 4H), 4.26-4.24 (m, 2H), 4.41 (s, 2H), 4.67 (s, 2H), 7.50-7.43 (m, 2H), 7.67-7.59 (m, 1H), 7.92-7.87 (m, 2H); <sup>13</sup>C NMR (CDCl<sub>3</sub>, 50 MHz) δ -5.2, 12.5, 18.3, 26.0, 47.4, 60.9, 68.5, 68.6, 69.8, 69.9, 81.1, 89.9, 110.5, 129.1, 130.4, 131.7, 134.9, 138.9, 149.8, 163.0, 169.1; MS (LC-MS) (*m/z*) Calcd for C<sub>30</sub>H<sub>36</sub>N<sub>2</sub>O<sub>4</sub>SiFe 572.55 [M<sup>+</sup>], Found 572.45 [M<sup>+</sup>]; Anal. calcd for C<sub>30</sub>H<sub>36</sub>N<sub>2</sub>O<sub>4</sub>SiFe: C, 62.93; H, 6.33; N, 4.89; Found: C, 62.68; H, 6.52; N, 4.78.

**1-(*N*3-Benzoylthyminylmethyl)-1'-(hydroxymethyl)ferrocene 23.**

(0-5 °C) solution of **22** (0.5 g, 0.87 mmol) in THF (10 mL) was added 1 M solution of TBAF (2.6 mL, 2.61 mmol) in THF and the resulting mixture was stirred at 0-5 °C for 3 h. Solvent was removed under reduced pressure and extracted with DCM (3 x 25 mL). The combined organic layer was washed with water and brine, dried over Na<sub>2</sub>SO<sub>4</sub>, and concentrated. The

crude product was chromatographed on a silica gel column, packed with petroleum ether/triethylamine (98:2), and eluted with ethyl acetate/petroleum ether (3:2) to give compound **23** as yellow foam. Yield 90%; IR (thin film) 3429, 1745, 1695, 1652 cm<sup>-1</sup>; <sup>1</sup>H NMR (CDCl<sub>3</sub>, 200 MHz) δ 1.90 (s, 3H), 4.17-4.19 (m, 2H), 4.23 (s, 4H), 4.31-4.29 (m, 2H), 4.35 (s, 2H), 4.69 (s, 2H), 7.05 (s, 2H), 7.52-7.44 (m, 2H), 7.69-7.60 (m, 1H), 7.93-7.89 (m, 2H); <sup>13</sup>C NMR (CDCl<sub>3</sub>, 125 MHz) δ 12.4, 47.3, 60.4, 68.5, 69.0, 69.4, 69.7, 81.5, 88.9, 110.7, 129.1, 130.4, 131.6, 134.9, 139.0, 149.9, 163.0, 169.1; MS (LC-MS) (*m/z*) Calcd for C<sub>24</sub>H<sub>22</sub>N<sub>2</sub>O<sub>4</sub>Fe 458.29 [M<sup>+</sup>], Found 458.32 [M<sup>+</sup>]; Anal. calcd for C<sub>24</sub>H<sub>22</sub>N<sub>2</sub>O<sub>4</sub>Fe: C, 62.90; H, 4.84; N, 6.11; Found: C, 62.81, H, 4.97, N, 5.98.

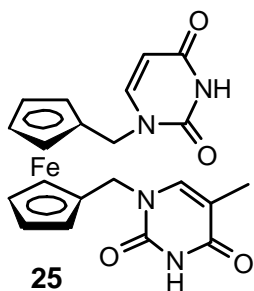
**1-(*N*3-Benzoylthyminylmethyl)-1'-(*N*3-benzoyluracilylmethyl)ferrocene 24.**

Experimental procedure is same as Mitsunobu reaction. The quantities of reagents used are as follow. *N*3-benzoyluracil (0.21 g, 0.99 mmol), triphenylphosphine (0.3 g, 1.14 mmol), alcohol **23** (0.35 g, 0.76 mmol), DIAD (0.23 mL, 1.14 mmol). The resulting solid was purified by flash chromatography on silica gel column, packing with petroleum ether/triethylamine

(98:2) and eluted with pet ether/ethyl acetate (1:4) to give ferrocene linked *N*3-benzoylprotected nucleobase **24** yellow solid. Yield 62%; mp 195-197 °C (DCM); IR (thin film) 1743, 1697, 1662 cm<sup>-1</sup>; <sup>1</sup>H NMR (CDCl<sub>3</sub>, 200 MHz) δ 1.90 (s, 3H), 4.23-4.29 (m, 8H), 4.65 (s, 2H), 4.67 (s, 2H), 5.74 (d, 1H, *J* = 8.0 Hz), 7.06 (s, 1H), 7.23 (d, 1H, *J* = 7.9 Hz), 7.57-7.43 (m, 4H), 7.72-7.61 (m, 2H), 7.98-7.86 (m, 4H); <sup>13</sup>C NMR (CDCl<sub>3</sub>, 50 MHz) δ 12.3, 47.0, 47.3, 69.77, 69.88, 69.93, 70.01, 81.7, 82.2, 101.9, 110.7, 129.11, 129.14, 130.32, 130.34, 131.3, 131.4, 135.05, 135.16, 139.4, 143.4, 149.73, 149.75, 162.3, 162.9, 169.0, 169.2; MS (LC-MS) (*m/z*) Calcd for C<sub>35</sub>H<sub>28</sub>N<sub>4</sub>O<sub>6</sub>Fe 656.47 [M<sup>+</sup>],

Found 655.98 [ $M^+$ ]; Anal. calcd for  $C_{35}H_{28}N_4O_6Fe$ : C, 64.04; H, 4.30; N, 8.53; Found: C, 64.23; H, 4.45; N, 8.49.

**1-(Thyminylmethyl)-1'-(uracilylmethyl)ferrocene 25.** The experimental procedure is



same as that for **20a** and **20b**. Yellow solid; Yield 83%; mp

240 °C (decomp) (DCM); IR (nujol) 3170, 1697, 1674  $cm^{-1}$ ;

$^1H$  NMR (DMSO- $d_6$ , 500 MHz)  $\delta$  1.77 (s, 3H), 4.23 (s, 4H),

4.37 (s, 4H), 5.54 (d, 1H,  $J = 7.7$  Hz), 7.62 (s, 1H), 7.74 (d,

1H,  $J = 7.8$  Hz);  $^{13}C$  NMR (DMSO- $d_6$ , 125 MHz)  $\delta$  12.2, 30.9,

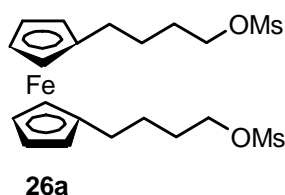
46.1, 46.4, 69.25, 69.28, 69.8, 83.5, 83.7, 101.2, 108.8, 141.1,

145.3, 150.9, 151.0, 163.9, 164.4; MS (LC-MS) ( $m/z$ ) Calcd for  $C_{21}H_{20}N_4O_4Fe$  448.25

[ $M^+$ ], Found 449.29 [ $M^+ + 1$ ], 471.30 [ $M^+ + Na$ ]; Anal. calcd for  $C_{21}H_{20}N_4O_4Fe$ : C,

56.27; H, 4.50; N, 12.50; Found: C, 56.34, H, 4.71, N, 12.66.

**1,1'-Bis(4-(methylsulfonyloxy)butyl)ferrocene 26a.** To a stirred solution of alcohol **6**



(0.33 g, 1.0 mmol) in dry DCM (4 mL) at 0-5 °C were added

$Et_3N$  (0.56 mL, 4.0 mmol) and a solution of mesyl chloride

(0.24 mL, 3.0 mmol) in dry DCM (4 mL). The resulting

mixture was stirred at 0-5 °C for 2 h. The solvent was removed

under reduced pressure and the resulting solid was extracted

with DCM (3  $\times$  15 mL). The combined organic phases were washed with 5 %  $KHSO_4$ ,

water, brine solution, dried over  $Na_2SO_4$  and concentrated. The crude product was

chromatographed on a silica gel column, packing with petroleum ether/triethylamine

(98:2) and eluted with pet ether/ethyl acetate (2:1) to give ferrocene linked mesyl

derivative **26a** as yellow solid. Yellow needles; Yield 89%; mp 64-66 °C (DCM); IR

(thin film) 3085, 3026, 2941, 2860, 1354, 1217, 1174  $cm^{-1}$ ;  $^1H$  NMR ( $CDCl_3$ , 200 MHz)

$\delta$  1.66-1.52 (m, 4H), 1.84-1.70 (m, 4H), 2.36 (t, 2H,  $J = 7.3$  Hz), 2.99 (s, 6H), 3.99 (br s,

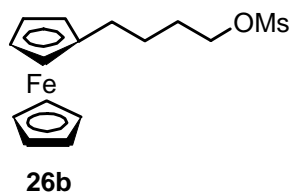
8H), 4.22 (t, 4H,  $J = 6.3$  Hz);  $^{13}C$  NMR ( $CDCl_3$ , 50 MHz)  $\delta$  27.0, 28.7, 37.3, 68.2, 68.9,

69.9, 88.6; MS (LC-MS) ( $m/z$ ) Calcd for  $C_{20}H_{30}O_6S_2Fe$  486.43 [ $M^+$ ], Found 486.67

[ $M^+$ ]; Anal. calcd for  $C_{20}H_{30}O_6S_2Fe$ : C, 49.38; H, 6.22; S, 13.18; Found: C, 49.55; H,

6.51; S, 13.12.

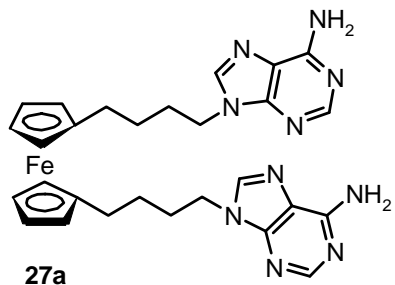
**1-(Methylsulfonyloxybutyl)ferrocene 26b.** The experimental procedure is same as that



for **26a**. The quantities of reagents used are as follow. Alcohol **11** (0.36 g, 1.39 mmol), triethylamine (0.25 mL, 1.81 mmol), mesyl chloride (0.13 mL, 1.67 mmol). The crude product was purified by chromatography on silica gel column, packing with petroleum ether/triethylamine

(98:2) and eluted with ethyl acetate/pet ether (1:15) to give ferrocene linked mesyl derivative **26b**. Yield 93%; mp 41-43 °C (DCM); IR (thin film) 3093, 3026, 2939, 2860, 1352, 1218, 1174  $\text{cm}^{-1}$ ;  $^1\text{H}$  NMR ( $\text{CDCl}_3$ , 200 MHz)  $\delta$  1.67-1.52 (m, 2H), 1.84-1.71 (m, 2H), 2.41-2.33 (m, 2H), 2.99 (s, 3H), 4.12-4.08 (m, 9H), 4.25-4.19 (m, 2H);  $^{13}\text{C}$  NMR ( $\text{CDCl}_3$ , 50 MHz)  $\delta$  26.9, 28.8, 28.9, 37.3, 67.3, 68.2, 68.6, 69.8, 88.4; MS (LC-MS) ( $m/z$ ) calcd for  $\text{C}_{15}\text{H}_{20}\text{O}_3\text{SFe}$  336.23 [ $\text{M}^+$ ], found 336.12 [ $\text{M}^+$ ]; Anal. Calcd for  $\text{C}_{15}\text{H}_{20}\text{O}_3\text{SFe}$ : C, 53.58; H, 5.99; S, 9.54; found: C, 53.72; H, 6.21; S, 9.43.

**1,1'-Bis(4-(adeninyl)butyl)ferrocene 27a.** To a suspension of adenine (0.33 g, 2.42

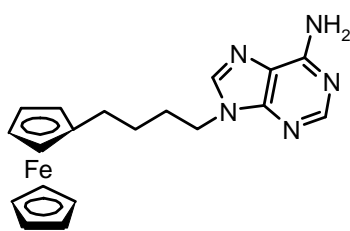


mmol) in DMF (8 mL) at 75 °C was slowly added NaH (0.11 g (60%), 2.75 mmol) and stirred for 30 min. When the formation of sodium salt of nucleobase was complete which was indicated by ceased effervescence, solution of mesyl derivative **26a** (0.54 g, 1.1 mmol) in DMF (8 mL) was added.

After stirring it for 5 h at 75 °C the reaction was allowed to gradually reach room temperature and then quenched with crushed ice. The solvent was removed under reduced pressure and the resulting solid was extracted with ethyl acetate (5 × 50 mL). The combined organic phases were washed with brine solution, dried over  $\text{Na}_2\text{SO}_4$  and concentrated. The crude product was chromatographed on a silica gel column, packing with petroleum ether/triethylamine (98:2) and eluted with ethyl acetate/pet ether (3:1) to give **27a** as yellow solid. Yield 63%; mp 265 °C (decomp); IR (nujol) 3326, 3269, 3147, 1656, 1598, 1571  $\text{cm}^{-1}$ ;  $^1\text{H}$  NMR ( $\text{DMSO}-d_6$  + few drops of  $\text{CD}_3\text{OD}$ , 400 MHz)  $\delta$  1.31-1.24 (m, 4H), 1.72-1.64 (m, 4H), 2.13-2.09 (m, 4H), 3.74-3.71 (m, 8H), 4.00-3.96 (m, 4H), 7.64 (s, 2H), 8.06 (s, 2H);  $^{13}\text{C}$  NMR ( $\text{DMSO}-d_6$  + few drops of  $\text{CD}_3\text{OD}$ , 100 MHz)  $\delta$  27.9, 28.4, 29.3, 43.5, 67.6, 68.3, 87.8, 118.6,

140.1, 149.2, 152.2, 155.2; MS (LC-MS) ( $m/z$ ) Calcd for  $C_{28}H_{32}N_{10}Fe$  564.47 [ $M^+$ ], Found 564.53 [ $M^+$ ]; Anal. calcd for  $C_{28}H_{32}N_{10}Fe$ : C, 59.58; H, 5.71; N, 24.81; Found: C, 59.77; H, 5.82; N, 24.78.

**1-(4-(Adeninyl)butyl)ferrocene 27b.** The experimental procedure is same as that for



**27b**

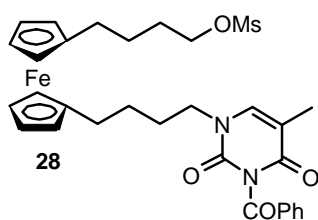
**27a.** The quantities of reagents used are as follow.

Mesyl derivative **26b** (0.47 g, 1.40 mmol), adenine (0.21 g, 1.54 mmol), NaH (0.07 g (60%), 1.68 mmol).

The crude product was purified by chromatography on silica gel column, packing with petroleum ether/triethylamine (98:2) and eluted with ethyl

acetate/pet ether (2:3) to give compound **27b** as orange solid. Recrystallization from ethyl acetate/pet ether gives orange needles. Orange needles; Yield 78%; mp 179-181 °C (ethyl acetate/pet ether); IR (thin film) 3415, 3353, 3321, 1650, 1647, 1635  $cm^{-1}$ ;  $^1H$  NMR ( $CDCl_3$ , 200 MHz)  $\delta$  1.59-1.45 (m, 2H), 1.98-1.84 (m, 2H), 2.39-2.34 (m, 2H), 4.08-4.06 (m, 9H), 4.21-4.16 (m, 2H), 6.34 (s, 2H), 7.78 (s, 1H), 8.33 (s, 1H);  $^{13}C$  NMR ( $CDCl_3$ , 50 MHz)  $\delta$  27.3, 28.1, 29.0, 42.7, 66.3, 67.2, 67.6, 87.5, 118.5, 139.5, 148.9, 151.9, 155.1; MS (LC-MS) ( $m/z$ ) Calcd for  $C_{19}H_{21}N_5Fe$  375.26 [ $M^+$ ], Found 375.89 [ $M^+$ ]; Anal. calcd for  $C_{19}H_{21}N_5Fe$ : C, 60.81; H, 5.64; N, 18.66; Found: C, 60.99; H, 5.88; N, 18.62.

**1-(4-(N3-Benzoylthyminy)butyl)-1'-(4-(methylsulfonyloxy)butyl)ferrocene 28.** The



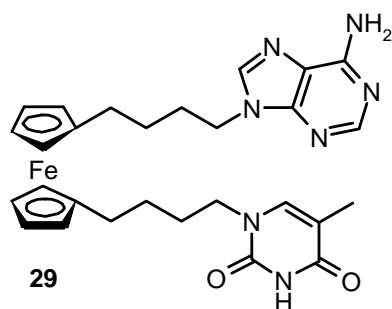
**28**

experimental procedure is same as that for **26a**. The quantities of reagents used are as follow. Alcohol **15** (0.98 g, 1.8 mmol), triethylamine (0.5 mL, 3.6 mmol), mesyl chloride (0.2 mL, 2.7 mmol). The resulting solid was purified by chromatography on silica gel column, packing

with petroleum ether/triethylamine (98:2) and eluted with ethyl acetate/pet ether (2:3) to give compound **28** as reddish-yellow oil. Yield 72%; IR (thin film) 3076, 3014, 2935, 2858, 1747, 1697, 1658, 1650, 1255, 1226, 1174  $cm^{-1}$ ;  $^1H$  NMR ( $CDCl_3$ , 200 MHz)  $\delta$  1.65-1.43 (m, 4H), 1.82-1.69 (m, 4H), 1.95 (s, 3H), 2.39-2.30 (m, 4H), 2.89 (s, 3H), 3.75-3.67 (m, 2H), 4.0 (br s, 8H), 4.24-4.18 (m, 2H), 7.05 (s, 1H), 7.52-7.45 (m, 2H),

7.68-7.61 (m, 1H), 7.93-7.90 (m, 2H);  $^{13}\text{C}$  NMR ( $\text{CDCl}_3$ , 50 MHz)  $\delta$  12.3, 26.9, 28.0, 28.56, 28.60, 28.66, 28.80, 37.2, 48.4, 60.3, 68.1, 68.9, 69.9, 88.5, 110.4, 129.0, 130.2, 131.5, 134.9, 140.2, 149.7, 163.1, 169.1; MS (LC-MS) ( $m/z$ ) Calcd for  $\text{C}_{31}\text{H}_{36}\text{N}_2\text{O}_6\text{SFe}$  620.54 [ $\text{M}^+$ ], Found 620.73 [ $\text{M}^+$ ]; Anal. calcd for  $\text{C}_{31}\text{H}_{36}\text{N}_2\text{O}_6\text{Sfe}$ : C, 60.00; H, 5.85; N, 4.51; S, 5.17; Found: C, 60.23; H, 5.98; N, 4.50; S, 5.08.

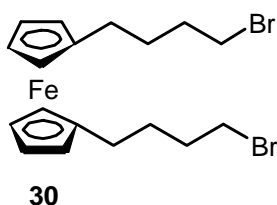
**1-(4-(Thyminyl)butyl)-1'-(4-(adeninyl)butyl)ferrocene 29.** The experimental



procedure is same as that for **27a**. The quantities of reagents used are as follow. Compound **28** (1.1 g, 1.77 mmol), adenine (0.26 g, 1.95 mmol), NaH (0.09 g, 2.30 mmol). The resulting solid was purified by chromatography on silica gel column, packing with petroleum ether/triethylamine (98:2) and eluted with ethyl acetate/pet ether (4:1) to give

compound **29** as yellow solid. Yield 46%; mp 235 °C (decomp); IR (nujol) 3380, 3342, 3259, 3217, 1685, 1681, 1654, 1650, 1598, 1573  $\text{cm}^{-1}$ ;  $^1\text{H}$  NMR ( $\text{DMSO}-d_6$ , 500 MHz)  $\delta$  1.41-1.37 (m, 4H), 1.59-1.53 (m, 2H), 1.75 (s, 3H), 1.85-1.79 (m, 2H), 2.28-2.21 (m, 4H), 3.63-3.61 (m, 2H), 3.93-3.90 (m, 8H), 4.17-4.14 (m, 2H), 7.20 (s, 1H), 7.54 (s, 1H), 8.14 (s, 1H), 8.15 (s, 1H), 11.25 (s, 1H);  $^{13}\text{C}$  NMR ( $\text{DMSO}-d_6$ , 125 MHz)  $\delta$  12.1, 27.7, 27.8, 28.3, 28.45, 28.51, 29.5, 42.9, 47.2, 67.6, 68.4, 68.5, 88.6, 108.6, 118.9, 141.0, 141.7, 149.8, 151.1, 152.5, 156.1, 164.5; MS (LC-MS) ( $m/z$ ) Calcd for  $\text{C}_{28}\text{H}_{33}\text{N}_7\text{O}_2\text{Fe}$  555.46 [ $\text{M}^+$ ], Found 555.46 [ $\text{M}^+$ ]; Anal. calcd for  $\text{C}_{28}\text{H}_{33}\text{N}_7\text{O}_2\text{Fe}$ : C, 60.55; H, 5.99; N, 17.65; Found: C, 60.59; H, 6.10; N, 17.61.

**1, 1'-Bis-(4-bromobutyl)ferrocene 30.** To the cooled mixture of diol **6** (0.5 g, 1.51



mmol) and carbon tetrabromide (3.06 g, 9.24 mmol) in dry DCM (7.5 mL) at 0 °C,  $\text{PPh}_3$  (2.46 g, 9.36 mmol) dissolve in dry DCM (7.5 mL) was added drop by drop. The reaction was stirred at room temperature for 15 h. Ethanol (0.5 mL) was added and the solution was stirred for 2 h. After

completion of reaction, it was concentrated and the crude product was purified by chromatography on silica gel column, packing with petroleum ether and eluted with the ethyl acetate/petroleum ether (1:49) to give compound **30** as reddish yellow oil. Yield

87%; IR (thin film) 825, 808, 769, 738, 669, 651  $\text{cm}^{-1}$ ;  $^1\text{H}$  NMR ( $\text{CDCl}_3$ , 200 MHz)  $\delta$  1.71-1.60 (m, 4H), 1.96-1.81 (m, 4H), 2.34 (t, 4H,  $J = 7.6$  Hz), 3.42 (t, 4H,  $J = 6.7$  Hz), 4.00 (s, 8H);  $^{13}\text{C}$  NMR ( $\text{CDCl}_3$ , 50 MHz)  $\delta$  28.5, 29.6, 32.5, 33.8, 68.00, 68.7, 88.6; MS (LC-MS) ( $m/z$ ) Calcd for  $\text{C}_{18}\text{H}_{24}\text{Br}_2\text{Fe}$  456.04 [ $\text{M}^+$ ], Found 456.19 [ $\text{M}^+$ ].

## 2.8 References

1. Steed, J. W.; Atwood, J. L. In *Supramolecular Chemistry*. Wiley, Chichester, **2000**; J.-M. Lehn, In *Supramolecular Chemistry-Concepts and Perspectives*. VCH, Weinheim, **1995**, Ch. 9.
2. Saenger, W. *Principles of Nucleic Acid Structure*; Springer-Verlag: New York, 1984; Leonard, G. A.; Zhang, S.; Peterson, M. R.; Harrop, S. J.; Helliwell, J. R.; Cruse, W. B.; d' Estaintot, B. L.; Kennard, O.; Brown, T.; Hunter, W. N. *Structure* **1995**, 3 (4), 335-340.
3. (a) Fan, E.; Vicent, C.; Geib, S. J.; Hamilton, A. D. *Chem. Mater.* **1994**, 6, 1113-1117. (b) Cooke, G.; Rotello, V. M. *Chem. Soc. Rev.* **2002**, 31, 275-286.
4. Sivakova, S.; Rowan, S. J. *Chem. Soc. Rev.* **2005**, 34, 9-21.
5. (a) Davis, J. T. *Angew. Chem., Int. Ed.* **2004**, 43, 668-698. (b) Krishnan-Ghosh, Y.; Liu, D.; Balasubramanian, S. *J. Am. Chem. Soc.* **2004**, 126, 11009-11016.
6. White, C. M.; Gonzalez, M. F.; Bradwell, D. A.; Rees, L. H.; Jeffrey, J.; Ward, M. D.; Armaroli, N.; Calogero, G.; Barigelletti, F. *J. Chem. Soc., Dalton Trans.* **1997**, 727-735.
7. Ghodke, H. B.; Krishnan, R.; Vignesh, K.; Pavan Kumar, G. V.; Narayana, C.; Krishnan, Y. *Angew. Chem., Int. Ed.* **2007**, 46, 2646-2649.
8. Sharma, N. K.; Ganesh, K. N. *Chem. Commun.* **2005**, 4330-4332.
9. Sessler, J. L.; Lawrence, C. M.; Jayawickramarajah, J. *Chem. Soc. Rev.* **2007**, 36, 314-325.
10. Paukstelis, P. J.; Nowakowski, J.; Birktoft, J. J.; Seeman, N. C. *Chem. Biol.* **2004**, 11, 1119-1126.
11. Noll, D. M.; Webba da Silva, M.; Noronha, A. M.; Wilds, C. J.; Michael Colvin, O.; Gamesik, M. P.; Miller, P. S. *Biochemistry* **2005**, 44, 6764-6775.
12. Fish, R. H.; Jaouen, G. *Organometallics* **2003**, 22, 2166-2177.

13. Schlotter, K.; Boeckler, F.; Hübner, H.; Gmeiner, P. *J. Med. Chem.* **2005**, *48*, 3696-3699.
14. Pike, A. R.; Ryder, L. C.; Horrocks, B. R.; Clegg, W.; Elsegood, M. R. J.; Connolly, B. A.; Houlton, A. *Chem. Eur. J.* **2002**, *8*, 2891-2899.
15. Van Staveren, D. R.; Metzler-Nolte, N. *Chem. Rev.* **2004**, *104*, 5931-5986.
16. (a) Westwood, J.; Coles, S. J.; Collinson, S. R.; Gasser, G.; Green, S. J.; Hursthouse, M. B.; Light, M. E.; Tucker, J. H. R. *Organometallics* **2004**, *23*, 946-951. (b) Li, C.; Medina, J. C.; Maguire, G. E. M.; Abel, E.; Gokel, G. W. *J. Am. Chem. Soc.* **1997**, *119*, 1609-1618. (c) Inouye, M.; Takase, M. *Angew. Chem., Int. Ed.* **2001**, *40*, 1746-1748.
17. Houlton, A.; Isaac, C. J.; Gibson, A. E.; Horrocks, B. R.; Clegg, W.; Elsegood, M. R. *J. J. Chem. Soc., Dalton Trans.* **1999**, 3229-3234.
18. (a) Patwa, A. N.; Gupta, S.; Gonnade, R. G.; Kumar, V. A.; Bhadbhade, M. M.; Ganesh, K. N. *J. Org. Chem.* **2008**, *73*, 1508-1515. (b) Kumar, J.; Purohit, C. S.; Verma, S. *Chem. Commun.* **2008**, 2526-2528.
19. Deeming, J. In *Comprehensive Organometallic Chemistry, Vol. 4.* (ed.) Wilkinson, G.; Stone, F. G. A. Pergamon, Oxford, **1982**, 475
20. (a) Graham, P. J.; Lindsey, R. V.; Parshall, G. W.; Peterson, M. L.; Whitman, G. M. *J. Am. Chem. Soc.* **1957**, *79*, 3416-3420. (b) Thomson, J. B. *Chem & Ind.*, **1959**, 1122.
21. (a) Cruickshank, K. A.; Jiricny, J.; Reese, C. B.; *Tetrahedron Lett.* **1984**, *25*, 681-684. (b) Rabinowitz, J. L.; Gurin, S. *J. Am. Chem. Soc.*, **1953**, *75*, 5758-5759.
22. Balavoine, G. G. A.; Doisneau, G.; Filleben-Khan, T. *J. Organomet. Chem.* **1991**, *412*, 381-382.
23. MacDonald, J. C.; Whitesides, G. M. *Chem. Rev.* **1994**, *94*, 2383-2420.
24. Ranganathan, A.; Pedireddi, V. R.; Rao, C. N. R. *J. Am. Chem. Soc.* **1999**, *120*, 1752-1753.
25. (a) Ranganathan, A.; Pedireddi, V. R.; Sanjayan, G.; Ganesh, K. N.; Rao, C. N. R. *J. Mol. Struct.* **2000**, *522*, 87-94. (b) Coppens, P.; Vos, A. *Acta Crystallogr.* **1971**, *B27*, 146-158. (c) Pedireddi, V. R.; Ranganathan, A.; Ganesh, K. N. *Org. Lett.* **2001**, *3*, 99-102.



26. (a) Vysabhatar, R.; Ganesh, K. N. *Tetrahedron Lett.* **2008**, *49*, 1314-1318. (b) Koskinen, A. M. P.; Helaja, J.; Kumpulainen, E. T. T.; Koivisto, J.; Mansikkamaki, H.; Rissanen, K. *J. Org. Chem.* **2005**, *70*, 6447-6453.
27. Wahl, M. C.; Rao, S. T.; Sundaralingam, M. *Nature Structural Biology*, **1996**, *3*, 24-31.
28. Moriuchi, T.; Nagai, T.; Hirao, T. *Org. Lett.* **2006**, *8*, 31-34.

## 2.9 Appendix

Sr. No.	Details	Page No.
01	Crystallographic data for <b>1a, 1b, 1c, 1d, 2a, 2b, 20a, 20b, 27b</b>	107-112
02	Crystallographic data for <b>31a (Form I and Form II)</b>	113-114
03	$^1\text{H}$ , $^{13}\text{C}$ and DEPT NMR photocopy of compound <b>4</b>	115
04	$^1\text{H}$ , $^{13}\text{C}$ and DEPT NMR photocopy of compound <b>5</b>	116
05	$^1\text{H}$ , $^{13}\text{C}$ and DEPT NMR photocopy of compound <b>6</b>	117
06	$^1\text{H}$ , $^{13}\text{C}$ and DEPT NMR photocopy of compound <b>7a, 7b, 7c</b>	118-120
07	$^1\text{H}$ , $^{13}\text{C}$ and DEPT NMR photocopy of compound <b>1a, 1b</b>	121-122
08	$^1\text{H}$ NMR photocopy of compound <b>1c</b>	123
09	$^1\text{H}$ NMR photocopy of compound <b>8</b>	123
10	$^1\text{H}$ , $^{13}\text{C}$ and DEPT NMR photocopy of compound <b>9</b>	124
11	$^1\text{H}$ , $^{13}\text{C}$ and DEPT NMR photocopy of compound <b>10</b>	125
12	$^1\text{H}$ , $^{13}\text{C}$ and DEPT NMR photocopy of compound <b>11</b>	126
13	$^1\text{H}$ , $^{13}\text{C}$ and DEPT NMR photocopy of compound <b>12a, 12b</b>	127-128
14	$^1\text{H}$ NMR photocopy of compound <b>2a</b>	129
15	$^1\text{H}$ , $^{13}\text{C}$ and DEPT NMR photocopy of compound <b>2b</b>	130
16	$^1\text{H}$ , $^{13}\text{C}$ and DEPT NMR photocopy of compound <b>13</b>	131
17	$^1\text{H}$ , $^{13}\text{C}$ and DEPT NMR photocopy of compound <b>14</b>	132
18	$^1\text{H}$ , $^{13}\text{C}$ and DEPT NMR photocopy of compound <b>15</b>	133
19	$^1\text{H}$ , $^{13}\text{C}$ and DEPT NMR photocopy of compound <b>16</b>	134
20	$^1\text{H}$ , $^{13}\text{C}$ and DEPT NMR photocopy of compound <b>1d</b>	135
21	$^1\text{H}$ , $^{13}\text{C}$ and DEPT NMR photocopy of compound <b>17</b>	136
22	$^1\text{H}$ , $^{13}\text{C}$ and DEPT NMR photocopy of compound <b>18</b>	137
23	$^1\text{H}$ , $^{13}\text{C}$ and DEPT NMR photocopy of compound <b>19a, 19b</b>	138-139
24	$^1\text{H}$ , $^{13}\text{C}$ and DEPT NMR photocopy of compound <b>20a, 20b</b>	140-141
25	$^1\text{H}$ , $^{13}\text{C}$ and DEPT NMR photocopy of compound <b>21</b>	142
26	$^1\text{H}$ , $^{13}\text{C}$ and DEPT NMR photocopy of compound <b>22</b>	143
27	$^1\text{H}$ , $^{13}\text{C}$ and DEPT NMR photocopy of compound <b>23</b>	144
28	$^1\text{H}$ , $^{13}\text{C}$ and DEPT NMR photocopy of compound <b>24</b>	145
29	$^1\text{H}$ , $^{13}\text{C}$ and DEPT NMR photocopy of compound <b>25</b>	146
30	$^1\text{H}$ , $^{13}\text{C}$ and DEPT NMR photocopy of compound <b>26a, 26b</b>	147-148
31	$^1\text{H}$ , $^{13}\text{C}$ and DEPT NMR photocopy of compound <b>27a, 27b</b>	149-150

<b>Sr. No.</b>	<b>Details</b>	<b>Page No.</b>
32	$^1\text{H}$ , $^{13}\text{C}$ and DEPT NMR photocopy of compound <b>28</b>	151
33	$^1\text{H}$ , $^{13}\text{C}$ and DEPT NMR photocopy of compound <b>29</b>	152
34	$^1\text{H}$ , $^{13}\text{C}$ and DEPT NMR photocopy of compound <b>30</b>	153
35	Mass spectra of <b>4, 5, 6</b>	154
36	Mass spectra of <b>7a, 7b, 7c</b>	155
37	Mass spectra of <b>1a, 1b, 1c</b>	156
38	Mass spectra of <b>8, 9, 10</b>	157
39	Mass spectra of <b>11, 12a, 12b</b>	158
40	Mass spectra of <b>2a, 2b, 13</b>	159
41	Mass spectra of <b>14, 15, 16</b>	160
42	Mass spectra of <b>1d, 17, 18</b>	161
43	Mass spectra of <b>19a, 19b, 20a</b>	162
44	Mass spectra of <b>20b, 21, 22</b>	163
45	Mass spectra of <b>23, 24, 25</b>	164
46	Mass spectra of <b>26a, 26b, 27a</b>	165
47	Mass spectra of <b>27b, 28, 29</b>	166
48	Mass spectra of <b>30</b>	167

**Table 1.1:** Crystal data for compounds **1a**, **1b** and **1c**

Crystal data	<b>1a</b>	<b>1b</b>	<b>1c</b>
Molecular Formula	C <sub>28</sub> H <sub>34</sub> FeN <sub>4</sub> O <sub>4</sub>	C <sub>26</sub> H <sub>30</sub> FeN <sub>4</sub> O <sub>4</sub>	C <sub>26</sub> H <sub>28</sub> Br <sub>2</sub> FeN <sub>4</sub> O <sub>4</sub>
Molecular Mass	546.44	518.39	676.19
Crystal size, mm	0.74 x 0.13 x 0.11	0.71 x 0.12 x 0.11	0.61 x 0.13 x 0.08
Temp. (K)	297(2)	297(2)	297(2)
Crystal system	Orthorhombic	Triclinic	Orthorhombic
Space group	<i>Pccn</i>	<i>P</i> -1	<i>Pccn</i>
<i>a</i> [Å]	14.074(5)	8.403(3)	14.408(4)
<i>b</i> [Å]	14.676(5)	9.705(4)	14.455(4)
<i>c</i> [Å]	13.252(5)	16.496(6)	13.137(4)
$\alpha$ [°]	90	98.201(7)	90
$\beta$ [°]	90	92.759(7)	90
$\gamma$ [°]	90	111.989(7)	90
<i>V</i> [Å <sup>3</sup> ]	2737.1(17)	1227.1(8)	2736.1(14)
<i>Z</i>	4	2	4
<i>F</i> (000)	1152	544	1360
<i>d</i> <sub>calc</sub> [g cm <sup>-3</sup> ]	1.326	1.403	1.642
$\mu$ [mm <sup>-1</sup> ]	0.591	0.655	3.511
Absorption correction	multi-scan	multi-scan	multi-scan
<i>T</i> <sub>min</sub>	0.6690	0.6529	0.2221
<i>T</i> <sub>max</sub>	0.9390	0.9333	0.7665
Reflns. Collected	12686	14903	12682
Unique reflns.	2400	4308	2406
Observed reflns.	1790	2971	1747
Index range (hkl)	(-16,12) (-17,17) (-15,14)	(-9,9) (-11,11) (-19,19)	(-17,17) (-15,17) (-12,15)
<i>R</i> <sub>1</sub> [ <i>I</i> >2 $\sigma$ ( <i>I</i> )]	0.0412	0.0486	0.0420
<i>wR</i> <sub>2</sub>	0.1011	0.0958	0.0964
Goodness-of-fit on <i>F</i> <sup>2</sup>	1.034	1.003	1.017
$\Delta\rho_{max}, \Delta\rho_{min}$ (e Å <sup>-3</sup> )	0.372, -0.169	0.385, -0.191	0.561, -0.253

**Table 1.2:** Crystal data for compounds **1d**, **2a** and **2b**

Crystal data	<b>1d</b>	<b>2a</b>	<b>2b</b>
Molecular Formula	C <sub>27</sub> H <sub>32</sub> FeN <sub>4</sub> O <sub>4</sub>	C <sub>19</sub> H <sub>22</sub> FeN <sub>2</sub> O <sub>2</sub>	C <sub>18</sub> H <sub>20</sub> FeN <sub>2</sub> O <sub>2</sub>
Molecular Mass	531.41	366.24	352.21
Crystal size, mm	0.89 x 0.45 x 0.05	0.32 x 0.23 x 0.05	0.32 x 0.11 x 0.04
Temp. (K)	297(2)	297(2)	297(2)
Crystal system	Orthorhombic	Triclinic	Triclinic
Space group	<i>Pccn</i>	<i>P</i> -1	<i>P</i> -1
<i>a</i> [Å]	13.675(3)	7.588(3)	7.376(2)
<i>b</i> [Å]	14.687(3)	9.813(5)	9.785(3)
<i>c</i> [Å]	13.361(3)	12.300(6)	11.757(3)
$\alpha$ [°]	90	67.192(7)	108.301(5)
$\beta$ [°]	90	89.527(8)	94.061(6)
$\gamma$ [°]	90	86.364(8)	91.481(6)
<i>V</i> [Å <sup>3</sup> ]	2683.6(9)	842.4(7)	802.6(4)
<i>Z</i>	4	2	2
<i>F</i> (000)	1116	384	368
<i>d</i> <sub>calc</sub> [g cm <sup>-3</sup> ]	1.315	1.444	1.457
$\mu$ [mm <sup>-1</sup> ]	0.600	0.908	0.950
Absorption correction	multi-scan	multi-scan	multi-scan
<i>T</i> <sub>min</sub>	0.6174	0.7610	0.7501
<i>T</i> <sub>max</sub>	0.9677	0.9603	0.9630
Reflns. Collected	12682	8042	7510
Unique reflns.	2362	2937	2799
Observed reflns.	1957	2667	2226
Index range (hkl)	(-15,16) (-9,17) (-14,15)	(-9,9) (-11,11) (-14,14)	(-8,8) (-11,11) (-13,13)
<i>R</i> <sub>1</sub> [ <i>I</i> >2 $\sigma$ ( <i>I</i> )]	0.0472	0.0363	0.0587
<i>wR</i> <sub>2</sub>	0.1068	0.0877	0.1163
Goodness-of-fit on <i>F</i> <sup>2</sup>	1.199	1.087	1.124
$\Delta\rho_{max}, \Delta\rho_{min}$ (e Å <sup>-3</sup> )	0.362, -0.153	0.407, -0.164	0.375, -0.252

**Table 1.3:** Crystal data for compounds **5a** and **5b**

Crystal data	20a	20b	27b
Molecular Formula	C <sub>22</sub> H <sub>22</sub> FeN <sub>4</sub> O <sub>4</sub> ·(0.5)O <sub>4</sub>	C <sub>20</sub> H <sub>18</sub> FeN <sub>4</sub> O <sub>4</sub>	C <sub>19</sub> H <sub>21</sub> FeN <sub>5</sub>
Molecular Mass	494.29	434.23	375.26
Crystal size, mm	0.45 x 0.19 x 0.07	0.35 x 0.23 x 0.02	0.65 x 0.13 x 0.03
Temp. (K)	297(2)	297(2)	297(2)
Crystal system	Monoclinic	Monoclinic	Triclinic
Space group	<i>P</i> 2 <sub>1</sub> / <i>n</i>	<i>P</i> 2 <sub>1</sub> / <i>c</i>	<i>P</i> -1
<i>a</i> [Å]	11.529(5)	12.917(10)	7.616(5)
<i>b</i> [Å]	12.016(5)	6.740(5)	11.983(8)
<i>c</i> [Å]	16.731(7)	25.088(16)	19.467(13)
$\alpha$ [°]	90	90	72.428(11)
$\beta$ [°]	109.697(7)	119.87(3)	83.649(12)
$\gamma$ [°]	90	90	86.800(11)
<i>V</i> [Å <sup>3</sup> ]	2182.2(16)	1894(2)	1683(2)
<i>Z</i>	4	4	4
<i>F</i> (000)	1024	896	784
<i>d</i> <sub>calc</sub> [g cm <sup>-3</sup> ]	1.504	1.523	1.481
$\mu$ [mm <sup>-1</sup> ]	0.739	0.832	0.908
Absorption correction	multi-scan	multi-scan	multi-scan
<i>T</i> <sub>min</sub>	0.7322	0.7594	0.5899
<i>T</i> <sub>max</sub>	0.9501	0.9836	0.9733
Reflns. Collected	15270	12958	14249
Unique reflns.	3808	3313	5683
Observed reflns.	3252	2589	3882
Index range (hkl)	(-13,13) (-14,14) (-19,19)	(-15,15) (-8,8) (-29,29)	(-9,9) (-14,14) (-22,23)
<i>R</i> <sub>1</sub> [ <i>I</i> >2 $\sigma$ ( <i>I</i> )]	0.0367	0.0490	0.0679
<i>wR</i> <sub>2</sub>	0.0920	0.1136	0.1243
Goodness-of-fit on <i>F</i> <sup>2</sup>	1.038	1.045	1.001
$\Delta\rho_{max}, \Delta\rho_{min}$ (e Å <sup>-3</sup> )	0.371, -0.294	0.972, -0.380	0.589, -325

**Table 1.4:** Bonds lengths (Å) dihedral angles (°) for intermolecular interactions.

Compound	D-H...A	D-H (Å)	H...A (Å)	D...A (Å)	D-H...A (°)
<b>1a</b>	N3-H3...O2#1	0.79(3)	2.14(3)	2.913(3)	169(3)
	C6-H6...O4#2	0.93	2.38	3.265(4)	160
	C8-H8A...O4#2	0.97	2.71	3.464(3)	135
	C14-H14...O2#3	0.98	2.74	3.515(4)	136
<b>1b</b>	N3-H3...O2#4	0.75(3)	2.17(3)	2.915(4)	176(3)
	N3'-H3'...O4'#5	0.81(3)	2.05(3)	2.845(4)	169(3)
	C6-H6...O2'	0.93	2.29	3.209(4)	171
	C5-H5...O4'#6	0.93	2.41	3.265(4)	152
	C10-H10B...O2#7	0.97	2.72	3.527(4)	141
	C15'-H15'...O4#7	0.93	2.56	3.368(4)	145
C16'-H16'...O4'#6	0.93	2.70	3.565(4)	154	
<b>1c</b>	N3-H3...O2#8	0.70(4)	2.23(4)	2.919(5)	170(5)
	C6-H6...O4#9	0.93(4)	2.27(4)	3.189(5)	168(3)
	C8-H8A...O4#9	0.91(4)	2.72(4)	3.478(5)	141(3)
	C14-H14...O2#10	0.94(4)	2.80(4)	3.523(6)	134(3)
	C10-H10A...Br1#9	0.97(3)	3.00(3)	3.786(4)	139(2)
	C16-H16...Br1#9	0.99(4)	3.02(4)	3.783(4)	135(3)
<b>1d</b>	N3-H3...O2#8	0.76(3)	2.16(3)	2.909(4)	168(3)
	C6-H6...O4#11	0.86(3)	2.45(3)	3.280(4)	164(2)
	C8-H8A...O4#11	0.95(3)	2.65(3)	3.367(4)	132(2)
	C14-H14...O2#12	0.97(4)	2.75(4)	3.453(5)	130(3)

Symmetry transformations used to generate equivalent atoms:

#1 -x+2,-y+2,-z	#2 -x+3/2,y,z+1/2	#3 -x+5/2,y,z+1/2	#4 -x+2,-y+2,-z
#5 -x+3,-y+3,-z+1	#6 -x+2,-y+2,-z+1	#7 -x+5/2,y,z+1/2	#8 -x,-y+1,-z
#9 -x-1/2,y,z-1/2	#10 -x+1/2,y,z-1/2	#11 -x+1/2,y,z+1/2	#12 -x-1/2,y,z+1/2

**Table 1.5:** Bonds lengths (Å) dihedral angles (°) for intermolecular interactions.

Compound	D-H...A	D-H (Å)	H...A (Å)	D...A (Å)	D-H...A (°)
<b>2a</b>	N3-H3...O4#1	0.71(2)	2.14(3)	2.847(3)	175(3)
	C14-H14...O4#2	0.95(3)	2.78(3)	3.424(4)	126(2)
	C13-H13...O2#3	0.87(3)	2.73(3)	3.340(4)	129(2)
	C12'-H12'...O2#4	0.74(3)	2.66(3)	3.363(4)	160(3)
	C13'-H13'...O2#5	0.87(3)	2.74(3)	3.463(4)	141(3)
	C7-H7...N1#6	0.96	2.80	3.705(4)	156.7
<b>2b</b>	C15-H15...O4#2	0.98	2.79	3.445(6)	125.0
	C9-H9A...O4#7	0.97	2.63	3.536(5)	155.9
	C16'-H16'...O2#8	0.98	2.55	3.388(8)	144.0
	C12'-H12'...O2#4	0.98	2.39	3.357(6)	168.7
	C16-H16...O2#9	0.98	2.47	3.312(6)	143.7
	C3-H3...O4#5	0.86	2.02	2.878(4)	172.9

Symmetry transformations used to generate equivalent atoms:

#1 -x-1,-y,-z+2	#2 x+1,y,z-1	#3 -x,-y,-z+1	#4 x+1,y,z
#5 -x,-y+1,-z+1	#6 -x,-y,-z+2	#7 -x+1,-y+1,-z+1	#8 -x+1,-y,-z
#9 -x+1,-y+1,-z			



**Table 1.6:** Bonds lengths (Å) dihedral angles (°) for intermolecular interactions.

Compound	D-H...A	D-H (Å)	H...A (Å)	D...A (Å)	D-H...A (°)
<b>20a</b>	C11A-H11E...O1#1	0.96	2.68	3.600(3)	159.7
	C11-H11B...O2#2	0.96	2.65	3.577(4)	163.7
	C7-H7...O2A#3	0.93	2.20	3.115(3)	167.0
	C7A-H7A...O2#4	0.93	2.18	3.089(3)	165.4
	N2-H2N...O1A#5	0.86	2.03	2.869(3)	165.9
	N2A-H2NA...O1#6	0.86	1.99	2.847(3)	174.9
<b>20b</b>	C7-H7...O1#5	0.93	2.62	3.260(5)	126.5
	C8-H8...O2#7	0.93	2.53	3.321(4)	143.3
	N2-H2N...O2#8	0.86	1.96	2.807(4)	169.8
	C7A-H7A...O1A#6	0.93	2.55	3.247(5)	132.4
	C8A-H8A...O2A#9	0.93	2.57	3.347(4)	141.3
	N2A-H2NA...O2A#10	0.86	2.01	2.853(4)	165.1
<b>27b</b>	N(5)-H(5B)...N(4')#11	0.837(19)	2.31(2)	3.142(5)	175(4)
	N(5)-H(5A)...N(3')#12	0.837(18)	2.34(3)	3.041(5)	142(3)
	C(14)-H(14A)...N(4')#13	0.97	2.74	3.632(5)	152.5
	N(5')-H(5'B)...N(4)#11	0.850(18)	2.23(2)	3.061(5)	166(4)
	N(5')-H(5'A)...N(3)	0.836(18)	2.41(2)	3.174(5)	153(3)
	C(2')-H(2')...N(3)#5	0.93	2.67	3.557(6)	160.7

Symmetry transformations used to generate equivalent atoms:

#1 -x+2,-y+2,-z+1	#2 -x+1,-y+1,-z	#3 x-1/2,-y+5/2,z-1/2
#4 x+1/2,-y+3/2,z+1/2	#5 x,y-1,z	#6 x,y+1,z
#7 -x+1,y-1/2,-z-1/2	#8 -x+1,y+1/2,-z-1/2	#9 -x+2,-y+1,-z+1
#10 -x+2,-y,-z+1	#11 -x+1,-y+2,-z+1	#12 x-1,y+1,z
#13 x-1,y,z		

**Table 1.7:** Crystal data for compounds **31a (Form I and Form II)**

<b>Crystal data</b>	<b>Form I</b>	<b>Form II</b>
Molecular Formula	C <sub>21</sub> H <sub>25</sub> FeN <sub>3</sub> O <sub>3</sub>	C <sub>21</sub> H <sub>25</sub> FeN <sub>3</sub> O <sub>3</sub>
Molecular Mass	423.29	423.29
Crystal size, mm	0.24 x 0.24 x 0.06	0.77 x 0.08 x 0.07
Temp. (K)	297 (2)	297 (2)
Morphology	Blocks	Needles
Crystal system	Triclinic	Monoclinic
Space group	<i>P</i> -1	<i>P</i> 2 <sub>1</sub> / <i>c</i>
<i>a</i> [Å]	5.822(2)	5.8621(9)
<i>b</i> [Å]	9.953(4)	36.209(5)
<i>c</i> [Å]	17.303(7)	26.887(4)
$\alpha$ [°]	101.982(8)	90
$\beta$ [°]	91.486(8)	90.742(4)
$\gamma$ [°]	102.308(8)	90
<i>V</i> [Å <sup>3</sup> ]	955.7(6)	5706.6(15)
<i>Z</i> ' , <i>Z</i>	1, 2	3, 12
<i>F</i> (000)	444	2664
<i>d</i> <sub>calc</sub> [g cm <sup>-3</sup> ]	1.471	1.478
$\mu$ [mm <sup>-1</sup> ]	0.817	0.821
Absorption correction	Multi-scan	Multi-scan
<i>T</i> <sub>min</sub>	0.8268	0.5706
<i>T</i> <sub>max</sub>	0.9526	0.9448
Reflns. Collected	9636	28582
Unique reflns.	3324	9987
Observed reflns.	2471	6570
Index range (hkl)	(-6,6) (-11,11) (-20,20)	(-6,6) (-36,43) (-25,31)
<i>R</i> <sub>1</sub> [ <i>I</i> >2 $\sigma$ ( <i>I</i> )]	0.0478	0.0766
<i>wR</i> <sub>2</sub>	0.0892	0.1266
Goodness-of-fit on <i>F</i> <sup>2</sup>	1.011	1.073
$\Delta\rho_{max}$ , $\Delta\rho_{min}$ (e Å <sup>-3</sup> )	0.318, -0.261	0.524, -0.411

**Table 1.8:** Bonds lengths (Å) dihedral angles (°) for intermolecular interactions.

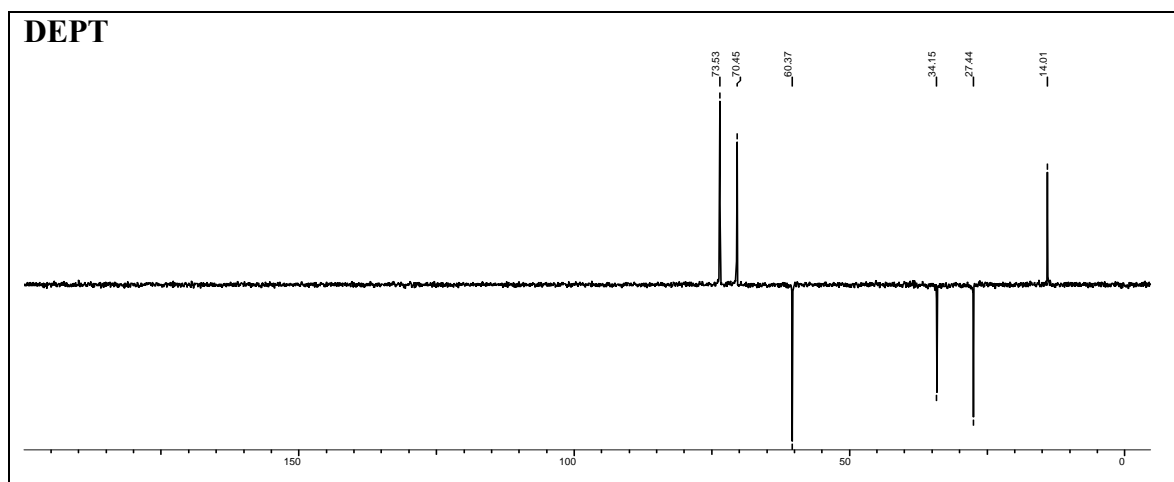
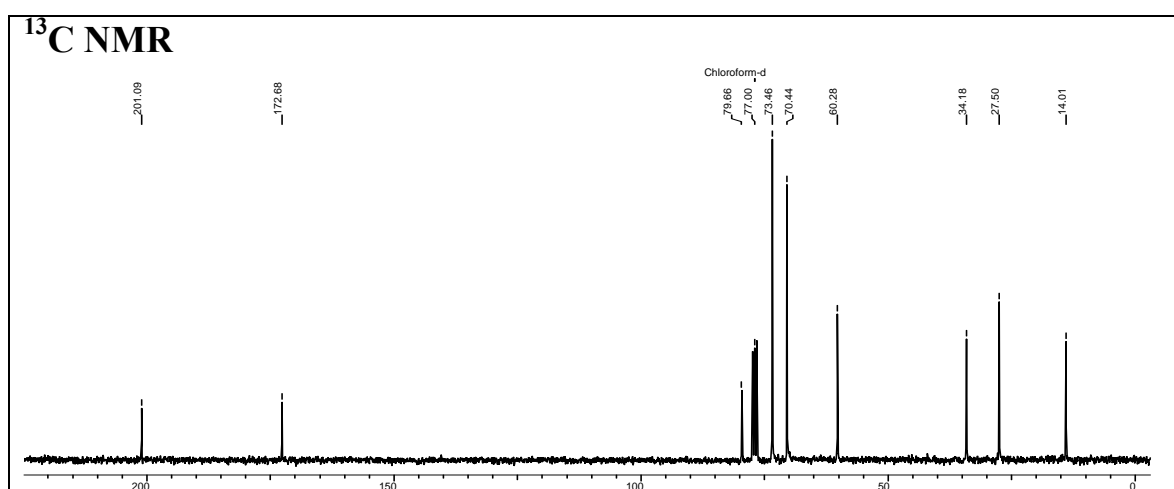
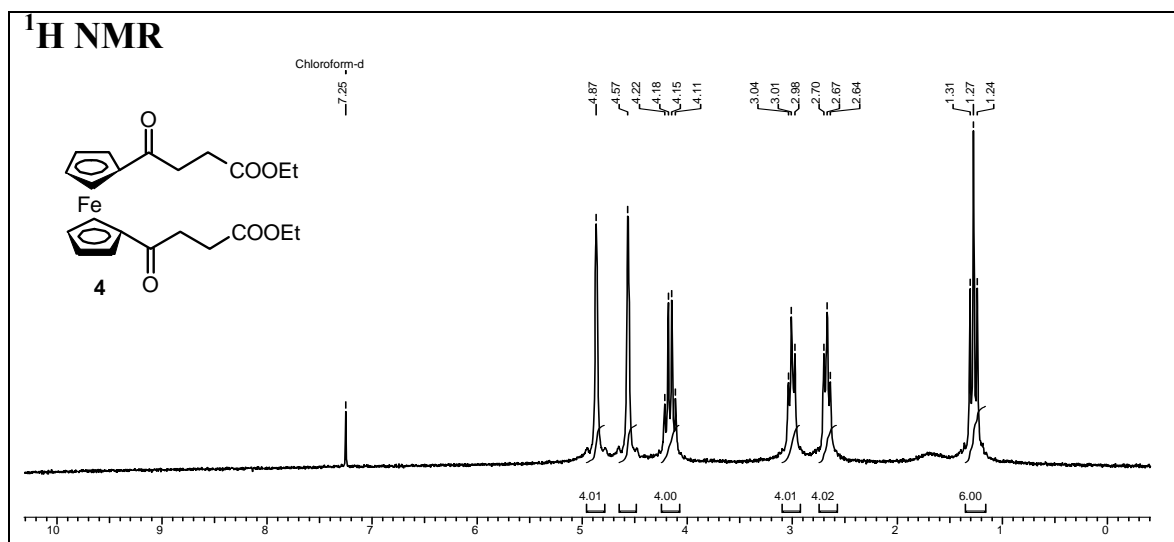
Compound	D-H...A	D-H (Å)	H...A (Å)	D...A (Å)	D-H...A (°)
<b>31a</b> <b>(Form I)</b>	N(3)-H(3N)...O(2)#1	0.86	1.98	2.836(4)	170.3
	N(3A)-H(3'A)...O(2B)#2	0.86	1.99	2.842(6)	170.9
	N(3B)-H(3'B)...O(2A)#3	0.86	1.96	2.815(6)	170.6
	N(3C)-H(3'C)...O(3C)#1	0.86	2.00	2.858(7)	172.4
<b>31<sup>a</sup></b> <b>(Form II)</b>	C(9A')-H(9'A)...O(3B)#4	0.97	2.64	3.347(7)	130.4
	C(8B')-H(8'B)...O(1B)#5	0.97	2.56	3.391(7)	143.8
	C(8B)-H(8B1)...O(2C)	0.97	2.72	3.453(9)	133.2
	C(8C')-H(8'C)...O(3B)	0.97	2.70	3.418(8)	131.2

Symmetry transformations used to generate equivalent atoms:

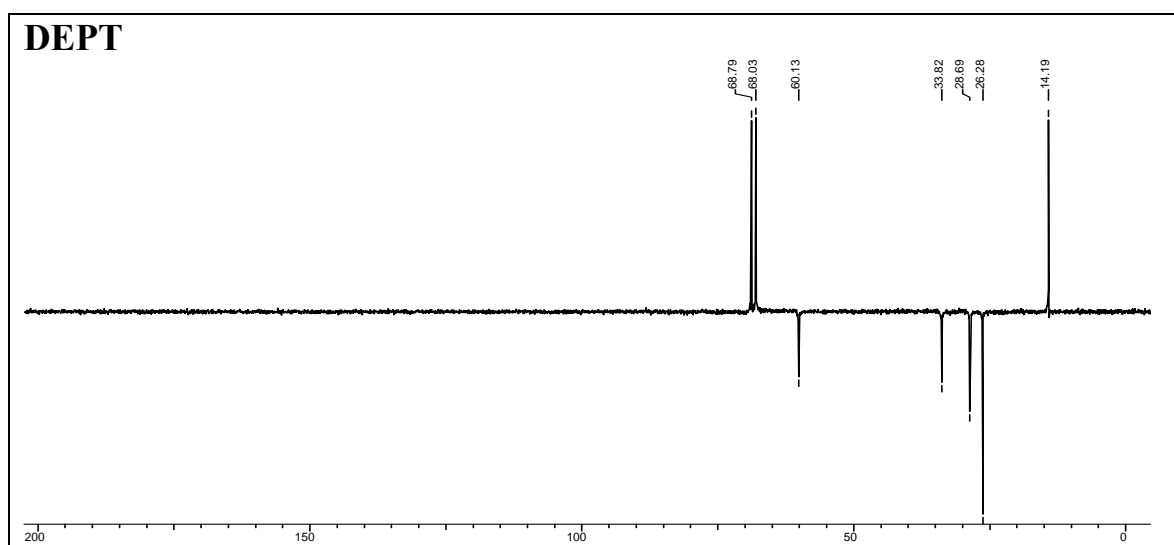
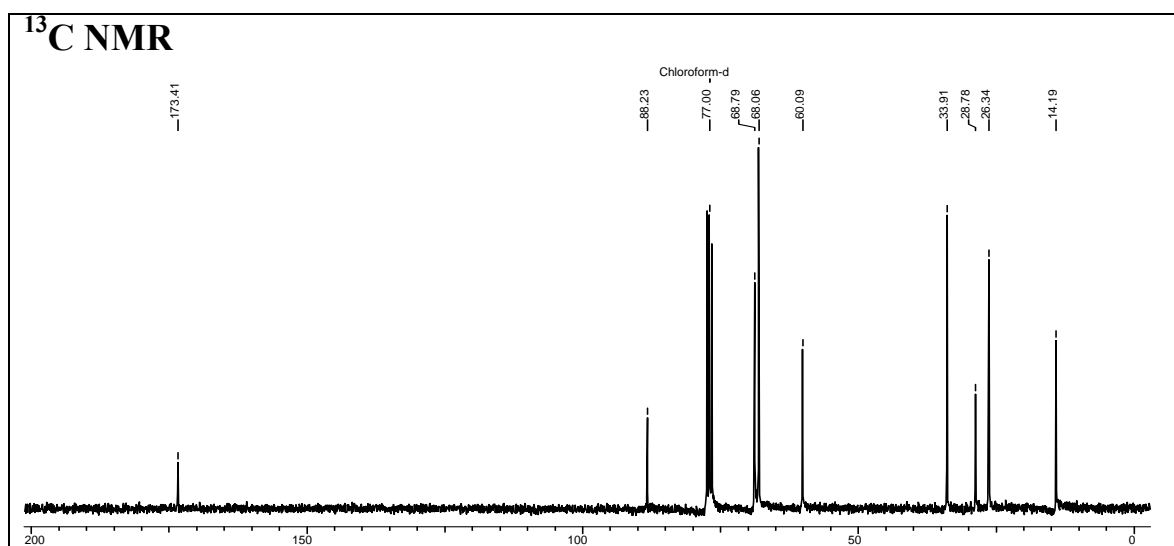
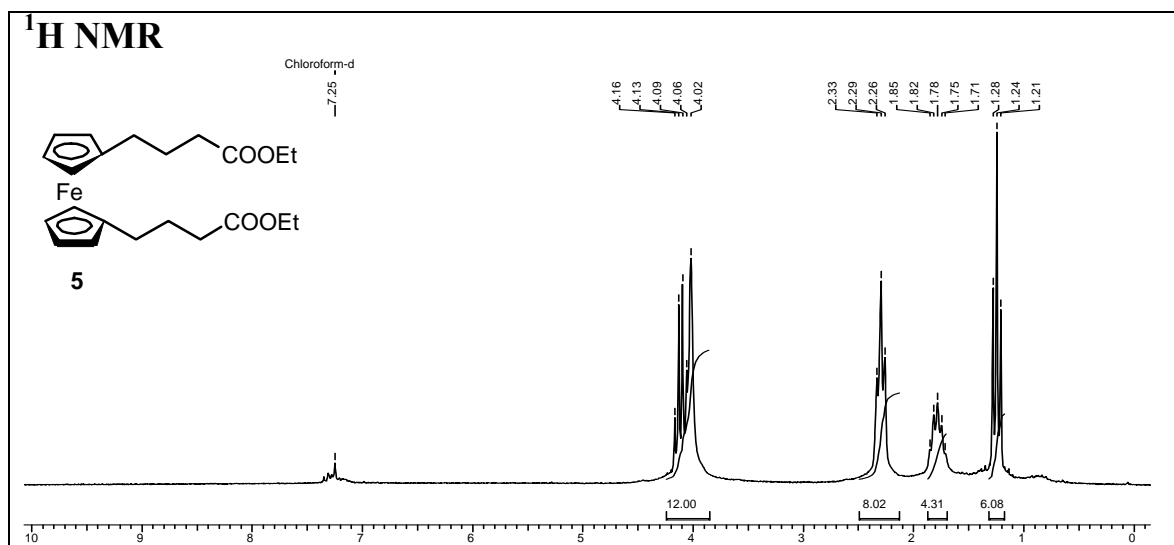
#1 -x+1,-y+1,-z+1    #2 -x,y+1/2,-z+1/2    #3 -x,y-1/2,-z+1/2    #4 -x+1,y+1/2,-z+1/2  
#5 x-1,y,z

Spectra ( $^1\text{H}$  NMR,  $^{13}\text{C}$  NMR and DEPT)

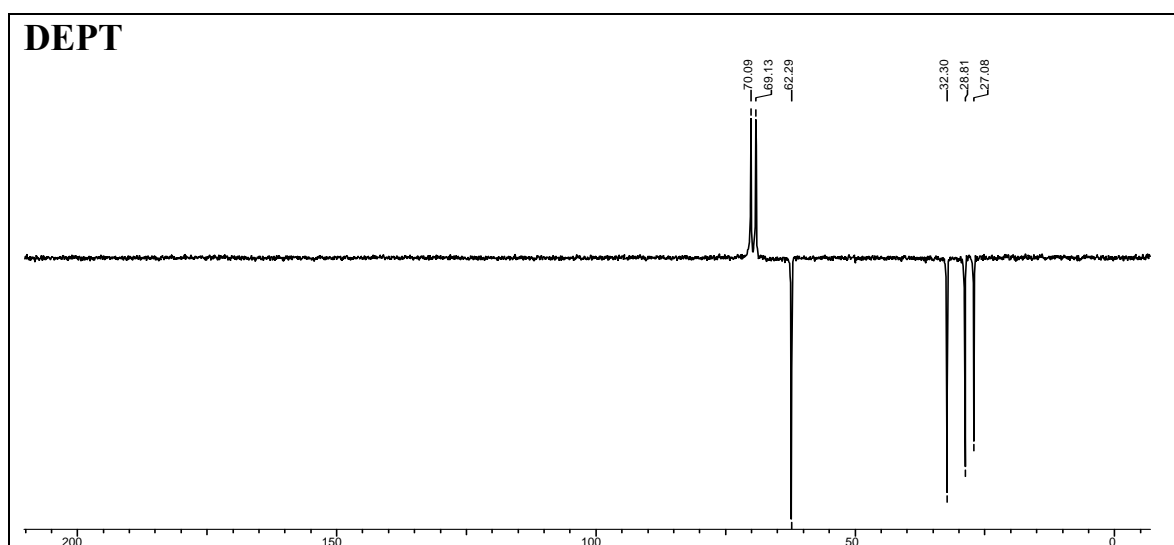
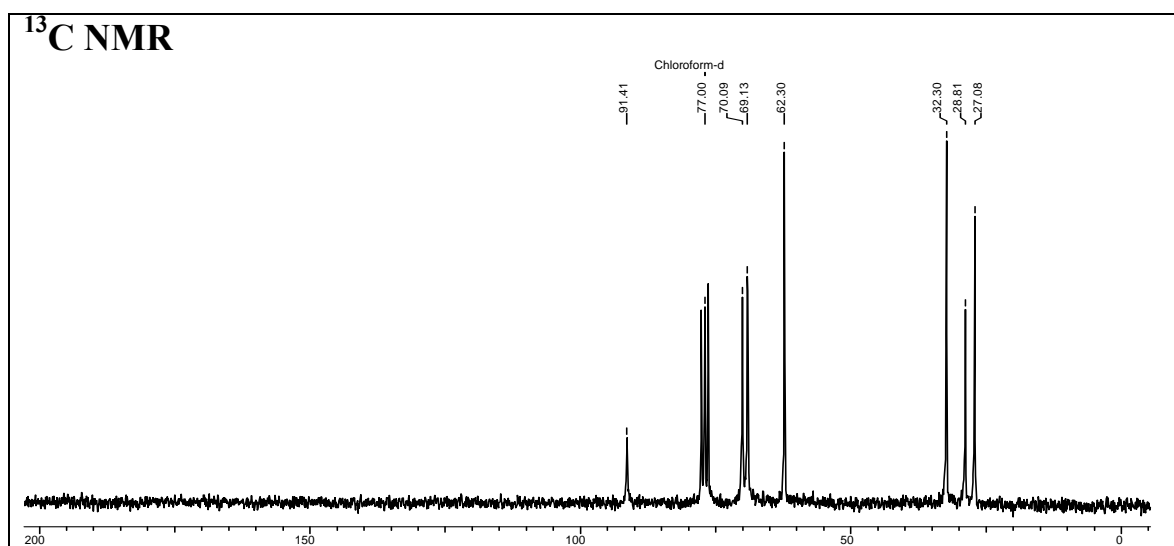
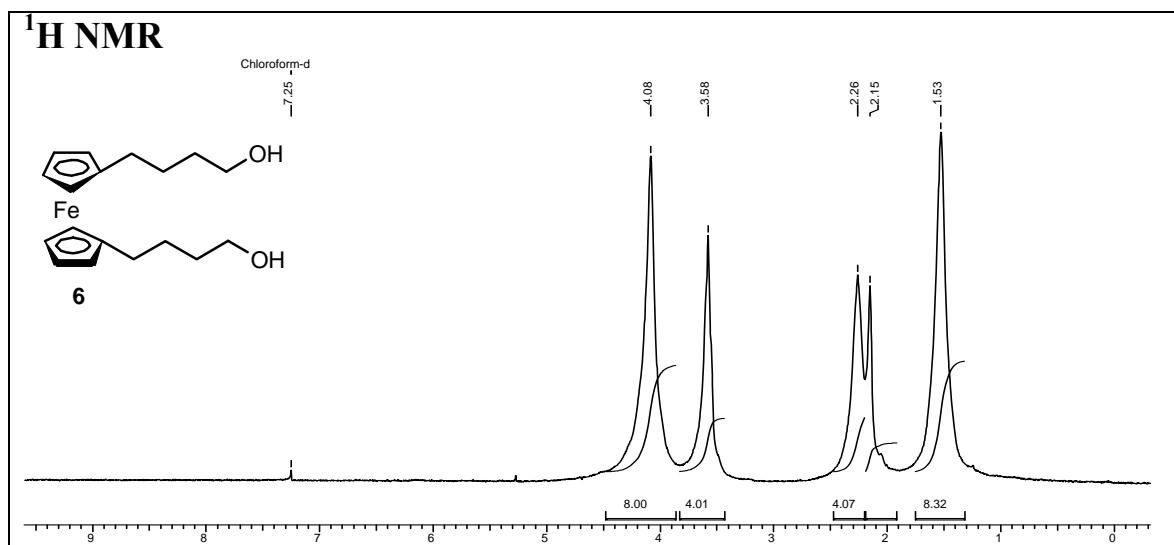
## 1, 1'-Bis-(3-carbethoxypropionyl)ferrocene (4)

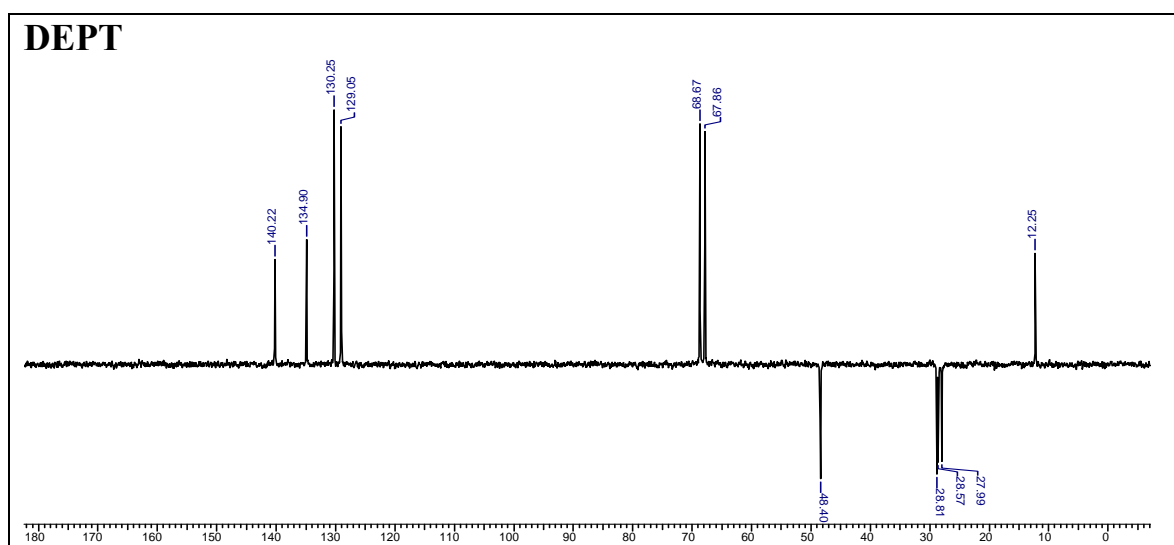
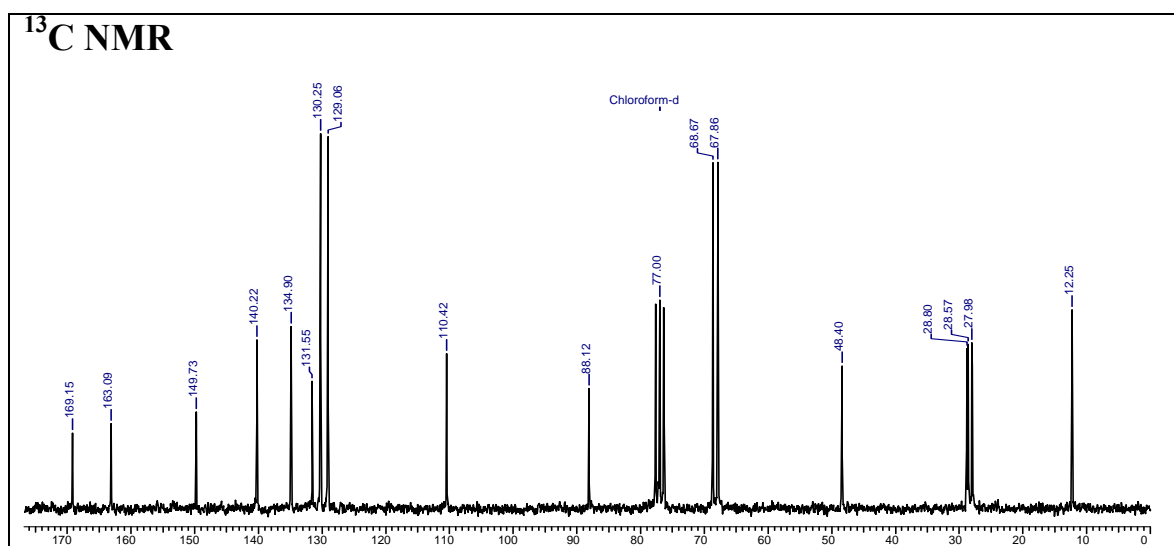
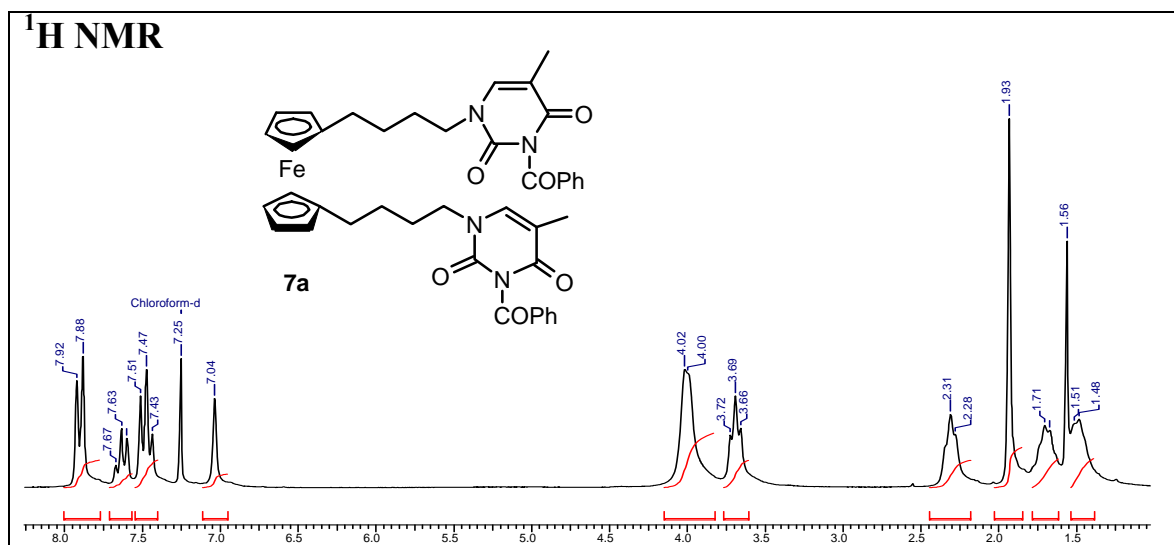


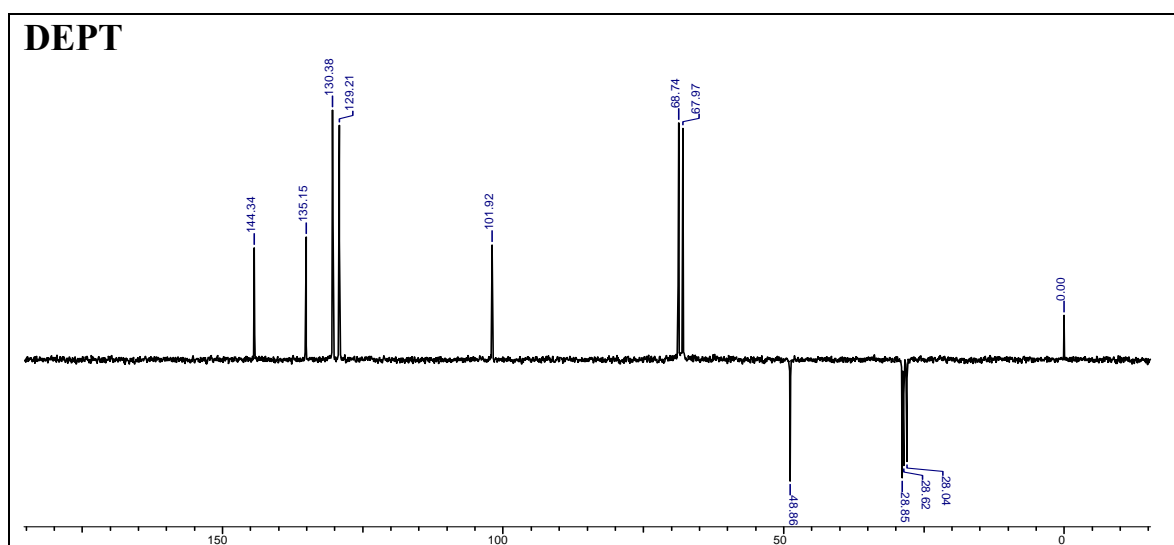
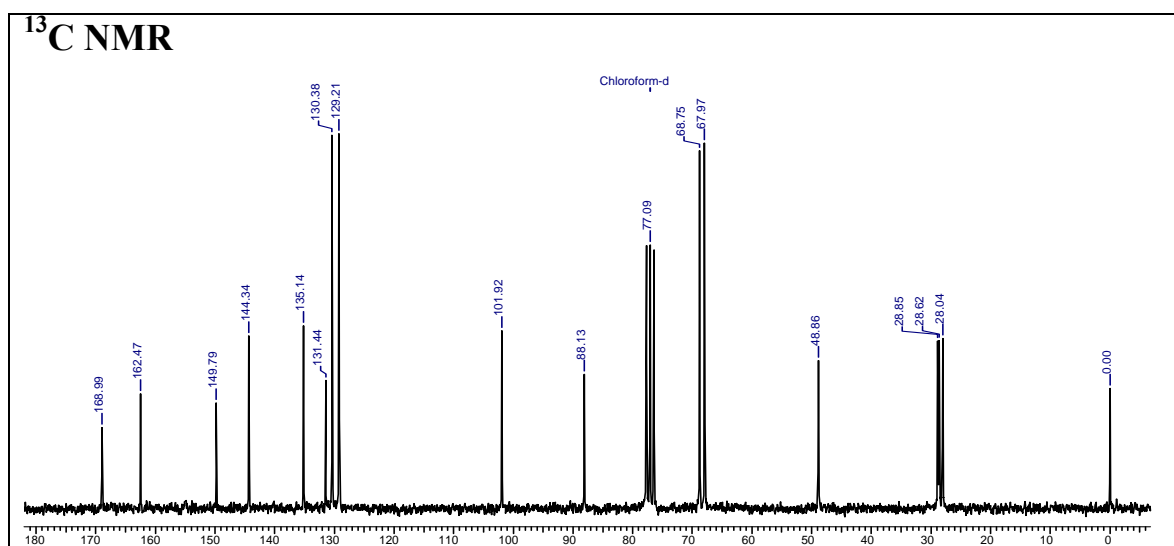
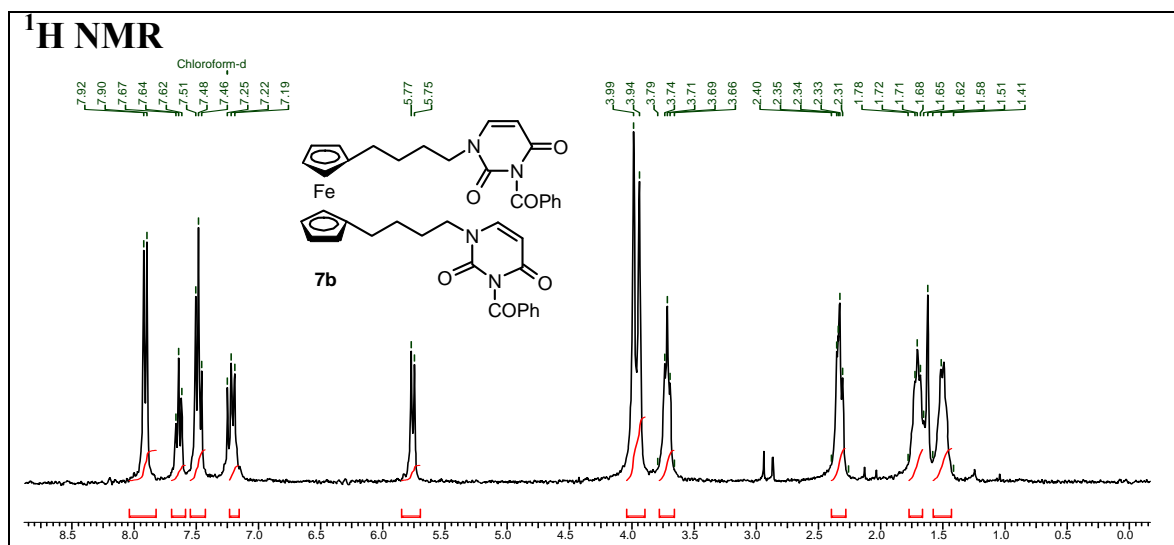
## 1, 1'-Bis-(3-carbethoxypropyl)ferrocene (5)



## 1, 1'-Bis-(4-hydroxybutyl)ferrocene (6)

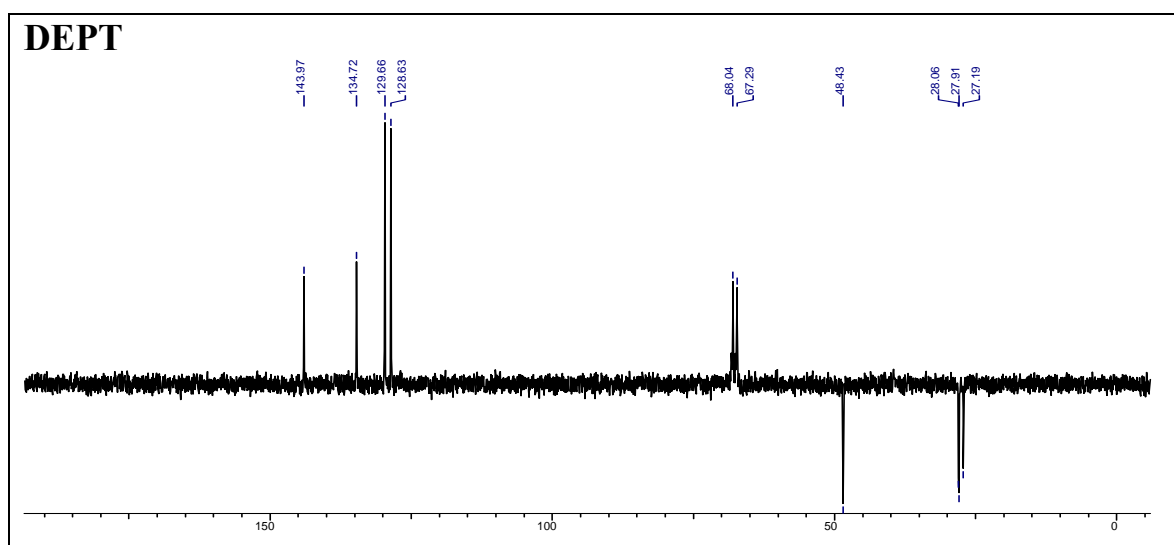
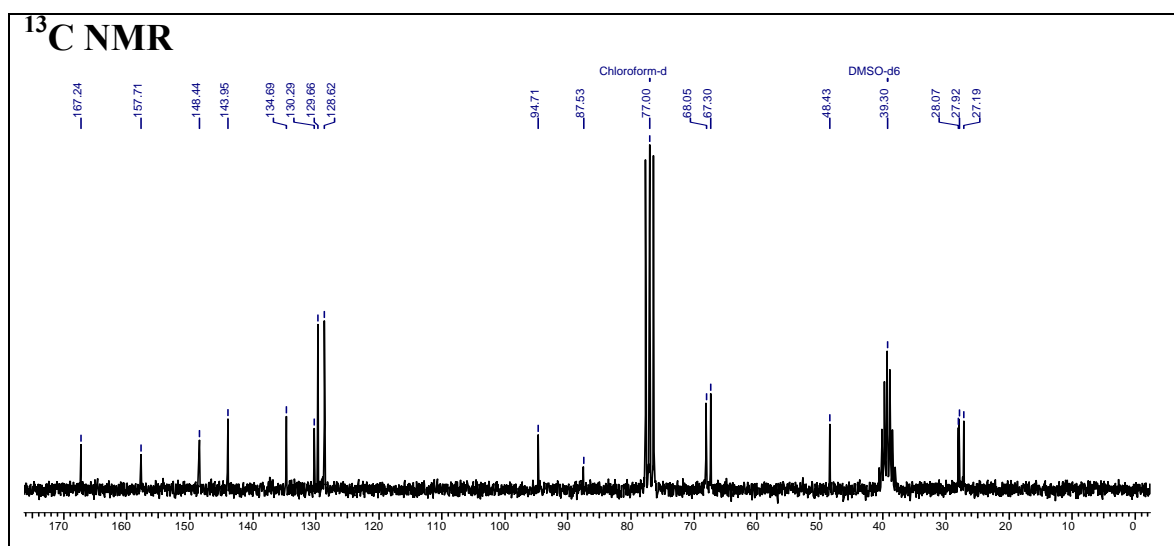
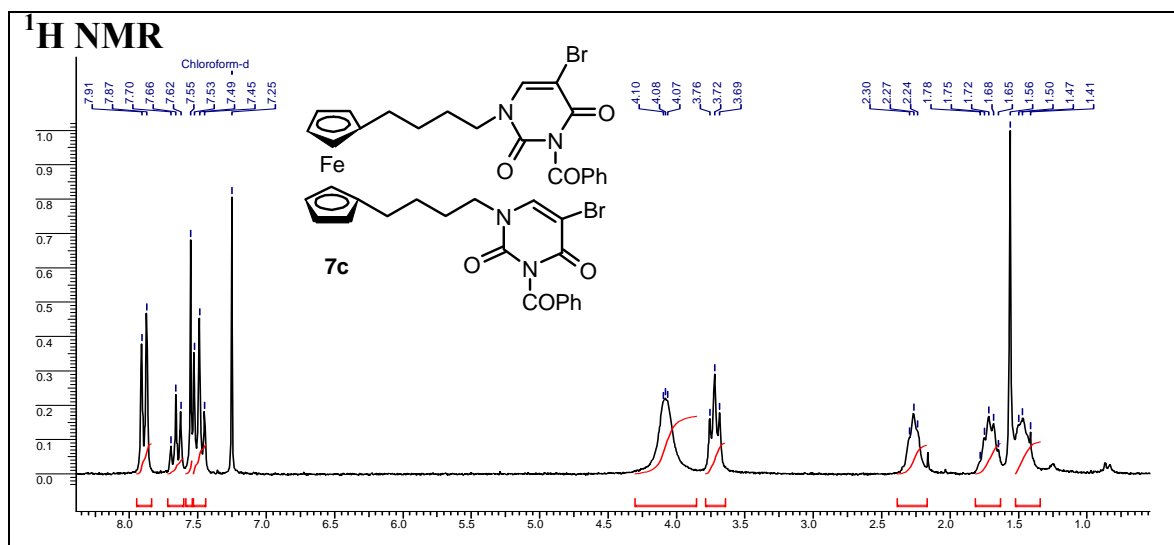


1, 1'-Bis-(4-(*N*3-benzoylthyminy)butyl)ferrocene (7a)

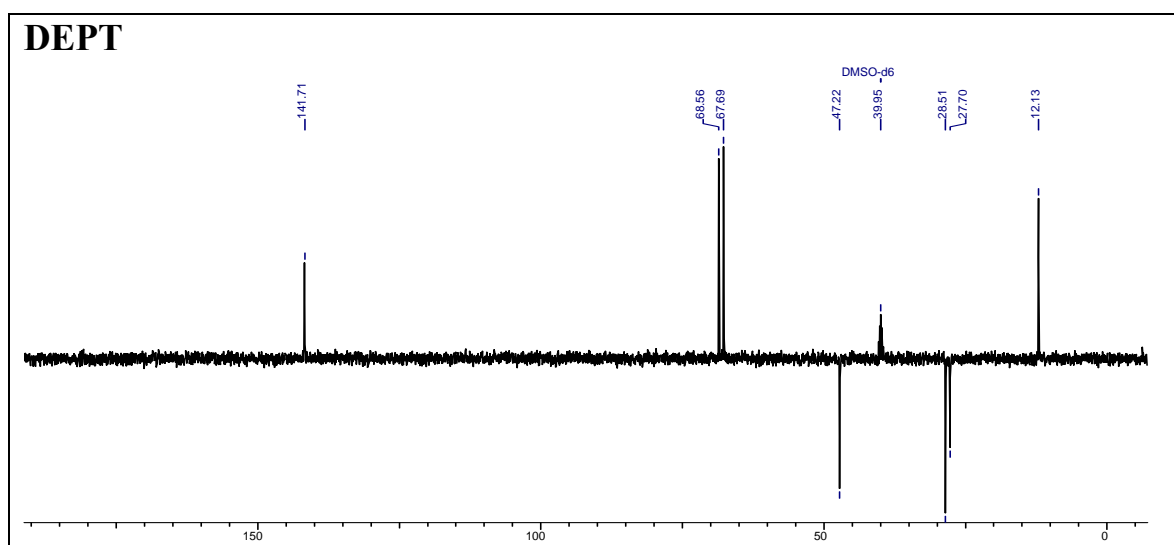
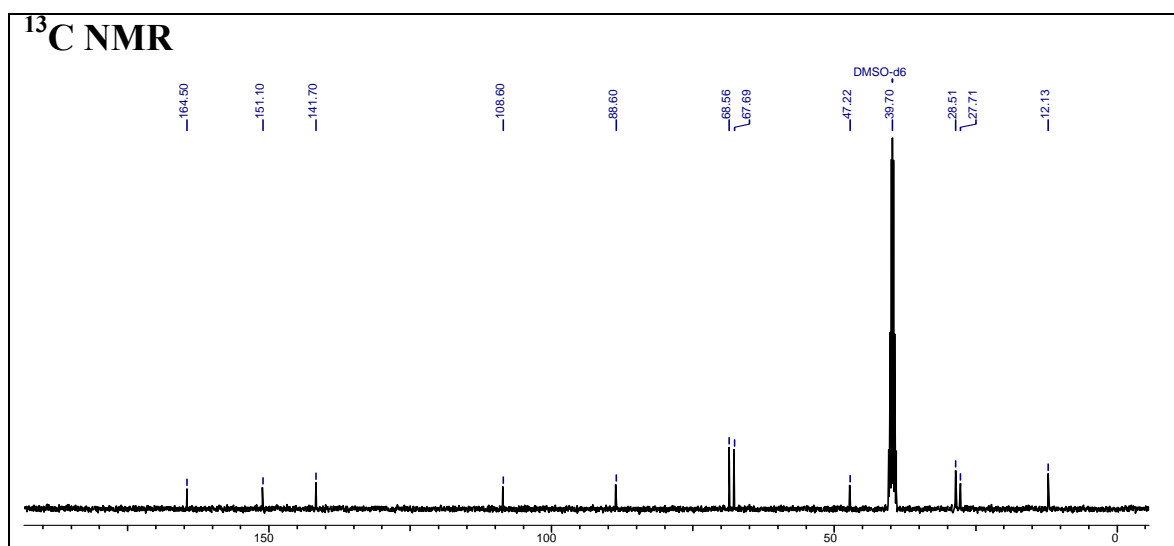
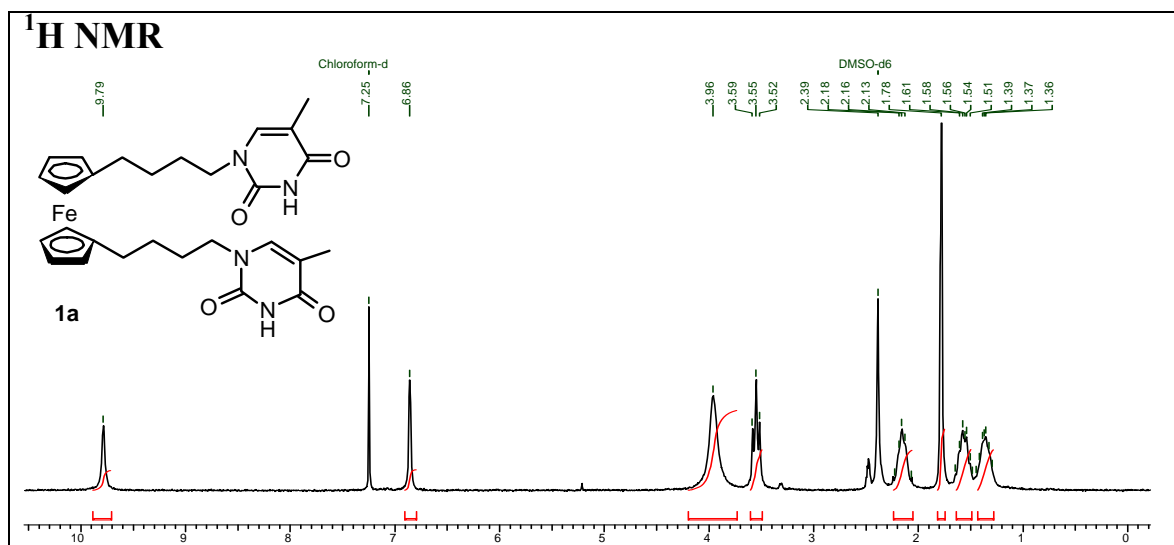
1, 1'-Bis-(4-(*N*3-benzoyluracilyl)butyl)ferrocene (**7b**)

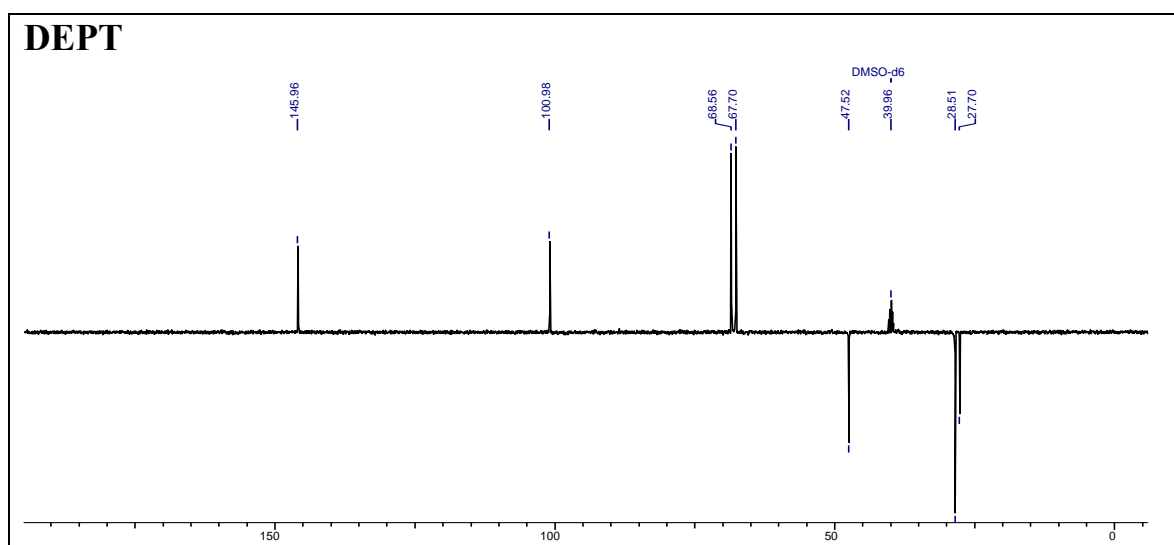
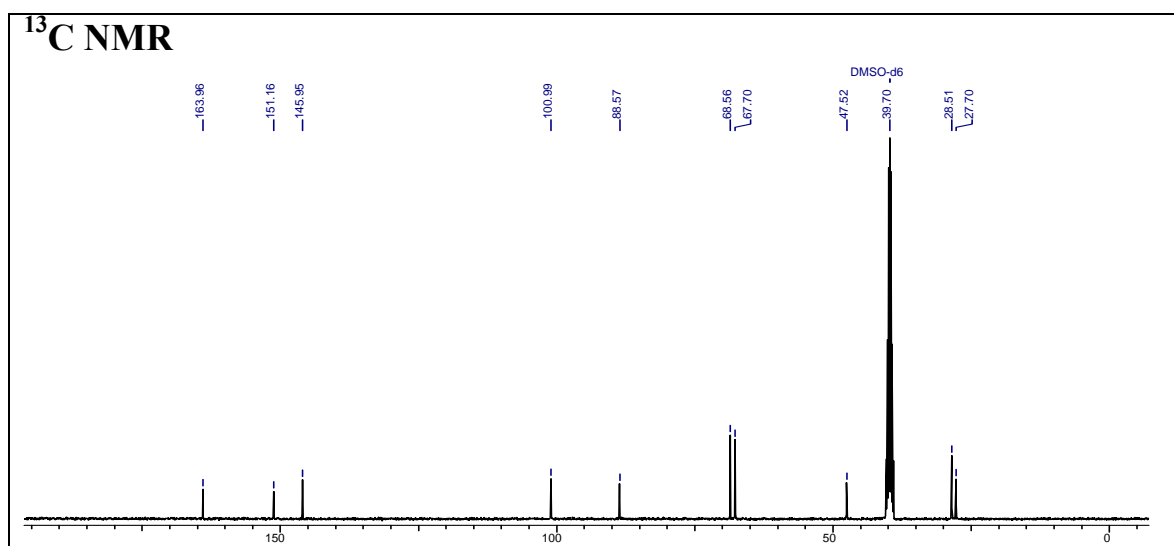
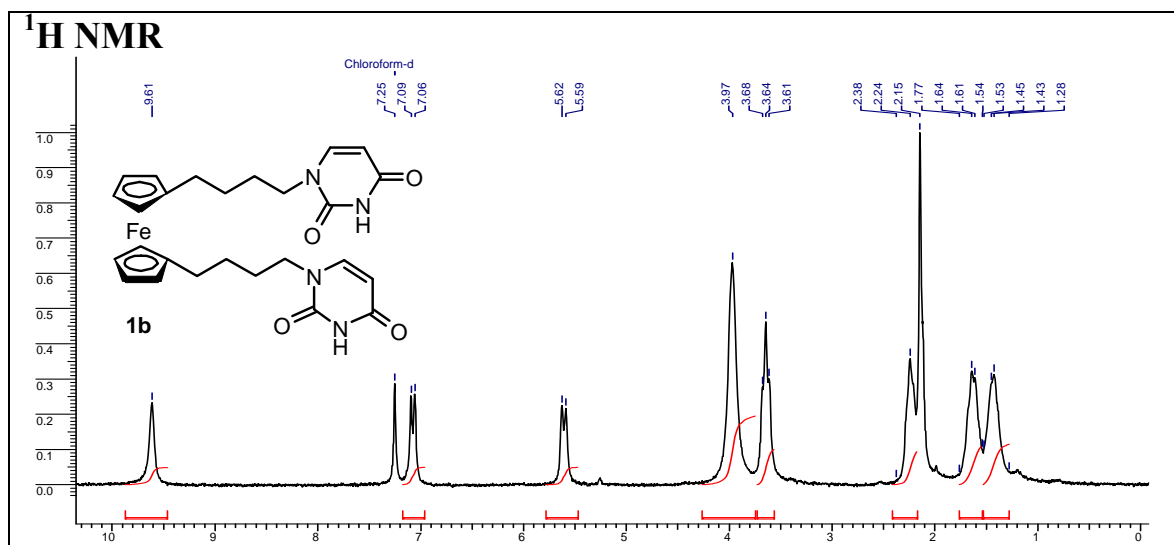


## 1, 1'-Bis-[(4-(N3-benzoyl)-5-bromouracyl)n-butyl]ferrocene (7c)

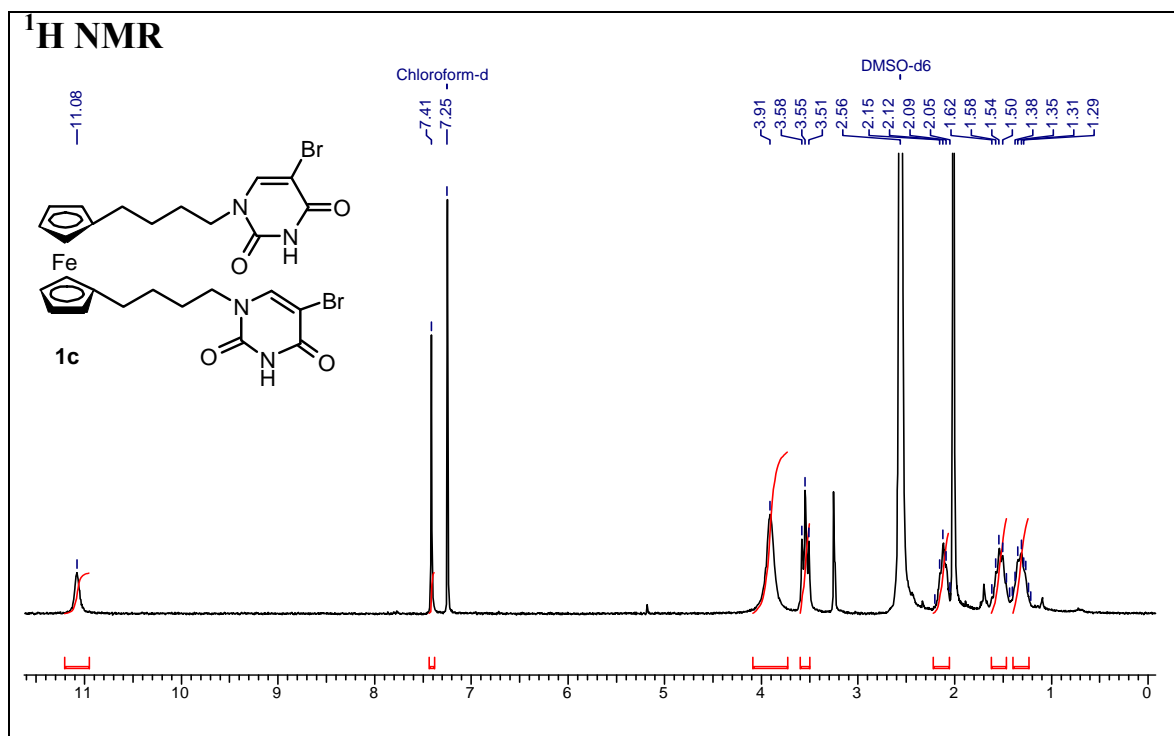


## 1, 1'-Bis-(4-(thyminy)butyl)ferrocene (1a)

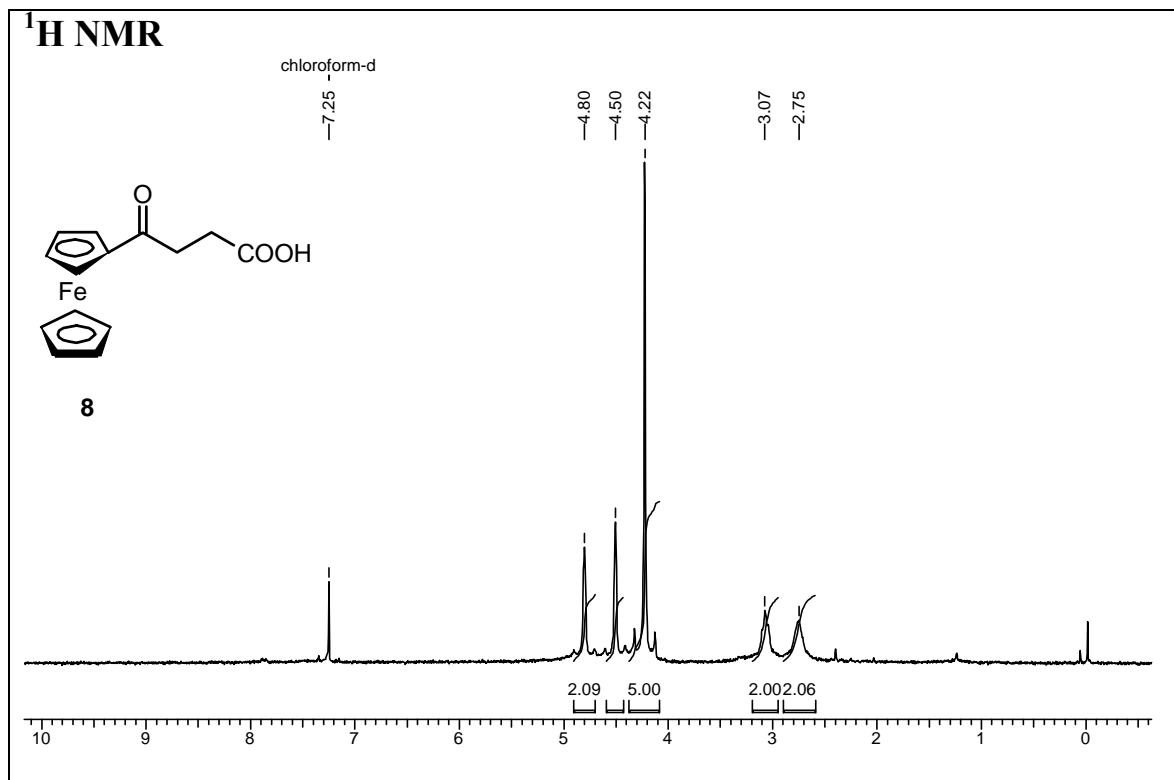


1,1'-Bis-(4-(uracilyl)butyl)ferrocene (**1b**)

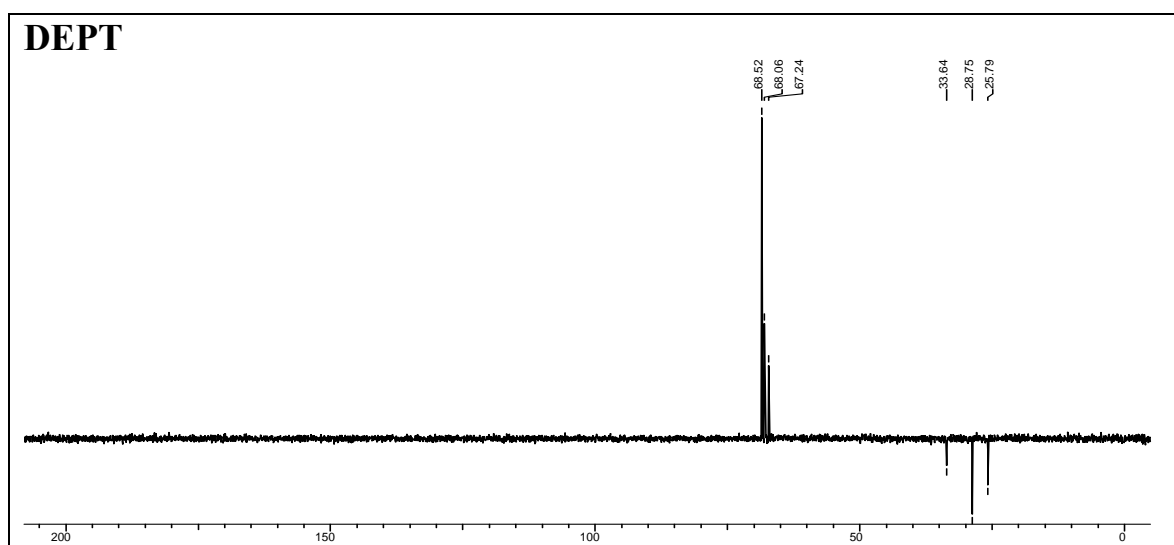
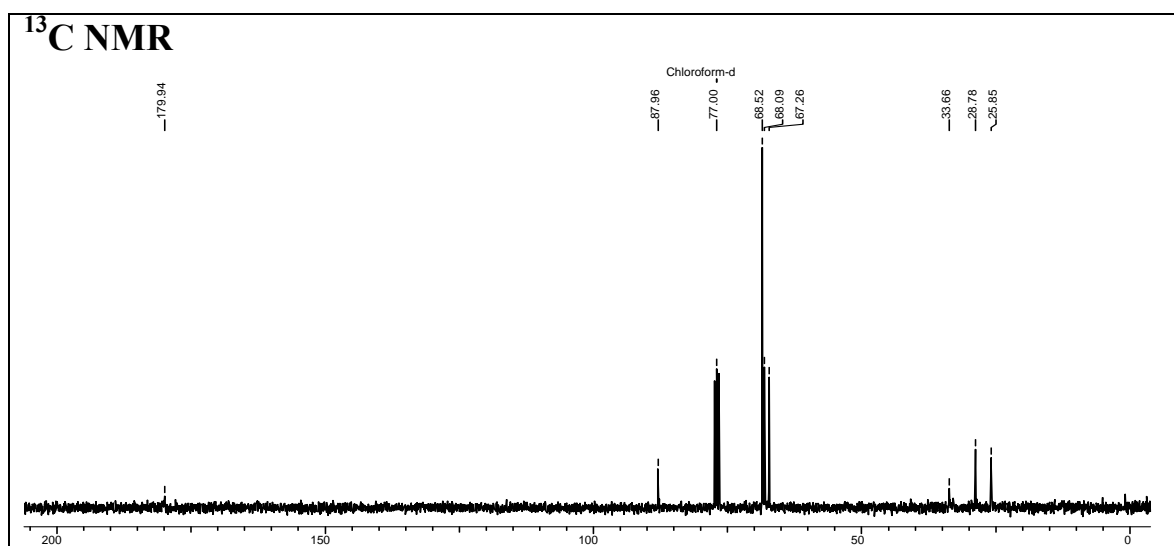
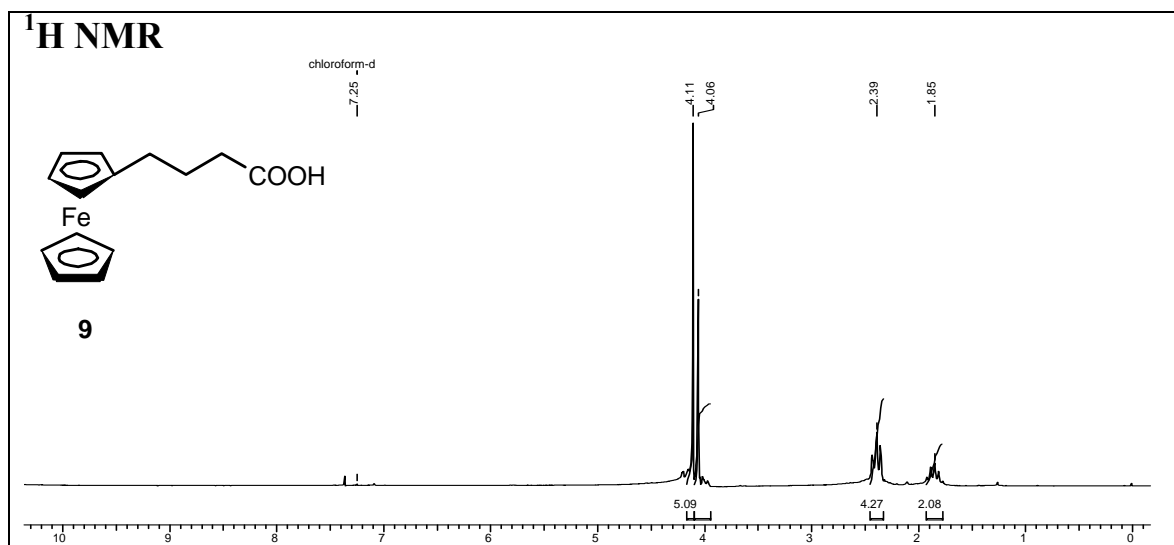
## 1, 1'-Bis-[4-(5-bromouracyl)butyl]ferrocene (1c)



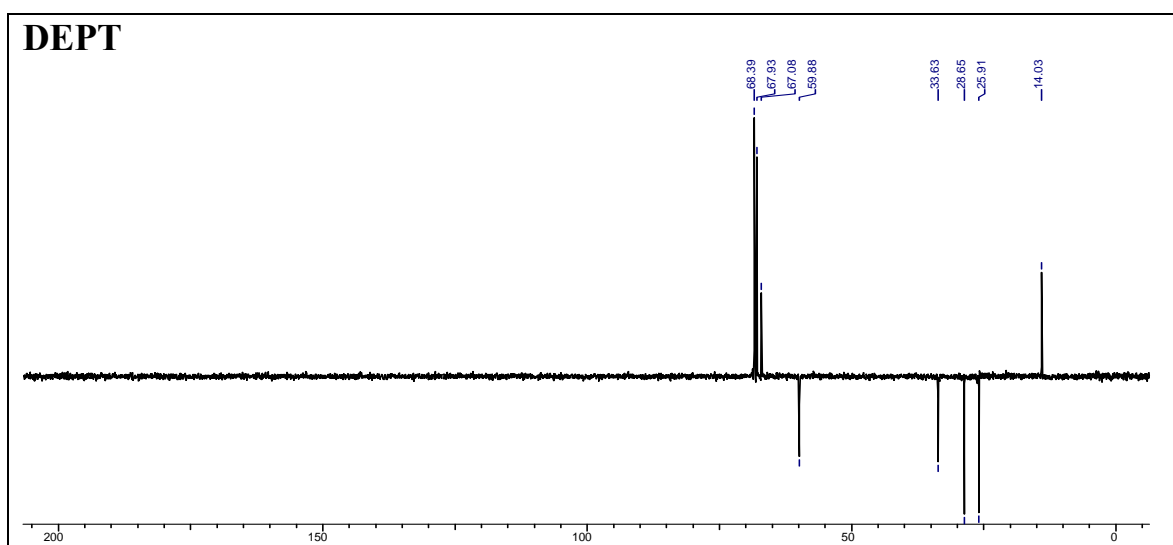
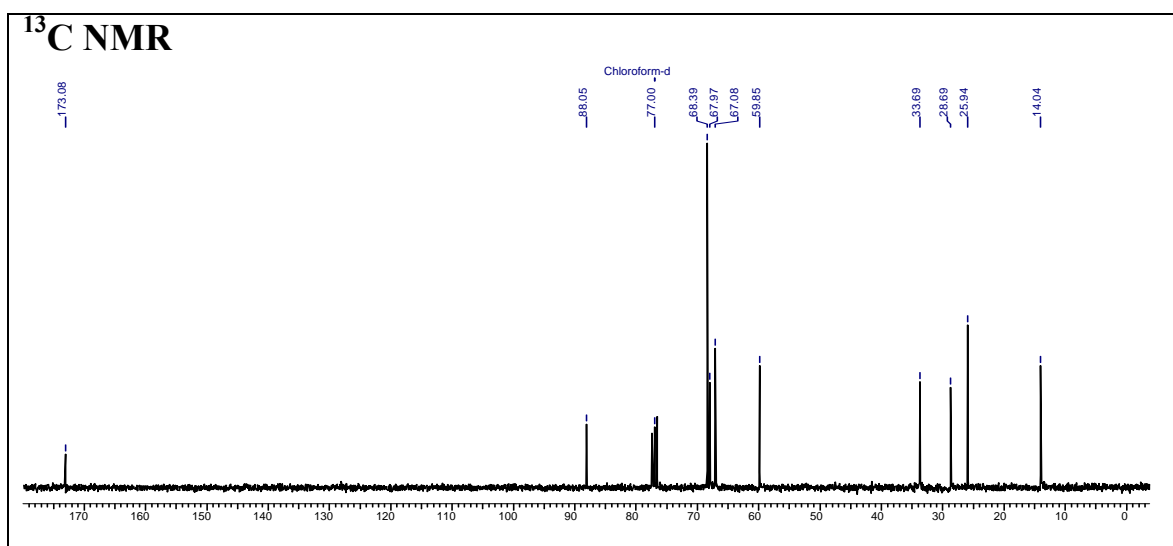
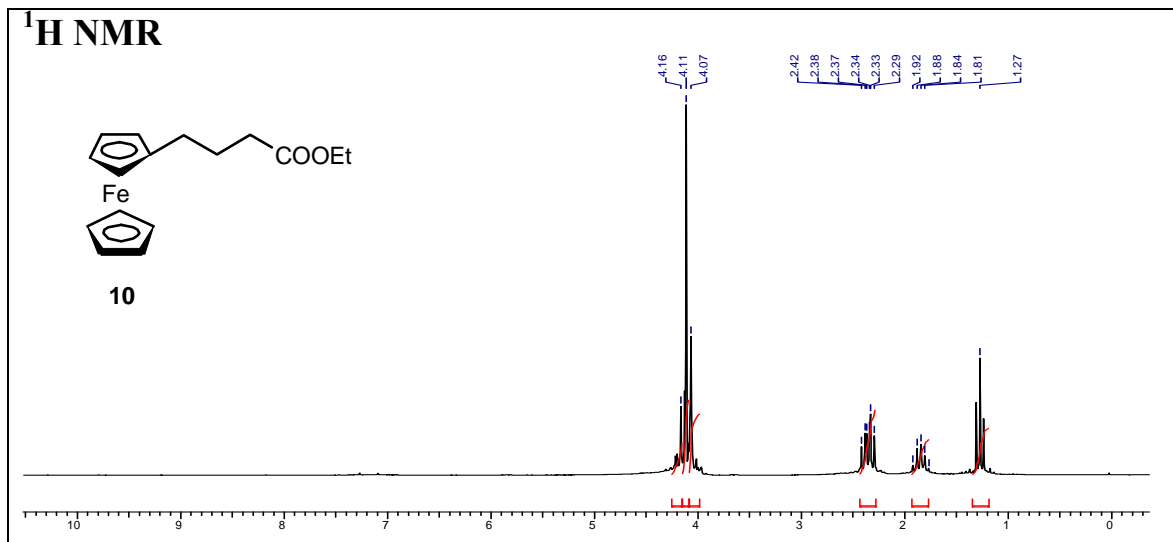
## 1-(3-Carboxypropionyl)ferrocene (8)



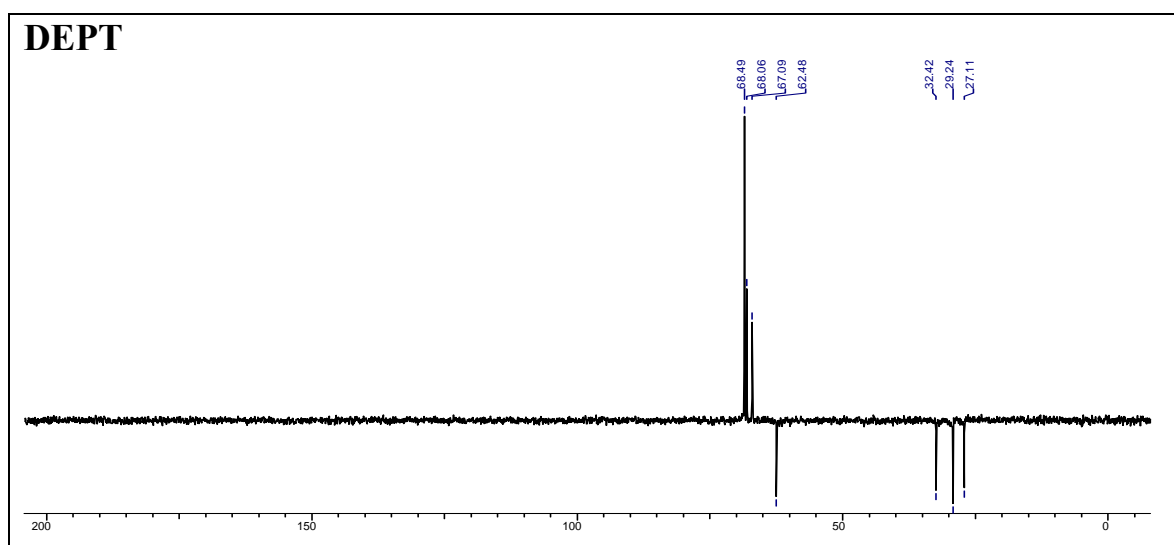
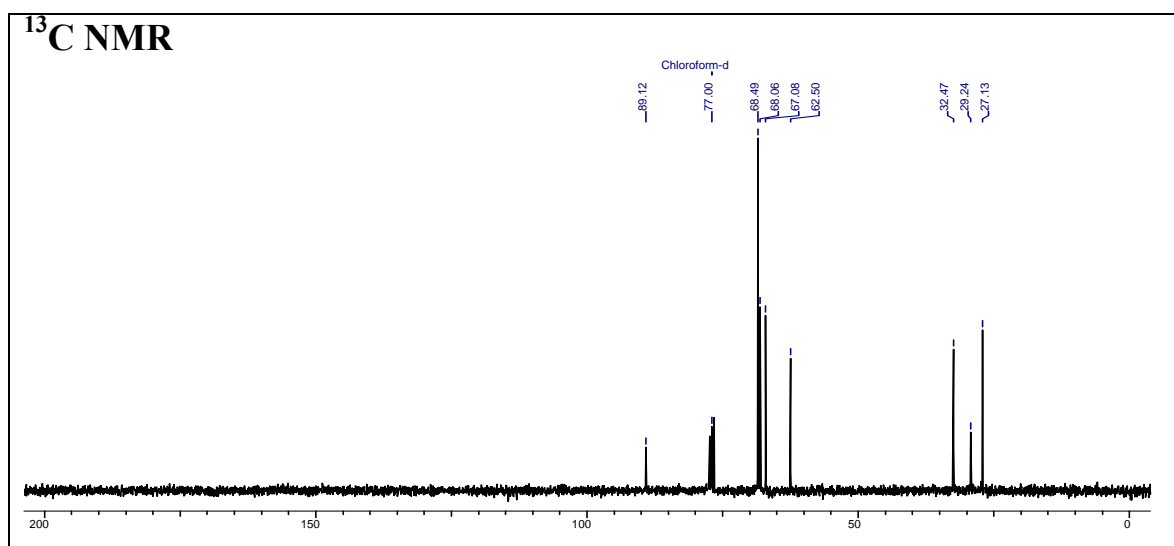
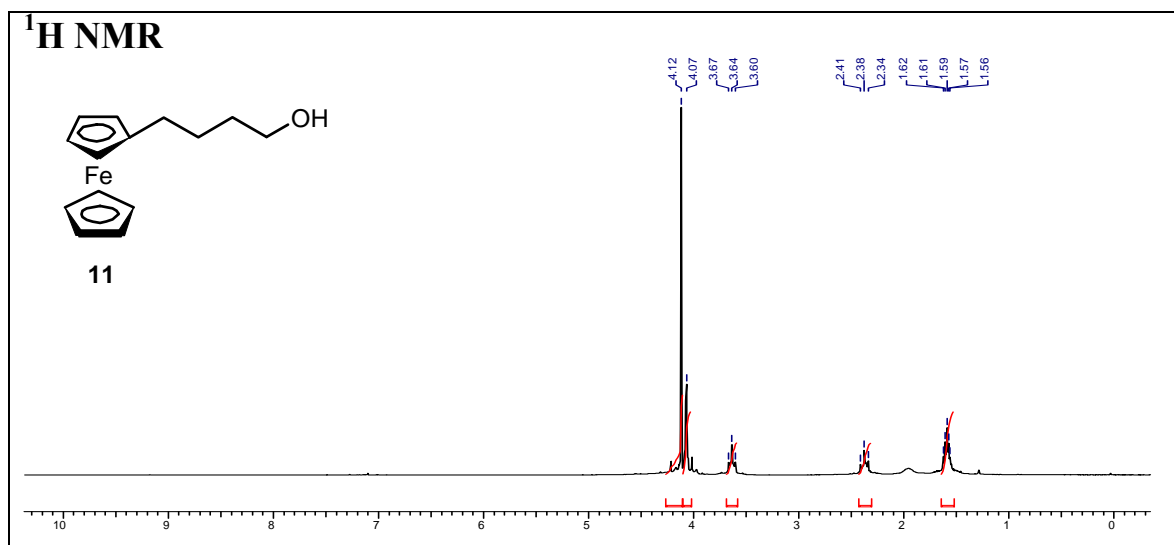
## 1-(3-Carboxypropyl)ferrocene (9)

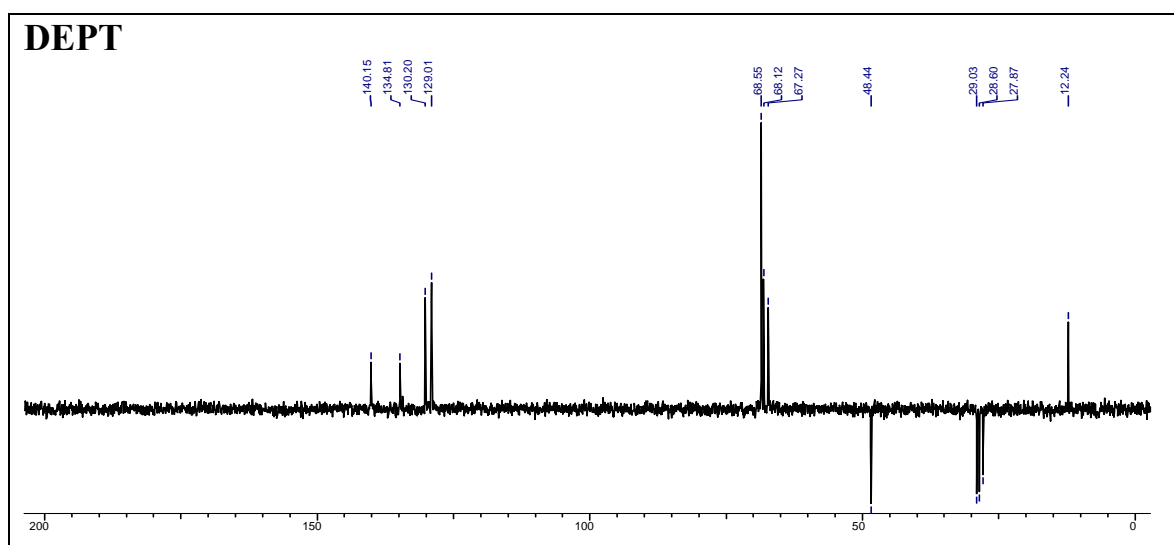
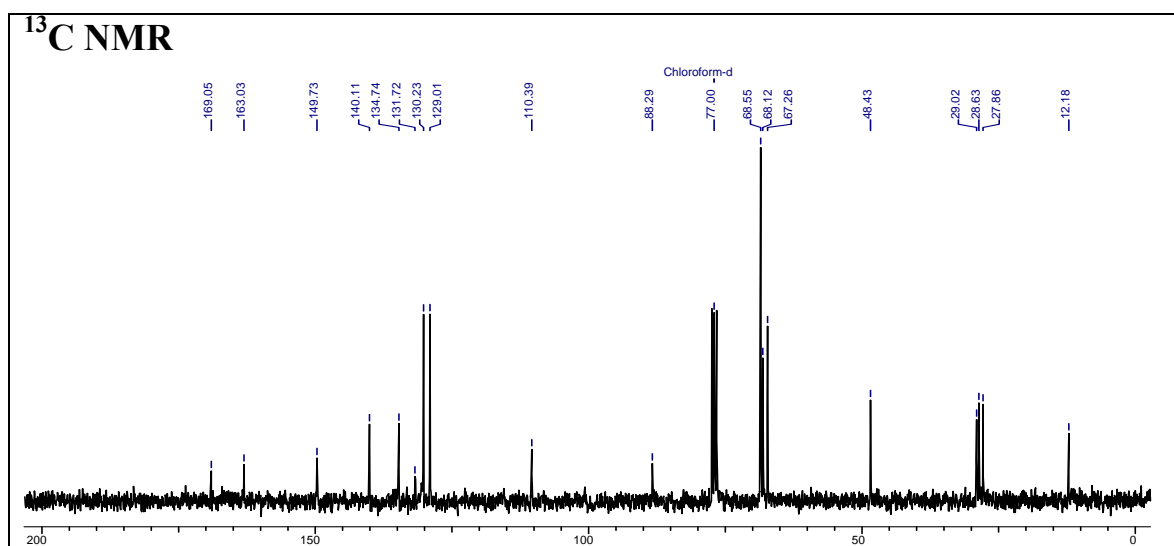
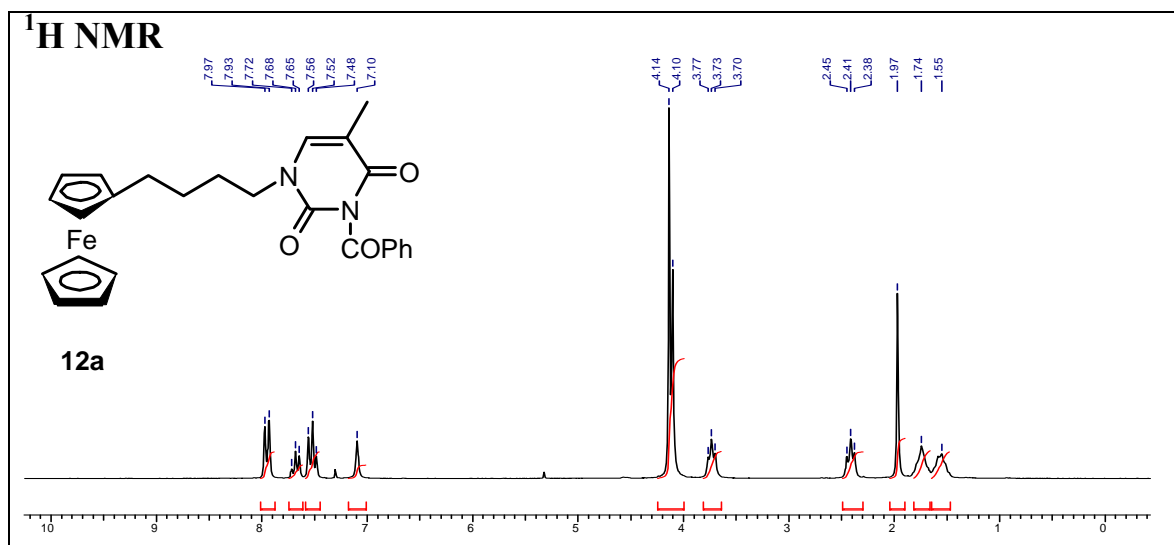


## 1-(3-Carbethoxypropyl)ferrocene (10)

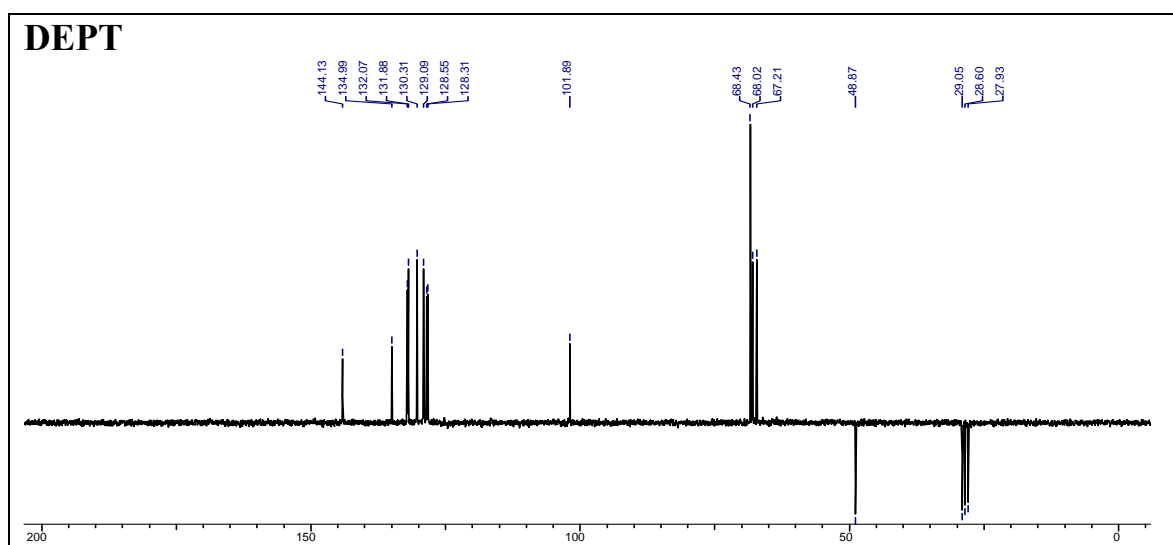
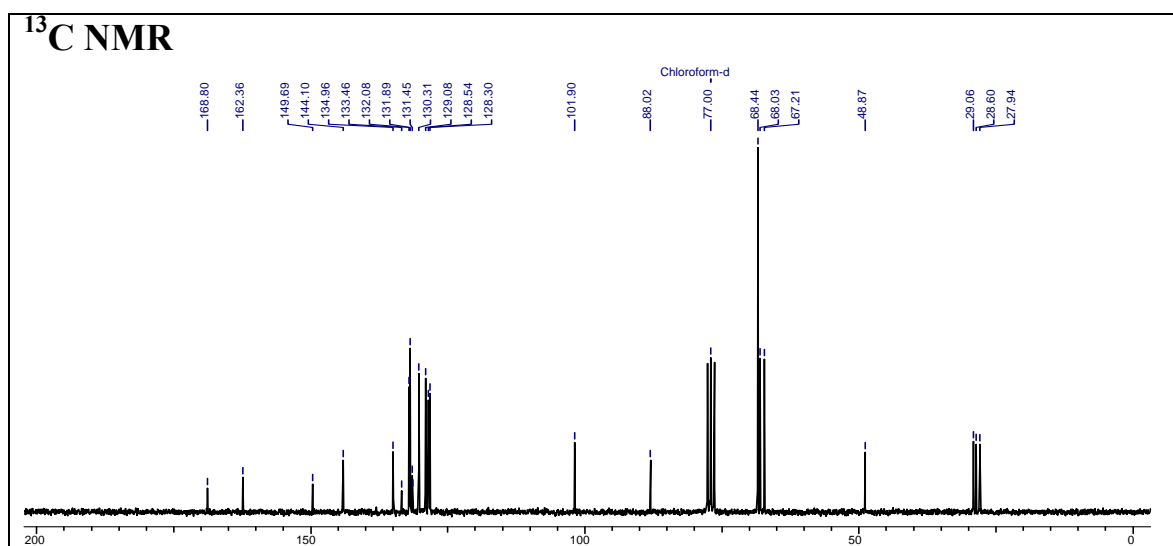
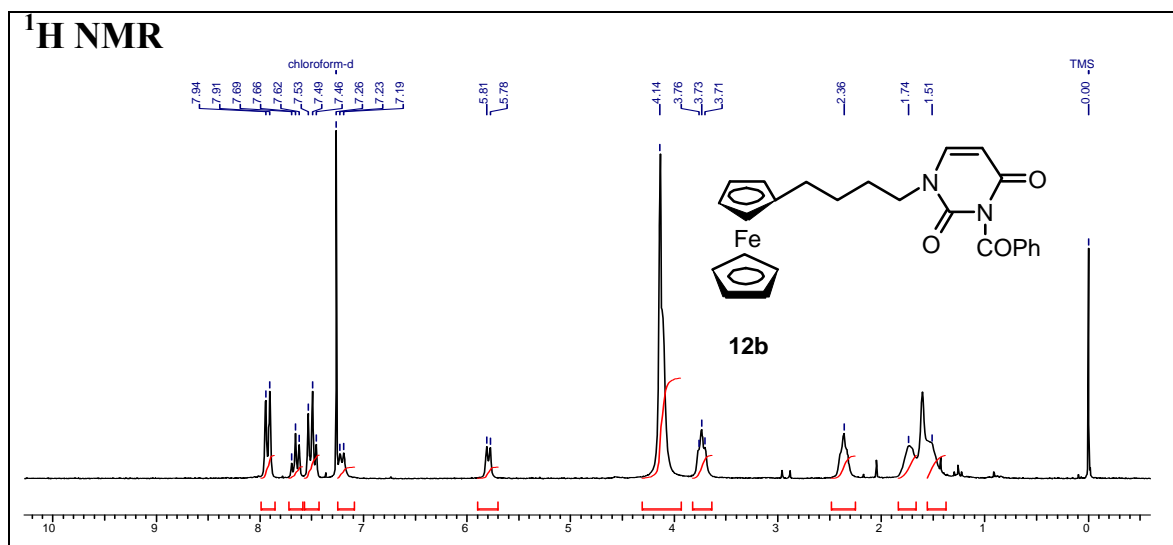


## 1-(4-Hydroxybutyl)ferrocene (11)

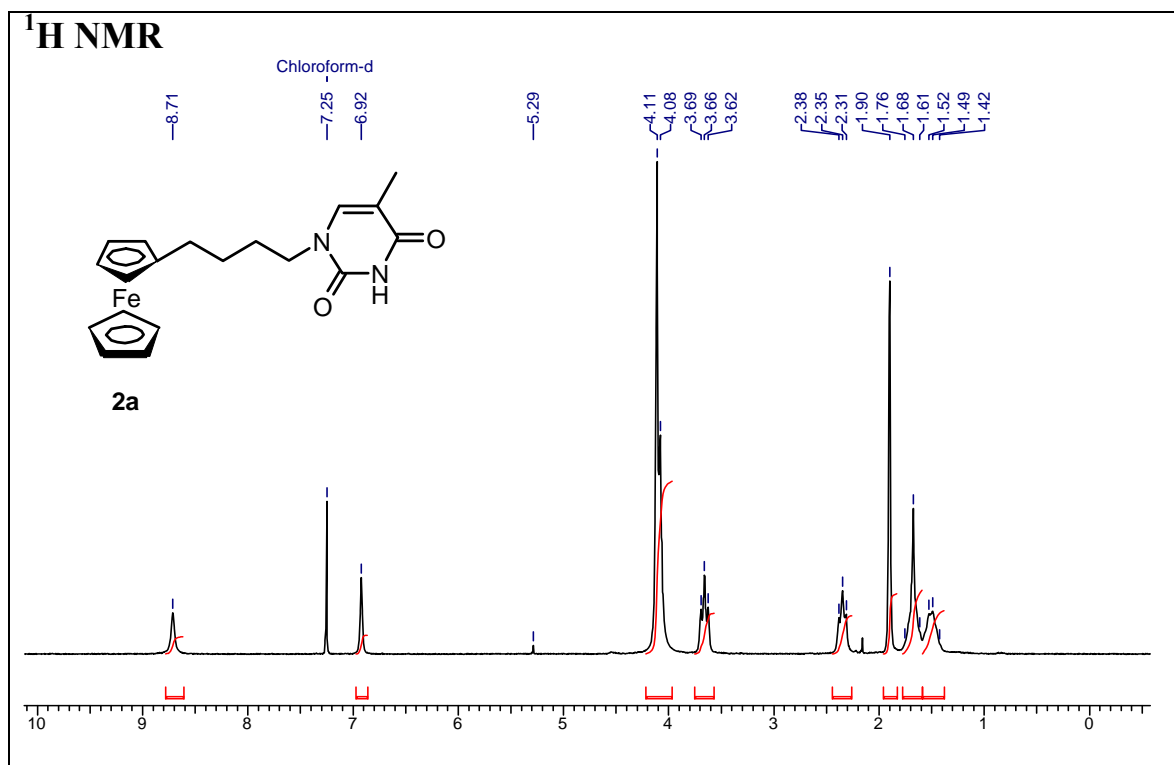


1-(4-(*N*3-benzoylthyminyl)butyl)ferrocene (12a)

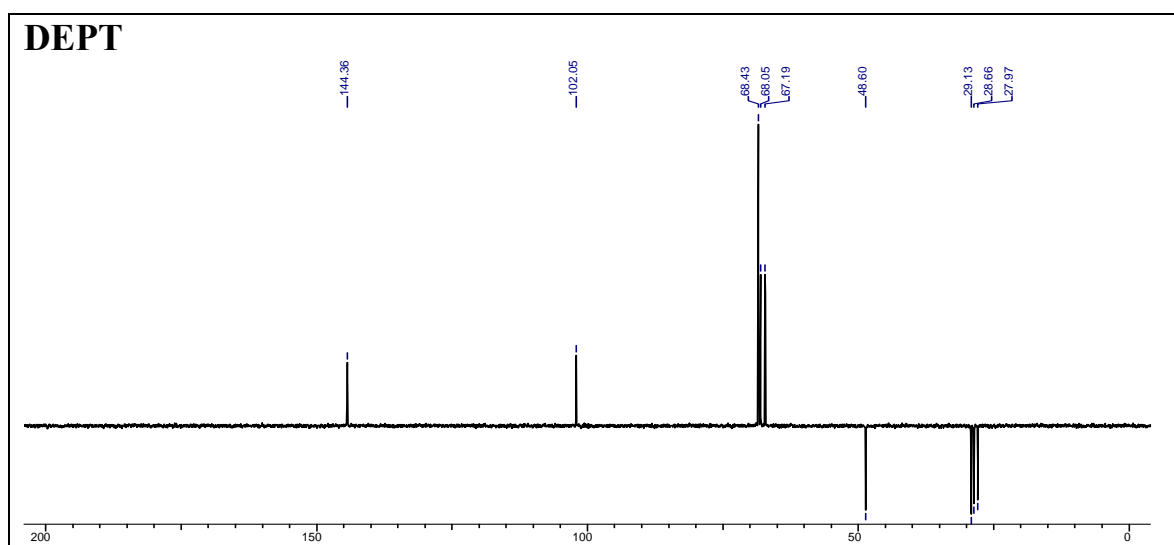
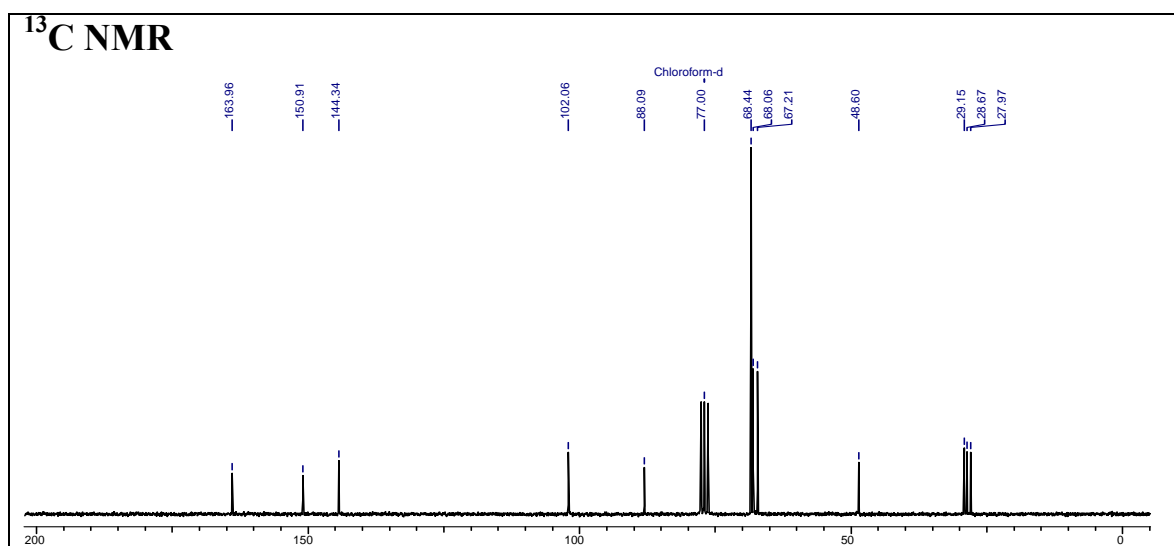
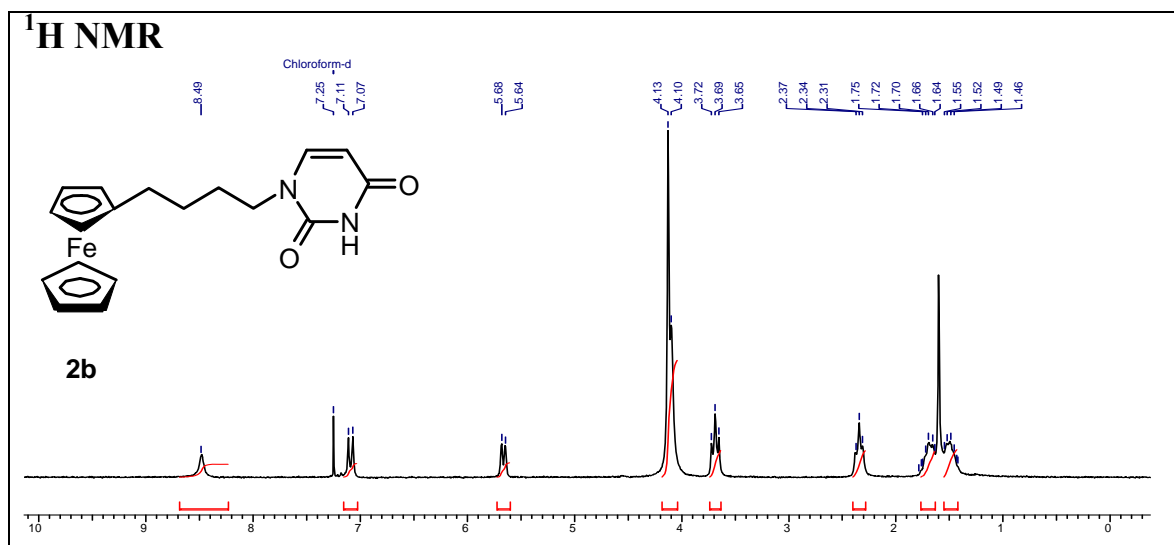


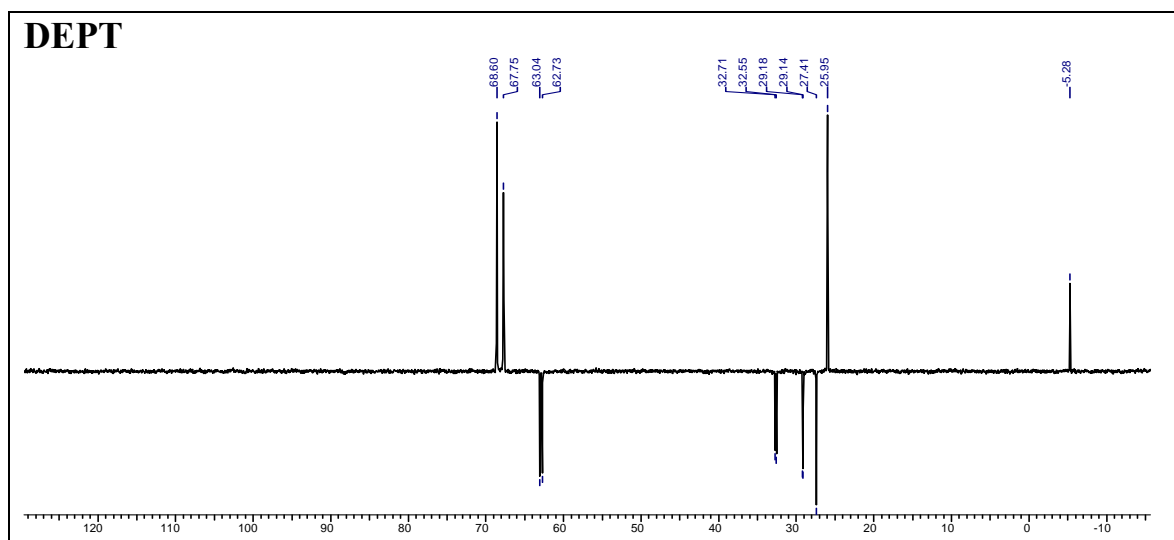
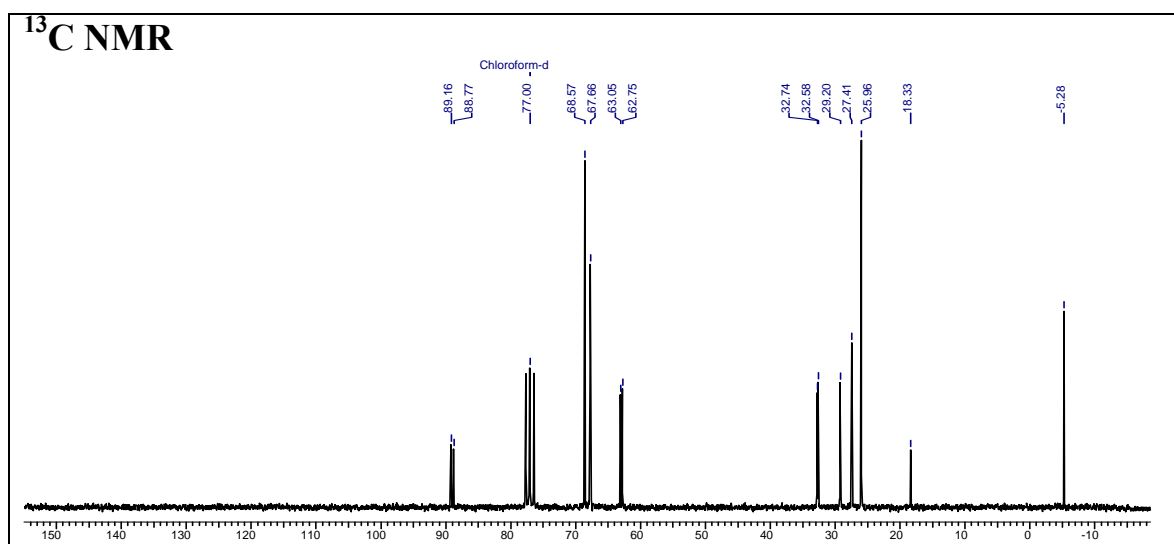
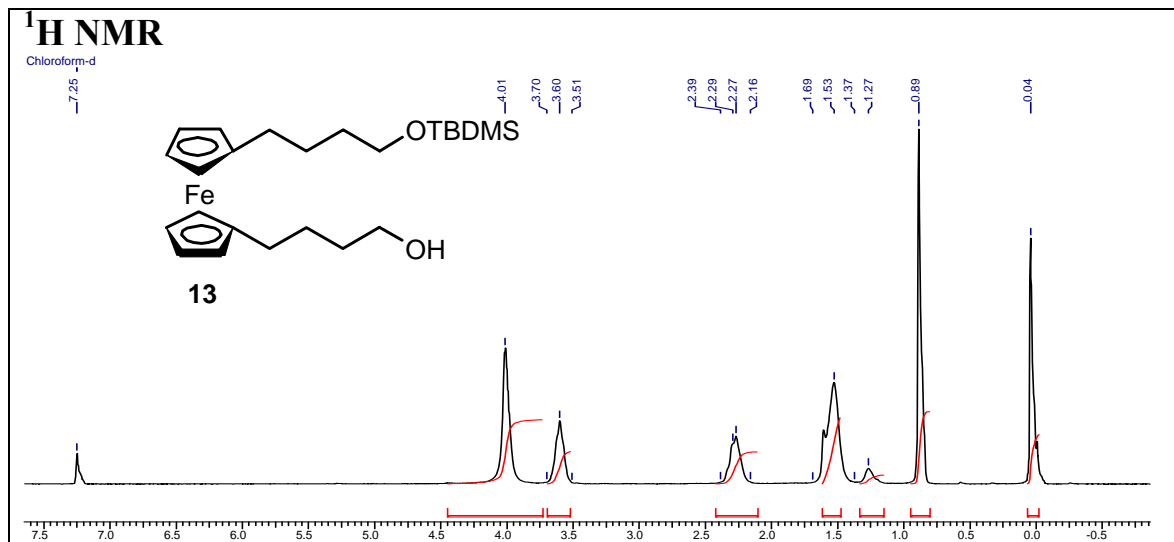
1-(4-(*N*3-benzoyluracilyl)butyl)ferrocene (**12b**)

## 1-(4-(Thyminyl)butyl)ferrocene (2a)

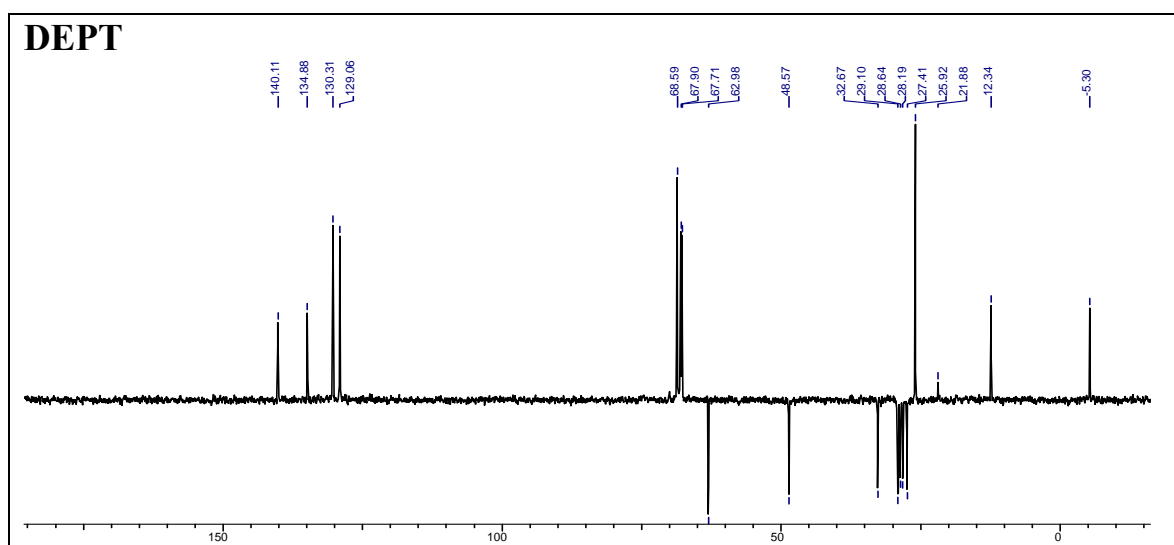
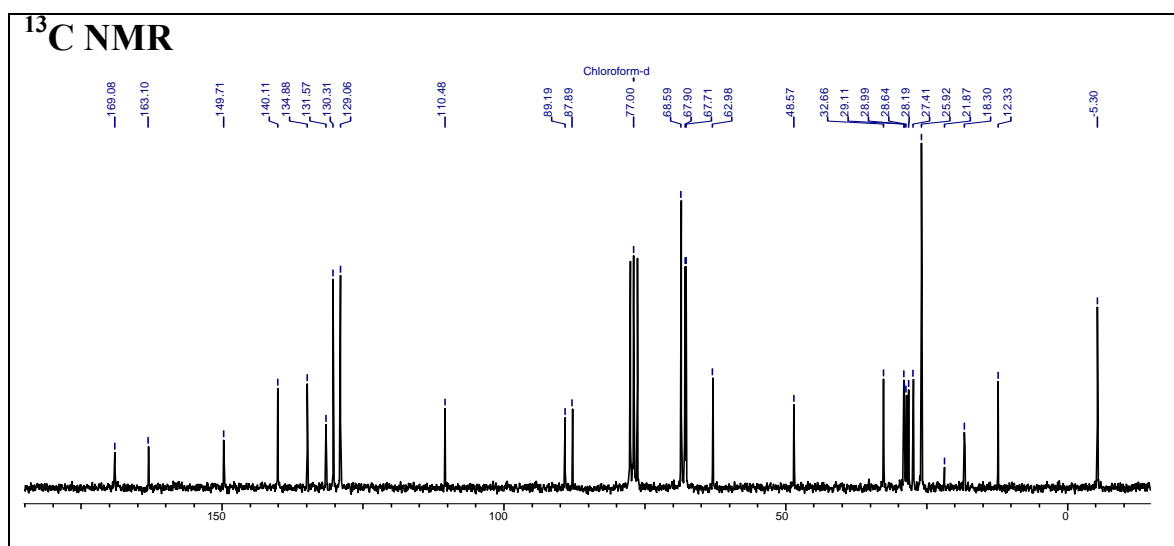
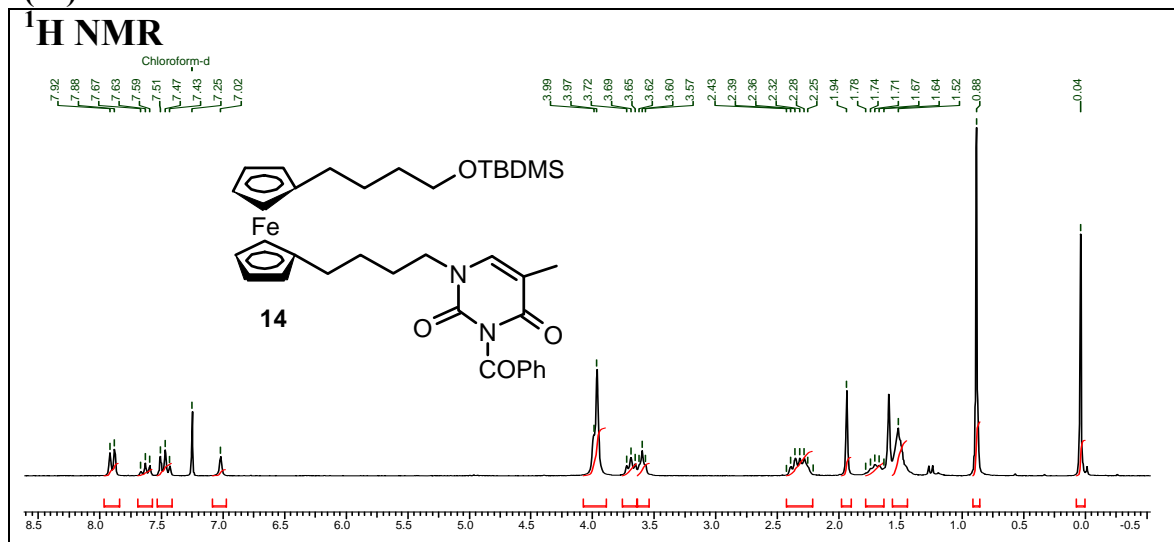


## 1-(4-(Uracilyl)butyl)ferrocene (2b)

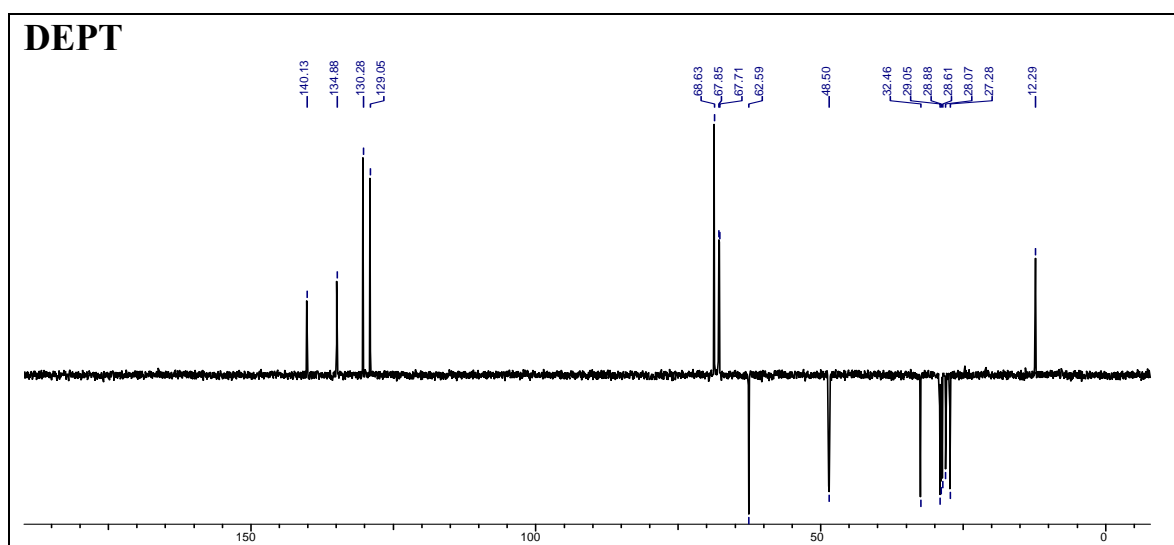
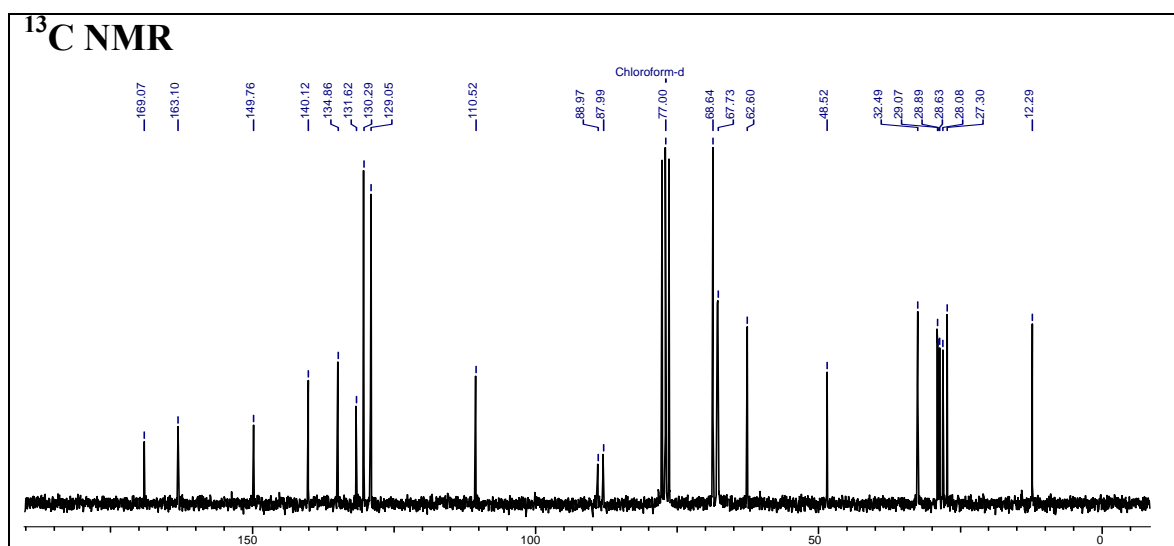
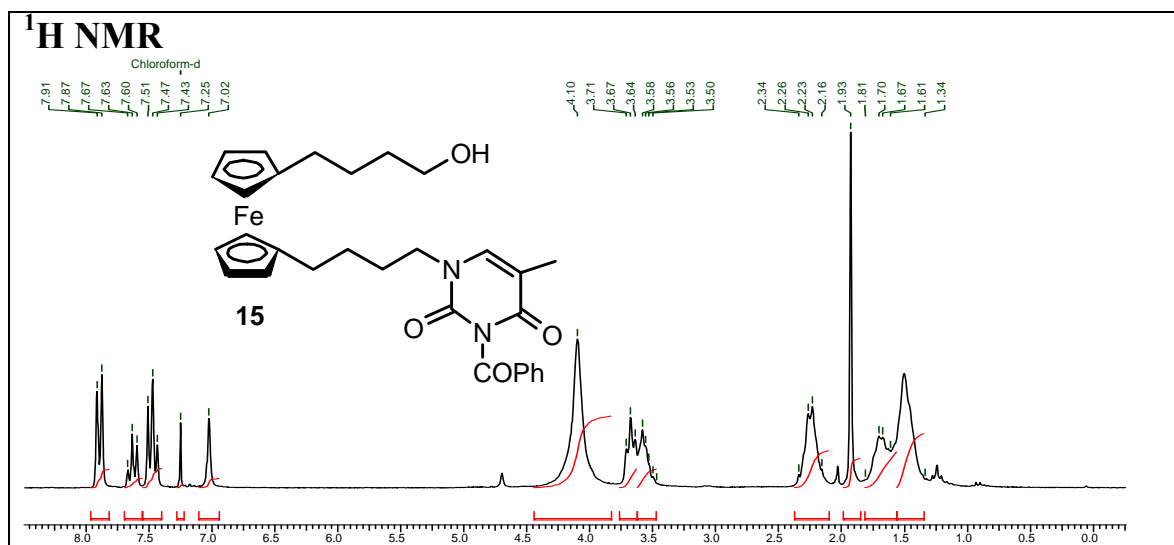


1-(4-Hydroxybutyl)-1'-(4-(*tert*-butyldimethylsilyloxy)butyl)ferrocene (13)

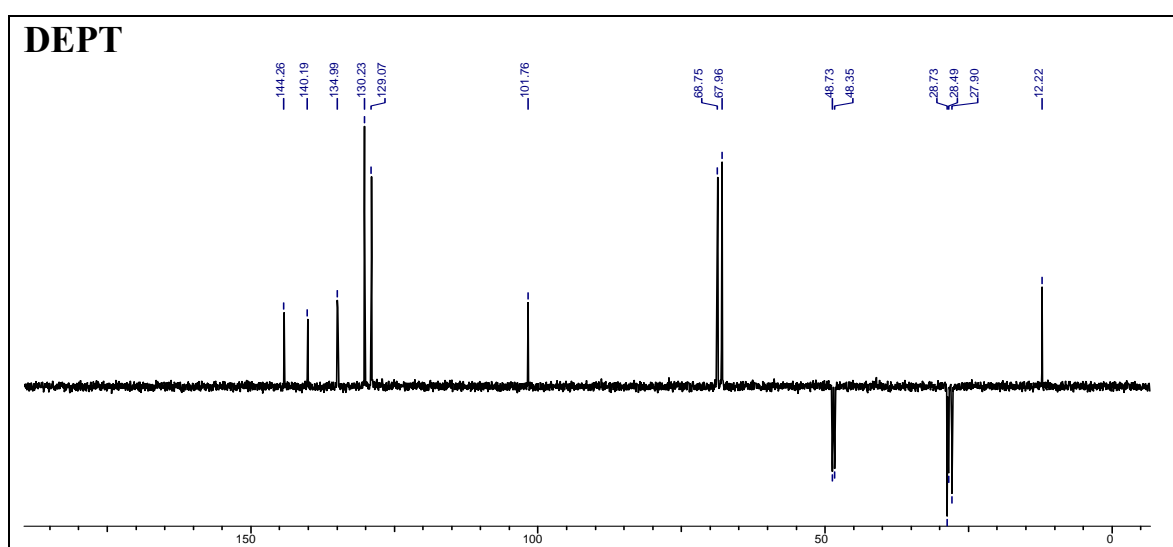
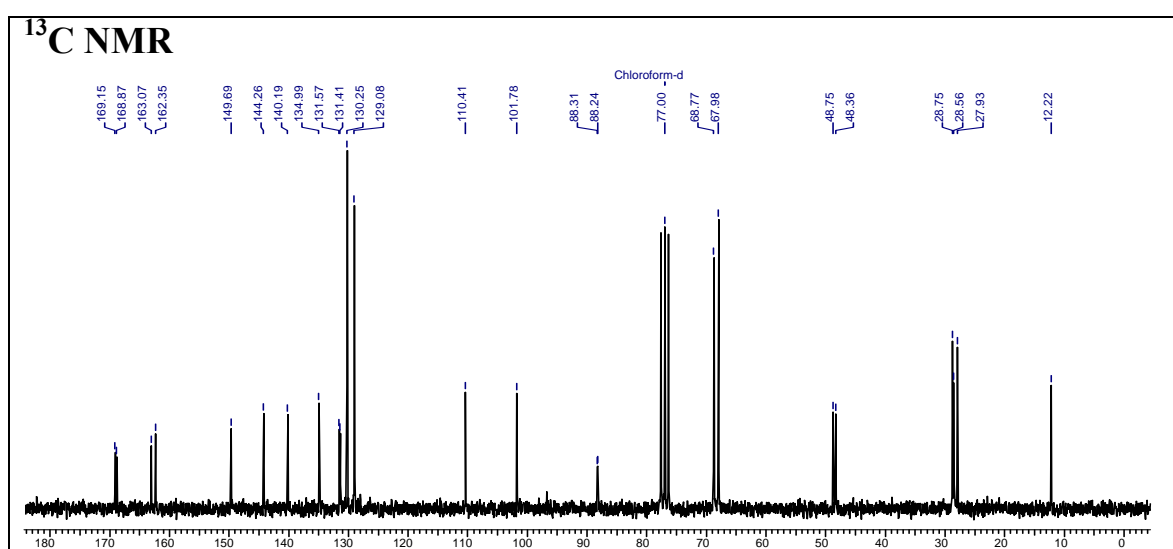
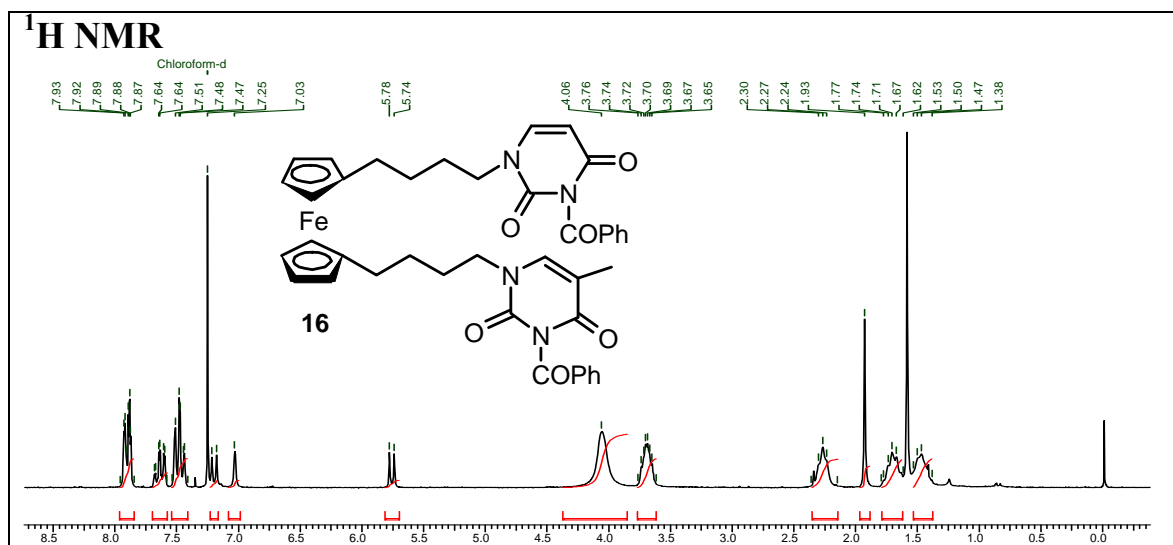
**1-(4-(*N*3-Benzoylthyminy)butyl)-1'-(4-(*tert*-butyldimethylsilyloxy)butyl)ferrocene (14)**



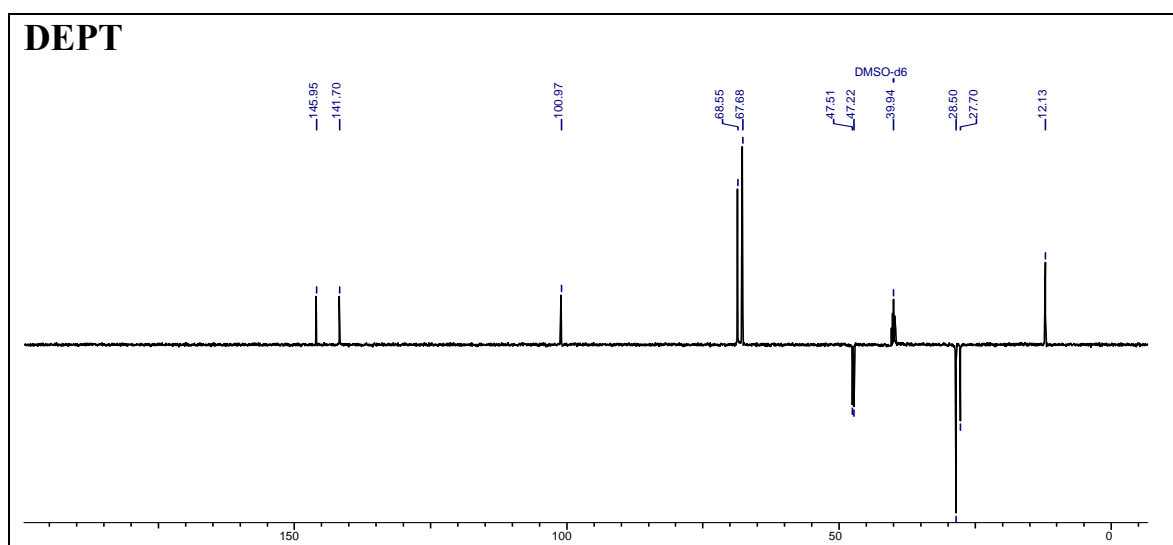
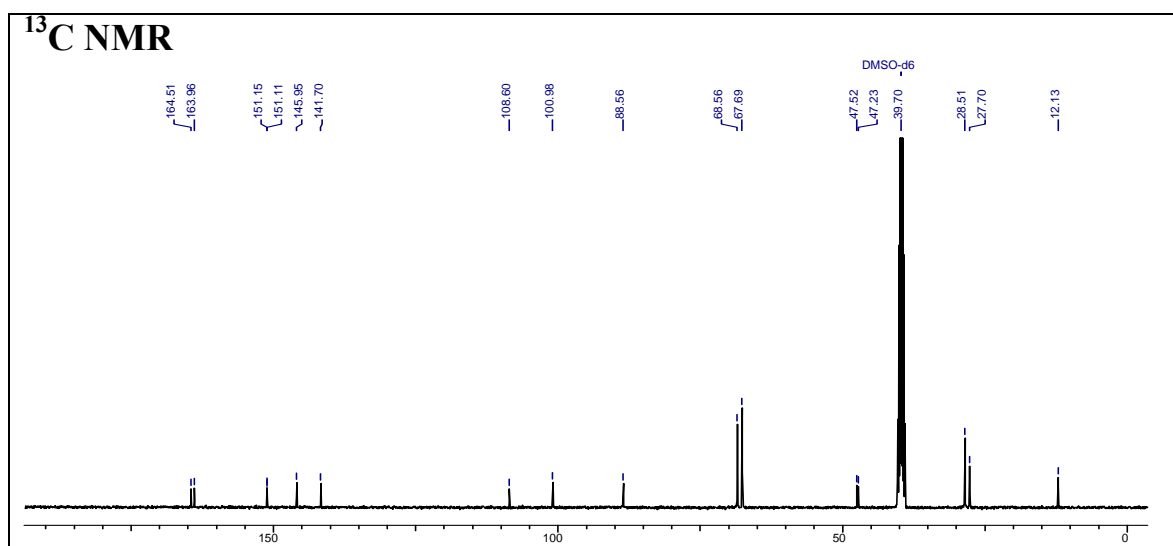
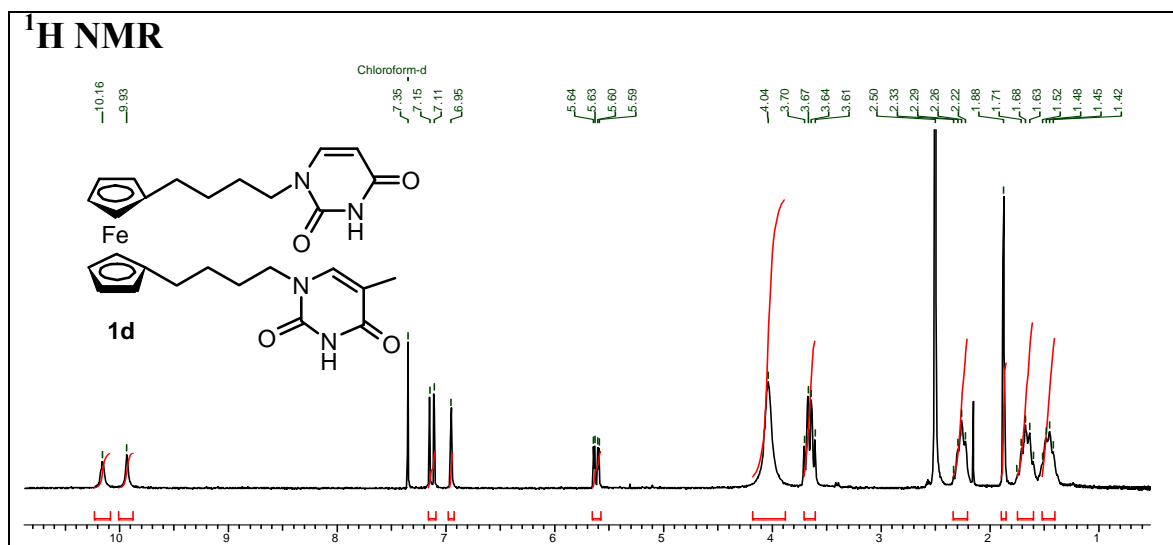
## 1-(4-(N3-Benzoylthyminy)butyl)-1'-(4-hydroxybutyl)ferrocene (15)



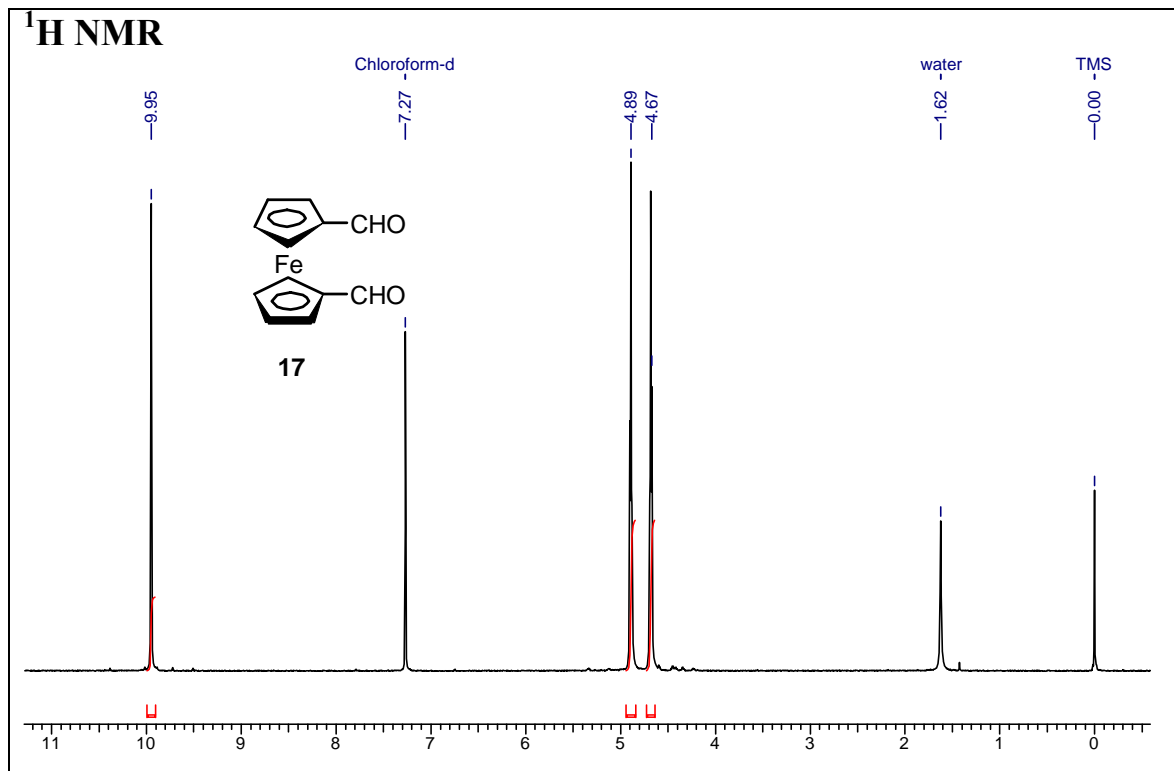
## 1-(4-(N3-Benzoylthyminy)butyl)-1'-(4-(N3-benzoyluracily)butyl)ferrocene (16)



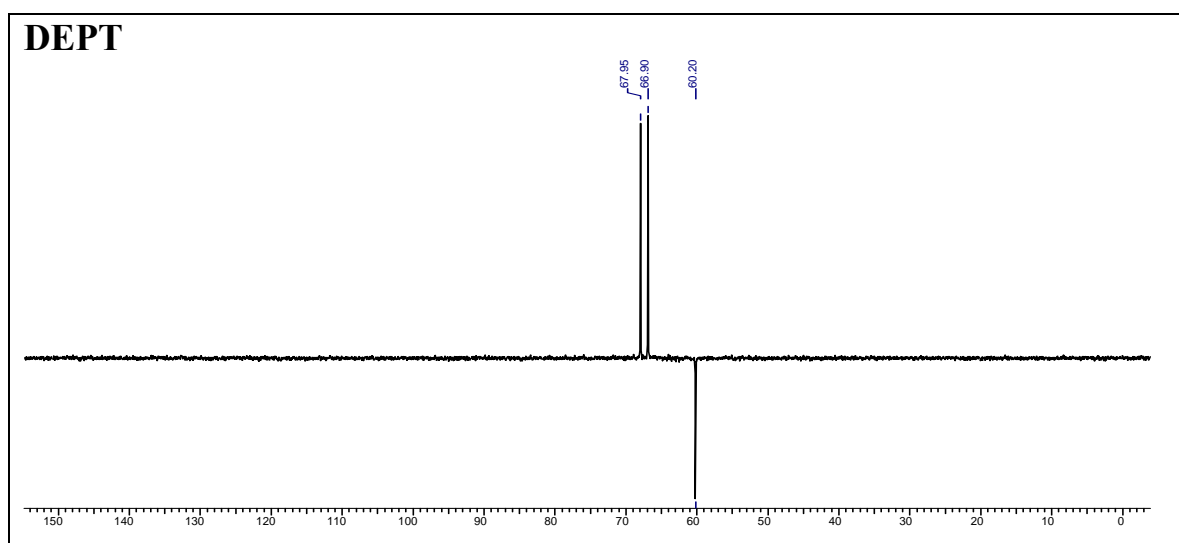
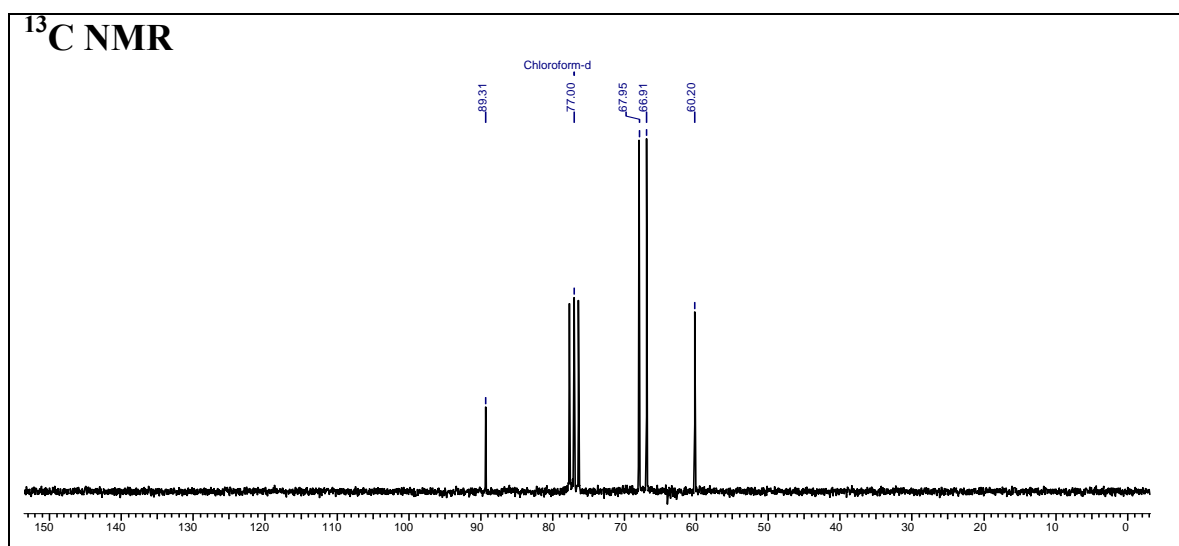
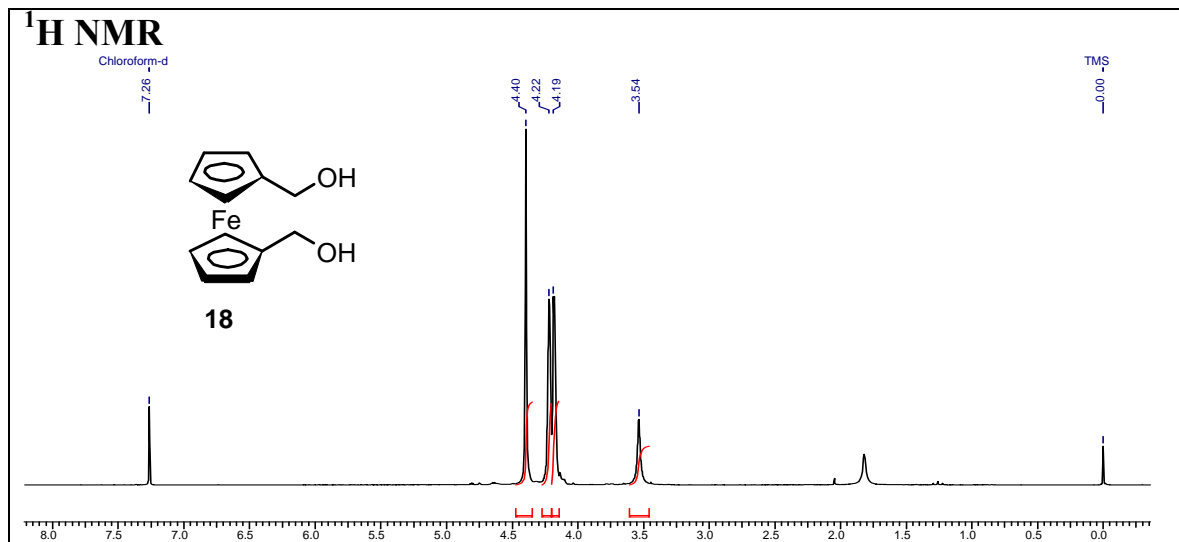
## 1-(4-(Thyminyl)butyl)-1'-(4-(uracilyl)butyl)ferrocene (1d)

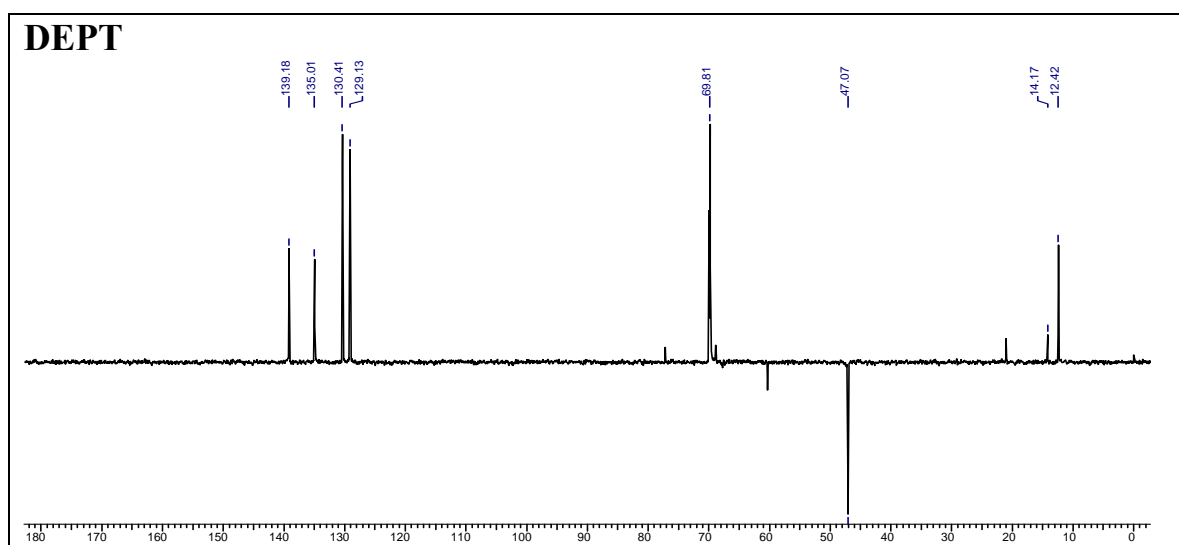
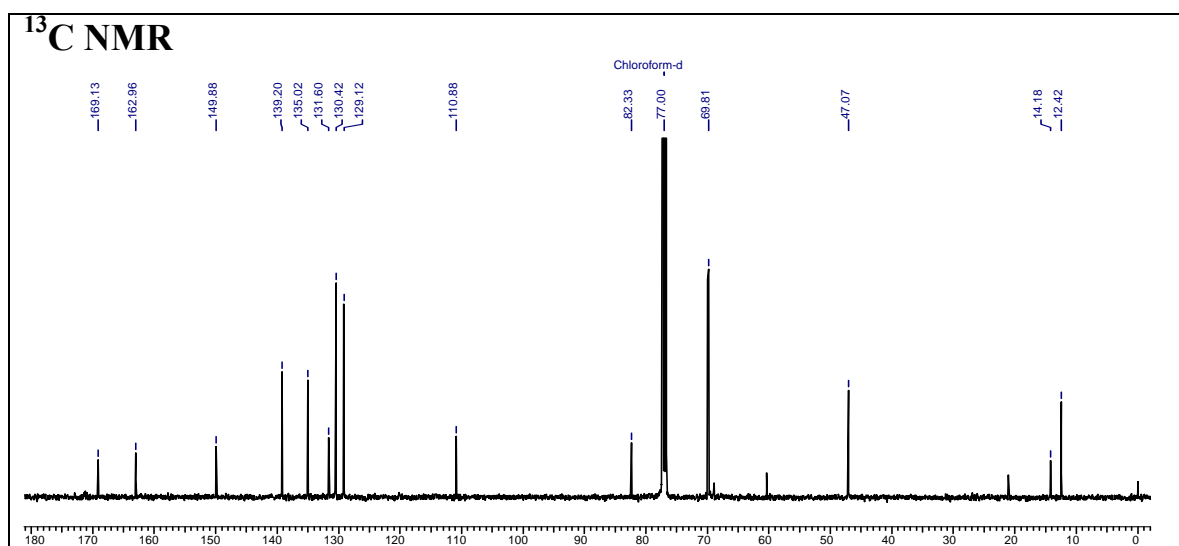
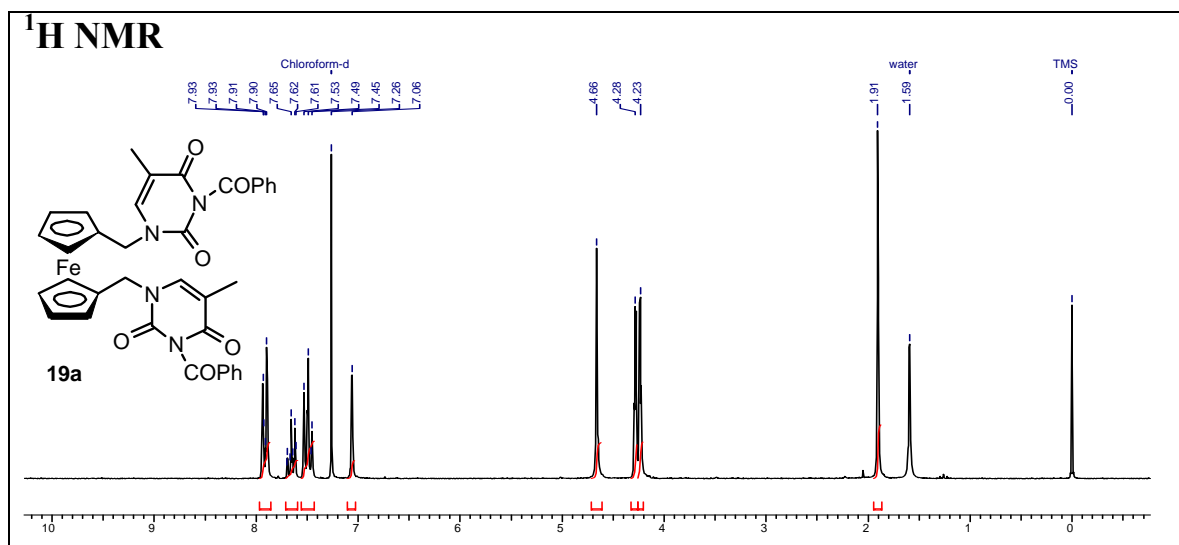


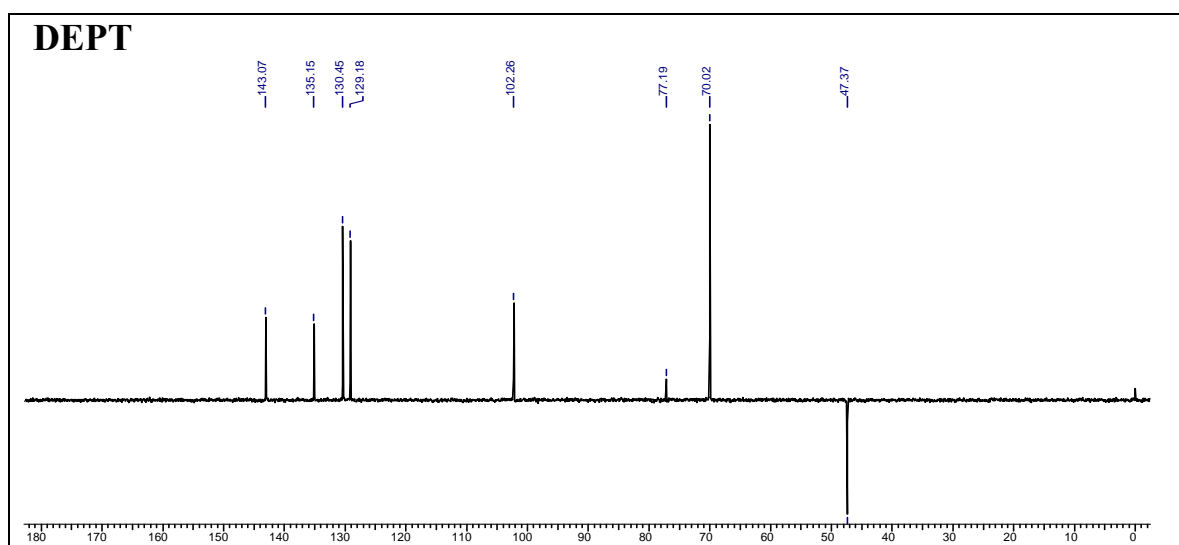
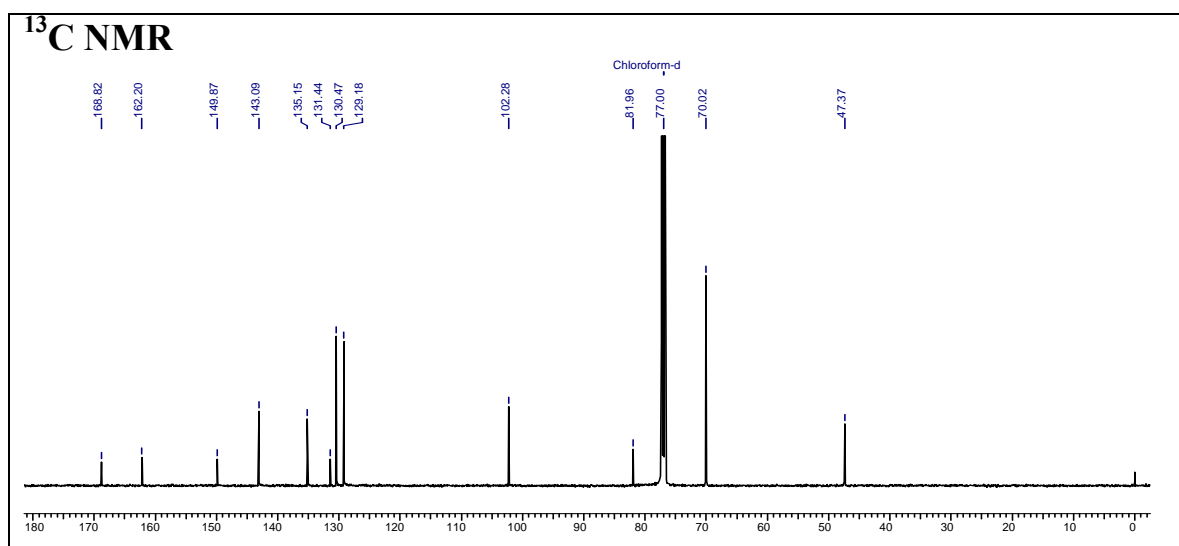
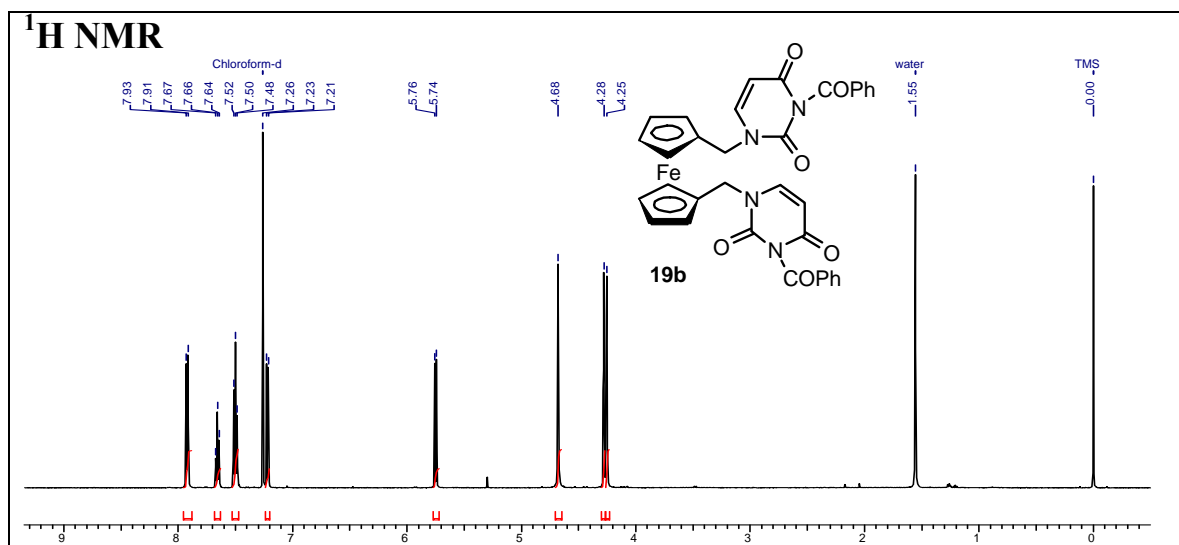


**1,1'-Ferrocenecarboxaldehyde (17)**

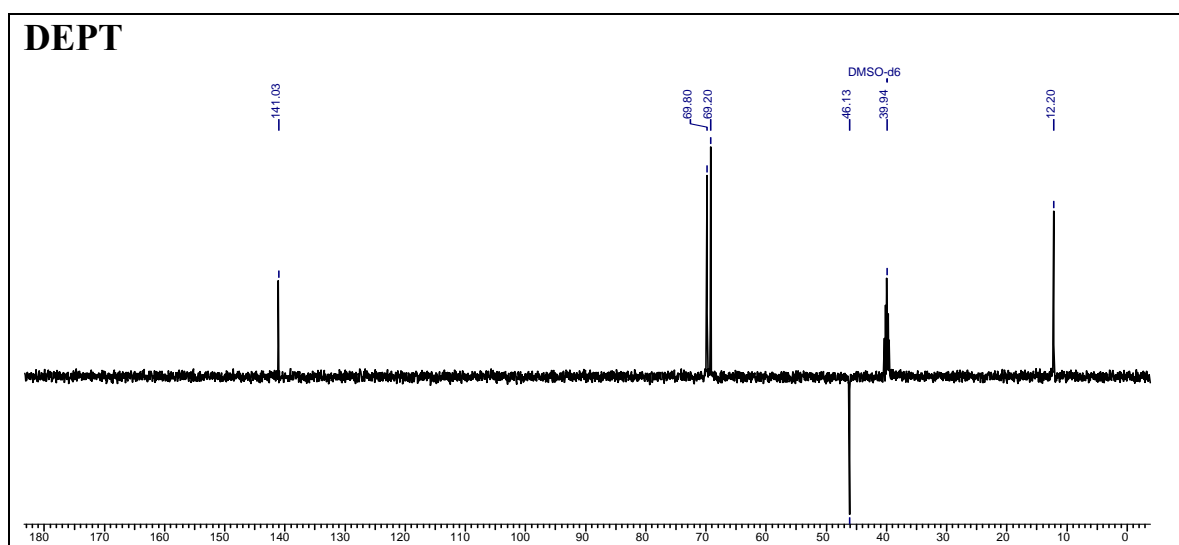
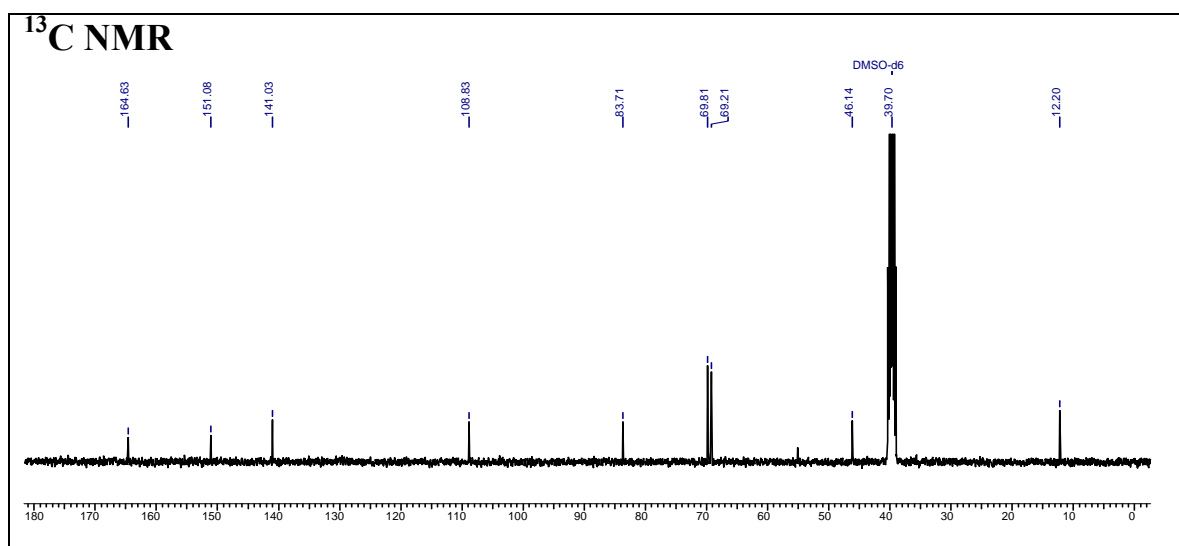
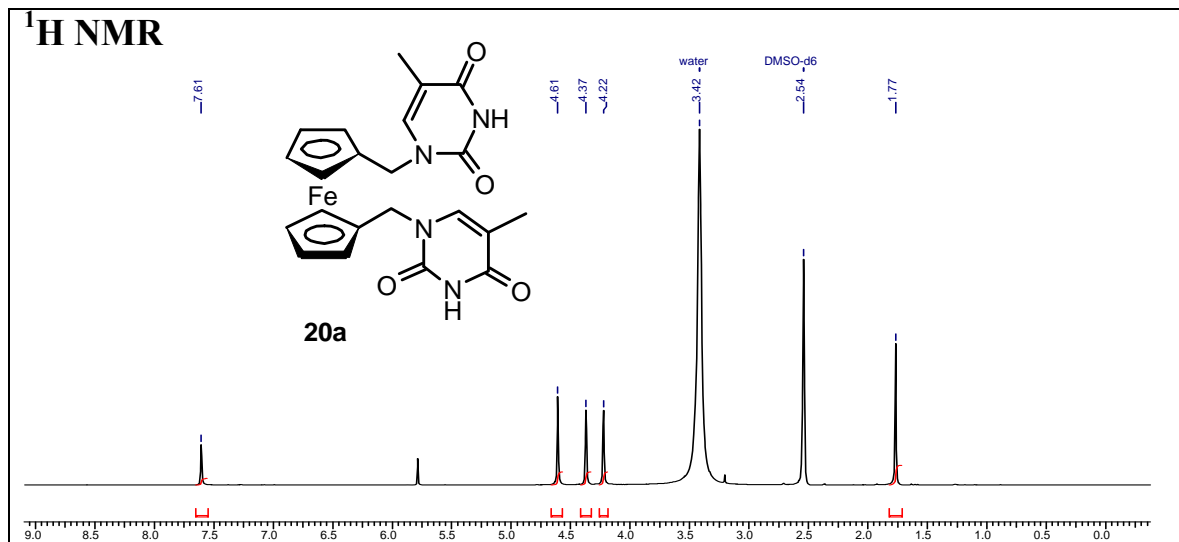
## 1,1'-Bis(hydroxymethyl)ferrocene (18)



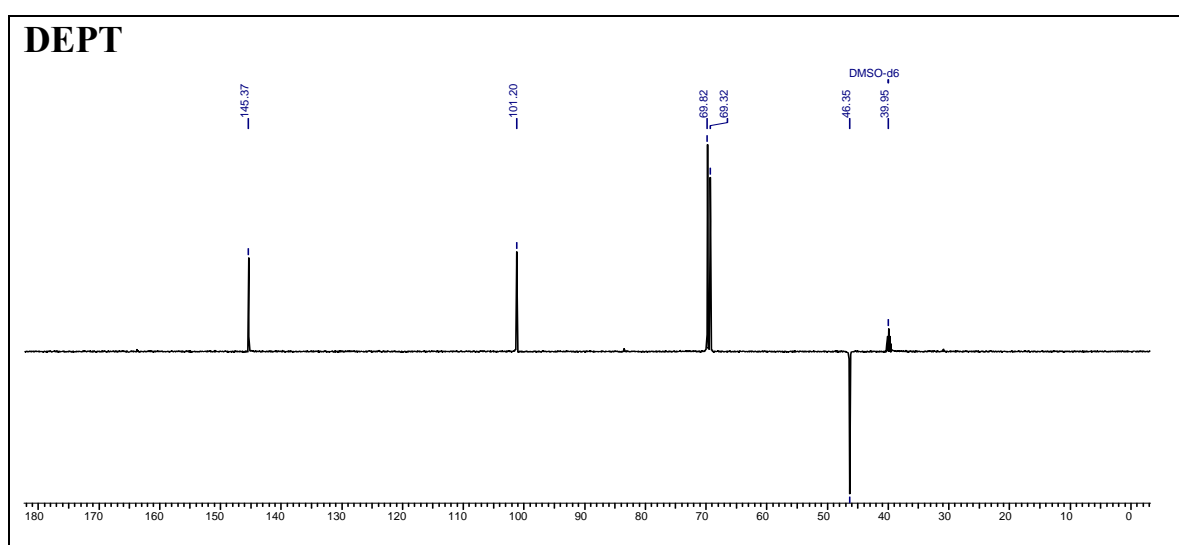
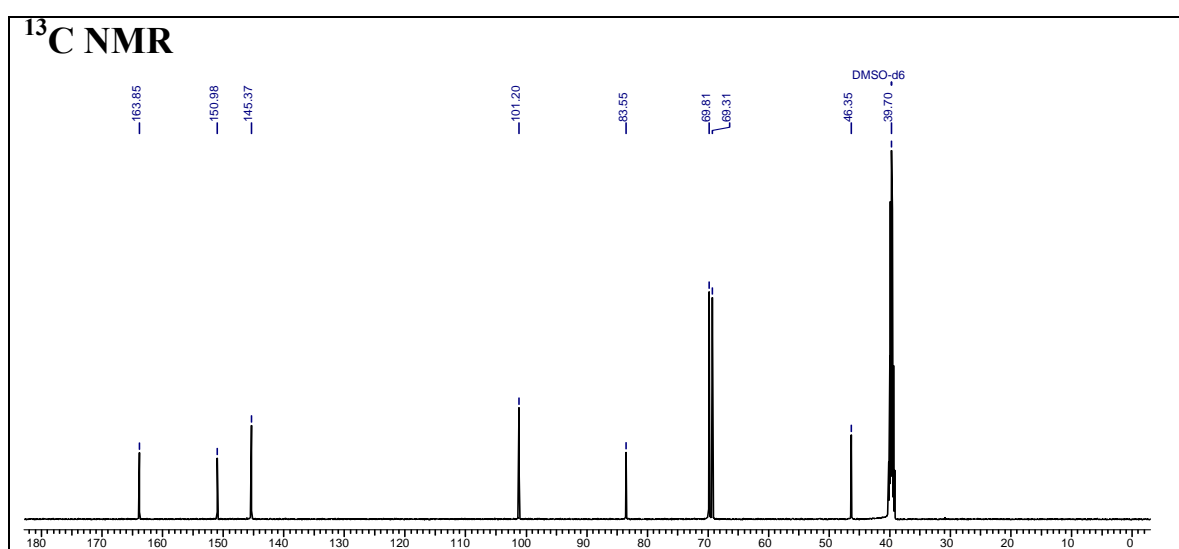
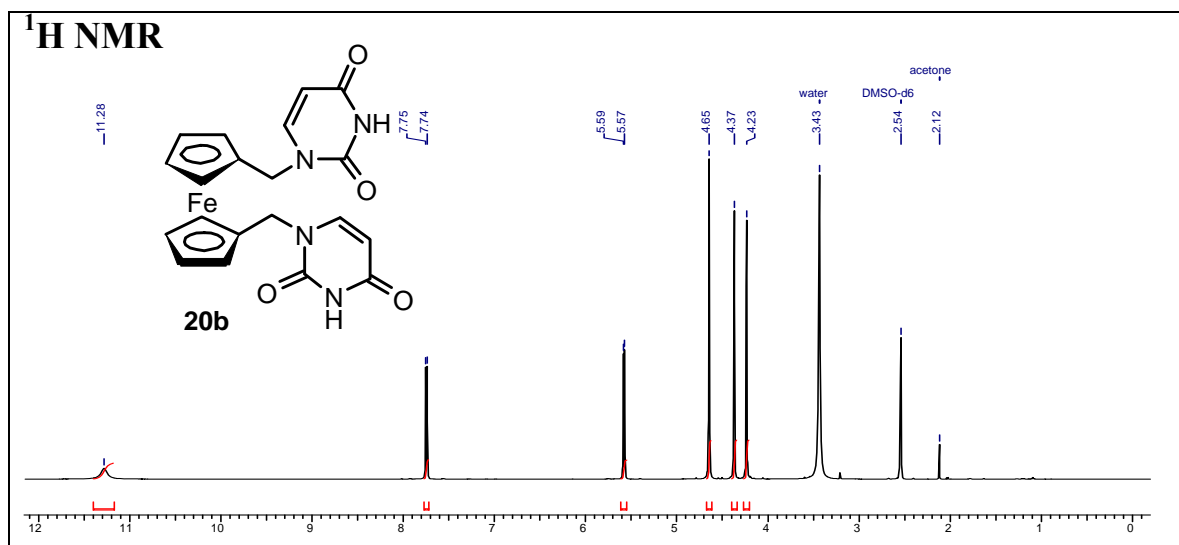
**1,1'-Bis(*N*3-benzoylthyminylmethyl)ferrocene (19a)**

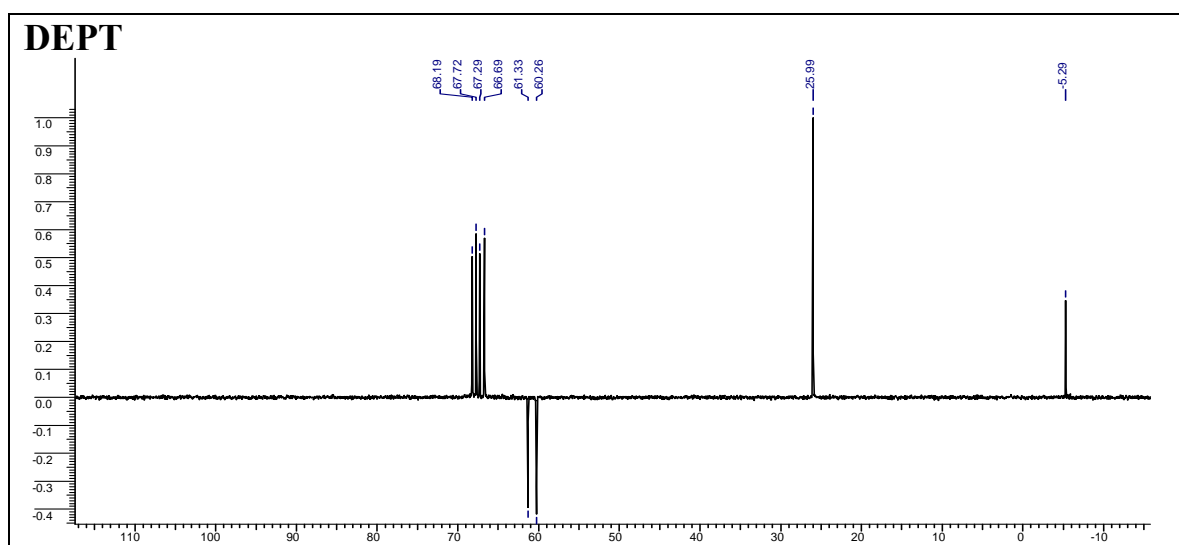
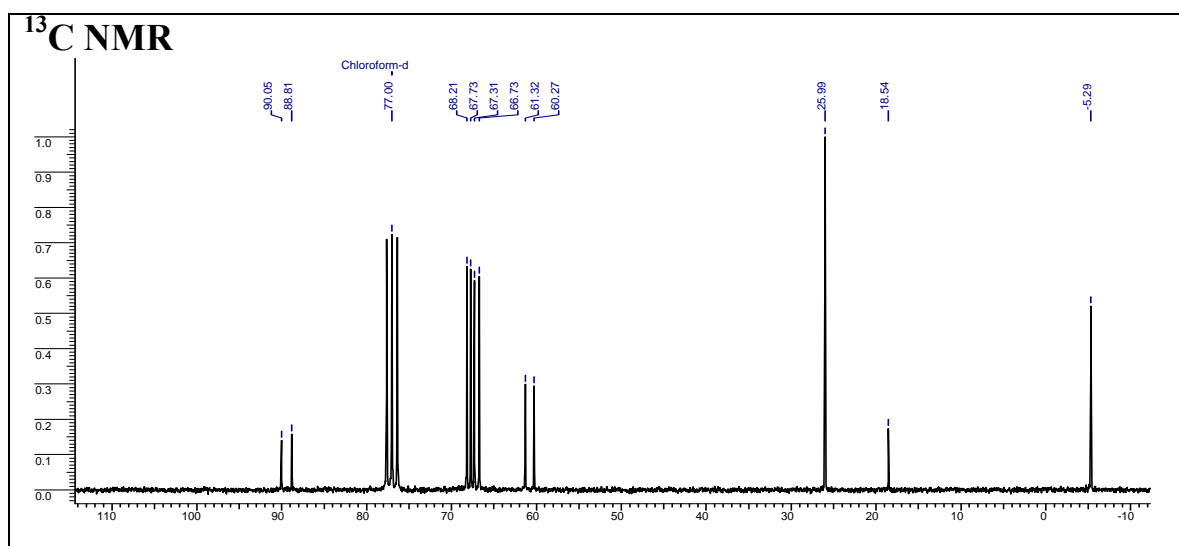
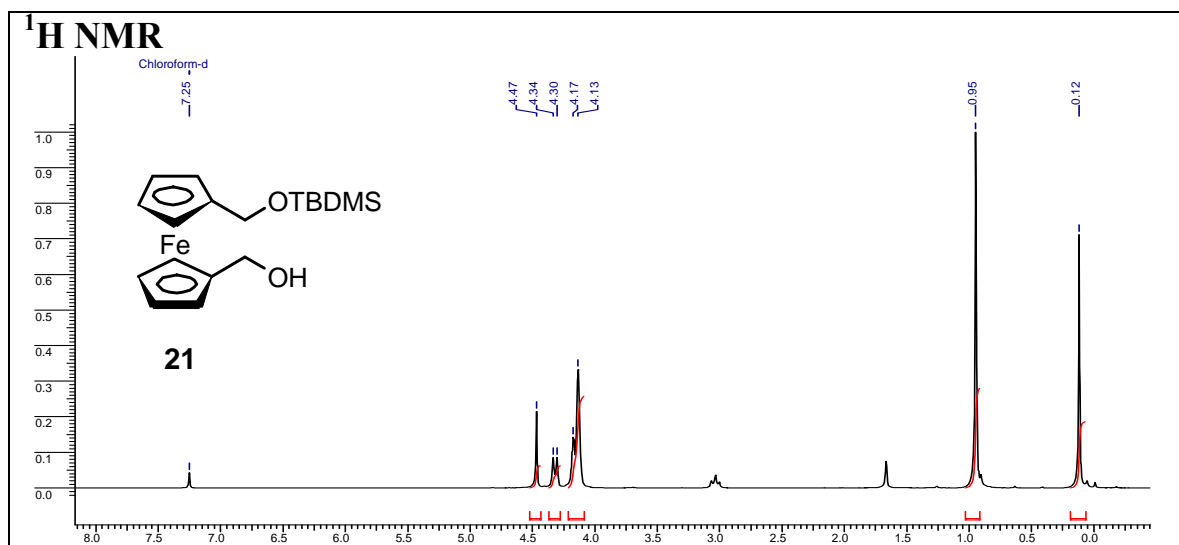
**1,1'-Bis(*N*3-benzoyluracilylmethyl)ferrocene (19b)**

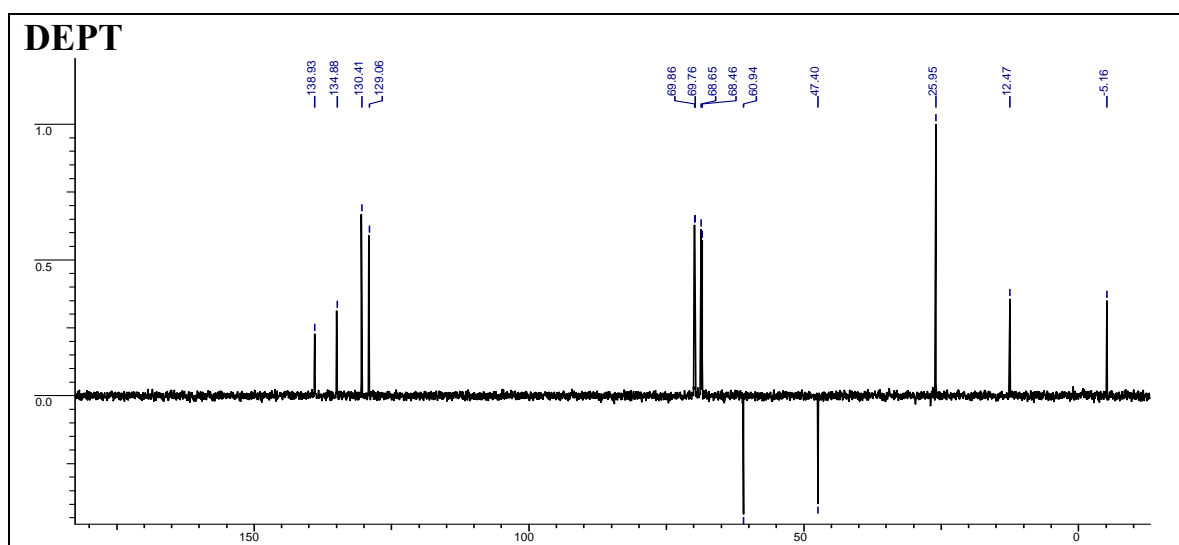
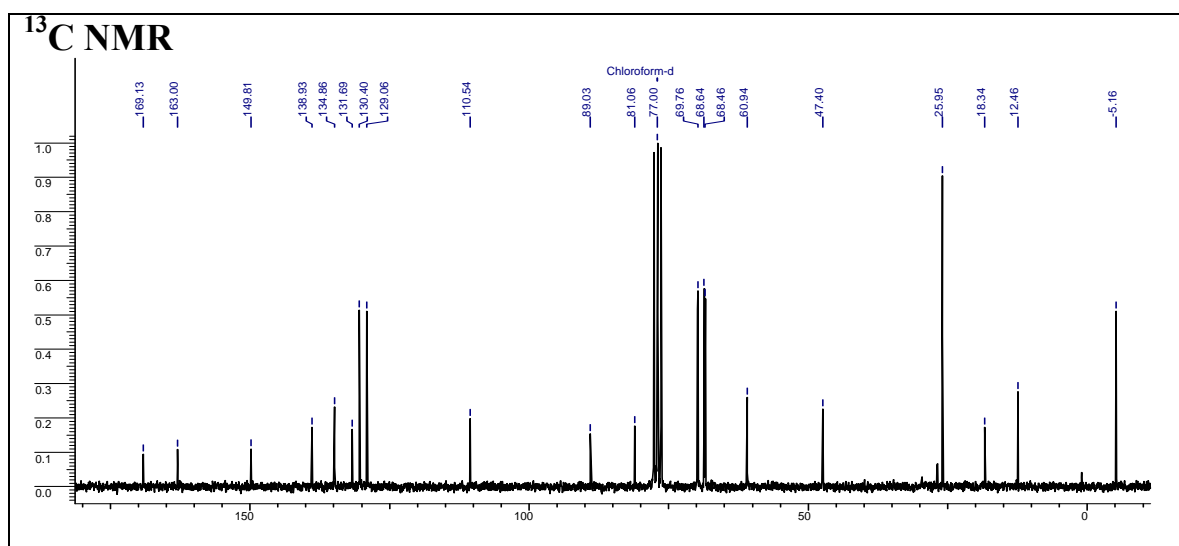
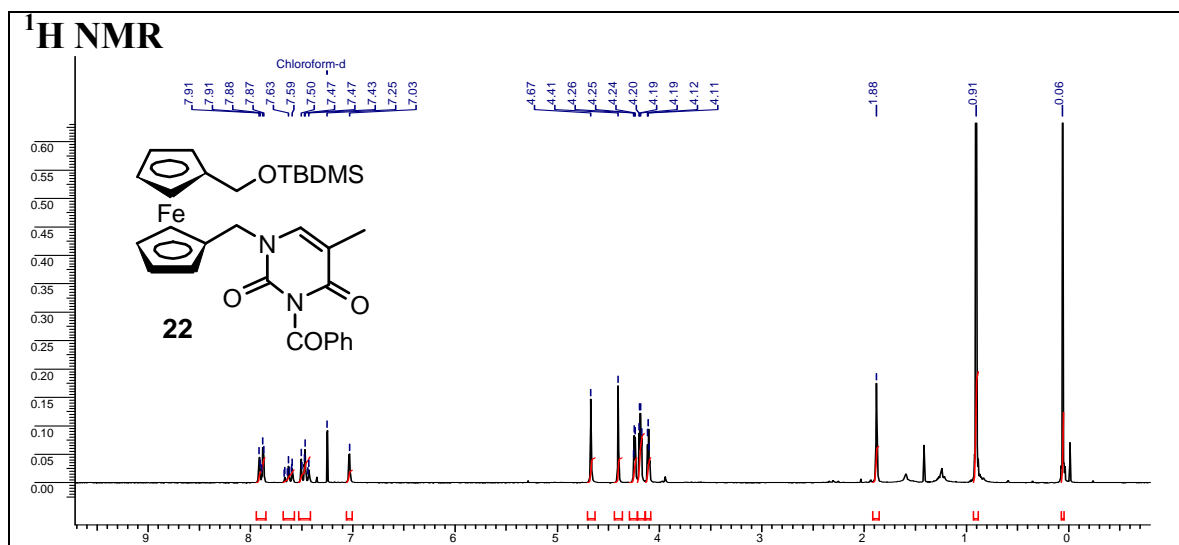
## 1,1'-Bis(thyminylmethyl)ferrocene (20a)



## 1,1'-Bis(uracilylmethyl)ferrocene (20b)

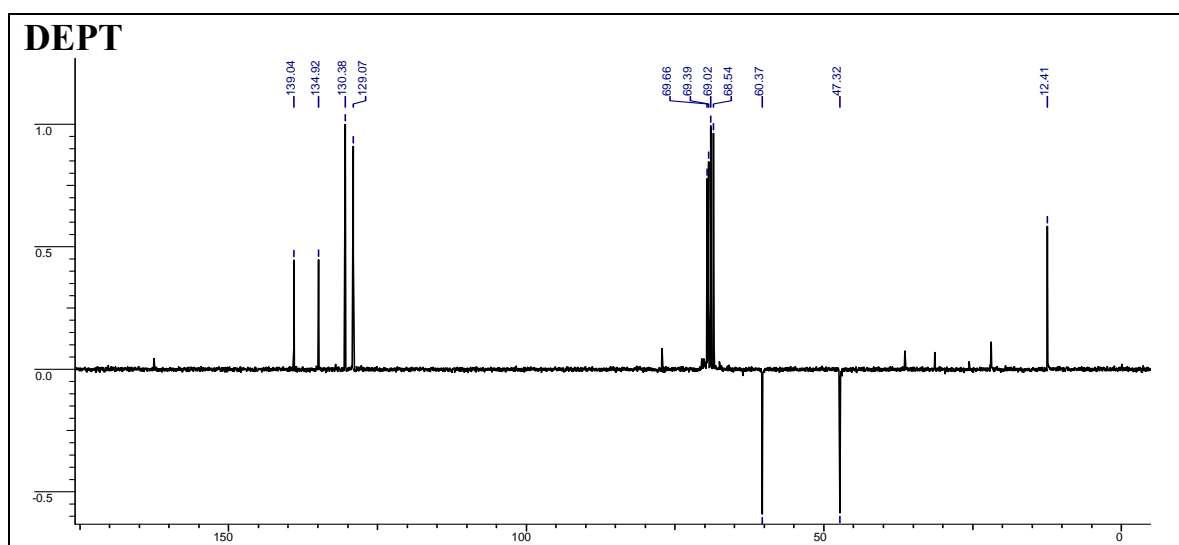
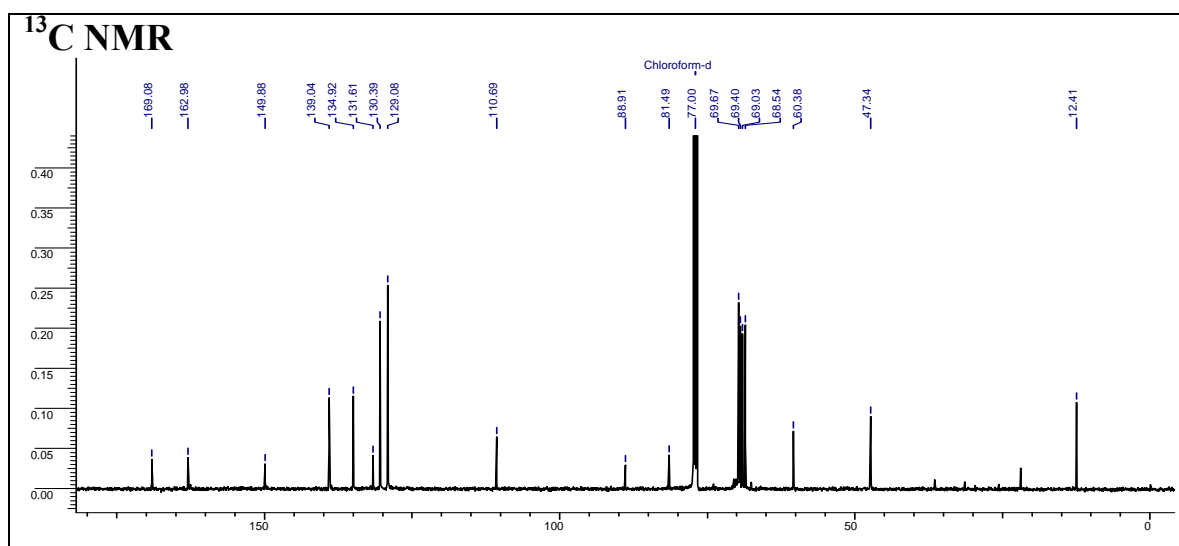
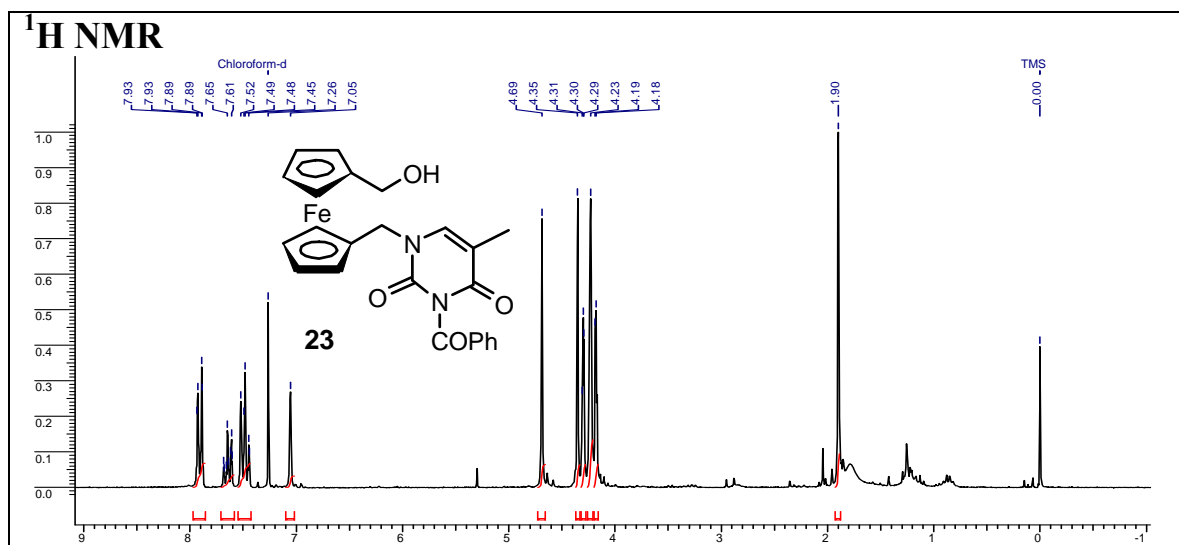


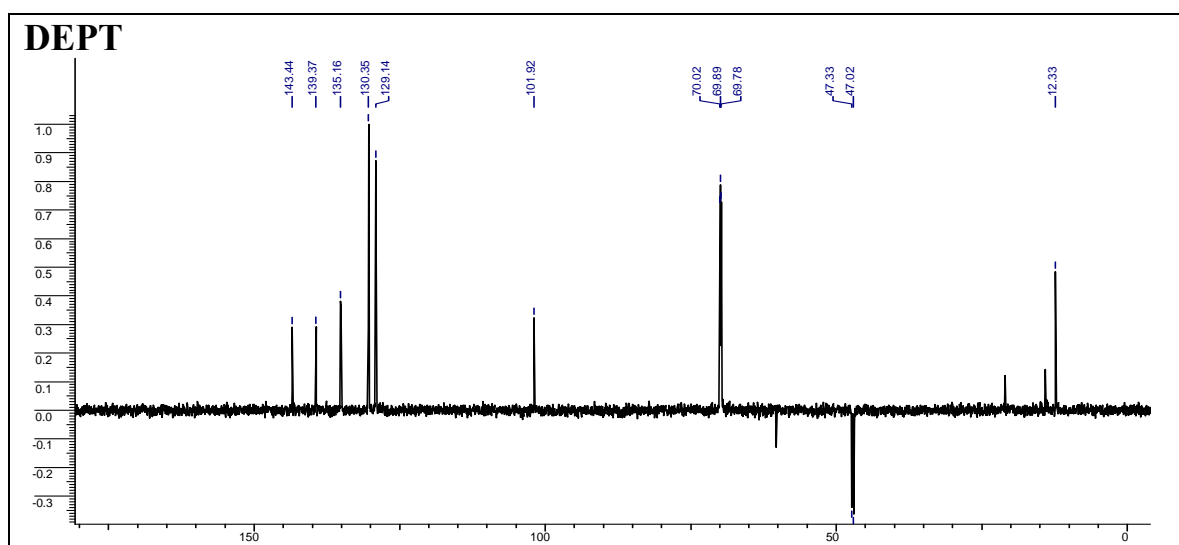
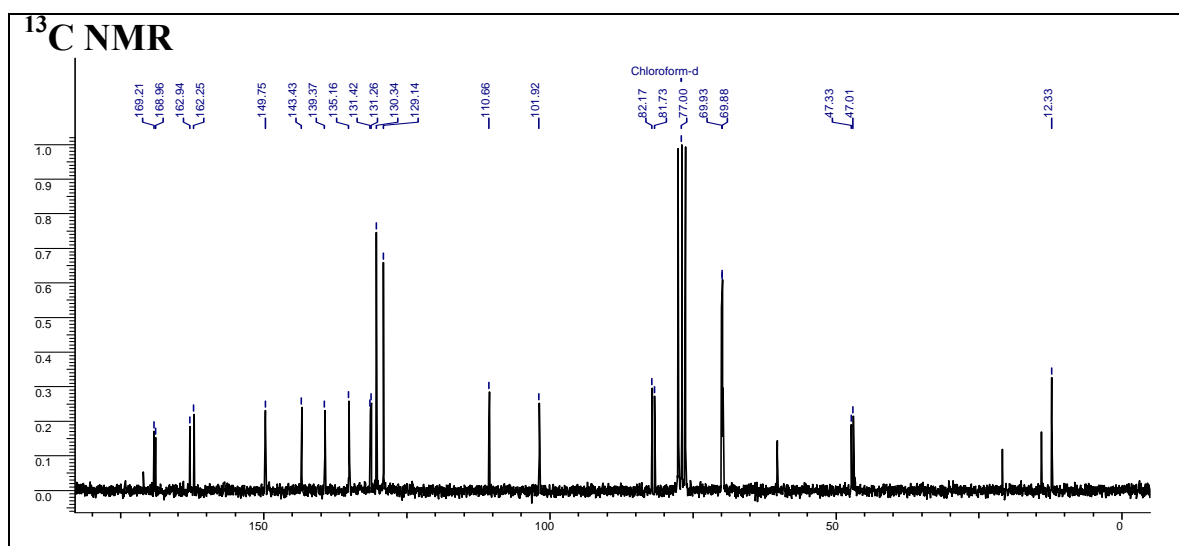
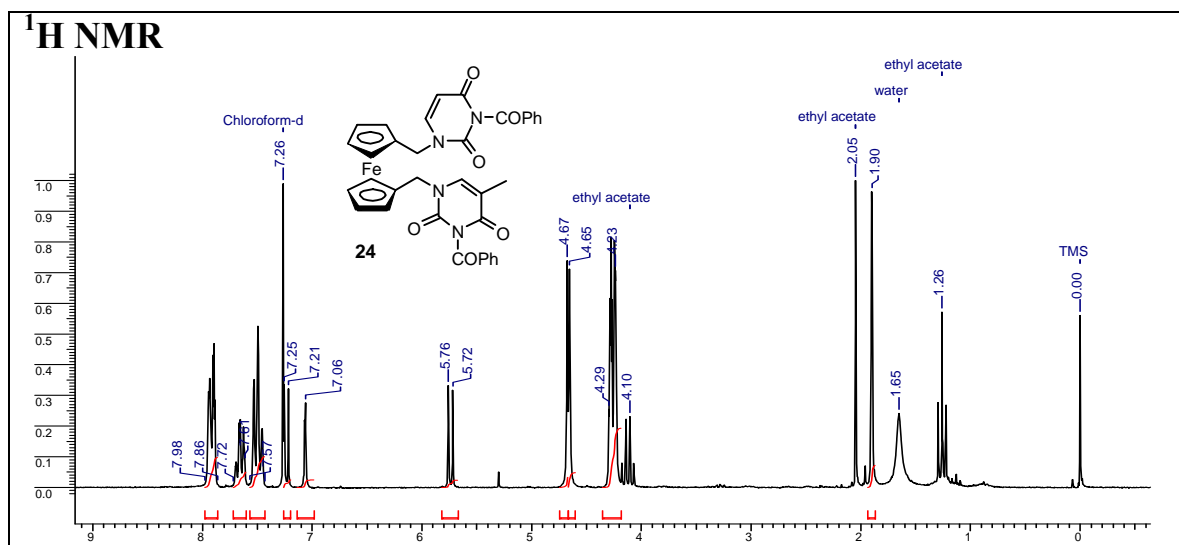
1-(Hydroxymethyl)-1'-(*tert*-butyldimethylsilyloxymethyl)ferrocene (21)

1-(*N*3-Benzoylthyminylmethyl)-1'-(*tert*-butyldimethylsilyloxymethyl)ferrocene (**22**)

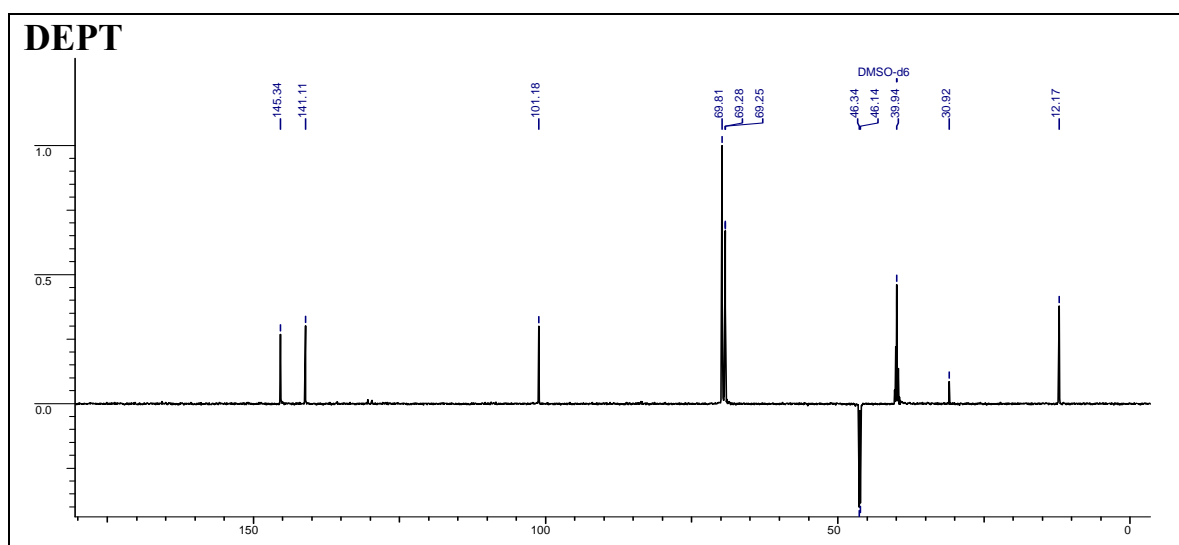
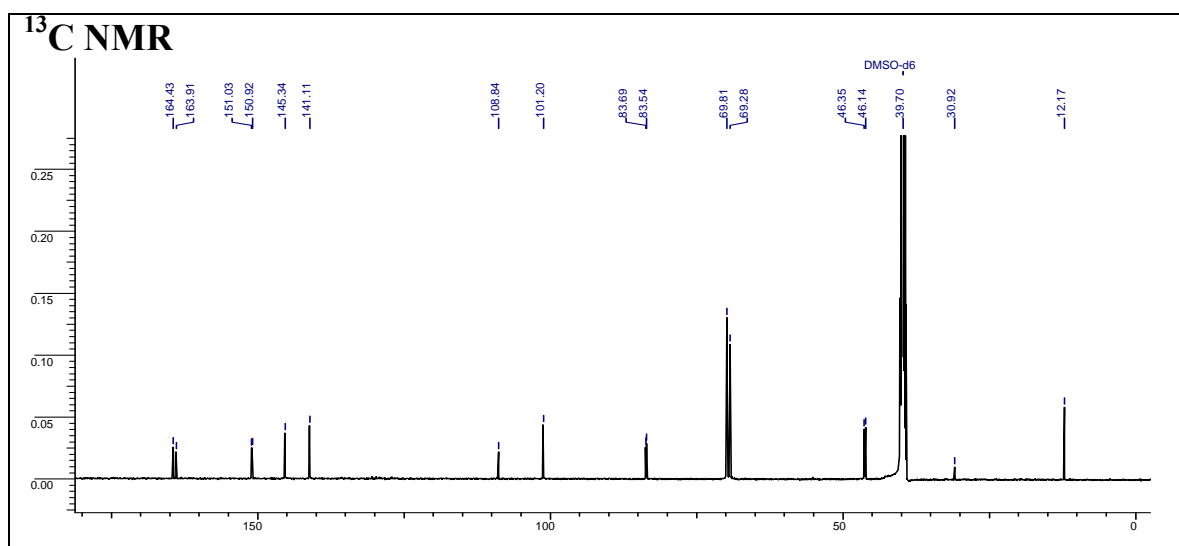
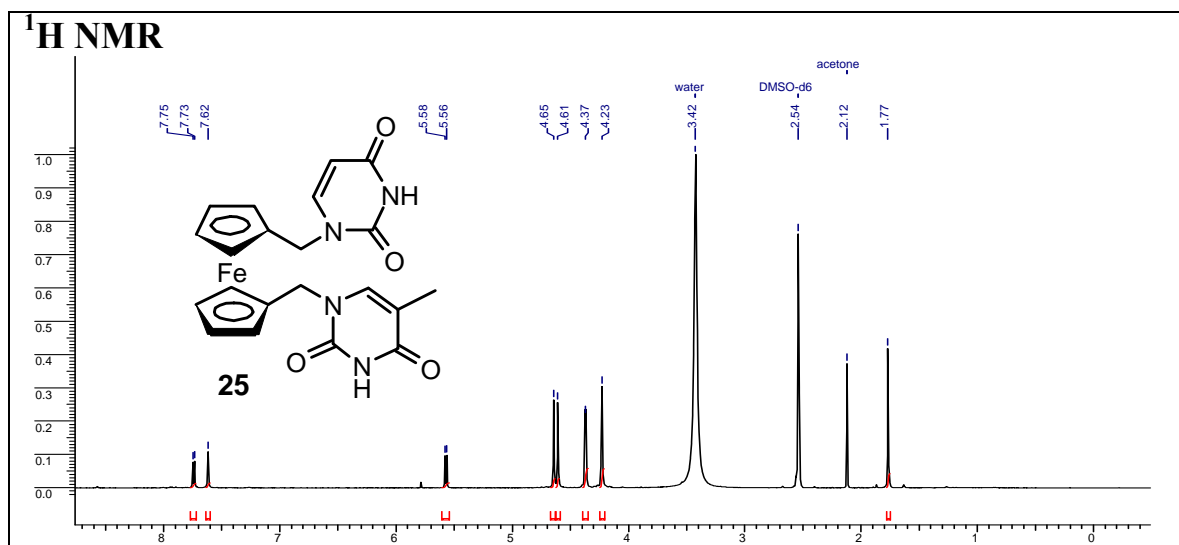


## 1-(N3-Benzoylthyminylmethyl)-1'-(hydroxymethyl)ferrocene (23)

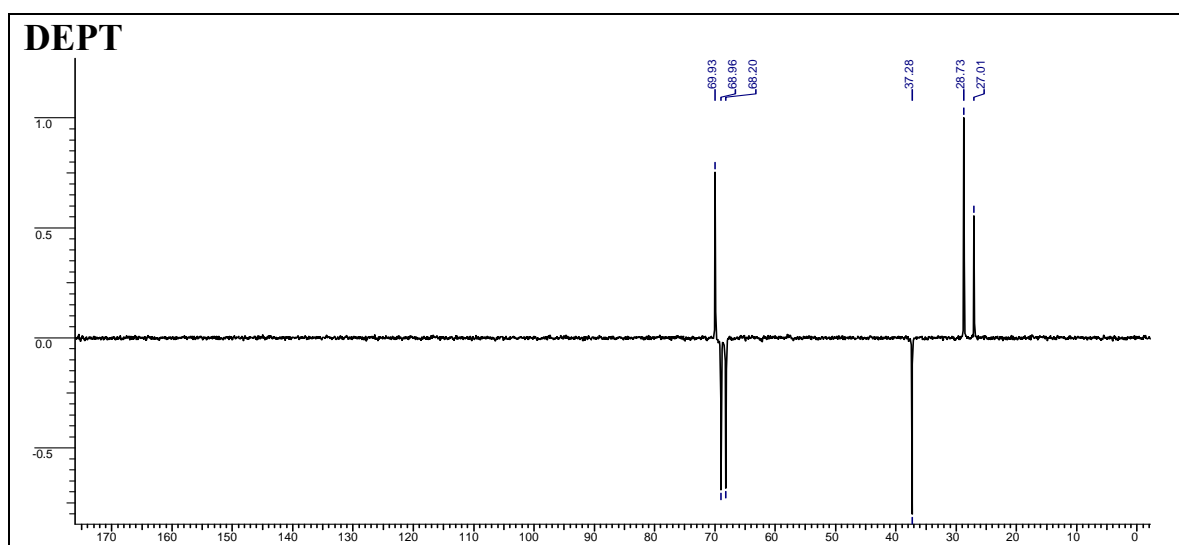
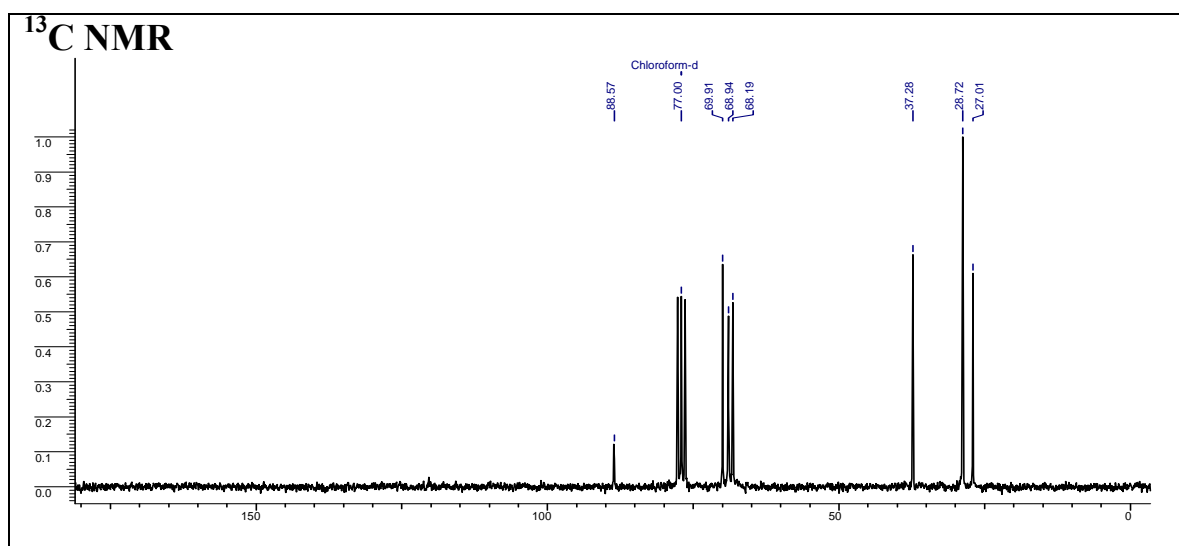
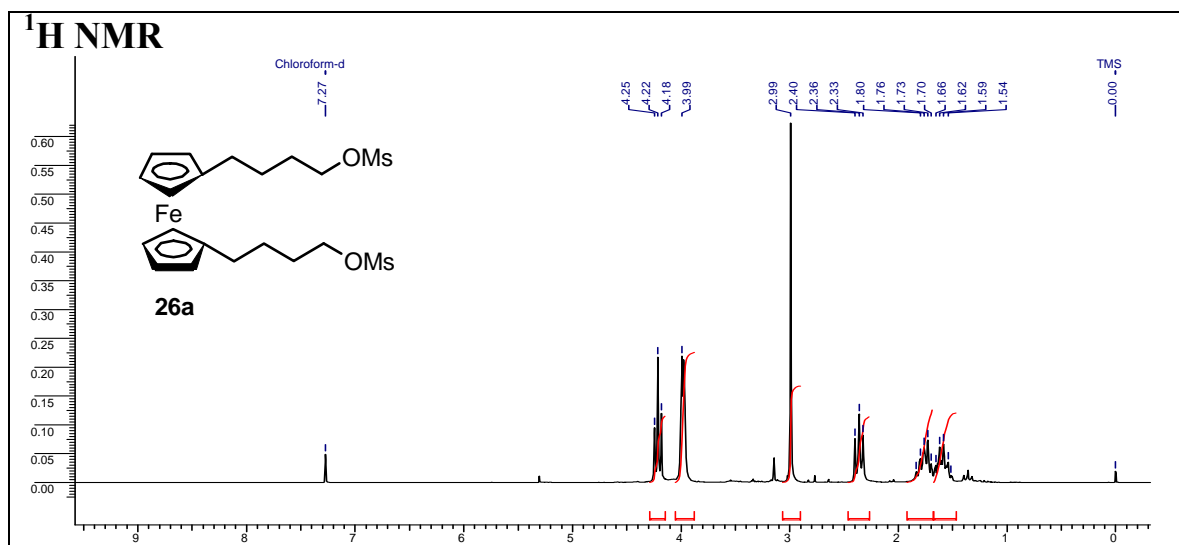


1-(*N*3-Benzoylthyminylmethyl)-1'-(*N*3-benzoyluracilylmethyl)ferrocene (**24**)

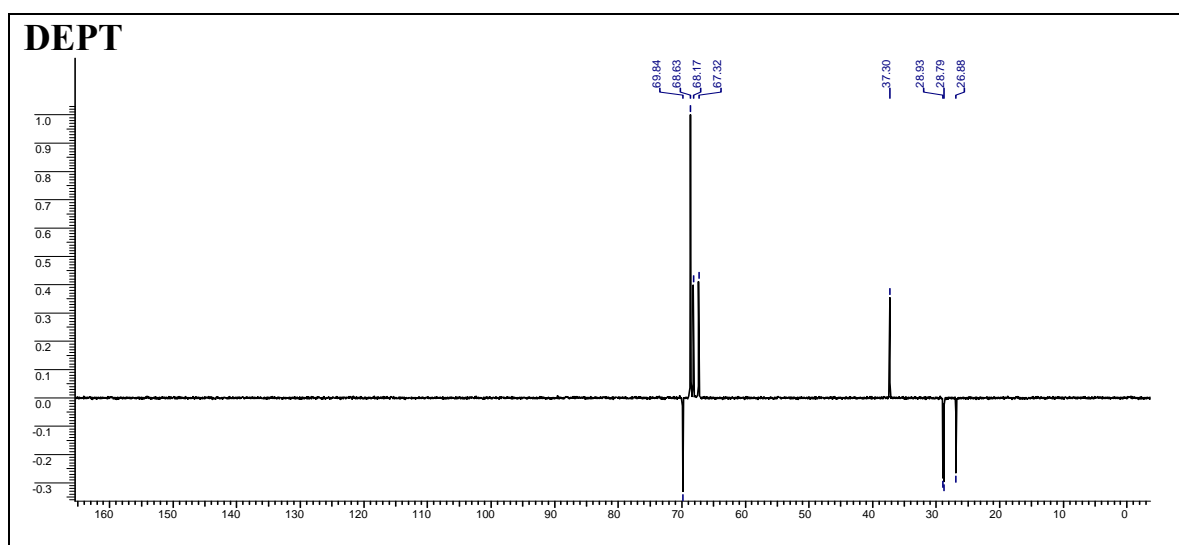
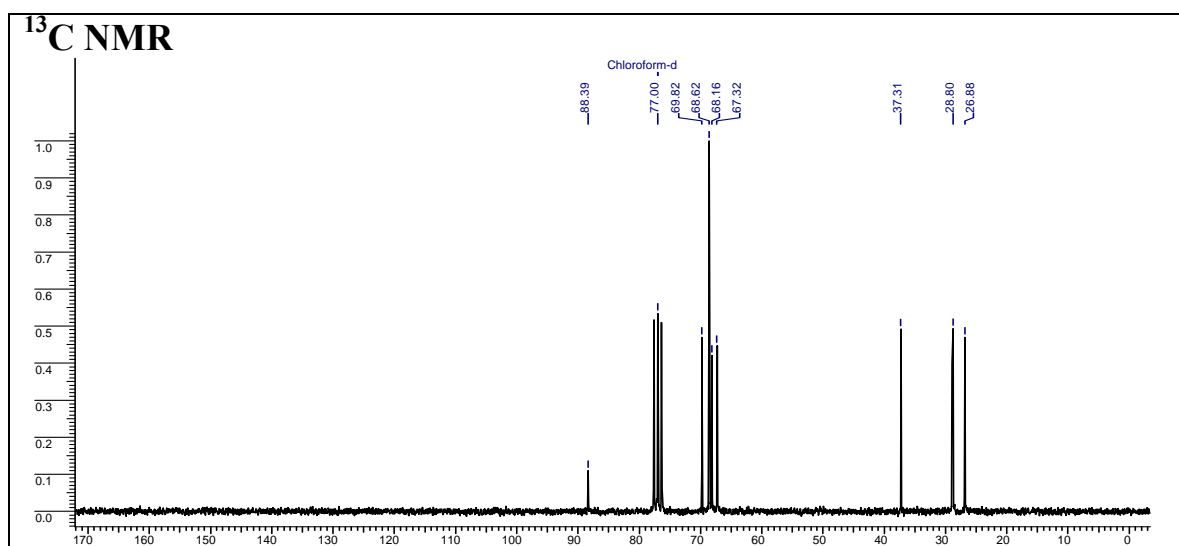
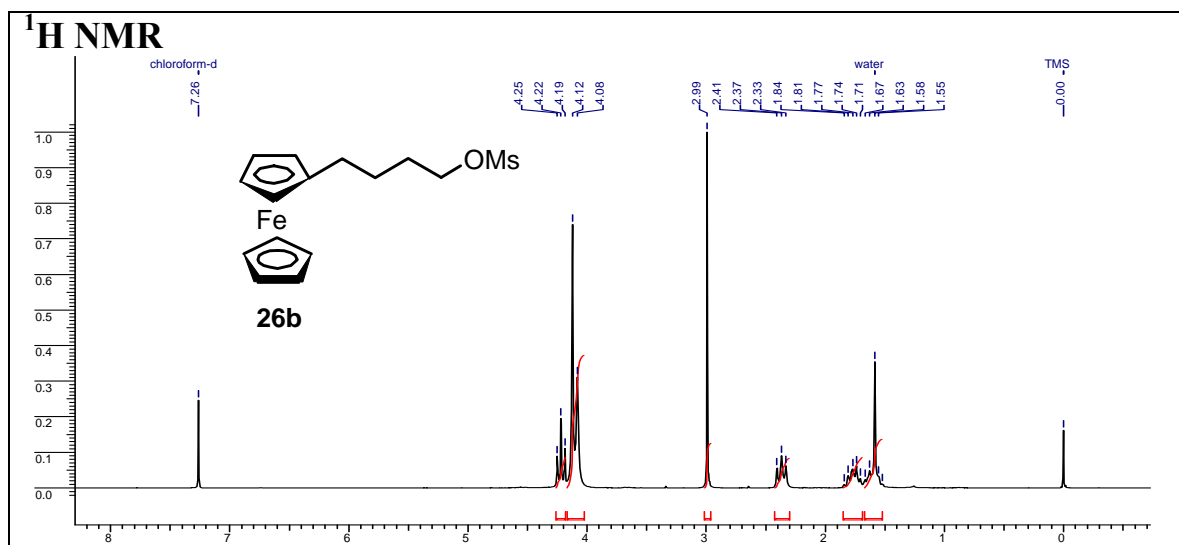
## 1-(Thyminylmethyl)-1'-(uracilylmethyl)ferrocene (25)



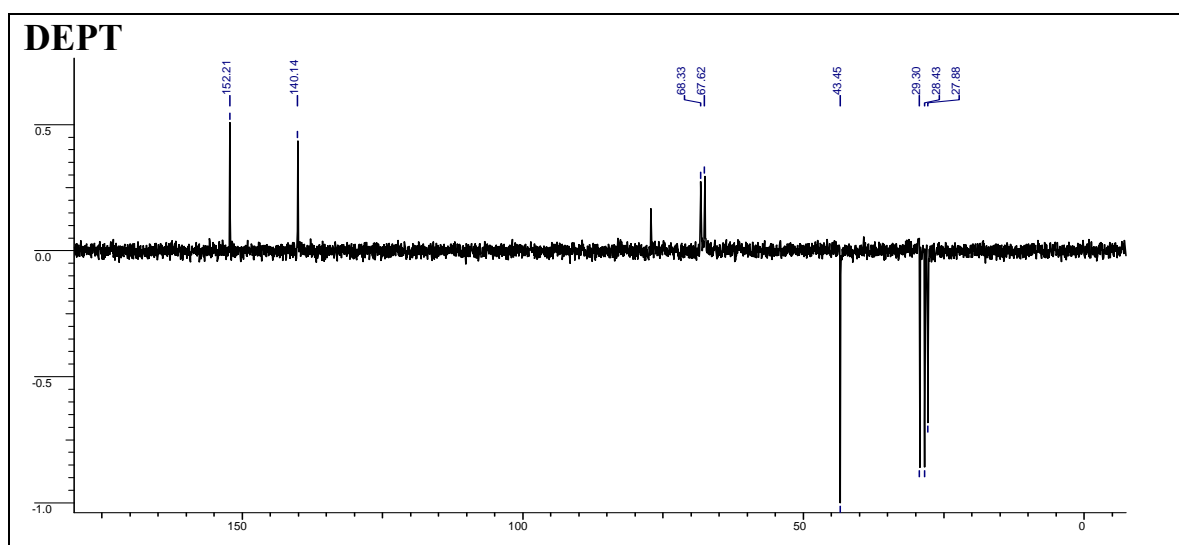
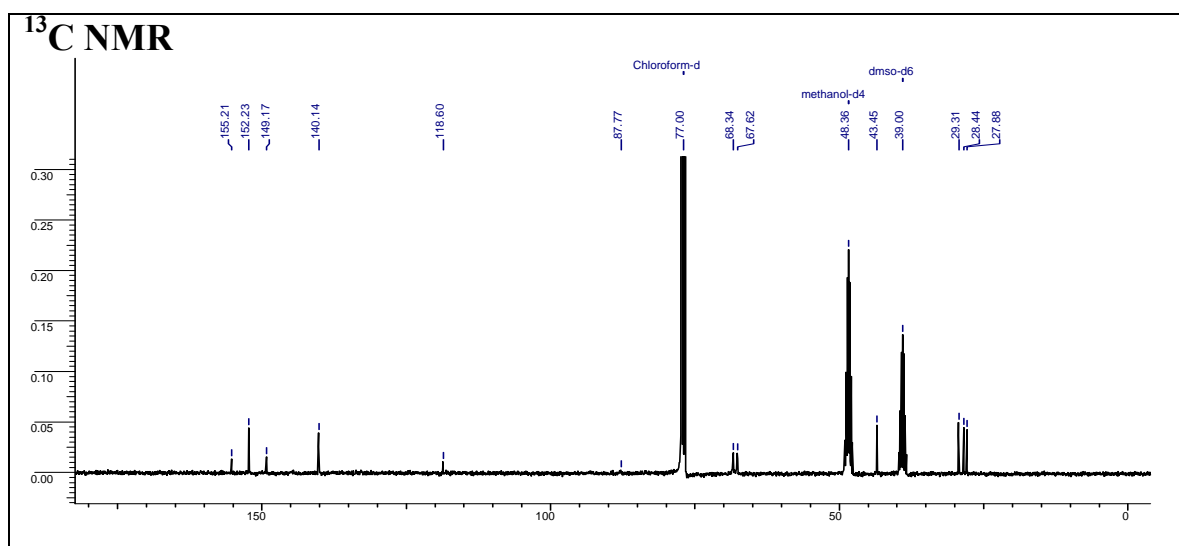
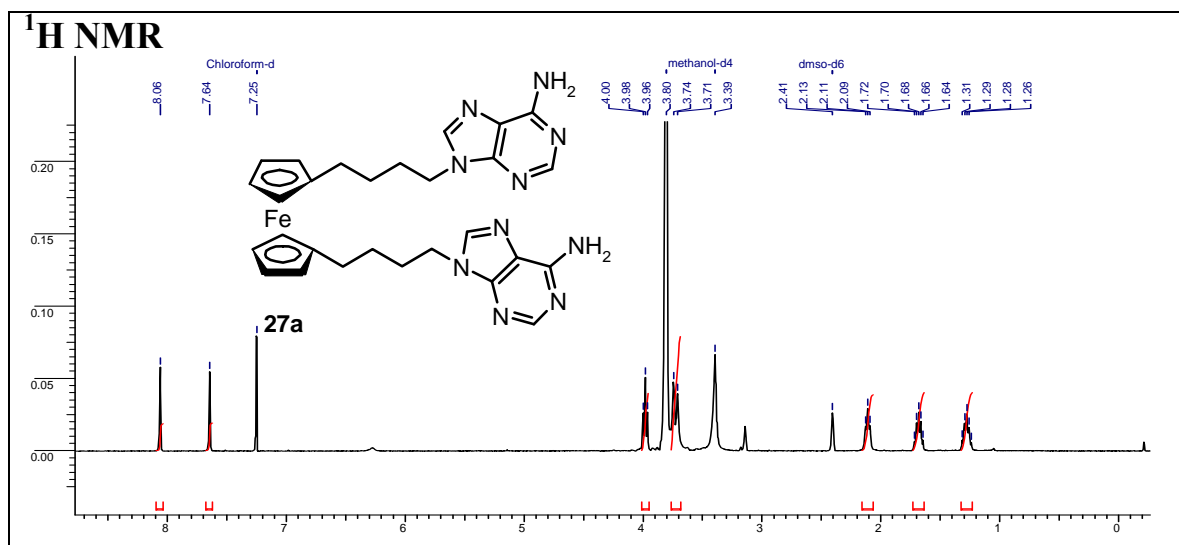
## 1,1'-Bis(4-(methylsulfonyloxy)butyl)ferrocene (26a)



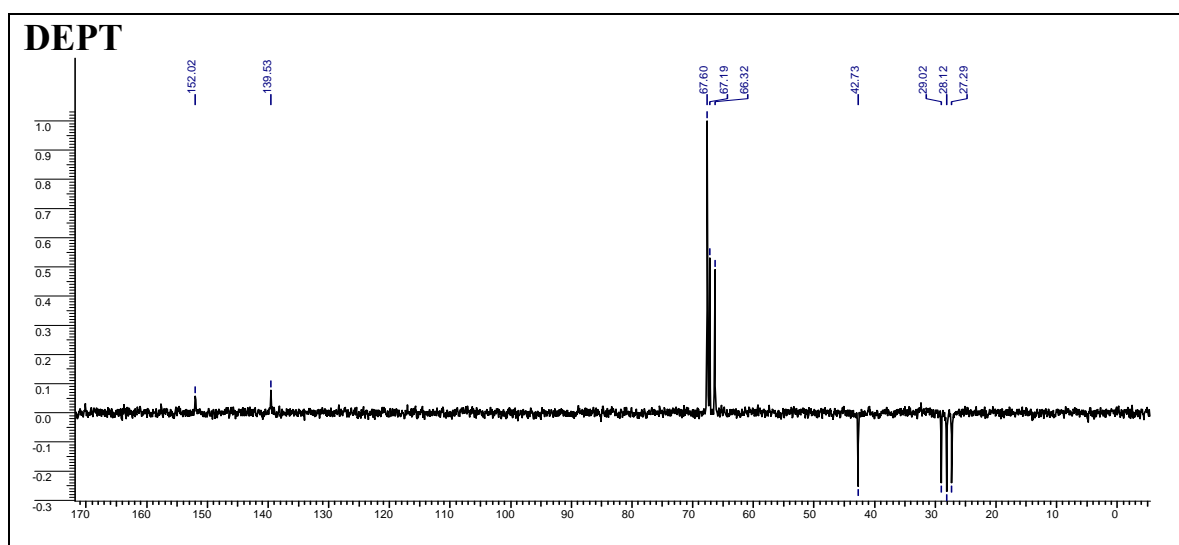
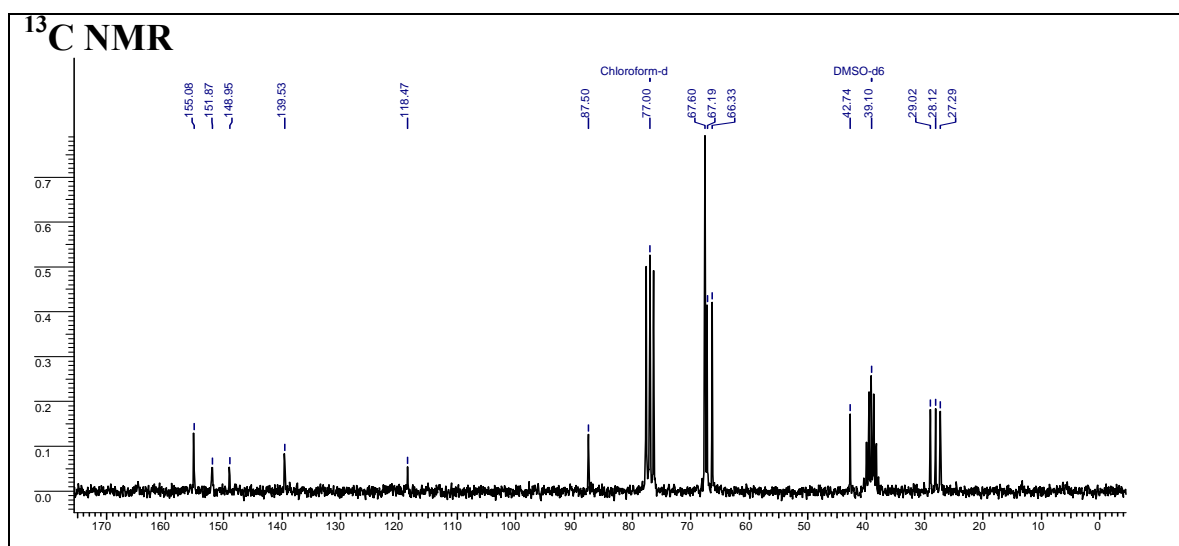
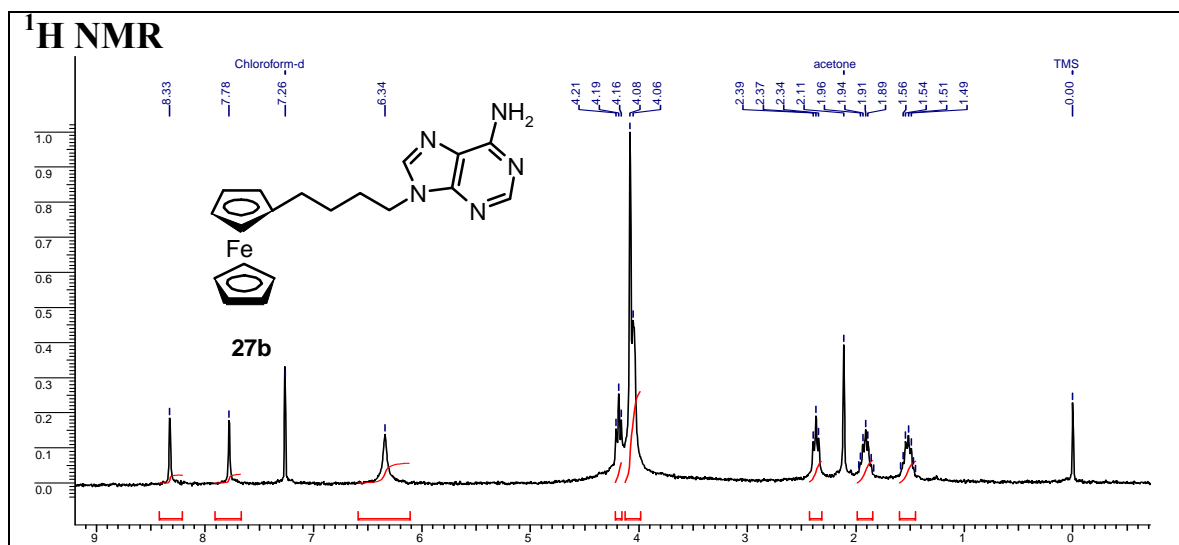
## 1-(Methylsulfonyloxybutyl)ferrocene (26b)

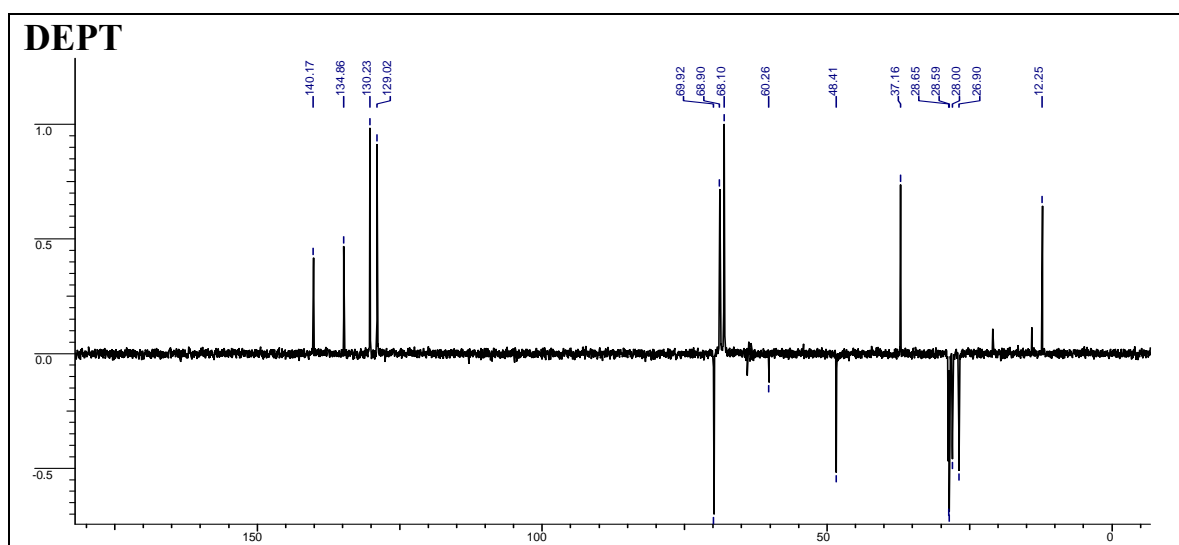
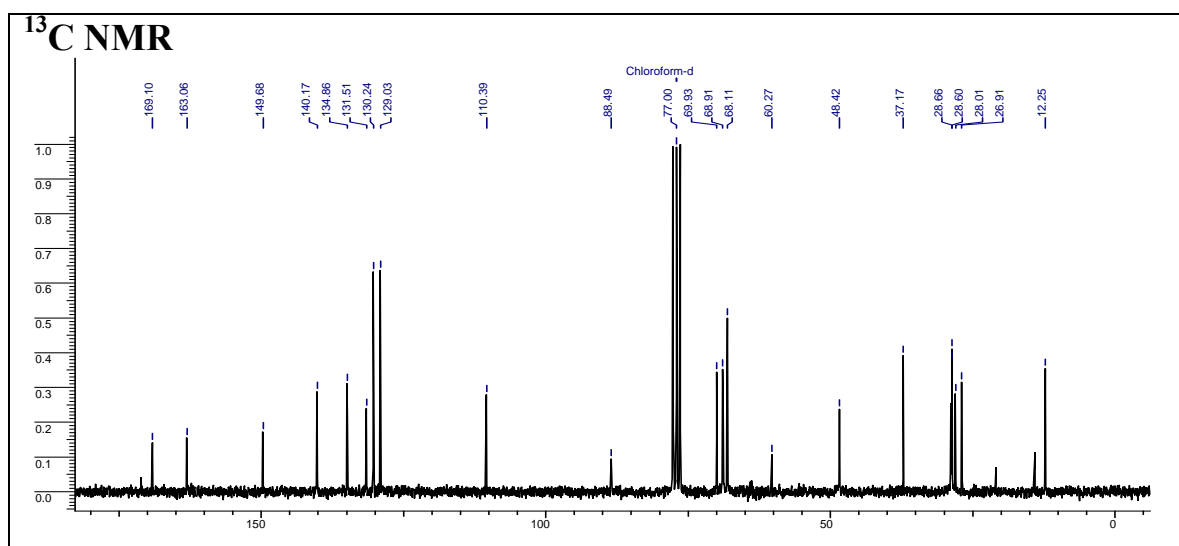
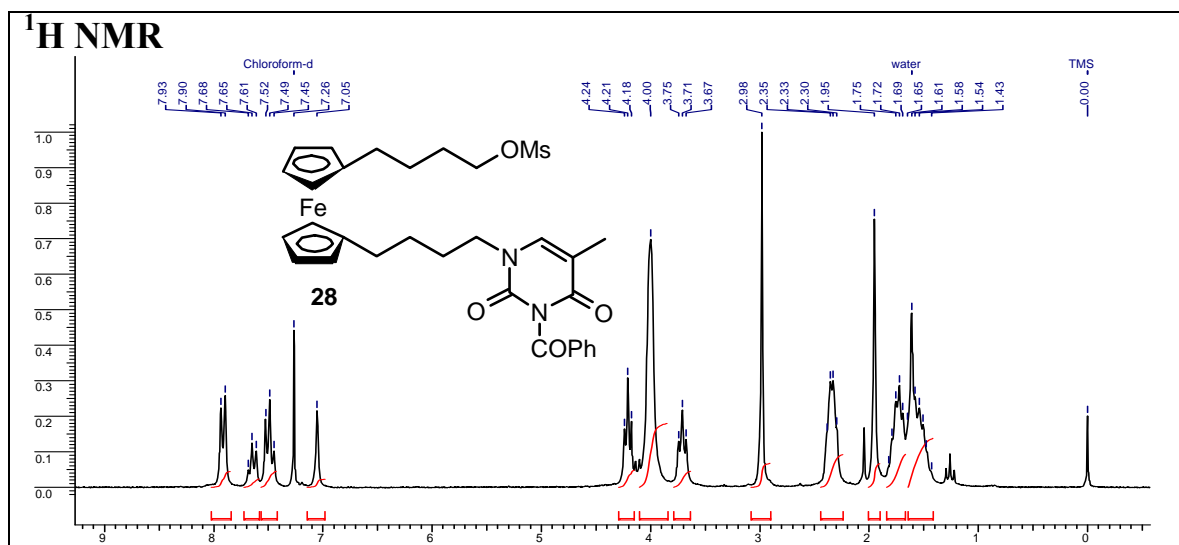


## 1,1'-Bis(4-(adeninyl)butyl)ferrocene (27a)



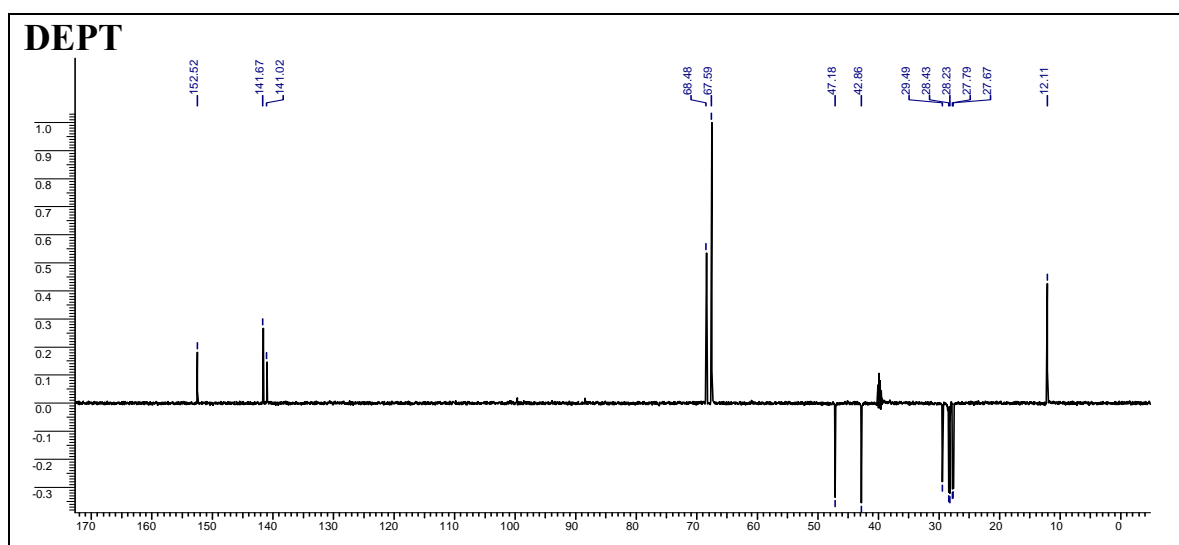
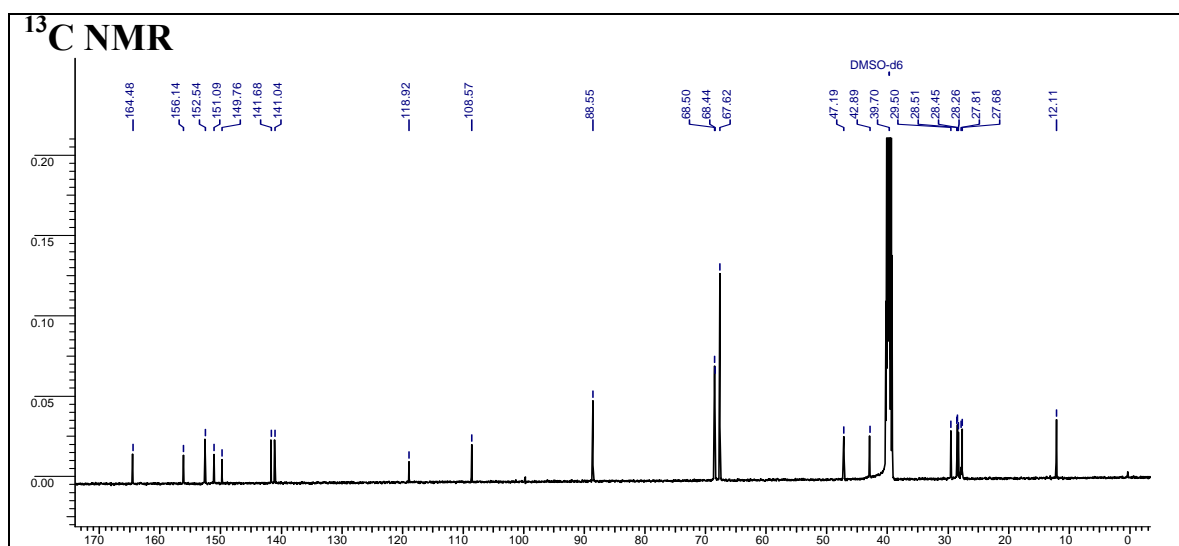
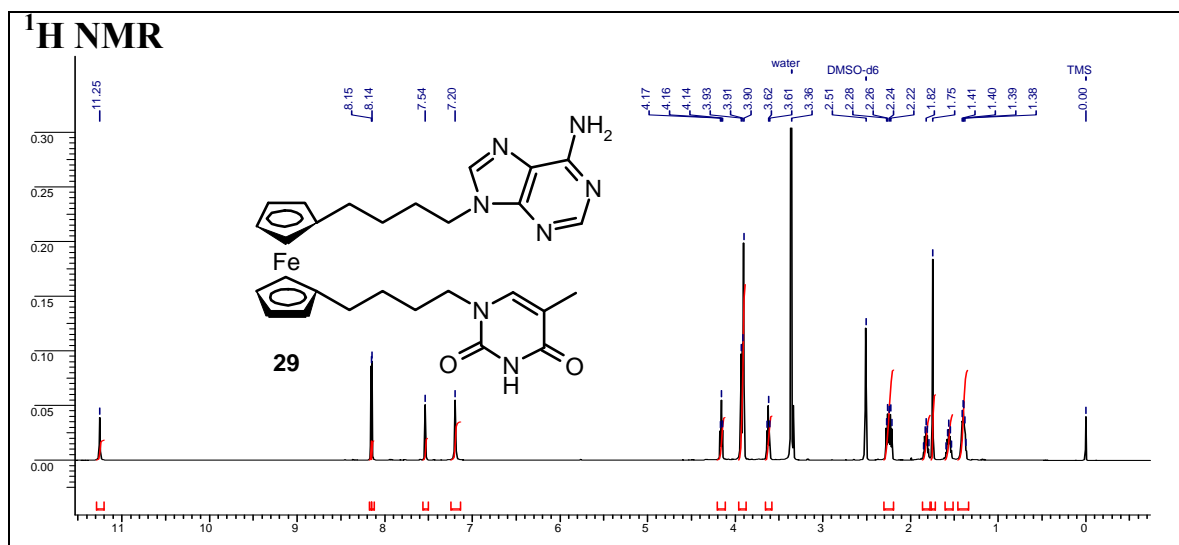
## 1-(4-(Adeninyl)butyl)ferrocene (27b)



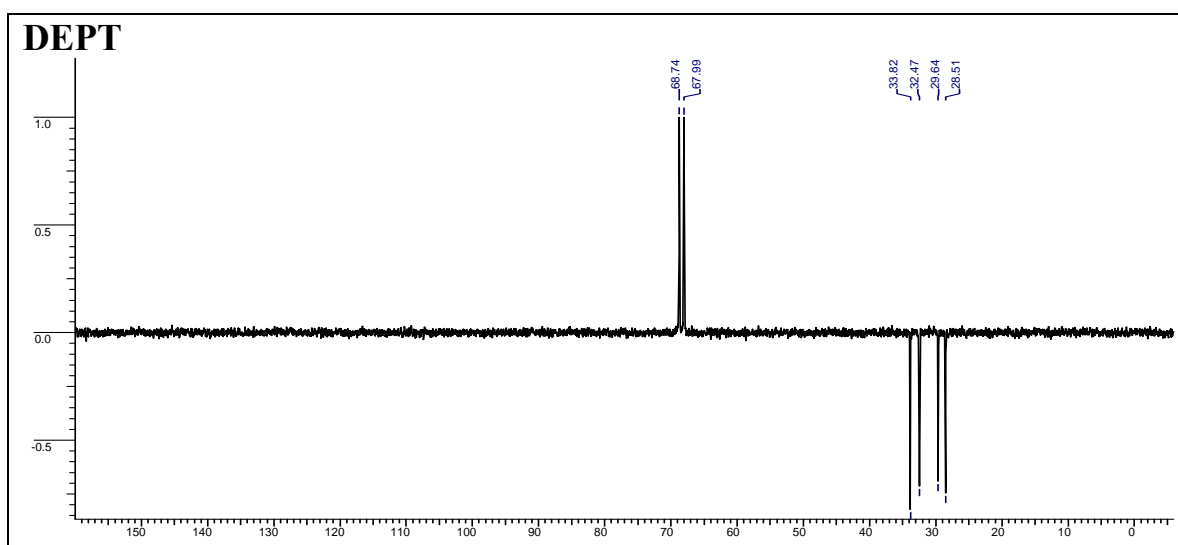
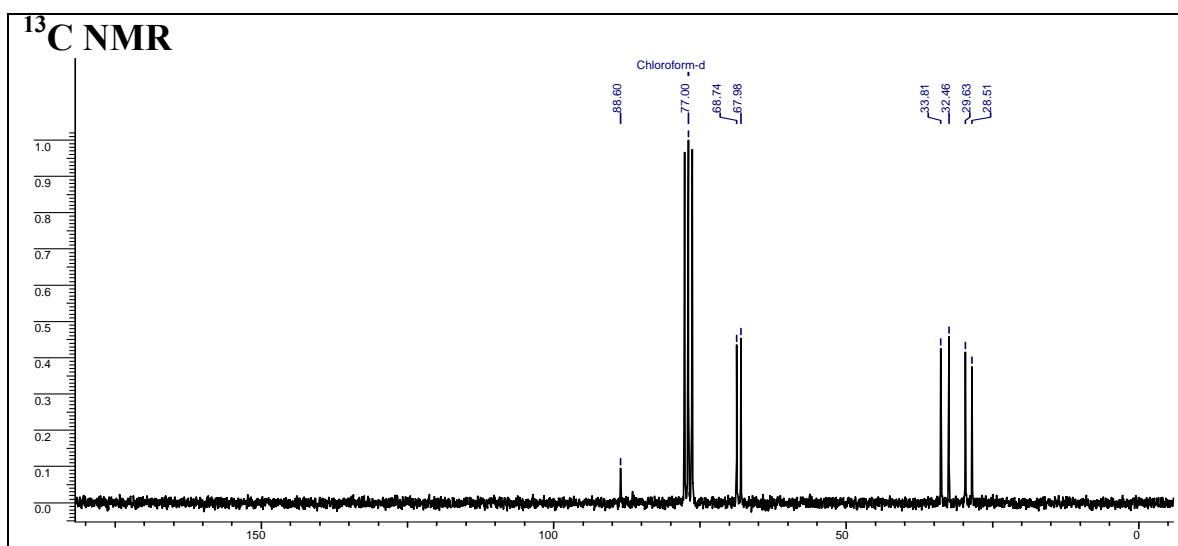
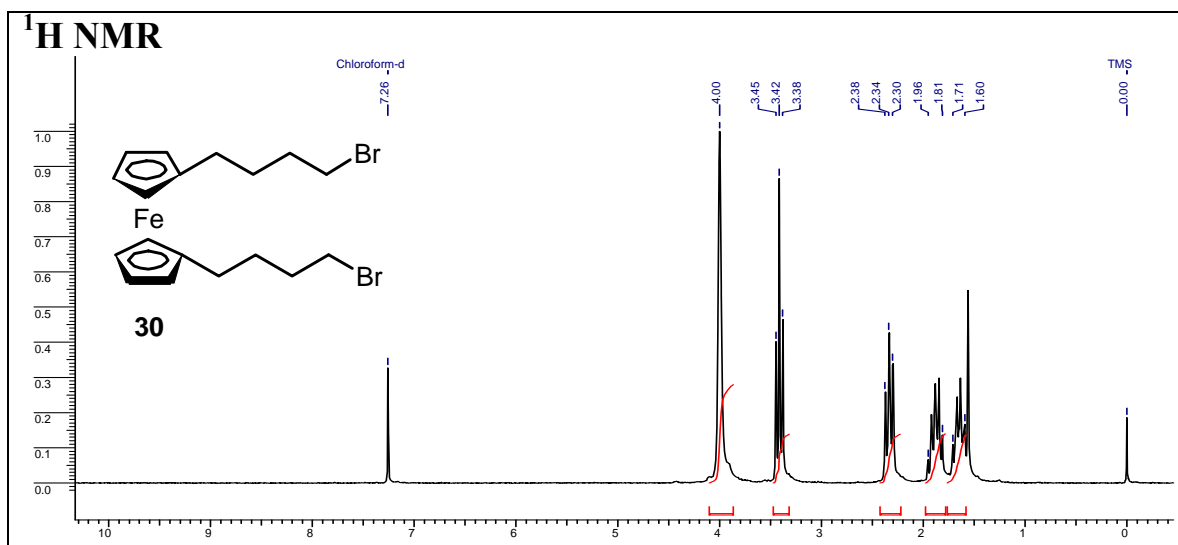
1-(4-(*N*3-Benzoylthyminy)butyl)-1'-(4-(methylsulfonyloxy)butyl)ferrocene (28)



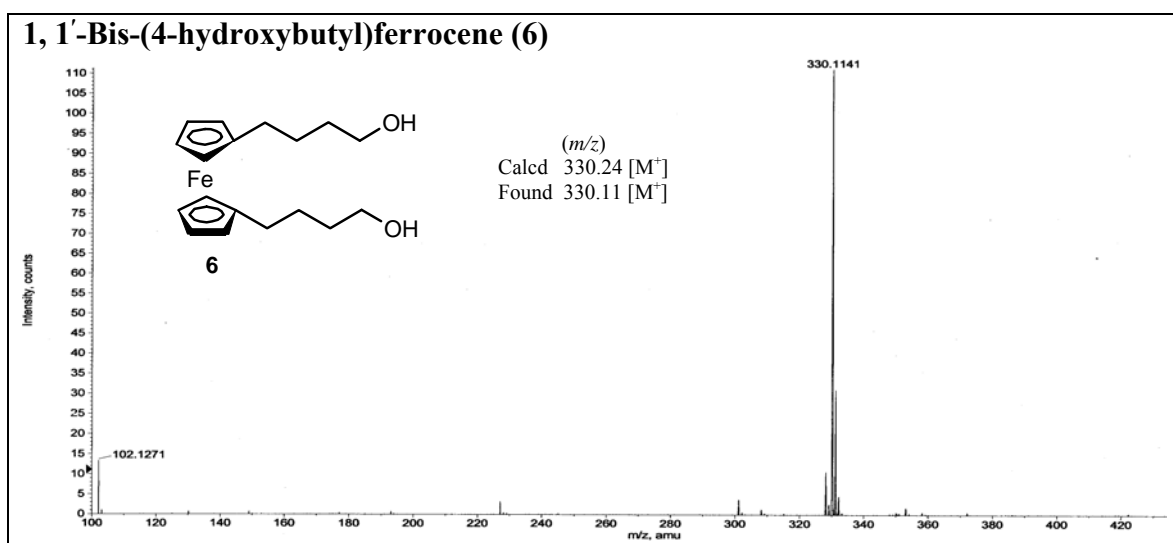
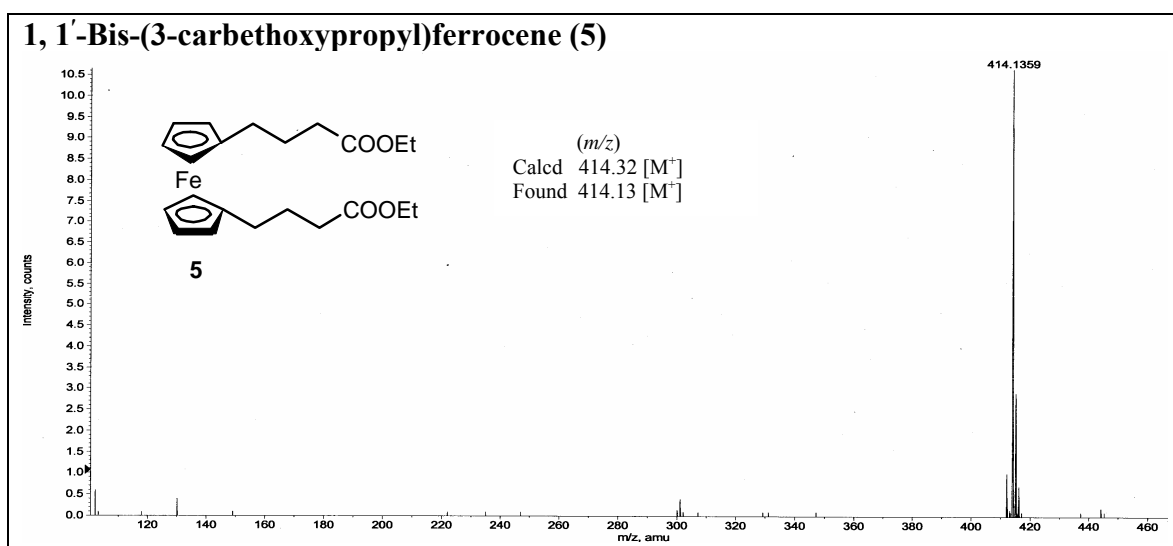
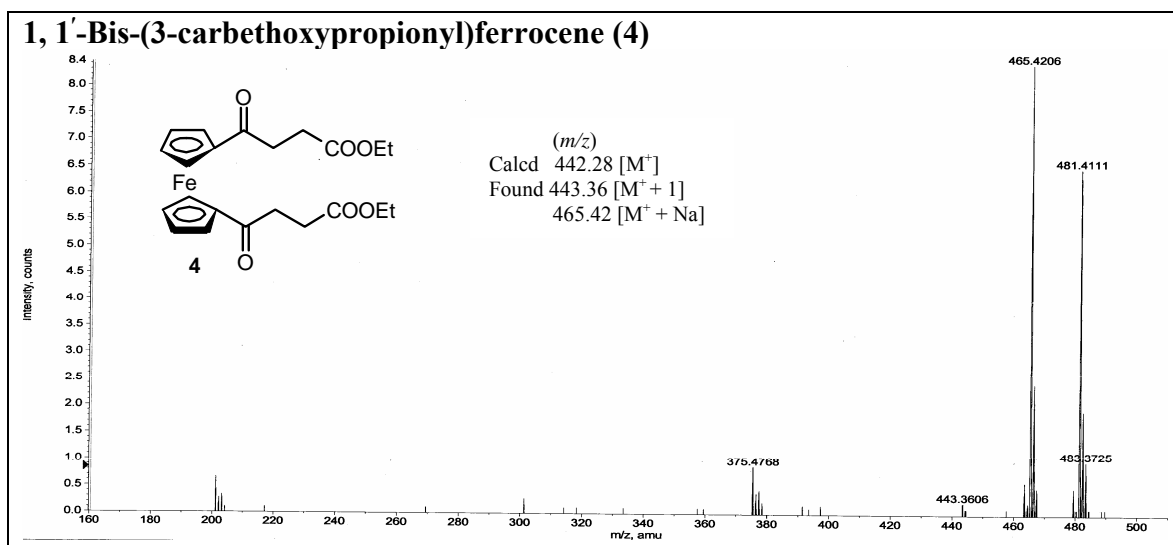
## 1-(4-(Thyminy)butyl)-1'-(4-(adeniny)butyl)ferrocene (29)

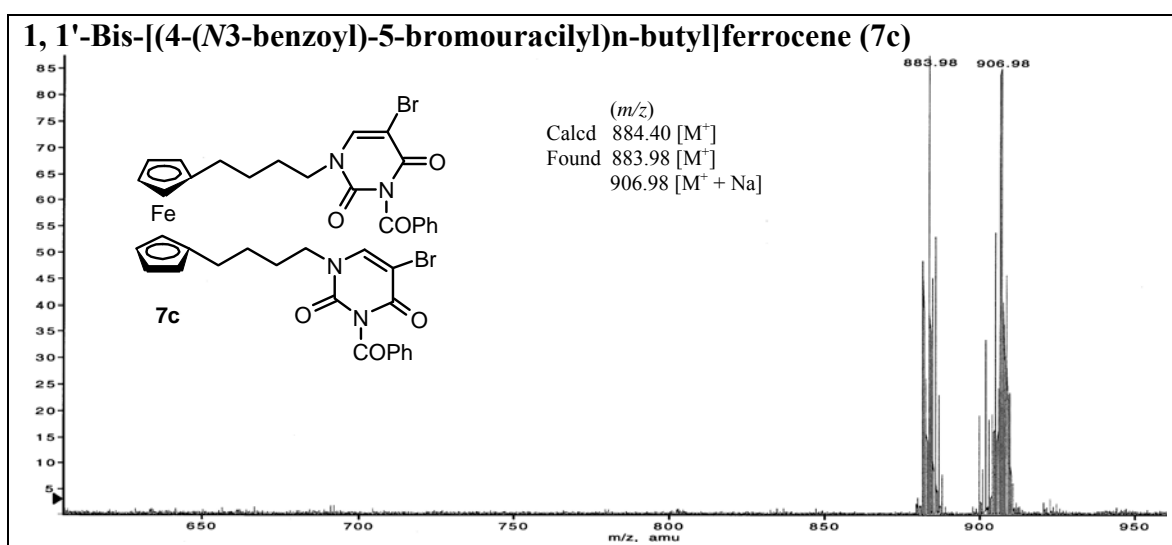
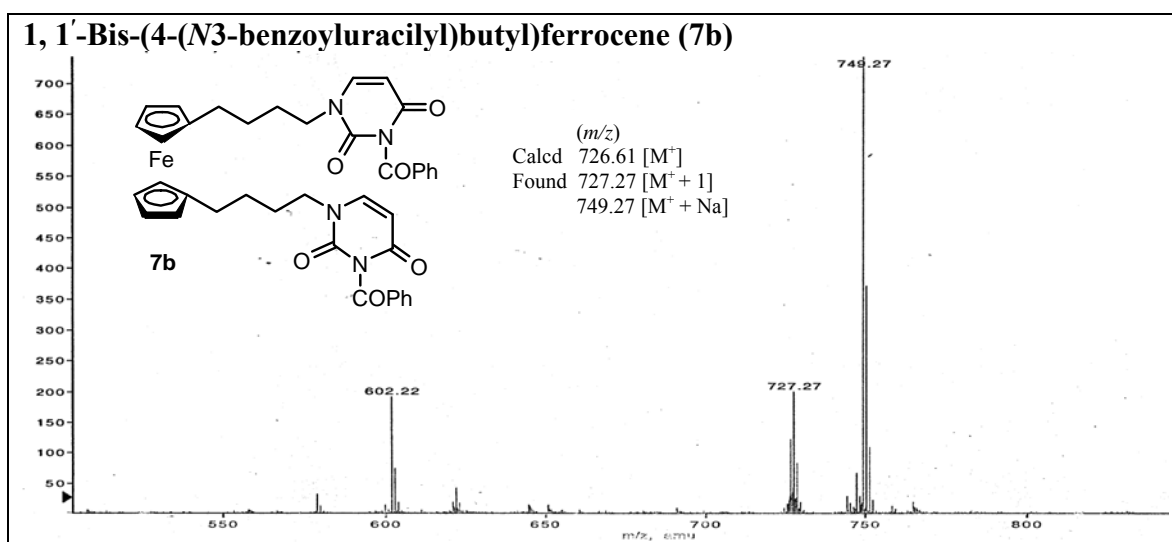
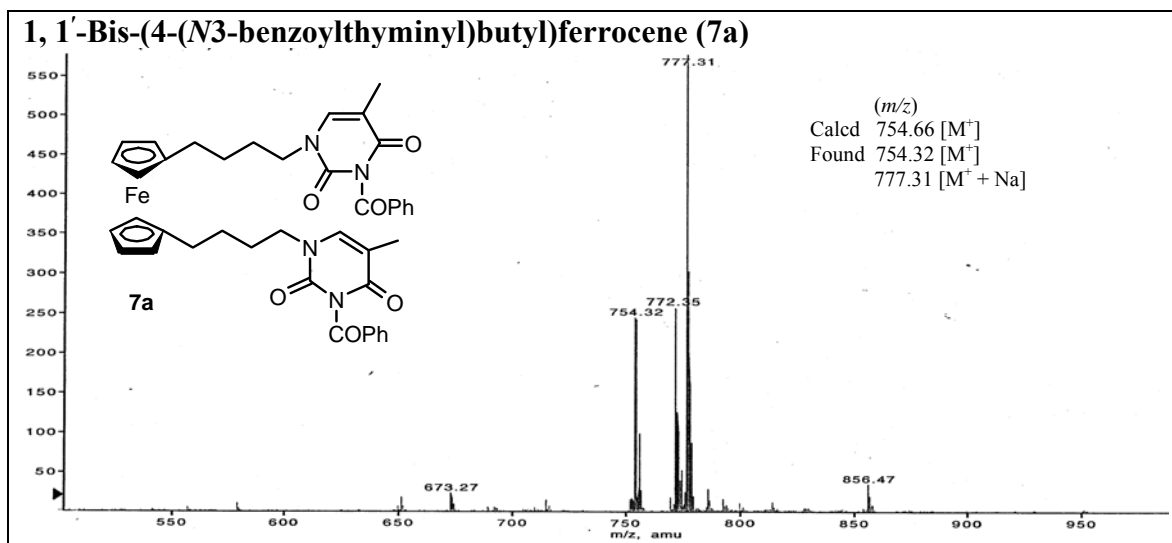


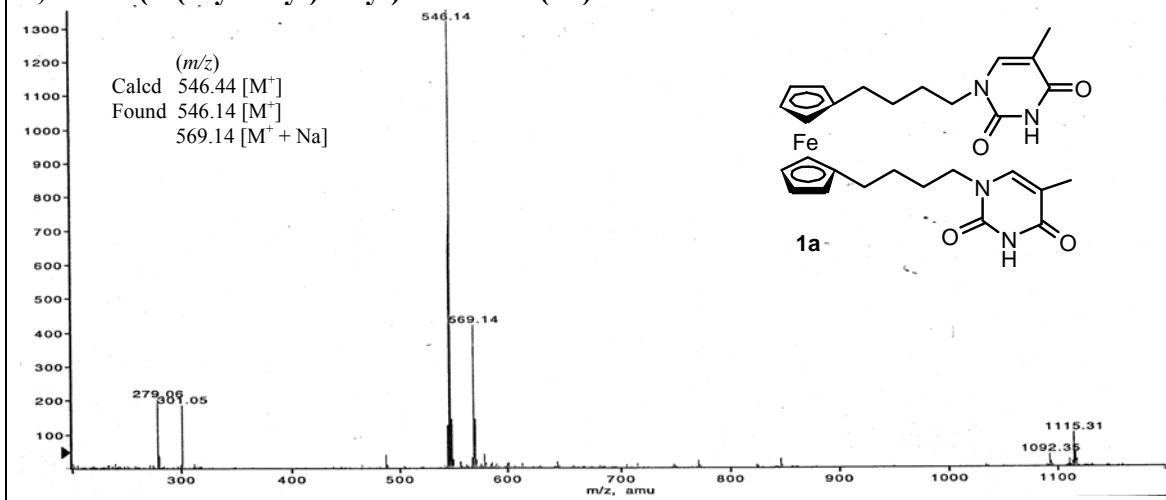
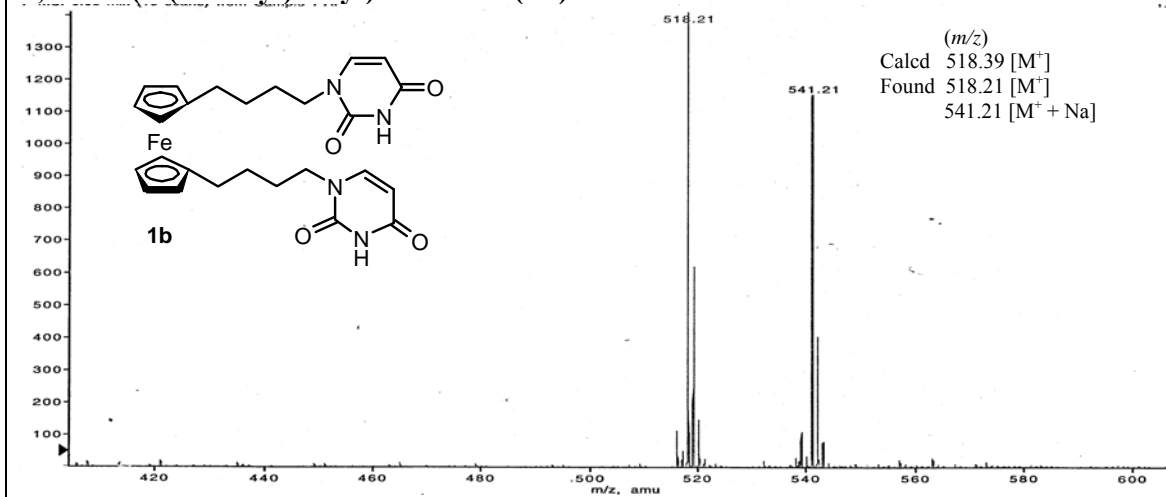
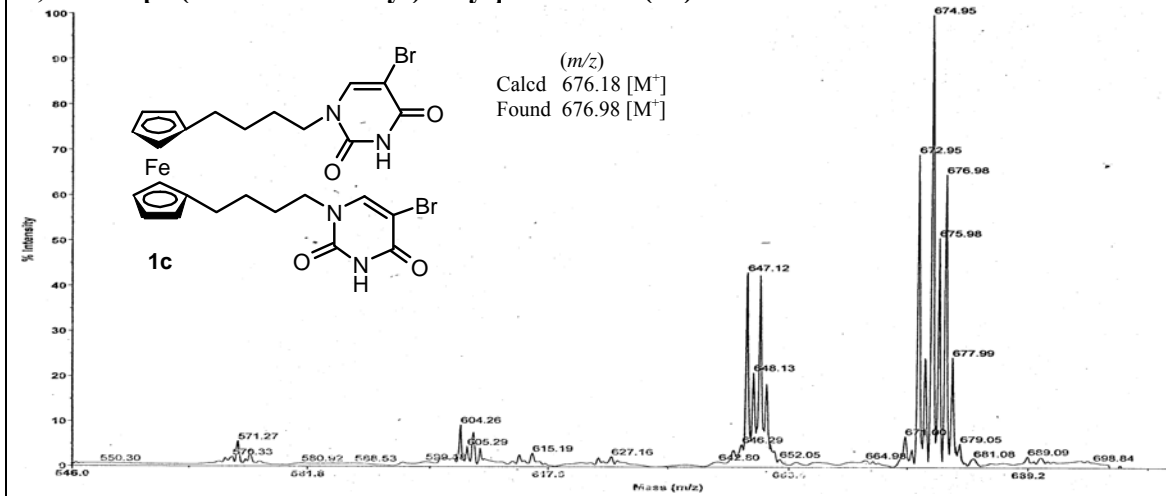
## 1, 1'-Bis-(4-bromobutyl)ferrocene (30)



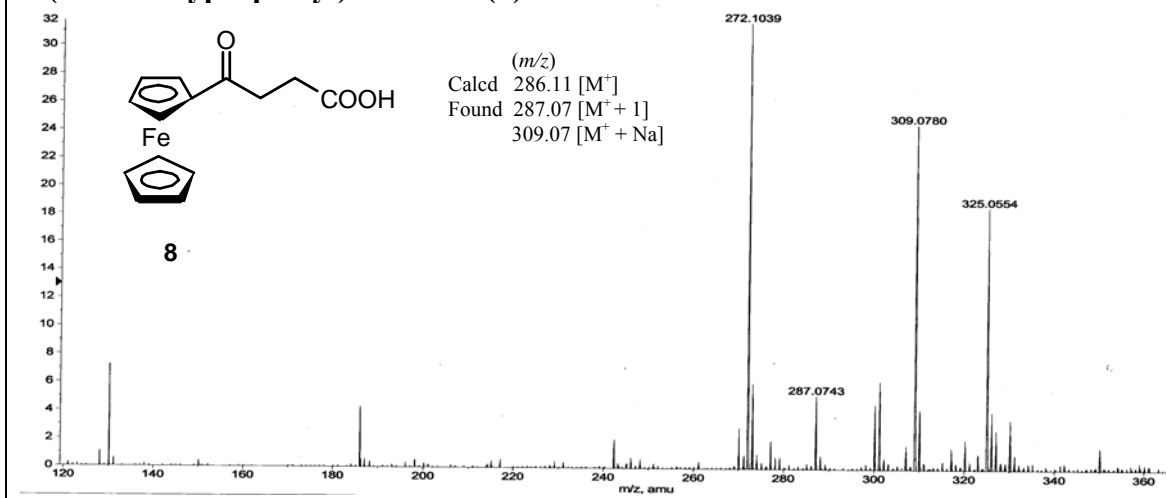
## Mass spectra



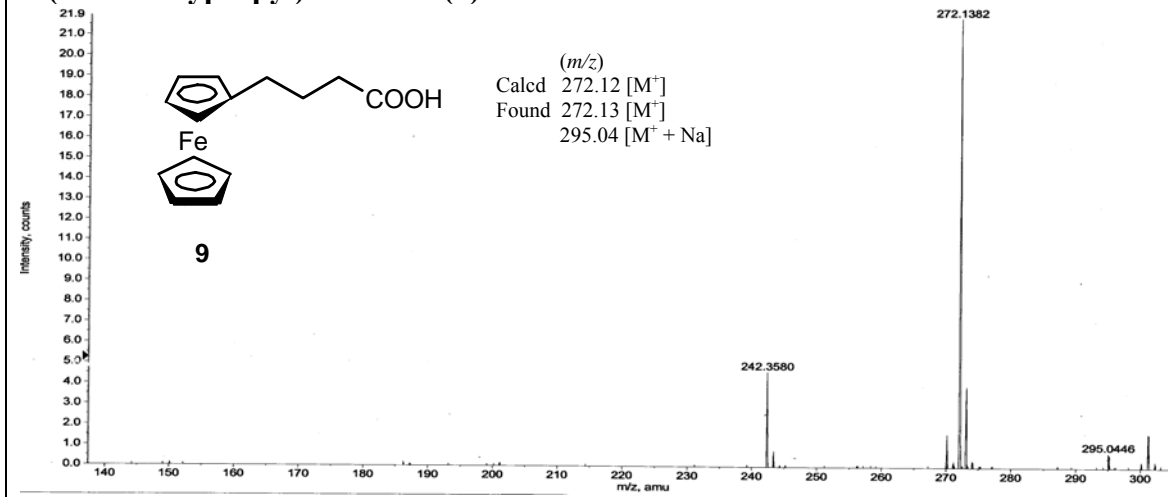


**1, 1'-Bis-(4-(thyminy)butyl)ferrocene (1a)****1, 1'-Bis-(4-(uracily)butyl)ferrocene (1b)****1, 1'-Bis-[4-(5-bromouracily)butyl]ferrocene (1c)**

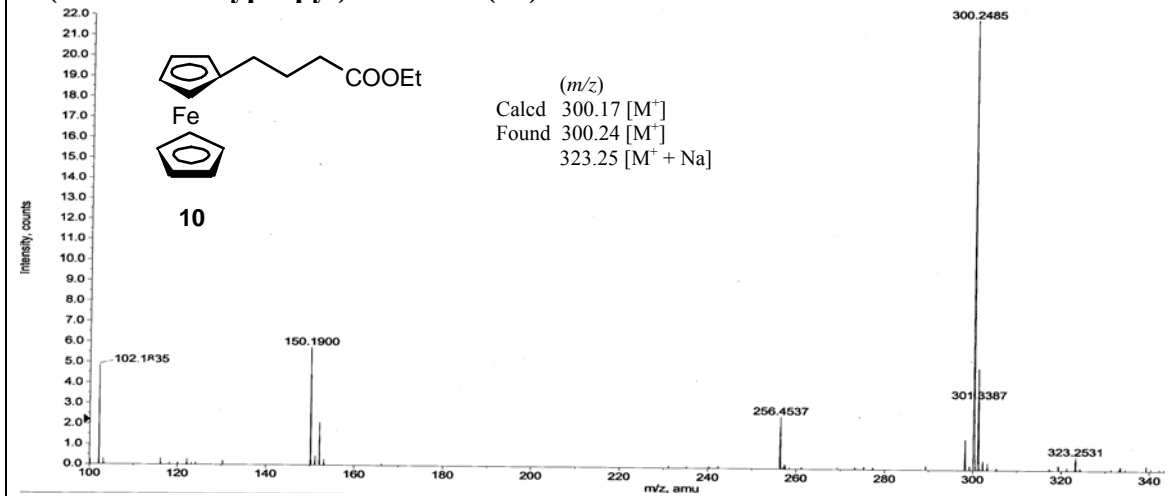
## 1-(3-Carboxypropionyl)ferrocene (8)



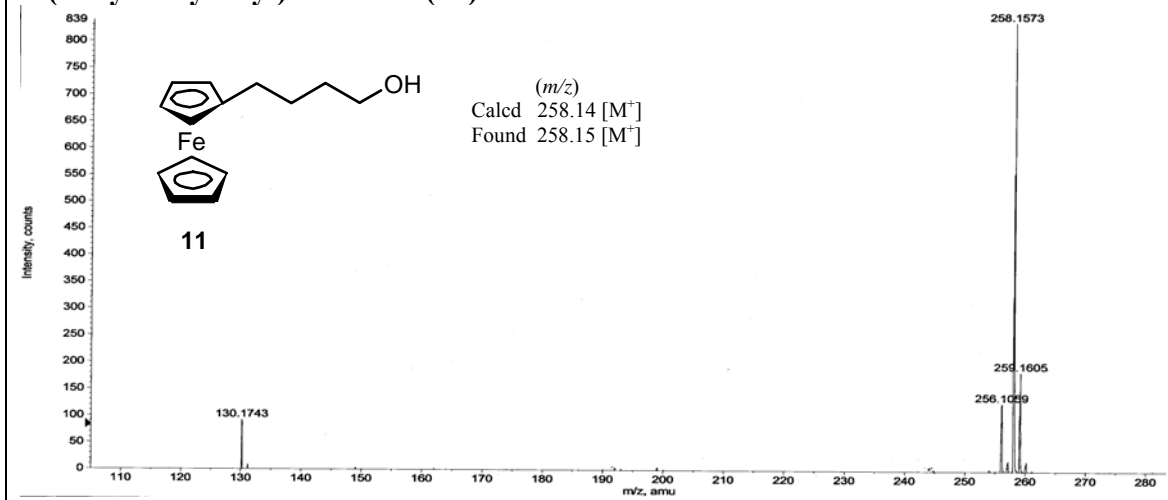
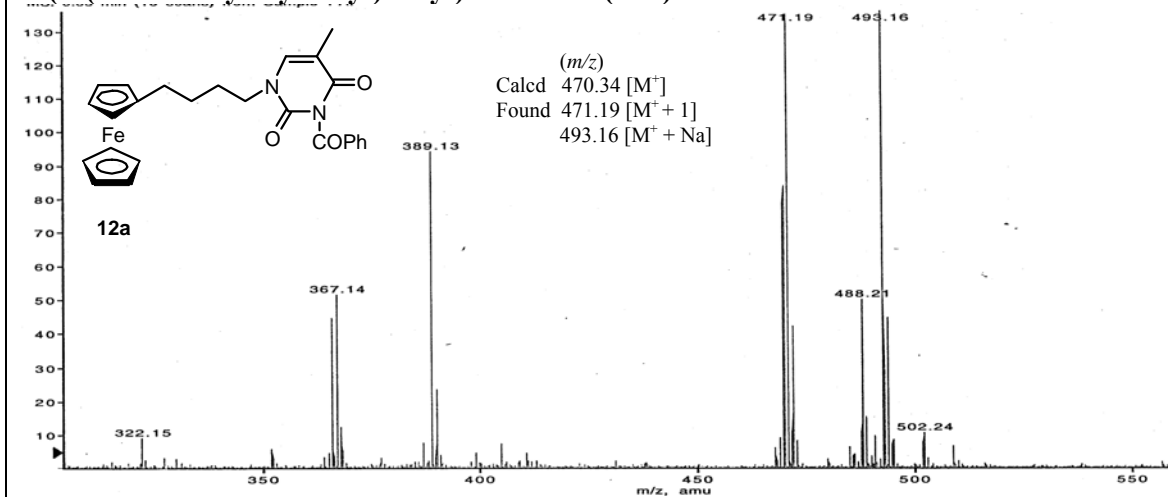
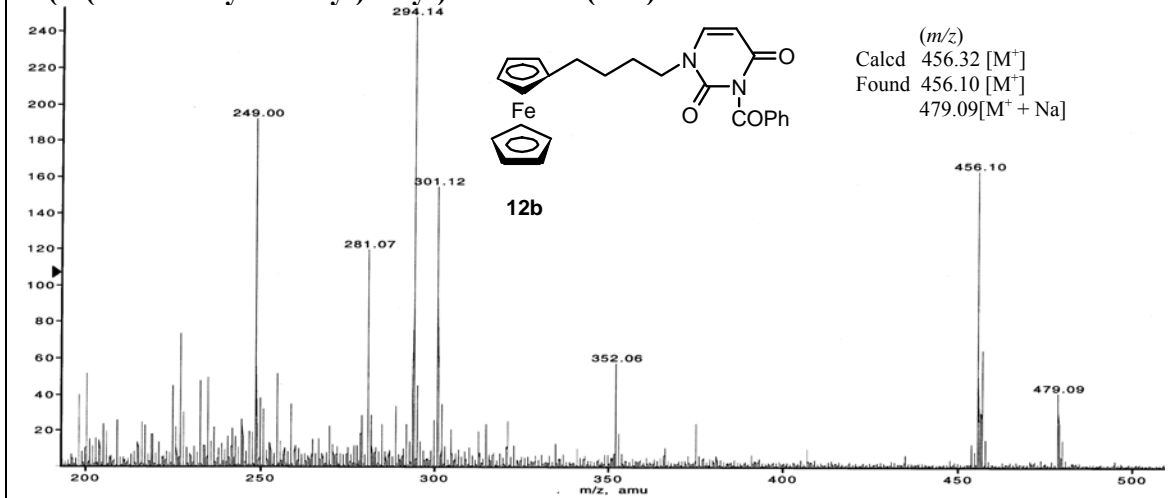
## 1-(3-Carboxypropyl)ferrocene (9)

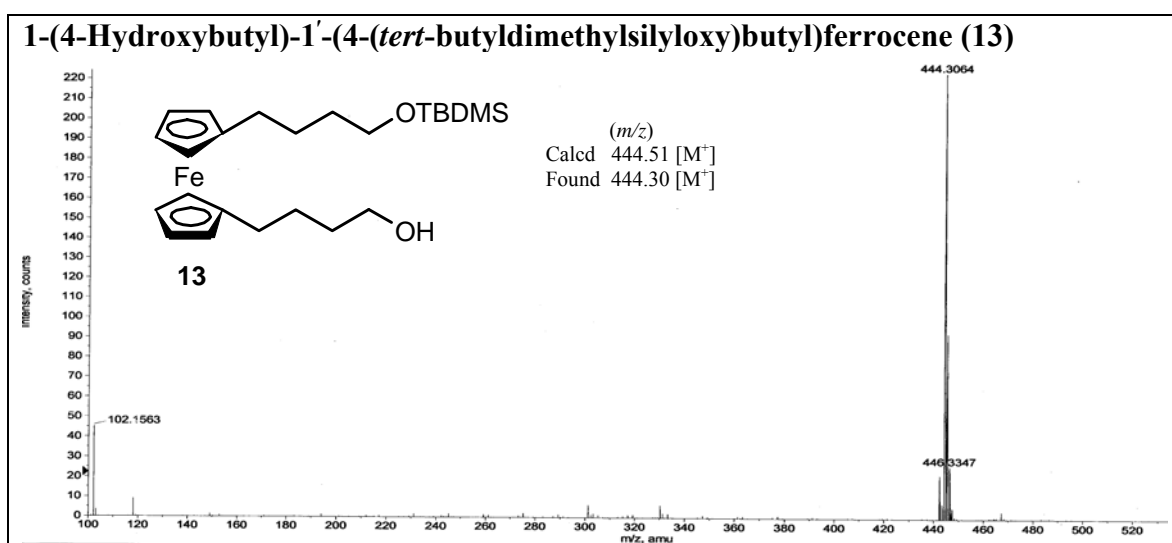
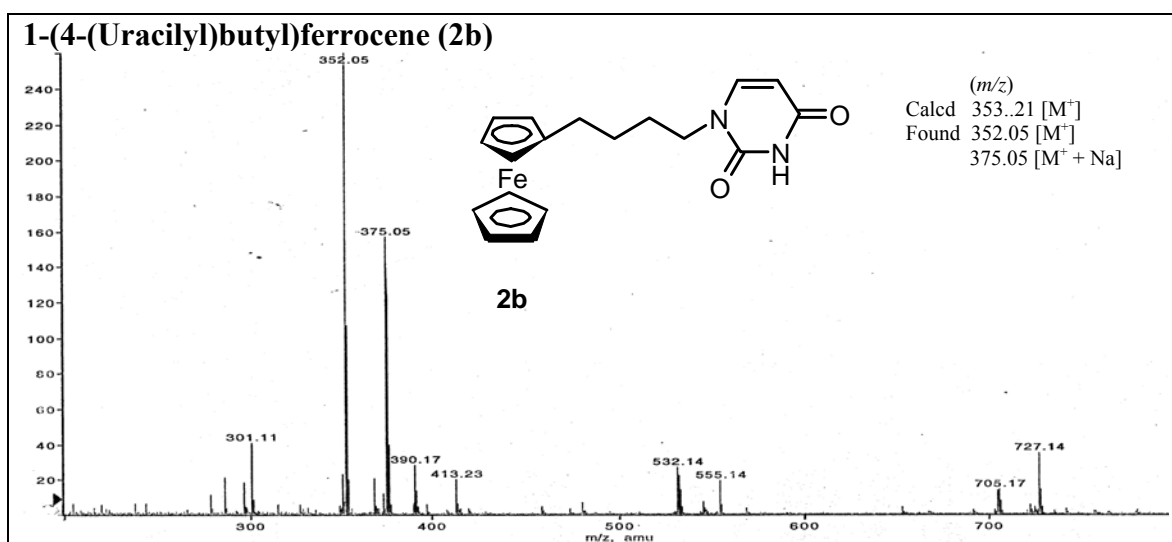
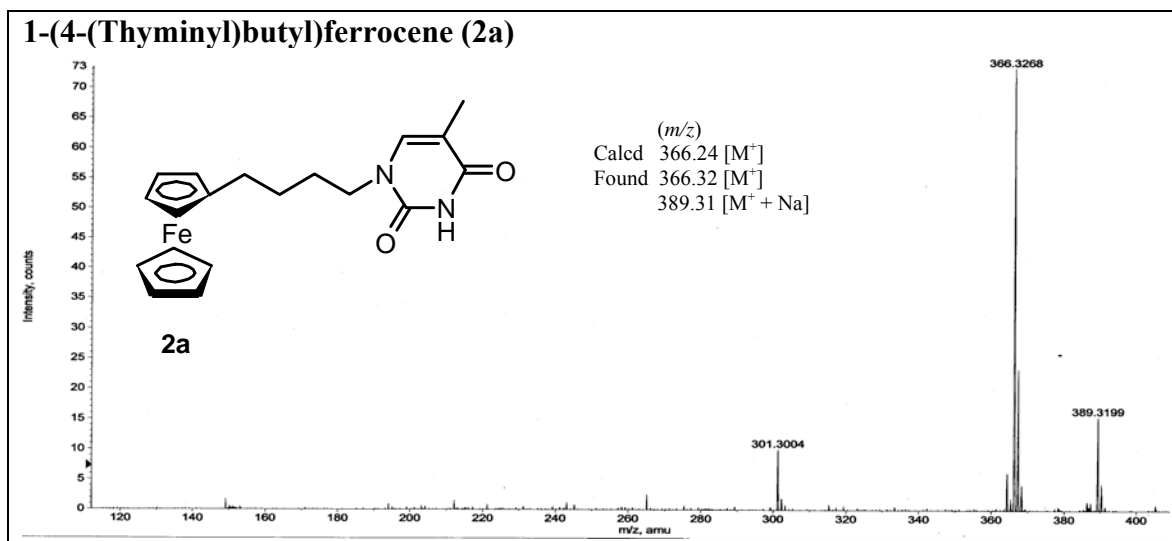


## 1-(3-Carboethoxypropyl)ferrocene (10)

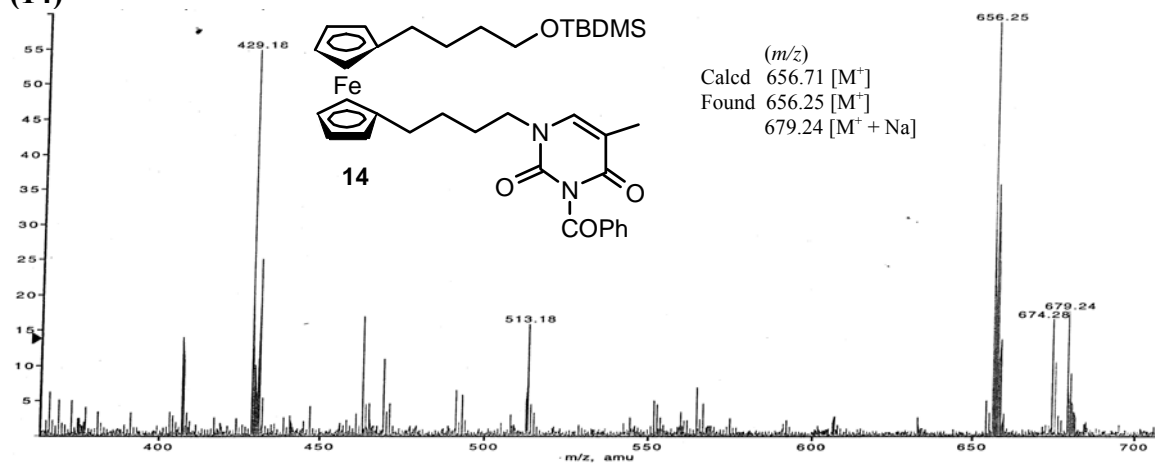
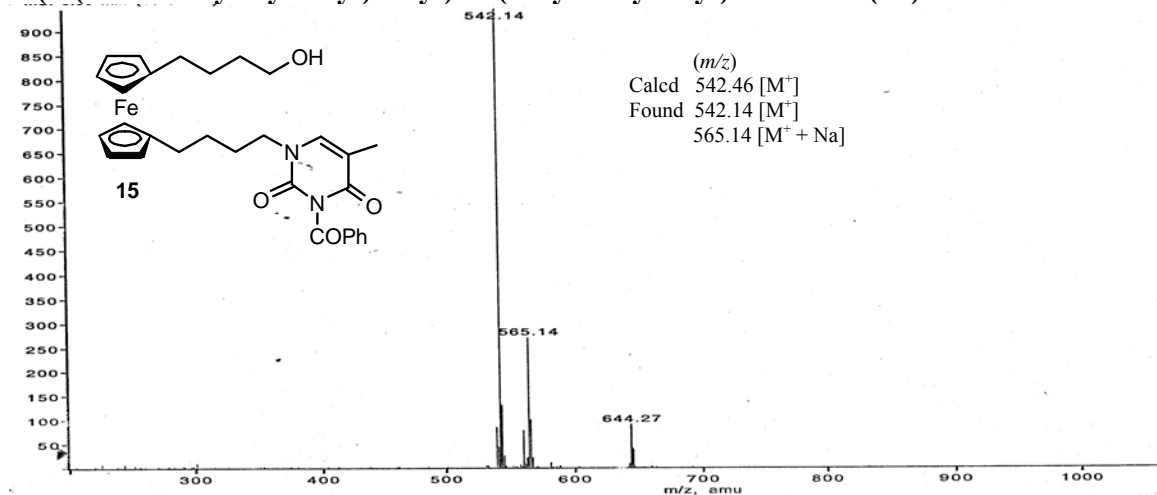
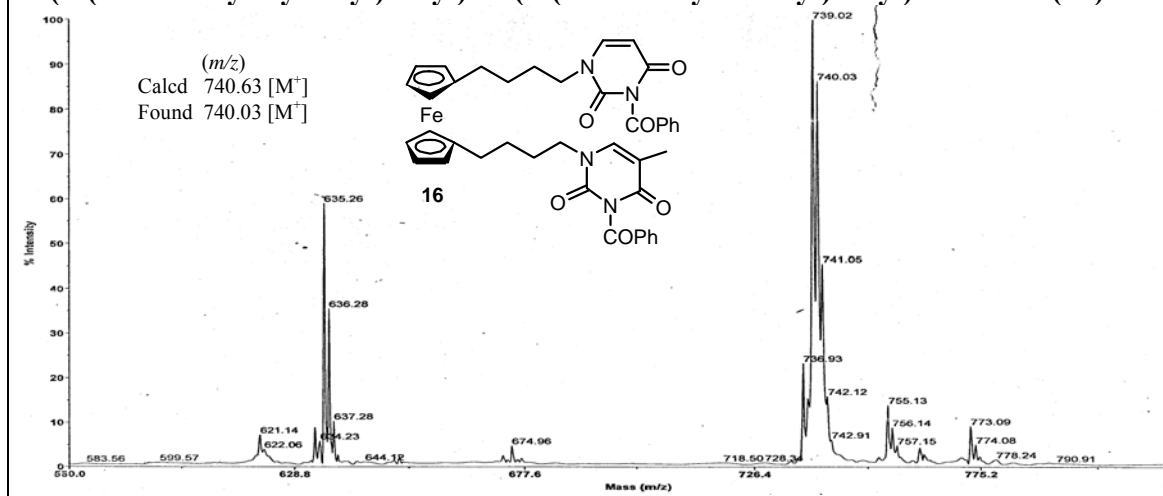


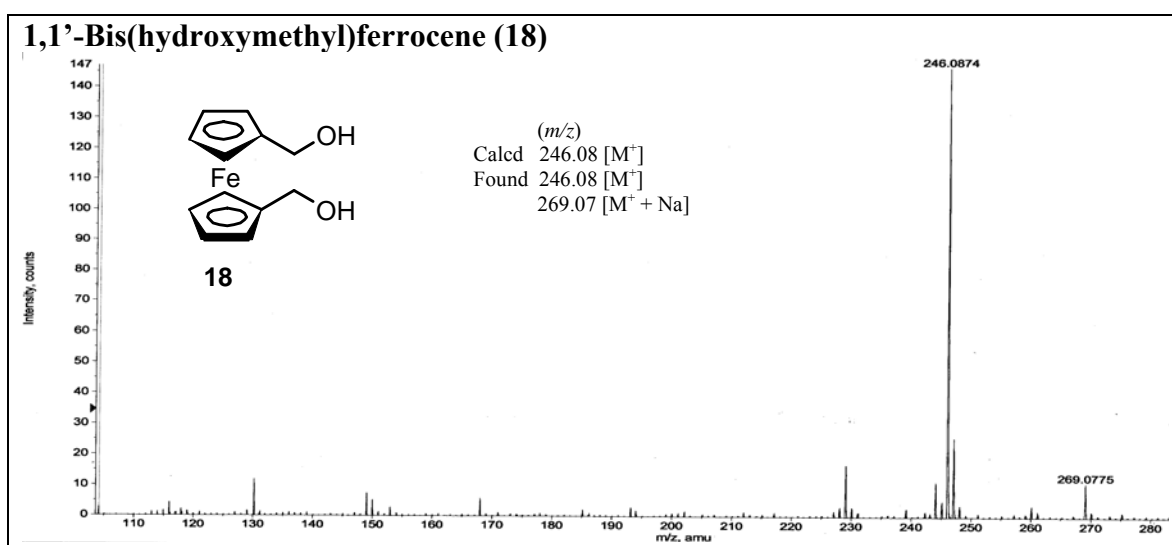
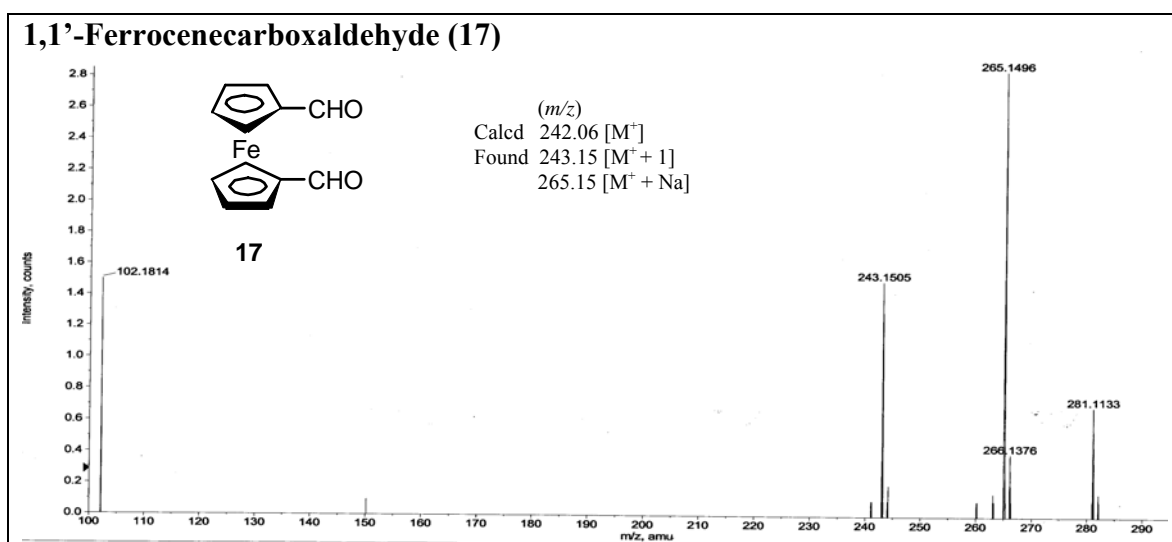
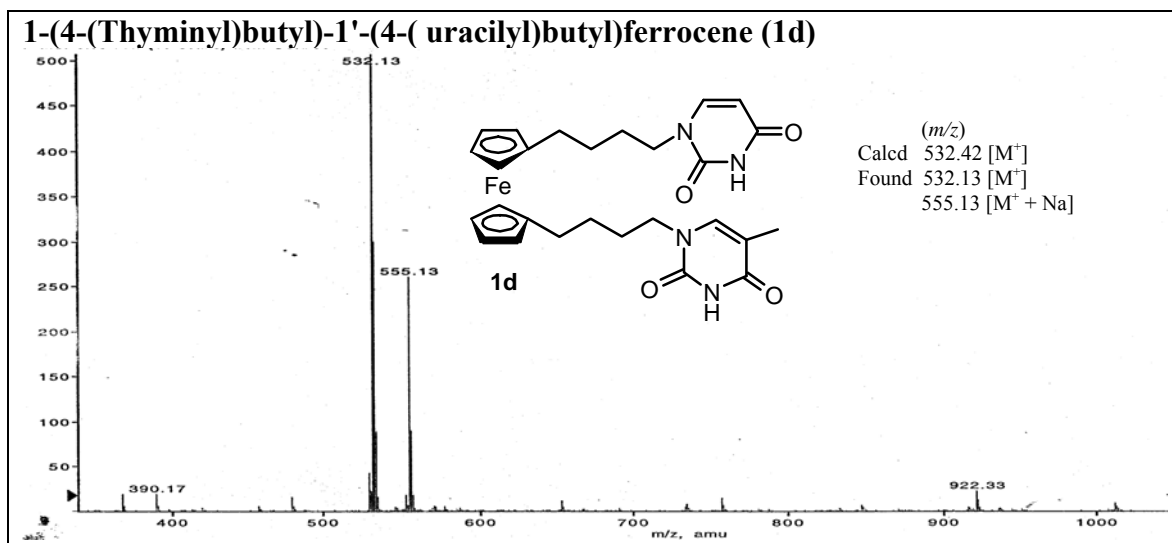
## 1-(4-Hydroxybutyl)ferrocene (11)

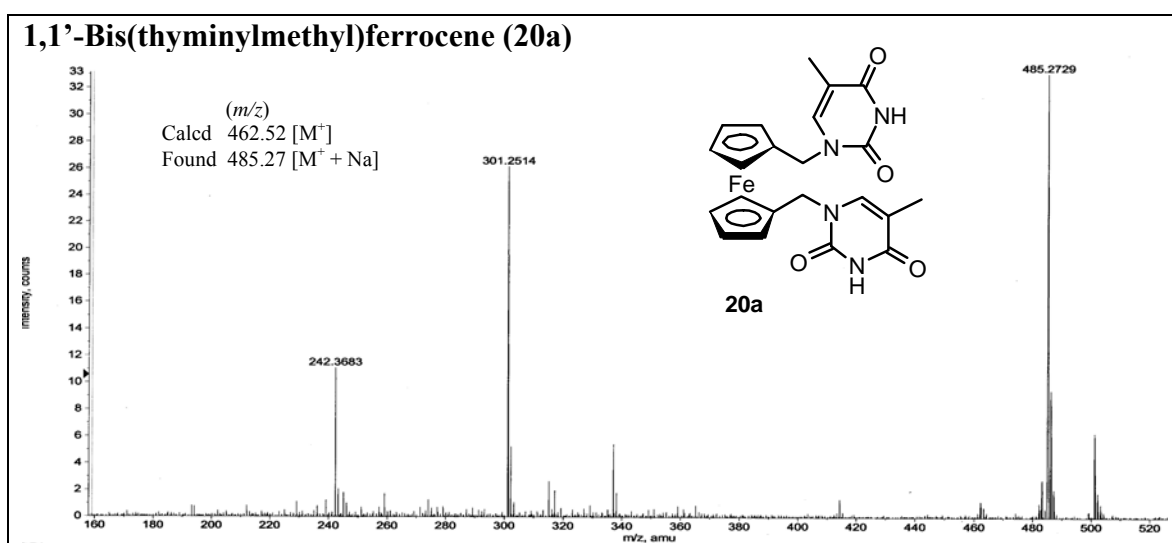
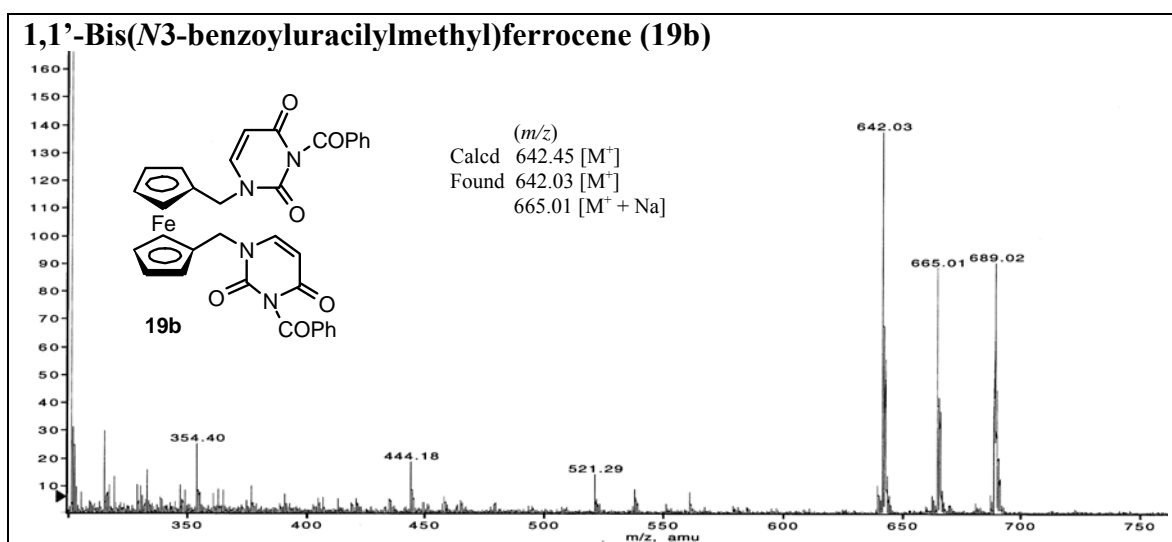
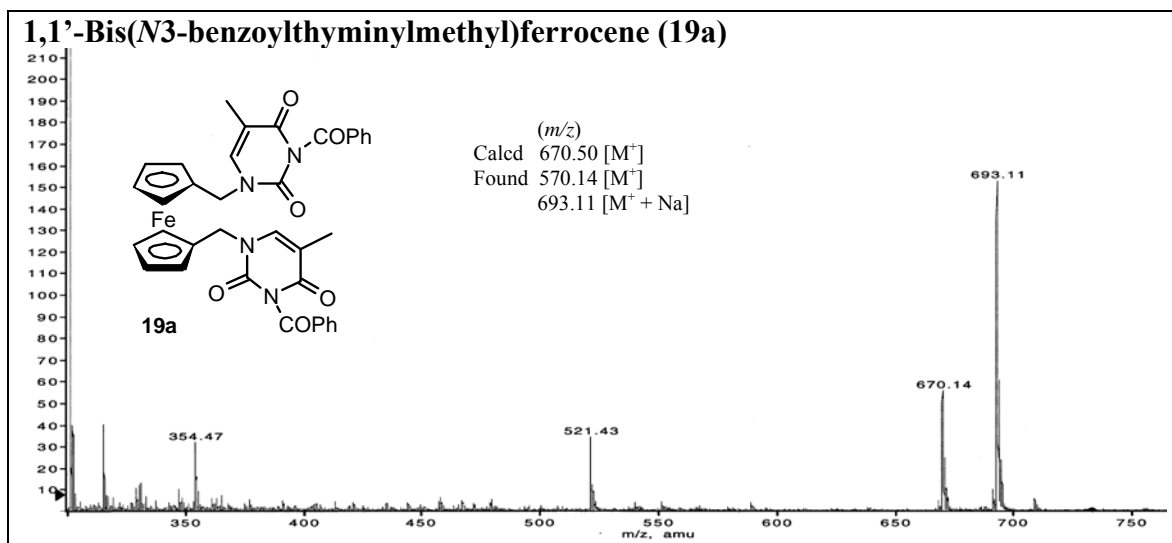
1-(4-(*N*3-benzoylthyminy)butyl)ferrocene (12a)1-(4-(*N*3-benzoyluracilyl)butyl)ferrocene (12b)

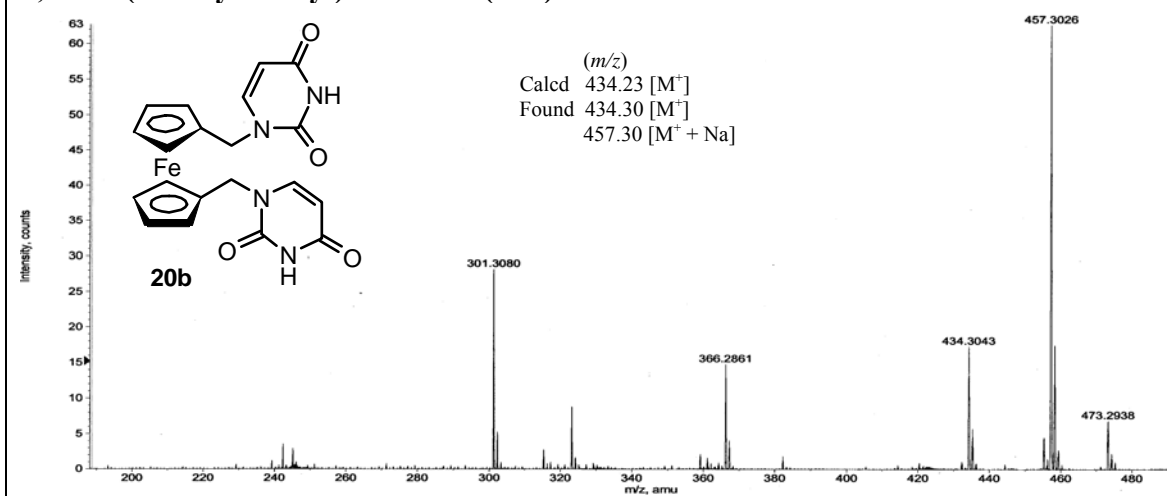
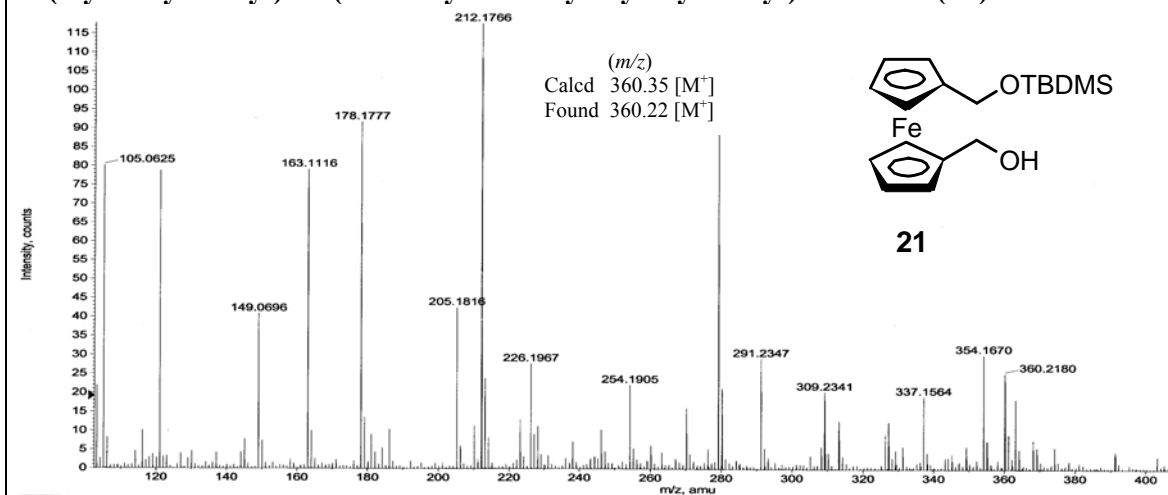
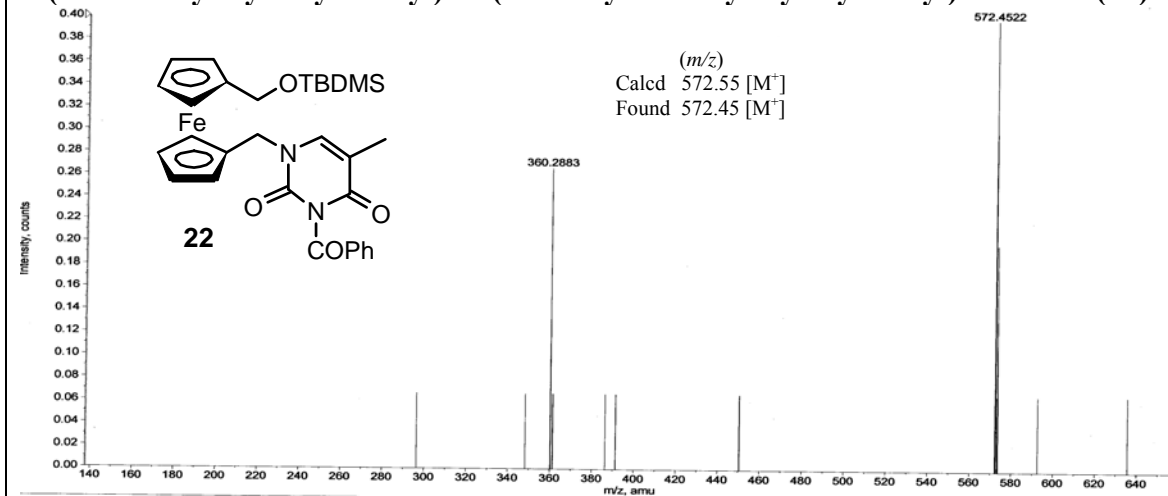


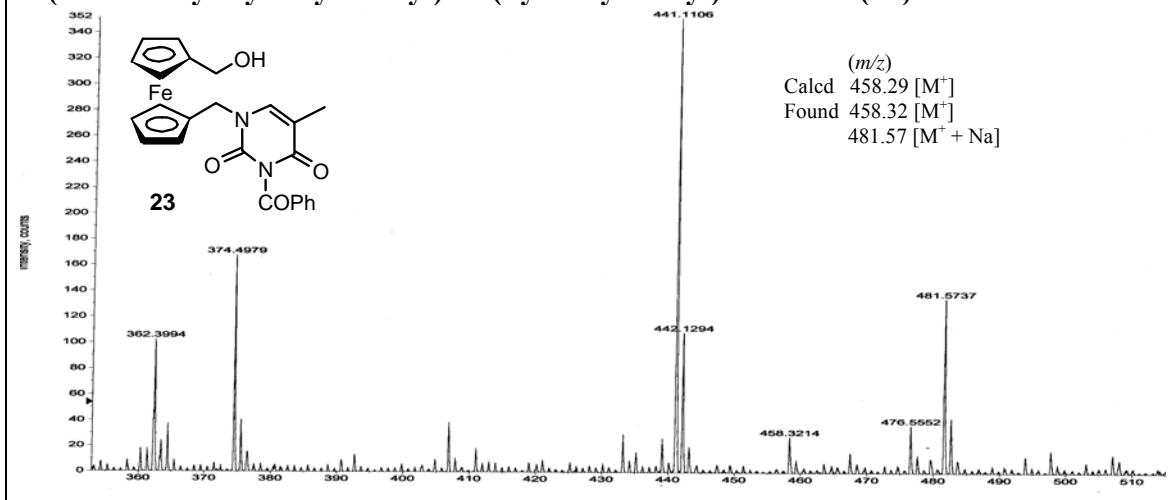
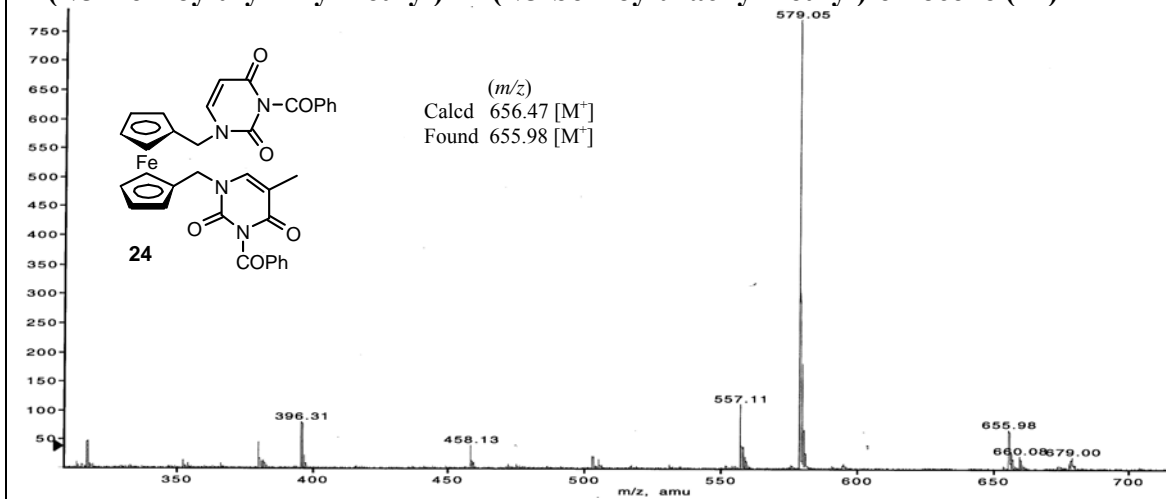


**1-(4-(*N*3-benzoylthyminyl)butyl)-1'-(4-(*tert*-butyldimethylsilyloxy)butyl)ferrocene (14)**

**1-(4-(*N*3-benzoylthyminyl)butyl)-1'-(4-hydroxybutyl)ferrocene (15)**

**1-(4-(*N*3-benzoylthyminyl)butyl)-1'-(4-(*N*3-benzoyluracilyl)butyl)ferrocene (16)**


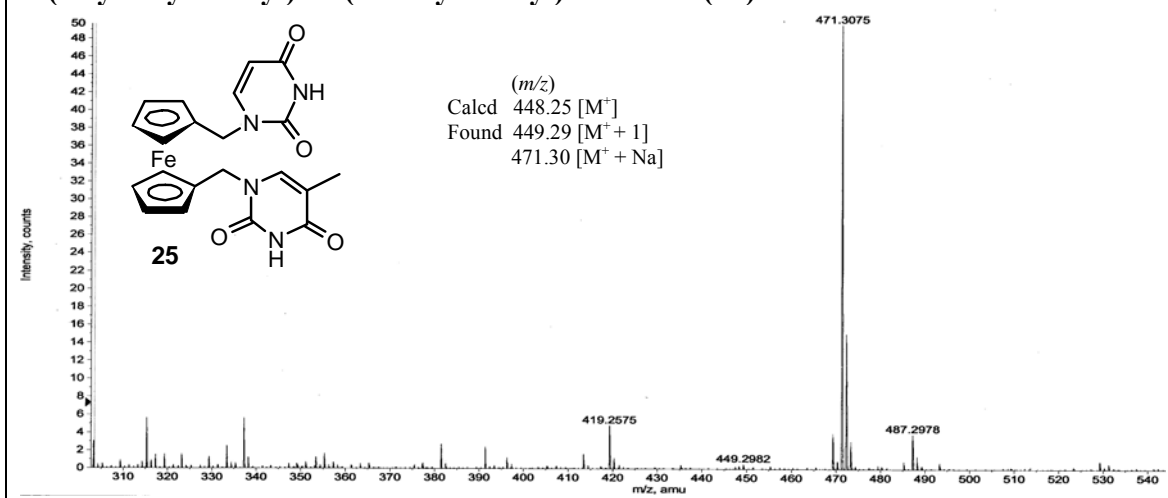


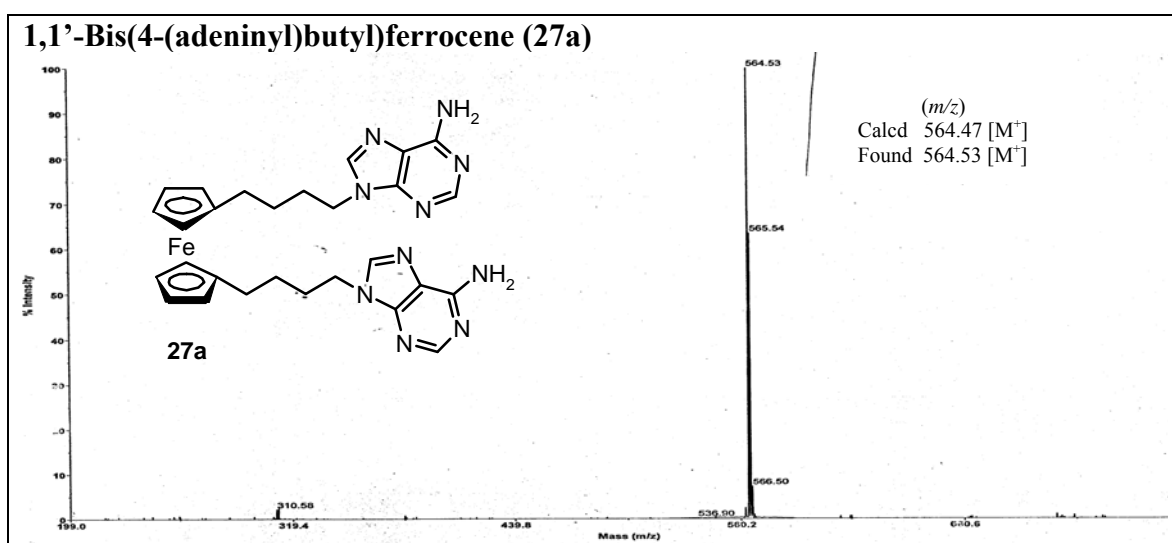
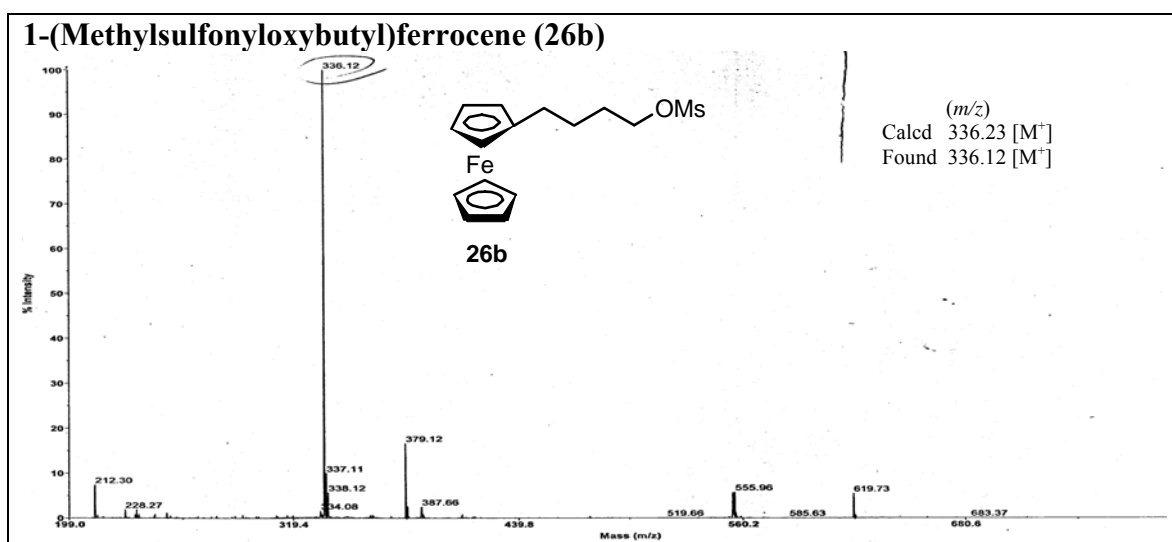
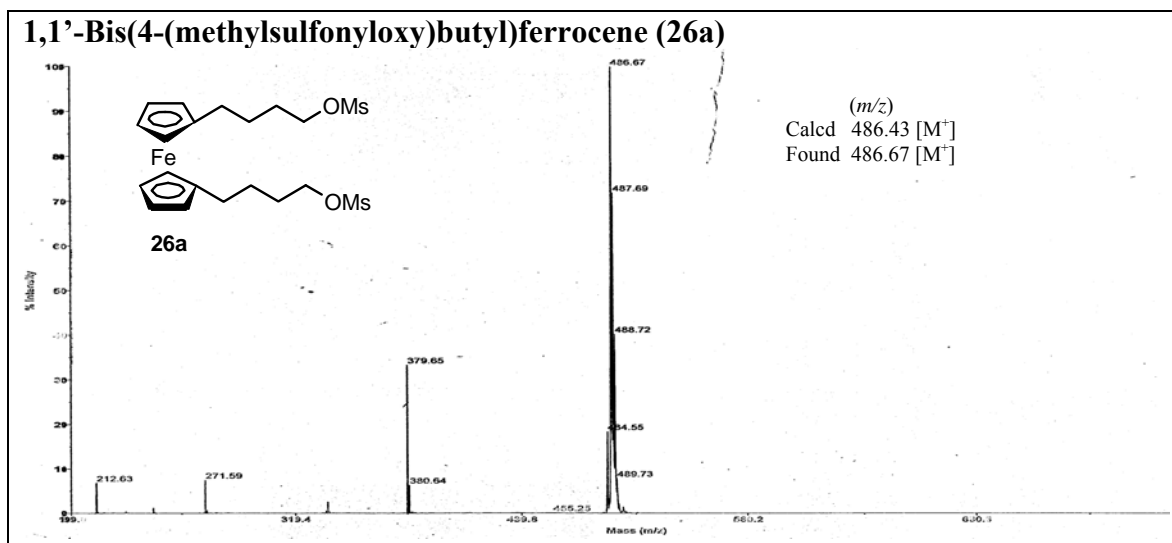


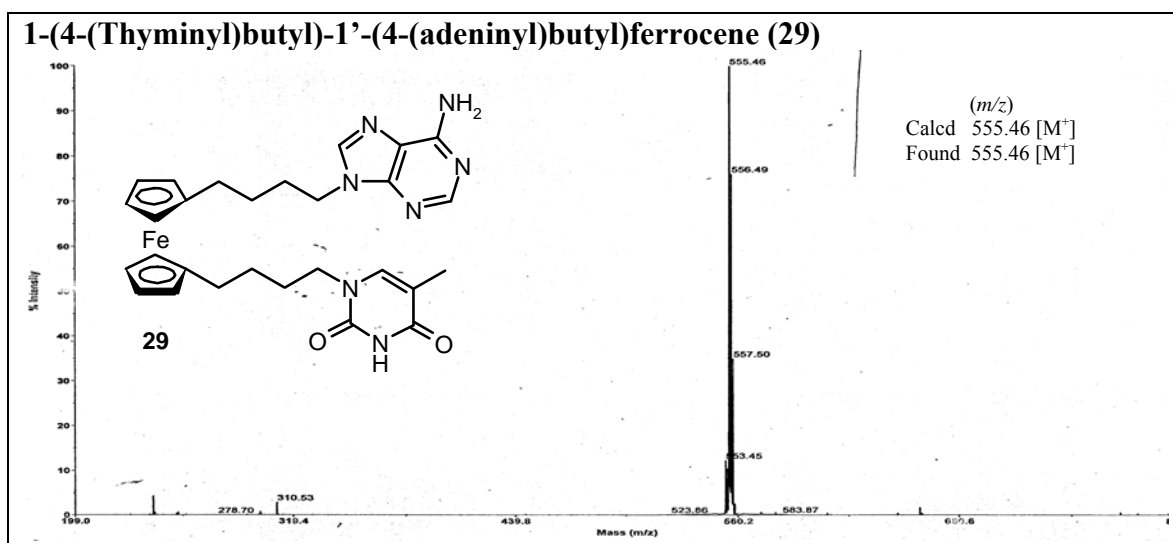
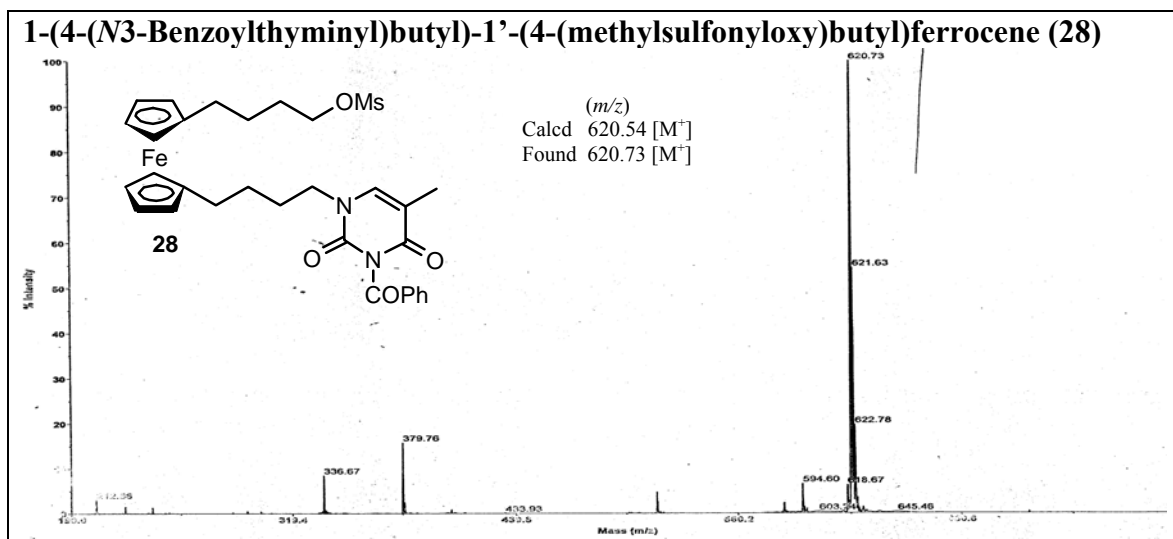
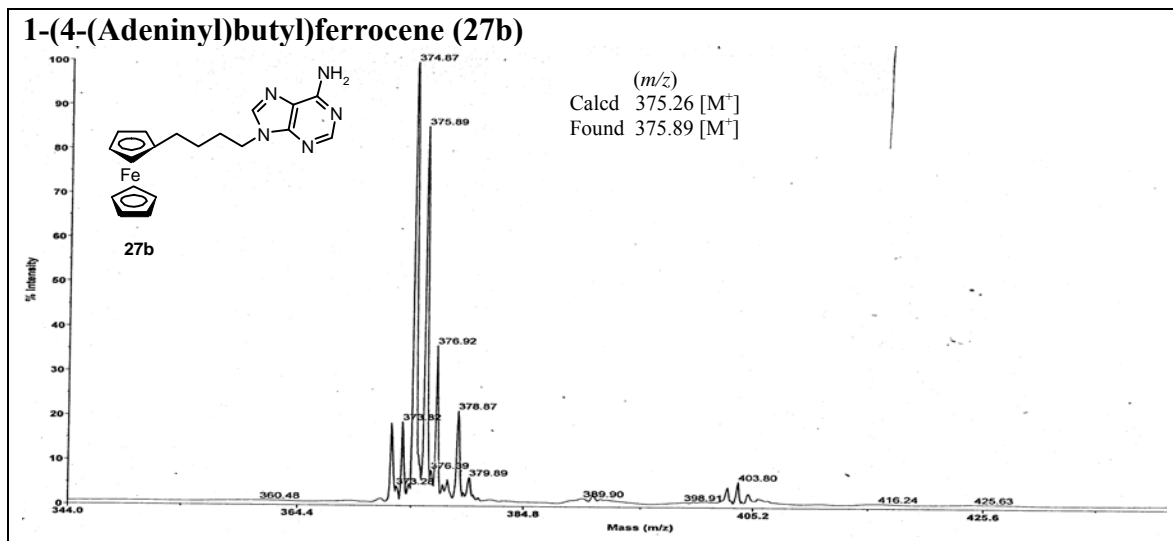
**1,1'-Bis(uracilylmethyl)ferrocene (20b)****1-(Hydroxymethyl)-1'-(*tert*-butyldimethylsilyloxymethyl)ferrocene (21)****1-(*N*3-Benzoylthyminylmethyl)-1'-(*tert*-butyldimethylsilyloxymethyl)ferrocene (22)**

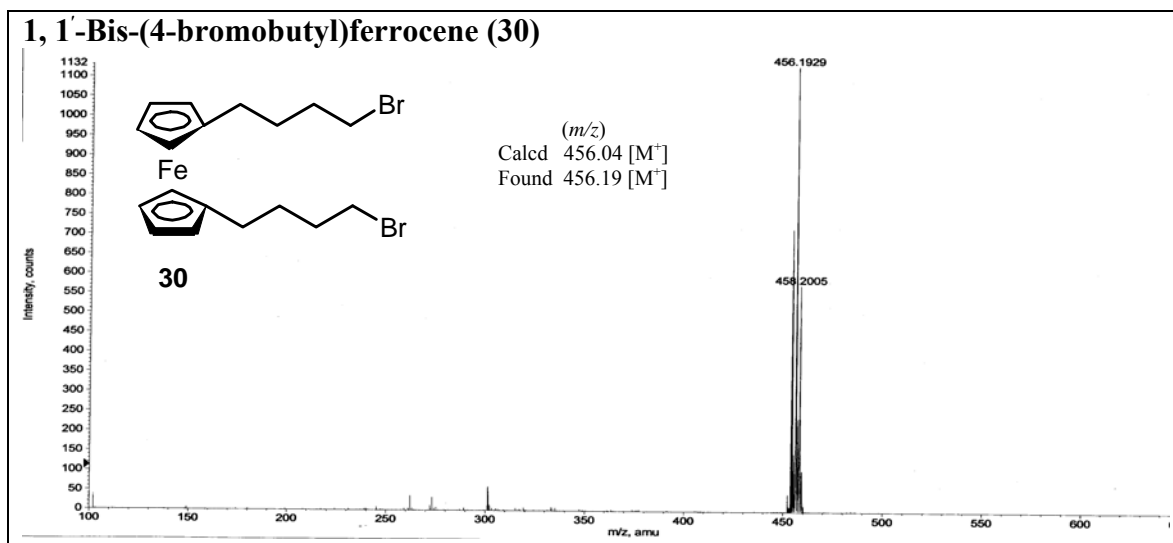
1-(*N*3-Benzoylthyminylmethyl)-1'-(hydroxymethyl)ferrocene (23)1-(*N*3-Benzoylthyminylmethyl)-1'-(*N*3-benzoyluracilylmethyl)ferrocene (24)

## 1-(Thyminylmethyl)-1'-(uracilylmethyl)ferrocene (25)











## **CHAPTER 3**

# **FERROCENE-OLIGONUCLEOTIDE CONJUGATES: SYNTHESIS, CHARACTERIZATION AND BIOPHYSICAL STUDIES**

### 3.1 Introduction

One of the major interests in redox labeled oligonucleotide derivatives is for electrochemical DNA sensors and is also important in studies on DNA mediated electron transfer processes, which has large potential for biomedical application. The detection of specific DNA sequences using real-time methods offer exciting potential application in clinical diagnostics, environmental protection, food quality control and forensic science.<sup>1</sup> Detection methods based on radioactive isotopes (RI) are widely used due to their high detection sensitivity but are also hazardous, having short shelf life, and not well suited for *in situ* measurements. The alternative non-radioactive detection methods such as luminescence, fluorescence<sup>2</sup> or quartz crystal microbalance measurements<sup>3</sup> are also recognized in literature. In this context, electrochemical methods have received particular attention due to their high sensitivity.<sup>4</sup>

The study of energy and electron transfer process through the DNA duplex, the development of DNA hybridization probes and electrochemical sensors have resulted in the synthesis of numerous transition metal (Ru, Os, Fe, Rh and Cu complexes) modified oligonucleotides.<sup>5-7</sup> One of the approaches of screening the DNA hybridization with a complementary strand is based on the change of the electrochemical response of labeling DNA with redox active compounds. Ferrocene and its derivatives have received a lot of importance because the two cyclopentadienyl rings can mutually rotate around the Fe atom which acts as ball bearing and they are attractive electrochemical probes as a result of their stability and convenient synthetic chemistry. In context to DNA, ferrocene has added attraction since the inter-ring spacing between the two cyclopentadienyl (Cp) rings in ferrocene is 0.35 nm which is almost the same as the distance between the stacked base pairs in DNA (Figure 1.13, Chapter 1).<sup>8</sup>

#### 3.1.1 Spectroscopic methods for studying DNA interaction

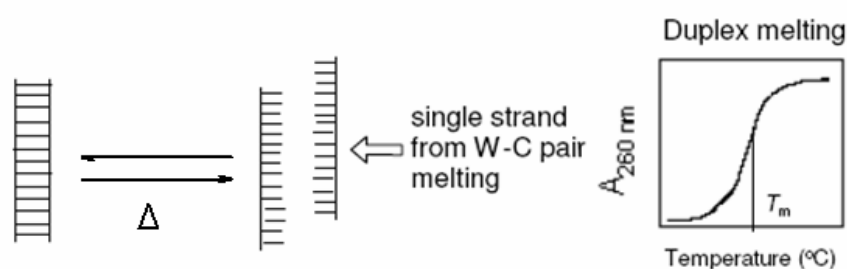
The ability of oligonucleotides to bind *in vitro* the target DNA can be detected by UV-Spectroscopy.

##### *UV-Spectroscopy*

Nucleic acid complexes have lower UV absorption than that predicted from the sum of their constituent base extinction coefficients that is usually measured at 260 nm. This phenomenon known as “hypsochromicity” results from coupling of the transition

dipoles between neighbouring stacked bases. As a result, the UV absorption of DNA duplex increases typically by 20-30 % when it is denatured. This transition from a helix to an unstacked, strand-separated coil has strong entropic component and so is temperature dependent.

The melting temperature ( $T_m$ ) is defined as the temperature at which half of the DNA strands are in the double-helical state and half are in the “random-coil” states. The melting temperature depends on both the length of the sequence as well as the base composition of the sequence.



**Figure 3.1:** Schematic representation of DNA duplex melting

The DNA melting is readily monitored by measuring its absorbance at a wavelength of 260 nm. A plot of absorbance against the temperature of measurement gives a sigmoidal curve in the case of duplexes and the midpoint of the transition gives the  $T_m$  (Figure 3.1).

Recently, Warren A. Kibbe from Northwestern University has developed OligoCalc as a web-accessible, client-based computational engine for reporting DNA and RNA single-stranded and double-stranded properties, including molecular weight, solution concentration, melting temperature, estimated absorbance coefficients, intermolecular self-complementarity estimation and intramolecular hairpin loop formation.<sup>9</sup> OligoCalc has a familiar ‘calculator’ look and feel, making it readily understandable and usable. OligoCalc incorporates three common methods for calculating oligonucleotide-melting temperatures, including a nearest-neighbour thermodynamic model for melting temperature. Since it first came online in 1997, there have been more than 900,000 accesses of OligoCalc from nearly 200,000 distinct hosts, excluding search engines. OligoCalc is available at <http://www.basic.northwestern.edu/biotools/oligocalc.html> with links to the full source code, usage patterns and statistics at that link as well.

### 3.1.2 Gel electrophoresis

Cross-linked chains of polyacrylamide, introduced as matrices for electrophoresis by Raymond and Weintraub in 1959, are used as electrically neutral matrices to separate double stranded DNA fragments according to size and single-stranded DNAs according to size and conformation.

Polyacrylamide gels have the following three major advantages over agarose gels:

- 1) Their resolving power is so great that they can separate molecules of DNA whose lengths differ by as little as 0.1 % (i.e., 1 bp in 1000 bp).
- 2) They can accommodate much larger quantities of DNA than agarose gels. Up to 10  $\mu\text{g}$  of DNA can be applied to a single slot (1 cm x 1 mm) of typical polyacrylamide gels without significant loss of resolution.
- 3) DNA recovered from polyacrylamide gels is extremely pure and can be used for the most demanding purposes (e.g. microinjection of mouse embryos)

There are two types of polyacrylamide gels.

#### *Denaturing polyacrylamide gels*

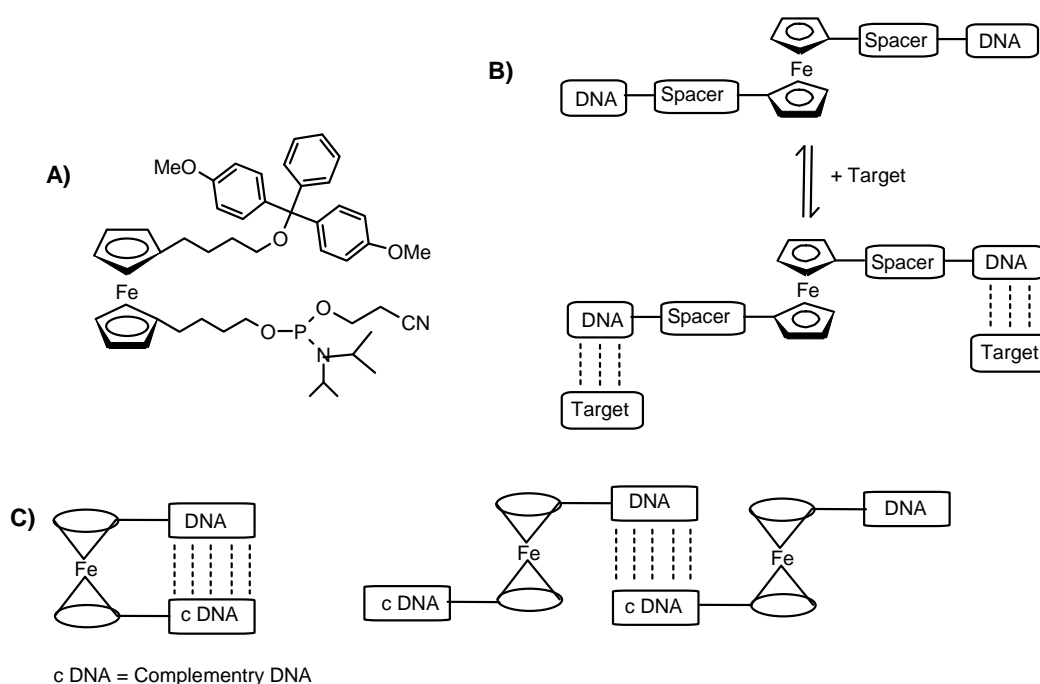
Denaturing polyacrylamide gels are used for the separation and purification of single-stranded fragments of DNA. These gels are polymerized in the presence of an agent (urea and/or, less frequently, formamide) that suppresses base pairing in nucleic acids. Denatured DNA migrates through these gels at a rate that is almost completely independent of its base composition and sequence.

#### *Nondenaturing polyacrylamide gels*

Nondenaturing polyacrylamide gels are used for the separation and purification of fragments of double-stranded DNA. As a general rule, double-stranded DNAs migrate through nondenaturing polyacrylamide gels at rates that are inversely proportional to the  $\log_{10}$  of their size. However, electrophoretic mobility is also affected by their base composition and sequence, so that duplex DNAs of exactly the same size can differ in mobility by up to 10 %. Nondenaturing polyacrylamide gels are used chiefly to prepare highly purified fragments of DNA and to detect protein-DNA complexes.

### 3.2 Present Work: Rationale and Objective

Recently there has been great interest in testing DNA molecules for electrical/charge conductance. Several theories have been formulated to understand the mechanism of conductance. In present research, it is proposed to conjugate ferrocene to oligonucleotides (ODNs) at desired positions to influence the conductance ability of ODNs and these molecules may help to test some of the hypothesis in mechanism of electron conduction in DNA. Towards developing of convenient method for microanalysis of DNA, ferrocenyl-modified oligonucleotides (FcODNs) were synthesized. Ferrocenyl-oligonucleotides obtained by the coupling of amino-terminated ODNs with a ferrocene derivative bearing an activated ester have been developed.<sup>10</sup> Yu *et al.*<sup>11</sup> have developed a similar approach in which the redox-active ferrocenyl-modified ODN was directly prepared using a DNA/RNA synthesizer and a nucleoside phosphoramidite bearing a ferrocenyl moiety at the 2' position. This latter strategy has the advantage of giving access to ODNs containing ferrocene at various positions but is chemically more difficult.<sup>11,12</sup> In such approaches, the electroactive marker is bound on a sugar or nucleic base of nucleotides, using different coupling strategies, i.e. prior<sup>11,12</sup> to, during<sup>13</sup> or after<sup>14</sup> the ODN synthesis on DNA/RNA synthesizer.



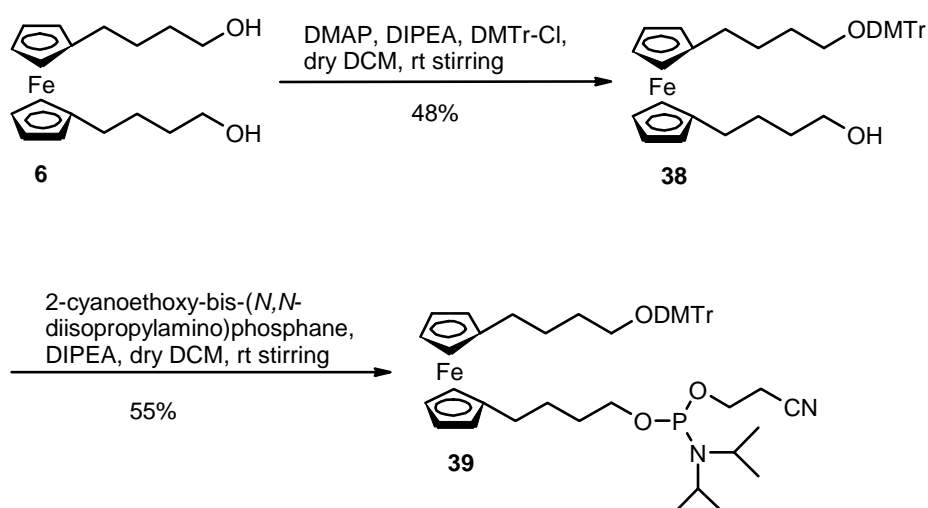
**Figure 3.2:** A) Ferrocene-phosphoramidite (monomer unit), B & C) Ferrocene unit incorporated in DNA sequences (ferrocene linked oligonucleotide).

In order to simplify the chemical synthesis and to increase the selectivity and sensitivity of such electronic microsensors, a new strategy has been developed to elaborate ferrocenyl-modified ODN based on a replacement of a nucleotide by an electroactive marker. This is directly inserted during the DNA synthesis.

Accordingly the aim was to prepare suitable monomers (Figure 3.2A). These can be incorporated into DNA sequence and the properties of resulting DNA conjugates were investigated using various techniques such as UV, CD, fluorescence and cyclic voltammetry. The results were aimed at understanding the mechanism of DNA conductance. These electrochemically active DNA probes may overcome most of the drawbacks and disadvantages of the conventional methods. In fact, several demonstrations for this expectation have been reported in literature.<sup>15</sup>

### 3.3 Synthesis of Ferrocene-Phosphoramidite Monomer Unit (39)

The synthesis of **6** has already been reported. The phosphoramidite **39** has been synthesized from **6** in two steps involving the protection of one hydroxyl group by dimethoxytrityl chloride (DMTr-Cl) to give 1-[4-*O*-dimethoxytritylbutyl]-1'-[4'-hydroxybutyl]ferrocene **38**<sup>16</sup> followed by reaction with 2-cyanoethoxy-bis-(*N,N*-diisopropylamino)-phosphane to yield 1-[4-*O*-dimethoxytritylbutyl]-1'-[4'-*O*-(2-cyanoethyl-*N,N*-diisopropylphosphoramidityl)butyl]ferrocene **39**<sup>17</sup> (Scheme 3.1).



**Scheme 3.1:** Synthesis of ferrocene-phosphoramidite monomer unit **39**

First step, protection of one hydroxyl group with DMTr-Cl, also gave some unreacted starting material **6** along with a compound containing both the hydroxyl group protected with DMTr-Cl.

Formation of DMT protected alcohol **38** was confirmed by  $^1\text{H}$  NMR spectrum showing singlet at  $\delta$  3.80 for  $-\text{OCH}_3$  of dimethoxytrityl (DMTr) group. Formation of ferrocene-phosphoramidite monomer unit **39** was confirmed by  $^1\text{H}$  NMR spectrum showing two singlets at  $\delta$  1.18 and 1.22 for two isopropyl group attached to nitrogen and further confirmed by  $^{31}\text{P}$  NMR spectrum showing singlet at  $\delta$  147.72 for trivalent phosphorous. Further, formation of conjugates **28** and **29** were confirmed by mass spectra analysis having mass ( $m/z$ ) at 632.15 [ $\text{M}^+$ ] and 832.84 [ $\text{M}^+$ ] respectively.

### 3.4 Synthesis, Purification and Characterization of Ferrocenyl-Modified Oligonucleotides

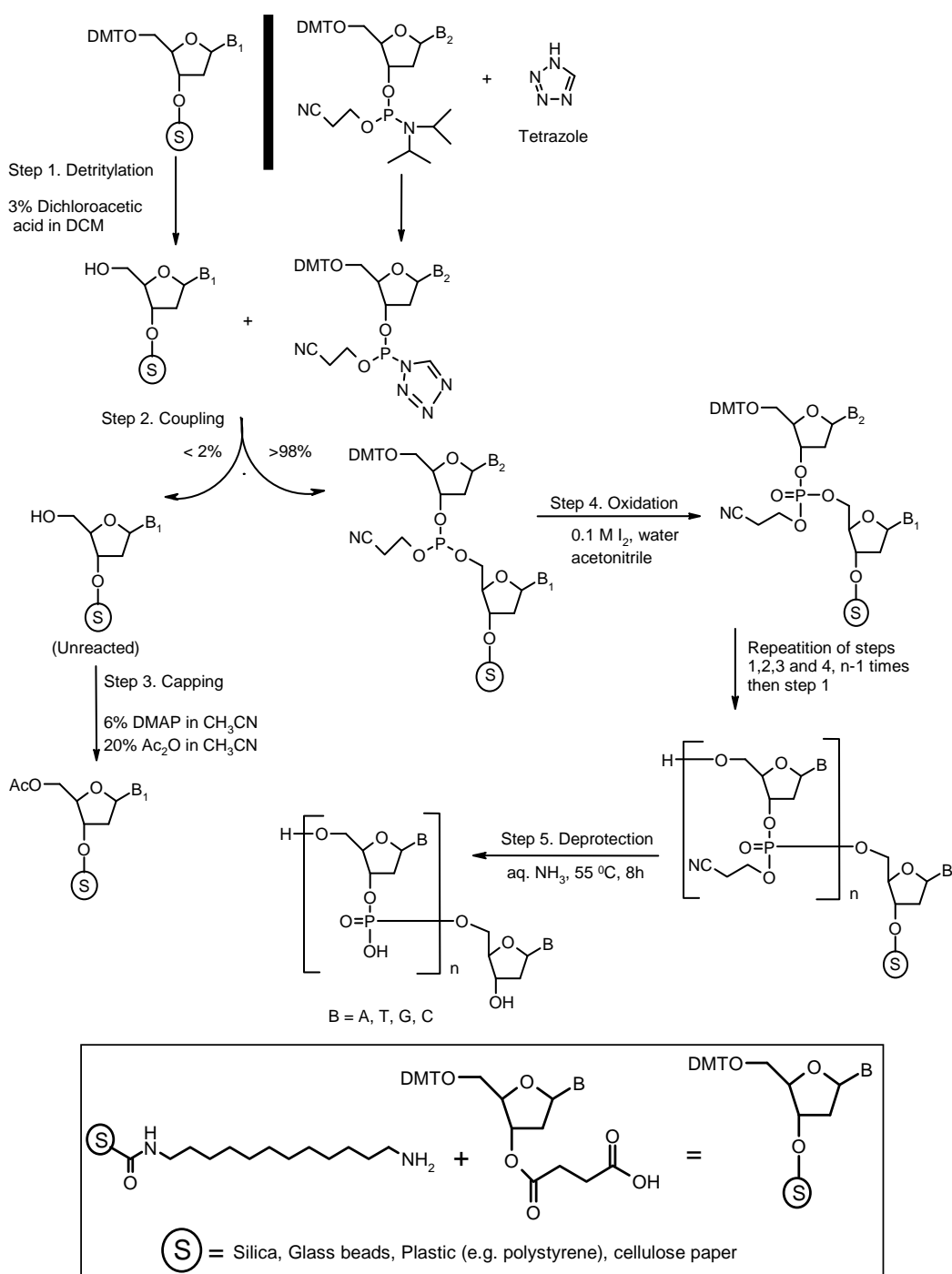
A bisfunctional ferrocene containing phosphoramidite and dimethoxytrityl (DMTr) **39** has been synthesized. This ferrocenyl-phosphoramidites has been directly employed in an automated solid-phase DNA synthesizer using phosphoramidite chemistry to synthesize ferrocenyl-modified oligonucleotides (entry 1-5, Table 3.1).

**Table 3.1:** HPLC and MALDI-TOF mass spectral analysis of oligonucleotides.

Entry	Code No.	Sequences	Retention time (min)	Calculated MW	Measured MW
1	ODN-1	5'-AGA AAA GGA-3'	6.344	2804.97	2807.67
2	ODN-2	5'-TCC TTT TCT-3'	7.474	2630.81	2634.15
3	FcODN-1	5'-AGA AAA GGA--Fc--TCC TTT TCT-3'	10.823	5889.85	5889.28
4	FcODN-2	5'-Fc-AGA AAA GGA-3'	14.698	3197.18	3198.57
5	FcODN-3	5'-TCC TTT TCT-Fc-T-3'	13.144	3327.17	3328.28

The oligonucleotides were synthesized on Applied Biosystems ABI 3900 high throughput DNA synthesizer using standard  $\beta$ -cyanoethyl phosphoramidite chemistry (Figure 3.3).<sup>18</sup> The oligomers were synthesized in 3' to 5' direction on polystyrene solid support, followed by ammonia treatment. The oligonucleotides were desalted by gel filtration. The purity of the so obtained oligomers was checked by analytical reverse

phase HPLC, which shows more than 65-70% purity. These were subsequently purified by RP-HPLC on a preparative column. The purity of the oligomers was again ascertained by analytical RP-HPLC and their integrity was confirmed by MALDI-TOF mass spectrometric analysis (Table 3.1).



**Figure 3.3:** Solid-phase syntheses of oligodeoxynucleotides by phosphoramidite method.



### 3.5 Results and Discussion

#### 3.5.1 Gel shift assays

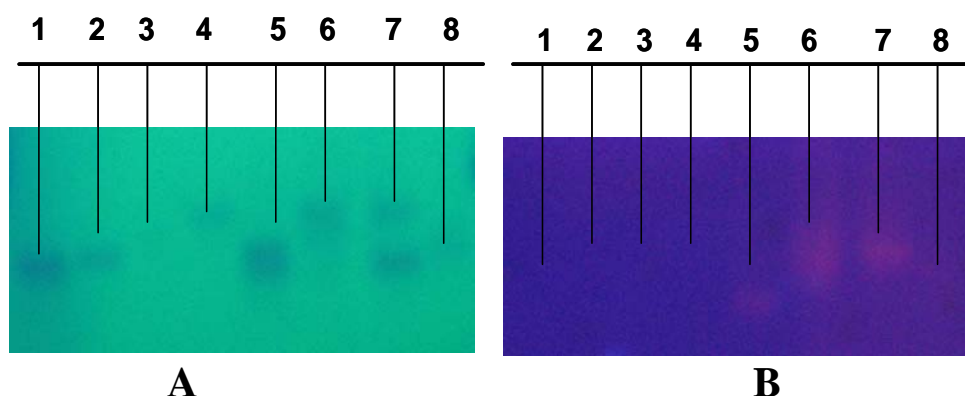
Ferrocenyl-phosphoramidite **39** was incorporated into oligodeoxyribonucleotides using an automated DNA synthesizer. Table 3.1 lists the sequences of the synthesized ferrocenyl-oligonucleotides (FcODNs; entry 3, 4 and 5). Normal oligonucleotides (ODNs, without ferrocene unit) were synthesized using the same protocol (entry 1 and 2). Different sequences of FcODNs and ODNs were prepared and the purity and ability of various FcODNs to form intramolecular secondary structures or intermolecular duplexes with complementary strands was evaluated through denaturing and non denaturing gel electrophoresis.

**Table 3.2:** Ferrocenyl-modified oligonucleotide and DNA sequences used for gel electrophoresis.

Entry	Code No.	Sequence
1	ODN-1	5'-AGA AAA GGA-3'
2	ODN-2	5'-TCC TTT TCT-3'
3	FcODN-2	5'- <b>Fc</b> -AGA AAA GGA-3'
4	FcODN-3	5'-TCC TTT TCT - <b>Fc</b> - T-3'
5	ODN-1 ODN-2	5'-AGA AAA GGA-3' 3'-TCT TTT CCT-5'
6	FcODN-2 FcODN-3	5'- <b>Fc</b> -AGA AAA GGA-3' 3'-T- <b>Fc</b> - TCT TTT CCT-5'
7	ODN-1 FcODN-3	5'-AGA AAA GGA-3' 3'-T- <b>Fc</b> - TCT TTT CCT-5'
8	ODN-2 FcODN-2	5'-TCC TTT TCT-3' 3'-AGG AAA AGA- <b>Fc</b> -5'

The different combinations of FcODN-2, FcODN-3, ODN-1 and ODN-2 used for generating duplexes, are listed in Table 3.2 (entry 1 to 8). Nondenaturing polyacrylamide gels were used for hybridization studies. The spots were visualized through UV shadowing by illumination of the gels placed on a fluorescent silica gel plate using UV-light. Lane 1 to 8 in Figure 3.4A corresponds to entry 1 to 8 (Table 3.2). Lane 1 to 4 corresponding to the single strands show different mobilities for different sequences. In

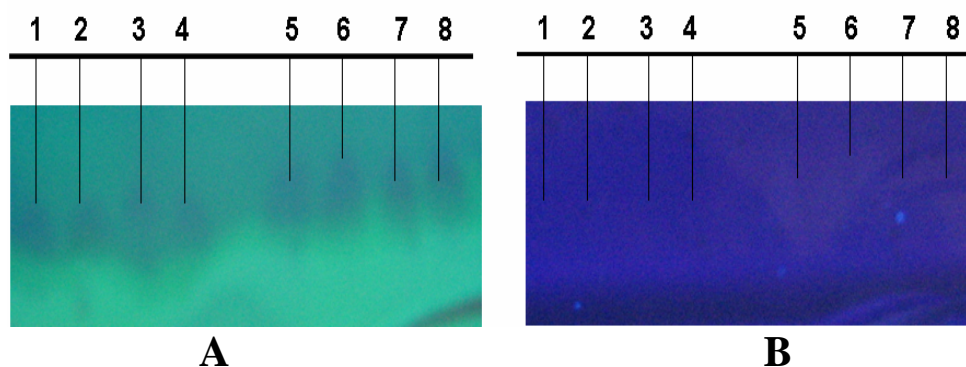
polyacrylamide gel, migration rates of single strand oligonucleotides is directly proportional to charge and inversely proportional to  $\log_{10}$  of size. ODN-1, having all purine bases, (entry 1, Table 3.2) being more polar moved slightly faster than ODN-2, having all pyrimidine bases (entry 2, Table 3.2) (lane 1 and 2, Figure 3.4A). Ferrocenyl-oligonucleotide FcODN-2 and FcODN-3 (entry 3 and 4 respectively, Table 3.2) migrated comparatively slower and this may be due to the presence of nonpolar ferrocene moiety with *n*-butyl spacer (lane 3 and 4, Figure 3.4A). The formation of duplexes between ferrocenyl-modified oligonucleotide and complementary oligonucleotides were accompanied by the disappearance of the bands due to corresponding single strands and appearance of a lower migrating band due to duplexes. Lanes 5 to 8 (Figure 3.4A) correspond to the double strand complexes, which was significantly retarded in the gel as compared to corresponding individual single strands. The duplexes from FcODN-2 and FcODN-3 (entry 6, Table 3.2) was retarded most perhaps due to having two nonpolar ferrocene units (lane 6, Figure 3.4A). The formation of duplexes was further confirmed by staining the gel with the indicator ethidium bromide and the spots were visualized through UV shadowing. Only the duplexes were observed as fluorescent bands because of intercalation, while the single strands were not stained and hence non-fluorescent. Lanes 5 to 8 show fluorescent bands (Figure 3.4B) corresponding to successful formation of duplexes (entry 5 to 8 respectively, Table 3.2).



**Figure 3.4:** Gel shift assay (nondenaturing gel) of ferrocenyl-oligonucleotide (entry 1-8, Table 3.2) (A) under UV shadow (B) after stained with ethidium bromide

Two bands appear in lane 7 (Figure 3.4A), where the faster migrating band corresponds to excess of the single strand ODN-1 (entry 1, Table 3.2) that did not show any fluorescent band after ethidium bromide staining (Figure 3.4B). The lower migrating

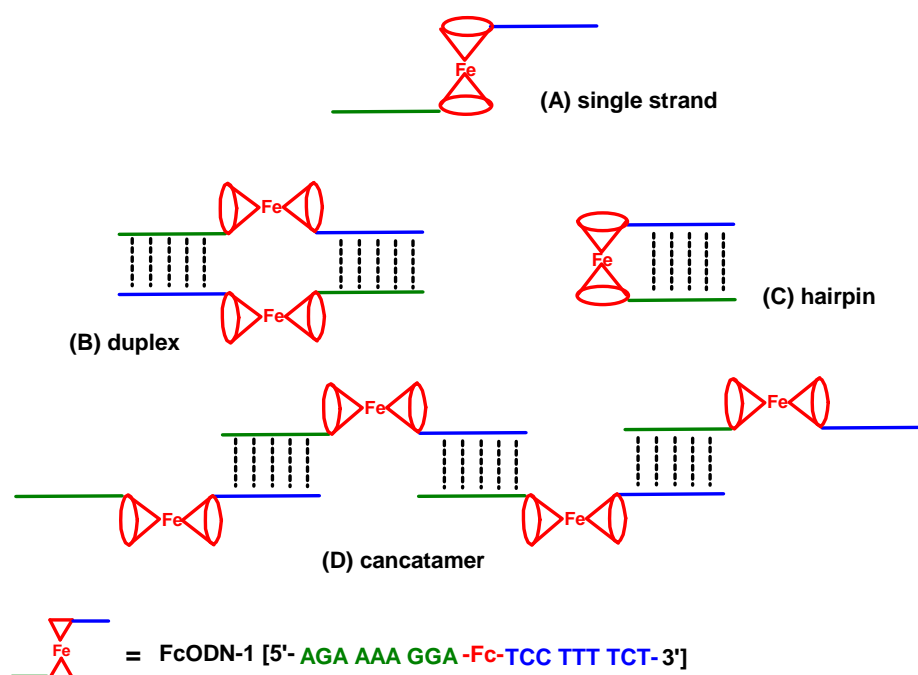
band which showed fluorescence after ethidium bromide staining (Figure 3.4B) corresponds to duplex in entry 7 (Table 3.2).



**Figure 3.5:** Gel shift assay (denaturing gel) of ferrocenyl-oligonucleotide (entry 1-10, Table 3.3) (A) under UV shadow (B) after stained with ethidium bromide

The fluorescent band arising after ethidium bromide staining was exclusively due to duplex formation was also confirmed by running denaturing polyacrylamide gels. These gels containing a denaturant urea did not favour formation of duplexes. Figure 3.5 (A and B) shows denaturing polyacrylamide gel for entry 1 to 8 (Table 3.2) before and after ethidium bromide staining respectively. Slight broadening of the bands was observed (lane 1 to 8, Figure 3.5A) and no fluorescent bands were seen after ethidium bromide staining (Figure 3.5B), indicating absence of duplexes in the presence of urea (Figure 3.5B).

The above gel experiments were carried out with ferrocenyl-oligonucleotides (FcODNs) having ferrocene moiety either at 5' end (FcODN-2, entry 4, Table 3.3) or at 3' end (FcODN-3, entry 5, Table 3.3). Ferrocenyl-oligonucleotide (FcODN-1, entry 3, Table 3.3) is a self complementary having ferrocene moiety at middle position with complementary sequences stretched on both sides. When hybridized with any one of complementary oligonucleotides (entry 1, 2, 4 and 5, Table 3.3), FcODN-1 can form several intra and intermolecular duplexes (Figure 3.6). Polyacrylamide gels were used for distinguishing several hybridization modes, with the bands visualized through UV shadowing or fluorescent viewing after ethidium bromide staining.

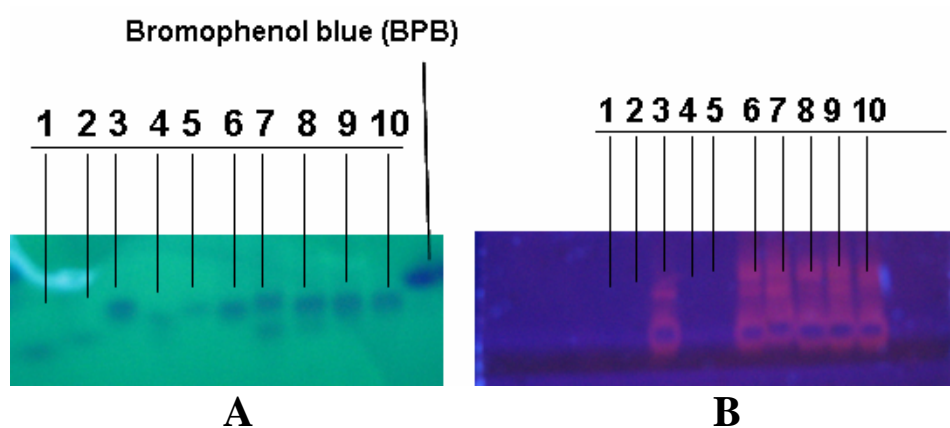


**Figure 3.6:** Different possible secondary structures for FcODN-1.

**Table 3.3:** Ferrocenyl-modified oligonucleotide and DNA sequences used for gel electrophoresis.

Entry	Code No.	Sequence
1	ODN-1	5'-AGA AAA GGA-3'
2	ODN-2	5'-TCC TTT TCT-3'
3	FcODN-1	5'-AGA AAA GGA-Fc-TCC TTT TCT-3'
4	FcODN-2	5'-Fc-AGA AAA GGA-3'
5	FcODN-3	5'-TCC TTT TCT -Fc- T-3'
6	FcODN-1	5'-AGA AAA GGA-Fc-TCC TTT TCT-3'
7	FcODN-1 ODN-1	5'-AGA AAA GGA-Fc-TCC TTT TCT-3' 3'-AGG AAA AGA-5'
8	FcODN-1 ODN-2	5'-AGA AAA GGA-Fc-TCC TTT TCT-3' 3'-TCT TTT CCT-5'
9	FcODN-1 FcODN-2	5'-AGA AAA GGA-Fc-TCC TTT TCT-3' 3'-Fc-AGG AAA AGA-5'
10	FcODN-1 FcODN-3	5'-AGA AAA GGA-Fc-TCC TTT TCT-3' 3'-T-Fc- TCT TTT CCT-5'

Lanes 1 to 10 in Figure 3.7A depict bands corresponding to entry 1 to 10 (Table 3.3). All double strands were significantly retarded in the gel corresponding to its two single strands. There was no significant difference between the migration rates of different double strands (lane 7 to 10, Figure 3.7A). The formation of double strands were confirmed by fluorescent bands upon ethidium bromide staining while bands due to unhybridized single strands were non-fluorescent (lane 7 to 10, Figure 3.7B).

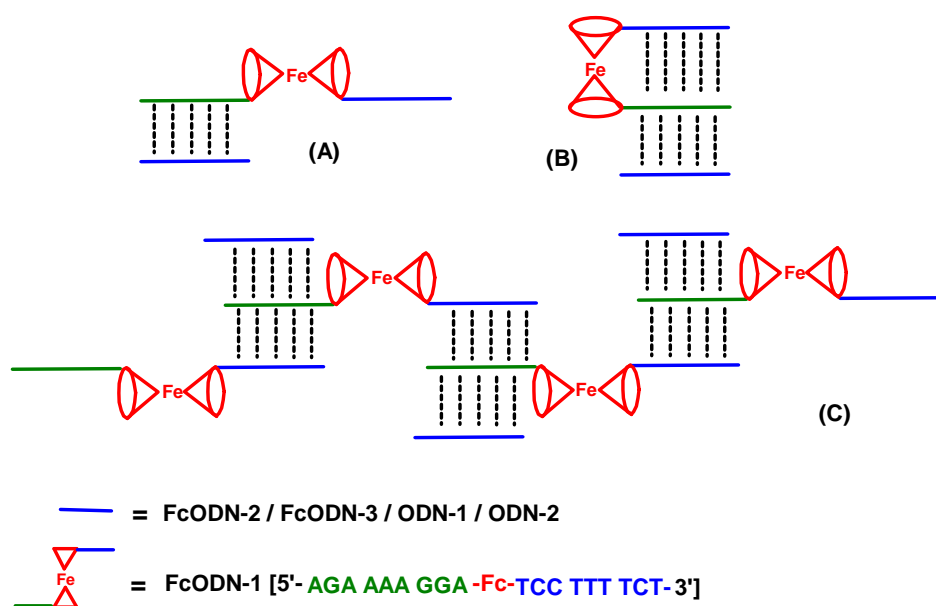


**Figure 3.7:** Gel shift assay (nondenaturing gel) of ferrocenyl-oligonucleotide (entry 1-10, Table 3.4) (A) under UV shadow (B) after stained with ethidium bromide.

FcODN-1 is a self complementary oligonucleotide with a possibility that it may remain as single strand (Figure 3.6A), exist as duplexes (Figure 3.6B), hairpin (Figure 3.6C) or concatameric structures (Figure 3.6D).

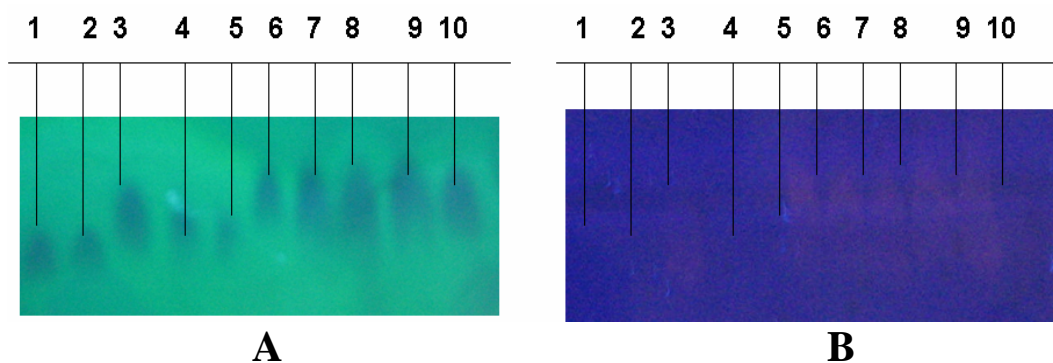
To distinguish the formation of single strand or duplex structure, FcODN-1 was spotted at low and high concentrations after the annealing process (entry 3 and entry 6, Table 3.3). Ethidium bromide staining indicated that both entry 3 and entry 6 (Table 3.3) does not exist as single strand but perhaps forms duplex structures that show fluorescent bands (Figure 3.7B). FcODN-1 alone (duplex) was retarded more than any other duplexes. In case of hairpin formation, it is expected to migrate faster than any of the double strands. Thus the possibility of formation of hairpin kind of structure of FcODN-1 was ruled out.

In case of entry 7 to 10 (Table 3.3), different secondary structures are possible (Figure 3.8). Two fluorescent bands (having significant difference in migration) appeared in lane 7 after ethidium bromide staining (Figure 3.7A), indicates the presence of different secondary structures.



**Figure 3.8:** Different possible secondary structures for entry 7 to 10 (Table 3.3).

In the denaturing gels, broadening of the bands were observed with no significant difference in migration among the different single (lane 1, 2, 4 and 5, Figure 3.9A) and double strand samples (lane 3, 6, 7, 8, 9 and 10, Figure 3.9A). No fluorescent bands were seen after ethidium bromide staining (Figure 3.9B) due to non-formation of duplexes in presence of urea and hence no intercalation of ethidium bromide moiety (Figure 3.9B).



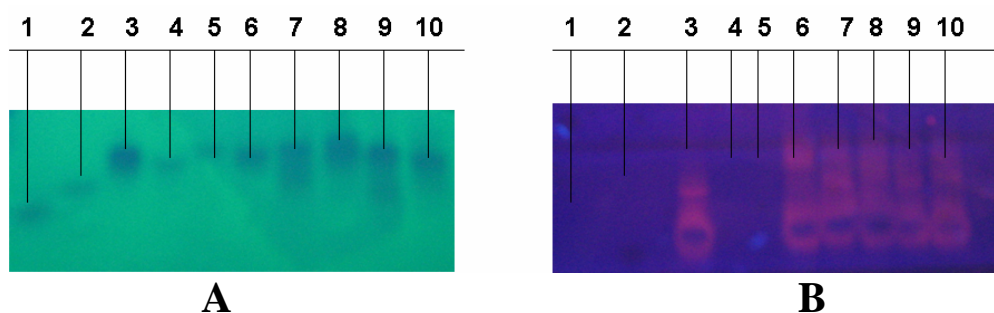
**Figure 3.9:** Gel shift assay (denaturing gel) of ferrocenyl-oligonucleotide (entry 1-10, Table 3.4) (A) under UV shadow (B) after stained with ethidium bromide

FcODN-1 (entry 3, Table 3.4) was hybridized with two different complementary oligonucleotides (entry 7, 8, 9 and 10, Table 3.4) and examined by non-denaturing polyacrylamide gel.

**Table 3.4:** Ferrocenyl-modified oligonucleotide and DNA sequences used for gel electrophoresis.

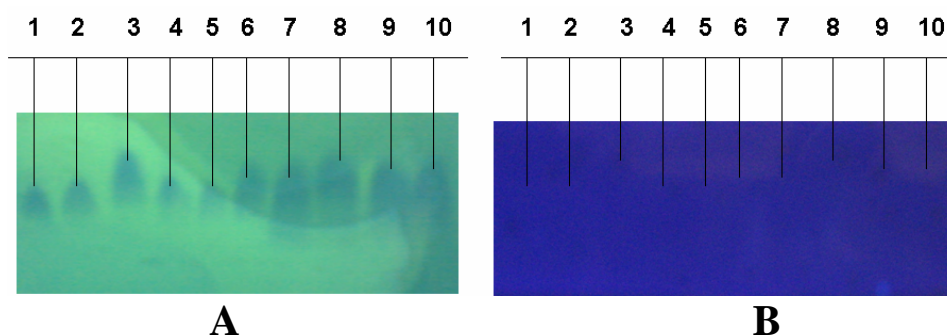
Entry	Code No.	Sequence
1	ODN-1	5'-AGA AAA GGA-3'
2	ODN-2	5'-TCC TTT TCT-3'
3	FcODN-1	5'-AGA AAA GGA- <b>Fc</b> -TCC TTT TCT-3'
4	FcODN-2	5'- <b>Fc</b> -AGA AAA GGA-3'
5	FcODN-3	5'-TCC TTT TCT - <b>Fc</b> - T-3'
6	FcODN-1	5'-AGA AAA GGA- <b>Fc</b> -TCC TTT TCT-3'
7	FcODN-1 ODN-1 ODN-2	5'-AGA AAA GGA- <b>Fc</b> -TCC TTT TCT-3' 3'-TCT TTT CCT-5' 3'-AGG AAA AGA-5'
8	FcODN-1 FcODN-2 FcODN-3	5'-AGA AAA GGA- <b>Fc</b> -TCC TTT TCT-3' 3'-T- <b>Fc</b> - TCT TTT CCT-5' 3'- <b>Fc</b> -AGG AAA AGA-5'
9	FcODN-1 ODN-1 FcODN-3	5'-AGA AAA GGA- <b>Fc</b> -TCC TTT TCT-3' 3'-T- <b>Fc</b> - TCT TTT CCT-5' 3'-AGG AAA AGA-5'
10	FcODN-1 ODN-2 FcODN-2	5'-AGA AAA GGA- <b>Fc</b> -TCC TTT TCT-3' 3'-TCT TTT CCT-5' 3'- <b>Fc</b> -AGG AAA AGA-5'

In lane 1 to 10 (Figure 3.10A) corresponding to entry 1 to 10 (Table 3.4) all double strands showed slower migration in the gel corresponding to its two single strands. The formation of double strands were further confirmed by ethidium bromide staining and visualization of the gel under UV where only the duplexes show up as fluorescent bands, while the single strands were not visible (lane 7 to 10, Figure 3.10B). The duplex (lane 8, Figure 3.10A) having three ferrocene moieties being more nonpolar (entry 8, Table 3.4) retarded most of all duplexes. There was no significant difference between the migration rates of other oligonucleotides (lane 3, 6, 7, 9 and 10, Figure 3.10A).



**Figure 3.10:** Gel shift assay (nondenaturing gel) of ferrocenyl-oligonucleotide (entry 1-10, Table 3.5) (A) under UV shadow (B) after stained with ethidium bromide

Under denaturing condition broadening of the bands were observed without significant difference in migration distances among the denatured strands (lane 1 to 10, Figure 3.11A). These also did not show any fluorescent band after ethidium bromide staining indicating absence of duplexes (Figure 3.11B). A combination of all these results clearly established cases where duplexes formed to enable meaningful interpretation of  $T_m$  results.



**Figure 3.11:** Gel shift assay (denaturing gel) of ferrocenyl-oligonucleotide (entry 1-10, Table 3.5) (A) under UV shadow (B) after stained with ethidium bromide

### 3.5.2 UV- $T_m$ studies

The stability of various intermolecular duplexes constituted from the synthesized oligonucleotides have evaluated through  $T_m$ 's obtained from temperature dependent UV-absorbance experiments. FcODN-1 (entry 1, Table 3.5) having self complementary sequence and hence capable of forming duplex had  $T_m$  of 52.4 °C (entry 1, Table 3.5). When it was complexed with ODN-1, complementary to the 3'-terminus, the  $T_m$  of the duplex was enhanced by 3.0 °C (entry 2, Table 3.5). Upon complexing with ODN-2, which is a 5'-complementary oligonucleotide to FcODN-1, stabilized the constituted



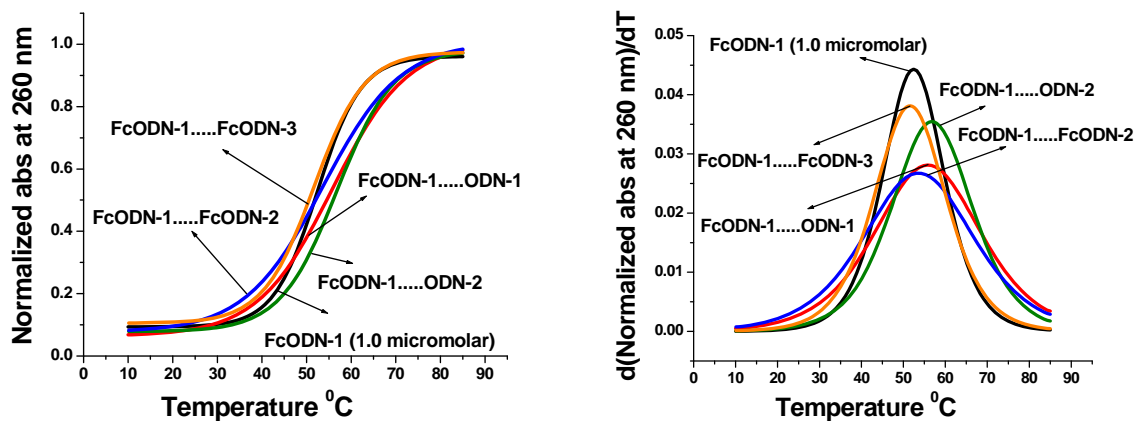
duplex slightly by 4.6 °C (entry 3, Table 3.5). However simultaneous complementation of both ODN-1 and ODN-2 with FcODN-1, did not have constitutive additive effect and the net stabilization upon FcODN-1 duplexes was only 3.8 °C (entry 4, Table 3.5).

FcODN-1 was complexed with the ferrocene conjugated ODN-1 (i.e. FcODN-2) and ODN-2 (i.e. FcODN-3). It was noticed that the derived duplexes entry 5 and entry 6 (Table 3.5) was slightly less stable than that without ferrocene conjugate and the 5'-complement FcODN-3 actually destabilized the corresponding duplex by 0.7 °C (entry 6, Table 3.5). Simultaneous complexation also leads to destabilization of the duplex by 1.5 °C (entry 7, Table 3.5). However combination of 3'-ferrocene + 5'-ODN and 5'-ferrocene + 3'-ODN conjugates with FcODN-1 showed stabilization by 3.0 – 3.8 °C (entry 8 and 9 respectively, Table 3.5).

**Table 3.5:** UV-Melting temperature ( $T_m$  values) of complementary oligonucleotide duplexes.

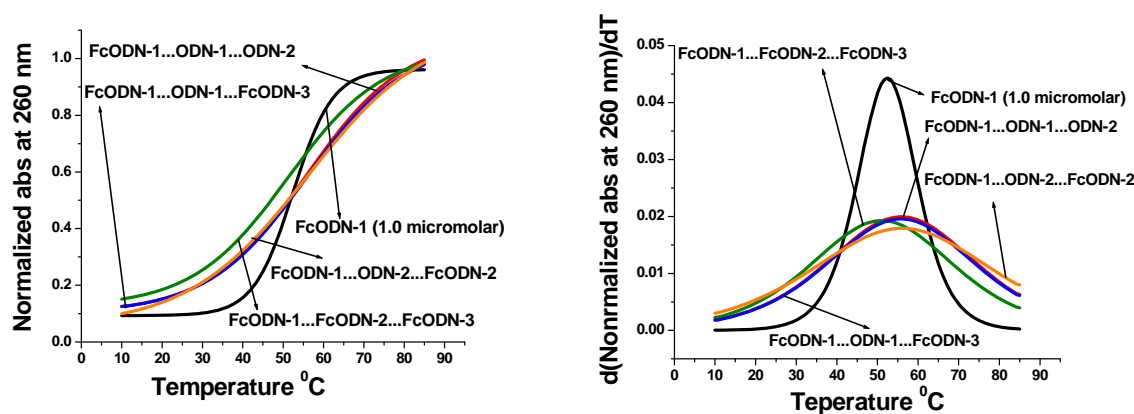
Entry	Code No.	Sequences	Melting Temp. $T_m$ (°C)	$\Delta T_m$ (w.r.t FcODN-1)
1	FcODN-1 (1.0 $\mu$ M)	5'-AGA AAA GGA-Fc-TCC TTT TCT-3'	52.4	duplex
2	FcODN-1 ODN-1	5'-AGA AAA GGA----Fc----TCC TTT TCT-3' 3'-AGG AAA AGA-5'	55.4	3'-duplex + 3 °C
3	FcODN-1 ODN-2	5'-AGA AAA GGA----Fc----TCC TTT TCT-3' 3'-TCT TTT CCT-5'	57.0	5'-duplex + 4.6 °C
4	FcODN-1 ODN-2 ODN-1	5'-AGA AAA GGA----Fc----TCC TTT TCT-3' 3'-TCT TTT CCT-5' 3'-AGG AAA AGA-5'	56.2	5',3'-duplex + 3.8 °C
5	FcODN-1 FcODN-2	5'-AGA AAA GGA----Fc----TCC TTT TCT-3' 3'-AGG AAA AGA-Fc-5'	54.0	3'-Fc-duplex + 1.6 °C
6	FcODN-1 FcODN-3	5'-AGA AAA GGA----Fc----TCC TTT TCT-3' 3'-T-Fc-TCT TTT CCT-5'	51.7	5'-Fc-duplex - 0.7 °C
7	FcODN-1 FcODN-3 FcODN-2	5'-AGA AAA GGA----Fc----TCC TTT TCT-3' 3'-T-Fc-TCT TTT CCT-5' 3'-AGG AAA AGA-Fc-5'	50.9	5',3'-Fc-duplex - 1.5 °C
8	FcODN-1 FcODN-3 ODN-1	5'-AGA AAA GGA----Fc----TCC TTT TCT-3' 3'-T-Fc-TCT TTT CCT-5' 3'-AGG AAA AGA-5'	55.4	5'-Fc-3'-duplex + 3 °C
9	FcODN-1 ODN-2 FcODN-2	5'-AGA AAA GGA----Fc----TCC TTT TCT-3' 3'-TCT TTT CCT-5' 3'-AGG AAA AGA-Fc-5'	56.2	3'-Fc-5'-duplex + 3.8 °C

The UV-melting profiles of intermolecular duplexes (entry 1 to 5, Table 3.5) constituted from the synthesized oligonucleotides are shown in Figure 3.12.



**Figure 3.12:** UV- $T_m$  curves of ferrocenyl-oligonucleotide (entry 1-5, Table 3.5).

The UV-melting profiles of intermolecular duplexes (entry 1, Entry 6 to 9, Table 3.5) constituted from the synthesized oligonucleotides are shown in Figure 3.13.



**Figure 3.13:** UV- $T_m$  curves of ferrocenyl-oligonucleotide (Entry 1, 6-9, Table 3.5)

The transitions corresponding to termolecular duplexes were generally broader than those with bimolecular duplexes.

### 3.6 Conclusions

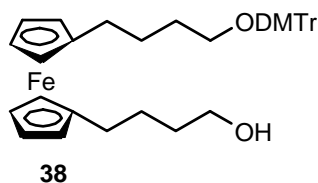
Bis functional ferrocene containing phosphoramidite and dimethoxytrityl (DMTr) groups has been synthesized and characterized. This ferrocenyl-phosphoramidite has been directly employed in an automated solid-phase DNA synthesizer using phosphoramidite chemistry. The advantages of this method are that it allows a non-specialist in nucleotide chemistry to access labeled ODNs. Ferrocenyl-phosphoramidite has been incorporated during automated DNA synthesis at various positions along the ODN sequence. ODNs modified at middle, 3' or 5' extremities have been prepared. Gel shift assays have been carried out and results demonstrate the formation of several inter and intramolecular duplexes with ferrocenyl modified ODNs. The thermal stability of these ferrocenyl modified ODNs were analyzed. Melting temperature measurements demonstrated that the introduction of a ferrocenyl group at the 3' position or at 5' position has no drastic effect on the thermal stability of DNA duplex. The transitions corresponding to termolecular duplexes were generally broader than those with bimolecular duplexes. At this stage it was decided to study the electrochemical properties of these ferrocenyl modified ODNs before and after hybridization with different ODNs as it appear to be extremely important for application as probe for electrochemical sensors.

### 3.7 General Experimental Methods

The chemicals used were of laboratory or analytical grade. All solvents used were purified according to the literature procedure. Reactions were monitored by TLC. Usual reaction work up involved sequential washing of the organic extract with water, brine followed by drying over anhydrous  $\text{Na}_2\text{SO}_4$ , and evaporation of the solvent under vacuum. Infrared spectra (IR) were recorded on Shimadzu 8400 series FTIR instrument.  $^1\text{H}$  and  $^{13}\text{C}$  NMR spectra were recorded on a Bruker AC-200, AC-400 and AC-500 spectrometer. The chemical shifts are given in delta ( $\delta$ ) ppm values and relative to internal standard tetramethylsilane for  $^1\text{H}$ . Mass spectra were recorded on LC-MS/MS-TOF API QSTAR PULSAR spectrometer. Elemental analyses were performed by CHNS-O EA1108 elemental analyzer. All reactions were monitored by analytical thin-layer chromatography (TLC) on Merck Aluminium precoated plates of silica gel 60 F<sub>254</sub> (Product Code. 1.05554.0007) with detection by either viewing under UV light or treating with an ethanolic solution of phosphomolybdic acid. Oligomers were characterized by RP-HPLC (Hewlett Packard) C18 column and MALDI-TOF mass spectrometry. The MALDI-TOF spectra were recorded on Voyager-De-STR (Applied Biosystems) MALDI-TOF instrument. UV-melting experiments were carried out on Perkin-Elmer Lambda-35 UV-spectrophotometer.

### 3.8 Experimental

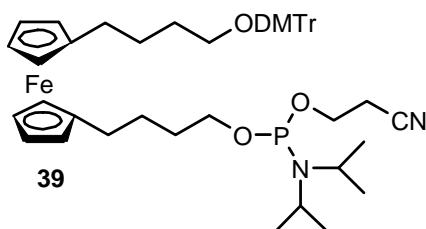
#### 1-[4-*O*-Dimethoxytritylbutyl]-1'-[4'-hydroxybutyl]ferrocene **38**<sup>16</sup>



To a solution of **1** (3.2 g, 9.7 mmol), DMAP (23.6 mg, 0.19 mmol), and DIPEA (8.4 mL, 48.5 mmol) in dried DCM (80 mL) cooled into an ice-water bath was added DMT-Cl (3.45 g, 10.2 mmol) portion wise. The reaction mixture was warmed to room temperature and stirred for 1 h, followed by adding DCM (65 mL) and methanol (6.5 mL). This mixture was washed with 5 %  $\text{NaHCO}_3$  aqueous solution and brine, dried over  $\text{Na}_2\text{SO}_4$ , and concentrated. The crude product was purified on silica gel column, which was packed with petroleum ether/triethylamine (98:2) and eluted with dichloromethane/petroleum ether (1:3) to give compound **2** as reddish-yellow oil. Yield 48%; IR (thin film)  $\text{cm}^{-1}$  2837 (OMe), 1606, 1581, 1508 (Ar), 1249, 1176, 1035 (C-O-C), 827 (4-OMe);  $^1\text{H}$  NMR ( $\text{CDCl}_3$ , 200 MHz)

$\delta$  1.81-1.35 (m, 8H), 2.41-2.17 (m, 4H), 3.08 (t, 2H,  $J = 5.1$  Hz), 3.63 (t, 2H,  $J = 5.4$  Hz), 3.80 (s, 6H), 4.15-4.00 (m, 8H), 6.87-6.83 (m, 4H), 7.49-7.19 (m, 9H);  $^{13}\text{C}$  NMR ( $\text{CDCl}_3$ , 50 MHz)  $\delta$  27.1, 27.2, 27.8, 29.0, 29.8, 32.4, 55.1, 62.6, 63.0, 68.3, 68.7, 69.2, 69.7, 70.8, 85.5, 90.7, 112.8, 126.4, 127.6, 128.1, 129.9, 136.6, 145.3, 158.2; MS (LC-MS) ( $m/z$ ) Calcd for  $\text{C}_{39}\text{H}_{44}\text{O}_4\text{Fe}$  632.62 [ $\text{M}^+$ ], Found 632.15 [ $\text{M}^+$ ]; Anal. calcd for  $\text{C}_{39}\text{H}_{44}\text{O}_4\text{Fe}$ : C, 74.05; H, 7.01; Found: C, 74.32; H, 7.06.

**1-[4-*O*-Dimethoxytritylbutyl]-1'-[4'-*O*-(2-cyanoethyl-*N,N*-diisopropylphosphoramidyl)butyl]ferrocene **39**<sup>17</sup>**



To a solution of **2** (2.85 g, 4.5 mmol) in dry acetonitrile/DCM (1:1, v:v, 30 mL) under argon was added tetrazole (0.32 g, 4.6 mmol) followed by 2-cyanoethoxy-bis-(*N,N*-diisopropylamino)-phosphane (2.26g, 7.5 mmol). After stirring for 1 h at rt, the reaction was stopped by adding *n*-

butanol (1.5 mL). The solution was diluted with ethyl acetate (450 mL), washed with 5 % aqueous  $\text{NaHCO}_3$  (60 mL) and saturated brine (150 mL), shortly dried with  $\text{Na}_2\text{SO}_4$  (30 minutes) and evaporated in vacuo to oil. The crude product was purified on neutral alumina column, which was packed with petroleum ether/triethylamine (98:2) and eluted with ethylacetate/petroleum ether (1:9) to give compound **3** as reddish-yellow oil. Yield 55%; IR (thin film)  $\text{cm}^{-1}$  2252 ( $\text{C}\equiv\text{N}$ ), 975 ( $\text{P}-\text{O}$ );  $^1\text{H}$  NMR ( $\text{CDCl}_3$ , 200 MHz)  $\delta$  1.18 (s, 6H), 1.22 (s, 6H), 1.62 (bs, 8H), 2.38-2.26 (m, 4H), 2.63 (t, 2H,  $J = 6.6$  Hz), 3.06 (t, 2H,  $J = 5.4$  Hz), 3.77-3.39 (m, 6H), 3.80 (s, 1H), 3.97 (s, 8H), 6.86-6.82 (m, 4H), 7.48-7.21 (m, 9H);  $^{31}\text{P}$  NMR ( $\text{CDCl}_3$ , 200 MHz)  $\delta$  147.7 (s, 1P);  $^{13}\text{C}$  NMR ( $\text{CDCl}_3$ , 50 MHz)  $\delta$  20.3, 24.6, 27.6, 28.0, 29.1, 29.2, 29.9, 31.1, 42.9, 43.0, 55.1, 58.3, 63.1, 63.5, 67.66, 67.72, 68.6, 85.6, 88.8, 89.0, 112.9, 117.6, 126.5, 127.6, 128.1, 130.0, 136.6, 145.4, 158.2; MS (LC-MS) ( $m/z$ ) Calcd for  $\text{C}_{48}\text{H}_{61}\text{N}_2\text{O}_5\text{PFe}$  832.84 [ $\text{M}^+$ ], Found 832.76 [ $\text{M}^+$ ]; Anal. calcd for  $\text{C}_{48}\text{H}_{61}\text{N}_2\text{O}_5\text{PFe}$ : C, 69.22; H, 7.38; N, 3.36 Found: C, 69.54; H, 7.21; N, 3.32.

### Oligomer Synthesis

Base protected standard nucleotide phosphoramidites (A, T, G, C) and nucleoside derivatized controlled pore glass supports were used. The DNA synthesis was carried out on an Applied Biosystems 3900 DNA synthesizer at 40 nmol scale. Dry solvents were used for synthesis. The commercially available amidites (0.1 M) were dissolved in dry acetonitrile while 0.15 M solution was prepared for ferrocenyl-phosphoramidite **39** and 4Å molecular sieves were added to it to remove traces of moisture. The solid phase synthesis protocol is summarized in Figure 3.3. The oligomers were cleaved from the support by treatment with concentrated aqueous NH<sub>3</sub> for 8 h. The cleaved oligomers were subjected to initial gel filtration and then purified by RP-HPLC.

### HPLC Analysis

To check the purity of oligonucleotides, RP-HPLC (Hewlett Packard) C18 column was used. A gradient elution method with A to B in 20 min. was used, where buffer A was 5% acetonitrile in 0.05 M TEAA (triethylammonium acetate) and buffer B was 30% acetonitrile in 0.05 M TEAA with a flow rate of 1.5 mL/min. The HP 1050 multiwavelength UV detector was used which was set at a wavelength of 254 nm.

### MALDI-TOF mass spectrometry

Mass spectral analysis was performed on a Voyager-De-STR (Applied Biosystems) MALDI-TOF. A nitrogen laser (337 nm) was used for desorption and ionization. Spectra were acquired in a linear mode. The matrixes used for analysis were THAP (2,4,6-trihydroxyacetophenone). Diammonium citrate was used as an additive. The samples were prepared by mixing 10 µL of matrix (0.5 M solution), 5 µL of diammonium citrate (0.1 M) and 1 µL oligonucleotides (OD 5-10/mL or 150-300 µg/mL) and spotted 1 µL on a stainless plate for analysis.

### UV-*T<sub>m</sub>* studies

The hybridization studies of ferrocenyl-modified oligonucleotides with complementary DNA sequences were done by temperature dependent UV-absorbance experiments. The concentration was calculated on the basis of absorbance from the molar extinction coefficients of the corresponding nucleobases (i.e., T, 8.8 cm<sup>2</sup>/µmol; C, 7.3

cm<sup>2</sup>/μmol; G, 11.7 cm<sup>2</sup>/μmol; and A, 15.4 cm<sup>2</sup>/μmol). The complexes were prepared in 10 mM sodium phosphate buffer, pH 7.4 containing NaCl (10 mM) and were annealed by keeping the samples at 85 °C for 5 minutes followed by slow cooling to room temperature (annealing). Absorbance versus temperature profiles were obtained by monitoring at 260 nm with Perkin-Elmer *Lambda 35 UV-VIS* spectrophotometer scanning from 5 to 85 °C at a ramp rate of 0.2 °C per minute. The data were processed using Origin 6.1 and  $T_m$  values derived from the derivative curves.

#### **Buffer for UV- $T_m$ studies**

##### ***Phosphate buffer (pH = 7.4, 10 mmol NaCl) (100 mL)***

Na<sub>2</sub>HPO<sub>4</sub> (110 mg), NaH<sub>2</sub>PO<sub>4</sub>·2H<sub>2</sub>O (35.3 mg), NaCl (58.5 mg) was dissolved in minimum quantity of water and the total volume was made 100 mL. The pH of the solution was adjusted 7.4 with concentrated NaOH solution (in DI water).

##### ***Phosphate buffer (pH = 7.4, 100 mmol NaCl) (100 mL)***

Na<sub>2</sub>HPO<sub>4</sub> (110 mg), NaH<sub>2</sub>PO<sub>4</sub>·2H<sub>2</sub>O (35.3 mg), NaCl (585.0 mg) was dissolved in minimum quantity of water and the total volume was made 100 mL. The pH of the solution was adjusted 7.4 with concentrated NaOH solution (in DI water).

#### **Electrophoretic Gel shift assay**

Electrophoretic gel mobility assay was used for the hybridization studies of different ferrocenyl-modified oligonucleotide to the complementary oligonucleotide (DNA). Ferrocenyl-modified oligonucleotides were individually mixed with complementary DNA in 1:1 ratio (each strand 0.4 mM) in water. The samples were lyophilized to dryness and re-suspended in sodium phosphate buffer (10 mM, pH 7.4, 4 μl) containing NaCl (10 mM). The samples were annealed by heating to 85 °C for 5 min followed by slow cooling to RT and refrigeration at 4 °C overnight. To this, 4 μl of 40 % sucrose in 5xTBE buffer (pH 8.0) was added and sample was loaded on the gel. Bromophenol blue (BPB) was used as the tracer dye and separately loaded in an adjacent well. Gel electrophoresis was performed on 20 % nondenaturing polyacrylamide gel (acrylamide:*N,N'*-methylenebisacrylamide, 29:1) at constant power supply of 200 V and 10 mA, until the BPB migrated to three-fourth of the gel length. During electrophoresis

the temperature was maintained at 10 °C. The spots were visualized through UV shadowing by illumination the gel placed on a fluorescent silica gel plate, GF<sub>254</sub> using UV-light.

### **Buffer and solutions for gel electrophoresis**

#### ***Acrylamide:bisacrylamide (29:1) (100 mL)***

The mixture of acrylamide (29.0 g) and *N,N'*-methylenebisacrylamide (1.0 g) was dissolved in minimum amount of DI water (15-20 mL) and the total volume was made 100 mL with DI water.

#### ***Ammonium persulfate (10 % w/v)***

Ammonium persulfate was used as a catalyst for the copolymerization of acrylamide and bisacrylamide gels. The polymerization reaction was driven by free radicals that were generated by an oxido-reduction reaction in which a diamine (e.g., TMEDA) was used as the adjunct catalyst.

#### ***5x TBE electrophoresis buffer (500 mL)***

The mixture of tris(hydroxymethyl)amino methane (tris-base) (27.0 g), boric acid (H<sub>3</sub>BO<sub>3</sub>) (13.75 g) and EDTA (1.4625 g) was dissolved in minimum quantity of water and the total volume was made 500 mL. Polyacrylamide gels were run in 1x TBE to prevent denaturation of small fragments of DNA by Joulic heating. 1x TBE buffer was used to ensure that adequate buffering capacity is available throughout the run. To make 1x TBE, take 5x TBE (100 mL) and dilute it upto 500 mL with DI water.

#### ***Casting the nondenaturing polyacrylamide gels (10 mL)***

Acrylamide:bisacrylamide (29:1) (6.66 mL), DI water (1.27 mL), 5x TBE (2.0 mL) was mixed and degassed it by applying vacuum under stirring. Then ammonium persulfate solution (10 %) (70 µL) and TMEDA (4.6 µL) was added. It was shaken properly and immediately poured in between two gel glass plates. It was kept for 5 to 15 minutes when the vinyl polymerization of monomer to cross-linked polymer was complete and it formed a gel.



### Casting the denaturing polyacrylamide gels (10 mL)

Acrylamide:bisacrylamide (29:1) (6.66 mL), urea (4.2 g, 7.0 M), 5x TBE (500  $\mu$ L) was mixed and degassed it by applying vacuum under stirring. Then ammonium persulfate solution (10 %) (70  $\mu$ L) and TMEDA (4.6  $\mu$ L) was added. It was shaken properly and immediately poured in between two gel glass plates. It was kept for 5 to 15 minutes when the vinyl polymerization of monomer to cross-linked polymer was complete and it formed a gel.

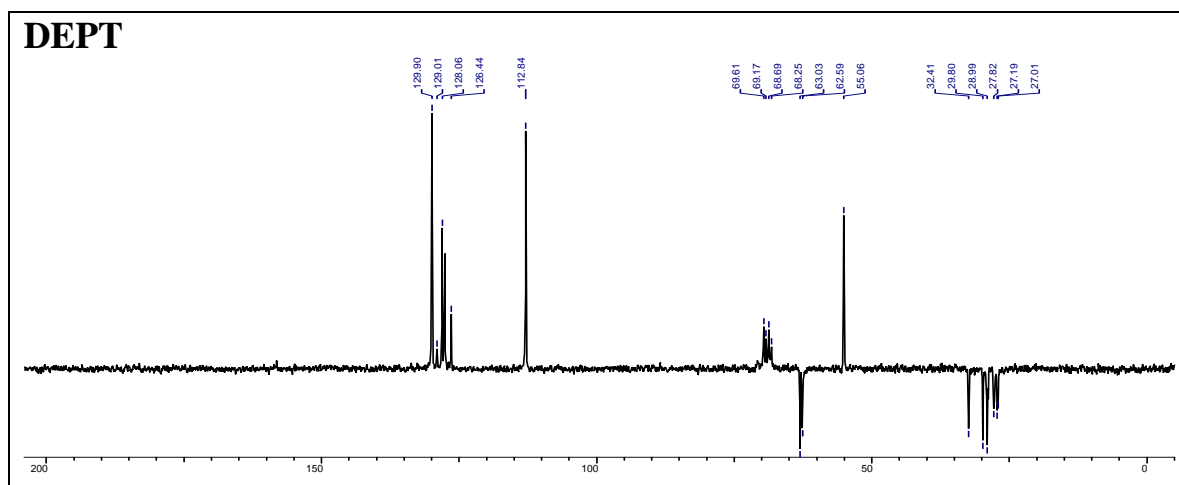
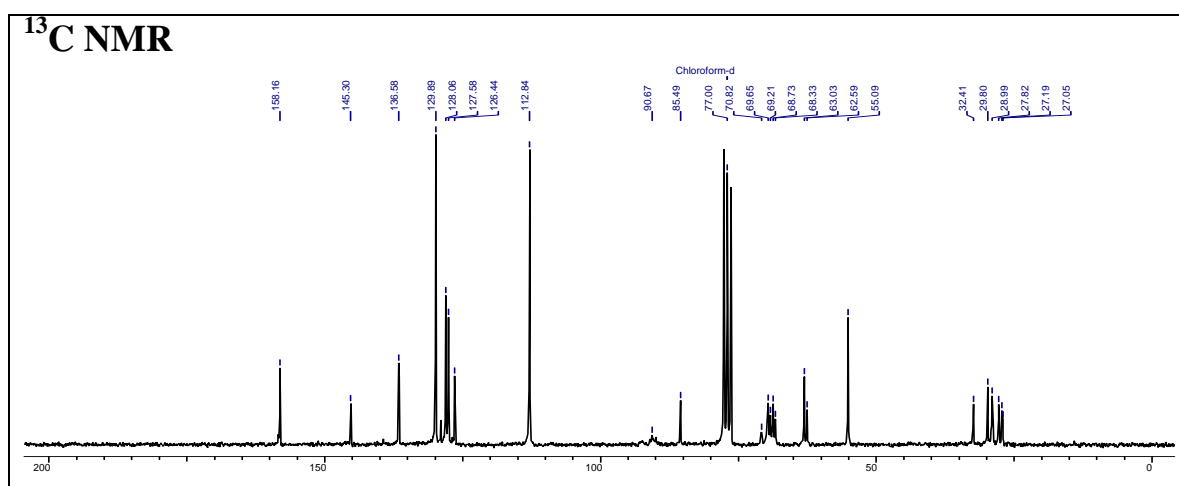
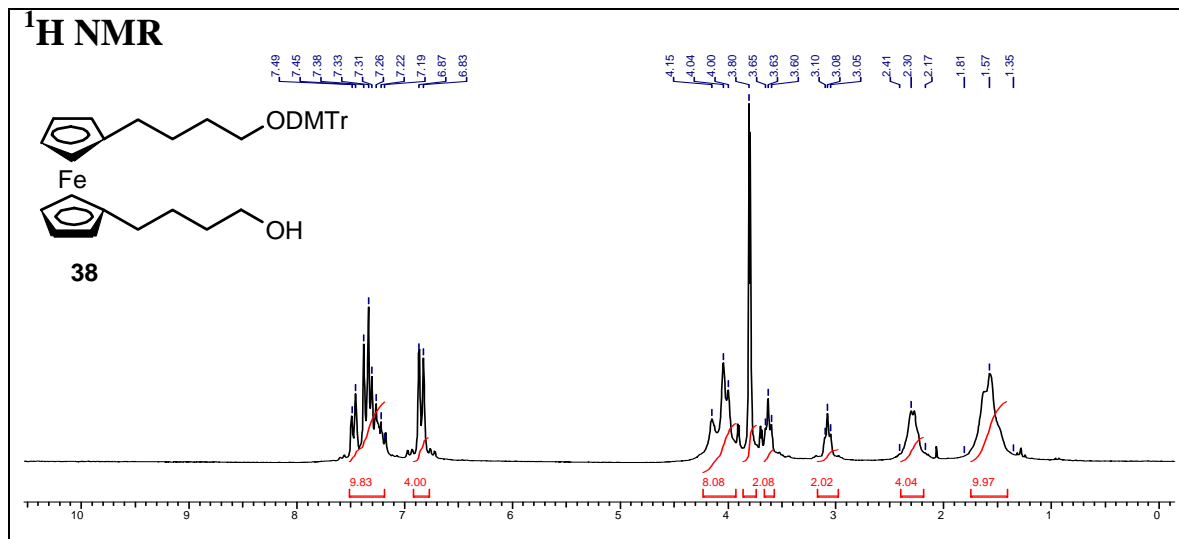
### 3.9 References

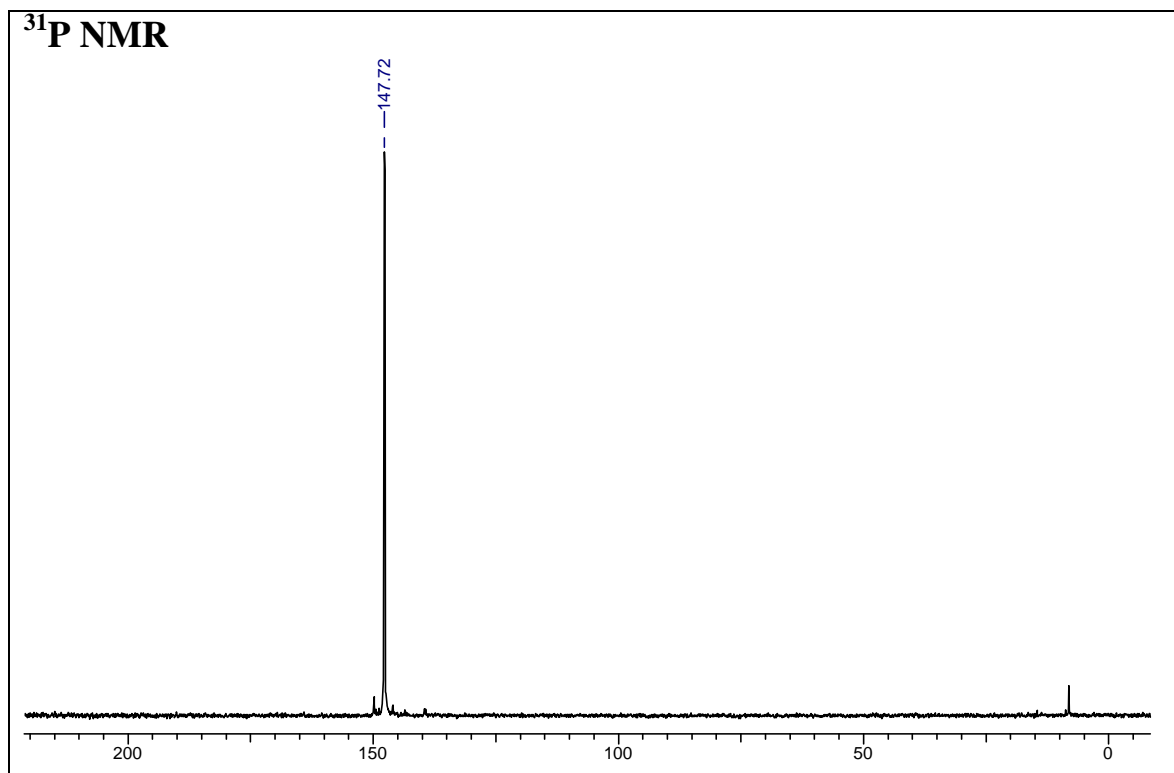
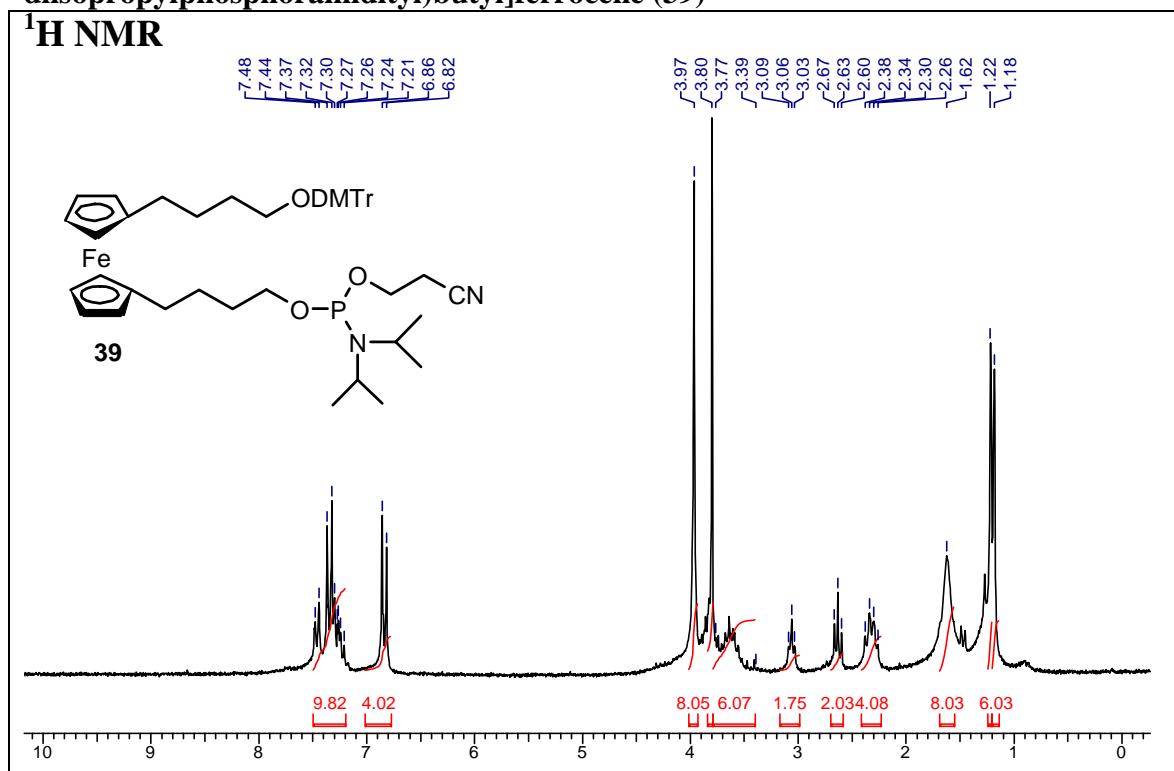
1. Navarro, A-E.; Spinelli, N.; Chaix, C.; Moustrou, C.; Mandrand, B.; Brisset, H. *Nucleic Acids Res.* **2004**, *32*, 5310-5319.
2. Abel, A. P.; Weller, M.G.; Duveneck, G. L.; Ehrat, M.; Widmer, H. M. *Anal. Chem.* **1996**, *68*, 2905–2912.
3. Fawcett, N. C.; Evans, J. A.; Chien, L. C.; Flowers, N. *Anal. Lett.* **1988**, *21*, 1099–1114.
4. Mikkelsen, S. R. *Electroanalysis* **1996**, *8*, 15-19.
5. Rack, J. J.; Krider, E. S.; Meade, T. J. *J. Am. Chem. Soc.* **2000**, *122*, 6287 – 6288.
6. Holmlin, R. E.; Yao, J. A.; Barton, J. K. *Inorg. Chem.* **1999**, *38*, 174-189.
7. Mucic, R. C.; Herrlein, M. K.; Mirkin, C. A.; Letsinger, R. L. *Chem. Commun.* **1996**, 555-557.
8. Deeming, A. J. In *Comprehensive Organometallic Chemistry Vol.4*; Wilkinson, G., Stone, F. G. A. (eds.) Pergamon Press: Oxford, **1982**; pp 475.
9. Kibbe, W. A. *Nucleic Acids Res.* **2007**, *35*, W43–W46.
10. (a) Ihara, T.; Maruo, Y.; Takenaka, S.; Takagi, M. *Nucleic Acids Res.* **1996**, *24*, 4273-4281. (b) Ihara, T.; Nakayama, M.; Murata, M.; Nakano, K. Maeda, M. *Chem. Commun.* **1997**, 1609-1610. (c) Nakayama, M.; Ihara, T.; Nakano, K.; Maeda, M. *Talanta*, **2002**, *56*, 857-866.
11. Yu, C. J.; Wang, H.; Wan, Y.; Yowanto, H.; Kim, J. C.; Donilon, L. H.; Tao, C.; Strong, M.; Chong, Y. *J. Org. Chem.* **2001**, *66*, 2937-2942.

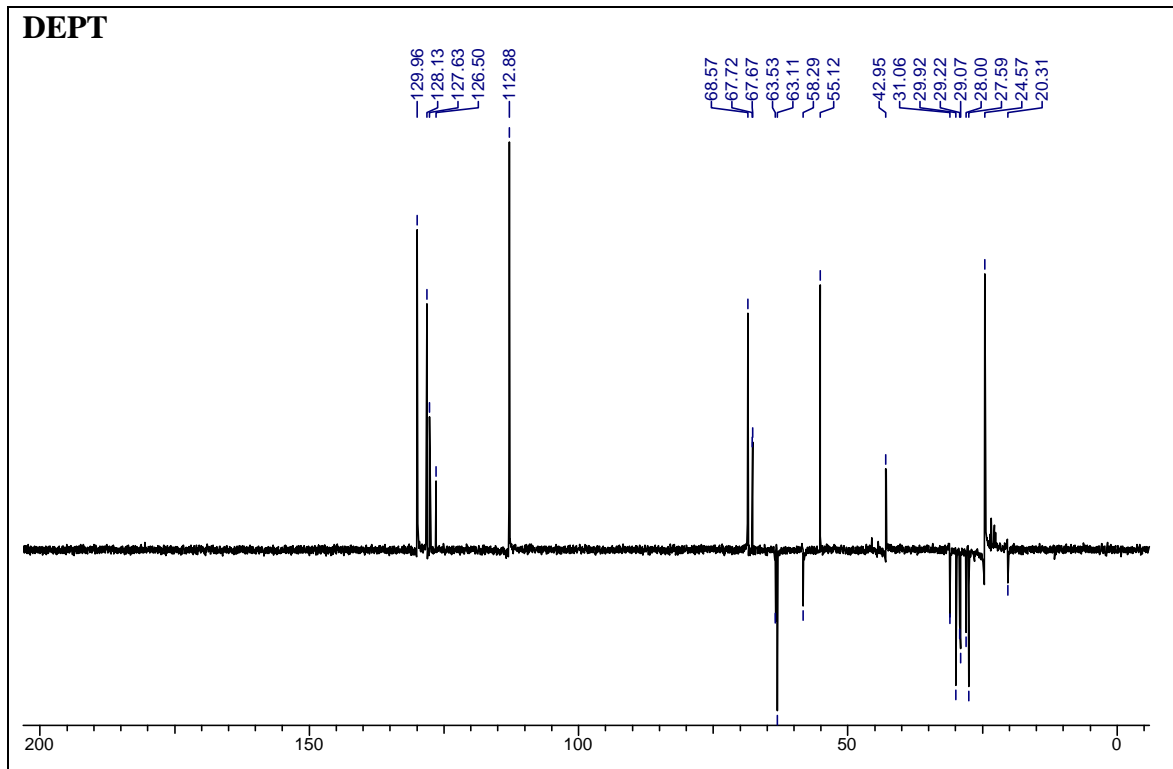
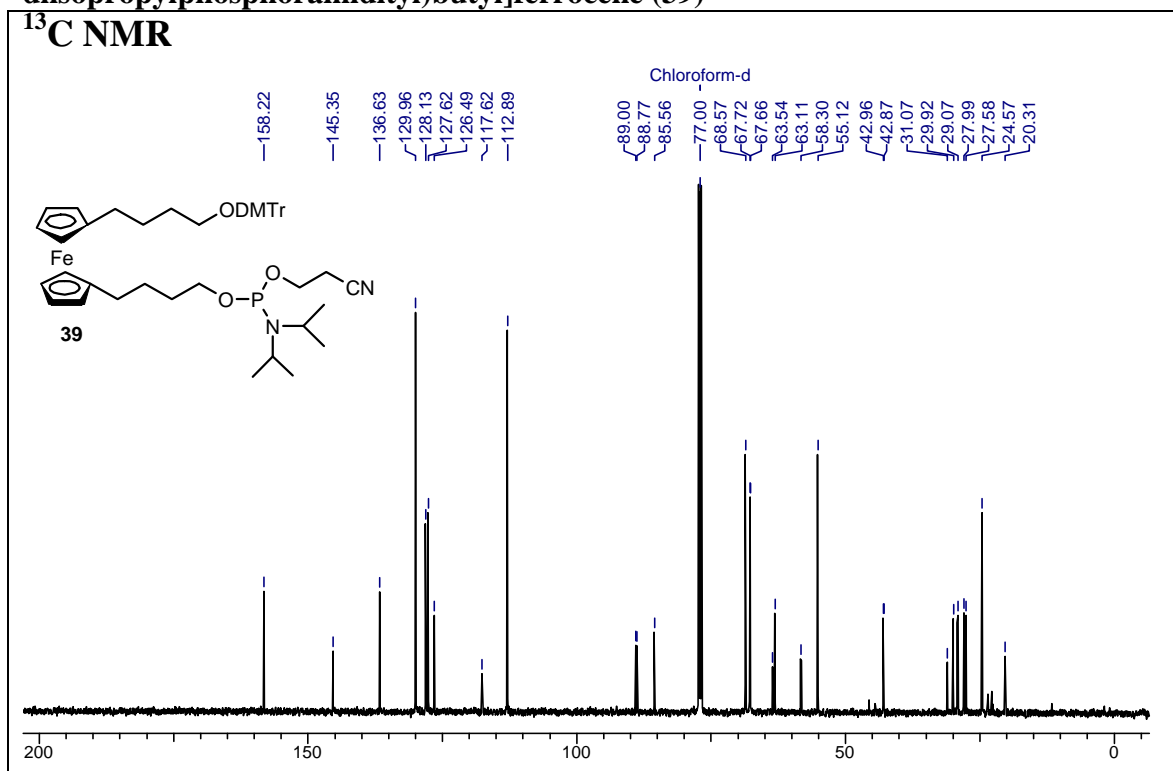
12. Umek, R. M.; Lin, S. W.; Vielmetter, J.; Terbrueggen, R. H.; Irvine, B.; Yu, C. J.; Kayyem, J. F. Yowanto, K.; Blackburn, G. F.; Farkas, D. H.; Chen, Y.-P. *J. Mol. Diagn.* **2001**, *3*, 74-84.
13. (a) Kim, K.; Yang, H.; Park, S. H.; Lee, D-S.; Kim, S-J.; Taik Lim, Y.; Tae Kim, Y. *Chem. Commun.* **2004**, *13*, 1466-1467 (b) Khan, S. I.; Grinstaff, M. W. *J. Am. Chem. Soc.* **1999**, *121*, 4704-4705.
14. Belstein, A. E.; Grinstaff, M. W. *Chem. Commun.* **2000**, 509-510.
15. Takenaka, S.; Uto, Y.; Kondo, H.; Ihara, T.; Takagi, M. *Anal. Biochem.* **1994**, *218*, 436-43.
16. Yu, C. J.; Wan, Y.; Yowanto, H.; Li, J.; Tao, C.; James, M. D.; Tan, C. L.; Blackburn, G. F.; Meade, T. J. *J. Am. Chem. Soc.* **2001**, *123*, 11155-11161.
17. Mag, M.; Lüking, S.; Engels, J. W. *Nucleic Acids Res.* **1991**, *19*, 1437-1441.
18. (a) Gait, J. M. *Oligonucleotide synthesis: A practical approach*; IRL Press: Oxford, UK 217, **1984**. (b) Agrawal, S: In *Protocols for oligonucleotides and analogs: Synthesis and properties; Methods in Molecular Biology Vol. 20*; Agrawal, S. (ed.) Totowa, NJ. Humana Press, Inc., **1993**.

**3.10 Appendix**

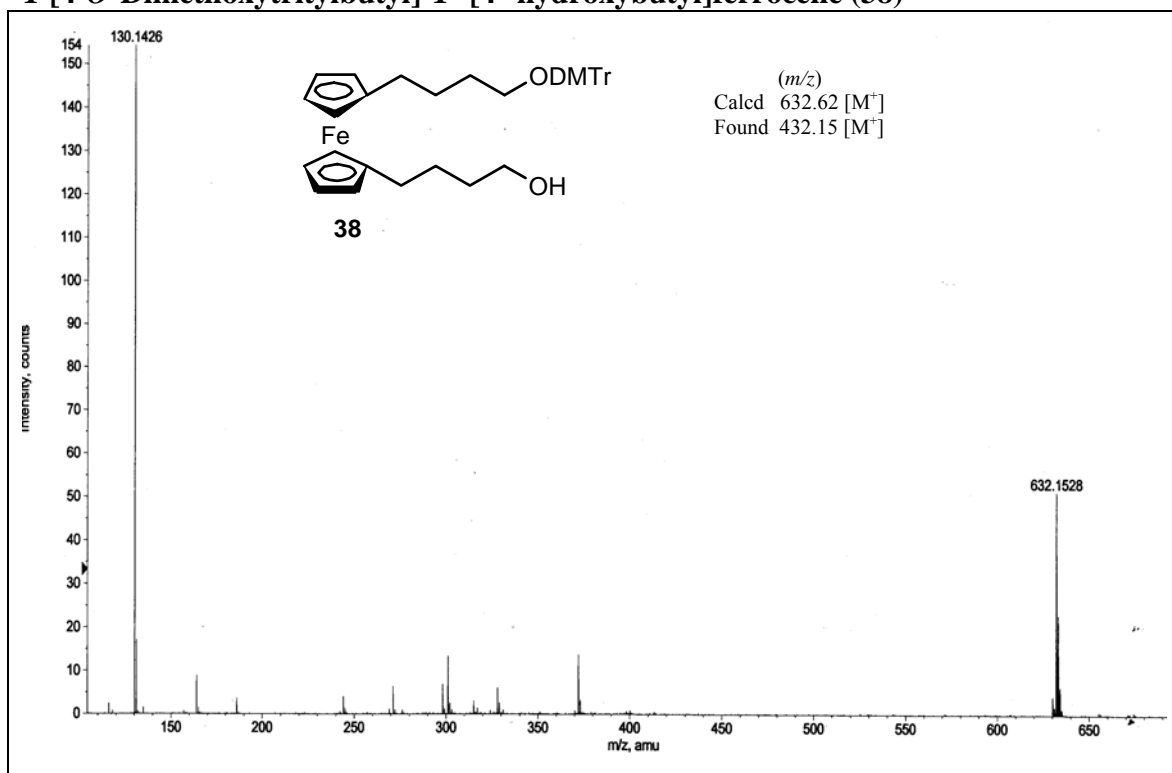
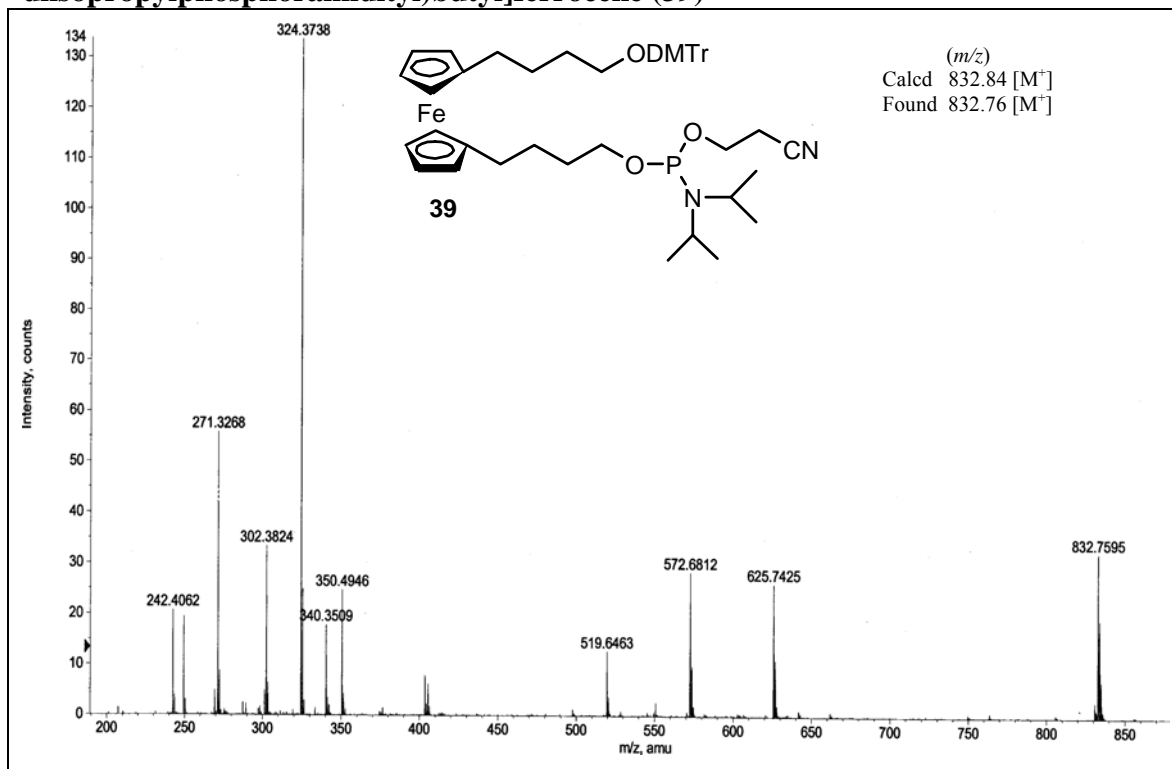
<b>Sr. No.</b>	<b>Details</b>	<b>Page No.</b>
01	$^1\text{H}$ , $^{13}\text{C}$ and DEPT NMR photocopy of compound <b>38</b>	194
02	$^1\text{H}$ and $^{31}\text{P}$ NMR photocopy of compound <b>39</b>	195
03	$^{13}\text{C}$ and DEPT NMR photocopy of compound <b>39</b>	196
04	Mass spectra of <b>38</b> , <b>39</b>	197
05	HPLC profiles of <b>ODN-1</b> , <b>ODN-2</b>	198
06	HPLC profiles of <b>FcODN-1</b> , <b>FcODN-2</b>	199
07	HPLC profiles of <b>FcODN-3</b>	200
08	MALDI-TOF spectra of <b>ODN-1</b> , <b>ODN-2</b>	201
09	MALDI-TOF spectra of <b>FcODN-1</b> , <b>FcODN-2</b>	202
10	MALDI-TOF spectra of <b>FcODN-3</b>	203

$^1\text{H}$ ,  $^{31}\text{P}$ ,  $^{13}\text{C}$ , DEPT NMR Spectra1-[4-*O*-Dimethoxytritylbutyl]-1'-[4'-hydroxybutyl]ferrocene (**38**)

**1-[4-*O*-Dimethoxytritylbutyl]-1'-[4'-*O*-(2-cyanoethyl-*N,N*-diisopropylphosphoramidite)butyl]ferrocene (39)**

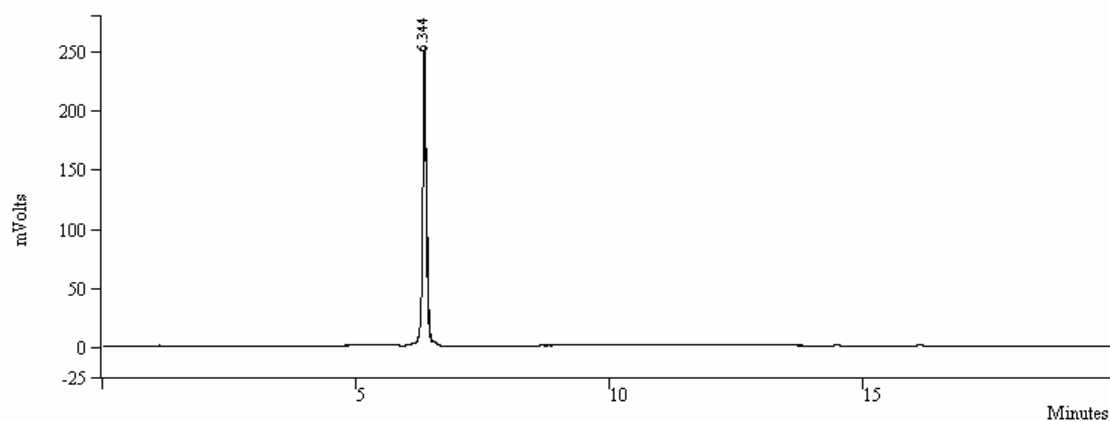
**1-[4-*O*-Dimethoxytritylbutyl]-1'-[4'-*O*-(2-cyanoethyl-*N,N*-diisopropylphosphoramidyl)butyl]ferrocene (39)**

## Mass spectra

1-[4-*O*-Dimethoxytritylbutyl]-1'-[4'-hydroxybutyl]ferrocene (38)1-[4-*O*-Dimethoxytritylbutyl]-1'-[4'-*O*-(2-cyanoethyl-*N,N*-diisopropylphosphoramidyl)butyl]ferrocene (39)

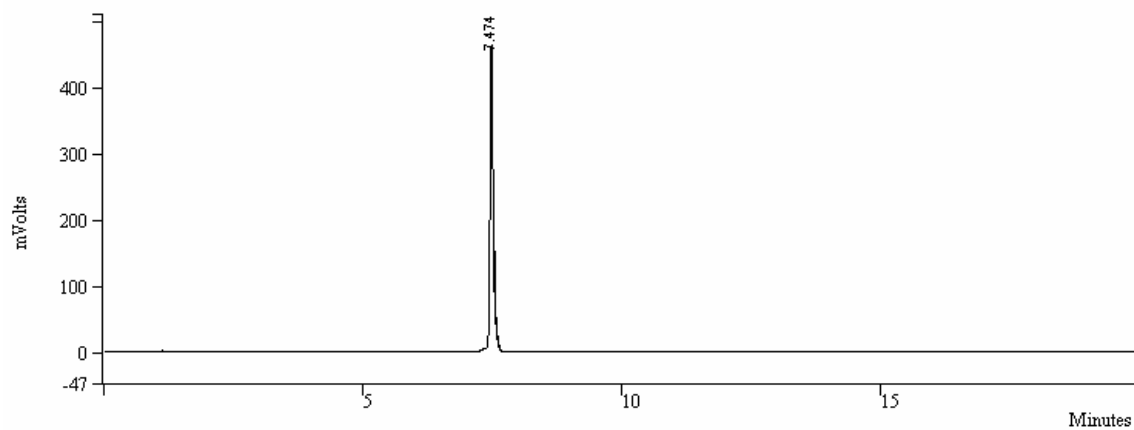
## HPLC Profiles

## ODN-1 [5'-AGA AAA GGA-3']



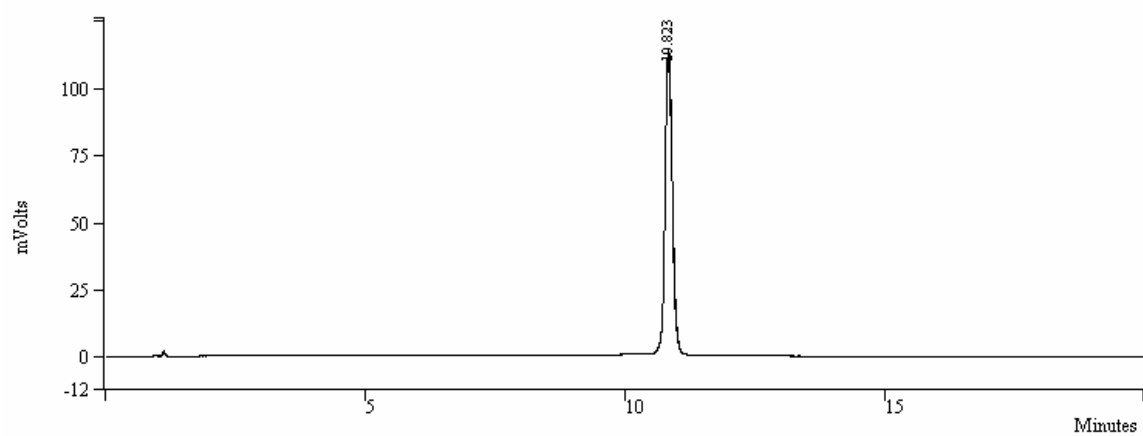
Peak No	Ret. Time (min)	Width 1/2 (sec)	Peak Area (counts)	Result (%)
1	6.344	4.3	1262383	100.0000
			<b>1262383</b>	<b>100.0000</b>

## ODN-2[5'-TCC TTT TCT-3']

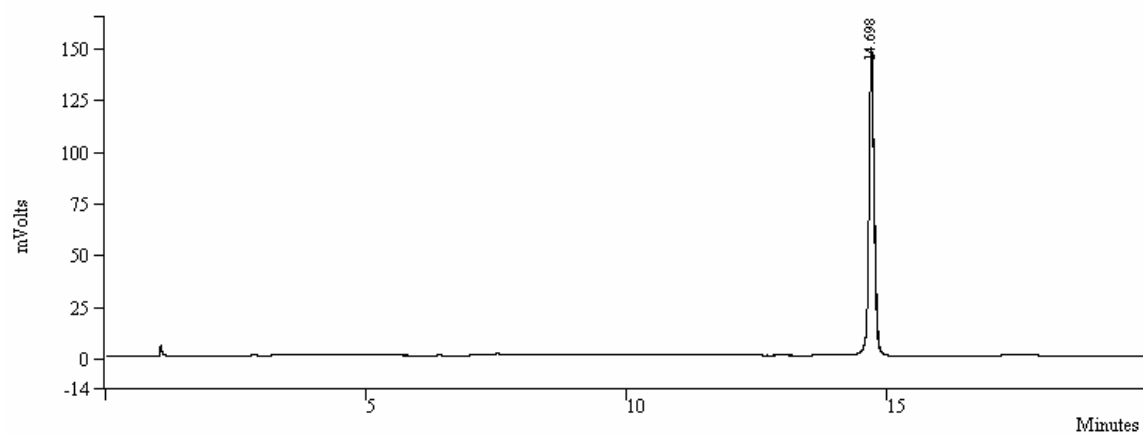


Peak No	Ret. Time (min)	Width 1/2 (sec)	Peak Area (counts)	Result (%)
1	7.474	3.8	2042890	100.0000
			<b>2042890</b>	<b>100.0000</b>

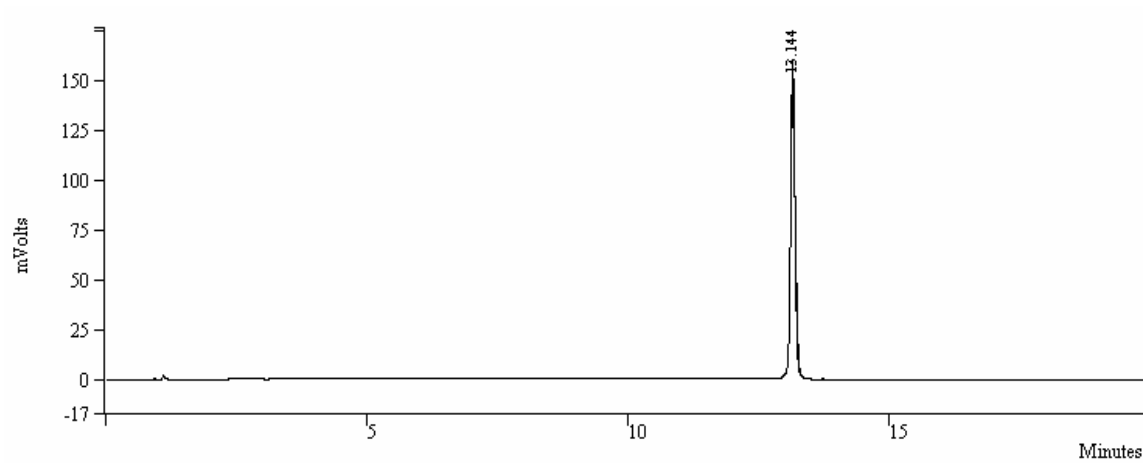


**FcODN-1 [5'-AGA AAA GGA--Fc--TCC TTT TCT-3']**

Peak No	Ret. Time (min)	Width 1/2 (sec)	Peak Area (counts)	Result (%)
1	10.823	8.8	1104590	100.0000
			<b>1104590</b>	<b>100.0000</b>

**FcODN-2 [5'-Fc-AGA AAA GGA-3']**

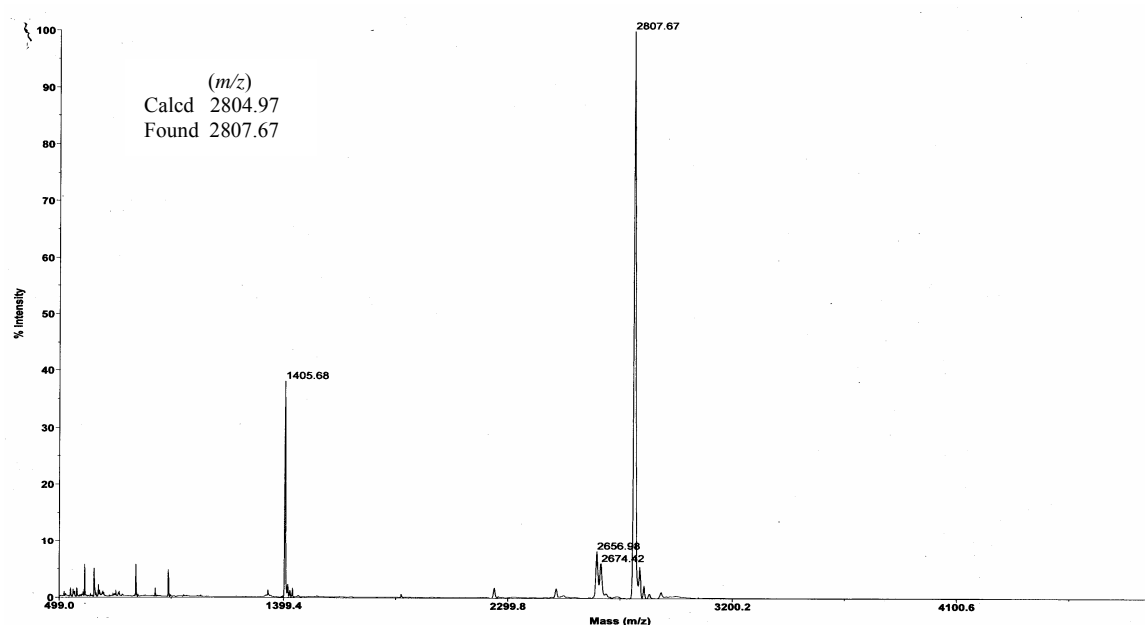
Peak No	Ret. Time (min)	Width 1/2 (sec)	Peak Area (counts)	Result (%)
1	14.698	6.2	1037908	100.0000
			<b>1037908</b>	<b>100.0000</b>

**FcODN-3 [5'-TCC TTT TCT-Fc-T-3']**

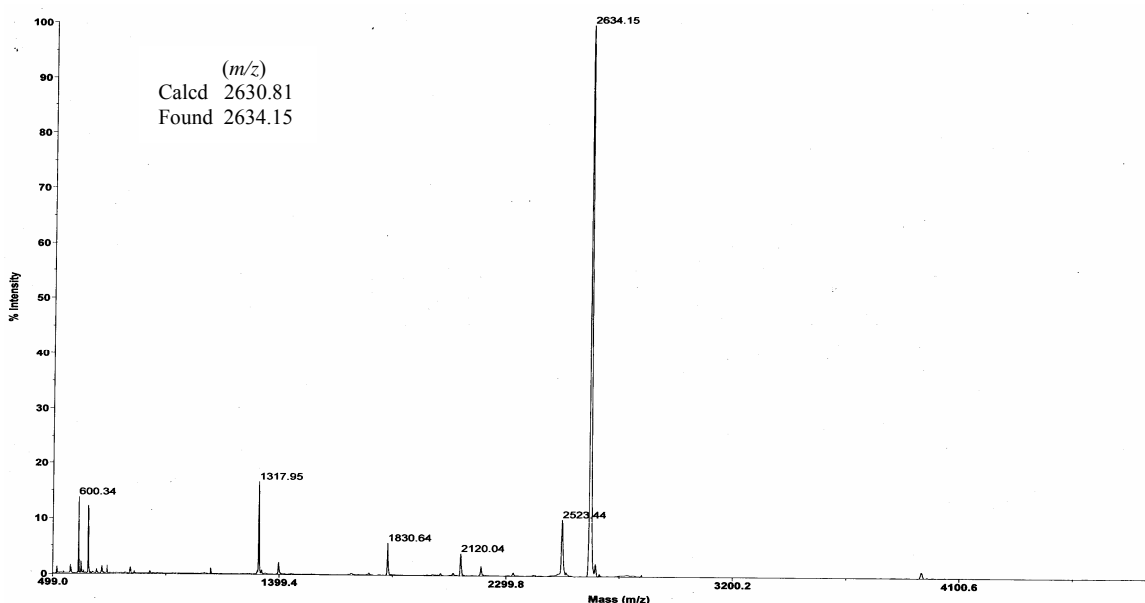
Peak No	Ret. Time (min)	Width 1/2 (sec)	Peak Area (counts)	Result (%)
1	13.144	5.4	953648	100.0000
			<b>953648</b>	<b>100.0000</b>

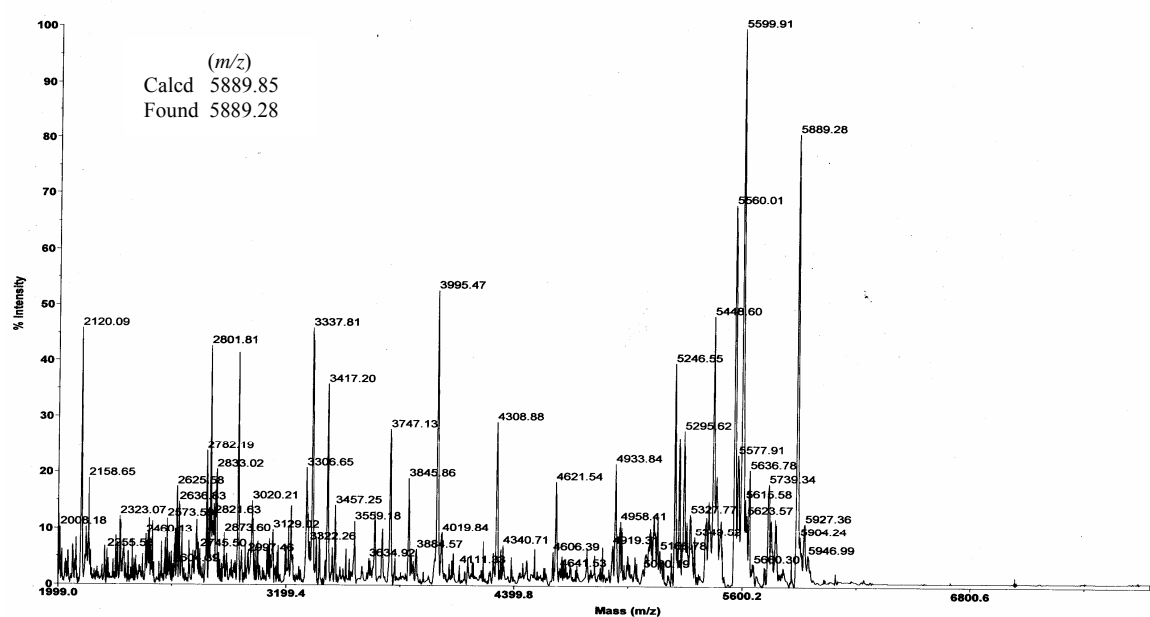
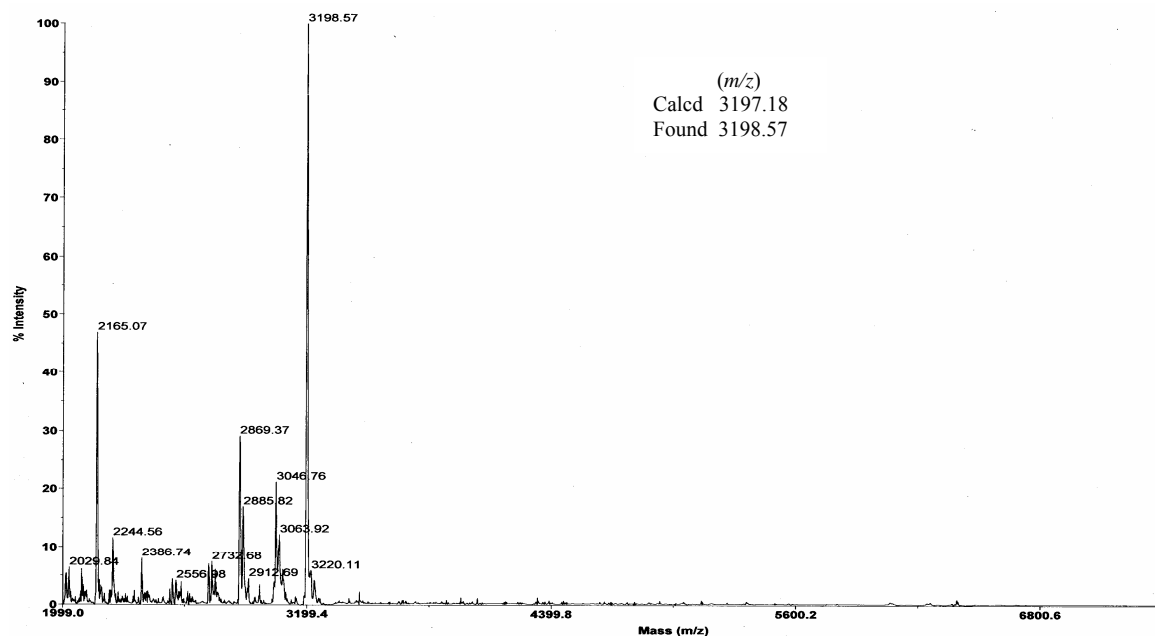
## MALDI-TOF Spectra

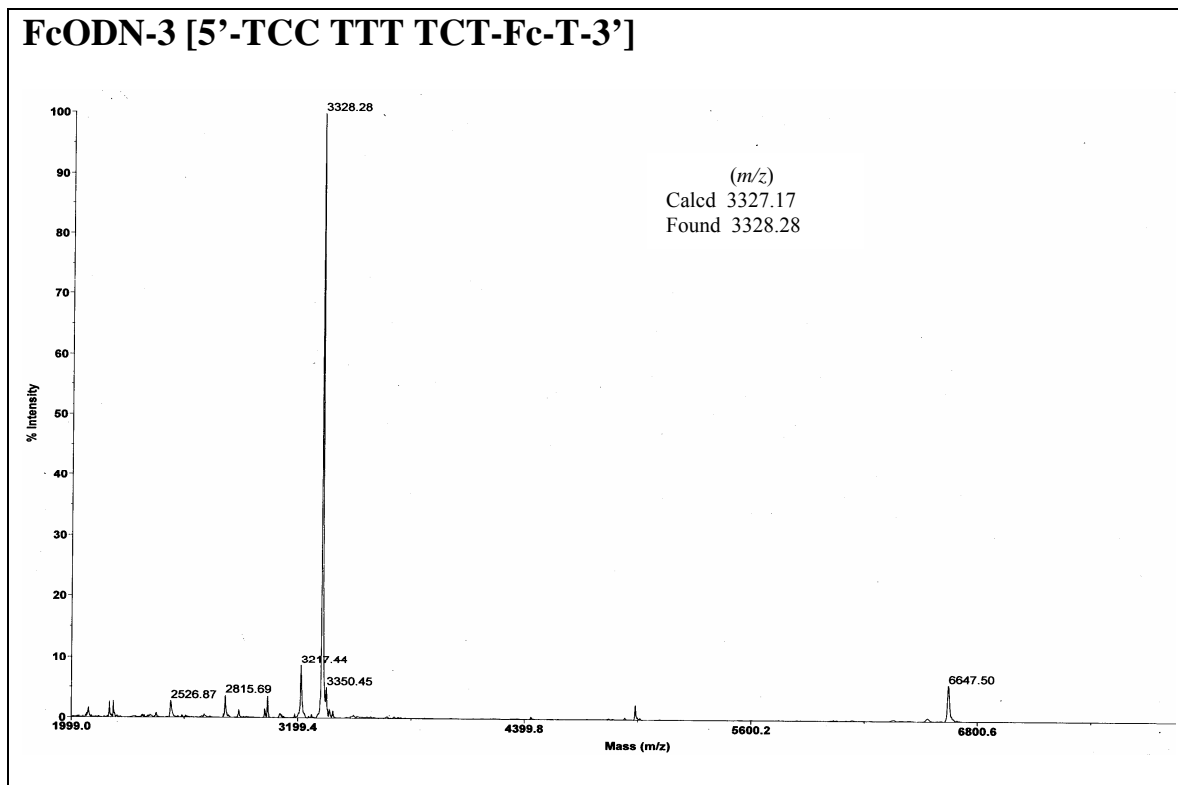
## ODN-1 [5'-AGA AAA GGA-3']



## ODN-2 [5'-TCC TTT TCT-3']



**FcODN-1 [5'-AGA AAA GGA--Fc--TCC TTT TCT-3']****FcODN-2 [5'-Fc-AGA AAA GGA-3']**



## **CHAPTER 4**

# **FERROCENE-NUCLEOBASE AND FERROCENE-OLIGONUCLEOTIDE CONJUGATES: ELECTROCHEMICAL INVESTIGATION**

## 4.1 Introduction

Previous chapters describe synthesis, structural properties of ferrocene-nucleobase conjugates and biophysical properties ferrocene-oligonucleotide conjugates. This chapter describes the results of electrochemical studies on these ferrocene conjugates.

### 4.1.1 Bioelectrochemistry: DNA and nucleobase electrochemistry trends

In a double-stranded DNA molecule, the nucleobase pairs are stacked on one another that there is an inter-base hybridization of  $\pi_z$  orbitals lying in a plane perpendicular to the plane of base-pair stacking, which has been suggested to be responsible for its conducting properties.<sup>1</sup> The highly specific binding between nucleobases of two single strands of DNA, its related self-assembly properties, and the ability to synthesize DNA in whatever desired sequence have made it a suitable candidate for the development of DNA-based molecular electronics.<sup>2</sup> Electrochemists are exploring the efficiency of DNA for application in electrochemical gene sensors to accomplish sequence specific detection of target DNA.<sup>3</sup> Sequence-specific detection of target DNA molecule is required for application like diagnosis of genetically inherited diseases, detecting bacterial or viral DNA or RNA in the environment and forensic investigations.

Over the past 20 years, many important technological advances have been made that provided us with the tools needed to develop new techniques to monitor biorecognition and interaction events on solid devices and in solution. Biosensing offers unprecedented opportunities for genetic screening and detection coupled with the ability to fabricate features on solid substrates with nanoscale precision. The inherent charge distribution associated with the sequence recognition of DNA strand for the biological functions has opened up new horizons in the field of bioelectrochemistry.

All molecular-based biosensors rely on highly specific recognition events to detect their target analytes. The essential role of the sensor is to provide a suitable platform that facilitates formation of the probe-target complex in such a way that the binding event triggers a usable signal for electronic readout. Molecular recognition layer and a signal transducer are the minimal elements of any biosensor that can be coupled to an appropriate readout device. How recognition event is reported depends ultimately on

the method of signal transduction, whether it be optical,<sup>4</sup> mechanical<sup>5</sup> or electrochemical.<sup>6</sup>

Optical biosensors based on fluorescence are extraordinarily sensitive, with detection limits approaching  $\sim 10^7$  molecules/cm<sup>2</sup>, and arrays containing thousands of unique probe sequences have been constructed.<sup>7</sup> Moreover, for such technology, instrument required is sophisticated and expensive. Besides the cost and sophistication of the instrumentation, the inconsistent yields of target synthesis and labeling, as well as nonuniform rates of fluorophore photobleaching can result in readout accuracies lower than what is required.<sup>8</sup> Another optical technique is surface plasmon resonance (SPR) which reports changes in the refractive index of a thin metal film substrate that occur upon adsorption of the analyte and is suitable for target detection in an array-based format.<sup>9</sup> It is usually necessary to amplify the hybridization signal to achieve detection limits sufficient for a diagnostically useful signal. Both, fluorescence-based techniques and SPR systems are costly, making them generally more suitable for research applications only.

An alternative readout strategy is to monitor mass changes in the immobilized recognition layer that occur upon target binding, most frequently using a quartz crystal microbalance (QCM).<sup>10</sup> Though these devices are sensitive and can provide real-time monitoring of hybridization events, reliable operation of the QCM in aqueous solution has been a technical challenge. New amplification strategies may overcome this limitation.<sup>11</sup> Change in mass can also be measured using microfabricated cantilevers.<sup>12</sup> Here, the increase in mass that accompanies hybridization is detected by the deflection of a laser beam reflected from the cantilever surface. The primary limitations of microcantilever techniques again are the expensive instrumentation and the technical difficulties involved with fabricating the cantilever features.

**Electrochemical methods** are well suited for DNA diagnostics. Electrochemical detection offers an alternative means of detection due to their high sensitivity and the simplicity of the detection apparatus. There is no need for expensive signal transduction equipment because electrochemical reactions give an electronic signal directly. Moreover, because immobilized probe sequences can be readily confined to a variety of electrode substrates, detection can be accomplished with an inexpensive electrochemical analyzer. Compared to fluorescence spectroscopy, electrochemical detection is more



robust and less prone to errors. Therefore, electrochemical methods have received particular attention in the development of inexpensive and compact devices. In fact, portable systems for clinical testing and on-site environmental monitoring are now being developed.<sup>13</sup>

#### 4.1.2 Redox labeling approach for direct electrochemistry of DNA

Developing electrochemical sensors for efficient detection of DNA hybridization, gene damage detection and fast, toxicity screening assays has recently emerged as an active area.<sup>14</sup> This is due to the attractive features of electrochemical techniques which enable direct electronic read-out of the biosensing events with high sensitivity and its versatility toward miniaturization for achieving of 'lab-on-a-chip' technology. Several protocols have been developed for electrochemical DNA detection assays like, direct label-free DNA detection,<sup>15</sup> intercalation of dye molecules<sup>16</sup> and metallocene conjugates of DNA duplexes etc. Among the various protocols, labeling DNA molecules with conjugate redox labels like metallocenes and quinones<sup>17</sup> is very attractive owing to the stability of the conjugates, sensitivity for high-throughput assays and reliability of the devices.

Such approach relies on mutual electronic interactions of two parts of a molecular system where an incorporated redox probe is able to reflect electronic changes that occur in the other part of the molecule by its changed electrochemical response. With ferrocene as a redox probe, this approach is proven to be effective because of its extraordinary sensitivity of the redox state to chemical and biological interactions in conjugated biomolecules and vice versa. Since the discovery of ferrocene in 1951, many of its derivatives are of considerable interest in various areas of research and applications, like asymmetric catalysis,<sup>18</sup> electrochemistry,<sup>19</sup> functional biomaterials<sup>20</sup> and even for medical purposes. A large variety of attractive analytical applications of ferrocene and its derivatives have been reported as well.

For example, Abbott *et al.*<sup>21</sup> have recently exploited this sensitivity to achieve controlled gene transfection across mammalian cell membranes. Particularly interesting are the reports on ferrocene tethered nucleotide, FcdUTP by King *et al.*<sup>17e</sup> wherein the efficiency of the reporter groups in the electrochemical transduction of the hybridization events has been demonstrated. King *et al.* have also demonstrated the application of

FcdUTP for real time detection of proteins on circular aptamers<sup>17f</sup> and FcUTP for RNA-detection,<sup>17g</sup> while Willner *et al.*<sup>17h</sup> and co-workers have employed redox active nucleic-acid replica for amplified detection of viral DNA.

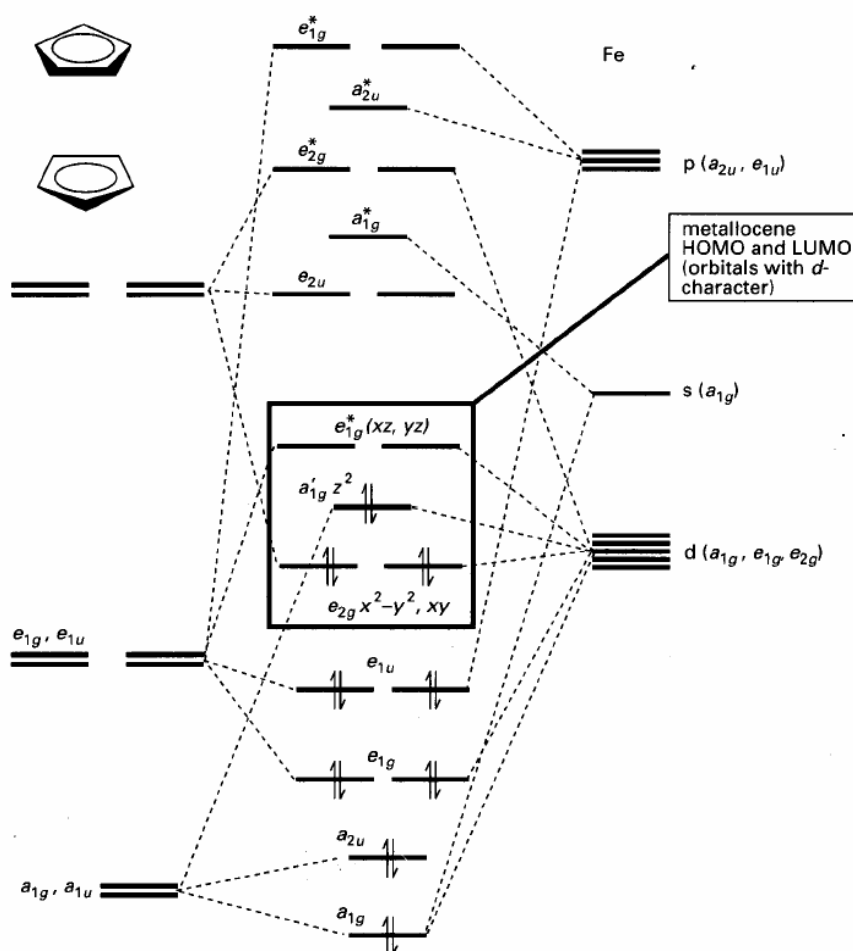
### 4.1.3 Why ferrocene?

Ferrocene-based derivatization has raised considerable interest in many fields of analytical chemistry. **Why ferrocene (Fc) is extensively used as a standard redox probe in electrochemistry?** The chemistry of ferrocenes is well explored and a large variety of ferrocene derivatives is easily accessible *via* established synthetic routes. Ferrocene and its derivatives mostly are neutral compounds and, unlike many other organometallics, are stable in the presence of water and air. An ideal electrochemical standard should not interact with other species in solution and ferrocene adequately fills this criteria. It shows reversible electrochemistry characterized with cyclic voltammetry peak separations,  $(\Delta E_p) = 59$  mV, corresponding to one electron redox process. A unique property of metallocenes is the possibility of introducing substituents on one or both of the cyclopentadienyl (Cp) rings while holding the properties of a simple one-electron redox couple. The redox behavior of ferrocene is sensitive to its covalent or noncovalent binding to other molecules.

The Fc/Fc<sup>+</sup> couple shows solvent-independent redox potentials. This is due to the fact that the activity of a univalent, large, symmetrical ion, with the charge deeply buried is the same as that of an uncharged molecule of the same size and structure in all solvents. The most fundamental reason behind these experimental observations could be understood from the electron structure of ferrocene from a Molecular Orbital (MO) Theory perspective. A typical MO diagram for ferrocene is shown (Figure 4.1).

From the simple MO picture, it is clear why ferrocene is the most stable of all the metallocenes; it has an ideal number of electrons for Cp<sub>2</sub>Fe complexes. If each C<sub>5</sub>H<sub>5</sub><sup>-</sup> ligand is considered as a six-electron donor and this coupled with the six *d* electrons of Fe (II), then the molecule has 18 valence electrons. These nine pairs are accommodated precisely by filling all the bonding and non-bonding molecular orbitals and none of the anti-bonding ones. The *frontier orbitals* can be regarded as bonding (*e*<sub>2</sub>), non-bonding (*a*<sub>1</sub>) and anti-bonding (*e*<sub>1</sub>\*). The scheme is, of course, applicable to other metallocene of *D*<sub>5d</sub> symmetry. The molecular orbital energy level diagrams indicate that chemically

relevant frontier orbitals are neither strongly bonding nor anti-bonding, and this characteristic permits the possibility of the existence of metallocenes that diverge from the 18-electron rule. Deviations from the rule do lead to significant changes in M–C bond lengths that correlate quite well with the MO scheme. For instance, the short M–C distance in ferrocene results from the  $a'_{1g}$  frontier orbitals and all lower orbitals being full; and the  $e^*_{1g}$  frontier orbital and all higher orbitals being empty. Similarly, the redox properties of the complexes can also be understood in terms of electronic structure.



**Figure 4.1:** A qualitative molecular orbital diagram for ferrocene.<sup>22</sup>

Metal complexes are often classified as inner sphere and outer sphere redox couples based on whether their ligands are involved in the electron transfer step or not. In this case, the excellent stability of ferrocene arising from its 18-electron structure ensures that there are no structural rearrangements during the event of electron transfer.

This property, in fact, makes ferrocene a perfect outer-sphere reversible redox probe. This could also be compared with the Frank-Condon principle of electronic “excitation” wherein the electronic transition, which does not accompany any nuclear rearrangements, has the maximum probability. More interestingly, this very fact deems ferrocene as an excellent candidate for verifying standard theories of electron transfer like the Marcus theory, which is based on the criteria that there should not be much nuclear rearrangement during the actual electron transfer event.

In the case of other metallocenes with 15, 16 and 17 valence electrons, the non-bonding nature of the metal  $a'_{1g}$  and  $e_{2g}$  orbitals make them electron deficient, paramagnetic and highly reactive with the three non-bonding orbitals being only partly filled. Due to such reasons, ferrocene occupies a unique position as a standard redox probe in electrochemistry and allows the use of a large variety of electrochemical detection (ECD) techniques, including amperometry or voltammetry.<sup>23</sup>

This chapter presents an electrochemical investigation of ferrocene-nucleobase conjugates and ferrocene-oligonucleotide conjugates using cyclic voltammetry to understand the redox behavior of the systems.

## **4.2 Electrochemical Investigation of Ferrocene-Nucleobase Conjugates and Ferrocene-Oligonucleotide Conjugates**

The work presented in this chapter consists of studies on electrochemical investigation of structural conjugates of ferrocene with nucleobases and nucleic acids. This section gives an overview on background literature of ferrocene-nucleobase conjugates and ferrocene-oligonucleotide conjugates and also describes a rationale and objective for undertaking the research work.

### **4.2.1 Ferrocene-nucleobase conjugates**

The ferrocene-conjugated nucleobases presented in chapter 2 are examples where the hydrogen bonding groups of the nucleobases are not coordinated by the metal and engage in complementary hydrogen bonding. The metal is remote from the hydrogen bonding sites and may act as a receptor of base pairing. In this context, it is important to understand the effect of interactions between the tethered nucleobase moieties on the charge transfer behaviour of ferrocene. While the electrochemistry of nucleobases alone

has been an area of immense research interest<sup>24,25</sup> and first principle calculation of their redox behaviour is available,<sup>26,27</sup> only a few reports exist on the electrochemistry of ferrocene-derivatized nucleobases.<sup>28,29</sup> For instance, Hocek *et al.*<sup>29</sup> have investigated ferrocene derivatized purines having ethyl and ethynyl spacers, in which, only thermodynamics of charge transfer has been analyzed in terms of formal potentials without any systematic analysis of the kinetics. Nevertheless to our knowledge, no rigorous quantitative treatment exists correlating the electrochemical behaviour of ferrocene to the structure and molecular interactions of purine and pyrimidine substituents, except for a few recent reports on structure-activity correlations of ferrocene derivatized PNA monomers.<sup>30,31</sup>

In this regard, it was decided to study the synthesized ferrocene-nucleobase conjugates to investigate the electrochemical behaviour of such redox conjugates. In this chapter, the results of an electrochemical investigation of mono and bis-functional ferrocene-nucleobase conjugates with different spacer chain using cyclic voltammetry in nonaqueous media (*viz.* acetonitrile and DMF) are reported. The redox behaviour of the system was understood in terms of the quantitative functional parameters derived from experimental electrochemical data, which has been correlated with their molecular structure, especially the nature of the nucleobase moiety. Such information may be valuable for rational design of linkers to tether the nucleobases to the ferrocene moiety for achieving highly stable and reversible systems, crucial from the viewpoint of DNA detection assays. More significantly, the sensitivity of redox kinetics of the ferrocene label to the environment (like different electron tunneling distances, conformational changes, etc.) might help to separate the substituent electronic effects from steric effects on the electron transfer rate. Thus, the results of these investigations would be useful in deciding the mode and site of attachment of ferrocene label to the oligonucleotide strand for application in DNA biosensors.

#### 4.2.2 Ferrocene-oligonucleotide conjugates

DNA hybridization biosensors commonly rely on the immobilization of a single-stranded (ss) oligonucleotide probe onto a transducer surface to recognize—by hybridization—its complementary target sequence. Extensive research has been directed towards the detection of specific DNA sequences using real-time methods without

radioactive isotopes, for applications in clinical diagnostics,<sup>32</sup> environmental protection,<sup>33</sup> food quality control<sup>34</sup> and forensic science.<sup>35</sup> The binding of the surface-confined probe and its complementary target strand is translated into a useful electrical signal. Transducing elements reported in the literature have included optical, electrochemical, and micro-gravimetric devices. Of the above methods of transduction, the electroanalytical techniques are the best suited for DNA hybridization detection owing to their simplicity, ease of micro-fabrication, low cost and provision for array detection. Excellent reviews on DNA hybridization-biosensors have appeared in recent years.<sup>36</sup>

Thus the change of the electrochemical response of labeling DNA with metal complexes<sup>37</sup> or electroactive compounds<sup>38,39</sup> is one to the strategies for monitoring the DNA hybridization with a complementary strand. In this conjugation, ferrocene as label has been the subject of intense investigation due to its good stability, which affords convenient synthetic chemistry. The main interest in ferrocenyl-modified oligonucleotide (ODN) is for electrochemical DNA sensors and is also important in studies on DNA mediated electron transfer. Generally, the electroactive marker is bound on sugar or nucleic base of nucleotides, in using different coupling strategies that is, prior to, during or after the ODN synthesis on DNA/RNA synthesizer.

To simplify the chemical approach of ferrocene-labelled oligonucleotide, a strategy based on a replacement of a nucleotide directly by a ferrocene unit during automated solid-phase DNA synthesis has been developed (Chapter 3). Furthermore, an increase of detection sensitivity can be considered by an easy incorporation of several electroactive markers at any position of the sequence.

In this regard, ferrocenyl-oligonucleotides were synthesized and steady state cyclic voltammetry was performed to study the electrochemical behaviour of ferrocene-oligonucleotide conjugates. The electrochemical properties of these ferrocene-oligonucleotide conjugates were analyzed before and after hybridization with different oligonucleotides. In this chapter, the results of an electrochemical investigation of different ferrocenyl-oligonucleotides in aqueous media have been illustrated and the ability of using these ferrocenyl-labeled oligonucleotides in DNA sensors has been demonstrated.

### 4.3 Electrochemical Techniques

Electrochemistry is a powerful and sensitive analytical tool used for both qualitative and quantitative analysis. The utility of electrochemical methods is not only because of their sensitivity to trace amounts of species and simple instrumentation, but also because these methods can be used for separation of ionic species in addition to detection.

Different types are:

- Potentiometry is based on the measurement of solution potential in the absence of an appreciable current. These methods often employ ion selective electrodes for fast simple measurements of certain ionic species in solution.
- Coulometry measures the current passed through an indicator electrode while it is held at a fixed potential. By appropriate choice of potential, quantitative determination is achieved by simply integrating the current with time in order to calculate the charge passed.
- Voltammetry refers to method in which the current in an electrochemical system is measured as the voltage of the system is changed.

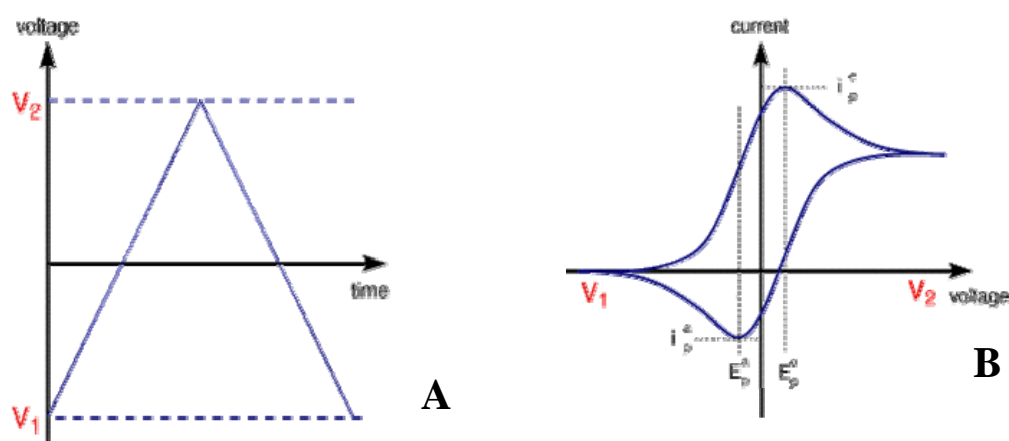
Voltammetry is one of the most useful electro-analytical techniques for obtaining fundamental information about electron transfer like redox potential and free energy changes. The technique involves monitoring the current response as a function of applied potential either by applying a potential ramp (Cyclic voltammetry) or a tiny differential pulse (Differential Pulse Voltammetry).

#### 4.3.1 Cyclic voltammetry

Cyclic voltammetry (CV) was performed to study electrochemical behaviour of ferrocene-nucleobase conjugates. Cyclic voltammetry involves the application of a cyclic potential sweep within a fixed potential window at a particular scan rate. The input potential waveform and the current-potential behavior obtained in a typical CV, particularly when the scan rate matches with the rate of electron transfer are shown in panels A and B of Figure 4.2.

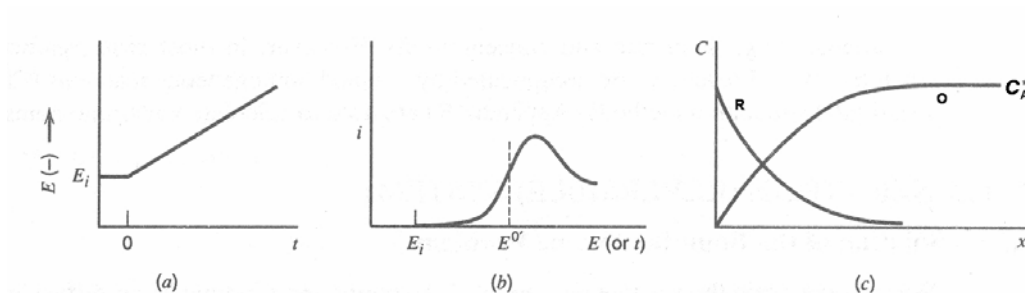
Cyclic voltammetry is used to determine the capacitance of electrochemical interfaces, to determine formal potentials and diffusion coefficients and to understand various electrochemical reactions taking place in the system. It is the most widely used

technique for acquiring qualitative information about electrochemical reaction. The power of CV results from ability to rapidly give considerable information on the thermodynamics of redox processes and the kinetics of heterogeneous electron transfer reaction and on coupled chemical reaction or absorption process. It offers a rapid location of redox potentials of the electro-active species, and convenient evaluation of the effect of media upon the reaction.



**Figure 4.2:** (A) Cyclic potential sweep, the voltage is swept between two values at a fixed rate, however now when the voltage reaches  $V_2$  the scan is reversed and the voltage is swept back to  $V_1$  (B) Resulting cyclic voltammogram is shown on the right hand side, where  $E_p^a$ ,  $E_p^c$  are anodic and cathodic peak potentials and  $I_p^a$ ,  $I_p^c$  are anodic and cathodic peak currents.

In these experiments current is recorded as a function of potential, which is equivalent to recording current vs. time. This technique known as linear potential sweep chronoamperometry also called linear sweep voltammetry.



**Figure 4.3:** (a) Linear potential sweep or ramp starting at  $E_i$  (b) Resulting  $i$ - $E$  curve (c) Concentration profiles of O and R for potential beyond the peak.

Let us consider a reaction  $O + e^- \rightarrow R$  with a formal redox potential  $E^{\circ'}$ ,



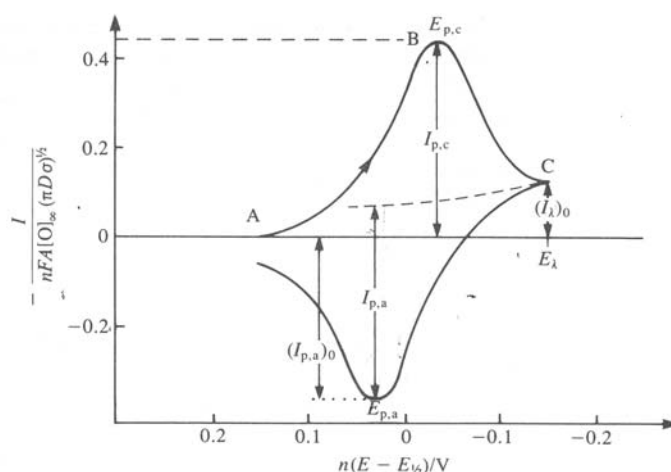
If the scan is begun at a potential more positive of  $E^{\circ'}$  for reduction, only nonfaradaic current will flow for a while. When the electrode potential reaches the vicinity of  $E^{\circ'}$ , the reduction begins and current starts to flow. As the potential continues to grow more negative, the surface concentration of oxidized species must drop: hence the flux to the surface (and current) increases. As the potential moves past  $E^{\circ'}$ , the surface concentration drops nearly to zero, mass transfer of oxidized species to the surface reaches a maximum rate and then it declines as the depletion effect sets in. The observation is therefore a peaked current potential curve like that in Figure 4.3b. At this point the concentration profiles near the electrode are like those in Figure 4.3c.

If we reverse the potential scan, the potential is swept in a positive direction and in the electrode vicinity there is a large concentration of reduced species. As the potential approaches and then passes  $E^{\circ'}$ , the electrochemical balance at the surface grows more and more current flows. This reversed current has a shape much like that of the forward peak for essentially the same reason. This experiment, which is called cyclic voltammetry, is a reversal technique.

#### 4.3.1A Classification of electrochemical systems

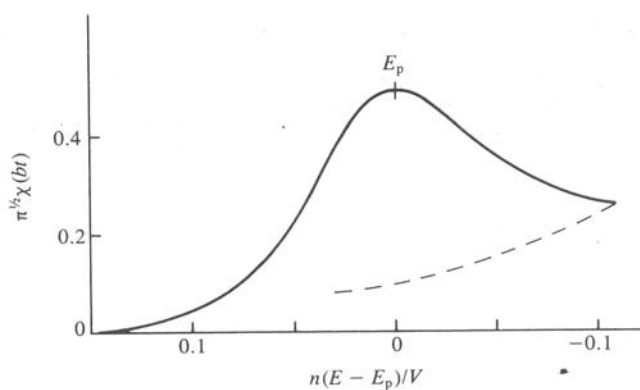
Based on their rate, the redox processes could be classified into reversible ( $k \sim 10^{-3}$  cm/s), irreversible ( $k \sim 10^{-9}$  cm/s) and quasi-reversible reactions ( $k \sim 10^{-3}$  to  $10^{-5}$  cm/s). For linear sweep and cyclic voltammograms of reversible reactions:

1.  $I_p \propto \nu^{1/2}$  ( $I_p$  is the peak current and  $\nu$  is the sweep rate)
  2.  $E_p$  independent of  $\nu$  ( $E_p$  is the peak potential)
  3.  $|E_p - E_{p/2}| = 56.6/n$  mV
- and for cyclic voltammetry,
4.  $E_{p,a} - E_{p,c} = 57.0/n$  ( $E_{\lambda} \gg E_{p,a}$  or  $E_{\lambda} \ll E_{p,c}$ ) ( $E_{\lambda}$  is the switching potential)
  5.  $|I_{p,a}/I_{p,c}| = 1$



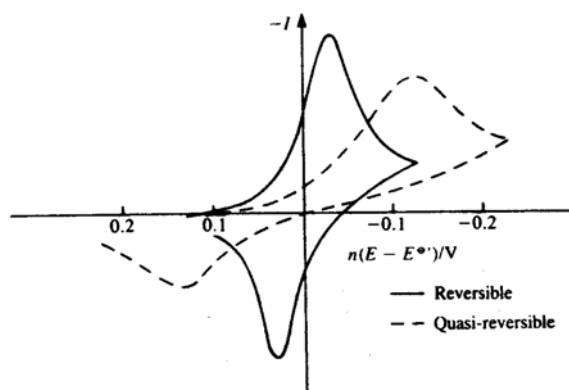
**Figure 4.4:** Cyclic voltammogram for a reversible system.

In the case of an irreversible reaction (Figure 4.5) or the type,  $O + ne^- \rightarrow R$ , linear sweep and cyclic voltammetry lead to the same voltammetric profile, since no inverse peak appears on inverting the scan direction. For an irreversible system ( $O + ne^- \rightarrow R$ ), in cyclic voltammetry, on inverting the sweep direction, one obtains only the continuation of current decay (Figure 4.5)



**Figure 4.5:** Linear sweep voltammogram for an irreversible system ( $O + ne^- \rightarrow R$ ). In cyclic voltammetry, on inverting the sweep direction, one obtains only the continuation of current decay (-----).

For quasi-reversible systems (Figure 4.6) the kinetics of the oxidation-reduction reactions has to be considered simultaneously. The extent of irreversibility increases with increase in sweep rate, while at the same time there is a decrease in the peak current relative to the reversible case and an increase in separation between anodic and cathodic peaks.

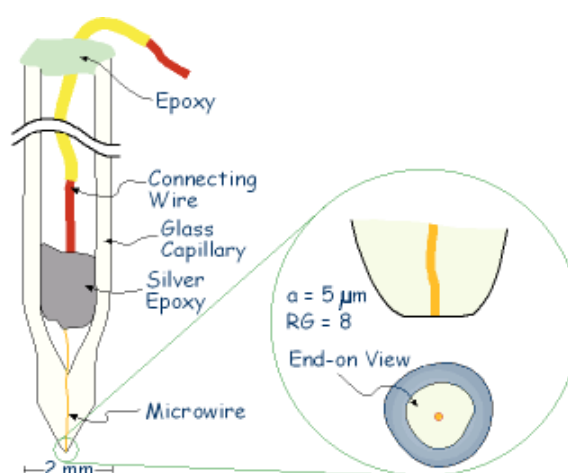


**Figure 4.6:** The effect of increasing irreversibility on the shape of cyclic voltammograms.

#### 4.3.2 Ultramicroelectrode voltammetry (steady-state voltammetry)

Steady-state cyclic voltammetry was performed to study electrochemical behaviour of ferrocene-oligonucleotide conjugates. Steady state cyclic voltammograms were recorded by fixing the ultramicroelectrode (UME) as tip. The tip signal is a Faradaic current from electrolysis of solution species. Microelectrodes, also commonly known as ultramicroelectrodes, may be defined as electrodes whose critical dimension is in the micrometer range, although electrodes with radii as small as  $10 \text{ \AA}$  have been fabricated.

A commonly used tip is based on an embedded disk-shaped geometry. A typical disk electrode would have a radius,  $a$ , of 1 to  $25 \text{ \mu m}$ . An insulator radius of 3 to 10 times larger than the electrode radius (the RG ratio) is desirable (Figure 4.7).

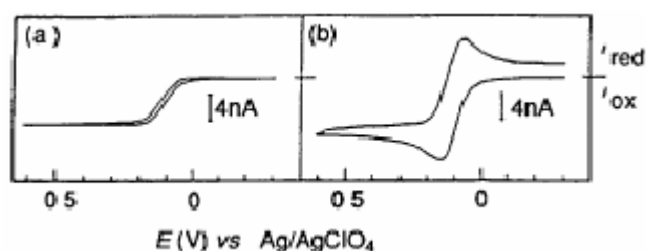


**Figure 4.7:** Schematic diagram of ultramicroelectrode.

The small size of microelectrodes makes diffusional mass transport extremely efficient. At relatively long experimental timescales, the dimensions of diffusion layer exceed the radius of the microelectrode, and the originally planar diffusion field transforms into a spherical diffusion field. Consequently, the flux of electroactive species to the electrode is substantially higher than for the pure planar diffusion case that is typical of a macroelectrode. This efficient mass transport allows one to observe steady-state responses when the applied potential is slowly scanned in cyclic voltammetry. The steady-state limiting current is directly proportional to the analyte concentration, making it useful for analysis. Another distinctive feature of microelectrodes is their ability to respond rapidly to changes in the applied potential, which makes them particularly useful in dynamic studies of short timescale homogeneous and heterogeneous electron-transfer processes.

The steady-state response arises because the electrolysis rate is equal to the rate at which molecules diffuse to the electrode surface. Steady-state is a stage when current is independent of time and is not observed for macroelectrodes but steady-state responses are easily observed for microelectrodes. To answer this difference, it is useful to determine the time over which steady-state behaviour will predominate and how this time regime is affected by the electrode radius.<sup>40</sup> To calculate a lower time limit at which the steady-state current contribution will dominate the total current, the ratio of the transient to steady-state contributions is useful parameter which gives dimensionless parameters. For example, taking a typical value of diffusion coefficient for an aqueous solution, then for a 5 mm radius electrode the experimental timescale must be longer than 80 seconds. Therefore, steady-state is not observed for macroelectrodes at the tens of milliseconds timescale typical of conventional electrochemical experiments.

However, reducing the electrode radius by a factor of a thousand to 5  $\mu\text{m}$ , means that a steady-state response can be observed for times longer than 80  $\mu\text{s}$ . Since, the steady-state current becomes more dominant with increasing time, steady-state responses are easily observed for microelectrodes in conventional electrochemical experiments. The unique voltammetric response of ultramicroelectrodes is an essential part of the steady-state voltammetry. The sigmoidal-shape of the wave indicates the current reaches a steady state in which the current is independent of time (Figure 4.8).



**Figure 4.8:** Cyclic voltammetric response at slow scan rates for the oxidation of 1.0 mM ferrocene at a gold disk microelectrode ( $r = 6.5 \mu\text{m}$ ). Supporting electrolyte is 0.1 M tetrabutyl ammonium perchlorate in acetonitrile.<sup>41</sup> (a) Scan rate is  $0.1 \text{ V s}^{-1}$  (b) scan rate is  $10 \text{ V s}^{-1}$ .

Sigmoidal-shaped response also indicates steady-state mass transfer is observed in slow scan-rate cyclic voltammetry. In contrast, at short experimental timescales (high scan-rates) peaked responses similar to those observed at conventional macroelectrodes are observed (Figure 4.8).

#### 4.3.2A Properties of Microelectrode

##### ✚ Reduced Capacitance

When an electrode comes into contact with an electrolytic solution, a double layer is formed at the interface, in which the charge present on the metal electrode is compensated by a layer of oppositely charged ions in the solution.<sup>42</sup> In many respects, this electrochemical double layer behaves like an electrolytic capacitor. In particular, when the applied potential is changed, a current flows to charge the double layer capacitance. This charging process complicates the electrochemical measurement.

The current required to charge the double layer of capacitance  $C$  must flow through a resistance  $R$  corresponding to the total cell resistance. The product  $RC$  represents the cell time constant. Now the question is what will be the effect of shrinking the electrode radius to the micrometer scale on the cell time constant? The electrode capacitance is an extensive property, and is proportional to the electrode area, thus the product  $RC$  decreases with decreasing electrode radius. The smaller  $RC$  cell time constants of microelectrodes means that they respond more rapidly to changes in the applied potential than their macroscopic counter parts. This ability to respond to changes in the applied potential at short timescales makes microelectrodes very attractive for investigating high-speed electron-transfer reactions.

### *Ohmic Effect*

When Faradaic and charging currents flow through a solution, they generate a potential that acts to weaken the applied potential, which can lead to severe distortions of experimental responses. Microelectrodes significantly reduce these Ohmic effects because the Faradaic currents observed are typically six orders of magnitude smaller than those at macroelectrodes. The immunity of microelectrodes to ‘Ohmic drop’ phenomena allows one to perform amperometric experiments in previously inaccessible samples such as non-polar solvents, supercritical fluids and solids.

#### **4.3.2B Applications**

Microelectrodes are predominantly used to determine analyte concentrations. The steady-state limiting current is directly proportional to both the diffusion coefficient and the concentration of the electroactive species. If the radius, the concentration and the steady-state current are known, it is possible to determine the diffusion coefficient. On the other hand if one knows the diffusion coefficient, then the analyte concentration can be determined.

The steady-state responses observed in slow-scan-rate cyclic voltammetry are also popular for determining heterogeneous electron-transfer rates of redox-active species. Using the steady-state response means that the voltammograms do not require correction for resistance and capacitance effects, and high-speed instrumentation is not needed.

## **4.4 Present Work: Experimental Section**

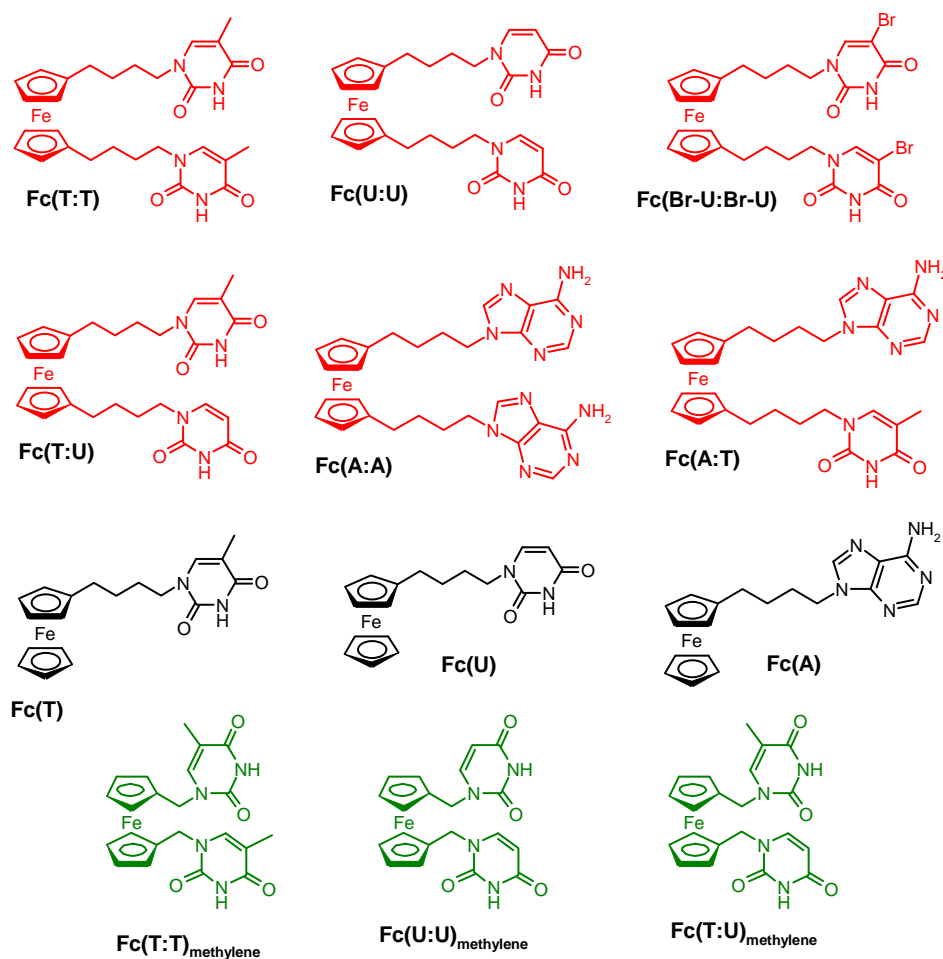
This section describes different electrochemical methods and chemical materials employed for investigation of electrochemical behaviour of ferrocene-nucleobase as well as ferrocenyl-oligonucleotides conjugates.

### **4.4.1 Electrochemical experiments for ferrocene-nucleobase conjugates**

#### **Chemical Materials**

Mono and bis-functional ferrocene-nucleobase conjugates with different spacer chain listed in Figure 4.9 were synthesized according to literature procedures.<sup>43</sup> Acetonitrile and DMF were of general reagent grade and were procured from Merck

limited, Mumbai, India. Acetonitrile and DMF were dried and distilled over  $\text{CaH}_2$  stored over Linde type 4Å molecular sieves in an atmosphere of argon. Lithium perchlorate ( $\text{LiClO}_4$ ) and ferrocene were of analytical grade, procured from Aldrich chemicals. Argon gas used for displacing dissolved oxygen in the electrolyte was of 99 % pure UHP grade.



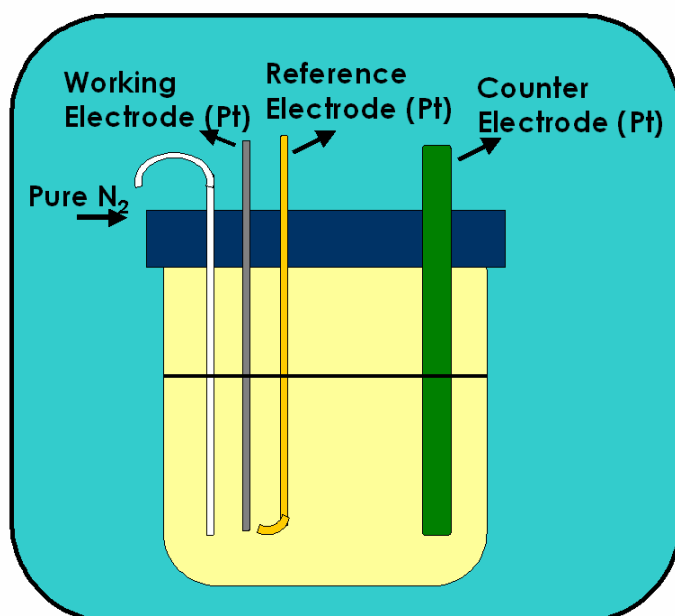
**Figure 4.9:** Ferrocene-linked mono and bis-nucleobase conjugates.

#### ✚ **Method: Cyclic Voltammetry (CV)**

Cyclic voltammetry (CV) is an important technique to study the redox behavior of the system. The electrochemical behaviour of ferrocene linked mono and bis nucleobase conjugates were studied by recording the cyclic voltammograms. All voltammograms were recorded using an Autolab PGSTAT30 (ECO CHEMIE) instrument. A conventional three-electrode setup with a Pt disk as working electrode (1.5

mm diameter), a rectangular Pt foil (2 x 1 cm) counter electrode and a Pt wire (0.5 mm thickness) as a quasi reference electrode (QRE) (calibrated using ferrocene/ferrocinium couple and the potentials were reported with respect to this couple), with 0.1M LiClO<sub>4</sub> (supporting electrolyte) dissolved in acetonitrile (in the case of Fc(T:T), Fc(U:U), Fc(T:U), Fc(A:A), Fc(A:T), Fc(T), Fc(U), Fc(A) with butyl spacer, Figure 4.9) and 0.1 M LiClO<sub>4</sub> dissolved in dry-distilled DMF (in the case of Fc(Br-U:Br-U, Figure 4.9) with butyl spacer and Fc(T:T)<sub>methylene</sub>, Fc(U:U)<sub>methylene</sub>, Fc(T:U)<sub>methylene</sub> with methylene spacer, Figure 4.9) containing 0.0227 mmol compound dissolved in the electrolyte in both the cases was used for the electrochemical investigations.

All the voltammograms were recorded after purging the electrolyte with pure argon. Each time, the working electrode was polished manually using 0.5 μm alumina slurry over a fine polishing cloth, washed by sonication in deionized water (Millipore, 18 MΩ), dried and rinsed with the solvent. The QRE was calibrated using cyclic voltammetry of 9 x 10<sup>-4</sup> M solution of ferrocene in the same electrolyte. The formal potential,  $E_{1/2}$  of the Fc<sup>0/1+</sup> couple was found to be 0.204 V (Vs Pt QRE) with respect to which, the potentials of the systems under investigation are reported throughout. The schematic representation of CV apparatus has shown (Figure 4.10).



**Figure 4.10:** Model of CV apparatus.



#### 4.4.2 Electrochemical experiments for ferrocene-oligonucleotide conjugates

##### ✚ Chemical materials

Ferrocene methanol was procured from Sigma-Aldrich chemicals. All aqueous solutions were made with MilliQ purified water. Buffer for steady-state voltammetry experiments were prepared as follow:

##### ❖ Phosphate buffer (pH = 7.4, 10 mmol NaCl) (100 mL)

$\text{Na}_2\text{HPO}_4$  (110 mg),  $\text{NaH}_2\text{PO}_4 \cdot 2\text{H}_2\text{O}$  (35.3 mg), NaCl (58.5 mg) was dissolved in minimum quantity of water and the total volume was made 100 mL. The pH of the solution was adjusted 7.4 with concentrated NaOH solution (in DI water).

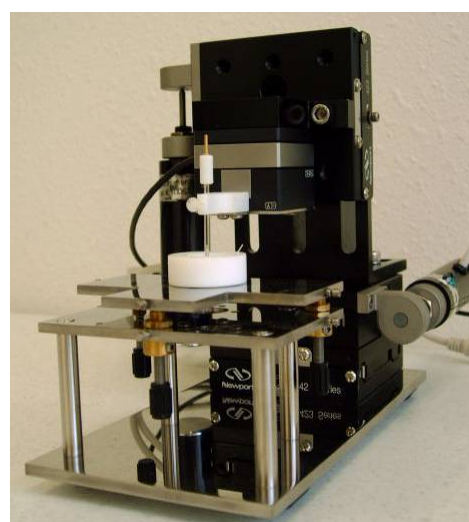
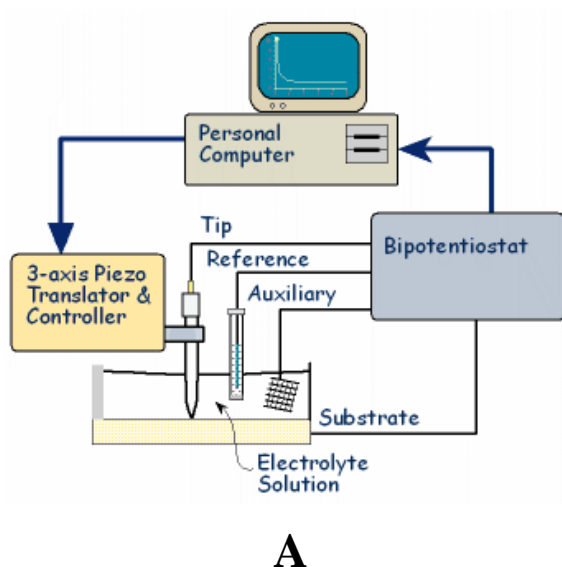
Oligonucleotide were synthesized and purified as mentioned in Chapter 3, Section 3.8.

##### ❖ Phosphate buffer (pH = 7.4, 10 mmol NaCl) (100 mL)

$\text{Na}_2\text{HPO}_4$  (110 mg),  $\text{NaH}_2\text{PO}_4 \cdot 2\text{H}_2\text{O}$  (35.3 mg), NaCl (585.0 mg) was dissolved in minimum quantity of water and the total volume was made 100 mL. The pH of the solution was adjusted 7.4 with concentrated NaOH solution (in DI water).

##### ✚ Method: Steady-state voltammetry

The instrument and schematic diagram for steady-state voltammetry is shown (Figure 4.11).



**Figure 4.11:** Schematic diagram of (A) steady-state voltammetry technique and (B) actual photograph of steady-state voltammetry instrument.

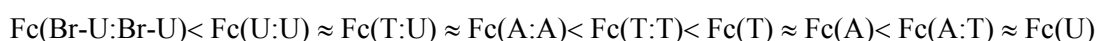
Steady-state voltammetry was performed using a model 900B CH Instruments bipotentiostat (Austin, TX, USA) with a three-electrode setup. A 25  $\mu\text{m}$  diameter Pt disk ultramicroelectrode procured from CH Instruments was used as the working electrode, a Pt wire counter electrode and Ag/AgCl, saturated KCl, reference electrode with ferrocene-oligonucleotide in aqueous buffer solution [2.5  $\mu\text{M}$  in phosphate buffer (pH 7.4), NaCl 10 mM]. The experiments were performed at room temperature (25  $^{\circ}\text{C}$ ).

## 4.5 Results and Discussion

The results of electrochemical investigation of ferrocene-nucleobase conjugates and ferrocene-oligonucleotide conjugates are summarized in this section.

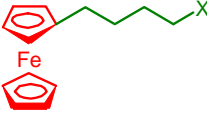
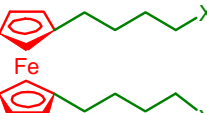
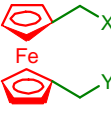
### 4.5.1 Ferrocene-nucleobae conjugates: electrochemical investigation

The electrochemical behaviour of mono and bis-functional ferrocene-nucleobase conjugates with different spacer chain (Figure 4.9) were studied by recording the cyclic voltammograms. The monofunctional ferrocene conjugates of Thymine Fc(T), Uracil Fc(U) and Adenine Fc(A) were found to exhibit a quasi-reversible redox behaviour similar to that reported for ferrocene<sup>44</sup> at a planar macroelectrode, the cyclic voltammograms (at 100  $\text{mV s}^{-1}$ ) of which are shown in Figure 4.12A. Also, compared to the monofunctional derivatives, the bifunctional derivatives of Thymine and Uracil-Fc(T:T), Fc(U:U) and Fc(T:U) showed an enhancement in peak currents in the respective CVs (Figure 4.12B and C), which implies better reactivity of the disubstituted derivatives compared to their monofunctional analogues. The formal potentials do not differ much with the nature of the nucleobase substituent, or mono or di substituents but from ferrocene the potentials were 70 mV less positive which means that there is an overall decrease in redox activity. However they could be arranged in the following order



The formal potentials of all the derivatives obtained from cyclic voltammetry are compiled in Table 4.1.

**Table 4.1:** Electrochemical data for ferrocene-nucleobase conjugate.

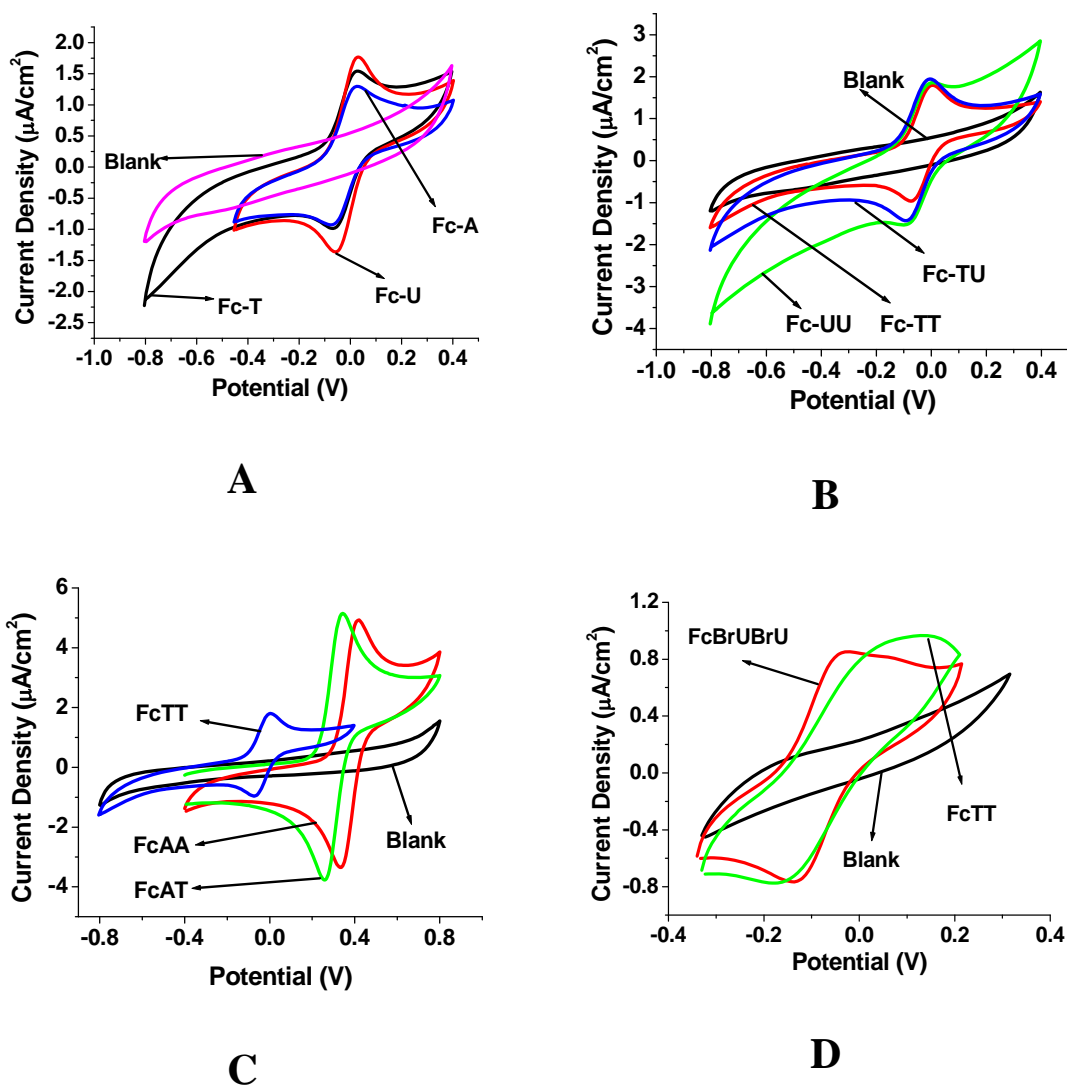
	Entry	Compound (calibrated to DMF)	$E_{1/2}$ (V) vs Pt QRE
	1	X = T	+ 0.29
	2	X = A	+ 0.29
	3	X = U	+ 0.30
	4	X = Y = T	+ 0.28
	5	X = Y = U	+ 0.27
	6	X = T, Y = U	+ 0.27
	7	X = Y = (Br)U	+ 0.26
	8	X = T, Y = A	+ 0.30
	9	X = Y = A	+ 0.27
	10	X = Y = T	+ 0.57
	11	X = Y = U	+ 0.55
	12	X = T, Y = U	+ 0.54
	13	Ferrocene (Acetonitrile)	+ 0.23
	14	Ferrocene (DMF)	+ 0.34

Analysis of this order provides considerable insight into the dependence of thermodynamic feasibility of charge transfer on the hydrogen bonding interactions of the tethered substituents. The less facile electron transfer in the bifunctional compounds, compared to that in the mono-functional ones could be attributed to a restriction in the charge induced reorientation about the n-butyl chain, owing to intramolecular hydrogen bonding present in the former. Also, single crystal X-ray diffraction analysis of the bifunctional conjugates shows a similar order in intramolecular hydrogen bonding,<sup>42</sup> which strongly supports the above interpretation of the trend in formal potentials.

The formal potentials of all these derivatives are slightly more negative than that of ferrocene, in contradiction to a report by Hocek *et al.*<sup>29</sup> on Adenine derivatized ferrocene, which has a more positive formal potential than that of ferrocene. Since the only difference in the experimental conditions between the reported work and present work is the supporting electrolyte, this behavioral change could be attributed to the

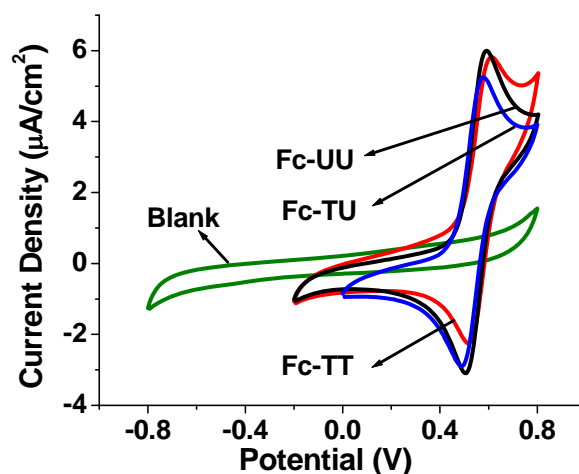
specific interactions between the supporting electrolyte and the redox species.<sup>45</sup> For example, lithium ions in non-aqueous solvents are reported to have strong interactions with intermediate radical anions produced during the redox process of some electroactive species.<sup>46</sup>

Figure 4.12D shows the cyclic voltammograms of Fc(T:T) and Fc(Br-U:Br-U) in DMF. A comparison of formal potentials shows that the dithymine derivative has a more facile charge transfer than that of the bis-bromouracil derivative and the electron transfer thermodynamics of Fc(T:T) does not show any significant solvent dependence, which is consistent with the solvent independent redox behavior of the Fc<sup>0/1+</sup> couple.<sup>47</sup>

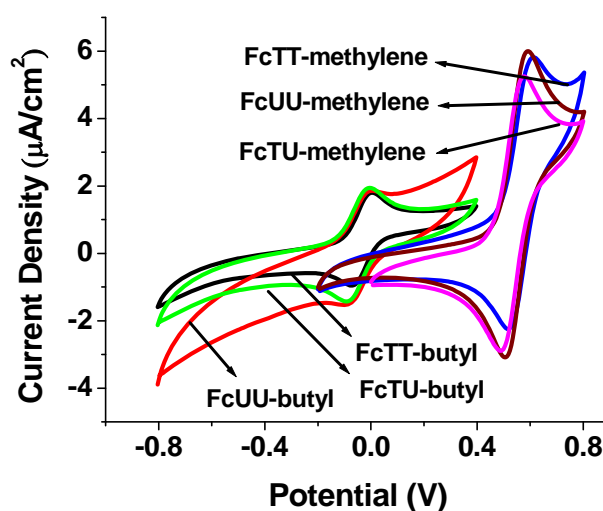


**Figure 4.12:** Cyclic voltammogram for ferrocene-nucleobase conjugates with *n*-butyl spacer for (A) entry 1 to 3, (B) entry 4 to 6, (C) entry 4,8 and 9, (D) entry 4 and 7 (Table 4.1).

Within methylene spacers also, there was no significant effect of change in bases; but the potentials were 200 mV more positive than that of ferrocene (Figure 4.13). There was a significant shift between methylene and butylenes compounds by +300 mV (Figure 4.14), which is very interesting. Thus it is apparent that ferrocene-nucleobase conjugates with methylene spacer are more easily oxidizable than ferrocene-nucleobase conjugates with butyl spacer.



**Figure 4.13:** Cyclic voltammogram for ferrocene-nucleobase conjugates with methylene spacer (entry 10-12, Table 4.1)



**Figure 4.14:** Comparison between the cyclic voltammograms of ferrocene-bis(nucleobase) conjugates with *n*-butyl spacer (entry 4-6, Table 4.1) and methylene spacer (entry 10-12, Table 4.1).

#### 4.5.2 Ferrocene-oligonucleotide conjugates: electrochemical investigation

The electrochemical responses of the ferrocene modified ODN were investigated by steady-state voltammetry (ultamicroelectrode voltammetry) experiments in buffered aqueous solution [2.5  $\mu$ M in phosphate buffer (pH 7.4)] at two different salt (NaCl) concentration [NaCl-10 mM and 100 mM] at 25 °C. Only one concentration of FcODN was used because each labeled ODN was synthesized in small quantities. Ferrocene modified oligonucleotide having ferrocene unit at different places (3' end, 5' end and middle position) were synthesized (Table 4.2, for synthesis see Chapter 3).

**Table 4.2:** Ferrocene-oligonucleotides conjugates

Entry	Code No.	Sequences
1	ODN-1	5'-AGA AAA GGA-3'
2	ODN-2	5'-TCC TTT TCT-3'
3	FcODN-1	5'-AGA AAA GGA— <b>Fc</b> --TCC TTT TCT-3'
4	FcODN-2	5'- <b>Fc</b> -AGA AAA GGA-3
5	FcODN-3	5'-TCC TTT TCT- <b>Fc</b> -T-3'

Different combinations were made for FcODNs (for 10mM and 100mM NaCl) (Table 4.3) and steady-state voltammetry was performed to examine the electrochemical response. The electrochemical response was also investigated before and after hybridization.

The OCV (at 100 mM NaCl) of FcODN-2 (entry 2) (OCV = 0.1 V) with ODN-1 (entry 16) (OCV = 0.03 V) and FcODN-3 (entry 3) (OCV = 0.12 V) with ODN-2 (entry 17) (OCV = 0.09 V) was then correlated. The difference in OCV [ $\Delta$ (OCV)] between FcODN-2 (entry 2) and ODN-1 (entry 16) was 70 mV and between FcODN-3 (entry 3) and ODN-2 (entry 17) was 30 mV. Thus more positive the OCV, more is the redox activity and the similar trend was observed with same oligonucleotide in buffer with 10 mM NaCl.

The  $E_{1/2}$  and OCV values of FcODN-2...FcODN-3 (entry 4) (10 mM NaCl:  $E_{1/2}$  = -0.2 V, OCV = 0.06 V; 100 mM NaCl:  $E_{1/2}$  = -0.13 V, OCV = 0.09 V) and ODN-1...ODN-2 (entry 18) (10 mM NaCl:  $E_{1/2}$  = -0.07 V, OCV = 0.05 V; 100 mM NaCl:  $E_{1/2}$  = -0.1 V, OCV = 0.03 V) was then correlated. The difference between these two sets was

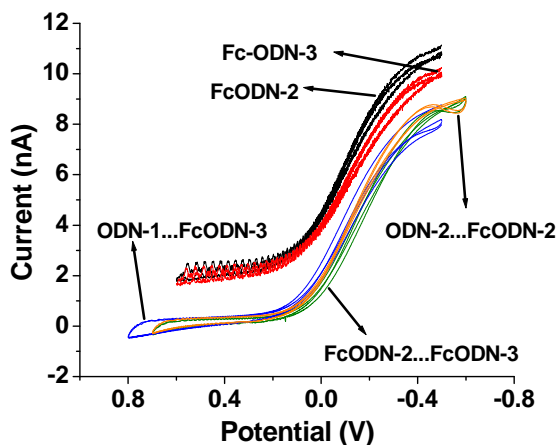
only the ferrocene unit content; one was ferrocenyl-modified oligonucleotide while other was normal oligonucleotide (without ferrocene unit). Here, with respect to change in  $T_m$  there was a shift in the  $E_{1/2}$  and OCV of Fc-containing sequences. The changes were appreciable only in the case of FcODNs and not for simple ODNs, which means that Fc-attachment is very useful for DNA hybridization sensors.

**Table 4.3:** Electrochemical data for ferrocene-oligonucleotide conjugate

Entry	Oligonucleotides	$E_{1/2}$ (vs Ag/AgCl) (V)		OCV (V)	
		10 mM NaCl	100 mM NaCl	10 mM NaCl	100 mM NaCl
1	FcODN-1	-0.09	-0.13	0.23	0.04
2	FcODN-2	-0.12	-0.04	0.12	0.10
3	FcODN-3	-0.14	-0.06	0.17	0.12
4	FcODN-2...FcODN-3	-0.2	-0.13	0.06	0.09
5	ODN-1...FcODN-3	-0.12	-0.12	0.05	0.10
6	ODN-2...FcODN-2	-0.15	-0.10	0.03	0.15
7	FcODN-1 (self complementary)	-0.10	-0.12	0.03	0.14
8	FcODN-1...ODN-1	-0.13	-0.10	0.02	0.14
9	FcODN-1...ODN-2	-0.15	-0.12	0.10	0.08
10	FcODN-1...FcODN-2	-0.13	-0.13	0.15	0.15
11	FcODN-1...FcODN-3	-0.18	-0.18	0.14	0.14
12	FcODN-1...ODN-1...ODN-2	-0.10	-0.10	0.16	0.16
13	FcODN-1...FcODN-2...FcODN-3	-0.15	-0.15	0.15	0.15
14	FcODN-1...ODN-1...FcODN-3	-0.13	-0.13	0.15	0.15
15	FcODN-1...ODN-2...FcODN-2	-0.13	-0.13	0.14	0.14
16	ODN-1	-0.13	-0.05	0.19	0.03
17	ODN-2	-0.04	-0.07	0.18	0.09
18	ODN-1...ODN-2	-0.07	-0.10	0.05	0.03
19	Ferrocene methanol std	+0.28		0.16	

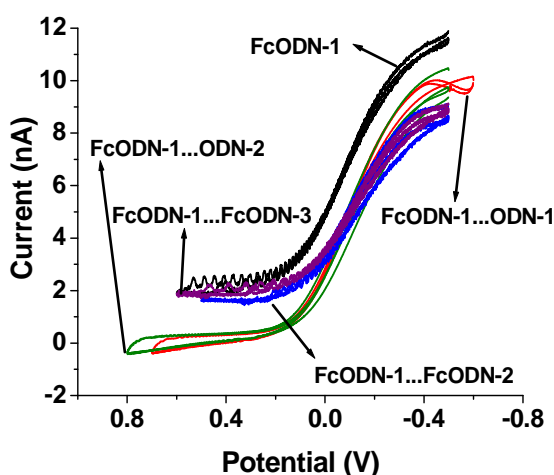
To show how electrochemical response changes with the number of Fc unit, OCV of FcODN-1, FcODN-2, FcODN-1...FcODN-2 and FcODN-1...FcODN-2...FcODN-3 (entry 1, entry 2, entry 10 and entry 13 respectively) at 100 mM NaCl which were 0.04, 0.1, 0.15, 0.15 V respectively was compared. OCV became more positive when two Fc units were present. However, when a third Fc unit was added, there was not much

change in  $E_{1/2}$  or OCV, which may be due to some structural feature that precluded the redox communication of all the three Fc units. The steady state cyclic voltammograms of intermolecular duplexes (entry 2-6, Table 4.3) constituted from the synthesized oligonucleotides are shown in Figure 4.15.



**Figure 4.15:** Steady state voltammograms of FcODN-2, FcODN-3, FcODN-2...FcODN-3, ODN-1...FcODN-3, ODN-2...FcODN-2 (entry 2, 3, 4, 5 and 6 respectively, Table 4.3) at a scan rate of 25 mV/s

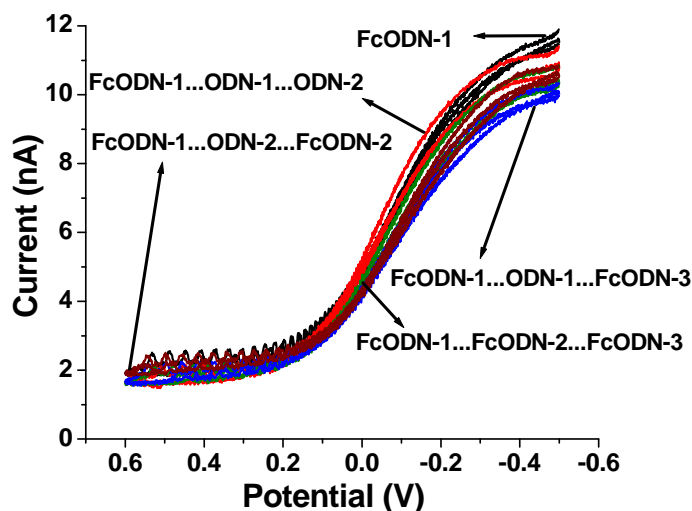
The steady state cyclic voltammograms of intermolecular duplexes (entry 1 and 8-11, Table 4.3) constituted from the synthesized oligonucleotides are shown in Figure 4.16.



**Figure 4.16:** Steady state voltammograms of FcODN-1, FcODN-1... ODN-1, FcODN-1...ODN-2, FcODN-1...FcODN-2, FcODN-1...FcODN-3 (entry 1, 8, 9, 10, and 11 respectively, Table 4.3) at a scan rate of 25 mV/s



The steady state cyclic voltammograms of intermolecular duplexes (entry 1 and 12 to 15, Table 4.3) constituted from the synthesized oligonucleotides are shown in Figure 4.17.



**Figure 4.17:** Steady state voltammograms of FcODN-1, FcODN-1... ODN-1...ODN-2, FcODN-1...Fc-ODN-2...FcODN-3, FcODN-1...ODN-1...FcODN-3, FcODN-1...ODN-2...FcODN-2 (entry 1, 12, 13, 14 and 15 respectively, Table 4.3) at a scan rate of 25 mV/s

All the Fc-ODNs have a more negative  $E_{1/2}$  than Fc-CH<sub>2</sub>OH (ferrocene methanol) indicating a reduction in redox activity of Fc moiety because of the attachment of oligonucleotides.

## 4.6 Conclusions

In the case of ferrocene-nucleobase conjugates, a significant shift in the formal potentials was seen depends on the spacer chain. In the case of ferrocene-nucleobase conjugates with *n*-butyl spacer, the formal potentials did not differ much with the nature of the nucleobase substituents or mono/di substituents, but from ferrocene the potentials were 70 mV less positive, which means that there is an overall decrease in redox activity. Within methylene spacers also, there was no significant effect of change in bases; but the potentials were 200 mV more positive than that for ferrocene. It is noticeable that there was a significant shift between methylene and butylenes conjugates by +300 mV, which is very interesting. Thus it is apparent that ferrocene-nucleobase conjugates with

*methylene spacer are more easily oxidizable than ferrocene-nucleobase conjugates with butyl spacer.*

In the case of ferrocene-conjugated oligonucleotides, there was a significant shift in the  $E_{1/2}$  value with hybridization. In a given buffer, there was a shift in  $E_{1/2}$  by about 70 mV after incorporating ferrocene to a simple oligonucleotide. All the ferrocene-tethered oligonucleotides have a more negative redox potential compared to ferrocene methanol standard, indicating that there is an overall decrease in redox activity of the ferrocene moiety after attaching to the oligonucleotides strands. In most of the cases, the redox potential became more positive after adding an extra ferrocene unit by hybridizing two ferrocene containing strands. These results demonstrate that all ferrocene-modified oligonucleotides are electrochemically detectable and can be used as signaling probes in the electronic detection of nucleic acids.

## 4.7 References

1. Eley, D. D.; Spivey, D. I. *Trans. Faraday Soc.* **1962**, *58*, 411-415.
2. (a) Wang, J. *Chem Eur. J.* **1999**, *5*, 1681-1685. (b) Braun, E.; Eichen, Y.; Sivan, U.; Ben-Yoseph, G. *Nature* **1998**, *391*, 775-778. (c) Pike, A. R.; Connolly, B. A.; Horrocks, B. R.; Houlton, A. *Aust. J. Chem.* **2002**, *55*, 191-194. (d) Storhoff, J. J.; Mirkin, C. A. *Chem. Rev.* **1999**, *99*, 1849-1862. (e) Mirkin, C. A. *Inorg. Chem.* **2000**, *39*, 2258-2272.
3. Mikkelsen, S. R. *Electroanalysis* **1996**, *8*, 15-19.
4. Piunno, P.; Krull, U.; Hudson, R.; Damha, M.; Cohen, H. *Anal. Chem.* **1995**, *67*, 2635-2643.
5. Okahata, Y.; Matsunobo, Y.; Ijio, K.; Mukae, M.; Murkami, A.; Makino, K. *J. Am. Chem. Soc.* **1992**, *114*, 8299-8300.
6. Wang, J. *Chem Eur. J.* **1999**, *5*, 1681-1685.
7. Epstein, J. R.; Biran, I.; Walt, D. R. *Anal. Chem. Acta.* **2002**, *469*, 3-36.
8. Fryer, R. M.; Randall, J.; Yoshida, T.; Hsiao, L.-L.; Blumenstock, J.; Jensen, K. E.; Dimofte, T.; Jensen, R. V.; Gullans, S. R. *Exp. Nephrol.* **2002**, *10*, 64-74.
9. McDonnell, J. M. *Curr. Opin. Chem. Biol.* **2001**, *5*, 572-577.
10. Wang, J.; Jiang, M.; Palecek, E. *Bioelectrochem. Bioenergetics* **1999**, *4*, 477-480.
11. Patolsky, F.; Lichtenstein, A.; Willner, I. *J. Am. Chem. Soc.* **2001**, *123*, 5194-5205.

12. Fritz, J.; Baller, M. K.; Lang, H. P.; Rothusizen, H.; Vettiger, P.; Meyer, E.; Guntherodt, H. -J.; Gerber, Ch.; Gimzewski, J. K. *Science* **2000**, 288, 316-318.
13. Wang, J. *Trends Anal. Chem.* **2002**, 21, 226-232.
14. Drummond, T. G.; Hill, M. G.; Barton, J. K. *Nat. Biotechnol.* **2003**, 21, 1192-1199.
15. Ozkan, D.; Erdem, A.; Kara, P.; Kerman, K.; Meric, B.; Hassmann, J.; Ozsoz, M. *Anal. Chem.* **2002**, 74, 5931-5936.
16. Boon, E. M.; Ceres, D. M.; Drummond, T. G.; Hill, M. G.; Barton, J. K. *Nat. Biotechnol.* **2000**, 18, 1096-1100.
17. (a) Wang, J.; *Nucleic Acids Res.* **2000**, 28, 3011-3016. (b) Mao, Y.; Luo, C.; Ouyang, Q. *Nucleic Acids Res.* **2003**, 31, e108. (c) Ihara, T.; Maruo, Y.; Takenaka, S.; Takagi, M. *Nucleic Acids Res.* **1996**, 24, 4273-4280. (d) Nagy, A. G.; Toma, S. J. *Organomet. Chem.* **1984**, 266, 257-268. (e) Wlassoff, W. A.; King, G. C. *Nucleic Acids Res.* **2002**, 30, e58. (f) Di Guisto, D. A.; Wjatschesslaw, A.; Gooding, J. J.; Messerle, B. A.; King, G. C. *Nucleic Acids Res.* **2005**, 33, e64. (g) Di Guisto, D. A.; Wlassoff, W. A.; Giesebrecht, S.; Gooding, J. J.; King, G. C. *J. Am. Chem. Soc.* **2004**, 126, 4120-4121. (h) Patolsky, F.; Weismann, Y.; Willner, I. *J. Am. Chem. Soc.* **2002**, 124, 770-772.
18. Arrayas, G. R.; Adrio, J.; Carretero, J. C. *Angew. Chem., Int. Ed. Engl.* **2006**, 45, 7674-7715.
19. Astruc, D. *Electron transfer and radical processes in transition-metal chemistry*; Wiley-VCH: New York, **1995**.
20. Van Staveren, D. R.; Metzler-Nolte, N. *Chem. Rev.* **2004**, 104, 5931-5985.
21. Abbott, N. L.; Jewell, C. M.; Hays, M. E.; Kondo, Y.; Lynn, D. M. *J. Am. Chem. Soc.* **2005**, 127, 11576-11577.
22. Long, N. J. In *Metallocenes: an introduction to sandwich complexes*. Blackwell Science Ltd., Oxford, **1998**.
23. Ciszowska, M.; Stojek, Z. *Anal. Chem.* **2000**, 754A-760A.
24. Santhanam, K. S. V.; Elving, P. J. *J. Am. Chem. Soc.* **1974**, 96, 1653-1660.
25. O'Reilly, J. E.; Elving, P. J. *J. Am. Chem. Soc.* **1971**, 93, 1871-1879.
26. Llano, J.; Eriksson, L. A. *Phys. Chem. Chem. Phys.* **2004**, 6, 4707-4713.
27. Llano, J.; Eriksson, L. A. *Phys. Chem. Chem. Phys.* **2004**, 6, 2426-2433.

28. Houlton, A.; Isaac, C. J.; Gibson, A. E.; Horrocks, B. R.; Clegg, W.; Elsegood, M. R. *J. J. Chem. Soc., Dalton Trans.* **1999**, 3229-3234.
29. Hocek, M.; Stepnicka, P.; Ludvik, J.; Cisarova, I.; Votruba, I.; Reha, D.; Hobza, P. *Chem. Eur. J.* **2004**, *10*, 2058-2066.
30. Baldoli, C.; Falciola, L.; Licandro, E.; Maiorana, S.; Mussini, P.; Ramani, P.; Rigamonti, C.; Zinzalla, G. *J. Organomet. Chem.* **2004**, *689*, 4791-4802.
31. Baldoli, C.; Licandro, E.; Maiorana, S.; Resemini, D.; Rigamonti, C.; Falciola, L.; Longhi, M.; Mussini, P. R. *J. Electroanal. Chem.* **2005**, *585*, 197-205.
32. MacPherson, J. M.; Gajadhar, A. A. *Mol. Cell. Probes* **1993**, *7*, 97-103.
33. Lucarelli, F.; Palchetti, I.; Marrazza, G.; Mascini, M. *Talanta* **2002**, *56*, 949-957.
34. Carnegie, P. R. *Australas. Biotechnol.* **1994**, *4*, 146-149.
35. Rao-Coticone, S.; Collins, P.; Dimsoski, P.; Ganong, C.; Leibelt, L.; Hennessy, C.; Shadravan, G.; Reeder, D. *Int. Congr. Ser.* **2003**, *3*, 1239.
36. (a) Gooding, J. J. *Electroanalysis* **2002**, *14*, 1149-1156. (b) Wang, J. *Anal. Chim. Acta* **2002**, *469*, 63-71. (c) Palecek, E.; Jelen, F. *Crit. Rev. Anal. Chem.* **2002**, *32*, 261-270.
37. (a) Cater, M. T.; Bard, A. J. *J. Am. Chem. Soc.* **1987**, *109*, 7528-7530. (b) Xu, X.-H. Bard, A. J. *J. Am. Chem. Soc.* **1995**, *117*, 2627-2631. (c) Millan, K. M.; Mikkelsen, S. R. *Anal. Chem.* **1993**, *65*, 2317-2323. (d) Hurley, D. J.; Tor, Y. *J. Am. Chem. Soc.* **1998**, *120*, 2194-2195. (e) Napier, M. E.; Loomis, C. R.; Sistare, M. F.; Kim, J.; Eckhardt, A. E.; Thorp, H. H. *Bioconjug. Chem.* **1997**, *8*, 906-913. (f) Armistead, P. A.; Thorp, H. H. *Anal. Chem.* **2001**, *73*, 558-564. (g) Lewis, F. D.; Helvoigt, S. A.; Letsinger, R. L. *Chem. Commun.* **1999**, 327-328.
38. (a) Whittemore, N. A.; Mullenix, A. N.; Inamati, G. B.; Manoharan, M.; Cook, P. D.; Tuinman, A. A.; Baker, D. C.; Chambers, J. Q. *Bioconjug. Chem.* **1999**, *10*, 261-270. (b) Mucic, R. C.; Herrlein, M. K.; Mirkin, C. A.; Letsinger, R. L. *Chem. Commun.* **1996**, 555-557. (c) Uto, Y.; Kondo, H.; Abe, M.; Suzuki, T.; Takenaka, S. *Anal. Biochem.* **1997**, *250*, 122-124. (d) Ihara, T.; Maruo, Y.; Takenaka, S.; Takagi, M. *Nucleic Acids Res.* **1996**, *24*, 4273-4281.
39. (a) Ihara, T.; Nakayama, M.; Murata, M.; Nakano, K.; Maeda, M. *Chem. Commun.* **1997**, 1609-1610. (b) Yu, C. J.; Wang, H.; Wan, Y.; Yowanto, H.; Kim, J. C.; Donilon, L. H.; Tao, C.; Strong, M.; Chong, Y. *J. Org. Chem.* **2001**, *66*, 2937-2942.

- (c) Anne, A.; Blanc, B.; Moiroux, J. *Bioconjug. Chem.* **2001**, *12*, 396-405. (d) Kim, K.; Yang, H.; Park, S. H.; Lee, D-S.; Kim, S-J.; Taik Lim, Y.; Tae Kim, Y. *Chem. Commun.* **2004**, *13*, 1466-1467. (e) Khan, S. I.; Grinstaff, M. W. *J. Am. Chem. Soc.* **1999**, *121*, 4704-4705.
40. Longmire, M. L.; Watanabe, M.; Zhang, H.; Wooster, T. T.; Murray, R. W. *Anal. Chem.* **1990**, *62*, 747.
41. Howell, J. O.; Wightman, R. M. *Anal. Chem.* **1984**, *56*, 524.
42. Bard, A. J.; Faulkner, L. R. *Electrochemical Methods*, Wiley, New York, **1980**.
43. Patwa, A. N.; Gupta, S.; Gonnade, R. G.; Kumar, V. A.; Bhadbhade, M. M.; Ganesh, K. N. *J. Org. Chem.* **2008**, *73*, 1508-1515.
44. Bond, A. M.; Hendersen, T. L. E.; Mann, D. R.; Mann, T. F.; Thormann, W.; Zoski, C. G. *Anal. Chem.* **1988**, *60*, 1878-1882.
45. Zuman, P. *Electrochim. Acta* **1976**, *21*, 687-692.
46. Holleck, L.; Becher, D. *J. Electroanal. Chem.* **1962**, *4*, 321-331.
47. Diggle, J. W.; Parker, A. J. *Electrochim. Acta* **1973**, *18*, 975-979.

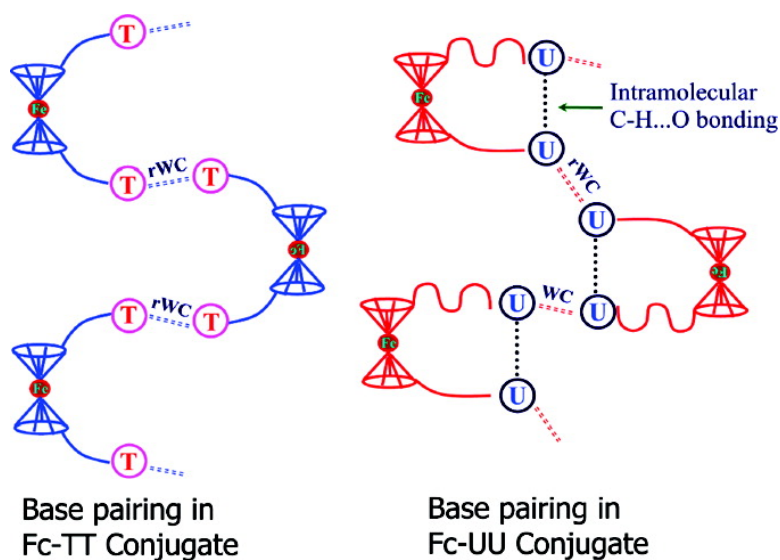
# Erratum

## Ferrocene-Linked Thymine/Uracil Conjugates: Base Pairing Directed Self-Assembly and Supramolecular Packing

Amit N. Patwa, Susmita Gupta, Rajesh G. Gonnade, Vaijayanti A. Kumar, Mohan M. Bhadbhade, and Krishna N. Ganesh

*J. Org. Chem.*, 2008, 73 (4), 1508-1515 • DOI: 10.1021/jo7023416 • Publication Date (Web): 23 January 2008

Downloaded from <http://pubs.acs.org> on April 6, 2009



### More About This Article

Additional resources and features associated with this article are available within the HTML version:

- Supporting Information
- Links to the 1 articles that cite this article, as of the time of this article download
- Access to high resolution figures
- Links to articles and content related to this article
- Copyright permission to reproduce figures and/or text from this article

[View the Full Text HTML](#)

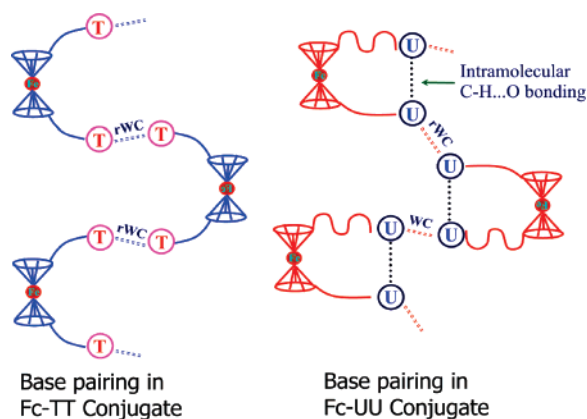
## Ferrocene-Linked Thymine/Uracil Conjugates: Base Pairing Directed Self-Assembly and Supramolecular Packing

Amit N. Patwa,<sup>†</sup> Susmita Gupta,<sup>†</sup> Rajesh G. Gonnade,<sup>‡</sup> Vaijayanti A. Kumar,<sup>†</sup>  
Mohan M. Bhadbhade,<sup>\*,‡</sup> and Krishna N. Ganesh<sup>\*,†,§</sup>

Division of Organic Synthesis and Center for Materials Characterization,  
National Chemical Laboratory, Pune 411008, India and Indian Institute of Science Education  
and Research, 900, NCL Innovation Park, Dr Homi Bhabha Road, Pune 411008, India

kn.ganesh@iiserpune.ac.in

Received October 30, 2007



Ferrocene-linked bis(nucleobase) (**1a–c**) and chimeric nucleobase (**1d**) conjugates have been synthesized from mono- and bis(hydroxybutyl)ferrocene **6** via Mitsunobu reaction as the key step. X-ray crystallographic studies of ferrocene bis(nucleobase) conjugates reveal two-dimensional supramolecular organizations of backbones through self-assembled Watson–Crick and reverse Watson–Crick type pairs. Ferrocene–bis(thymine) conjugate self-assembles by reverse Watson–Crick pairing, while the corresponding bis(uracil) conjugate self-assembles by alternating WC and reverse WC type pairing. Such continuous assemblies are not seen in monosubstituted ferrocene nucleobase conjugates which form only planar sheets. The results are interesting from the point of understanding and engineering supramolecular assemblies through rational design of base pairing patterns.

Development of supramolecular assemblies into well-defined architecture has been a subject of great interest in recent years in view of both its importance in the synthesis of artificial models for natural processes and its significance to obtain insight into the conformational features of biomolecules such as proteins, lipids, and nucleic acids.<sup>1</sup> A system of evolutionary perfection for molecular self-assembly is DNA/RNA.<sup>2</sup> The two antiparallel strands of DNA are held together by A:T and C:G base pairs to form the double helix where hydrogen bonding

between complementary bases and  $\pi$ -stacking interactions between the adjacent and stacked base pairs stabilize the double helical architecture.<sup>2</sup> Given the four natural nucleobases A, G, C, and T/U, at least 28 types of base pair modes are possible involving all combinations of self-base pairing and complementary base pairing through the diverse hydrogen bond donor–acceptor sites.<sup>2</sup> However, nature prefers only two types in the form of the canonical Watson–Crick (WC) and Hoogsteen (HG) complementary base pairing in most DNA/RNA structures. Hydrogen bond mediated supramolecular interactions have

<sup>†</sup> Division of Organic Synthesis.

<sup>‡</sup> Center for Materials Characterization.

<sup>§</sup> Indian Institute of Science Education and Research.

(1) Steed, J. W.; Atwood, J. L. *Supramolecular Chemistry*; Wiley: Chichester, UK, 2000. Lehn, J.-M. *Supramolecular Chemistry—Concepts and Perspectives*; VCH: Weinheim, Germany, 1995; Chapter 9.

(2) Saenger, W. *Principles of Nucleic Acid Structure*; Springer-Verlag: New York, 1984. Leonard, G. A.; Zhang, S.; Peterson, M. R.; Harrop, S. J.; Helliwell, J. R.; Cruse, W. B.; d'Estaintot, B. L.; Kennard, O.; Brown, T.; Hunter, W. N. *Structure* **1995**, 3 (4), 335–340.



provided inspiration to design a number of novel self-assembling systems.<sup>3</sup> Incorporation of the common nucleobases A, G, C, and T (or U) in the supramolecular environment enables exploration of different pairing characteristics of these nucleobases.<sup>4</sup> Guanine derivative self-assembles through Hoogsteen interaction into either linear tapes or macrocycles.<sup>5</sup> Self-pairing of adenine<sup>6</sup> as well as the 1-dimensional i-motif from C:C<sup>+</sup> base pairing via non-Watson–Crick base pairing in DNA<sup>7</sup> and PNA<sup>8</sup> have been reported. In view of these findings, there has been a great interest in developing novel approaches to self-assembled superstructures directed by nucleobase pairing in systems where the sugar–phosphate backbone is modified or replaced by synthetic linkers.<sup>9</sup> Studies of such designed systems are unraveling the importance of non-canonical, unusual modes of base pairing of the nucleobases, which have been recently detected in abundance in continuous 3-dimensional DNA lattice<sup>10</sup> and in DNA complexes having interstrand crosses.<sup>11</sup> Thus the study of unusual base pairings in nucleic acids and their model systems assumes new significance.

Currently bioorganometallic chemistry is growing rapidly, networking classical organometallic chemistry to biology, medicine, and molecular biotechnology.<sup>12–15</sup> Ferrocene and its derivatives have received a lot of importance in molecular recognition research, due to their redox characteristics.<sup>3,15,16</sup> Synthesis and self-association motifs of ferrocene-linked mono-(nucleobase) conjugates with a single carbon methylene spacer have been reported by Houlton's group.<sup>17</sup> An attractive feature of ferrocene is that the two cyclopentadienyl (Cp) rings can rotate around the Fe atom, which can act as a ball bearing,<sup>17</sup> and the vertical distance between the two Cp rings in ferrocene is 0.35 nm, which is similar to the distance between the stacked base pairs in DNA.<sup>2,18</sup> The redox active ferrocene units linked to self-base pairing nucleobases or DNA/RNA with a designed

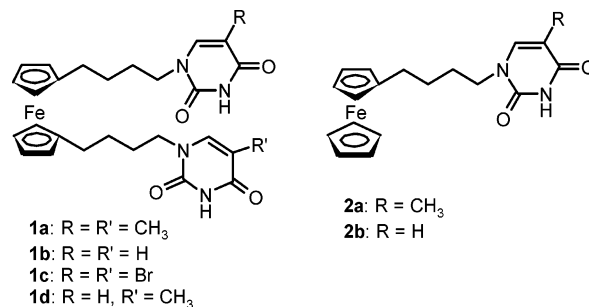


FIGURE 1. Structures of **1a–d** and **2a,b**.

spacer could therefore be useful building blocks in supramolecular chemistry coupling molecular recognition with electrochemistry, leading to novel applications for the electrochemical recognition of a large variety of DNA/RNA binding substrates.

In this paper, we report the construction of a series of new ferrocene-linked bisconjugates 1,1'-bis(*N*1-butylthymine) **1a**, 1,1'-bis(*N*1-butyluracil) **1b**, 1,1'-bis(*N*1-butyl-5-bromouracil) **1c**, and the chimeric 1-(*N*1-butyluracil)-1'-(*N*1-butylthymine) **1d** derivatives, in addition to the monoconjugates 1-(4-(thyminyl)butyl)ferrocene **2a** and 1-(4-(uracil)butyl)ferrocene **2b** (Figure 1). X-ray crystallographic analyses of these ferrocene–nucleobase conjugates reveal highly ordered and self-assembled structures arising from self-pairing of nucleobases in contiguous helical backbones via Watson–Crick (WC) and reverse Watson–Crick (rWC) type base pairings, leading to nucleobase-dependent differential supramolecular packing.

We chose a simple *n*-alkyl spacer to connect ferrocene with the nucleobases T and U and the *n*-butyl chain provided the appropriate hydrophobicity to enhance the solubility of the ferrocene-linked bis(nucleobase) conjugates in common organic solvents. The synthetic route for the bis(nucleobase) ferrocene target compounds involved the key intermediate 1,1'-bis(4-hydroxybutyl)ferrocene **6**<sup>19</sup> while the mono(nucleobase) ferrocene was synthesized from 1-(4-hydroxybutyl)ferrocene **11**. Compounds **6** and **11** were obtained from ferrocene, by reacting with either 1 or 2 equiv of succinic anhydride under Friedel–Craft reaction conditions followed by Zn/Hg reduction of carbonyl group and LAH reduction of the carboxylic acid to the corresponding alcohol, which was reacted with *N*3-protected T/U/5-BrU, under Mitsunobu reaction conditions, to yield **7a–c** and **12a,b**. This was followed by *N*3-debenzoylation with aq K<sub>2</sub>CO<sub>3</sub> in methanol–toluene or LiOH in THF–methanol to afford the target compounds **1a–c** and **2a,b** (Scheme 1). Compound **16** was synthesized from **6** in four steps involving protection of one hydroxyl with the TBDMS group to desymmetrize the molecule, Mitsunobu reaction of the second hydroxyl with *N*3-benzoylthymine, desilylation with TBAF, and reaction of the resulting hydroxyl with *N*3-benzoyluracil under Mitsunobu condition, followed by debenzoylation to obtain the chimeric mixed base ferrocene derivative **1d** (Scheme 2).

The crystal structures of **1a–d** were determined by single-crystal X-ray diffraction analysis (Supporting Information). The bis(thyminyl) ferrocene compound **1a** occupies crystallographic 2-fold symmetry axis passing through the central Fe atom of the ferrocene moiety with the *n*-butyl chains in the extended

(3) (a) Fan, E.; Vicent, C.; Geib, S. J.; Hamilton, A. D. *Chem. Mater.* **1994**, *6*, 1113–1117. (b) Cooke, G.; Rotello, V. M. *Chem. Soc. Rev.* **2002**, *31*, 275–286.

(4) Sivakova, S.; Rowan, S. J. *Chem. Soc. Rev.* **2005**, *34*, 9–21.

(5) (a) Davis, J. T. *Angew. Chem., Int. Ed.* **2004**, *43*, 668–698. (b) Krishnan-Ghosh, Y.; Liu, D.; Balasubramanian, S. *J. Am. Chem. Soc.* **2004**, *126*, 11009–11016.

(6) White, C. M.; Gonzalez, M. F.; Bradwell, D. A.; Rees, L. H.; Jeffrey, J.; Ward, M. D.; Armaroli, N.; Calogero, G.; Barigelletti, F. *J. Chem. Soc., Dalton Trans.* **1997**, 727–735.

(7) Ghodke, H. B.; Krishnan, R.; Vignesh, K.; Pavan Kumar, G. V.; Narayana, C.; Krishnan, Y. *Angew. Chem., Int. Ed.* **2007**, *46*, 2646–2649.

(8) Sharma, N. K.; Ganesh, K. N. *Chem. Commun.* **2005**, 4330–4332.

(9) Sessler, J. L.; Lawrence, C. M.; Jayawickramarajah, J. *Chem. Soc. Rev.* **2007**, *36*, 314–325.

(10) Paukstelis, P. J.; Nowakowski, J.; Birktoft, J. J.; Seeman, N. C. *Chem. Biol.* **2004**, *11*, 1119–1126.

(11) Noll, D. M.; Webba da Silva, M.; Noronha, A. M.; Wilds, C. J.; Michael Colvin, O.; Gamsik, M. P.; Miller, P. S. *Biochemistry* **2005**, *44*, 6764–6775.

(12) Fish, R. H.; Jaouen, G. *Organometallics* **2003**, *22*, 2166–2177.

(13) Schlotter, K.; Boeckler, F.; Hübner, H.; Gmeiner, P. *J. Med. Chem.* **2005**, *48*, 3696–3699.

(14) Pike, A. R.; Ryder, L. C.; Horrocks, B. R.; Clegg, W.; Elsegood, M. R. J.; Connolly, B. A.; Houlton, A. *Chem. Eur. J.* **2002**, *8*, 2891–2899.

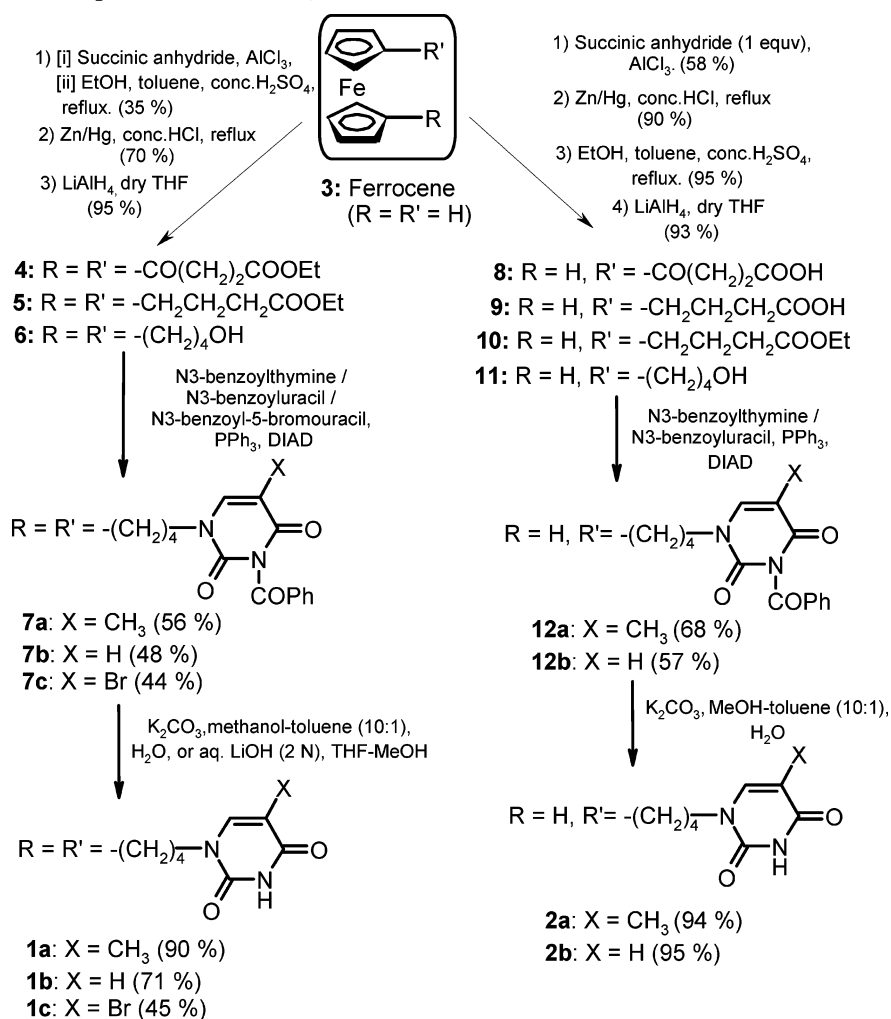
(15) Van Staveren, D. R.; Metzler-Nolte, N. *Chem. Rev.* **2004**, *104*, 5931–5986.

(16) Westwood, J.; Coles, S. J.; Collinson, S. R.; Gasser, G.; Green, S. J.; Hursthouse, M. B.; Light, M. E.; Tucker, J. H. R. *Organometallics* **2004**, *23*, 946–951. Li, C.; Medina, J. C.; Maguire, G. E. M.; Abel, E.; Gokel, G. W. *J. Am. Chem. Soc.* **1997**, *119*, 1609–1618. Inouye, M.; Takase, M. *Angew. Chem., Int. Ed.* **2001**, *40*, 1746–1748.

(17) Houlton, A.; Isaac, C. J.; Gibson, A. E.; Horrocks, B. R.; Clegg, W.; Elsegood, M. R. *J. Chem. Soc., Dalton Trans.* **1999**, 3229–3234.

(18) Deeming, J. In *Comprehensive Organometallic Chemistry*; Wilkinson, G.; Stone, F. G. A., Eds.; Pergamon: Oxford, UK, 1982; Vol. 4, p 475.

(19) Graham, P. J.; Lindsey, R. V.; Parshall, G. W.; Peterson, M. L.; Whitman, G. M. *J. Am. Chem. Soc.* **1957**, *79*, 3416–3420. Thomson, J. B. *Chem. Ind.* **1959**, 1122. Martin, E. L. *Organic Reactions*; J. Wiley & Sons, Inc.: New York, 1942; Vol. 1, pp 155–209.

SCHEME 1. Synthesis of Compounds 1a–c and 2a,b<sup>a</sup>

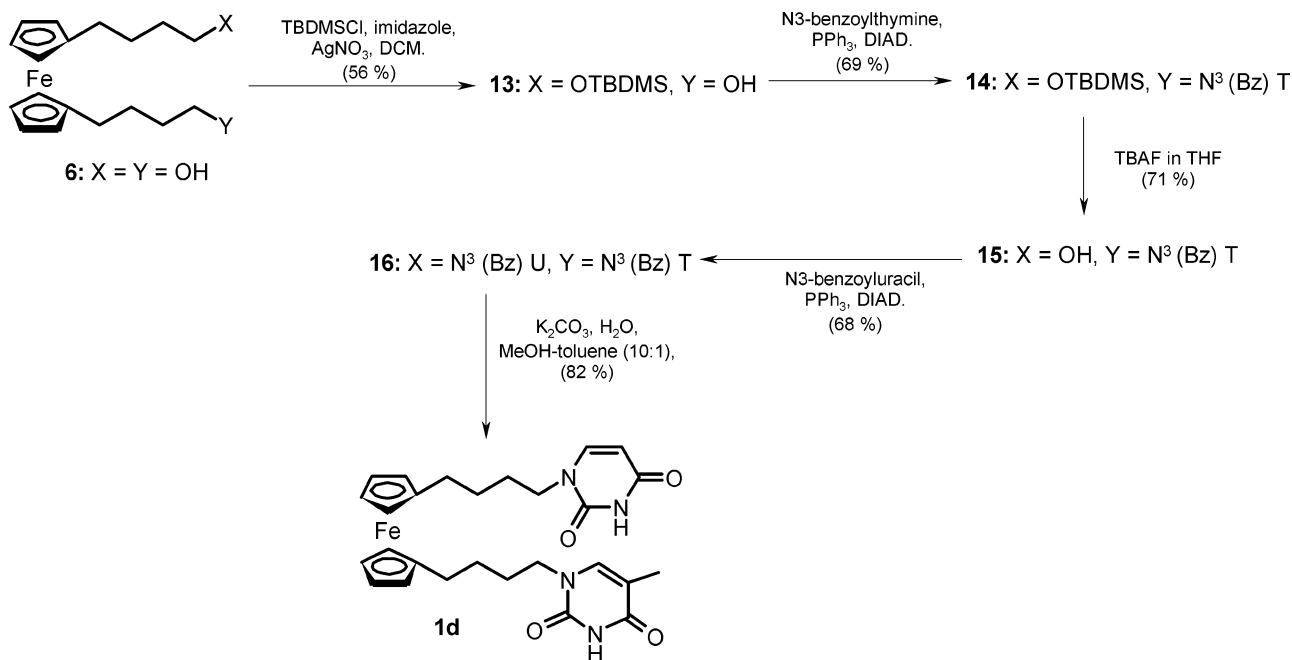
<sup>a</sup> Values in parentheses in each step indicate yields. For details see the experimental procedures.

conformation. A contiguous centrosymmetric, self-base pairing was seen via two N3–H3···O2 hydrogen bonds (H3···O2 = 2.14(3) Å, N3···O2 = 2.913(3) Å, and N3–H3···O2 = 169-(3)°, constituting “reverse Watson–Crick” (rWC defined as pairing involving O2 of T/U) type pairing (Figure 2A).<sup>2,15,17</sup> This self-pairing motif seems to be a dominant synthon in the self-assembly process during crystallization that leads to a regular helical backbone (Figure 2B). The bis-substituents linked to the Cp rings of ferrocene are staggered by ~67° around the ferrocene ring, with the methyl groups attached to the C5 atom of thymine bases pointing away from each other (Figure 3A).

**Self-Assembly in Bis(ferrocene) Conjugates.** The structure of bis(uracil) conjugate **1b** (Figure 2C) was devoid of 2-fold symmetry, with one of the *n*-butyl chains adopting an extended conformation and the other chain in the folded state. The U of the folded chain exhibited WC type self-pairing through O4 rather than O2 and making N3'–H3'···O4' interaction with U on the folded chain of the next molecule. Interestingly, the U on the extended chain formed a rWC type pairing with the U of the extended chain of the neighboring molecule via N3–H3···O2 hydrogen bond, in comparison to the WC type base pairing of U in the folded chains. This contiguous, alternating WC and rWC pairing motif formed the synthon of the bis(uracil) ferrocene helical backbone. The folded spacer chain conforma-

tion leads to additional intramolecular C6–H6···O2' interaction, which is absent in **1a** and results in relatively eclipsed orientation (~19°) of the two spacer chains in **1b** (Figure 3B).

The presence of the 5-methyl group in **1a** seems to sterically preclude the intermolecular (C5–H5···O4') and intramolecular (C6–H6···O2') interactions seen in **1b**, which perhaps leads to two different base pairings in the helical assembly of **1b**. To examine this, the 5-methyl in **1a** was replaced by 5-bromo in **1c**, whose crystal structure was found to be almost identical with that of **1a** (Supporting Information), reiterating the steric role of the 5-substituent in preventing the additional interactions seen in U:U pairings. Additionally, we also examined the crystal structure of the chimeric conjugate **1d**, in which one of the chains carried a thymine residue and the other a uracil moiety. Remarkably, the structure of **1d** was isomorphous to that of **1a**. The chimeric **1d**, which chemically lacks a 2-fold symmetry, acquired it in crystal structure by statistically distributing itself over two equally occupied orientations with the methyl group C7 having only half the occupancy (Supporting Information). Unlike **1b** that had alternate WC and rWC type pairings, compound **1d** exhibited only rWC type hydrogen bonding, in spite of having U:U base pairs as in analogous **1b**. There can be four possibilities of base pairings in **1d**, namely T:T, U:U, T:U, and U:T, but the observed structure corresponded to an average base pairing of 1/2(T+U)···1/2(T+U).

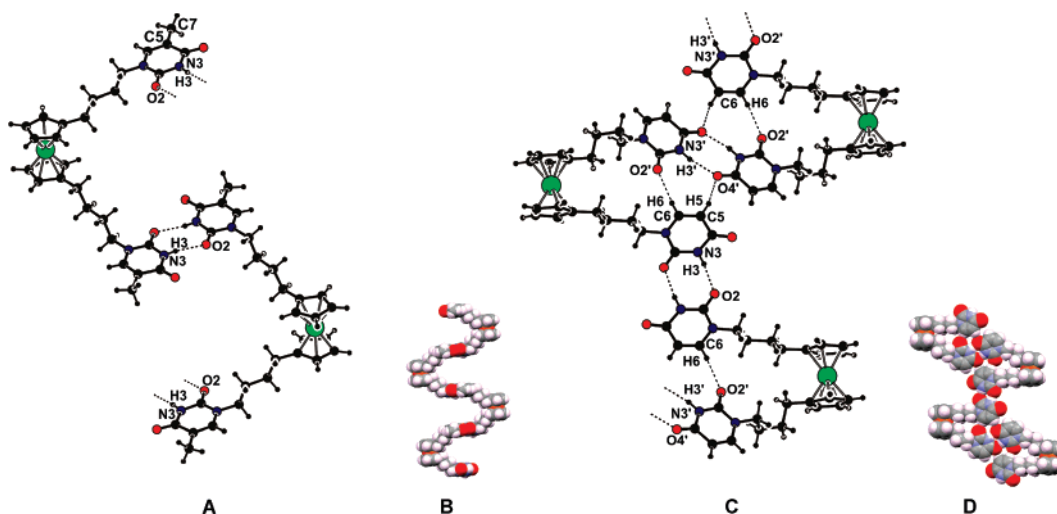
SCHEME 2. Synthesis Of compound **1d**<sup>a</sup>

<sup>a</sup> Values in parentheses in each step indicate yields.

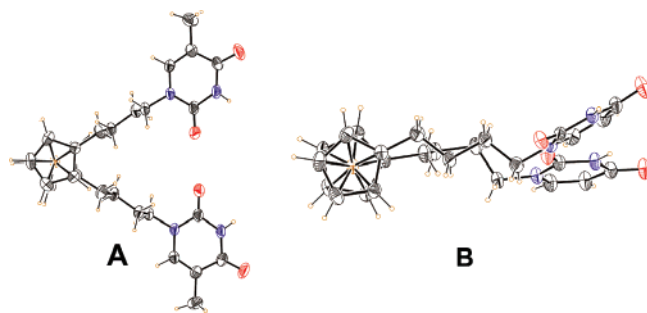
The accurate geometries of the T:T, U:U, and T:U base pairings are of considerable structural interest because of their presence in nucleic acids.<sup>2,20</sup> Very interestingly, the bis(uracil) derivative **1b** shows two different types of U:U base pairings in the same crystal form: a centrosymmetric rWC type with two N3–H3···O2 intermolecular contacts (H3···N2 = 2.13(3) Å, N3···O2 = 2.915(4) Å, and N3–H3···O2 = 176(3)°) as in **1a/1c/1d** and the other being centrosymmetric WC type pairing through two N3'–H3'···O4' H-bonds (H3'···O4' = 2.05(3) Å, N3'···O4' = 2.845(4) Å, and N3'–H3'···O4' = 169(3)° (Figure 2C). O4' participating in WC motif is involved in bifurcated hydrogen bonding via C5–H5···O4' interactions (H5···O4' = 2.41 Å, C5···O4' = 3.265(4) Å, and C5–H5···O4' = 152°). A weak C–H···O interaction of C5–H5 in uracil, possibly due to the absence of the methyl group, seems to cause a bending

of one of the side chains in bis(uracil) **1b** causing additional helical twist.

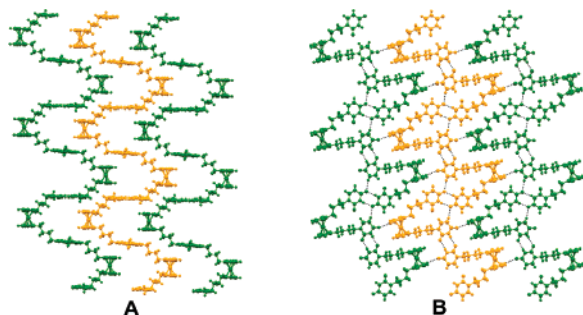
Sheets of infinite one-dimensional chains, self-assembled via base pairings, are shown (Figure 4). In **1a**, a regular helix with a pitch of ~20.33 Å has its bases almost perpendicular to the helical axis with no significant interhelical interactions in the sheet (Figure 4A). However, there are various C–H···O interactions made by a perpendicular interpenetrated sheet (Supporting Information). The planar sheet in **1b** with each helix having two types of U:U pairings almost in the plane of the sheet makes one C15–H15···O4 interhelical adhesion in this planar arrangement (Figure 4B) with a lower helical pitch of ~17.9 Å. **1a/1c/1d** show a single string of a regular helix (Figure 2B) while in **1b**, the helix is of “zigzag” type (Figure 2D); the absence of C5-methyl in **1b** provides possibilities for additional



**FIGURE 2.** T:T and U:U self-base pairing in **1a** (A) and **1b** (C). Molecule **1b** makes an intramolecular C6–H6···O2' contact. The inset shows the CPK model of a single helical strand for **1a** (B) and **1b** (D).



**FIGURE 3.** ORTEP of **1a** (A) and **1b** (B) viewed perpendicular to Cp rings.



**FIGURE 4.** A sheet of chain assemblies showing differences in architecture in **1a** (A) and **1b** (B).

interactions. Although coordination-induced self-assembly of helical chains is well-known, this is a novel example where self-base pairing present within the backbone leads to helical assemblies. The slightly different geometries of T:T and U:U base pairs lead to variations in interchain contacts causing different supramolecular structures.

#### Self-Assembly in Monosubstituted Ferrocene Conjugates.

Crystal structures of mono(thyminyl) ferrocene **2a** and mono(uracilyl) ferrocene **2b** were also determined by single-crystal X-ray diffraction method. Both the compounds are almost isostructural. Notably, molecules in both **2a** and **2b** form dimeric centrosymmetric self-base pairing of WC type via N3–H3···O4 (H3···O2 = 2.14(3) Å, N3···O2 = 2.847(3) Å, and N3–H3···O2 = 173(3)°) for **2a** and (H3···O2 = 2.02 Å, N3···O2 = 2.878(4) Å, and N3–H3···O2 = 173°) for **2b** hydrogen bond (Figure 5). These dimeric base pairs in **2a** and **2b** are held together with various C–H···O and C–H··· $\pi$  interactions forming planer sheet unlike **1a** and **1b** where molecules form helical assembly (Figure 6). The methyl group at C5 in **2a** did not make much effect in molecular packing. In **2b**, the side chain is in the extended form involved in WC type base pairing while in the corresponding bisconjugate **1b**, the WC type base pairing is observed with the side chain in folded form. The T:T and U:U base pairing seen in monosubstituted *n*-butyl spacer ferrocene conjugates is similar to that seen earlier in the mono(cytosinyl) ferrocene conjugates with methylene spacer chain.

In conclusion, the newly designed ferrocene-linked mono- and bis(nucleobase) conjugates show different supramolecular assemblies mediated via centrosymmetric base pairings (T:T, BrU:BrU, T:U) of rWC type and U:U pairings of both WC and rWC types. The structure of ferrocene–bis(uracil) **1b** is perhaps

the first example of WC and rWC like pairings being simultaneously present within the same crystal lattice. The comparison of structures clearly delineates the steric role of the 5-substituent in influencing the supramolecular packing by inhibiting specific inter- and intramolecular C–H···O contacts. The base pairing-directed self-assemblies are seen only in bis-substituted ferrocene conjugates and this topology is influenced by the C5 substituents. The self-assembly occurs through the use of all available hydrogen-bonding donors in the solid state. Such self-assembling organometallic units have utility in inducing chain reversal<sup>21</sup> and in building supramolecular scaffolds. Studies on different possible analogous base:base interactions in the ferrocene-linked complementary nucleobase (A:T/C:G) conjugates with different spacer chains including introduction of conjugation and their electrochemical studies are underway.

#### Experimental Section

**1,1'-Bis(3-carbethoxypropionyl)ferrocene (4).**<sup>19</sup> (A) A mixture of anhydrous aluminum chloride (96 g, 0.72 mol) in 200 mL of methylene chloride was treated with succinic anhydride (36 g, 0.36 mol). The mixture was stirred and shaken a few minutes and a solution of ferrocene **3** (33.3 g, 0.18 mol) in 200 mL of methylene chloride was added in small portions over a 10-min period. Hydrogen chloride gas was evolved and the heat of reaction brought the mixture to 35 °C. The dark violet viscous solution was allowed to stand 7 h at room temperature, poured onto ice, and filtered. The air-dried solid (yield 46 g) was extracted once with 800 mL of boiling water and twice with 150 mL of boiling water. The combined extract was cooled in an ice bath and filtered to obtain 19.7 g (38% yield) of crystalline 1,1'-bis(3-carboxypropionyl)ferrocene, mp 164–166 °C dec. (B) The above diacid was converted to the corresponding diethyl ester by slowly distilling a solution of the acid (21.3 g, 0.055 mol), sulfuric acid (1.5 g, 0.015 mol), ethyl alcohol (200 mL), and toluene (250 mL) through a small still. After slow distillation for 4 h, the remaining solution was cooled to room temperature and washed with 10% aqueous sodium carbonate solution (75 mL). The toluene solution was dried over magnesium sulfate, filtered, and evaporated at room temperature to obtain 23 g (94%) of red brown crystals of **4**, which were recrystallized from ethyl alcohol as shiny orange-brown platelets, mp 134–136 °C (ethyl alcohol). Yield 35% (combine two steps). <sup>1</sup>H NMR (CDCl<sub>3</sub>, 200 MHz)  $\delta$  1.27 (t, 6H,  $J$  = 7.1 Hz), 2.67 (t, 4H,  $J$  = 6.2 Hz), 3.01 (t, 4H,  $J$  = 6.0 Hz), 4.18 (q, 4H,  $J$  = 7.1 Hz), 4.57 (2, 4H), 4.87 (s, 4H). <sup>13</sup>C NMR (CDCl<sub>3</sub>, 50 MHz)  $\delta$  14.0, 27.5, 34.2, 60.3, 70.4, 73.5, 79.7, 172.7, 201.1. MS (LC-MS) ( $m/z$ ) calcd for C<sub>22</sub>H<sub>26</sub>O<sub>6</sub>Fe 442.28 [M<sup>+</sup>], found 443.36 [M<sup>+</sup> + 1], 465.42 [M<sup>+</sup> + Na]. Anal. Calcd for C<sub>22</sub>H<sub>26</sub>O<sub>6</sub>Fe: C, 59.73; H, 5.92. Found: C, 60.1; H, 5.81.

**1,1'-Bis(3-carbethoxypropyl)ferrocene (5).** To zinc amalgam (5.0 g) in water (3.0 mL), conc HCl (7.0 mL), benzene (5.0 mL), and ethanol (4.0 mL) is added **4** (2.5 g, 5.65 mmol). The mixture was refluxed briskly for 24–30 h, during which time conc HCl (2.5 mL) was added every 6 h. The solution was cooled to room temperature; the aqueous layer was separated, diluted with water (5.0 mL), and extracted with ether (3  $\times$  3.0 mL). The combined ether and benzene solutions are washed with water and dried over calcium chloride. The solvents are removed by distillation under diminished pressure, and the residue is purified by column chromatography on silica gel, and eluted with petroleum ether/ethyl acetate (8:2) to give **5** as reddish yellow oil. Yield 70%. <sup>1</sup>H NMR (CDCl<sub>3</sub>, 200 MHz)  $\delta$  1.24 (t, 6H,  $J$  = 7.0 Hz), 1.71–1.85 (m, 4H), 2.26–2.33 (m, 8H), 4.02 (s, 8H), 4.13 (q, 4H,  $J$  = 7.0 Hz). <sup>13</sup>C NMR (CDCl<sub>3</sub>, 50 MHz)  $\delta$  14.2, 26.3, 28.8, 33.9, 60.1, 68.1, 68.8, 88.2, 173.4. MS (LC-MS) ( $m/z$ ) calcd for C<sub>22</sub>H<sub>30</sub>O<sub>4</sub>Fe 414.32 [M<sup>+</sup>],

(20) Wahl, M. C.; Rao, S. T.; Sundaralingam, M. *Nat. Struct. Biol.* **1996**, *3*, 24–31.

(21) Moriuchi, T.; Nagai, T.; Hirao, T. *Org. Lett.* **2006**, *8*, 31–34.

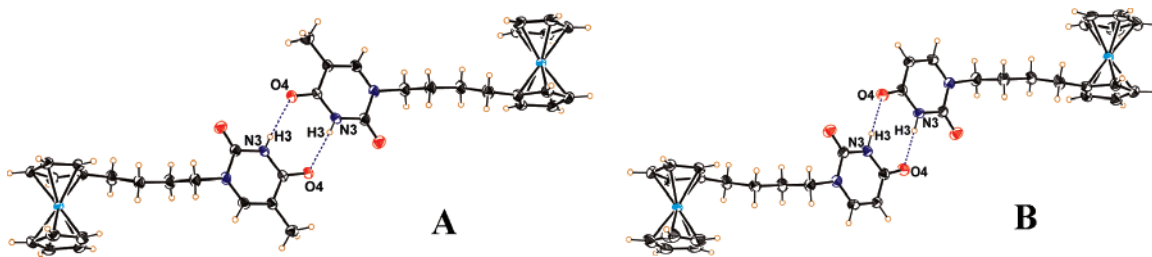


FIGURE 5. Self-base pairing in monosubstituted ferrocene conjugates **2a** (A) and **2b** (B).

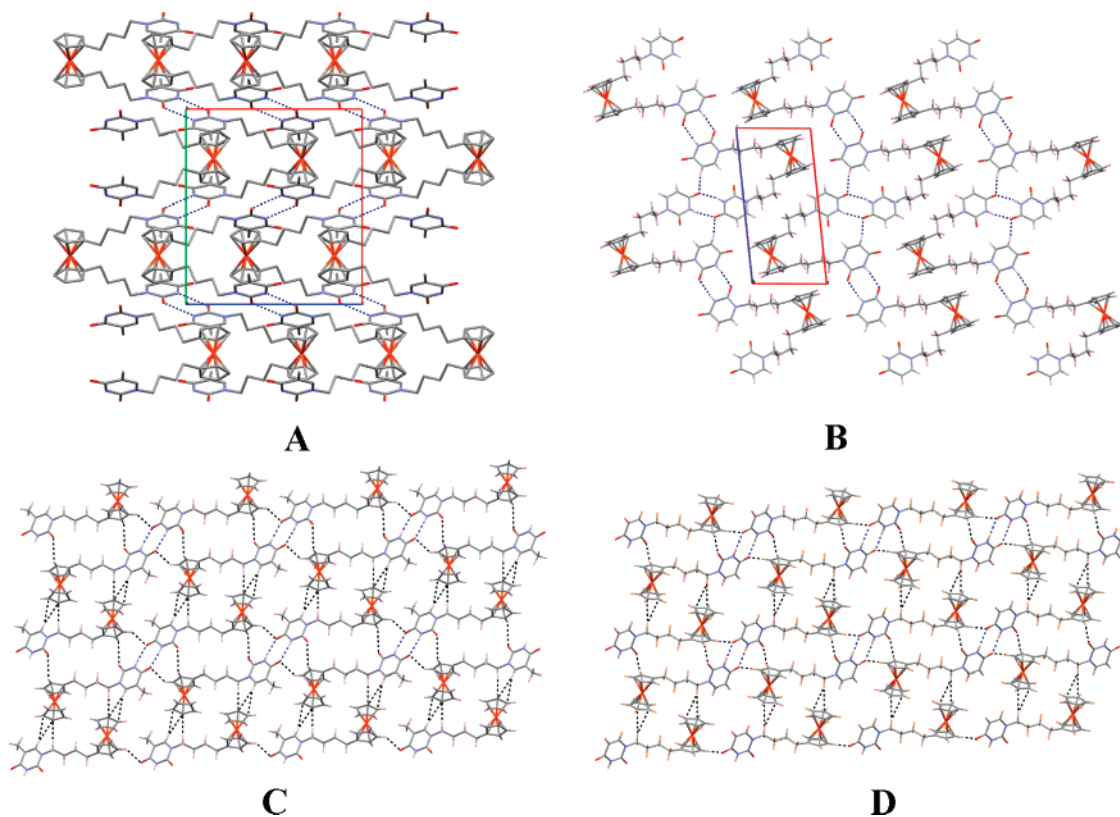


FIGURE 6. Molecular packing diagram of **1a** (A), **1b** (B), **2a** (C), and **2b** (D).

found 414.13 [M<sup>+</sup>]. Anal. Calcd for C<sub>22</sub>H<sub>30</sub>O<sub>4</sub>Fe: C, 63.76; H, 7.24. Found: C, 63.61; H, 7.62.

**1,1'-Bis(4-hydroxybutyl)ferrocene (6).** LiAlH<sub>4</sub> (1.22 g, 32.1 mmol) in dry THF (40 mL) was stirred for 10 min and a solution of **5** (2.2 g, 5.3 mmol) in dry THF (15 mL) was added drop by drop at such a rate to maintain gentle THF reflux. The reaction mixture was stirred for 3 to 4 h at room temperature followed by cooling in an ice-bath, quenching with slow addition of ice, and stirring for 1 h. The reaction mixture was filtered and washed with ether. The solvents are removed by distillation under diminished pressure, and the residue is purified by column chromatography on silica gel and eluted with petroleum ether/ethyl acetate (3:2) to give **6** as reddish-yellow oil: Yield 95%. <sup>1</sup>H NMR (CDCl<sub>3</sub>, 200 MHz) δ 1.53 (m, 8H), 2.26 (m, 4H), 3.58 (m, 4H), 4.08 (s, 8H). <sup>13</sup>C NMR (CDCl<sub>3</sub>, 50 MHz) δ 27.1, 28.6, 32.3, 62.3, 69.1, 70.1, 91.4. MS (LC-MS) (*m/z*) calcd for C<sub>18</sub>H<sub>26</sub>O<sub>2</sub>Fe 330.24 [M<sup>+</sup>], found 330.11 [M<sup>+</sup>]. Anal. calcd for C<sub>18</sub>H<sub>26</sub>O<sub>2</sub>Fe: C, 65.45; H, 7.87. Found: C, 65.11; H, 8.22.

**General Procedure for the Preparation of 7a–c via Mitsunobu Reaction.** *N*3-Benzoylthymine/*N*3-benzoyluracil (1.89 mmol) and triphenylphosphine (0.60 g, 2.27 mmol) were dissolved in dry THF (10 mL) and the solution was cooled to 0 °C. At this temperature alcohol **6** (0.25 g, 0.75 mmol), dissolved in dry THF (4 mL), was added to the stirred solution followed by dropwise

addition of DIAD (0.45 mL, 2.27 mmol). The solution was allowed to gradually reach room temperature and stirring was continued overnight. The solvent was removed under reduced pressure and the resulting solid was purified by flash chromatography on silica gel, packing with petroleum ether/triethylamine (98:2) and eluting with petroleum ether/ethyl acetate (7:3) to give ferrocene-linked *N*3-benzoylprotected nucleobase **7a–c**.

**1,1'-Bis(4-(*N*3-benzoylthyminyl)butyl)ferrocene (7a):** Yellow foam. Yield 56%. IR (thin film) 1745, 1695, 1650 cm<sup>-1</sup>. <sup>1</sup>H NMR (CDCl<sub>3</sub>, 200 MHz) δ 1.51–1.36 (m, 4H), 1.80–1.60 (m, 4H), 1.93 (s, 6H), 2.42–2.18 (m, 4H), 3.69 (t, 4H, *J* = 6.9 Hz), 4.02 (br s, 8H), 7.04 (s, 2H), 7.51–7.43 (m, 4H), 7.67–7.60 (m, 2H), 7.90 (d, 4H, *J* = 7.8 Hz). <sup>13</sup>C NMR (CDCl<sub>3</sub>, 50 MHz) δ 12.3, 28.0, 28.6, 28.8, 48.4, 67.9, 68.7, 88.1, 110.4, 129.1, 130.3, 131.6, 134.9, 140.2, 149.7, 163.1, 169.2. MS (LC-MS) (*m/z*) calcd for C<sub>42</sub>H<sub>42</sub>N<sub>4</sub>O<sub>6</sub>Fe 754.66 [M<sup>+</sup>], found 754.32 [M<sup>+</sup>], 777.21 (M<sup>+</sup> + Na).

**1,1'-Bis(4-(*N*3-benzoyluracyl)butyl)ferrocene (7b):** Orange foam. Yield 48%. IR (thin film) 1745, 1703, 1660 cm<sup>-1</sup>. <sup>1</sup>H NMR (CDCl<sub>3</sub>, 200 MHz) δ 1.58–1.41 (m, 4H), 1.78–1.65 (m, 4H), 2.40–2.26 (m, 4H), 3.79–3.66 (m, 4H), 3.99 (s, 8H), 5.76 (d, 2H, *J* = 8.1 Hz), 7.21 (d, 2H, *J* = 8 Hz), 7.51–7.46 (m, 4H), 7.67–7.62 (m, 2H), 7.91 (d, 4H, *J* = 7.4 Hz). <sup>13</sup>C NMR (CDCl<sub>3</sub>, 50 MHz) δ 28.0, 28.6, 28.9, 48.9, 68.0, 68.8, 88.1, 101.9, 129.2, 130.4, 131.4, 135.1, 144.3, 149.8, 162.5, 169.0. MS (LC-MS) (*m/z*) calcd



67.2, 68.1, 68.4, 88.1, 102.1, 144.3, 150.9, 164.0. MS (LC-MS) ( $m/z$ ) calcd for  $C_{18}H_{20}N_2O_2Fe$  352.21 [ $M^+$ ], found 352.05 [ $M^+$ ]. Anal. Calcd for  $C_{18}H_{20}N_2O_2Fe$ : C, 61.36; H, 5.68; N, 7.95. Found: C, 61.53; H, 5.52; N, 7.62.

**1-(4-Hydroxybutyl)-1'-(4-(tert-butyl)dimethylsilyloxy)butylferrocene (13).** Compound **6** (0.68 g, 2.06 mmol), imidazole (0.42 g, 6.18 mmol), and  $AgNO_3$  (0.17 g, 1.03 mmol) were dissolved in 20 mL of DCM and the resulting mixture was stirred at 0 °C. Then TBDMSCl (0.34 g, 2.266 mmol) in 10 mL of DCM was added dropwise and the reaction mixture was allowed to come to rt and stirred overnight, then extracted with DCM (3 × 20 mL), and the combined organic layer was washed with water and brine, dried over  $Na_2SO_4$ , and concentrated. The crude product was chromatographed on a silica gel column, packing with petroleum ether/triethylamine (98:2) and eluted with ethyl acetate/petroleum ether (1:19) to give compound **13** (515 mg, 56%). Reddish-yellow oil. Yield 56%.  $^1H$  NMR ( $CDCl_3$ , 200 MHz)  $\delta$  0.04 (s, 6H), 0.89 (s, 9H), 1.27 (br s, 1H), 1.69–1.37 (m, 8H), 2.39–2.16 (m, 4H), 3.70–3.51 (m, 4H), 4.01 (s, 8H).  $^{13}C$  NMR ( $CDCl_3$ , 50 MHz)  $\delta$  –5.3, 18.3, 26.0, 27.4, 29.2, 29.2, 32.6, 32.7, 62.8, 63.1, 67.66, 67.72, 68.6, 88.8, 89.2. MS (LC-MS) ( $m/z$ ) calcd for  $C_{24}H_{40}O_2SiFe$  444.51 [ $M^+$ ], found 444.30 [ $M^+$ ].

**1-(4-(N3-Benzoylthyminy)butyl)-1'-(4-(tert-butyl)dimethylsilyloxy)butylferrocene (14).** For the experimental procedure and setup see the Experimental Section in the Supporting Information. Brown oil. Yield 69%. IR (KBr) 1747, 1697, 1658  $cm^{-1}$ .  $^1H$  NMR ( $CDCl_3$ , 200 MHz)  $\delta$  0.04 (s, 6H), 0.88 (s, 9H), 1.57–1.45 (m, 6H), 1.78–1.64 (m, 2H), 1.94 (s, 3H), 2.43–2.21 (m, 4H), 3.60 (t, 2H,  $J = 5.4$  Hz), 3.69 (t, 2H,  $J = 7$  Hz), 3.97 (s, 8H), 7.02 (s, 1H), 7.51–7.43 (m, 2H), 7.67–7.59 (m, 1H), 7.90 (d, 2H,  $J = 7.3$  Hz).  $^{13}C$  NMR ( $CDCl_3$ , 50 MHz)  $\delta$  –5.3, 12.3, 18.3, 21.9, 25.9, 27.4, 28.2, 28.6, 29.0, 29.1, 32.7, 48.6, 63.0, 67.7, 67.9, 68.6, 87.9, 89.2, 110.5, 129.1, 130.3, 131.6, 134.9, 140.1, 149.7, 163.1, 169.1. MS (LC-MS) ( $m/z$ ) calcd for  $C_{36}H_{48}N_2O_4SiFe$  656.71 [ $M^+$ ], found 656.25 [ $M^+$ ], 679.24 [ $M^+ + Na$ ].

**1-(4-(N3-Benzoylthyminy)butyl)-1'-(4-hydroxybutyl)ferrocene (15).** To a stirred, cooled (0–5 °C) solution of **14** (0.29 g, 0.44 mmol) in THF (5 mL) was added 1 M solution of TBAF (1.3 mL, 1.32 mmol) in THF and the resulting mixture was stirred at 0–5 °C for 3 h. Solvent was removed under reduced pressure and extracted with DCM (3 × 10 mL). The combined organic layer was washed with water and brine, dried over  $Na_2SO_4$ , and concentrated. The crude product was chromatographed on a silica gel column, packed with petroleum ether/triethylamine (98:2), and eluted with ethyl acetate/petroleum ether (1:1) to give compound **15** (170 mg, 71%). Brown oil. Yield 71%. IR (KBr) 3431, 1747,

1697, 1650  $cm^{-1}$ .  $^1H$  NMR ( $CDCl_3$ , 200 MHz)  $\delta$  1.56–1.34 (m, 4H), 1.81–1.61 (m, 4H), 1.93 (s, 3H), 2.34–2.16 (m, 4H), 3.61–3.47 (m, 2H), 3.67 (t, 2H,  $J = 6.95$  Hz), 4.10 (s, 8H), 7.02 (s, 1H), 7.51–7.43 (m, 2H), 7.67–7.60 (m, 1H), 7.89 (d, 2H,  $J = 7.7$  Hz).  $^{13}C$  NMR ( $CDCl_3$ , 50 MHz)  $\delta$  12.3, 27.3, 28.1, 28.6, 28.9, 29.1, 32.5, 48.5, 62.6, 67.7, 67.9, 68.6, 88.0, 89.0, 110.5, 129.1, 130.3, 131.6, 134.9, 140.1, 149.8, 163.1, 169.1. MS (LC-MS) ( $m/z$ ) calcd for  $C_{30}H_{34}N_2O_4Fe$  542.46 [ $M^+$ ], found 542.14 [ $M^+$ ], 565.14 [ $M^+ + Na$ ].

**1-(4-(N3-Benzoylthyminy)butyl)-1'-(4-(N3-benzoyluracyl)butyl)ferrocene (16).** For the experimental procedure and setup see the Experimental Section in the Supporting Information. Yellow foam. Yield 68%. IR (thin film) 1747, 1699, 1660  $cm^{-1}$ .  $^1H$  NMR ( $CDCl_3$ , 200 MHz)  $\delta$  1.53–1.38 (m, 4H), 1.77–1.62 (m, 4H), 1.93 (s, 3H), 2.36–2.15 (m, 4H), 3.76–3.62 (m, 4H), 4.06 (br s, 8H), 5.76 (d, 1H,  $J = 7.8$  Hz), 7.03 (s, 1H), 7.20 (d, 2H,  $J = 7.8$  Hz), 7.54–7.41 (m, 4H), 7.69–7.58 (m, 2H), 7.96–7.85 (m, 4H).  $^{13}C$  NMR ( $CDCl_3$ , 50 MHz)  $\delta$  12.2, 27.9, 28.5, 28.6, 28.8, 48.4, 48.8, 68.0, 68.8, 88.2, 88.3, 101.8, 110.4, 129.1, 129.1, 130.3, 131.4, 131.6, 134.9, 135.0, 140.2, 144.3, 149.7, 149.7, 162.4, 163.1, 168.9, 169.2. MS (MALDI-TOF) ( $m/z$ ) calcd for  $C_{41}H_{40}N_4O_6Fe$  740.63 [ $M^+$ ], found 740.03 [ $M^+$ ].

**1-(4-(Thyminy)butyl)-1'-(4-(uracyl)butyl)ferrocene (1d).** The experimental procedure and setup are the same as those for **1a,b**. Yellow needle, mp 162–164 °C (DCM/methanol/toluene). Yield 82%. IR (thin film) 3184, 1697, 1674  $cm^{-1}$ .  $^1H$  NMR ( $CDCl_3 + 3-4$  drops of  $DMSO-d_6$ , 200 MHz)  $\delta$  1.52–1.42 (m, 4H), 1.75–1.60 (m, 4H), 1.88 (s, 3H), 2.33–2.20 (m, 4H), 3.70–3.61 (m, 4H), 4.04 (br s, 8H), 5.62 (dd, 1H,  $J = 2, 7.8$  Hz), 6.95 (s, 1H), 7.13 (d, 1H,  $J = 7.8$  Hz), 9.93 (br s, 1H), 10.06 (br s, 1H).  $^{13}C$  NMR ( $DMSO-d_6$ , 50 MHz)  $\delta$  12.1, 27.7, 28.5, 47.2, 47.5, 67.7, 68.6, 88.56, 88.60, 101.0, 108.6, 141.7, 145.9, 151.1, 151.2, 164.0, 164.5. MS (LC-MS) ( $m/z$ ) calcd for  $C_{27}H_{32}N_4O_4Fe$  532.42 [ $M^+$ ], found 532.13 [ $M^+$ ], 555.13 [ $M^+ + Na$ ]. Anal. Calcd for  $C_{27}H_{32}N_4O_4Fe$ : C, 60.90; H, 6.05; N, 10.52. Found: 60.58, 6.05, 10.33.

**Acknowledgment.** The authors thank CSIR-UGC, New Delhi for research fellowship (A.N.P. and S.G.) and K.N.G. acknowledges the Department of Science and Technology, New Delhi, for award of the JC Bose Fellowship.

**Supporting Information Available:** Experimental procedures, spectroscopic details of new compounds, and data for single crystal X-ray analysis of **1a–d** (CIF). This material is available free of charge via the Internet at <http://pubs.acs.org>.

JO7023416